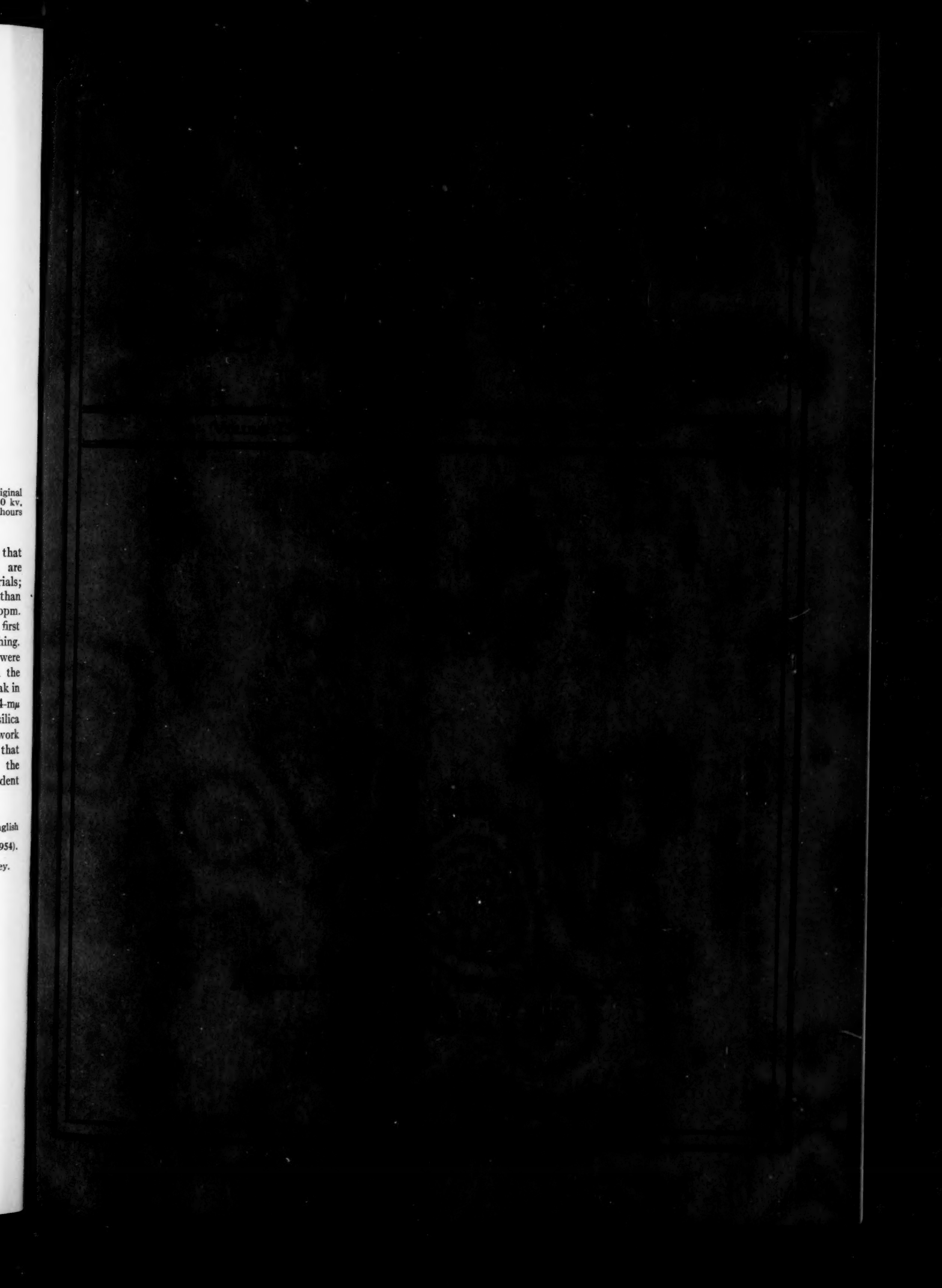

Volum

IN rec
molec
in the ass
states of
of these
view of s

The n
been des
ized exc
descripti
to expla
spectra c
arising f
only a sn
band, eq
the unit
approacl
method
transitio

The el
interest
has beer
transitio

[1] J. Fre
Physik 13
[2] A. S.
(1948).
[3] H. Wi

THE JOURNAL
OF
CHEMICAL PHYSICS

VOLUME 23, NUMBER 5 MAY, 1955

Theory of the Lower Excited Electronic States of the Benzene Crystal

DAVID FOX, *Department of Physics*
AND
OTTO SCHNEPP, *Laboratory of Physical Chemistry, Israel Institute of Technology, Haifa, Israel*
(Received September 27, 1954)

For the two lowest exciton bands of benzene, calculations have been carried out for the band widths and for the energies of the levels to which dipole transitions from the ground state are allowed. Expressions have been derived for the intensities of crystal transitions corresponding to both allowed and forbidden molecular transitions and have been applied to the case of the benzene crystal. Comparison is made with available experimental data and additional experiments are suggested so that further comparison may be made. From the band widths, evidence is obtained that the lowest excited state of the benzene molecule belongs to the B_{2u} representation of the molecular group, D_{6h}.

I. INTRODUCTION

IN recent years the investigation of the spectra of molecular crystals has become of interest as an aid in the assignment of symmetries of the excited electronic states of the constituent molecules. The excited states of these crystals are also of interest from the point of view of solid-state theory.

The nonconducting states of molecular crystals have been described in terms of exciton states, i.e., nonlocalized excitation waves.[1] Davydov[2] has applied this description to crystals of aromatic molecules in order to explain sharp structure in the low-temperature spectra of these crystals. He showed that selection rules arising from considerations of crystal symmetry allow only a small number of transitions to levels in the crystal band, equal to or less than the number of molecules in the unit cell. Winston[3] developed a group theoretical approach to the same problem and found a simple method for determining the number of allowed crystal transitions and their polarizations.

The electronic spectrum of solid benzene is of special interest because of the large amount of work which has been done on the molecular spectrum. The first transition in solid benzene was first observed by Kronenberger,[4] and more recently by Broude, Medvedev, and Prikhot'ko[5] who used single crystals and polarized light. Davydov,[6] using the results of his earlier work, applied group theoretical methods to find the number and polarizations of the allowed components of the 0—0 transition; comparing his predictions with the observations of Broude *et al.*, he concluded that the lowest excited molecular state belongs to the irreducible representation B_{2u} of the molecular symmetry group D_{6h}. In his treatment he made an approximation with respect to the crystal structure which is not justified in the light of the most recent x-ray determination.[7] Winston[3] applied his method to benzene and his results are not in agreement with those of Davydov.

In this paper we shall calculate the energies of the benzene crystal states to which dipole transitions from the ground state are allowed. The bands corresponding to the B_{1u} and B_{2u} molecular states will be considered and the exciton band widths for each will be calculated. A preliminary report of these results has been published.[7a] Expressions will be derived for the intensities of crystal transitions corresponding to both allowed and

[1] J. Frenkel, Phys. Rev. **37**, 17, 1276 (1931); R. Peierls, Ann. Physik **13**, 905 (1932).
[2] A. S. Davydov, J. Exptl. Theoret. Phys. (U.S.S.R.) **18**, 210 (1948).
[3] H. Winston, J. Chem. Phys. **19**, 156 (1951).
[4] A. Kronenberger, Z. Physik **63**, 497 (1930).
[5] Broude, Medvedev, and Prikhot'ko, J. Exptl. Theoret. Phys. (U.S.S.R.) **21**, 665 (1951).
[6] A. S. Davydov, J. Exptl. Theoret. Phys. (U.S.S.R.) **21**, 673 (1951).
[7] E. G. Cox and J. A. S. Smith, Nature **173**, 75 (1954); E. G. Cox (private communication).
[7a] D. Fox and O. Schnepp, Phys. Rev. **96**, 1196 (1954).

forbidden molecular transitions and will be applied to the case of the benzene crystal. We shall discuss the revisions that are required in Davydov's work[2,6] by the latest crystallographic determination,[7] as well as by the refinements discussed by Winston.

Because of the smallness of the perturbation on the molecule by the crystal field, each crystal exciton band is readily correlated with a molecular state. The electronic states of the benzene molecule have been studied by many investigators, both theoretically and experimentally. Theoretical calculations by the molecular orbital method were carried out using the wave functions of Mayer and Sklar.[8,9] These calculations predict that the lowest excited states belong, in order of increasing energies, to the representations B_{2u}, B_{1u}, and E_{1u} of the symmetry group D_{6h}. Theoretical investigations by the valence-bond method, with considerable refinements, lead to the same results.[9] At the present time, such calculations cannot be considered as conclusive, and much emphasis must be placed on experimental results in the identification of excited electronic states of molecules.

The absorption spectrum of the benzene molecule in the ultraviolet[10] begins at about 2600 A with a weak system with a maximum absorption coefficient of 200. A second band system occurs at about 2200 A with absorption coefficient about 30 times as large as that of the first system. At 1700 A, a very intense absorption has been observed,[11] which has an f-number close to one.[12] Platt gives the f-numbers of the other two transitions as 0.002 and 0.1 respectively. Sponer, Nordheim, Sklar, and Teller[10] have carried out a vibrational analysis of the first two absorption systems and have arrived at the conclusion that they represent forbidden transitions made allowed by vibrational perturbation which allows the mixing in of the allowed and intense transition at 1700 A. They conclude that the lowest state belongs to B_{2u} and the second lowest state to B_{1u}. It must be remembered, however, that the vibrational analysis can in no way differentiate between these two symmetries and therefore this experimental evidence cannot determine the symmetries of these states unambiguously. Recently, Albrecht and Simpson[13] have presented indirect experimental evidence to show that the lowest excited state does indeed belong to B_{2u}. One of the aims of the present investigation was to help clarify this question of assignment of the excited electronic states of the benzene molecule.

[8] M. Goeppert-Mayer and A. L. Sklar, J. Chem. Phys. **6**, 645 (1938).
[9] Parr, Craig, and Ross, J. Chem. Phys. **18**, 1561 (1950).
[10] Sponer, Nordheim, Sklar, and Teller, J. Chem. Phys. **7**, 207 (1939).
[11] W. C. Price and R. W. Wood, J. Chem. Phys. **3**, 439 (1935).
[12] J. R. Platt and H. B. Klevens, Chem. Revs. **41**, 301 (1948); J. R. Platt, J. Chem. Phys. **17**, 484 (1949).
[13] A. C. Albrecht and W. T. Simpson, J. Chem. Phys. **21**, 940 (1953).

II. ENERGIES OF BAND LEVELS

A. General Theory

The derivation of the expression for the energies of the band levels was carried out by Davydov[2]; however, he did not use the sufficiently general form of the exciton wave function in his development. We shall therefore outline his derivation, but, in setting up the wave functions, we shall be guided by the discussion of Winston.[3]

The Schroedinger equation of the electrons of the crystal may be written as

$$(\sum_k H_k+\sum_{k<l} V_{kl}-E)\Phi=(H-E)\Phi=0, \tag{1}$$

where H is the crystal Hamiltonian, H_k is the Hamiltonian of the kth molecule, V_{kl} is the interaction energy between the kth and lth molecules, and E is the energy of the state Φ. If Φ is antisymmetrized, as required by the Pauli principle, then V_{kl} is to be interpreted as involving those electrons which, in a given permutation, find themselves on molecules k and l.

We shall treat the sum of molecular interactions as a perturbation. The zero-order wave functions will thus be eigenfunctions of the sum of molecular Hamiltonians. As zero-order ground state, we may take

$$\Phi_0=\prod_s \psi_0^s \tag{2}$$

where ψ_0^s is the ground-state molecular wave function of molecule s (the index s designating both the unit cell and the molecular site within that cell), and the product is taken over all molecules of the crystal.

The function

$$\Psi_j^{n\mu}=\psi_j^{n\mu}\prod_{s\neq(n\mu)} \psi_0^s \tag{3}$$

is a zero-order solution representing a localized excitation, where $\psi_j^{n\mu}$ is the wave function of the molecule at the μth site of the nth unit cell, excited to the jth molecular state. If there are N unit cells in the crystal and t molecular sites per unit cell, there are tN degenerate states of the form (3), corresponding to all possible values of n and μ. The zero-order wave functions must be appropriate linear combinations of these degenerate states.

The order of the secular equations may be partially reduced by group theoretical means. The solutions must belong to the irreducible representations of the crystal symmetry group. We construct the functions

$$\zeta_j^{\mathbf{K}\mu}=1/\sqrt{N}\sum_{n=1}^{N} e^{i\mathbf{K}\cdot\mathbf{n}}\Psi_j^{n\mu} \tag{4}$$

where $\mathbf{n}$ is the position of the center of the nth unit cell. The function (4) belongs to the irreducible $\mathbf{K}$-representation of the translation group of the crystal and represents an excitation wave over all μth site molecules;

we shall call such functions "one-site excitons." The problem of finding the appropriate linear combinations of the degenerate states has been reduced to finding the combinations of one-site excitons with fixed j and $\mathbf{K}$:

$$\Phi_j^{\mathbf{K}g}=\sum_{\mu=1}^{l} B_\mu{}^g\zeta_j^{\mathbf{K}\mu} \quad g=1, 2, \cdots, l. \tag{5}$$

The one-site excitons are orthonormal; if the exciton wave functions (5) are also to be orthonormal, $B_\mu{}^g$ must form a unitary matrix. These coefficients are functions of j and of $\mathbf{K}$.

If the molecular function ψ_j is one of a degenerate set, there will be additional localized excitations which are degenerate with (3), constructed from molecular states which are degenerate with ψ_j. In that case, we must also sum the right side of Eq. (5) over all j contained in the set of degenerate molecular functions, with an index j added to the coefficients. Unless otherwise noted, it will be assumed that the molecular state is nondegenerate.

Winston[3] has pointed out that for the most general $\mathbf{K}$, symmetry conditions will give no further aid in determining the coefficients in Eq. (5), or in the more general equation discussed in the preceding paragraph. Except for particular values of $\mathbf{K}$, no operation of the space group can transform a one-site exciton into another on a different site without changing $\mathbf{K}$. On the other hand, two one-site excitons with the same $\mathbf{K}$ have, in general, the same transformation properties, so that any linear combination of two such functions will also have the same transformation properties. Therefore, we cannot use the symmetry properties to complete the solution of the secular equations. However, for special values of $\mathbf{K}$, the vector may be transformed into itself under an operation which transforms one molecular site into another; for example, $\mathbf{K}$ may lie on an axis of rotational symmetry. In such cases, the preceding arguments break down, and linear combinations of one-site excitons with the same $\mathbf{K}$ may belong to reduced representations. In a subsequent paragraph we shall discuss the reduction of the representation in the case $\mathbf{K}=0$.

In constructing his exciton functions, Davydov[2,6] did not take all of the aforementioned considerations into account. As a result, his functions are not correct in the general case. However, they are correct for the special case, $\mathbf{K}=0$, to which he eventually restricts his discussion.*

The functions (5) must be antisymmetrized with respect to all the electrons. This leads to the addition of energy terms containing overlap or electron exchange integrals; since these terms were found to be small, we shall not write the antisymmetrization explicitly.

From first-order perturbation theory, the excitation energy of the state (5) was found to be:

$$E-E_0=\epsilon_j-\epsilon_0+D+M, \tag{6}$$

where E and E_0 are the energies of the states (5) and (2), respectively, ϵ_j and ϵ_0 are the energies of the jth excited state and of the ground state of the molecule, respectively, and

$$D=\sum_m \sum_{\mu,\nu} |B_\nu{}^g|^2 \int [|\psi_j{}^{n\nu}\psi_0{}^{m\mu}|^2-|\psi_0{}^{n\nu}\psi_0{}^{m\mu}|^2] \times V_{n\nu,m\mu}d\tau \tag{7}$$

$$M=\sum_m \sum_{\mu,\nu} B_\nu{}^{g*}B_\mu{}^g \exp[i\mathbf{K}\cdot(\mathbf{m}-\mathbf{n})] \times \int (\psi_j{}^{n\nu}\psi_0{}^{m\mu})^* V_{n\nu,m\mu}\psi_0{}^{n\nu}\psi_j{}^{m\mu}d\tau. \tag{8}$$

E, D, and M are characteristic of the state (5), but for simplicity the indices j, $\mathbf{K}$, and g are omitted. D and M represent interaction terms between the molecules of an arbitrary unit cell, n, and all the other molecules of the crystal. If all the molecular sites have the same environment, the summation over ν and the factor $|B_\nu{}^g|^2$ may be omitted from Eq. (7); the index ν then designates an arbitrarily chosen molecule of cell n.

The term D is independent of $\mathbf{K}$ and therefore does not remove the degeneracy of the localized excited states. On the other hand, M is dependent on $\mathbf{K}$ and therefore splits the degenerate level into a band. Each matrix element contained in M is an excitation exchange integral; that is, the excitation is exchanged between the pair of interacting molecules. The terms of D will be called band-shift terms; those of M, band-splitting terms.

In many molecules the lower excited states may, to a good approximation, be described in terms of excitations of a limited number of electrons only. In the benzene molecule, for example, these electrons are the carbon $2p\pi$ electrons. It may be shown in the case of crystals made up of such molecules that the molecular wave functions in Eqs. (7) and (8) may be replaced by appropriate $2p\pi$ wave functions, with the exception of the factors of $|\psi_0{}^{m\mu}|^2$ in (7), which must always be interpreted as the square of the ground-state wave function of all the electrons and nuclei of molecule $m\mu$. With this exception, terms involving electron interactions in which at least one of the electrons is not in a $2p\pi$ state vanish, either through subtraction of equal terms or because of the orthogonality or near-orthogonality of molecular states.

We shall be interested in the position of optically active levels within the band, i.e., levels to which dipole transitions are allowed from the crystal ground state. The dipole matrix element for the transition between

* In the case of benzene, later work by one of us showed that Davydov's functions (reference 2 but not reference 6) are correct for all $\mathbf{K}$ in the approximation of near-neighbor interaction used in obtaining Eq. (11). In a later paper on the complete band structure it will be shown that the validity of these functions arises from a special symmetry of the near-neighbors.

states (5) and (2) is

$$(\mathbf{R})_{j\mathbf{K}g;0}=\int\Phi_j^{\mathbf{K}g*}(\sum_{n=1}^{N}\sum_{\nu=1}^{t}\mathbf{r}_{n\nu})\Phi_0 d\tau, \tag{9}$$

where the summation is over all molecules of the crystal and $\mathbf{r}_{n\nu}$ is the sum of dipole moment operators of all electrons in molecule $n\nu$. Davydov[2] has shown that transitions are forbidden to all but a small number of levels in the crystal band, for the following reason: both Φ_0 and the sum of dipole moments belong to the totally symmetric representation of the translation group, so that $\Phi_j^{\mathbf{K}g}$ must also belong to this representation in order for the matrix element not to vanish; that is, $\mathbf{K}$ must equal zero. In addition, the integrand must belong to the totally symmetric representation of the factor group; this requirement may restrict the allowed values of the index g. Winston has developed a group theoretical method for predicting the number and polarizations of optically active states in the crystal band (as given by these two selection rules) directly from character tables. He showed that those one-site excitons, (4), of a given band which belong to the completely symmetric representation of the translation group ($\mathbf{K}=0$) form a basis for a reducible representation of the factor group; the character, ${}^q\chi^{f\cdot g\cdot}(S)$, of this reducible representation may be found from Eq. (3) of reference 3:

$${}^q\chi^{f\cdot g\cdot}(S)=\sum_{\mu}\delta_\mu(S)\chi_{q\mu}{}^{s\cdot g\cdot}(S) \tag{10}$$

where $\chi_{q\mu}{}^{s\cdot g\cdot}(S)$ is the character of the qth representation of the site group of the μth molecular site (the representation to which the molecular wave function $\psi_j{}^{m\mu}$ belongs) and δ_μ is 1 if the operation S of the factor group is also contained in the μth site group, and is 0 otherwise. The functions (4), with $\mathbf{K}=0$, form the basis of the reducible representation; after reduction, the basis functions of the irreducible representations will be of the form (5), with the reduction determining the values of the coefficients $B_\mu{}^g$.

B. Application to the Benzene Crystal

The crystal structure of benzene has been investigated by Cox[14] and by Cox and Smith.[7] The structure is orthorhombic bipyramidal and belongs to the space group P_{bca} ($D_{2h}{}^{15}$, $V_h{}^{15}$) with four molecules per unit cell. The dimensions of the unit cell are: $a=7.460$ A, $b=9.666$ A, $c=7.034$ A.

The coordinate axes u, v, w will be taken in the crystal directions c, b, a, respectively. The four molecules in a unit cell will be designated as $\mu=$ I, II, III, IV; the coordinates of their centers are I: (0,0,0); II: ($c/2$,0,$a/2$); III: ($c/2$,$b/2$,0); IV: (0,$b/2$,$a/2$). The equation of the plane of a molecule of type I is

$$0.6671u+0.2229v+0.7109w=0.$$

[14] E. G. Cox, Proc. Roy. Soc. (London) **A135**, 491 (1932).

The coordinates in A units of the atoms in a molecule of type I, referred to its center of symmetry, are

	u	v	w
C_1	−0.04073	1.33043	−0.38098
C_2	0.86399	0.46445	−0.95421
C_3	0.90577	−0.86569	−0.58069

1. Investigation of the Band Structure

The structures of the bands corresponding to the B_{1u} and B_{2u} molecular states will now be investigated. The labor involved in calculating the band-splitting term, M, becomes excessive if one attempts to attain better than about 10 percent accuracy. For this reason, all contributions which were expected to be less than 10 percent of the largest terms were omitted:

(a) An estimated upper limit of the electron exchange terms omitted from M was very much smaller than 10 percent of M.

(b) The perturbation energy was expanded in a series of multipole-multipole interaction terms, and only the lowest-order nonvanishing terms were retained. Since the molecules are invariant to inversion, the molecular states are either g or u, so that only even or only odd molecular multipole matrix elements between a given pair of states will be nonvanishing. Therefore, the largest neglected terms will be two orders of the expansion parameter smaller than those retained. If this parameter is taken to be the radius of the $2p\pi$ molecular orbital (1.4 A) divided by the nearest-neighbor distance (5.1 A), its square is 7 percent.

(c) The interaction terms were calculated only for pairs of interacting molecules in the same or adjacent cells. The convergence with distance between molecules was about as expected. Terms smaller than 6 percent of the largest terms were dropped.

(d) As will be shown, the lowest nonvanishing band-splitting terms are octupole-octupole. In the benzene crystal, a dipole-dipole interaction in second-order perturbation may be as large as a quadrupole-quadrupole interaction in first order. It was therefore necessary to examine higher-order perturbation terms. It was found that there could be appreciable contributions to the band-shift terms, but that the additions to the band splitting should be at least an order of magnitude smaller than the value found in first-order perturbation.

By successively applying various symmetry operations to the exciton exchange integrands on the right side of Eq. (8), one can determine which of these integrals are equal to one another. In this way, Eq. (8) can be rewritten as

$$\begin{aligned}M=&2Re\{F(K_a a)[B_I{}^{g*}B_{II}{}^{g}F(K_c c)\\&+B_{III}{}^{g*}B_{IV}{}^{g}F^*(K_c c)]\}M_{I\,II}+2Re\{F(K_c c)\\&\times[B_I{}^{g*}B_{III}{}^{g}F(K_b b)+B_{IV}{}^{g*}B_{II}{}^{g}F^*(K_b b)]\}M_{I\,III}\\&+2Re\{F(K_b b)[B_I{}^{g*}B_{IV}{}^{g}F(K_a a)\\&+B_{II}{}^{g*}B_{III}{}^{g}F^*(K_a a)]\}M_{I\,IV}\end{aligned} \tag{11}$$

where $M_{\mu\nu}$ is the excitation exchange integral between a molecule of type μ and its nearest neighbor of type ν; interactions between more distant molecules are neglected. K_a, K_b, K_c, are the components of $\mathbf{K}$ along the crystal axes and

$$F(x)=1+\exp(-ix).$$

When the multipole-multipole expansion is carried out, $M_{\mu\nu}$ becomes a sum of terms, each of the form

$$\int \psi_j^{n\nu *} f^s(\mathbf{r}_i)\psi_0^{n\nu} d\tau_{n\nu} \int \psi_0^{m\mu *} g^t(\mathbf{r}_k)\psi_j^{m\mu} d\tau_{m\mu}, \quad (12)$$

where $\mathbf{r}_i$ and $\mathbf{r}_k$ are the coordinates of electron i on molecule $n\nu$ and of electron k on molecule $m\mu$ respectively, with the origin of each molecular coordinate system at the center of the molecule; $f^s(\mathbf{r}_i)$ and $g^t(\mathbf{r}_k)$ are homogeneous polynomials of degree s and t in the components of their respective arguments.

The lowest value of s or t which gives nonvanishing matrix elements was determined group theoretically, with the aid of the character table of the point group, D_{6h}, of the benzene molecule. State $\psi_0^{m\mu}$ belongs to the representation A_{1g} while $\psi_j^{m\mu}$ belongs to representation B_{1u} (for $j=1$) or to B_{2u} (for $j=2$). The group theoretical notation used is that of Eyring, Walter, and Kimball.[15] For either value of j, the product of wave functions in the integrand of each matrix element is odd to inversion; therefore, the value of s or t must also be odd. The dipole matrix elements vanish (forbidden transitions). We therefore examine the octupole terms. An investigation of the transformation properties of the third-degree terms leads to the conclusion that only the functions x^3, x^2y, xy^2, and y^3 belong to a representation containing the irreducible representations B_{1u} and B_{2u}. (Here, the x- and y-axes lie in the molecular plane, with the y-axis passing through C atoms.) Reduction leads to the result: (x^3-3xy^2) belongs to B_{2u}, (y^3-3x^2y) belongs to B_{1u}, and (x^3+xy^2) and (x^2y+y^3) belong to E_{1u}. We define $(g^t)_{ij}$ as the matrix element of g^t between the ith and jth molecular states. The requirement that $(g^t)_{01}$ must vanish unless g^t contains B_{1u} leads to the conclusion that

$$(x^3)_{01}=(xy^2)_{01}=0; \quad (x^2y)_{01}=-(y^3)_{01}.$$

Similarly,

$$(x^2y)_{02}=(y^3)_{02}=0; \quad (x^3)_{02}=-(xy^2)_{02}.$$

All other third-degree matrix elements vanish. Therefore, for each of the states 1 and 2, there is only one independent octopole transition matrix element to the ground state; the other elements are either proportional to it or are zero. The lowest order terms of form (12) (octupole-octupole) may therefore each be written as a constant, dependent only on the intermolecular distances, times $|(y^3)_{01}|^2$ in the case of the B_{1u} state, or a constant times $|(x^3)_{02}|^2$ in the case of the B_{2u} state. Then the members of Eq. (11) are equal to the square of the appropriate molecular matrix element times a function of $\mathbf{K}$ and $B_\mu{}^g$. The matrix element squared thus enters as a scale factor, so that the relative band structure can be determined from $\mathbf{K}$ and $B_\mu{}^g$ alone. It was shown that for the optically active levels $\mathbf{K}=0$, while the $B_\mu{}^g$ can be obtained group theoretically, so that the relative spacings between observed levels can be calculated from crystal data alone, without knowledge of the molecular wave functions.

To evaluate the scale factors, the molecular benzene wave functions of Mayer and Sklar[8] were used. The remaining factors in the energy expression were calculated from the crystal data of Cox and Smith.[7] The results were:

$$B_{1u}: \quad M_{\mathrm{I\,II}}=-10Y \text{ cm}^{-1}; \quad M_{\mathrm{I\,III}}=30Y \text{ cm}^{-1}; \quad Y\equiv|(y^3)_{01}|^2=2.2 \text{ A}^6. \quad (13)$$

$$B_{2u}: \quad M_{\mathrm{I\,III}}=-33X \text{ cm}^{-1}; \quad M_{\mathrm{I\,IV}}=20X \text{ cm}^{-1}; \quad X\equiv|(x^3)_{02}|^2=0.14 \text{ A}^6. \quad (14)$$

The omitted $M_{\mu\nu}$'s were too small to be considered. The energies are given in wave numbers.

In benzene, the site group for each site is C_i, which contains the identity operation and inversion. The factor group is D_{2h}. Using Eq. (10) it is found, as Winston[3] reported, that the irreducible representations A_{1u}, B_{1u}, B_{2u}, and B_{3u} of the factor group D_{2h} are each contained once; the last three are optically active, with polarizations a, b, and c, respectively.

The basis functions (5) are found in this case to have the following values of $\mathbf{K}$ and $B_\mu{}^g$:

$$\mathbf{K}=0, \quad B_\mu{}^g=\begin{pmatrix} \frac{1}{2} & \frac{1}{2} & \frac{1}{2} & \frac{1}{2} \\ \frac{1}{2} & -\frac{1}{2} & -\frac{1}{2} & \frac{1}{2} \\ \frac{1}{2} & -\frac{1}{2} & \frac{1}{2} & -\frac{1}{2} \\ \frac{1}{2} & \frac{1}{2} & -\frac{1}{2} & -\frac{1}{2} \end{pmatrix}, \quad \text{with } g=\alpha,\beta,\gamma,\delta \quad \mu=\mathrm{I, II, III, IV}. \quad (15)$$

That is, the states are:

$$\begin{aligned} \Phi_j{}^{0\alpha}&=\tfrac{1}{2}(\zeta_j{}^{0\mathrm{I}}+\zeta_j{}^{0\mathrm{II}}+\zeta_j{}^{0\mathrm{III}}+\zeta_j{}^{0\mathrm{IV}}) \\ \Phi_j{}^{0\beta}&=\tfrac{1}{2}(\zeta_j{}^{0\mathrm{I}}-\zeta_j{}^{0\mathrm{II}}-\zeta_j{}^{0\mathrm{III}}+\zeta_j{}^{0\mathrm{IV}}) \\ \Phi_j{}^{0\gamma}&=\tfrac{1}{2}(\zeta_j{}^{0\mathrm{I}}-\zeta_j{}^{0\mathrm{II}}+\zeta_j{}^{0\mathrm{III}}-\zeta_j{}^{0\mathrm{IV}}) \\ \Phi_j{}^{0\delta}&=\tfrac{1}{2}(\zeta_j{}^{0\mathrm{I}}+\zeta_j{}^{0\mathrm{II}}-\zeta_j{}^{0\mathrm{III}}-\zeta_j{}^{0\mathrm{IV}}) \end{aligned} \quad (16)$$

In determining the symmetry properties of these functions under the operations of the factor group, D_{2h}, it should be remembered that the functions are affected by the operations in two ways: first, each molecular term is subjected to a suitable operation of the molecular symmetry group, and second, molecules of the unit cell are interchanged by the operations. The effects of the necessary factor group operations are summarized in Table I. The correspondence between columns 1 and 2 of the table is dependent on the choice of relative directions of positive axes of different molecules. By

[15] Eyring, Walter, and Kimball, *Quantum Chemistry* (John Wiley and Sons, Inc., New York, 1949), pp. 281, 386, 387.

TABLE I. Correspondence between symmetry operations on the benzene crystal and operations on the constituent molecules.

Factor group operation	Corresponding molecular point group operation	Interchange of molecules in the unit cell
C_2^a	C_2^z	I↔IV, II↔III
C_2^b	C_2^y	I↔III, II↔IV
i	i	no interchange

applying the information of Table I, the irreducible representations of D_{2h} to which the functions (16) belong were determined. The results are listed in the second columns of Tables II and III for exciton functions constructed from molecular states of symmetry B_{1u} and B_{2u}, respectively. It is seen that the results agree with those of Winston. The third columns of these tables give the polarizations of the allowed crystal transitions from the totally symmetric ground state. The energies of the states (16), measured from $\epsilon_j-\epsilon_0+D$ [see Eq. (6)], are listed in the fourth columns. These energies are found from Eq. (11) by inserting the numerical values given in Eqs. (13), (14), and (15).

Comparison of the calculated separations with an observed value[5] of 25 cm^{-1} in the lowest band proves that the lowest molecular level belongs to B_{2u}. The calculated separations for the B_{1u} case are of a different order of magnitude.

We shall use Eq. (11) to determine the band width without explicitly calculating the energies of levels with $\mathbf{K}\neq 0$. The maximum absolute value of each coefficient of the $M_{I\nu}$ in Eq. (11) (subject to the restriction that $B_\mu{}^\rho$ is a unitary matrix) occurs when the parameters have the values given in Eq. (15). Since the $M_{I\nu}$ and their coefficients are real, a sufficient condition that one of the $\mathbf{K}=0$ states lies at the top (bottom) of the band is that $M_{I\nu}$ has the same (opposite) sign as its coefficient in (11) for that state. If, for each band, only two of the $M_{I\nu}$ are large enough to be taken into consideration as is indicated in Eqs. (13) and (14), it is always possible to satisfy the maximum condition with one of the states (16), and the minimum condition with another. Therefore, within the accuracy of the calculation, the band width is equal to the energy difference between the lowest and highest states with $\mathbf{K}=0$.

2. Band Shift

In investigating the band-shift term, D, [Eq. (7)], the interaction energy was expanded in a multipole-multipole series. From the symmetry properties of the wave functions it may be shown that the lowest nonvanishing terms of the integral are quadrupole-quadrupole. One of the quadrupole matrix elements, $(z^2-x^2)_{00}$, does not lend itself to calculation, since it involves all the electrons and nuclei of the molecule; small changes in the bond wave functions lead to large changes in the value of this matrix element and may even change its sign. In addition, it can be shown that there are contributions in second-order perturbation theory of the same order of magnitude as the terms considered here.

3. Limiting Case for Simplified Crystal Structure

Davydov[6] based his discussion of the benzene crystal on the early work of Cox.[14] On the basis of those data, Davydov apparently made the approximation that the four molecules in the unit cell can be divided into two pairs of parallel molecules. From the more recent data[7] used in the present paper, it may be seen that this approximation is not justified. However, in order to facilitate the comparison of the results obtained here with those of Davydov, the limiting case will be briefly considered in which the molecular planes are parallel to the b-axis in the benzene crystal. The unit cell then contains only two molecules. The factor group is still D_{2h}. The method of Winston will be used to determine the allowed crystal transitions. The site group includes the operations E, $C_2{}^b$, σ^b, i. In the case of the molecular B_{1u} state the corresponding character of the irreducible site group representation is: 1, 1, −1, −1, whereas in the case of the molecular B_{2u} state it is: 1, −1, 1, −1. Using these results in Winston's Eq. (3) [our Eq. (10)] and reducing the resulting factor group representation, one obtains in the first case the irreducible representations A_{1u} (inactive), B_{2u} (b-polarized). In the second case one obtains the representations B_{1u} (a-polarized) and B_{3u} (c-polarized).

These results are identical with Davydov's final conclusions but his procedure is misleading. He takes the nearly parallel molecules as equivalent in performing the symmetry operations. This requires the application of a different space group in which only two of the original four wave functions belong to completely symmetric representations of the translation group. Nevertheless he continues to use the space group P_{bca}, treating all four functions as translationally invariant. In this manner he obtains two functions belonging to each of the above one-dimensional irreducible representations of the factor group and concludes without further explanation that there will be only one observable transition for each of the polarizations as given in the preceding paragraph.

TABLE II. Symmetries and energies of translationally invariant states in the B_{1u} band, and polarizations and intensities of the transitions from the ground state to these levels.

Wave f'n	Repr. in D_{2h}	Polariz. of trans.	M (cm^{-1})	Intensity ratio ×10^4
$\Phi_1{}^{0\alpha}$	B_{2u}	b	+180	$\lvert+4.3A-1.4L_1\rvert^2=\lvert+0.09Q-2.9\rvert^2=8$
$\Phi_1{}^{0\beta}$	B_{2u}	c	−180	$\lvert-0.9A+2.0L_1\rvert^2=\lvert-0.02Q+4.1\rvert^2=17$
$\Phi_1{}^{0\gamma}$	A_{1u}	forbidden	+360	0
$\Phi_1{}^{0\delta}$	B_{1u}	a	−360	$\lvert-0.5A+2.6L_1\rvert^2=\lvert-0.01Q+5.4\rvert^2=29$

III. INTENSITIES

A. General Theory

To calculate the matrix element for a transition from the ground state to a crystal excited state, one of the excited-state functions (5) with $\mathbf{K}=0$ and the ground-state function (2) are substituted in Eq. (9). Expressing the function (5) in terms of molecular wave functions and summing over the N unit cells, we obtain

$$(\mathbf{R})_{j0g;0}=\sqrt{N}\sum_{\mu=1}^{t} B_\mu{}^g(\mathbf{r}_\mu)_{j0}, \tag{17}$$

where $(\mathbf{r}_\mu)_{j0}$ is the molecular transition dipole moment, between states ψ_j and ψ_0, of a molecule at site μ of any cell. It is thus found that for exciton states the transition moment of the crystal transition is obtained from a vector addition of the molecular moments $(\mathbf{r}_\mu)_{j0}$.

Equation (17) is useful only if the molecular transition is allowed.† For forbidden molecular transitions, $(\mathbf{R})_{j0g;0}$ vanishes because of the vanishing of the molecular moment. If such a transition is made allowed by the crystal field, Eq. (5) must be corrected to first-order of perturbation theory before it is substituted in Eq. (9). The perturbed crystal function $(\Phi_j{}^{0g})'$ may be written to first order as:

$$(\Phi_j{}^{0g})'=\Phi_j{}^{0g}+\sum_l C_{jl}\Phi_l{}^{0h}, \tag{18}$$

where a sum over h is not required since for each l there will be only one value of h for which $\Phi_j{}^{0g}$ and $\Phi_l{}^{0h}$ belong to the same representation. That they must belong to the same representation follows from the fact that the perturbation coefficient

$$C_{jl}=(E_j{}^{0g}-E_l{}^{0h})^{-1}\int \Phi_l{}^{0h*}\sum_{i<k} V_{ik}\Phi_j{}^{0g}d\tau \tag{19}$$

will vanish otherwise, since the interaction energy belongs to the completely symmetric representation of the crystal group. C_{jl} is dependent on g, but the additional index has been omitted for simplicity. The transition matrix element is now written

$$(\mathbf{R})_{(j0g)';0}=\sum_l C_{jl}(\mathbf{R})_{l0h;0}. \tag{20}$$

To evaluate the perturbation coefficient, C_{jl}, one follows a parallel procedure to that used in calculating the transition energy. The crystal functions (5) are substituted in (19) and the integral is reduced to the sums of matrix elements of the interaction between pairs of molecules. For $\mathbf{K}=0$,

$$C_{jl}=(E_j{}^{0g}-E_l{}^{0h})^{-1}\sum_{n,\nu}\Big[\sum_\mu B_\mu{}^{h*}B_\mu{}^g \times\int(\psi_l{}^{m\mu}\psi_0{}^{n\nu})^*\Big]V_{m\mu,n\nu}\psi_j{}^{m\mu}\psi_0{}^{n\nu}d\tau +\sum_\mu B_\nu{}^{h*}B_\mu{}^g\int(\psi_0{}^{m\mu}\psi_l{}^{n\nu})^*V_{m\mu,n\nu}\psi_j{}^{m\mu}\psi_0{}^{n\nu}d\tau. \tag{21}$$

If every site has the same environment, as is the case in benzene, the summation over μ and the factor of $B_\mu{}^{h*}B_\mu{}^g$ may be omitted from the first term.

For light polarized in the allowed direction, the integrated absorption strength of a crystal transition is

$$\int\epsilon d\nu=(tN)^{-1}(8\pi^3e^2\nu/ch)\,|\,(\mathbf{R})_{j0g;0}\,|^2 \tag{22}$$

while that of a molecular transition, for any direction of polarization, is[16]

$$\int\epsilon^0 d\nu^0=(8\pi^3e^2\nu/3ch)\,|\,(\mathbf{r})_{j0}\,|^2G^0. \tag{23}$$

Here ν and ν^0 are the frequencies of the crystal and molecular transitions, respectively, and G^0 is the degeneracy of the molecular level. The factor of $\frac{1}{3}$, which appears only in the molecular case, arises from the averaging of orientations of gas molecules; it would also appear in the crystal case if we were dealing with a polycrystal containing randomly oriented crystallites. The factor of $1/tN$ appears only in the crystal case, for the following reason: In the molecular case, every molecule is able to absorb the radiation, if oriented properly; in the crystal, only one state in (tN) may absorb radiation of a given polarization. However, the ratio of the square of the matrix element appearing in (22) to that in (23) is of the order of tN, as may be seen from Eq. (17) so that, in general, the intensities will be of the same order of magnitude in the two cases. For a transition forbidden in the molecule Eq. (22) becomes

$$\int\epsilon' d\nu'=(tN)^{-1}(8\pi^3e^2\nu'/ch)\,|\sum_l C_{jl}(\mathbf{R})_{l0h;0}\,|^2. \tag{24}$$

TABLE III. Symmetries and energies of translationally invariant states in the B_{2u} band, and polarizations and intensities of the transitions from the ground state to these levels.

Wave f'n	Repr. in D_{2h}	Polariz. of trans.	M (cm^{-1})	Intensity ratio $\times10^4$
$\Phi_2{}^0\alpha$	B_{3u}	c	-7	$\|-1.9B-0.5L_2\|^2=\|-1.9Q-0.3\|^2$
$\Phi_2{}^0\beta$	B_{2u}	b	$+29$	$\|-0.2B+2.9L_2\|^2=\|-0.2Q+1.5\|^2$
$\Phi_2{}^0\gamma$	B_{1u}	a	-29	$\|+1.8B-1.9L_2\|^2=\|+1.8Q-1.0\|^2$
$\Phi_2{}^0\delta$	A_{1u}	forbidden	$+7$	0

† If the exciton states are built from perturbed molecular wave functions, as is done in reference 3, rather than from functions of the free molecule, then Eq. (17) may also be applied to crystal transitions forbidden in the molecule. The final results would be the same as those developed here.

[16] R. S. Mulliken, J. Chem. Phys. 7, 14 (1939).

B. Application to Benzene

We shall now apply the results of the preceding section to the benzene crystal states derived from the molecular states belonging to B_{1u} and B_{2u}. Since the molecular transitions from the ground state are forbidden, we must carry out calculations as indicated in Eq. (24); i.e., we must evaluate the perturbation coefficients (21) and the transition matrix elements (17) for the perturbing states. It will be assumed that the only perturbing states are those constructed from the doubly degenerate molecular state belonging to the representation E_{1u} of the free molecule. This assumption seems justified by the facts that this level is the lowest optically active state and that its transition from the ground state is by far the most intense. Since the molecular coordinates x and y are also partners belonging to this representation, we may, for convenience, choose ψ_x and ψ_y, having the symmetries of x and y, respectively, as the degenerate molecular states from which to build the perturbing crystal states. The perturbing potential is invariant to all space group operations; therefore the perturbed and the perturbing states must belong to the same representation of the space group. With $\mathbf{K}=0$ we can build one exciton state with the required factor group symmetry from each of the above chosen molecular states. Strictly speaking, we should diagonalize the portion of the energy matrix corresponding to these two exciton states, according to the discussion on degenerate molecular states following Eq. (5). If this is not done, the error in the perturbation calculation is of the order of the ratio of the energy difference between the two perturbing excitons to the energy difference between perturbed and perturbing states. It is not likely that this ratio can be observed experimentally, since it would require a crystal of 0.01μ thickness at most for direct observation of the splitting of the E_{1u} level. We shall assume that the ratio is small compared to 1, so that the diagonalization need not be performed.

From the manner in which ψ_x and ψ_y were chosen, it may be seen that the dipole transition moment from the molecular ground state to the former has only an x-component; to the latter, only a y-component; that is

$$(\mathbf{r})_{x0}=\mathbf{i}(x)_{x0};\ (\mathbf{r})_{y0}=\mathbf{j}(y)_{y0},\ \text{with}\ |(x)_{x0}|=|(y)_{y0}|, \quad (25)$$

where $\mathbf{i}$, $\mathbf{j}$, and $\mathbf{k}$ are the unit vectors in the x, y, and z directions, respectively. We have chosen the molecular axes in such a way that for every molecular site, $\mathbf{i}$ has a positive u-component, $\mathbf{j}$ has a positive v-component, and $\mathbf{k}$ has a positive w-component. On substituting (25) and the appropriate values of the $B_\mu{}^\varrho$'s in Eq. (17), we obtain the transition moments

$$\begin{aligned}
&(\mathbf{R})_{x0\alpha;0}=(4N)^{\frac{1}{2}}(x)_{x0}a_{11}\mathbf{u} && (\mathbf{R})_{y0\alpha;0}=(4N)^{\frac{1}{2}}(y)_{y0}a_{22}\mathbf{v}\\
&(\mathbf{R})_{x0\beta;0}=(4N)^{\frac{1}{2}}(x)_{x0}a_{12}\mathbf{v} && (\mathbf{R})_{y0\beta;0}=(4N)^{\frac{1}{2}}(y)_{y0}a_{21}\mathbf{u}\\
&(\mathbf{R})_{x0\gamma;0}=(4N)^{\frac{1}{2}}(x)_{x0}a_{13}\mathbf{w} && (\mathbf{R})_{y0\gamma;0}=0\\
&(\mathbf{R})_{x0\delta;0}=0 && (\mathbf{R})_{y0\delta;0}=(4N)^{\frac{1}{2}}(y)_{y0}a_{23}\mathbf{w}
\end{aligned} \quad (26)$$

where a_{ij} is the transformation from the crystal coordinate system u, v, w to the coordinates x, y, z of molecule I, and $\mathbf{u}$, $\mathbf{v}$, and $\mathbf{w}$ are the unit vectors in the crystal system.

We now substitute the values (26) in Eq. (24). Since in our approximation we limit ourselves to two terms of the summation over l, we obtain

$$\int \epsilon' d\nu' = (8\pi^3 e^2 \nu'/ch)\,|C_{jx}a_{1p}+C_{jy}a_{2p}|^2\,|(x)_{x0}|^2 \quad (27)$$

where the values of $p=1, 2, 3$, correspond to the polarizations of absorbed light along the crystal axes c, b, a respectively. The index j takes on the values 1 or 2 corresponding to B_{1u} or B_{2u} respectively.

The coefficients C_{jx} and C_{jy} are calculated from Eq. (21). The interaction potential energy is developed in a multipole-multipole expansion and only the lowest-order nonvanishing terms are calculated. These are quadrupole-quadrupole for the first term of (21), with the matrix elements taken between ground-state functions and again between perturbed and perturbing states. The second term of (21) is dipole-octupole, with the dipole matrix element taken between the ground and the perturbing states while the octupole moment is between ground and perturbed states. The products of molecular matrix elements which appear are

$$\begin{aligned}
A&=(x^2)_{1y}(z^2-x^2)_{00}=0.02Q\ \text{A}^4\\
B&=(y^2)_{2x}(z^2-x^2)_{00}=1.03Q\ \text{A}^4\\
L_1&=(y^3)_{10}(x)_{0x}=2.07\ \text{A}^4\\
L_2&=(x^3)_{20}(x)_{0x}=0.53\ \text{A}^4
\end{aligned} \quad (28)$$

where $Q=(z^2-x^2)_{00}$. Numerical values were obtained by using the Mayer and Sklar wave functions.[8] The value of Q was not calculated for the reason given in Sec. IIB2. In these calculations, the same approximations were made as in the calculations of the band energies. In addition, it was assumed that the energies of all perturbing crystal states constructed from the molecular E_{1u} states are the same.

The results of the intensity calculation are given in the last columns of Tables II and III as the ratios of the absorption strengths of the perturbed crystal states to the absorption strengths of the molecular E_{1u} states; i.e., as the ratio of (27) to (23), using (25):

$$\int \epsilon' d\nu' \Big/ \int \epsilon^0 d\nu^0 = (3\nu'/2\nu^0)\,|C_{jx}a_{1p}+C_{jy}a_{2p}|^2. \quad (29)$$

Experimentally,[4,5] the ratio (29) is of the order of 10^{-3} or less for the B_{2u} case. It may be seen from Table III that Q may not be larger than of the order of 1 in order to obtain agreement with experiment. For the B_{1u} case, the terms involving Q may be neglected; all the intensity ratios listed in Table II are of the order of 10^{-3}.

IV. DISCUSSION

A. Energies

It had been hoped that the identification of the B_{1u} and B_{2u} bands could be made from the relative positions of transitions of different polarizations. Unfortunately, this is not possible, as may be seen from Tables II and III; for each band, the predicted order of increasing energy is: polarizations *a*, *b*, *c*. Furthermore, the ratios of energy differences (from *a* to *c*/from *c* to *b*) are nearly equal in the two bands.

The band widths, however, seem to offer a more decisive criterion. As was stated earlier, two optically active levels have been observed in the lowest exciton band, with a separation of 25 cm^{-1}. Comparison with Tables II and III leads to the assignment of B_{2u} symmetry to the lowest excited molecular state. This assignment is not dependent on the specific choice of the Mayer and Sklar wave functions, but rather on the assumption that the charge of the $2p\pi$ electrons is concentrated near the carbon atoms of the benzene ring instead of near the bond centers. The band width and level separations are about 10 times as large in the B_{1u} case as are the corresponding quantities in the B_{2u} case. This large factor arises from the large ratio of octupole matrix elements [see Eqs. (13) and (14)]. If one assumes a charge concentration near the *C* atoms, then for any B_{1u} wave function, the leading term in the octupole matrix element $(y^3)_{01}$ is the cube of the radius of the benzene ring, which leads to separations comparable with those in Table II; for any B_{2u} wave function, the corresponding leading term in the matrix element $(x^3)_{02}$ vanishes, and the main contributions come from atomic overlap integrals, leading to much smaller level separations. In order to make the B_{1u} separations comparable with the experimental value, one would have to assume molecular wave functions with $2p\pi$ electrons concentrated near the centers of the C—C bonds. These results follow from the fact that a B_{1u} function has nodal planes perpendicular to the molecular plane and bisecting opposite C—C bonds, while the corresponding B_{2u} nodal planes pass through opposite C atoms.

It must be remembered that, in carrying out the calculations, terms an order of magnitude smaller than the largest ones were neglected. It is to be expected that the total error will not change the results by as much as a factor of two. An unfortunate accumulation of errors arising from these neglected terms, however, could affect the results to this extent. We may conclude then that the orders of magnitude of the band widths and level separations are correct and that the sequences of the levels in energy are probably correct.

B. Intensities

It has been shown that comparison with intensity observations on the B_{2u} band leads to a value of Q of the order of one or less. A rough theoretical calculation showed that this is a reasonable range of values for Q. If we accept this range, the terms involving Q for the B_{1u} case (Table II) may be neglected, and intensity ratios of the order of 10^{-3} are obtained.

The same considerations with regard to accuracy apply to the intensity formulas as to the expressions for the bond energies. The intensity ratios in Tables II and III should therefore be correct as to order of magnitude and are probably more accurate than that.

Broude, Medvedev, and Prikhot'ko[5] claimed to have identified the crystal directions from the relative intensities of the observed crystal absorptions of light polarized in these directions. Their arguments are implicitly based on the assumption that equations similar to (26) are valid, so that with known values of the a_{ij}, it is possible to identify the crystal directions from observed relative intensities of the 0—0 band components. For forbidden transitions, however, the calculation is more complex since Eq. (20) must be used. In this case, more is required than knowledge of crystal data to calculate relative intensities. Their observation of two active levels of different polarization in the lower band would have identified the *ac* plane (but not the axes within that plane) only in the limiting case of two molecules per unit cell. In this case, only the B_{2u} band contains two active levels; their polarizations are *a* and *c*.

In an experiment in which the crystal axes have been determined independently, more observations can be made than are necessary to calculate the parameters in the intensity and energy formulas. A self consistent set of results would be strong evidence for the validity of our approximations and at the same time would lend support to the assumption of the existence of exciton states in the benzene crystal.

V. ACKNOWLEDGMENTS

We would like to thank Dr. D. S. McClure, Dr. H. Winston, and Dr. P. Zilsel, who read the manuscript and offered valuable suggestions. We are also very grateful to Professor Cox for sending us unpublished data on the benzene crystal structure.

Charge Transfer Reactions in Monatomic and Diatomic Gases*

J. A. DILLON, JR., W. F. SHERIDAN, AND H. D. EDWARDS, *Geophysics Research Directorate, Air Force Cambridge Research Center, Air Research and Development Command*
AND
S. N. GHOSH, *Wentworth Institute, Boston, Massachusetts*†
(Received June 11, 1954)

Cross sections for charge transfer reactions between ions and neutral atoms and molecules have been measured in the energy range from 50 to 850 ev. Charge transfer cross sections for symmetrical reactions in monatomic and diatomic gases increase with increasing viscosity cross sections. The charge transfer cross sections decrease with increasing incident ion energy in conformity with the adiabatic criterion. For reactions in diatomic gases the charge transfer cross sections decrease as the changes in internuclear distance for the processes increase.

INTRODUCTION

THE importance of charge transfer processes has resulted in the accumulation of a large amount of data giving charge transfer cross sections for many reactions.[1] There is still need for further investigation because of the absence of data on some reactions and because of discrepancies among the data on others.[2] In the present paper the measurement of charge transfer cross sections using a simple apparatus is described. The results for a number of reactions are discussed with an emphasis on the influence of molecular parameters on the results obtained. Several workers have indicated the importance of the Franck-Condon principle in collisions involving charge transfer reactions,[3–5] and at least a qualitative agreement with this principle is found for reactions taking place in diatomic gases.

APPARATUS

With the exception of the ion source, accelerator, and collimator unit which consists of a modified radio frequency mass spectrometer,[6] the apparatus used in these measurements is similar to that reported by Keene.[7] The mass spectrometer is modified by substituting a collision chamber for the original ion collector, providing a means of varying the ion beam energy, and improving the collimation of the beam. By installing a collimating tube 2 cm long and 7 mm in diameter, the diameter of the ion beam is decreased from 2 cm to 7 mm. Attempts to further improve the collimation result in reduction of the beam current below a useful value and increase the energy spread of the beam. The ion beam can be accelerated to energies between 25 and 850 ev by applying a variable potential to a grid attached to the collimating tube. The collision chamber, shown in Fig. 1, consists of a system of semicylindrical brass elements. The ion beam passes through the collision chamber and is collected at the Faraday chamber FG. A transverse electric field is maintained between F and G to collect secondary electrons and ions formed in the region between the plates. Ions formed by charge transfer in the distance L are accelerated in the transverse field between plates C and G. Plate A is a guard ring which serves to maintain a uniform field over the distance L.

Measurements of charge transfer cross sections are made by comparing the charges collected on C and F by means of a balanced electrometer. Voltages developed by these charges leaking to ground through calibrated grid resistors are balanced by varying the value of the resistor in the Faraday chamber circuit. The resistor in the charge transfer circuit is a fixed 960 (± 1 percent) megohm unit. The balance condition is indicated on a galvanometer connected between the cathodes of the electrometer tubes. This charge collection system does not have the advantage of cancelling out the effects of ionization as does that of Hasted.[8] An earlier design, similar to Hasted's, was found to yield cross sections for the inert gases of the same values as those reported here but was less stable in operation than the present one. The fact that none of the reactions differs noticeably from the normal energy dependence suggests that ionization introduces negligible error in the range studied. For measurements at higher energies, however, use of the other arrangement would be advisable.

The collision chamber, battery box, and electrometer amplifier are electrostatically shielded. Shielded leads with the inner and outer conductors at the same potentials carry the small currents (10^{-10} to 10^{-12} amperes) from plates C and F. The guard ring A is at the same potential as C and terminates on the shield as shown in Fig. 1. The batteries are insulated from

* Presented in part at the Washington, D. C. meeting of the American Physical Society, April 29–May 1, 1954.

† Part of this research was supported under Contract AF19-(122)-40 by the Geophysics Research Directorate, Air Force Cambridge Research Center, Air Research and Development Command.

[1] H. S. W. Massey and E. H. S. Burhop, *Electronic and Ionic Impact Phenomena* (Oxford University Press, New York, 1952), 498 ff.

[2] See reference 1, pp. 519, 524.

[3] R. Meyerott, Phys. Rev. **70**, 671 (1946); Phys. Rev. **71**, 553 (1947).

[4] J. A. Hornbeck, J. Phys. Chem. **56**, 829 (1952).

[5] E. E. Muschlitz Jr., and J. H. Simons, J. Phys. Chem. **56**, 837 (1952).

[6] W. H. Bennett, J. Appl. Phys. **21**, 143 (1950).

[7] J. P. Keene, Phil. Mag. **40**, 369 (1949).

[8] J. B. Hasted, Proc. Roy. Soc. (London) **A205**, 421 (1951).

ground, and all leads are brought out through glass or polystyrene insulators.

To determine the proper operating point, a plot is made of the charge transfer current *versus* the potential applied between C and G. The saturation region of this curve is used. In the energy range studied, it was found that 30 volts provided the desired condition for all the ions considered. This same potential difference is maintained across the Faraday chamber.

All measurements are made at about 20°C and a pressure of the order 10^{-4} mm Hg. The fact that the observed cross sections are invariant to large changes in operating pressure and ion beam density suggests that pure charge transfer reactions are being observed. The ultimate vacuum attainable is about 5×10^{-7} mm Hg. With the exceptions of CO (96 percent pure), Cl_2 (99.5 percent pure), NO (98 percent pure), and Hg (triple distilled mercury), all the gases used are spectroscopically pure. The limit of accuracy of the apparatus is about ±10 percent. Because some uncertainty exists in the balancing process, the apparatus is calibrated in such a way that the value of Q obtained for the reaction $A^+ + A \rightarrow A + A^+$ at 450 ev is the same as that obtained by Hasted.[8]

RESULTS

If a uniform ion beam passes through a region of length dx which contains neutral atoms or molecules, the current strength of the ion beam is diminished, due to charge transfer, by an amount

$$dI_x = -NQ_1 I_x dx$$

where N is the number of neutral atoms or molecules per cubic centimeter, and Q_1 is the effective cross section per atom for the process. If the collision region is of length L, and the charge transfer current is I_e, the current reaching the Faraday chamber is

$$I_f = (I_f + I_e)e^{-NQ_1L}.$$

By equating the voltage drops across the grid resistors at the balance condition, it is seen that to a good approximation

$$Q_1 = (kT/cpL)\cdot(R/(960+R)).$$

R is the variable resistance in the Faraday chamber circuit in megohms, p is the pressure in mm Hg, c is the conversion factor between absolute pressure units and mm Hg, k is Boltzmann's constant, and T is the absolute temperature.

The total cross section, Q, is equal to Q_1 multiplied by the value of N at 1 mm Hg and 20°C.

$$Q = (1/pL)\cdot(R/(960+R)).$$

The units of p having been divided out in the multiplication of Q_1 by N, Q appears in units of cm^{-1}.

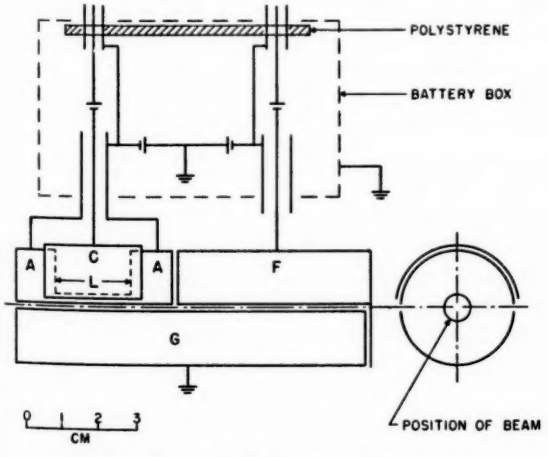

FIG. 1. Collision chamber.

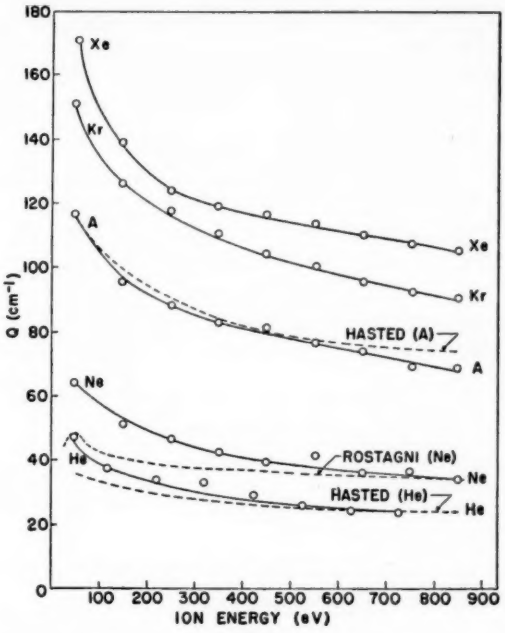

FIG. 2. Total charge transfer cross sections for symmetrical reactions involving the inert gases. In each case the reaction is of the type $X^+ + X \rightarrow X + X^+$.

SYMMETRICAL REACTIONS IN MONATOMIC GASES

Symmetrical charge transfer cross sections for the inert gases are shown in Fig. 2. Previously reported values for He, A (Hasted[8]), and Ne (Rostagni[9]) are shown for comparison. The cross sections for the He reaction are in closer agreement with the values of Hasted and others[10] rather than the higher values obtained by extrapolating the results of Keene[7] and Meyer.[11] Using the impact parameter method, Jackson[12] has recently made a theoretical calculation of the cross section for the helium reaction. His results are in general agreement with those of Hasted. Potter's[13] recent experimental results also support these lower

[9] A. Rostagni, Nuovo cimento **12**, 134 (1935).
[10] See reference 1, p. 519.
[11] H. Meyer, Ann. Physik **30**, 635 (1937).
[12] J. D. Jackson, Can. J. Phys. **32**, 60 (1954).
[13] R. F. Potter, J. Chem. Phys. **22**, 974 (1954).

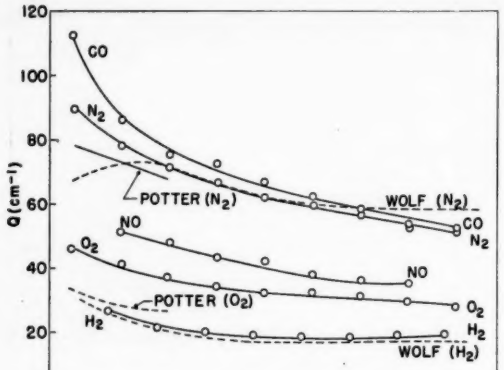

FIG. 3. Total charge transfer cross sections for symmetrical reactions involving diatomic gases. In each case the reaction is of the type $X_2^+ + X_2 \rightarrow X_2 + X_2^+$.

values for helium although his values for argon are somewhat lower than Hasted's.

It is found that a quadratic relationship exists between the measured values of Q and the atomic diameters computed from viscosity measurements.[14] In the energy range studied, the total cross sections for the inert gases follow approximately the empirical relationship given in Eq. (1).

$$Q=F(D,V)=(6D^2+12)(1-0.44\log_{10}(V/150)), \quad 50\leq V\leq 850. \quad (1)$$

D is the atomic diameter in angstrom units (A), and V is the energy of the incident ions in electron volts. For this group of gases the charge transfer cross sections vary linearly with the viscosity cross sections (πD^2), the effective values per atom varying from approximate equality with the viscosity cross sections at 50 ev to about half those values at 850 ev.

The decrease in Q with energy is in agreement with the theoretical considerations which utilize the approach to adiabatic conditions as a criterion for the magnitude of Q.[15] A maximum value of Q is expected somewhere near an incident ion velocity $v=a\Delta E/h$, where a is the interaction distance, ΔE is the difference between the ionization potentials of the interacting particles, and h is Planck's constant. When the velocity deviates much from this value, the cross section is small. For the symmetrical cases ($\Delta E=0$) the maximum value of Q should appear at zero energy. This criterion, although being of considerable interest and value, does not prescribe the magnitude of Q, the exact energy dependence, or the influence of molecular parameters on the value of Q.

TABLE I. Charge transfer cross sections for the reactions $Hg^+ + Hg \rightarrow Hg + Hg^+$ and $Cl_2^+ + Cl_2 \rightarrow Cl_2 + Cl_2^+$.

Ion energy (ev)	50	150	250	350	450	550	650	750	850
Q(cm^{-1})(Hg)		105	94	89	90	84	80	76	
Q(cm^{-1})(Cl_2)	95	80	73	70	65	59	55	54	52

Cross sections for the symmetrical charge transfer reaction in Hg, which are listed in Table I, deviate by about 25 percent from the values of Q computed from Eq. (1). These values are less reliable than the others because the error in pressure measurement is higher for mercury vapor than for the other gases used. No other data is available at present due to the experimental difficulties associated with the study of symmetrical monatomic reactions for cases other than those presented here.

SYMMETRICAL REACTIONS IN DIATOMIC GASES

Symmetrical charge transfer cross sections for a number of diatomic gases are shown in Fig. 3. A comparison is made with the results of Wolf[16] and Potter.[13] The cross sections for chlorine, which fall between those of nitrogen and carbon monoxide, are listed in Table I. In reactions involving diatomic gases, the change in internuclear distance resulting from transitions from the neutral to the ionized state must be considered in estimating the probability of a given reaction taking place. Processes of this type are governed by the Franck-Condon principle. The observed values for the total cross sections are lower in every case than the values computed from Eq. (1). A better estimate of the values can be obtained from Eq. (2).

TABLE II. Observed values of Q for diatomic reactions and the values computed from Eq. (2). In each case the reaction is of the type $X_2^+ + X_2 \rightarrow X_2 + X_2^+$.

Gas	Molecular diameter[a]	Δr[b]	Q(obs. at 150 ev)	Q(Eq. (2) at 150 ev)
H_2	2.730A	0.328A	25 cm^{-1}	23 cm^{-1}
O_2	3.620	0.085	41	46
NO	3.690	0.090[c]	51	48
N_2	3.756	0.022	78	72
CO	3.766	0.013	87	87
Cl_2	5.554	0.097	80	99

[a] From viscosity measurements, see reference 14.
[b] Absolute value of the change in internuclear distance between the neutral and first ionized ground states.
[c] Estimated from results of G. Glockler, J. Chem. Phys. **16**, 604 (1948).

$$Q=F(D,V)/(2.5-\log_{10}(0.32/\Delta r)), \quad 0.01<\Delta r. \quad (2).$$

$F(D,V)$ is defined in Eq. (1) and Δr is the absolute value of the difference in internuclear distance (in A) between the neutral and first ionized ground states as tabulated by Herzberg.[17] The comparison of observed and calculated values given in Table II indicates how well the diatomic reactions follow Eq. (2). The deviation in the case of chlorine may possibly be due to the

[14] S. Chapman and T. G. Cowling, *The Mathematical Theory of Non-Uniform Gases* (Cambridge University Press, London, 1952), 229.
[15] See reference 1, p. 513.
[16] F. Wolf, Ann. Physik **30**, 313 (1937).
[17] G. Herzberg, *Molecular Spectra and Molecular Structure* (D. Van Nostrand Company, Inc., New York, 1950), 501.

use of an incorrect value for the ground state level.[18] The correlation with experimental results may be improved if it is taken into consideration that some of the particles may be in excited states. Deciding a priori what these states should be can be difficult. Hasted[19] has recently shown that conformity of his results with the adiabatic criterion can be obtained for the reaction $O_2^+ + A \rightarrow O_2 + A^+$ if it is assumed that the incident ion is in the $^4\pi_u$ state. If the ion in the symmetrical oxygen reaction is also assumed to be in this state, the values computed from Eq. (2) are in better agreement with experiment than if the ionic ground state is used.

On the basis of the available data, the following conclusions can be drawn.

1. Charge transfer cross sections for symmetrical reactions in monatomic and diatomic gases increase with increasing viscosity cross section.
2. For diatomic gases the cross sections decrease as the changes in internuclear distances for the processes increase.
3. The cross sections decrease with increasing incident ion energy in conformity with the adiabatic criterion.

[18] A. Elliot and W. H. B. Cameron, Proc. Roy. Soc. (London) **A164**, 531 (1938).
[19] J. B. Hasted, Proc. Roy. Soc. (London) **A212**, 235 (1952).

THE JOURNAL OF CHEMICAL PHYSICS VOLUME 23, NUMBER 5 MAY, 1955

Crystal Structure and Quadrupole Coupling of Cyanogen Bromide, BrCN

S. GELLER AND A. L. SCHAWLOW
Bell Telephone Laboratories, Inc., Murray Hill, New Jersey
(Received September 1, 1954)

The crystal structure of BrCN has been determined from single-crystal x-ray data. BrCN belongs to space group $D_{2h}(13)-Pnmm$, with two molecules in a unit cell of dimensions: $a=5.80$, $b=6.02$, $c=4.12$ A (all ± 0.03 A). All atoms are in positions $2(a)$: $\pm(x, \frac{1}{4}, \frac{1}{4})$ with parameters $x_{Br}=0.144$, $x_C=0.45$, and $x_N=0.65$. The structure is made up of straight chains of BrCN molecules directed along the a-axis with the bromine atom of one molecule bonding weakly to the nitrogen of the next molecule in the same chain. The structure is consistent with recent measurements of quadrupole coupling for the Br and N nuclei.

INTRODUCTION

IF a nucleus has a nonspherical charge distribution, and hence, an electric quadrupole moment, its coupling to the electronic electric field can be used to measure the gradient of the field. This measurement can sometimes be made by microwave spectroscopy on a free molecule in the gaseous state. In this case the coupling is governed by the structure of the molecule. Measurements can also be made in the solid state by the method of pure quadrupole resonance.[1] The coupling in the solid state is often close to that of the free molecule particularly if the substance forms good molecular crystals with only very weak intermolecular binding. Usually it is a few percent less in the solid because weak interactions of neighboring molecules tend in general to make the field at the nucleus more nearly spherical. The iodine coupling in ICN, however, is an exception; in this case, it is five percent greater in the solid (at 293°K) than in the gas. This apparent anomaly has been explained by Townes and Dailey[2] on the assumption that there is some covalent bonding between the iodine atom of one molecule and the nitrogen atom of the next. This explanation is verified by examination of the crystal structure of ICN.[3] In this structure, molecules are arranged in straight chains with a distance between the iodine atom of one molecule and the nitrogen atom of the next molecule in the same chain of from 0.8–0.9 A less than the sum of the van der Waals radii of nitrogen and iodine.

ICN belongs to space group $C_{3v}(5)-R3m$ with a unimolecular unit cell. All atoms are in positions $1(a)$: (x,x,x). The quadrupole resonance measurements confirm the conclusion derived independently from x-ray data that all iodine atoms and consequently all nitrogen atoms and all carbon atoms occupy crystallographically equivalent positions. Were this not so, different resonances would be observed for the different positions. Because the experimental resolution is so high, even a weak intermolecular interaction would cause a detectable shift between resonances of nonequivalent nuclei. Only if the nucleus has spin one can a splitting of the resonance be caused by other than nonequivalent lattice positions. For example, in the case of nitrogen, the resonance may be split into two components by a departure from cylindrical symmetry of the field gradient at the nucleus. This kind of splitting cannot occur for halogen nuclei and does not occur for nitrogen in ICN because each nucleus is on the threefold axis.

Recently, measurements have been made of quad-

[1] H. G. Dehmelt, Am. J. Phys. **22**, 110 (1954).
[2] C. H. Townes and B. P. Dailey, J. Chem. Phys. **20**, 35 (1952).
[3] J. A. A. Ketelaar and J. W. Zwartsenberg, Rec. trav. chim. **58**, 449 (1939).

rupole resonances of nitrogen[4] and bromine[5] in solid BrCN. The nitrogen resonance frequency was found to be very near that observed in solid ICN, but two components were observed. The splitting between these components was sensitive to temperature and they coincided and crossed over near 0°C. The presence of two nitrogen resonances was sufficient to indicate that BrCN is not isostructural with ICN. Only one bromine resonance was observed, indicating that the bromine atoms occupy crystallographically equivalent positions, and therefore suggesting the cause of the nitrogen splitting to be field gradient asymmetry. The bromine quadrupole coupling in BrCN is also higher in the solid than in the gas.

It will be shown subsequently that the crystal structure and results of quadrupole resonance measurements of BrCN are consistent.

The structure of the BrCN molecule in the gaseous state has been determined in two ways. Beach and Turkevich[6] have determined the structure by electron diffraction and Townes, Holden, and Merritt[7] by microwave spectroscopy.

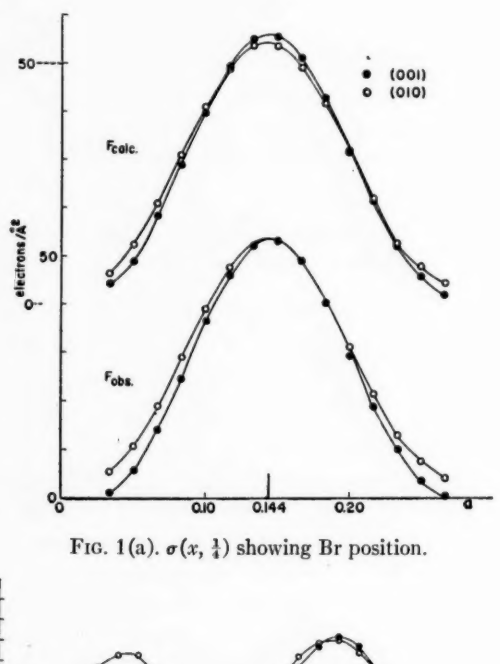

FIG. 1(a). $\sigma(x, \frac{1}{4})$ showing Br position.

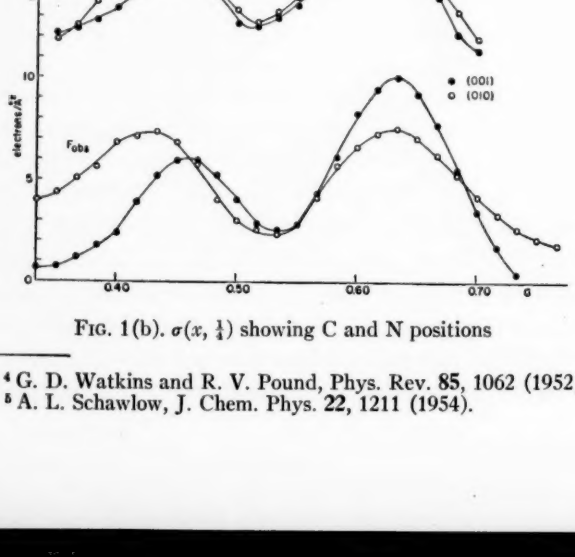

FIG. 1(b). $\sigma(x, \frac{1}{4})$ showing C and N positions

TABLE I. Parameters from F_{obs} Fourier syntheses.

Atom	Parameters (001)	(010)	$\frac{(001)+(010)}{2}$
Br	0.145	0.143	0.144
C	0.460	0.425	0.443
N	0.632	0.630	0.631

DETERMINATION OF THE STRUCTURE

A crystal of BrCN was grown by sublimation in a thin-walled glass capillary of 0.3 mm internal diameter. Thickness of capillary wall was about 0.02 mm. The crystal was mounted on a goniometer head and aligned by means of the Hendershot[8] method. A rational direction of the crystal was found to lie within a few degrees of the capillary axis. This rational direction had an identity period of 5.80A. Weissenberg photographs were taken with CuKα (Ni filtered) radiation. These established the diffraction symmetry $D_{2h}-mmm$ for the crystal. Precession photographs were taken with the other two axes as precession axes using MoKα radiation (Zr filtered). All x-ray data were obtained at room temperature.

The x-ray photographs indicated that reflections of the type $(0kl)$, $k+l$ odd are absent. Thus the probable space groups are $D_{2h}(13)-Pnmm$ or $C_{2v}(7)-Pnm$. The cell dimensions are $a=5.80$, $b=6.02$, $c=4.12\pm0.03$ A. Assuming two molecules in the unit cell, the x-ray density is 2.44 g/cc. This value is somewhat higher than the reported pycnometric density of 2.015 g/cc given in the handbooks (primary reference not available). This is not alarming however, because the crystals are very poor and some do show microscopic holes. In addition the BrCN is difficult to handle. Ketelaar and Zwartsenberg[3] found the same kind of discrepancy in the case of ICN. They found an x-ray density of 3.10 and a pycnometric density of 2.84 g/cc for that compound.

The structure of BrCN is a simple one. All atoms must be either in positions $2(a): \pm(x, \frac{1}{4}, \frac{1}{4})$ of *Pnmm* or in $2(a): xy0; \frac{1}{2}+x, \bar{y}, \frac{1}{2}$ of *Pnm*. (In the *Pnmm* case, the origin is taken at 1.) An examination of the 0-layer Weissenberg film indicated that the $(0kl)$ intensities were most likely independent of an irrational parameter, as would be expected if the correct space group were *Pnmm*. The precession photographs indicated that relative intensities amongst $(hk0)$ were similar to those amongst $(h0l)$ reflections, therefore also pointing to the centrosymmetric space group as the correct choice.

[4] G. D. Watkins and R. V. Pound, Phys. Rev. **85**, 1062 (1952).
[5] A. L. Schawlow, J. Chem. Phys. **22**, 1211 (1954).
[6] J. Y. Beach and A. Turkevich, J. Am. Chem. Soc. **61**, 299 (1939).
[7] Townes, Holden, and Merritt, Phys. Rev. **74**, 113 (1948).
[8] O. P. Hendershot, Rev. Sci. Instr. **8**, 436 (1937).

TABLE II. Parameters from F_{calc} Fourier syntheses.

Atom	Parameters (001)	(010)	$\frac{(001)+(010)}{2}$
Br	0.1437	0.1425	0.143
C	0.451	0.438	0.445
N	0.616	0.612	0.614

The ($hk0$) and ($h0l$) intensities were estimated visually by comparison with an intensity scale. Lorentz and polarization corrections were applied using the Waser chart.[9,10] The structure could easily have been determined by trial and error but in order to expedite the solution, the Patterson synthesis

$$p(x,\tfrac{1}{4})=\sum_h\sum_k |F_{hk0}|^2\cos 2\pi(hx+k/4)$$

was computed. Beevers-Lipson strips[11,12] were used for the computation. From this synthesis, it was possible to deduce the followimg parameters for the atoms $x_{Br}=0.144$, $x_C=0.45$, and $x_N=0.64$. These parameters were used to calculate reflection amplitudes. Values of the atom form factors for nitrogen and carbon were taken from McWeeny's[13] paper. The values for the atom form factors for the bromine are averages of those from the Internationale Tabellen[14] and from the paper of Pauling and Sherman.[15]

The observed reflection amplitudes were put on an absolute scale by comparison with the calculated values. Following this, a least-squares calculation was made applying equal weight to all ($h0l$) and ($hk0$) values. This resulted in the following:

$\Delta x_{Br}=0.000$, $\Delta x_C=-0.006$, $\Delta x_N=0.022$. The value obtained for the nitrogen leads to an impossible C≡N bond length. Actually, the only really meaningful result is that obtained for the bromine atom because the contributions from the nitrogen and carbon atoms to both the structure factors and to the first partial derivatives are very small as compared with that of the bromine atom.

Finally, Fourier syntheses (both F_{obs} and F_{calc}) were computed. These syntheses shown in Figs. 1(a) and 1(b),

$$\text{are } \sigma(x,\tfrac{1}{4})=\sum_h\sum_k F_{hk0}\cos 2\pi\left(hx+\frac{k}{4}\right),$$

$$\text{and } \sigma(x,\tfrac{1}{4})=\sum_h\sum_l F_{h0l}\cos 2\pi\left(hx+\frac{l}{4}\right).$$

The results are tabulated in Tables I and II.

All phases, of course, of the F_{obs} are determined by the bromine atom, so that the changes in the parameters shown in Table I from those deduced from the Patterson are final for the given data. The corrections obtained from the F_{calc} series are negligible for the bromine atom but appreciable for the carbon and nitrogen atoms.

The Fourier projections attest to the validity of the assumption that the correct choice of space group is the centrosymmetric one. This is so because the electron densities obtained from both the (001) and (010) projections are very close for the bromine and nitrogen atoms. This, of course, is hardly to be expected for the carbon atom.

The comparisons of the calculated with the observed reflection amplitudes are shown in Tables III and IV. The values for the discrepancy factors

$$(R=\Sigma||F_0|-|F_c||/\Sigma|F_0|)$$

are 0.14 for the ($hk0$) and 0.11 for the (h0l) reflections. (These exclude reflections too weak to be observed.) The values of B in the temperature factor,

$$\exp[-B\sin^2\theta/\lambda^2],$$

are 3.05×10^{-16} for the ($hk0$) and 2.95×10^{-16} for the ($h0l$) amplitudes. No corrections were made for absorption or extinction.

TABLE III. Comparison of calculated with observed ($hk0$) reflection amplitudes.

	(k)	Amplitude Obs	Calc		(k)	Amplitude Obs	Calc
$h=0$	2	56	−61	$h=4$	0	33	−29
	4	29	36		1	19	16
	6	14	−19		2	25	24
	8	<13	8		3	17	−12
					4	14	−17
$h=1$	0	24	23		5	<13	7
	1	37	−42		6	<13	8
	2	19	−22		7	<11	− 4
	3	24	28				
	4	12	15	$h=5$	0	<13	− 3
	5	11	−17		1	19	18
	6	<13	− 8		2	<13	3
	7	<13	− 8		3	14	−14
	8	<13	4		4	<13	− 2
					5	<13	9
$h=2$	0	13	− 9				
	1	51	−49	$h=6$	0	14	10
	2	11	8		1	15	13
	3	31	35		2	10	− 8
	4	<11	− 5		3	13	−10
	5	16	−21		4	<13	6
	6	<13	3				
	7	<13	8	$h=7$	0	11	10
	8	<11	− 1				
$h=3$	0	37	−35				
	1	17	−16				
	2	30	31				
	3	13	13				
	4	18	−20				
	5	<13	− 8				
	6	<14	11				
	7	<13	4				

[9] J. Waser, Rev. Sci. Instr. **22**, 467 (1951).
[10] J. Waser, Rev. Sci. Instr. **23**, 420 (1952).
[11] C. A. Beevers and H. Lipson, Proc. Phys. Soc. (London) **48**, 772 (1936).
[12] C. A. Beevers, Acta Cryst. **5**, 670 (1952).
[13] R. McWeeny, Acta Cryst. **4**, 513 (1951).
[14] *Internationale Tabellen zur Bestimming von Kristallstrukturen* (Edwards Brothers, Inc., Ann Arbor, Michigan, 1944), Vol. 2.
[15] L. Pauling and J. Sherman, Z. Krist. **81** (1932).

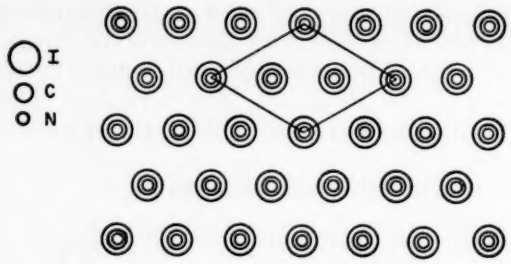

FIG 2(a). (00·1) projection of ICN structure.

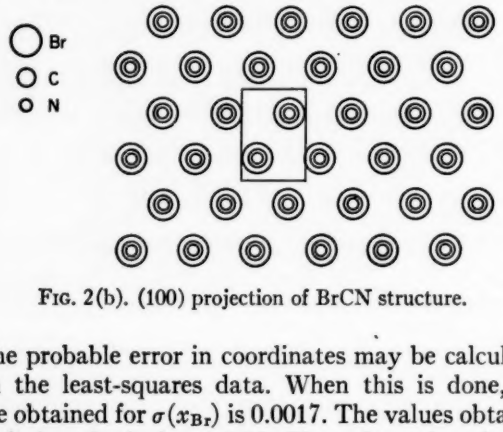

FIG. 2(b). (100) projection of BrCN structure.

The probable error in coordinates may be calculated from the least-squares data. When this is done, the value obtained for $\sigma(x_{Br})$ is 0.0017. The values obtained for $\sigma(x_C)$ and $\sigma(x_N)$ are 0.02. The value taken for the bromine parameter is therefore 0.144 ± 0.002. The results of either the least-squares or Fourier methods lead to the conclusion that one can say very little about the carbon and nitrogen parameters. The values of interatomic distances for Br−C, and for C≡N, from the microwave spectroscopic determination are 1.790 and 1.158 A, respectively. About 25 percent double-bond character is indicated for BrCN in the gaseous state. That is, the structure resonates between Br−C≡N(∼75 percent) and $Br^+=C=N$(∼25 percent). As will be shown from the quadrupole couplings, when the BrCN goes into the solid, the latter structure becomes less important and the additional structure $-Br^+-\bar{C}=N-$ comes into importance. The result is that the intramolecular interatomic distances should not be very different in the solid and gaseous states. On this assumption the carbon and nitrogen parameters should be 0.45 and 0.65 respectively.

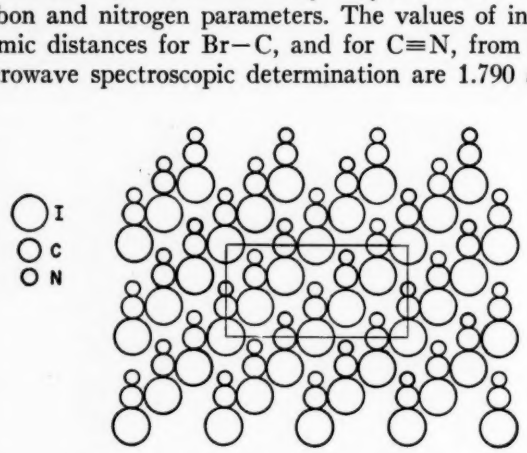

FIG. 3(a). ICN projection along [11·0].

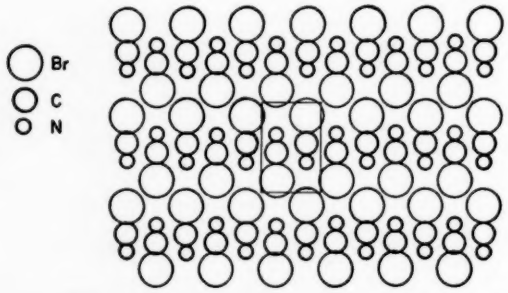

FIG. 3(b). BrCN projection along [010].

DISCUSSION

A summary of the measured couplings of Br and N in solid and gaseous BrCN is given in Table V. The couplings are also expressed in terms of U_p, the equivalent number of "unbalanced" p electrons. For this conversion, the quadrupole coupling of a Br^{81} nucleus with a single p electron is taken as 623.0 Mc, from atomic beam measurements.[16] For nitrogen, atomic beam measurements are not available, so the coupling of the nucleus with a single p electron is taken as 10 Mc. This value, together with a 50 percent s-hybridization of σ bonds has been shown by Townes and Dailey,[17] to be consistent with the quadrupole couplings observed in a number of nitrogen compounds.

The sign of the coupling cannot be determined in the solid, and so is assumed to be the same as in the gas.

It seems reasonable that, as proposed by Townes and Dailey for ICN, the bond structure in the solid

TABLE IV. Comparison of calculated with observed ($h0l$) reflection amplitudes.

		Amplitude				Amplitude	
	(l)	Obs	Calc		(l)	Obs	Calc
$h=0$	2	48	47	$h=4$	0	33	−29
	4	14	20		1	18	16
					2	19	19
$h=1$	0	24	23		3	<12	− 9
	1	43	−40		4	<12	9
	2	17	−19				
	3	18	21	$h=5$	0	<13	−3
	4	<12	9		1	18	18
	5	<14	− 7		2	<12	3
					3	<12	−11
$h=2$	0	13	− 9				
	1	51	−47	$h=6$	0	14	10
	2	9	7		1	12	12
	3	18	25		2	<12	− 7
	4	<12	− 3				
	5	<14	− 9	$h=7$	0	11	10
$h=3$	0	37	−35				
	1	16	−16				
	2	22	26				
	3	11	9				
	4	<13	11				
	5	<11	3				

[16] V. Jaccarino and J. G. King, Phys. Rev. **83**, 471 (1953), and private communication.

[17] C. H. Townes and B. P. Dailey, J. Chem. Phys. **17**, 782 (1949).

BrCN is a superposition of the three structures shown in Table VI. The third structure involves intermolecular covalent bonds between molecules in the chain. Assuming just these three structures, their relative importance can be determined from the two measured quadrupole couplings (Br and N). The values obtained in this way are included in the table.

In making these calculations, certain assumptions have been made.[17,18] These are: (1) Owing to the tightening of the p-electrons by a positive formal charge on the bromine atom, U_p is multiplied by 1.25. (2) In the third structure, the $-Br^+---$ bonding is linear and therefore 50 percent s-character for σ bonds to Br is assumed. (3) Apart from this case there is no s-character in the Br σ bonds. That there is a measure of arbitrariness in these assumptions is clearly understood, the goal being to show that such assumptions lead to plausible conclusions.

The fractional importance of the intermolecular bond is not large,* and would have little effect on the bond distances within the molecule. The nuclear quadrupole coupling for atomic iodine has been measured since the paper of Townes and Dailey was written. The value of eqQ for the atom, and hence, for a pure covalent p-bond is 2292 Mc, which is less than the coupling in either gaseous or solid ICN. Agreement with the experimental values, and a reasonable bond structure is obtained if the normal covalent iodine bond is assumed to have enough p-d hybridization to raise its coupling to 2500 Mc. Such p-d hybridization was discussed by Townes and Dailey,[17] and has recently been used to explain the structure of solid iodine.[19]

The crystalline structure of BrCN gives credence to the results expressed above. The structure [see Figs. 2(b) and 3(b)] consists of straight chains of BrCN molecules along the a-axis direction. Along the (100) pinacoid diagonal, these chains point alternately oppositely and are separated by 3.65 A on centers [Fig. 2(b)]. The distance between nearest chains in neighboring cells on two different diagonals is also 3.65 A, and these chains also point oppositely alternately. In exactly the c-axis direction, the chains point the same way and nearest chains are separated by 4.12 A, the length of the c-axis. Thus a given chain is surrounded by four chains pointing oppositely at 3.65 A and two pointing in the same way at 4.12 A.

TABLE V. Quadrupole couplings in BrCN.

State	Quadrupole coupling eqQ Mc/sec Br	N	U_p Br	N
Gas	−573	−3.85	0.891	−0.385
Solid	(−)598[a]	(−)3.37[a]	0.962	−0.337

[a] Extrapolated to 0° K.

TABLE VI. Percentage importance of structures in solid and gaseous BrCN.

Structure	U_p Br	U_p N[a]	Percent importance Solid	Percent importance Gas
$Br-C\equiv N$	1.0	−0.50	76	74
$Br^+=C=\bar{N}$	0.625	0	15	26
$-Br^+-\bar{C}=N-$	1.25	+0.50	9	

[a] 50 percent s-hybridization assumed for σ bonds to nitrogen.

The van der Waals radii of Br and N are 1.95 and 1.5 A respectively. With a Br—C distance of 1.79 A and a C—N distance of 1.15 A, the over-all length of a free molecule would be 6.4 A However, the a-axis is only 5.80 A long. The distance between the N atom of one molecule and the Br atom of the next molecule in the same chain is 2.87 A. It is seen therefore that there is some intermolecular bonding along the chains. This is in line with the results obtained from the quadrupole coupling data.

Each Br atom is surrounded by four other Br atoms at distance 4.01 A and two Br atoms at 4.12 A. In neighboring chains the distance of a N atom to the nearest Br atom is 4.64 A, to nearest C atom is 3.7 A, and to the nearest N atom is 4.0 A. Thus except along the chains the structure is a loose one.

As pointed out previously intermolecular bonding along chains occurs also in ICN. Figures 2(a) and 2(b) show the ICN and BrCN structures projected on the (00·1) and (100) faces respectively. (The ICN structure is referred to hexagonal axes for simplicity.) Figures 3(a) and 3(b) show the ICN and BrCN projections along [11·0] and [010] respectively. If the BrCN molecule is considered a unit, it is seen that the stacking of molecules in the two structures is strikingly similar.

ACKNOWLEDGMENTS

The authors wish to acknowledge helpful discussions with Dr. C. H. Townes, Dr. J. M. Mays, and Dr. P. Kisliuk.

We wish also to thank Miss E. G. Cheatham who programmed the least-squares calculation for the Digital Computer, Bell Telephone Laboratories Model No. 6, and Mr. G. J. Gass who made the glass apparatus used to obtain the BrCN crystal for x-ray photography.

[18] J. M. Mays and B. P. Dailey, J. Chem. Phys. **20**, 1695 (1952).

* In fact, the number indicated (9 percent) seems high, and may be a result of necessary simplifications in the assumptions.

[19] Robinson, Dehmelt, and Gordy, J. Chem. Phys. **22**, 511 (1954).

Production of Excited Hydroxyl Radicals in the Hydrogen Atom-Ozone Reaction*

J. D. McKinley, Jr., David Garvin, and M. J. Boudart
The James Forrestal Research Center, Princeton University, Princeton, New Jersey

(Received September 21, 1954)

Near-infrared emission spectrograms of vibrationally excited hydroxyl radicals in the ground state have been obtained upon mixing H atoms and ozone. A recent interpretation of a particular source of the night-sky radiation has been verified. A nonequilibrium distribution of energy between the reaction products is indicated.

SPECTROGRAMS showing the fine structure of the night-sky radiation in the near infrared have been obtained by Meinel.[1–3] These and other night-sky spectrograms have been identified by him[3] and by Herzberg[4] as radiation from vibrationally excited hydroxyl radicals in the $^2\Pi$ ground state. Band sequences corresponding to vibrational quantum jumps of $\Delta v=4$, 5, and 6 were observed. Rotational constants were derived from the 5, 1 and 6, 2 bands which are consistent with the recent values obtained by Herman and Hornbeck[5] from their accurate data on the hydroxyl radical spectrum produced by an oxy-acetylene flame.

Herzberg[4] has suggested two chemical mechanisms that could account for the production of these radicals in the upper atmosphere. One requires a direct reaction of hydrogen and oxygen atoms, (1), to form an unstable OH which then jumps to an upper vibrational level in the electronic ground state and undergoes the observed series of vibrational transitions.

$$\begin{aligned} &H+O\rightarrow OH(^2\Sigma^-)\rightarrow OH^*(^2\Pi)+h\nu \\ &OH^*(^2\Pi)\rightarrow OH(^2\Pi)+h\nu. \end{aligned} \qquad (1)$$

The second mechanism involves a reaction between ozone and hydrogen atoms to produce hydroxyl radicals in a high ($v=9$) vibrational level of the ground state consistent with the energy of the reaction.

$$\left.\begin{aligned} &H+O_3\rightarrow O_2+OH^*(^2\Pi) \\ &OH^*(^2\Pi)\rightarrow OH(^2\Pi)+h\nu \end{aligned}\right\}\Delta H=-3.57 \text{ ev.}\dagger \qquad (2)$$

A comparison of the intensities of the lines observed by Meinel with those calculated on the basis of this second mechanism[6] supported the reaction between ozone and atomic hydrogen.

We have examined reaction (2) in the laboratory, and have obtained near-infrared emission spectrograms that show substantially the same line structure as the plates obtained from the night sky. We believe that this is strong evidence for the occurrence of reaction (2) in the upper atmosphere, and also that it offers a unique opportunity for obtaining detailed information about the behavior of a free radical possessing a large excess of vibrational energy.

EXPERIMENTAL

The radiation was produced in a low-pressure flow system by injecting a stream of ozone through a small nozzle into an atmosphere of partially dissociated hydrogen. Essentially, the system was the type used for the study of Polanyi diffusion flames.[7] At and surrounding the tip of the ozone nozzle a faint reddish (7100 A) glow was observed. Figure 1 shows an infrared photograph of the radiation source used for the spectrography.

Hydrogen atoms were produced by flowing hydrogen, saturated with water at room temperature, through an uncoated pyrex Wood's discharge tube,[8] and then through the reaction chamber. Ozone was fed from a five-liter spherical flask through a flow-control capillary to the nozzle. In all cases the hydrogen-atom flow exceeded that of the ozone by more than a factor of four.

The ozone was prepared in a separate apparatus as follows. Electrolytic oxygen was passed over platinized asbestos at 300°C, through Drierite, and into a Siemen's ozonizer. The exit gases were condensed in a trap at liquid nitrogen temperature and at a pressure low enough to prevent appreciable condensation of oxygen. By pumping on the liquid nitrogen cooled sample additional amounts of oxygen were removed, and the concentrated product was finally distilled into the reservoir flask. The mole percent ozone in the reservoir at the time of use ranged from 80 to 95 depending on the length of time the sample was stored.

With a high-speed four-stage mercury diffusion pump, the pressure at the reaction zone was kept at 0.20 mm Hg. The average ozone flow rate was 2×10^{-6} mole/sec. The flow rate of undissociated hydrogen was 10×10^{-6}

* This research was supported by the United States Air Force under Contract No. AF 33(038)-23976 monitored by the Air Research and Development Command.

[1] A. B. Meinel, J. Astrophys. **111**, 207 (1950).
[2] A. B. Meinel, J. Astrophys. **111**, 433 (1950).
[3] A. B. Meinel, J. Astrophys. **111**, 555 (1950).
[4] G. Herzberg, J. Roy. Astron. Soc. Canada **45**, 100 (1951). See also D. R. Bates and M. Nicolet, Publ. Astron. Soc. Pac. **62**, 106 (1950).
[5] R. C. Herman and G. A. Hornbeck, J. Astrophys. **118**, 214 (1953); G. A. Hornbeck, Fifth Symposium on Combustion (International), Pittsburgh, Sept. 1954, Paper No. 56.
† This value is consistent with the newly determined dissociation energy of OH, see reference 5.
[6] H. S. Heaps and G. Herzberg, Z. Physik **133**, 48 (1952).
[7] M. Polanyi, *Atomic Reactions* (Williams and Norgate, London, 1932); L. Frommer and M. Polanyi, Trans. Faraday Soc. **30**, 519 (1934).
[8] R. W. Wood, Proc. Roy. Soc. (London) **A97**, 455 (1920).

mole/sec. The percentage of hydrogen dissociated at the mixing point was 50±5; this was determined in separate experiments by a calorimetric method.[9]

The radiation passed through the pyrex wall of the reaction vessel and was imaged by a small uncorrected glass lens upon the slit of the spectrograph, a small, Hilger, constant-deviation, glass prism wavelength spectrometer, similar to the D-186, (focal length 286 mm, $f/11$) with camera attachment. The dispersion of the instrument was 80 A/mm at 6500 A and 250 A/mm at 8500 A. Spectrograms were taken on Eastman Kodak type I–N and I–M spectrographic plates that had been hypersensitized with ammonia and pre-exposed to a density of 0.3 to 0.5 immediately before use. Due to the low brightness of the source, exposures were made for two or three hours. Reference spectra of argon were taken on each plate. These were easily obtained from a two-watt Western Electric "Point-o-lite" zircon arc (which has an argon atmosphere).

The products of the reaction were condensed in a trap held at liquid-nitrogen temperature, and then were analyzed. This phase of the work, which is not complete, will be reported later.

RESULTS

The better of two type I–N plates used in the analysis is reproduced in Fig. 2. The spectra were scanned with a Leeds and Northrup recording microphotometer, and with these tracings the positions of the features of the bands were measured. A slit width greater than the optimum value was employed to show clearly the weak lines in the P branches. A consequent loss in resolution caused overlapping of the relatively intense Q lines with the R branch heads; also the doublet splitting is obscured. The measured positions of the various band elements, and the assignments to the hydroxyl spectrum are listed in Table I. Included are two bands tentatively identified by analysis of a type I–M (8500–10 000 A) plate. The wavelengths reported by Meinel are shown for comparison. The wave numbers in column 6 of Table I were calculated from rotational and coupling constants compiled by Herzberg[10] together with the vibrational constants computed by Meinel[3] from his data. The agreement with the observed frequencies is satisfactory in view of the uncertainty in our measurements (±5 A) occasioned by the low resolution of the spectrographic arrangement.

No bands other than those recorded in Table I were observed; of the bands predicted in this spectral region for vibrational transitions of hydroxyl formed in the 9th level, all were observed with the exception of the 6,1 transition at 6500 A. This band could not be seen due to the presence of the strong $H\alpha$ line at 6560 A.

TABLE I. Near-infrared emission spectrum of OH.

Observed λ, A (air)	Observed ν, cm⁻¹ (vac)	Assignment Band	Branch	K	Observed by Meinel cm⁻¹ (vac)	Calculated cm⁻¹ (vac)
6235 } [a]	16 033					
6258 }	15 974	9,3	Q, R			15 975 (origin)
6560	15 240	$H\alpha$				15 233 [b]
6834 } [a]	14 629	7,2	Q, R			14 565
6879 }	14 532					(origin)
7288	13 717	8,3	Q		13 724.5	13 718.3
7328	646		P	2	650.7	655.3
7349	603		P	3	605.1	607.2
7374	557		P	4	554.2	554.0
7409	493		P	5	494.3	493.6
7471	13 381	4,0	R			13 389
7492	344		R			345
7523	289		Q			286
7574	199		P	2	13 193.9	197.2
7604	147		P	3		150.4
7756	12 890	9,4	Q		12 890.0	12 896.9
7800	818		P	2	818.6	820.5
7865	711	5,1	R			710.3
7877	691		R		696.6	691.8
7897	663	9,4	P	5	666.7	664.9
7966	12 550	5,1	P	2	12 545.9	12 550.6
8024	460		P	4	450.3	453.7
8067	393		P	5	394.2	396.4
8107	332		P	6	333.4	333.1
8298	048	6,2	R		044.8	053.8
8344	11 981	6,2	Q			11 982.7
8349	974		Q		11 976.6	971.3
8399	903		P	2	899.3	901.3
8464	811		P	4	806.8	806.9
8503	757		P	5	752.2	752.0
8552	11 690		P	6	11 691.8	11 689.3
8559	626		P	7	632.2	621.5
8772	397	7,3	R			398
8777	390		R		388.5	390
8792	371		R			371
8825	11 328		Q		11 322.8	11 320.2
8890	239		P	2	240.4	242.4
8928	198		P	3	203.1	199.9
8970	145		P	4	154.9	151.7
9006	101		P	5		097.3
9300 } [c]	10 752	8,4				10 658
9400 }	10 637					(origin)
10 000 [c]	10 000	9,5				9 986 (origin)

[a] Limits of unresolved emission band.
[b] *Handbook of Chemistry and Physics* (Chemical Rubber Publishing Company, Cleveland, Ohio), 35th edition.
[c] Observed on type I–M plate.

Comparison of our spectra with the near-infrared water-vapor emission bands[11] showed no similarities.

In separate experiments we have injected ozone into a stream of undissociated hydrogen under conditions comparable to those described above. An examination of the trapped exit gases showed no evidence of reaction. This is in agreement with some observations

[9] H. G. Poole, Proc. Roy. Soc. (London) **A163**, 404 (1937); H. Henkin and H. A. Taylor, J. Chem. Phys. **8**, 1 (1940).
[10] G. Herzberg, *Molecular Spectra and Molecular Structure I. Spectra of Diatomic Molecules* (D. Van Nostrand Company, Inc., New York, 1950), p. 561.
[11] A. G. Gaydon, Proc. Roy. Soc. (London) **181A**, 197 (1942).

FIG. 1. Ozone nozzle tip showing radiation source.

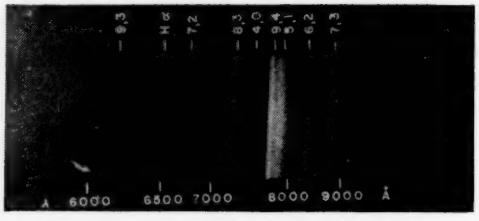

FIG. 2. The emission spectrum of hydroxyl in the near infrared.

of Lewis[12] on the explosion limits of ozone, hydrogen mixtures. On mixing pure oxygen and atomic hydrogen and photographing the emission spectrum on a type I–N plate, only the *Hα* line was observed after a one-hour exposure. In neither of these experiments was the red radiation characteristic of the H, O_3 reaction visible. The intensity of the 6500 A radiation was far greater in the ozone experiments than in that using oxygen. We believe that the *Hα* line observed in the latter is due to reflection from the Wood's discharge tube, and incline to Meinel's view that the 6,1 transition occurs.

The position of the radiation source leaves little doubt in our minds that reaction (2) is the immediate precursor of the OH radiation. The radiation emanated from a region immediately about the tip of the ozone nozzle and, in part, from within the end of the nozzle. Observations on other low-pressure diffusion flames indicate that the *initial reaction* between the reagents occurs in the region just described. In addition to reactions (1) and (2), the following possible initial reactions can be imagined

$$H+O_2=OH+O. \quad (3)$$

$$H+O_2+M=HO_2+M. \quad (4)$$

$$H_2+O_3=OH+HO_2. \quad (5)$$

These three reactions can be ruled out as radiation precursors because of the negative results in the control experiments described in the preceding paragraph. Reaction (1) requires the presence of oxygen atoms which must come from the disassociation of ozone within the nozzle. Were sufficient oxygen atoms produced from this source at room temperature we would expect to have observed reaction products upon mixing hydrogen (molecular) and ozone. If atomic hydrogen in the system can produce an extremely fast catalytic decomposition of ozone within the nozzle, a sufficient supply of oxygen atoms might be delivered to the nozzle mouth. However, the short contact time of ozone in the nozzle (4×10^{-5} sec) argues against this possibility. Upon these grounds, and the fact that H and O_3 are the major reagents, we conclude that reaction (2) is most probably the initial reaction and consequently is, in this system, the source of the radiating hydroxyls.

The source of the night-sky hydroxyls, however, cannot be positively identified as reaction (2) on the basis of these laboratory experiments alone. The general interpretation of the night-sky radiation in terms of reaction (2) has been criticized recently by Krasovskii.[13] On the other hand the production in the laboratory of a spectrum very similar to that of the night sky offers direct support to the mechanism implied in reaction (2).

One other conclusion, the consequences of which are now being investigated, stands out. In this system it appears that of the two molecules produced in the two-body collision, the hydroxyl radical carries off the bulk of the reaction energy. This is an extreme case of a nonequilibrium distribution of energy.

The absolute-rate theory, being an equilibrium theory, makes no prediction of the energy distribution among the immediate products of a reaction act. The detailed path by which activated complexes decompose is beyond the scope of the theory. Although speculations have been made concerning possible nonequilibrium distributions following reaction,[14] the reality of their existence for an elementary reaction had not been established in the laboratory. The success of these experiments possibly depends on the low probability for collisional deactivation of the hydroxyl radicals.[15]

We are indebted to Professor A. G. Shenstone of the Physics Department for the loan of the spectrograph, and to Dr. James A. Amick of the David Sarnoff Research Laboratories, Radio Corporation of America, for making the densitometric traces of our plates.

[12] B. Lewis, J. Am. Chem. Soc. **55**, 4001 (1933).

[13] V. I. Krasovskii, Usp. Fiz. Nauk **47**, 493 (1952).

[14] S. Golden and A. M. Peiser, J. Chem. Phys. **17**, 630 (1949).

[15] H. A. Bethe and E. Teller, BRL Report X-117.

Energy Transfer by Collisions in Vapors of Chlorinated Methanes*

D. SETTE,† A. BUSALA,‡ AND J. C. HUBBARD§
Department of Physics, Catholic University of America, Washington, D. C.
(Received June 7, 1954)

Ultrasonic velocity has been measured at 30°C in the four chlorinated methanes: methyl chloride, methylene chloride, chloroform, and carbon tetrachloride, at pressures from 1.5 cm Hg to more than one atmos in the case of methyl chloride, and with the others to the vapor pressures available up to 28°C and at frequencies from 0.2 to 2 Mc sec^{-1}. Dispersion of the velocity has been found in each case, the relaxation frequency/pressure ratios, correcting for departure from the ideal gas law, at 30° being in CH_3Cl, $CHCl_3$, and CCl_4 respectively 1.13, 27.3, and 23.3 Mc sec^{-1} $atmos^{-1}$. In CH_2Cl_2 two relaxations have been found with respective frequency/pressure ratios after similar corrections of 2.27 and 105 Mc sec^{-1} $atmos^{-1}$.

INTRODUCTION

THE process of energy transfer by collisions between gas molecules has recently received much attention. R. N. Schwartz, Z. I. Slawsky, and K. F. Herzfeld[1] have given a theory for the calculation of transition probabilities and relaxation times in the energy exchange between translation and vibration of gas molecules, which despite some simplifying and restrictive assumptions, is a noticeable advance over the preceding situation. It is evident, however, that further theoretical developments are needed to have a satisfactory picture of the phenomena. In the process of testing and developing new theories, it was felt by the authors that information on the behavior of a series of gases whose molecules had structures intimately related might be significant, and for that reason we have studied the four chlorinated methanes.

A previous investigation[2] by the present authors on the vapors of *cis*- and *trans*-dichloroethylenes succeeded in showing that the efficiency of collisions in those gases is essentially determined by short-range forces and that the dipole forces do not appreciably affect the magnitude of the transition probabilities. Boudart[3] has shown that when the correction is made for departure from the ideal gas law, only one relaxation time, within the precision of our experiments, is evident in any one vapor.

Recently J. D. Lambert and J. S. Rowlinson[4] have studied a large number of organic vapors and in each case in which they find acoustic dispersion it can be represented in terms of a single relaxation time characteristic of each vapor. At this writing (November, 1953) there has appeared a study by Fogg, Hanks, and Lambert[5] on the vapors of the halo-methanes. This includes data on all the substances discussed here as well as many others. They find: "Dispersion or incipient dispersion occurs in all cases. Each dispersion zone observed corresponds to a single relaxation time, involving disappearance of the whole of the molecular vibrational energy." Their measurements were made at a temperature of 100°C, and at pressures between 0.25 and 2 atmos, while the results presented here were obtained at 30°C and at pressures ranging from 1.4 cm Hg upward to one atmos in one case. S. Petralia[6] has studied the dispersion of sound in methyl chloride at 14°C, and his results and those of Fogg, Hanks, and Lambert[5] are later discussed with ours.

As has been discussed by Schaefer,[7] two extreme cases of dispersion are distinguished in polyatomic molecules. In one (parallel excitation) the energy is exchanged between translational and each vibrational degree of freedom independently. In the second case (series excitation) only one internal vibration mode exchanges energy with translation, and the energy subsequently flows from the first into the other vibrations. In real cases both processes may be present at the same time, but pertinent experimental data so far presented are not sufficient in quantity or precision to permit any generalization, and for this reason we undertook the present work.

METHOD OF MEASUREMENT

Sound velocity measurements were made with an acoustic resonator interferometer with short acoustic path and with construction insuring rigorous parallelism between the optically plane parallel piezoelectric X-cut quartz plates used and the moving piston. An improved drive for the latter developed here[8] was used in all the measurements presented in this paper. This drive consists of external gears working on a bent arm enclosed in a metal bellows so as to turn the micrometer screw inside the vacuum-tight enclosure of the interferometer. Further improvements were made during

* Work supported by Office of Naval Research.
† From the Instituto di Ultracustica, Rome, Italy.
‡ Now at Bell Telephone Laboratories, Murray Hill, New Jersey.
§ Died August 2, 1954.
[1] Schwartz, Slawsky, and Herzfeld, J. Chem. Phys. **20**, 1591–1599 (1952); R. N. Schwartz and K. F. Herzfeld, J. Chem. Phys. **22**, 767–773 (1954).
[2] Sette, Busala, and Hubbard, J. Chem. Phys. **20**, 1899–1902 (1952).
[3] M. Boudart, J. Chem. Phys. **21**, 955–956 (1953).
[4] J. D. Lambert and J. S. Rowlinson, Proc. Roy. Soc. (London) **A204**, 424–434 (1950–1951).
[5] Fogg, Hanks, and Lambert, Proc. Roy. Soc. (London) **A219**, 490–499 (1953).
[6] S. Petralia, Nuovo cimento **9**, 351 (1952).
[7] K. Schaefer, Z. physik Chem. **B46**, 212 (1940).
[8] W. J. Thaler, J. Acoust. Soc. Am. **24**, 15 (1952).

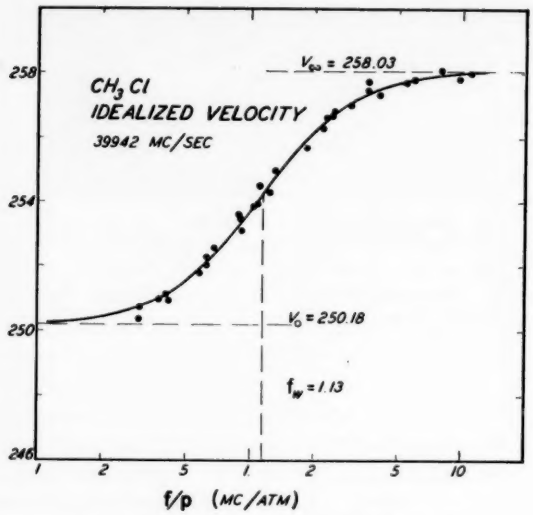

FIG. 1. Dispersion of ultrasonic velocity in methyl-chloride vapor at 30°C.

the course of the experiments: reducing areas of surfaces in contact inside the interferometer, a large portion of the contact of the piston with the sidewalls of the containing tube being cut away, openings made into cavities of the micrometer screw, and an enlarged duct made into the acoustic space between piston and reflector. These improvements have greatly reduced the time necessary for evacuation of the interferometer system and have correspondingly reduced the time needed for securing equilibrium of pressure of the vapors studied. A new method of measuring the positions of reaction peaks was adopted. This consists in moving the piston (upwards) toward the crystal when nearing a reaction peak and recording the screw and galvanometer readings just before the peak is reached; the screw is then carefully turned in the same direction until the same galvanometer reading is reached. The mean of the two screw readings is then taken as the peak reading.

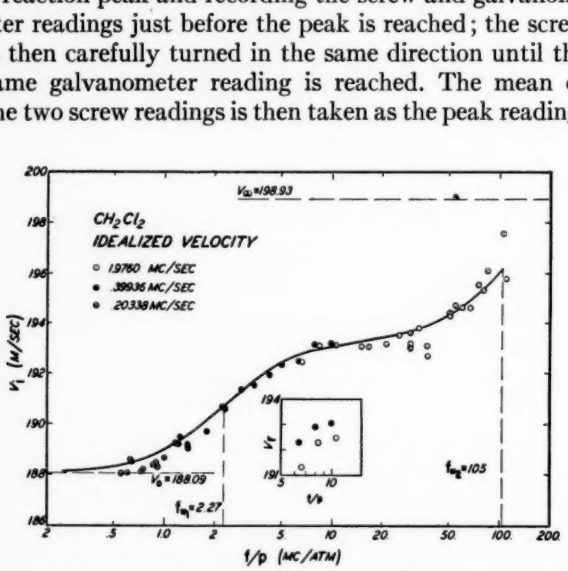

FIG. 2. Dispersion of ultrasonic velocity in methylene-chloride vapor at 30°C. Insert: three values of measured velocity (not idealized) for each of two-crystal frequencies at similar values of f/p, for comparison with the respective idealized velocities on the curve above.

The symmetry of the crevasse must be assured during this operation, otherwise the peaks will not be symmetrical at the top.[9]

This procedure has been tested under many conditions of pressure, and it is not too much to say that the gain in precision is nearly an order of magnitude. The convenient low-pressure limit for significant results has been pushed to about 0.5 cm. It should be emphasized that the force opposing motion of the micrometer screw is its own friction plus the weight of the piston and its friction. The frictions are remarkably constant where the motion is always upward towards the crystal.

TABLE I. Ultrasonic velocities in CH_2Cl_2 vapor at 30°C.

Frequency in Mc sec^{-1}	p cm Hg	f/p Mc sec^{-1} atmos^{-1}	V_r m sec^{-1}	V_i m sec^{-1}
0.20338	28.16	0.5489	186.63	188.04
	25.34	0.6070	186.82	188.08
	24.46	0.6319	187.38	188.60
	24.40	0.6335	187.31	188.54
	21.31	0.7253	187.04	188.11
	20.46	0.7555	187.19	188.21
	18.15	0.8516	187.63	188.40
	17.33	0.8919	187.65	188.52
	17.15	0.9013	187.49	188.34
	15.48	0.9985	187.93	188.70
	10.93	1.414	188.50	189.03
0.3975	16.86	1.792	188.88	189.74
	13.66	2.212	189.93	190.64
	13.13	2.301	189.93	190.60
	10.55	2.864	190.87	191.39
	8.79	3.437	191.13	191.56
	7.17	4.213	191.62	191.96
	5.98	5.052	192.05	192.34
	4.79	6.31	192.3	192.5
	3.78	7.99	192.9	193.1
	3.05	9.90	193.1	193.2
0.399356	25.62	1.179	187.93	189.22
	24.99	1.209	187.96	189.21
	24.38	1.239	188.29	189.50
	21.76	1.389	188.11	189.20
1.9760	22.75	6.601	191.28	192.43
	18.01	8.338	192.19	193.12
	14.14	10.62	192.42	193.15
	11.02	15.06	192.50	193.06
	9.00	16.69	192.62	193.08
	7.02	21.39	192.86	193.19
	5.92	25.37	193.25	193.54
	5.08	29.56	192.8	193.0
	5.05	29.74	192.9	193.2
	5.02	29.92	193.3	193.6
	4.50	33.37	193.6	193.8
	4.04	37.17	192.9	193.1
	4.02	37.36	192.5	192.7
	3.11	51.2	194.1	194.3
	2.97	50.6	194.3	194.4
	2.76	54.4	194.6	194.7
	2.51	59.8	194.6	194.6
	2.24	67.0	194.5	194.6
	2.00	75.1	195.4	195.5
	1.87	80.3	195.2	195.3
	1.77	84.8	196.0	196.1
	1.41	106.5	197.6	197.6
	1.34	112.0	195.7	195.8

[9] J. C. Hubbard, Phys. Rev. 41, 531 (1932).

The quartz crystals used had the resonance frequencies of approximately 0.2, 0.4, 1.0, and 2.0 Mc sec^{-1}. The pressure range was 2.7 to 100 cm Hg for CH_3Cl; 1.3 to 28 cm Hg for CH_2Cl_2; 2.9 to 13.9 cm Hg for $CHCl_3$; 1.5 to 12.1 cm Hg for CCl_4. Because the temperature of the laboratory reached 30°C at times, nearly all the measurements were made at temperatures between 31 and 32°C, controlled to 0.05°. The data were reduced to 30° with the help of standard corrections. The chemicals used were of analytical grade and furnished by the following manufacturers: methyl chloride from the Matheson Company, methylene chloride from Fisher and from Eastman, and chloroform and carbon tetrachloride from Fisher. The samples of methylene chloride used were obtained by distillation of the Eastman chemical at 40°C. Methyl chloride was distilled into a cooled vessel under pressure.

The method of admitting vapor to the interferometer system consists in first introducing the liquid, the vapor of which is to be studied, into a closed vessel which can be connected through a stopcock with the interferometer system. The system, except for the vessel mentioned, is pumped out through a trap cooled with a dry ice and alcohol mixture. The pump is then closed off as well as the interferometer system. The liquid vessel is opened for a moment, then closed, releasing air and some vapor which is condensed into the trap. The air is then pumped out, the vessel opened again for a moment, and closed, to release more air and some vapor. The cooling trap and connecting tubes are of such volume that in four or five steps the liquid begins distilling into the trap and the volume of liquid is reduced by about one fourth. The liquid container is then surrounded by a dry ice-alcohol bath and after some minutes is opened into the rest of the system for final pumping out. The last stage in this process consists in shutting off the trap and pump, removing the cooling bath from about the liquid container and allowing vapor to fill the interferometer system to a desired pressure; after this, the container is closed and the cooling bath replaced about it. It is usual to make determinations of velocity with several samples of vapor secured in this way before proceeding with a series of velocity determinations at different pressure reductions. The agreement of velocity determinations for different samples at approximately equal pressure is an indication of the relative purity of the samples, and corresponds closely to the precision expected from half-wave determinations.

EXPERIMENTAL RESULTS

In Table I the experimental values, V_r, of the sound velocity, and the idealized values, V_i, are given for CH_2Cl_2. The idealized velocity, V_i, for all four vapors is shown in Figs. 1, 2, 3, and 4, as function of

$$f^* = f/p \text{ sec}^{-1} \text{ atmos}^{-1}.$$

This variable is chosen because only the ratio of the period to the time between collisions—which is inversely proportional to p—matters. The present body of data together with much previous work, confirms this.[10]

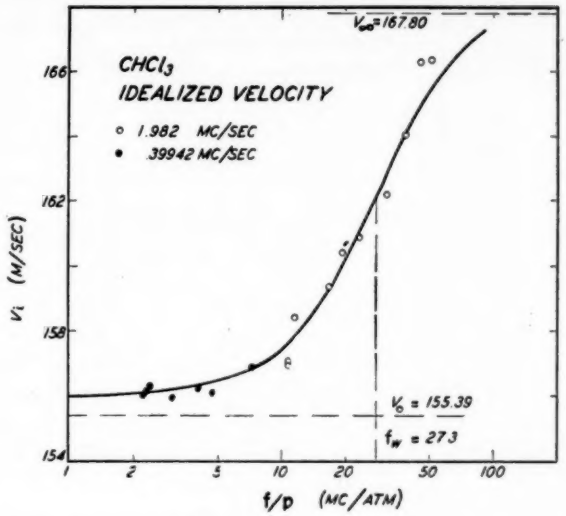

FIG. 3. Dispersion of ultrasonic velocity in chloroform vapor.

THE IDEALIZATION OF VELOCITIES

The idealized velocity, V_i, has been obtained from the measured value, V_r, by the relation

$$\frac{V_r}{V_i} = 1 + p\left[\frac{B}{RT} + \frac{1}{C_v^0}\left(\frac{dB}{dT} + \frac{RT}{2C_p^0}\cdot\frac{d^2B}{dT^2}\right)\right] = 1 - \alpha p, \quad (1)$$

where p is pressure, C_v^0 and C_p^0 are the low-frequency ideal specific heats which have been calculated from spectroscopic data, and B is the second virial coefficient. This formula does not take account of any variation

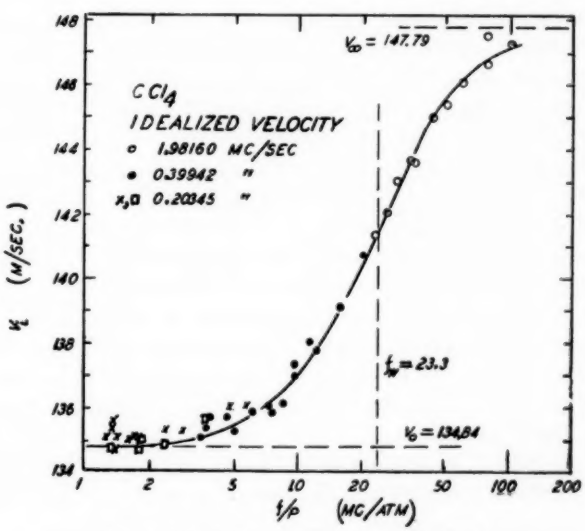

FIG. 4. Dispersion of ultrasonic velocity in carbon-tetrachloride vapor.

[10] See, e.g., W. T. Richards and J. A. Reid, J. Chem. Phys. 2, 193 (1934); Literature Review: W. T. Richards, Revs. Modern Phys. 11, 42, 49 (1939).

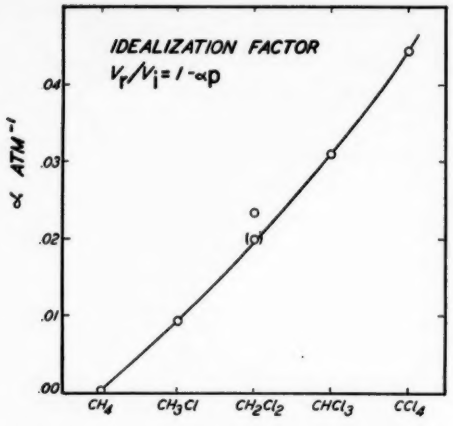

FIG. 5. Factor α for the "idealization" of measured acoustic velocities at small pressures, in methane and the vapors of the chlorinated methanes at 30°C.

of specific heats due to acoustic relaxation,[11] but, as was shown by R. T. Beyer,[12] this correction is very small and can be neglected. The determination of the second virial coefficient has been made using the Berthelot relation[13] and the critical pressure and temperature, thus:

$$B=\frac{9}{128}\frac{RT_c}{p_c}\left(1-\frac{6T_c^2}{T^2}\right). \qquad (2)$$

The critical data are available[14] for methyl chloride, chloroform, and carbon tetrachloride as indicated in Table II. For methylene chloride (CH_2Cl_2) the only critical datum we have found in the literature is the critical temperature. In order in this case to determine the idealization factor, α, we note that for CH_3Cl $CHCl_3$, and CCl_4 the entropy of vaporization is very near to 21 cal deg^{-1} mole^{-1}, as is usually the case for unassociated normal substances.[15] Because of this uniformity, and moreover because the idealization factor changes almost uniformly as the number of chlorine atoms increases for the three cases in which we have all the critical data, we could assume that the idealization factor of CH_2Cl_2 may be taken from the smooth curve of α *vs* the number of atoms of chlorine in the molecule, as shown in Fig. 5. The value of α for CH_2Cl_2 indicated in this manner is about 0.020 atmos^{-1}. As has been pointed out by Lambert and Rowlinson[4] a plot of V_r with p should give a straight line in the absence of acoustic dispersion and its extrapolation of $p \doteq 0$ gives V_0, the velocity of sound in the idealized vapor. Our data treated in this manner yield a slightly larger value of α.

However, since the low-frequency data given here are measurably within the dispersion zone, the value of α finally used for CH_2Cl_2 has been such as to bring the values of V_i into a single, uniform curve, Fig. 2. The value of α required for this is 0.0232 atmos^{-1}. An insert in this figure shows three values of V_r at two frequencies, in order to illustrate the match achieved in V_i using this value of α. Using the available critical constants in Table II and Eqs. (1) and (2), it corresponds to a critical pressure of 59.2 atmos, which is inserted in brackets in the table.

TABLE II. Idealization factors, α, for ultrasonic velocities.

	CH_4	CH_3Cl	CH_2Cl_2	$CHCl_3$	CCl_4
Critical temperature (°C)[a]	−82.5	143.1	245.1	262.5	283.1
Critical pressure (atmos)[b]	45.8	65.8	(59.2)[d]	53.8	44.98
ΔS, vaporization (cal/mole °K)[c]	17.51	20.7	21.4	20.99	20.5
C_v^0(30°C) (cal/mole °K)	6.69	7.84	10.36	13.85	18.12
α(atmos^{-1}) at 30°C	0.000424	0.00927	(0.0232)[d]	0.03086	0.04422

[a] From: International Critical Tables.
[b] From: Glasstone, reference 13, p. 457.
[c] All vaporization entropies at 760 mm Hg from Bur. Standards, selected values of chemical thermodynamic properties.
[d] Adjusted. See text, *Idealization of Velocities*.

DISCUSSION OF RESULTS

Plotted as a function of f/p Mc sec^{-1} atmos^{-1}, Figs. 1, 2, 3, and 4, the measured idealized ultrasonic velocities show a dispersion of values between theoretical limits that are calculated from the specific-heat change involved in the disappearance of the vibration levels of the molecules, these levels being determined from infrared and Raman spectra.[16] Table III gives the frequencies of the various modes of vibration of each molecule and their contributions to the specific heat at 30°C calculated with the Planck-Einstein formula. C_v^0 was obtained by adding the total vibrational specific heats, C_i, to $3R$ which is the translational and rotational contribution to the specific heat. In the table are also given the ratios of specific heats, γ_0, γ_∞, and the limiting velocities, V_0, V_∞ (two upper limits for CH_2Cl_2).

The calculated velocities both in the dispersion zones and in their limits agree excellently with the reduced measured velocities. It is therefore considered that the purity of the vapors is satisfactorily established. This fact seems to clear up some anomalies in Petralia's[6] experiments on CH_3Cl. From measurements of ultrasonic velocity he found for the specific heat of CH_3Cl at 14°C the respective low- and high-frequency values of $C_v^0=7.89$ cal mole^{-1} and $C_v^\infty=6.05$ cal mole^{-1}. The corresponding idealized limit velocities would be 241.78 m sec^{-1} and 250.61 m sec^{-1}, while in the values obtained from spectroscopic data the same temperature would be $V_0=244.34$ m sec^{-1} and $V_\infty=251.13$ m sec^{-1}. There is therefore a difference in both the values of the limit velocities and the increase of velocity due to relaxation. On the basis of the experimental results obtained by

[11] Otohiko Nomoto, Bull. Kobayasi Inst. **1**, 162 (1952).
[12] R. T. Beyer, J. Acoust. Soc. Am. **24**, 714 (1952).
[13] S. Glasstone, *Textbook of Physical Chemistry* (D. Van Nostrand Company, Inc., New York, 1946), second edition, p. 295.
[14] International Critical Tables.
[15] Reference 13, p. 457.
[16] G. Herzberg, *Infrared and Raman Spectra of Polyatomic Molecules* (D. Van Nostrand Company, Inc., New York, 1945).

us, it seems reasonable to attribute these discrepancies between Petralia's experiment and expectation to the presence of some impurities in the gas tested by Petralia.

V_i^2 is represented as a function of f^* by Eq. (3), where f_w^* is the value of f/p for the inflection point of the S-shaped curve corresponding to dispersion for a single relaxation time. The asymptotes of the single relaxation-time dispersion curve are represented by V_0 and V_∞.

$$V_i^2=\frac{V_\infty^2 f^{*2}+V_0^2 f_w^{*2}}{f^{*2}+f_w^{*2}}. \tag{3}$$

The inflection point occurs at the value of

$$V_w=[(V_0^2+V_\infty^2)/2]^{\frac{1}{2}}.$$

The relaxation curves, Figs. 1, 3, and 4, have been placed so as to represent the experimental results in the best manner. It is evident from Figs. 1, 3, and 4 that the experimental results for these gases are well represented within the experimental error by the assumption of a *single* relaxation time. The relaxation time, τ, can be calculated from f_w^* values with the relation

$$\tau=\frac{1}{2\pi f_w^*}\frac{C_v^0}{C_v^\infty}. \tag{4}$$

The case is different for CH_2Cl_2, in which two relaxation zones are clearly evident. The presence of a plateau in the dispersion line of CH_2Cl_2, Fig. 2, shows that the relaxation zones have at least two relaxation frequencies and that these are sufficiently far apart to consider the phenomena to be independent of each other. Under these circumstances Eq. (3) is to be replaced by (5):

$$V_i^2=V_0^2+\frac{a(f^*/f_{w_1}^*)^2}{1+(f^*/f_{w_1}^*)^2}+\frac{b(f^*/f_{w_2}^*)^2}{1+(f^*/f_{w_2}^*)^2}, \tag{5}$$

where

$$a=V_{\infty_1}^2-V_0^2; \qquad b=V_{\infty_2}^2-V_{\infty_1}^2, \tag{6}$$

and V_{∞_1} is at the same time the upper limit of velocity for the low-frequency relaxation and the lower limit for the higher frequency relaxation; V_{∞_2} is the upper limit of velocity for the high-frequency relaxation.

From Eq. (5) the curve V_i *vs* f/p has been drawn, Fig. 2. The two relaxation frequencies have been chosen with the criterion of best fit. From what has been mentioned before, $f_{w_1}^*$ and $f_{w_2}^*$ are the relaxation frequencies corresponding respectively to the relaxation times τ_1 and τ_2 given in Table IV.

The specific heat corresponding to the velocity, $V_{\infty_1}=193.30$ m sec^{-1}, is $C_v^{\infty_1}=3.86R$. This means that the vibrational specific heat, $C_v^0-C_v^{\infty_1}=(5.21-3.86)R=1.35R$, is involved in the low-frequency relaxation while the portion, $C_v^{\infty_1}-C_v^{\infty_2}=(3.86-3)R=0.86R$, is left for the high-frequency relaxation. The data on the contribution of the various vibration modes of CH_2Cl_2 to the specific heat (Table III) seem to indicate that all vibration modes except the lowest are involved in the first-relaxation phenomenon, leaving only the mode, $\nu_{\min}=283$ cm^{-1} for the high-frequency relaxation.

THE EXCITATION PROCESS OF VIBRATION MODES

In the sense that they are well represented by theoretical curves with a single relaxation time, the results on CH_3Cl, $CHCl_3$, and CCl_4 are in agreement with those obtained by Lambert and Rowlinson[4] in other polyatomic gases such as benzene and cyclopropane vapors.

TABLE III. Vibrational heats, specific heats, and ideal limiting sound velocities of chlorinated methanes.

CH_3Cl		CH_2Cl_2		$CHCl_3$		CCl_4	
$\bar{\nu}$ cm^{-1}	$\Delta C_i/R$	$\bar{\nu}$ cm^{-1}	$\Delta C_i/R$	$\bar{\nu}$ cm^{-1}	$\Delta C_i/R$	$\bar{\nu}$ cm^{-1}	$\Delta C_i/R$
732.1	0.3986	283	0.8626	260[a]	1.7648	218[a]	1.8306
1015.0[a]	0.3816	704	0.4246	364	0.7844	305[b]	2.5263
1354.9	0.0673	737	0.3937	667	0.4609	460	0.6822
1454.6[a]	0.0966	899	0.2623	760[a]	0.7460	775[b]	1.0797
2966.2	0.0001	1155	0.1263	1205[a]	0.2164	...	...
3041.8[a]	0.0002	1266	0.0894	3033	0.0001	C_i/R	6.1188
...	...	1429	0.0529	...	...		
C_i/R	0.9444	2984	0.0001	C_i/R	3.9726		
		3048	0.0001				
			...				
		C_i/R	2.2120				
C_v^0/R	3.9444		5.2120		6.9726		9.1188
C_p^0/R	4.9444		6.2120		7.9726		10.1188
γ_0	1.2535		1.1919		1.1434		1.1097
γ_{∞_1}	1.3333		1.2589		1.3333		1.3333
γ_{∞_2}			1.3333				
V_0	250.18		188.09		155.39		134.84
V_{∞_1}	258.03		193.30		167.80		147.79
V_{∞_2}			198.93				

[a] Double.
[b] Triple.

TABLE IV. Relaxation value of frequency/pressure, f_w^*; experimental relaxation time, τ; relaxation time for the exchange of energy between translation and the lowest vibrational mode, τ^*; molecular diameter, d; Sutherland's Constant, S; average number of collisions per sec, Z; average number of collisions for de-excitation of the lowest vibrational mode, Z_{10}^*; frequency of lowest vibrational mode, $\bar{\nu}_{\min}$; temperature, 30°C.

	$f_w^* \times 10^{-8}$ Mc sec^{-1} atmos^{-1}	$\tau \times 10^8$ sec	d[a] A	S[b]	$Z \times 10^{-10}$	$\tau^* \times 10^8$ sec	Z_{10}^*	$\bar{\nu}_{\min}$ cm^{-1}
CH_4		107	3.882	198	1.69	80.7	4800	1306.2
CH_3Cl	1.13	18.5	3.375	441	1.07	7.81	835	732.1
CH_2Cl_2	2.27	9.46	4.759	425	1.61	2.83	464	704
	105	0.195				0.195	31	283
$CHCl_3$	27.3	1.35	5.430	462	1.85	0.601	110	260
CCl_4	23.3	2.08	5.881	492	1.99	0.621	123	218

[a] Hirschfelder, Bird, and Spotz, Chem. Revs. **44**, 205 (1949).
[b] J. Braune and R. Linke, Z. physik Chem. **A148**, 195 (1930).

This conclusion is more widely confirmed by Fogg, Hanks, and Lambert[5] with respect to the ten methyl halides studied by them at 100°C, but their detailed conclusions as to relaxation time are somewhat different from ours, *viz.*, our values for $\tau \times 10^8$ sec for CH_3Cl, $CHCl_3$, and CCl_4 at 30°C are respectively 18.5, 1.35, and 2.08; theirs, at 100°C, 18, $\leqslant$2.8, 8.3. For CH_2Cl_2, we have the two relaxation times, $\tau \times 10^8$ sec, 9.46 and 0.195, while they give a single value, 8.4. The comparison of these results suggests that a study of temperature dependence of relaxation times of larger molecules is much needed.

The existence of only one relaxation time in CH_3Cl, $CHCl_3$, CCl_4 seems to indicate that the excitation process of the various modes of vibrations of these molecules is not a parallel process. In fact, if this were the case, the experimental results would mean that modes of different vibrational frequency would all have the same relaxation time, while it is expected that the different quanta involved in the transitions would produce different transition probabilities and different relaxation times.

It seems therefore that the experimental results in CH_3Cl, $CHCl_3$, CCl_4 are to be explained by assuming that the excitation process is a series one with the relaxation time for internal conversion very small.

This is a conclusion reached also by Lambert and Rowlinson considering many polyatomic molecules in which the relaxation phenomena occur with a single-relaxation time. These authors pointed out that in the cases examined by them the relaxation time itself as well as the average number of collisions needed for de-exciting a molecule decreases with the frequency of the lowest vibration mode. Accordingly they suggested the view that in these polyatomic molecules the energy is exchanged between translation and the mode of lowest frequency which is more easily activated; the energy flows then from this mode to the others and *vice versa* very rapidly.

For the case in which the observed single relaxation-time dispersion curve is related to a series process (i.e., only one vibrational mode exchanges with translation while the internal conversion relaxation times are very small), the relaxation time τ^* of the exchange translation-vibration mode is given by Eq. (7).

$$\tau^* = \frac{1}{2\pi f_w^*} \frac{C_v^0}{C_v^\infty} \frac{C^*}{C_i} = \tau \frac{C^*}{C_i}, \tag{7}$$

where C^* is taken as the contribution of that mode to the specific heat and C_i as the total vibrational specific heat.

The values of C^*, taking with Lambert and Rowlinson for C^* the contribution of the lowest vibration mode, are given in Table IV for CH_4, CH_3Cl, and CCl_4. The relaxation data on CH_4 at 30°C have been obtained by extrapolation of Eucken-Aybar's[17] results in the range 109–353°C. In the same table are calculated for the same molecules the average number of collisions, Z_{10}^*, to de-excite the lowest vibration mode:

$$Z_{10}^* = \tau^* Z, \tag{8}$$

Z being the average collision number per second,

$$Z = 2nd^2 \left(\frac{4RT}{M}\right)^{\frac{1}{2}} \left(1 + \frac{S}{T}\right) \tag{9}$$

and n, the number of molecules per cm^3; d, the diameter of the molecule; S, Sutherland's constant.

The results in CH_3Cl and $CHCl_3$ when compared with the data on CH_4 seem to confirm the view of Lambert and Rowlinson in the sense that an increase of efficiency of collisions (decrease of Z_{10}) corresponds to a decrease of $\nu_{\min}$. The results on CCl_4 compared with those on CH_4 show the same behavior, but if they are compared with those in $CHCl_3$ a decrease of efficiency corresponds to a decrease of $\nu_{\min}$. The change in mass between $CHCl_3$ and CCl_4 molecules, of course, acts by itself in the sense of decreasing the efficiency of CCl_4 collisions. Observing however that the percent change in mass between $CHCl_3$ and CCl_4 is much less than that between either CH_4 and CH_3Cl, or CH_3Cl

[17] A. Eucken and S. Aybar, Z. physik Chem. **B46**, 195 (1940).

and $CHCl_3$, it seems improbable that the different behavior of $CHCl_3$ and CCl_4 could be due entirely to a mass effect.

In contrast to the cases of CH_3Cl, $CHCl_3$, CCl_4, the experiment in CH_2Cl_2 vapor shows the presence of two well-distinguished relaxation times, and it is not possible to draw a definite conclusion as to the prevalent excitation process. A parallel excitation of at least two modes could be present. However in the light of the results obtained for other polyatomic gases, it seems likely that in CH_2Cl_2 also a series process is mainly effective with a finite relaxation time for some internal conversion. If this is true, the mode of lowest frequency, ν_4, exchanges energy with translation giving rise to the faster observed relaxation process τ_2, while the feeding of higher modes from the lowest is the origin of the low-frequency relaxation. In such a case it would of course be probable that the flow of energy towards the higher modes occurs also as a series process via the second low mode ν_3.

THE JOURNAL OF CHEMICAL PHYSICS VOLUME 23, NUMBER 5 MAY, 1955

Dipole Velocity and Dipole Length Matrix Elements in π Electron Systems and Configuration Interaction*

MAX WOLFSBERG
Chemistry Department, Brookhaven National Laboratory, Upton, Long Island, New York
(Received June 11, 1954)

Equations relating dipole velocity and dipole length matrix elements have been tested for π electron systems treated by a molecular orbital method. Considerable improvement in the validity of the equations is noted when configuration interaction is included in the calculations.

INTRODUCTION

TRANSITION probabilities in molecular systems have been computed usually with the use of the dipole moment operator in its dipole length form. Recently, Shull[1] has made calculations of transition probabilities in some simple diatomic molecules using the dipole moment operator in both its dipole length and its dipole velocity form. He has attempted to gain some insight into the form of ground and excited state wave functions by making use of the quantum mechanical relationship existing between the matrix elements of the two above mentioned types of dipole moment operators when one uses exact eigenfunctions of the Hamiltonian of the molecule treated. It appears that no computations of dipole velocity matrix elements in conjugated organic systems have as yet been carried out. Since these systems have received a major amount of attention in the study of molecular wave functions, it seemed worthwhile to study the two types of dipole moment matrix elements in these systems. Such a study might supply some information as to the reliability of the wave functions employed and might also be used in attempting to improve the wave functions.

PROCEDURE

If Ψ_a and Ψ_b are eigenfunctions of the Hamiltonian H with eigenvalues E_a and E_b, respectively, one finds[2]

$$\int \Psi_a^* \sum_j r_j \Psi_b d\tau = \frac{1}{E_b - E_a} \frac{h^2}{4\pi^2 m} \int \Psi_a^* \sum_j \frac{\partial}{\partial r_j} \Psi_b d\tau, \quad (1)$$

where r_j stands for a coordinate of the j's electron, j is to be summed over all electrons, and m is the electronic mass. If one now has wave functions ψ_a and ψ_b which are not true eigenfunctions of the Hamiltonian, these will satisfy the relations

$$\begin{aligned} H\psi_a &= H_{aa}\psi_a + H_{ac}\psi_c + H_{ad}\psi_d + \cdots = \sum_n H_{an}\psi_n, \\ H\psi_b &= H_{bb}\psi_b + H_{bk}\psi_k + H_{bl}\psi_l + \cdots = \sum_m H_{bm}\psi_m, \end{aligned} \quad (2)$$

with

$$H_{an} = \int \psi_n^* H \psi_a d\tau,$$

where one has expanded $H\psi_a$ and $H\psi_b$ in terms of some complete orthonormal set of ψ's. For these functions one finds by methods similar to those used in the derivation of Eq. (1), the relationship

$$\begin{aligned} \int \psi_a^* \sum_j r_j \psi_b d\tau = \frac{1}{H_{bb} - H_{aa}} \Bigg[\frac{h^2}{4\pi^2 m} \int \psi_a^* \\ \times \sum_j \frac{\partial}{\partial r_j} \psi_b d\tau - \sum_{m \neq b} H_{bm} \int \psi_a^* \sum_j r_j \psi_m d\tau \\ + \sum_{n \neq a} H_{an}^* \int \psi_n^* \sum_j r_j \psi_b d\tau \Bigg]. \end{aligned} \quad (3)$$

Equation (3) for the ψ's which are not eigenfunctions of the Hamiltonian is quite similar to Eq. (1) in that it only adds terms to the right-hand side of Eq. (1) which involve the expansion coefficients introduced in Eq. (2). With the H_{ad} integrals expressed in electron

* Work performed under the auspices of the U. S. Atomic Energy Commission.
[1] H. Shull, J. Chem. Phys. **20**, 18 (1952); **20**, 1095 (1952).
[2] See, for instance, L. I. Schiff, *Quantum Mechanics* (McGraw-Hill Book Company, Inc., New York, 1949), p. 247.

TABLE I.[a]

Molecule	Transition	Dipole length	Dipole velocity
ethylene	$I^1A_{1g}\rightarrow I^1B_{3u}$		
	without configuration interaction	1.000	0.492
	with configuration interaction	0.667	0.544
cyclobutadiene	$I^1B_{2g}\rightarrow I^1E_u$		
	without configuration interaction	1.00	0.39
	with configuration interaction	0.022	0.025
	$I^1A_{1g}\rightarrow I^1E_u$		
	without configuration interaction	1.00	0.56
	with configuration interaction	−0.014	−0.025

[a] Substitution of wave functions into the left- and right-hand sides of Eq. (1). The I's refer to the fact that in each case we are dealing with the lowest lying state of that symmetry classification.

volts,

$$\int \psi_a^* r \psi_b d\tau \text{ in A}, \quad \text{and} \quad \int \psi_a^* \frac{\partial}{\partial r_j} \psi_b d\tau \text{ in A}^{-1},$$

Eq. (3) becomes

$$\int \psi_a^* \sum_j r_j \psi_b d\tau = \frac{1}{H_{bb}-H_{aa}} \Big[7.618 \int \psi_a^* \times \sum_j \frac{\partial}{\partial r_j} \psi_b d\tau - \sum_{m \neq b} H_{bm} \int \psi_a^* \sum_j r_j \psi_m d\tau + \sum_{n \neq a} H_{an}^* \int \psi_n^* \sum_j r_j \psi_b d\tau \Big]. \quad (4)$$

In this paper we shall be dealing with molecular orbital wave functions. The functions ψ_a and ψ_b may then be considered to be single configuration functions (which we used as first-order approximations to good molecular wave functions) with the $\psi_{m's}$ and $\psi_{n's}$ being other configuration wave functions with which ψ_a and ψ_b interact. The H_{bm} and H_{an} are then the interaction integrals which occur when one carries out configuration interaction calculations in molecular orbital theory. In practice, in carrying out configuration interaction calculations on organic π electron systems using the LCAO approximation, only those states arising from the use of $2p\pi$ orbitals of the carbon atoms in the molecules have been drawn into consideration. In testing the validity of Eq. (3), we shall then only use these same configurations and assume that interaction integrals which connect the wave functions with yet other configurations are zero. In addition to testing Eq. (3) with single configuration molecular orbital wave functions, Eq. (1) will be tested in some cases using for Ψ_a and Ψ_b the final wave functions resulting from a configuration interaction calculation which has been restricted in the above mentioned manner.[3]

Configuration interaction calculations have been carried out previously on the molecules with which we deal in this note. They are *trans*-butadiene,[4] cyclobutadiene,[5] ethylene,[6] and benzene.[7] The calculations in this note made use of the same integrals as those used in the published calculations whenever these applied. Only one new type of integral appeared, $\int \psi_{a2p\pi} (\partial/\partial x_b) \psi_{b2p\pi} \times d\tau$. It can be easily evaluated by employing the method used in evaluating overlap integrals.[8]

The substitution of wave functions resulting from a configuration interaction calculation into Eq. (1) is quite straightforward and will not be further discussed. The use of Eq. (3) is simpler since it only requires a knowledge of the matrix elements involved in the secular equation without requiring its actual solution. We give as an example its application to the dipole velocity matrix element between the lowest lying configurations of symmetries $^1B_{2g}$ and ^1E_u in cyclobutadiene which will be referred to as I^1B_{2g} and I^1E_u. Higher lying states will be referred to as II^1B_{2g}, II^1E_u, etc. One then obtains

$$\int \psi^*(I^1B_{2g}) \sum_j x_j \psi(I^1E_u) d\tau = \frac{1}{H_{I,I}(^1E_u) - H_{I,I}(^1B_{2g})} \times \Big[\frac{h^2}{4\pi^2 m} \int \psi^*(I^1B_{2g}) \sum_j \frac{\partial}{\partial x_j} \psi(I^1E_u) d\tau - H_{I,II}(^1E_u) \int \psi^*(I^1B_{2g}) \sum_j x_j \psi(II^1E_u) d\tau + H_{I,II}(^1B_{2g}) \int \psi^*(II^1B_{2g}) \sum_j x_j \psi(I^1E_u) d\tau \Big]. \quad (5)$$

or,

$$\int \phi_1^* x \phi_2 d\tau = \frac{1}{H_{I,I}(^1E_u) - H_{I,I}(^1B_{2g})} \Big[\frac{h^2}{4\pi^2 m} \int \phi_1^* \frac{\partial}{\partial x} \phi_2 d\tau - H_{I,II}(^1E_u) \int \phi_0^* x \phi_1 d\tau + H_{I,II}(^1B_{2g}) \frac{6^{\frac{1}{2}}}{2} \int \phi_{-1}^* x \phi_0 d\tau \Big]. \quad (6)$$

[3] Such a test of Eq. (1) may of course be also considered a test of Eq. (3) for functions ψ_a and ψ_b for which all H_{bm} and H_{an} are zero.

[4] C. A. Coulson and J. Jacobs, Proc. Roy. Soc. (London) **A206**, 287 (1951).

[5] D. P. Craig, Proc. Roy. Soc. (London) **A202**, 498 (1950).

[6] R. G. Parr and B. L. Crawford, J. Chem. Phys. **16**, 526 (1948).

[7] Parr, Craig, and Ross, J. Chem. Phys. **18**, 1561 (1950).

[8] Mulliken, Rieke, Orloff, and Orloff, J. Chem. Phys. **17**, 1248 (1949).

TABLE II.[a]

Transition	$\int\psi_a^*\sum_j x_j\psi_b d\tau$	A $\frac{7.618}{H_{bb}-H_{aa}}\int\psi_a^*\sum_j\frac{\partial}{\partial x_j}\psi_b d\tau$	B $\frac{1}{H_{bb}-H_{aa}}\left(-\sum_{m\neq b}H_{bm}\int\psi_a^*\sum_j x_j\psi_m d\tau + \sum_{n\neq a}H_{an}^*\int\psi_n^*\sum_j x_j\psi_b d\tau\right)$	$A+B$
ethylene				
$I_1A_{1g}\rightarrow I^1B_{3u}$	1.000	0.492	0.407	0.899
cyclobutadiene				
$I^1B_{2g}\rightarrow I^1E_u$	1.000	0.390	0.496	0.886
$I^1A_{1g}\rightarrow I^1E_u$	1.000	0.563	0.345	0.908
$I^3A_{2g}\rightarrow I^3E_u$	1.000	0.833	0.000	0.833
$I^3A_{2g}\rightarrow II^3E_u$	1.000	0.799	0.000	0.799
benzene				
$I^1A_{1g}\rightarrow I^1E_u$	1.000	0.472	0.539	1.011

[a] Substitution into the left- and right-hand sides of Eq. (4). The symmetry designations refer to single configuration molecular orbital wave functions ψ_a and ψ_b, with I's referring to the lowest lying configuration of that symmetry and II to the next lowest lying configuration of the same symmetry.

In setting up Eq. (5), use is made of the vanishing of many integrals. The ϕ's in Eq. (6) refer to the individual molecular orbitals.[5]

RESULTS

The results of the calculations involving the substitution of configuration interaction wave functions into Eq. (1), and single configuration molecular orbital wave functions into Eq. (3) are given in Tables I and II, respectively. In Table I, the results for wave functions without configurational interaction are also shown explicitly. It is seen that in every case the introduction of configuration interaction either lessens the difference between the left and right sides of Eqs. (1) and (3) or does not change anything. In the cases when the contribution from

$$-\sum_{m\neq b}H_{bm}\int\psi_a^*\sum r_j\psi_m d\tau+\sum_{n\neq a}H_{an}^*\int\psi_n^*\sum r_j\psi_b d\tau$$

is zero in Eq. (3), the agreement between the right and left hand side of the equation is good, nevertheless. No numerical results for trans-butadiene are presented. Here it was attempted to use the configuration interaction wave functions given in the paper by Coulson and Jacobs.[4] While the results here again indicated that the agreement in Eq. (1) was much better when the configuration interaction functions were used rather then when the single configuration functions are used, the actual numbers are in some doubt since the data given by Coulson and Jacobs leaves the sign of the coefficients of some of the wave function in doubt. Since the actual magnitude (but not the relative values) of the integrals involved in Eq. (1) and (3) depends on the choice of the coordinate, and the form of the wave function ψ_b when ψ_b is a wave function of a degenerate state, we list in the Tables I and II all the results normalized to $\int\psi_a x\psi_b d\tau$ equal to 1 when ψ_a and ψ_b are the single configuration molecular orbital wave functions.

Analysis of the Near Ultraviolet Absorption Spectra of *ortho*- and *para*-Dichlorobenzene Vapors

TOSINOBU ANNO AND IKUO MATUBARA
Department of Chemistry, Faculty of Science, Kyushu University, Fukuoka, Japan
(Received August 16, 1954)

The absorption spectra of *o*- and *p*-dichlorobenzene vapors appearing in the region 2900–2400 A and 2950–2400 A, respectively, were photographed and measured. For the *ortho*-spectrum the band at 36 232 cm^{-1} is assigned as the 0−0 band. The progression with frequency intervals of 1089 cm^{-1} starts from the stronger bands. For the *para*-spectrum, the band at 35 750 cm^{-1} is taken to be the 0−0 band. The only progression-forming frequency is 1051 cm^{-1}. In both the spectra, most of the prominent bands are assigned to progressions or combinations of the possible fundamental frequencies. The fundamental frequencies are compared with the Raman values. From the vibrational analysis it is concluded that both molecules in the excited electronic states retain all their elements of symmetry in the ground states. For the *para*-compound the molecular structure in the upper state is discussed in some detail.

INTRODUCTION

THE near ultraviolet absorption spectra of the three isomeric-dichlorobenzene vapors were studied by Wollman (quoted by Sponer[1]); however, the detailed report has not yet been published. The ultraviolet absorption spectra of these substances in hexane solution have been studied by Conrad-Billroth.[2] The Raman spectra of dichlorobenzenes were reported by many authors[3] and the depolarization data are also available.[4] Lecomte[5] and Thompson[6] described the infrared absorption spectra of these compounds. Partial assignments of the fundamental frequencies to vibrational modes in the ground electronic state were given in different papers. They are collected in the Landolt-Börnstein Tables[7] and were taken from there. From the electron diffraction measurements of *o*-dichlorobenzene Brockway[8] derived a planar structure of this compound, while Hassel[9] concluded that the two chlorine atoms are out of the benzene plane in opposite directions.

In the present paper, detailed interpretations of ultraviolet absorption spectra of *o*- and *p*-dichlorobenzene will be described and a possible molecular structure of the *para*-compound in the upper electronic state will be discussed.

[1] H. Sponer, Revs. Modern Phys. **14**, 224 (1942).
[2] H. Conrad-Billroth, Z. physik. Chem. **B19**, 76 (1932).
[3] Dadieu, Kohlrausch, and Pongratz, Monatsh. **60**, 253, 426 (1932); J. W. Swaine and J. W. Murray, J. Chem. Phys. **1**, 512 (1933); O. Paulsen, Monatsh. **72**, 244 (1939); H. Sponer and J. S. Kirby-Smith, J. Chem. Phys. **9**, 667 (1941); E. Herz, Monatsh. **76**, 1 (1946); and Herz, Kohlrausch, and Vogel, Monatsh. **76**, 200 (1947).
[4] O. Paulsen, Monatsh. **72**, 244 (1939); E. Herz, Monatsh. **76**, 1 (1946); and H. Sponer and J. S. Kirby-Smith, J. Chem. Phys. **9**, 667 (1941).
[5] J. Lecomte, J. phys. radium **9**, 13 (1938).
[6] R. E. Richards and H. W. Thompson, Proc. Roy. Soc. (London) **A195**, 1 (1949).
[7] Landolt-Börnstein, *Zahlenwerte und Funktionen* (Springer-Verlag, Berlin, 1951), sixth edition, Vol. 1, Part II, p. 312.
[8] L. O. Brockway and K. J. Palmer, J. Am. Chem. Soc. **59**, 2181 (1937).
[9] O. Bastiansen and O. Hassel, Acta. Chem. Scand. **1**, 489 (1947).

EXPERIMENTAL

The samples of *o*- and *p*-dichlorobenzene were synthesized from the corresponding chloranilines by Sandmeyer reaction. The *o*-dichlorobenzene was distilled several times before use while the *p*-dichlorobenzene was purified by sublimation.

The spectrograph used for the *ortho*-compound was a Hilger E-II quartz spectrograph having a dispersion of 12 A/mm at 2600 A. The *para*-spectrum was taken by a quartz spectrograph whose dispersion at 2700 A is 8 A/mm. The absorption cell with quartz windows was 40 cm long, to which a small side tube was attached. A small glass ampoule containing the sample was placed in the side tube and the absorption cell was evacuated. After sealing off the cell the ampoule was broken, letting the vapor fill the entire cell.

The temperatures of the main cell and the reservoir were controlled independently by a nichrome-wired heater, always keeping the former about 10°C higher than the latter. When it was necessary to keep the reservoir cooler than the room temperature by means of an appropriate freezing mixture, the main cell was kept always at room temperature. The temperature of the reservoir was thus changed from 1° to 125°C for the *ortho*-compound, and from 0° to 200°C for the *para*-compound.

A hydrogen discharge lamp was used as a continuous light source and an iron arc supplied the comparison spectrum. Well-exposed plates, using Fuji process brand, were obtained in 40 min for the *ortho*-compound, and in one hour for the *para*-compound. Wavelengths were determined with a comparator supplied by Kagaku-Kenkyusho.

RESULTS

The *ortho*-spectrum appears in the region between 2900 and 2400 A. About 300 bands were observed. All bands have heads on the violet side. On a plate taken at 1°C only the stronger bands appear, of which the one at the longest wavelength, 2759.2 A (36 232 cm^{-1}), is taken as the 0−0 band. Other stronger bands ap-

pearing on the 1°C plate are at 36 539, 36 669, 36 842, 37 190, 37 321, 37 718, 37 760, 38 276, and 38 404 cm^{-1}. The frequency separations between any one of these stronger bands and its close-lying long wavelength companions are 24 and 59 cm^{-1} or their combinations. With increasing temperature of the reservoir, many more bands appear on the long-wave side of the 0—0 band, and at the same time the short-wave bands become more intense. The largest number of bands is observed on a plate taken at 35°C, and on plates taken at higher temperatures the absorption becomes so strong that the spectrum appears continuous (see Fig. 1).

The experimental data for the *ortho*-compound are given in Table I. Wavelengths and wave numbers of the observed bands are listed in columns one and two, respectively. The wave numbers are accurate to 2 or 3 cm^{-1} for the sharper bands. For each reservoir temperature visually estimated intensities are given in columns three, four, and five, in which: ew=extremely weak, vw=very weak, w=weak, mw=medium weak, m=medium, ms=medium strong, s=strong, vs=very strong, and es=extremely strong. Wave-number distances of each band from the 0—0 band at 36 232 cm^{-1} are given in column six while column seven contains vibrational assignments.

The *para*-spectrum appears in the region between 2950 and 2400 A, in which about 400 bands were observed. All bands are degraded towards the red. On a plate taken at 0°C, bands with wave numbers 35 750, 36 081, 36 278/86, 36 801, 36 811, 37 000/08, 37 211/16, 37 526, 37 538, 37 850, 37 863, 37 934/42, and 38 270/76 cm^{-1} are observed, of which the longest, 2796.4 A (35 750 cm^{-1}), is considered as the 0—0 band. Each of these bands is accompanied by satellites on the longer wavelength side, dominantly with separations 26 and 86 cm^{-1}. The effect of increasing the temperature is the same as in the case of the *ortho*-compound, and the largest number of bands are observed on a plate taken at 50°C (see Fig. 2).

The data for the *para*-compound are listed in Table II, in the same way as in Table I for the *ortho*-compound.

THEORETICAL CONSIDERATIONS

From the group theoretical considerations and the Franck-Condon principle applied to polyatomic molecules,[10] if the molecule in the excited state has the same symmetry elements as in the ground state, the only vibrations which appear in progression in the spectrum are the totally symmetrical ones, whose origins of the normal coordinates in the two states should be considerably different. The nontotally symmetrical vibrations should appear only in $v-v$ transitions, since, in this case, the normal coordinate origins of these vibrations are the same in the two states. The intensities of these $v-v$ transitions are determined by Boltzmann

[10] G. Herzberg and E. Teller, Z. physik. Chem. **B21**, 410 (1933) and H. Sponer and E. Teller, Revs. Modern Phys. **13**, 75 (1941).

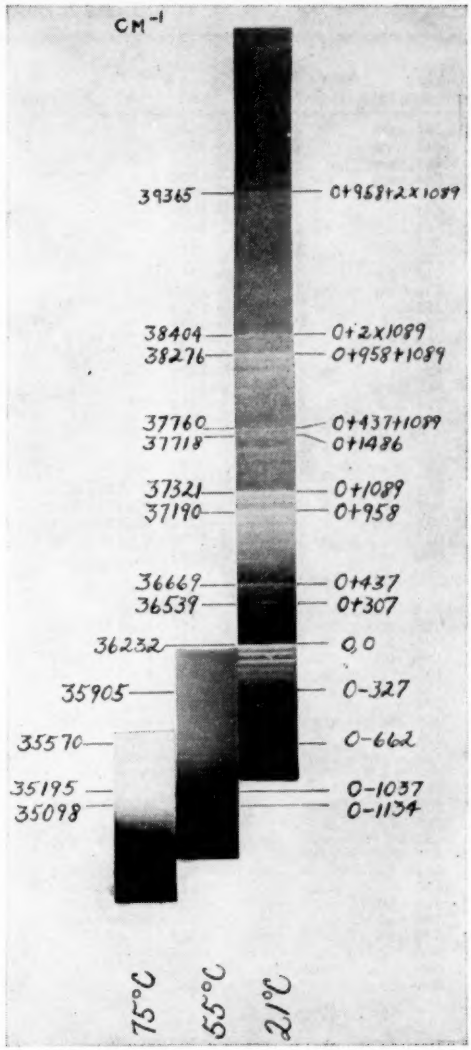

FIG. 1. Absorption bands of *o*-dichlorobenzene vapor.

factors of the nontotally symmetrical vibrations concerned. If the molecule belongs to different symmetry groups in the two electronic states, the progression-forming vibrations are totally symmetrical with respect to the lower symmetry group and may be nontotally symmetrical with respect to the higher one. The *p*-dichlorobenzene cannot have a symmetry higher than V_h, and *o*-dichlorobenzene not higher than C_{2v}.

Undoubtedly, *p*-dichlorobenzene belongs to V_h in the ground-electronic state and the fact that the only progression-forming vibration is a totally symmetrical one (Table II) shows that the molecule has the V_h symmetry also in the upper electronic state. As to *o*-dichlorobenzene, Brockway and Hassel suggested, as mentioned earlier, different models for its ground-electronic state. From the absorption spectrum it is interpreted that the only progression-forming vibration (Table I) is a totally symmetrical vibration of the C_{2v} model suggested by Brockway. This vibration, of course, is totally symmetrical in the C_2 model and we

TABLE I. Absorption bands of *o*-dichlorobenzene.

Wavelength in A	Wave numbers in cm^{-1}	Intensity 115°C	105°C	95°C	Separation from 0,0 band	Assignments
2906.9	34 391	vw			−1841	
02.7	441	vw			−1791	
00.4	468	vw			−1764	
2894.0	544	vw	vw	vw	−1688	
90.1	591	vw	vw		−1641	
87.4	623			vw	−1609	
86.5	634		vw		−1598	
81.4	695	vw			−1537	
80.6	705		vw		−1527	
79.8	715			w	−1517	
78.4	731	vw	vw		−1501	
76.7	752		vw		−1480	
75.7	764			w	−1468	
74.8	775			w	−1457	
73.9	786	vw		w	−1446	
72.4	804		vw		−1428	
71.5	815	vw			−1417	
69.1	844			w	−1388	
66.1	880	vw	vw	w	−1352	
		105°C	95°C	85°C		
64.0	906		mw		−1326	
61.9	932	vw	mw	w	−1300	0−1134−164
59.0	967		m		−1265	0−1134−136
57.3	988	vw	m	mw	−1244	0−1134−114
53.3	35 037		ms	mw	−1195	0−1134−59
52.6	046	vw			−1186	
		95°C	85°C	75°C		
51.7	057			vw	−1175	
50.2	075	s			−1157	0−1134−24
48.3	098	s	m	ms	−1134	0−1134
45.1	138	ms	mw	m	−1094	0−1037−59
42.9	165		m		−1067	0−1037−24
40.5	195	vs	s	s	−1037	0−1037
38.4	221			mw	−1011	
35.9	252	s	ms	m	−980	0−662−327
32.2	298			mw	−934	
		75°C	65°C	55°C		
30.9	314		w		−918	
27.8	353	s	mw	w	−879	0−662−226
25.2	385		w		−847	
23.6	405	s	mw	w	−827	0−662−3×59?
20.8	441		mw		−791	
19.2	461	es	ms	m	−771	0−662−114
16.9	490		mw		−742	0−662−24−59
15.1	512	vs	m	m	−720	0−662−59
12.4	546	vs	m	mw	−686	0−662−24
10.5	570	vs	s	ms	−662	0−662
08.5	596			w	−636	
07.5	608		mw		−624	
04.7	644		mw		−588	
		55°C	45°C	35°C		
02.8	668	mw	w	vw	−564	0−503−59
2798.0	729	s	m	vw	−503	0−503
94.6	773		ms		−459	0−436−24
92.8	796	s	s	w	−436	0−436
88.7	849	s	ms	w	−383	0−327−59
86.4	878		s	w	−354	0−327−24
84.3	905		vs	mw	−327	0−327
81.0	948			mw	−284	0−226−59
		35°C	21°C	1°C		
79.6	966	mw			−266	
76.5	36 006	s	mw	w	−226	0−226
74.3	035	ms	w	w	−197	
72.9	053	vs			−179	0−3×59?
71.7	068	vs	m	mw	−164	0−164
69.6	096	s	mw	w	−136	0−136; 0−2×59−24
67.9	118	es	s	m	−114	0−114; 0−2×59
65.5	149	s	mw	w	−83	0−83; 0−24−59
63.7	173	vs	s	m	−59	0−59
60.7	212	s	m	mw	−20	0−24
59.2	232	vs	vs	ms	0	0,0
		45°C	35°C	21°C		
56.7	265	vs	mw	w	33	0+92−59; 0+151−2×59
54.2	298	ms	w	w	66	0+92−24; 0+151−83
52.2	324	vs	mw	w	92	0+92; 0+151−59
49.7	357	s	w	w	125	0+151−24
47.7	383	vs	w	w	151	0+151
46.2	403	s	w	vw	171	0+195−24
44.4	427	vs	mw	w	195	0+195; 0+307−2×59
41.7	463		mw		231	
40.6	478	s	mw	w	246	0+307−59
37.9	514	s	mw	vw	282	0+307−24
36.0	539	vs	m	mw	307	0+307
34.2	563	m	vw		331	
32.4	587		vw		355	0+437−83
30.7	610	vs	m	mw	378	0+437−59
29.4	627		vw		395	
28.1	645	m	vw		413	0+437−24

Wavelength in A	Wave numbers in cm^{-1}	Intensity 35°C	21°C	1°C	Separation from 0,0 band	Assignments
26.3	669	ms	m	mw	437	0+437
23.4	708	w			476	0+610−136
21.8	730	mw	w	vw	498	0+610−2×59
19.2	765	w			533	
17.6	786	mw	w	vw	554	0+610−59
15.2	819	w	vw		587	0+610−24
13.5	842	m	mw	vw	610	0+610
11.3	872	mw	w	vw	640	
08.1	915	w			683	
05.5	951	mw	w	vw	719	
02.5	992	w			760	0−327+1089
00.8	37 015	mw	w		783	0+958−3×59?
2699.6	032	w		vw	800	
98.5	047	w			815	0+958−136
96.6	073	ms	m	w	841	0+958−2×59
92.5	129	ms	m	w	897	0+958−59
90.5	157	w	ms		925	0+1089−164
89.4	172	s	ms		940	0+958−24
88.1	190	s	ms	mw	958	0+958; 0+1089−136
87.1	204	ms	w		972	0+1089−2×59
85.6	225	w	w		993	0+610+437−59
84.3	243	w			1011	0+1089−83
83.1	259	ms	m	mw	1027	0+1089−59; 0+610 +437−24
81.5	282	mw	w		1050	0+610+437
80.3	298	w			1066	0+1089−24
78.7	321	s	ms	mw	1089	0+1089
76.4	353	w	vw		1121	
74.2	383	vw			1151	
72.0	414	w			1182	
70.3	438	w	vw		1206	
67.6	476	w			1244	0+151+1089
65.5	505	w	vw	vw	1273	0+437+958−2×59
61.0	569	mw	vw	vw	1337	0+437+958−59
59.7	587	w			1355	
58.1	610	m			1378	0+437+958−24
56.8	628	mw	w	vw	1396	0+307+1089; 0+437+958; 0+437+1089−136
56.0	639	vw			1407	0+1486−83
54.3	664	w	vw		1432	0+1486−59
51.9	698	mw	vw		1466	0+1486−24; 0+437 +1089−59
50.5	718	mw	mw	vw	1486	0+1486
47.5	760	w	mw	vw	1528	0+437+1089
46.3	777	vw			1545	
44.4	805	w	w		1573	0+610+1089−2×59
41.5	846	vw			1614	0+610+1089−83
40.1	866		w		1634	
39.4	876	vw			1644	0+610+1089−59
37.5	903	w			1671	0+610+1089−24
35.8	928	w	vw		1696	0+610+1089
33.9	955	w			1723	
33.2	965	w	vw		1733	
30.7	38 001	w			1769	
28.1	039	mw	w	vw	1807	0+437+1486−2×59
25.4	078	mw			1846	0+958+1089−197; 0−327+2×1089
24.2	096	mw	vw		1864	0+437+1486−59
226.	120	mw			1888	
21.3	138	mw			1906	0+958+1089−136; 0+437+1486−24; 0+2×958?
20.1	155	mw	w	vw	1923	0+958+1089−2×59; 0+437+1486
19.2	168	w			1936	
16.0	215	m	mw	vw	1983	0+958+1089−59
14.2	241	mw			2009	
11.8	276	ms	m	w	2044	0+958+1089
09.7	307	vw	vw		2075	
07.9	334	w	vw	vw	2102	
05.3	372	w	vw	vw	2140	0+2×1089−24; 0+610 +437+1089
03.1	404	mw	w	vw	2172	0+2×1089
		45°C	35°C	21°C		
00.4	444		vw		2212	
2599.2	462			vw	2230	
98.4	474		vw	vw	2242	
96.5	502			vw	2270	
94.9	526		vw		2294	
93.1	552		vw	vw	2320	0+307+2×1089−164
92.1	567		vw		2335	
90.9	585		vw	vw	2353	
90.3	594			vw	2362	
86.9	645		vw	vw	2413	
82.2	715	ms	w	vw	2483	0+307+2×1089; 0+437 +958+1089
80.3	744	m	vw	vw	2512	0+437+2×1089−2×59
79.0	763		vw		2531	
76.3	804	ms	w	vw	2572	0+437+2×1089−59; 0+1486+1089
72.6	860	m	vw	vw	2628	0+437+2×1089
70.8	887	m	vw	vw	2655	0+610+2×1089−2×59
69.4	908		vw		2676	
69.0	914		vw		2682	0+610+2×1089−83

TABLE I—*Continued.*

Wave-length in A	Wave numbers in cm^{-1}	Intensity 45°C	35°C	21°C	Separation from 0,0 band	Assignments
63.3	39 001		vw	vw	2769	0+610+2×1089
60.5	043		vw	ew	2811	
56.2	109		vw	ew	2877	0+3×958?
54.7	132		vw		2900	
52.7	163	ms	vw	ew	2931	0−327+3×1089
48.6	226	s	w	vw	2994	0+958+2×1089−136
45.6	272			ew	3040	
43.8	300		w		3068	
43.2	309		w	ew	3077	0+958+2×1089−59
42.0	327	s	w		3095	0+3×1089−163
39.6	365	s	w	vw	3133	0+958+2×1089
38.0	389	m			3157	
36.1	419	m	vw	ew	3187	
33.8	455		vw		3223	0+610+437+2×1089
31.5	490	m	vw	ew	3258	0+3×1089
		65°C	55°C	45°C		
27.4	555		w		3323	
24.4	602		mw	mw	3370	
23.6	614		w		3382	
22.0	639			mw	3407	
20.8	658	s	w		3426	
19.5	679		w		3447	
19.0	686		w		3454	
17.6	708		w	mw	3476	
13.6	772	ms	w		3540	0+307+3×1089−24
12.0	797	ms	w	mw	3565	0+307+3×1089
10.9	814		w		3582	
07.7	865		w		3633	
03.4	934	ms	w	w	3702	0+437+3×1089
01.0	972	ms	w		3740	
00.2	985		w		3753	
2498.3	40 015	ms	w		3783	
97.4	030		w		3798	0+610+3×1089−59
95.9	054	m	w		3822	
94.2	081	m	w		3849	
93.5	092	m	w		3860	0+610+3×1089
92.3	112	m	w		3880	
91.3	128	m	w		3896	
90.2	145		w		3913	
89.4	158		w		3926	
88.2	178	m	w		3946	
87.6	187	m	w		3955	
85.9	215	m	w		3983	
84.6	236		w		4004	
83.6	252	m	w		4020	0−327+4×1089
		75°C	65°C	55°C		
82.0	278	s		w	4046	
80.0	310	s	m	mw	4078	0+958+3×1089−136; 0+2×958+2×1089?
78.5	335		m		4103	0+958+3×1089−2×59
77.6	350		m	w	4118	
76.8	363	s	m	w	4131	0+958+3×1089−83
76.3	371	s			4139	
74.4	402	s	m	w	4170	0+958+3×1089−59
73.3	420	s	m	w	4188	
71.4	451	s	m	w	4219	0+958+3×1089
70.2	470			vw	4238	
68.3	502	s	mw		4270	
66.3	534		mw	vw	4302	
64.9	557	s	mw	vw	4325	
64.0	572		mw		4340	0+4×1089
62.3	600		mw	vw	4368	
61.1	620		mw		4388	

Wave-length in A	Wave numbers in cm^{-1}	Intensity 75°C	65°C	55°C	Separation from 0,0 band	Assignments
59.6	645	s	mw		4413	
58.9	656		mw		4424	
57.7	676	s	mw	vw	4444	
56.2	701			vw	4469	
55.4	714		mw	vw	4482	
54.2	734		mw	vw	4502	
53.7	742		mw		4510	
52.8	757	s			4525	
50.8	791	s	mw	vw	4559	
49.0	821	s		vw	4589	0+437+958+3×1089−164
47.6	844	s	mw	vw	4612	
46.4	864		mw		4632	
44.8	891	s	mw	vw	4659	0+437+958+3×1089; 0+307+4×1089
43.7	909		mw	vw	4677	
42.3	933		mw		4701	
41.2	951		mw	vw	4719	
40.5	963		mw		4731	
39.8	975	s	mw		4743	
38.9	990		mw		4758	
37.9	41 007	s	mw	vw	4775	0+437+4×1089
35.3	050	s	mw	vw	4818	
33.7	077	s	mw		4845	
31.8	109		mw		4877	
30.7	128	s	mw	vw	4896	
28.2	170		mw		4938	0+610+4×1089
26.6	197		mw	vw	4965	
26.0	208		mw		4976	0+3×958+2×1089−59?
25.2	221		mw	vw	4989	
23.7	247	s	mw	vw	5015	0+3×958+2×1089−24?
22.5	267		mw		5035	0+3×958+2×1089?
21.6	283	s	mw	vw	5051	
20.3	305		mw	vw	5073	
18.9	329		mw	vw	5097	0−327+5×1089
17.4	354	s	mw		5122	
16.5	370		mw	vw	5138	
16.0	378	s	mw		5146	0+2×958+3×1089−24?
15.3	390			vw	5158	
14.6	402	s	mw		5170	0+2×958+3×1089?
12.9	431		mw	vw	5199	0+958+4×1089−2×59
12.0	447		mw	vw	5215	0+958+4×1089−83
10.8	467	s	mw		5235	0+958+4×1089−59
10.0	481	s	mw	vw	5249	
09.5	490		mw		5258	
08.3	510	s	mw	vw	5278	0+958+4×1089−24
07.2	529		mw		5297	0+958+4×1089
05.9	552	s	mw		5320	
04.5	576		mw		5344	0+5×1089−83
02.8	605		mw		5373	0+5×1089−59
01.3	631		mw		5399	0+5×1089−24
00.1	652	s	mw		5420	0+5×1089
2399.3	666		mw		5434	
98.3	684	s			5452	
94.8	744	s	mw		5512	
93.9	760	s			5528	
91.5	802	s	mw		5570	
91.0	811	s			5579	
89.9	830		mw		5598	
89.3	841		mw		5609	
88.0	863	s	mw		5631	
86.8	884		mw		5652	
85.4	909	s			5677	
83.4	944	s			5712	
82.7	956	s			5724	
82.0	969	s	mw		5737	

can easily see that the symmetry group of *o*-dichlorobenzene is the same in the two electronic states. These considerations also show that, if Hassel's model is correct, the out-of-plane deviations of the Cl atoms are not very different in the two electronic states.

For the convenience of the following discussions, we should define the coordinate axes for both molecules. For the *ortho*-compound (C_{2v}) the z-axis is taken in the molecular plane bisecting the angle between the two C−Cl bonds. The molecular plane is denoted as the xz-plane. For the *para*-compound the z-axis is chosen perpendicular to the molecular plane, the y-axis passing through the two chlorine atoms. Then the symmetry notations used are the same as those given by Herzberg.[11]

In *o*-dichlorobenzene, the electronic transition which is expected to produce a spectrum in the 2600 A region is the allowed A_1-A_1 type with the transition moment in the z-direction. Also vibrations of β_1- or β_2-type may distort the benzene ring so that weak transitions may take place with their moments in the x- or y-directions, respectively. In the *para*-compound, the electronic transition with which we are concerned is the allowed A_g-B_{3u} type with the transition moment in the x-direction. The "forbidden parts" in this spectrum are caused by β_{1g}- or β_{2g}-type vibrations with their transition moments lying in the y- or z-directions, respectively.

[11] G. Herzberg, *Infrared and Raman Spectra of Polyatomic Molecules* (D. Van Nostrand Company, Inc., New York, 1945), Chap. II, Sec. 3d.

ANALYSIS AND DISCUSSION

o-Dichlorobenzene

The 36 232-cm^{-1} band is chosen as the 0−0 band. The pair of bands at 37 321=0+1089 and 35 098 =0−1134 cm^{-1} gives fundamental frequencies arising

TABLE II. Absorption bands of *p*-dichlorobenzene.

Wave-length in A	Wave numbers in cm^{-1}	Intensity 160°C	150°C	140°C	Separation from 0,0 band	Assignments
2933.6	34 078	vw			−1672	
32.5	091	vw			−1659	
31.0	108	w			−1642	
28.8	134	w			−1616	
26.5	161	mw			−1589	0−1589
23.6	194	m			−1556	
21.0	225	s	w		−1525	
19.1	247			vw	−1503	
18.6	253	vs	w		−1497	
16.4	279		mw	vw	−1471	
13.3	315		mw	w	−1435	
11.5	337		mw		−1413	
10.3	351			w	−1399	
		150°C	140°C	130°C		
08.6	371	mw	vw		−1379	
06.5	396	m		vw	−1354	
05.6	406		w		−1344	
03.8	428	m	w	vw	−1322	
02.9	438	ms	w		−1318	
00.8	463		w		−1287	
2898.5	491	vs		w	−1259	
97.8	499		mw		−1251	
96.1	519	es	m	w	−1231	
93.4	551	es	m	ms	−1199	
90.8	582		s	s	−1168	
90.5	586	es	s		−1164	0−1164
		140°C	130°C	120°C		
88.5	610	vs	s		−1140	
86.5	634	es		mw	−1116	
85.3	648		vs	w	−1102	0−1102
84.2	662	vs			−1088	0−755−331
83.3	672	es	vs	w	−1078	0−1078
82.5	682		ms		−1068	
81.0	700		vs		−1050	
76.6	753		es	mw	−997	0−755−247
74.0	785			vw	−965	
		110°C	90°C	80°C		
69.5	839	mw	vw		−911	0−755−86−3×26
67.7	861	m	vw		−889	0−755−86−2×26
65.7	885	m	w	vw	−865	0−755−86−26
63.7	910	s	mw	w	−840	0−755−86
62.8	921	w	w	vw	−829	0−755−3×26
62.1	929		w		−821	
60.6	947	ms	mw	w	−803	0−755−2×26
58.7	971	vs	m	mw	−779	0−755−26
56.7	995	es	ms	m	−755	0−755
55.8	35 006			vw	−744	0−631−86−26
53.5	034	s	mw	w	−716	0−631−86
51.3	061	vs	m	mw	−689	0−631−2×26
48.7	093		s	m	−657	0−631−26
46.6	119		ms	m	−631	0−631
46.2	124			w	−626	
44.1	150		vs	s	−600	0−486−86−26
41.8	179		vs	s	−571	0−486−86
		80°C	70°C	60°C		
39.7	205	m			−545	
39.3	210	mw	w	vw	−540	0−486−2×26
38.1	225	mw			−525	
37.1	237	s	m	vw	−513	0−486−26
35.9	252	ms	w	ew	−489	0−2×247
34.9	264	vs	ms	w	−486	0−486
33.9	277	s	mw	ew	−473	0−331−2×26−86
31.5	307		vs	mw	−443	0−331−26−86
29.1	337		vs	mw	−413	0−331−86
		60°C	50°C	40°C		
26.8	365	s	mw	w	−385	0−331−2×26
24.6	393	vs	ms	mw	−357	0−331−26
22.5	419	es	ms	mw	−331	0−331
20.2	448	s	m	w	−302	0−302
18.7	467	m	mw		−283	0−247−26−9
18.0	476	s	s	mw	−274	0−247−26
16.5	495	ms	m	vw	−255	0−247−9
15.8	503	vs	s	mw	−247	0−247
		50°C	40°C	30°C		
13.4	534	m	vw	ew	−216	0−86−5×26
11.9	553	m			−197	0−2×86−26
11.3	560	mw	vw	ew	−190	0−86−4×26
10.4	572	m			−178	
09.9	578	ms	vw	vw	−172	0−2×86
09.3	586	m	ew	ew	−164	0−86−3×26
		40°C	30°C	16.5°C		
08.3	598	ew			−152	0−86−2×26−16
07.2	612	w	w	vw	−138	0−86−2×26
06.4	622	vw			−128	0−86−26−16
05.8	630	vw			−120	0−86−26−9
05.2	638	m	mw	w	−112	0−86−26

Wave-length in A	Wave numbers in cm^{-1}	Intensity 40°C	30°C	16.5°C	Separation from 0,0 band	Assignments
04.4	648	vw	ew		−102	0−86−16
03.8	655	w	vw		−95	0−86−9
03.1	664	ms	m	mw	−86	0−86
02.5	672	mw	mw	w	−78	0−3×26
01.7	682	mw			−68	0−2×26−16
01.1	690	mw			−60	0−2×26−9
00.4	699	vs	s	m	−51	0−2×26
2799.2	714	s	vs		−36	0−26−9
98.4	724	es	es	s	−26	0−26
97.6	734	m	w		−16	0−16
97.1	741	s	vs	m	−9	0−9
96.4	750	es	es	vs	0	0−0
		60°C	50°C	40°C		
92.9	795	mw	ew		45	
92.2	805	w			55	
90.9	820	m	vw	ew	70	
88.6	850	ms	w	vw	100	
87.1	869	m			119	
86.9	872	m	vw	ew	122	
85.1	895	mw	ew	ew	145	
84.1	908	mw	ew		158	0+244−86
81.7	939	m	ew		189	0+244−2×26
79.5	967	ms	vw	ew	217	0+331−86−26; 0+244−26
77.4	994	vs	s	mw	244	0+331−86; 0+244
76.1	36 011			vw	261	
75.0	025	ms	mw		275	0+331−2×26?
73.7	042			ew	292	0+331−9
72.9	053	s	s	mw	303	0+331−26
70.7	081	es	vs	m	331	0+331
70.1	089	ms	mw	ew	339	0+528−190
67.9	118	m	w	vw	368	0+725−331−26
65.5	149	s	mw	vw	399	0+725−331
64.1	167			ew	417	0+528−86−26
63.6	174	ms	mw	ew	424	0+725−247−2×26
62.1	194	m	mw	ew	444	0+528−86
61.5	202	s	m	vw	452	0+725−247−26
59.3	230	s	m	w	480	0+725−247
57.6	253	vs	m	vw	503	0+528−26
57.1	259	ms	mw	ew	509	
55.7	278	vs	ms	mw	528	0+528
55.1	286	vs	m	w	536	
		50°C	40°C	30°C		
53.4	308	vw			555	
52.9	315	vw			565	
52.1	325	w	ew		575	
51.2	337	w	ew		587	0+725−86−2×26
50.1	352	mw	ew		602	
49.1	365	m	vw	ew	615	0+725−86−26
47.8	382		ew	ew	632	0+725−86−9
47.1	391	s	w	w	641	0+725−86
46.6	398	m	ew	ew	648	0+725−3×26
45.1	418		w	w	668	0+725−2×26−9?
44.6	424	vs	mw	w	674	0+725−2×26
43.3	442		w	mw	692	0+725−26−9
42.7	450	es	s	ms	700	0+725−26
41.9	460		mw		710	0+725−16
41.4	467		mw	mw	717	0+725−9
40.8	475	es	s	s	725	0+725
38.9	500	m	vw	vw	750	0+1051−247−2×26
36.8	528	s	w	w	778	0+1051−247−26
36.1	538		ew		788	0+1061−247−26
34.8	555	vs	mw	mw	805	0+1051−247
34.3	562	mw	vw	ew	812	0+1061−247
33.1	578	mw	vw	vw	828	
32.3	588	mw	vw	vw	838	0+1051−190−26
31.4	600	w	ew		850	
30.4	614	ms	vw	vw	864	0+1051−190
29.4	627	ms	vw	ew	877	0+1051−2×86
28.5	639	ms	vw	ew	889	0+1051−86−3×26; 0+1061−2×86
27.6	651	m	ew		901	0+1061−86−3×26
27.1	658	s	ew	ew	908	0+1051−86−2×26
		40°C	30°C	16.5°C		
25.8	676	ew	ew	ew	926	0+1061−86−2×26
24.8	689	w	w	w	939	0+1051−86−26
23.9	701	w	w	w	951	0+1061−86−26
22.8	716	mw	mw	mw	966	0+1051−86
22.1	725	mw	mw	mw	975	0+1061−86; 0+1051−3×26
21.3	736	vw	vw	vw	986	0+1061−3×26
20.4	748	m	mw	w	998	0+1051−2×26
19.5	761	m	m	w	1011	0+1061−2×26
18.5	774	s	s	m	1024	0+1051−26
17.6	786	s	ms	m	1036	0+1061−26
17.3	790			vw	1040	0+1051−9
16.5	801	es	vs	ms	1051	0+1051
15.8	811	vs	vs	m	1061	0+1061
		50°C	40°C	30°C		
14.6	827			vw	1077	
14.2	832	ms	w	w	1082	0+1089
13.7	839	ms	w	w	1089	

TABLE II—*Continued.*

Wavelength in A	Wave numbers in cm^{-1}	Intensity 50°C	40°C	30°C	Separation from 0,0 band	Assignments
12.1	861	w	vw		1111	0+1051+331−247−26
10.2	887	mw			1137	0+1051+331−247
09.4	898	w	vw		1148	0+1061+331−247
07.5	924	mw	vw	ew	1174	0+1051+331−190−26
06.0	944	mw	vw	ew	1194	0+1051+331−190
05.3	954		vw		1204	0+1061+331−190
04.4	966	m	vw	vw	1216	0+1461−247
03.7	975	mw	vw	vw	1225	0+528+725−26
03.1	984		ew	ew	1234	
01.9	37 000	ms	w	w	1250	0+528+725
01.3	008	m	w	w	1258	
2698.4	048	mw	ew		1298	0+1051+331−86
96.4	076	mw	ew	ew	1326	0+1051+331−2×26
94.4	103	s	vw	vw	1353	0+1051+331−26
93.4	117	ms	vw	vw	1367	0+1061+331−26
92.4	131	vs	mw	mw	1381	0+1051+331
91.6	142	ms	vw	ew	1392	0+1061+331
90.1	162		vw	vw	1412	0+1461−2×26
89.7	168	m	ew		1418	
89.4	172	mw			1422	
88.3	187	s	w	w	1437	0+1461−26
88.0	191	m	vw		1441	
87.5	198		vw		1448	0+2×725?
86.6	211	vs	m	mw	1461	0+1461
86.2	216	ms	mw	mw	1466	
83.6	252	mw	vw	vw	1502	0+528+1061−86
81.6	280	w	w	vw	1530	0+725+1051−247
81.1	287	vw	vw	vw	1537	0+528+1061−2×26
79.2	314	mw	mw	w	1564	0+528+1061−26
78.9	318			ew	1568	
77.4	339	m	mw	w	1589	0+528+1061
76.9	346		w	ew	1596	
75.3	368	vw	vw	vw	1618	0+725+1061−2×86
71.9	415	w	ew		1665	0+725+1051−86−26
71.1	427	m	ew	ew	1677	0+725+1061−86−26
70.1	441	ms	vw	ew	1691	0+725+1051−86
69.2	453	ms	vw	vw	1703	0+725+1061−86
68.2	467		ew	ew	1717	0+725+1061−3×26?
67.8	473		ew		1723	0+725+1051−2×26
66.9	486		ew	ew	1736	0+725+1061−2×26
65.9	500	s	mw	w	1750	0+725+1051−26
64.9	514	ms	mw	w	1764	0+725+1061−26
64.0	526	vs	m	m	1776	0+725+1051
63.2	538	s	mw	mw	1788	0+725+1061
61.7	559	w	vw	vw	1809	0+1089+725
61.2	566	vw	ew		1816	
60.5	576	ew	ew		1826	0+2×1051−247−26
58.5	604	m	vw		1854	
58.2	608		vw	vw	1858	0+2×1051−247
56.4	634	m	vw	vw	1884	0+528+1061+331−26
55.7	644	w		ew	1894	
54.4	662	mw			1912	0+528+1061+331
53.6	673	m	ew	vw	1923	
52.1	695	mw	ew		1945	0+1051+1061−86 −3×26
51.4	704	mw	ew	vw	1954	0+2×1051−86−2×26
49.9	726	ms	vw		1976	0+1051+1061−86 −2×26
49.3	735	ms	w	w	1985	0+2×1051−86−26
48.2	750	ms	vw		2000	0+1051+1061−86−26
47.3	763	s	w	w	2013	0+2×1051−86
46.2	780		vw	vw	2030	0+1051+1061−86
45.2	793			ew	2043	
45.0	796	vs	mw	w	2046	0+2×1051−2×26
43.8	813			w	2063	0+1051+1061−2×26
42.9	826	vs	m	m	2076	0+2×1051−26
42.1	837		m	m	2087	0+1051+1061−26
41.2	850	vs	ms	ms	2100	0+2×1051
40.3	863	vs	m	m	2113	0+1051+1061
39.3	878	s	mw	mw	2128	0+1089+1051
38.8	885	s	mw	mw	2135	
37.1	909	m	ew		2159	0+1461+725−26
36.7	915	w	ew	ew	2165	
35.4	934	s	mw	mw	2184	0+1461+725
34.8	942	m	w	w	2192	
33.1	967	mw	vw	ew	2217	0+1051+725+528−86
31.1	996	m	vw	vw	2246	0+1051+725+528 −2×26
30.4	38 006	vw			2256	0+1061+725+528 −2×26
29.4	020	m	w	w	2270	0+1051+725+528−26
28.2	038	w			2288	0+1061+725+528−26
26.6	061	m	w	vw	2311	0+1061+725+528
25.9	071	w	ew		2321	
24.3	094	w			2344	0+2×1051+331−86
23.8	101	vw	vw		2351	0+2×1051+331−3×26
22.0	127	vw	ew		2377	0+2×1051+331−2×26
20.8	145	w			2395	
20.3	152	mw	vw	ew	2402	
19.8	159	mw	vw		2409	0+2×1051+331−26
18.5	178	ms	mw	vw	2428	0+2×1051+331
17.7	190	mw	vw	ew	2440	0+1051+1061+331
16.8	203	w			2453	
15.7	219	mw	vw	vw	2469	0+1461+1061−2×26
14.7	234	w			2484	0+1461+1051−26
14.2	241	m			2491	
13.8	247	mw	w	vw	2497	0+1461+1061−26

Wavelength in A	Wave numbers in cm^{-1}	Intensity 60°C	50°C	40°C	Separation from 0,0 band	Assignments
12.9	260		w		2510	0+1461+1051
12.2	270	es	ms	w	2520	0+1461+1061
11.8	276	s	mw	vw	2526	
10.1	301	m	w	w	2551	0+725+2×1051−247−26
08.5	325	m	w	vw	2575	
08.3	328	m			2578	0+725+2×1051−247
06.8	350	m	w	vw	2600	
06.2	359	m	vw		2609	
04.0	391			vw	2641	0+528+1051+1061
03.6	397	m	vw	vw	2647	
01.5	428	m	vw	vw	2678	
00.3	446			vw	2696	
2599.5	457	ms	vw	vw	2707	0+725+1051+1061 −86−2×26
97.9	481	vs	w		2731	0+725+1051+1061 −86−26
96.5	502		w		2752	0+725+1051+1061−86
95.4	518	es	w	vw	2768	0+725+2×1051−2×26
93.5	546	es	m	w	2796	0+725+2×1051−26
92.3	564		w		2814	0+725+1051+1061−26
91.5	576	es	m	w	2826	0+725+2×1051
90.5	591	vs	mw	w	2841	0+725+1051+1061
89.9	600	ms	w		2850	0+1089+1051+725
89.4	607	ms	w	vw	2857	
89.0	613	m			2863	
87.8	631	m	w		2881	
87.3	639	mw		vw	2889	
86.0	658		w		2908	
85.5	666	ms	w	vw	2916	
84.7	678	m	vw		2928	
83.5	696	m	w	ew	2946	
82.9	705	m	vw		2955	
81.9	720	ms	w	ew	2970	
81.4	727			ew	2977	
80.5	741	s	mw		2991	0+3081−86
79.6	754	ms	vw	vw	3004	0+3081−3×26
78.8	766	m			3016	
77.8	781	ms	w	ew	3031	0+3081−2×26
76.1	807	s	w		3057	0+3081−26
75.7	813	m	vw	vw	3063	
74.5	831	vs	ms		3081	0+3081
73.9	840	s	w	w	3090	
72.9	855		vw	ew	3105	0+3×1051−2×26
71.8	872		vw		3122	
71.2	881	s	w	ew	3131	0+3×1051−26
70.2	896		m	vw	3146	0+1061+2×1051−26; 0+1089+2×1051−2×26
69.7	903	s	w		3153	0+3×1051
68.8	917		m		3167	0+1061+2×1051; 0+1089+2×1051−26
68.2	926	vs	m	vw	3176	
67.9	931		ew		3181	
67.0	944		vw	ew	3194	0+1089+2×1051
65.5	967	m			3217	0+1461+1061+725−26
64.6	981	m			3231	0+1461+1051+725
63.8	993	s	w	vw	3243	0+1461+1061+725
63.3	39 001	ms	vw	ew	3251	
62.1	019		vw		3269	0+725+528+2×1051
61.7	025	m	vw	ew	3275	−3×26
60.5	043	m		ew	3293	0+725+528+2×1051
59.9	052	m	vw		3302	−2×26
58.8	069	ms	w		3319	0+725+528+2×1051−26
58.3	077	m	ew	ew	3327	
56.0	112	w	vw	ew	3362	0+725+528+2×1051
54.4	136	w	vw	ew	3386	
50.8	192	mw			3442	
50.2	201	mw	ew		3451	
48.3	230	m	vw		3480	
46.8	253	m	vw	ew	3503	
45.0	281	m			3531	0+1461+2×1051−26
42.6	318	ms	w	ew	3568	0+1461+1061+1051
42.2	324		w		3574	
42.0	327	mw			3577	
40.6	349	mw			3599	
37.6	395		ew	ew	3645	
34.3	447	w			3697	
32.4	476	w	ew	ew	3726	
28.6	536	ms	vw		3786	
26.9	562	ms	w	ew	3812	
23.1	622	m			3872	0+725+3×1051
21.2	652	m	w	ew	3902	
18.6	693		ew		3943	
15.0	749	mw		ew	3999	
11.3	808	mw	ew	ew	4058	
09.2	841		ew		4091	
08.8	848	w	ew		4098	
07.7	865	mw	vw		4115	
05.8	895	m	w	ew	4145	
04.6	915	w			4165	
03.1	938	mw	ew	ew	4188	0+4×1051
00.9	974	mw	vw	ew	4224	0+3×1051+1061
2499.0	40 004	w			4254	0+1461+725+2 ×1051−26
96.9	038	m			4288	0+1461+725+2×1051
94.5	076	w	vw		4326	

TABLE II—*Continued.*

Wave-length in A	Wave numbers in cm^{-1}	Intensity 60°C	50°C	40°C	Separation from 0,0 band	Assignments
91.1	131	w			4381	
90.9	134	w			4384	
83.8	249	w			4499	
82.8	265	w			4515	
80.6	301	w			4551	
78.9	328	w			4578	0+1461+3×1051−26
77.0	359	w			4609	0+1461+3×1051
75.7	380	w			4630	0+1461+1061+2×1051
72.2	438	w			4688	
71.7	446	vw			4696	
70.6	464	w			4714	
66.9	524	vw			4774	
65.7	544	vw			4794	
64.2	569	w			4819	
62.6	595	w			4845	
61.2	618	w			4868	
60.8	625	vw			4875	
58.3	666	w			4916	0+4×1051+725
56.6	694	w			4944	0+3×1051+1061+725
55.1	719	vw			4969	
50.6	794	vw			5044	
50.0	804	vw			5054	
49.0	821	vw			5071	
47.3	849	vw			5099	
46.8	857	vw			5107	
46.1	869	vw			5119	
40.8	958	ew			5208	
39.8	975	ew			5225	
38.7	993	ew			5243	
35.2	41 052	ew			5302	
34.0	072	ew			5322	
32.3	101	ew			5351	
31.5	114	ew			5364	
30.3	135	ew			5385	
28.3	169	ew			5419	
26.5	199	ew			5449	

from the same vibration in the upper- and in the lower-electronic states of the molecule, which can be identified with the 1129-cm^{-1} Raman frequency assigned to a totally symmetrical vibration.[7] The progression with a 1089-cm^{-1} interval starts from all stronger bands. Considering the fact that the 992-cm^{-1} ground-state benzene frequency drops by 7 percent in the upper state,[12] the above correlation is justified by the resulting 4 percent drop of frequency and it is also confirmed that these frequencies are of a totally symmetrical ring vibration. Similarly another pair, 35 195=0−1037 and 37 190=0+958 cm^{-1} may arise from a totally symmetrical carbon vibration. The band at 37 718=0+1486 cm^{-1} may also be due to a totally symmetrical carbon vibration in the upper state, although the ground-state counterpart is not observed. Raman frequencies corresponding to these fundamentals are 1039 and 1575 cm^{-1}, respectively. The C−Cl stretching frequency in the ground state appears clearly in the band at 35 570 =0−662 cm^{-1}, the corresponding Raman value being 659 cm^{-1}. There is an ambiguity in deciding the corresponding upper-state frequency, since two bands 36 842 =0+610 and 36 872=0+640 cm^{-1} appear rather strongly and the progression with a 1089-cm^{-1} interval starts from either band. We tentatively take the stronger 36 842 cm^{-1} one and interpret the 610 cm^{-1} as the upper-state frequency. Another totally symmetrical vibration frequency is given by the band pair 36 427=0+195 and 36 006=0−226 cm^{-1}. This may be identified with the 240-cm^{-1} Raman frequency.

[12] Sponer, Nordheim, Sklar, and Teller, J. Chem. Phys. **7**, 207 (1939) and F. M. Garforth and C. K. Ingold, J. Chem. Soc. **1948**, 417.

A relatively weak band at 36 669=0+437 cm^{-1} may give the frequency of a nontotally symmetrical vibration forming the forbidden part of the spectrum. We refrain from interpreting the 35 729=0−503 cm^{-1} band as giving the corresponding ground-state frequency, as no Raman shift with this frequency is observed. We may alternatively choose the 469-cm^{-1} Raman frequency as the ground-state value, which is assigned to a β_1-type vibration,[7] although this frequency could not be observed on our plates, since the corresponding region is crowded with other broad and strong bands.

The bands at 35 796=0−436 and 36 539=0+307 cm^{-1} give the ground- and the excited-state frequencies of a fundamental vibration, corresponding to the Raman frequency of 428 cm^{-1} assigned to an α_2- or a β_2-type vibration.[7] The band at 35 905 cm^{-1}, relatively strong in this region, has a separation from the 0−0 band of 327 cm^{-1}, which may be identified with the 333-cm^{-1} Raman value assigned to a β_1-type vibration.[7] The corresponding upper-state frequency could not be found. The 1089-cm^{-1} progression also starts from this band.

On the red side of each of the aforementioned stronger bands, satellite bands appear with frequency separations of 24 and 59 cm^{-1}. These separations are certainly the result of the superposition of $v-v$ transitions of nontotally symmetrical vibrations, although their detailed interpretations cannot be given.

One thing should be mentioned about the structure of the *o*-dichlorobenzene molecule. In this molecule two chlorine atoms lie so close to each other that a repulsive force between them is expected. From our vibrational analysis of the spectrum it is apparent that the molecule has the same symmetry in the two electronic states. In the A_1-A_1 electronic transition of the C_{2v}-model, transitions involving an α_2-type vibration are forbidden. This type of vibration goes over into an α type in the C_2-model, and the transition involving it is allowed in the $A-A$ electronic transition. The only vibration assigned to the α_2 type in the C_{2v}-model is of the 153-cm^{-1} frequency.[7] Therefore, if a band with this fundamental frequency appears in the spectrum, the C_{2v}-model for this molecule should be excluded. Unfortunately it is impossible to ascertain the band with the 153-cm^{-1} frequency, since many strong bands cluster in the corresponding region. The 36 324-cm^{-1} band on the violet side of the 0−0 band gives the frequency separation of 92 cm^{-1}, which we cannot interpret appropriately. However, if it were the excited-state frequency corresponding to the 153-cm^{-1} ground-state value, we could give support to Hassel's C_2-model. Moreover, it may be noted that the frequency difference 153–92=61 cm^{-1} would explain the 59-cm^{-1} shifts of satellites from the main bands.

p-Dichlorobenzene

The 35 750-cm^{-1} band is taken as the 0−0 band. The pair of bands at 34 648=0−1102 and 36 801=0+1051

cm^{-1} gives fundamental frequencies in the ground and in the excited state, respectively, to which a polarized Raman line with 1108-cm^{-1} shift corresponds. The 1051-cm^{-1} frequency appears in progressions starting from all stronger bands. The resulting frequency drop of 5 percent in the excited state shows that this frequency is of a totally symmetrical ring vibration. In the Raman spectrum, strong polarized lines with shifts of 330, 750, and 1575 cm^{-1} are reported. Correspondingly, in uv absorption, bands shifted from the 0—0 band on the red side by 331, 755, and 1589 cm^{-1} are observed. While the 725 and 1461/66 cm^{-1} excited-state frequencies undoubtedly correspond to the 755 and 1589 cm^{-1} ground-state frequencies, respectively, it is difficult to interpret the observed 331-cm^{-1} excited-state frequency as corresponding to 331 cm^{-1} of the ground state, because then no frequency drop occurs. From its magnitude this vibration appears to be a benzene ring deformation vibration.[7] However, as the inplane deformation-force constant of benzene is known to decrease considerably in the excited state causing the frequency to drop by 10 percent or more,[13] we had better choose the 35 994=0+244-cm^{-1} band as giving the upper-state frequency of this vibration and interpret the 331-cm^{-1} separation on the violet side of the 0—0 band as the two-quanta combination of some unknown vibration whose single excitation is forbidden. The 34 586=0—1164-cm^{-1} band may give the ground-state fundamental which is correlated to the 1061-cm^{-1} upper-state frequency, to which a polarized-weak-Raman line 1172 cm^{-1} assigned to a CH inplane deformation vibration corresponds.

A depolarized-Raman line 630 cm^{-1} is reported. In uv absorption a relatively strong band is observed at 35 119 cm^{-1} separated by 631 cm^{-1} from the 0—0 band. The corresponding upper-state frequency is 528/36 cm^{-1}. This vibration may be of a β_{1g} type causing the appearance of the forbidden part of the spectrum. The 606-cm^{-1} ϵ_g^+-benzene vibration splits in this molecule into an α_g and a β_{1g} component by the removal of degeneracy caused by the reduction of symmetry from D_{6h} to V_h. Then the 631-cm^{-1} ground-state frequency may be the β_{1g} part of this splitting, and the α_g part may be the 331-cm^{-1} ground-state frequency previously described. It is interesting that the bands containing 528/36-cm^{-1} and 1461/66-cm^{-1} frequencies appear in doublets with the lower-frequency heads being stronger. We have used the stronger heads in our analysis.

The band 36 839=0+1089 cm^{-1} is also double as observed at reservoir temperatures higher than 16.5°C with a satellite on the red side at 7 cm^{-1} distance. Similar doublets are found at 37 559/66 and 37 878/85 cm^{-1}, the separations from the 0—0 band being 1809/16 and 2128/35 cm^{-1}, respectively. These shifts are interpreted as 1082/89+725=1807/14 and 1082/89+1051=2133/40 cm^{-1}, respectively, although 1082/89 cm^{-1} remains unassigned. If it were a fundamental, it must be a CH inplane-deformation vibration. Another possibility is to interpret it as the first overtone of a vibration whose single excitation is forbidden.

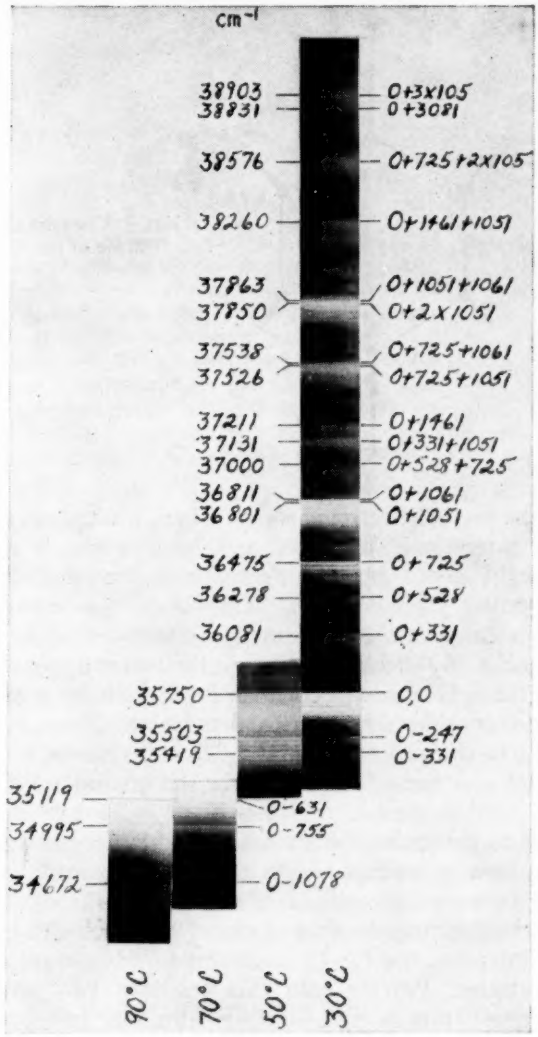

FIG. 2. Absorption bands of *p*-dichlorobenzene vapor.

Another doublet is observed at 38 831/40=0+3081/90 cm^{-1} which may give the excited-state frequency corresponding to the ground-state frequency 3072 cm^{-1} given by the Raman effect. This can be assigned to a CH-stretching vibration frequency which is considered to increase in magnitude in the excited state as in the case of the benzene molecule.[12]

Satellites accompanying prominent bands involve mostly the shifts of 26 and 86 cm^{-1} or their combinations. Other satellites with shifts of 9 or 16 cm^{-1} are also found to accompany sharper and stronger bands.

STRUCTURE OF THE *p*-DICHLOROBENZENE MOLECULE IN THE B_{3u} EXCITED STATE

As discussed above, the symmetry of the *p*-dichlorobenzene molecule is the same both in the ground- and

[13] Garforth, Ingold, and Poole, J. Chem. Soc. **1948**, 508.

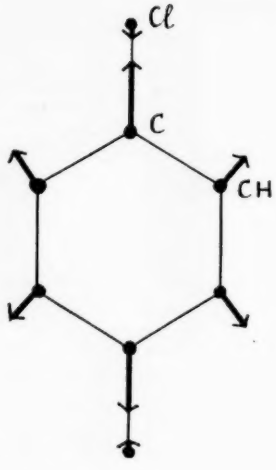

FIG. 3. Vibrational mode of ν_2.

in the excited-electronic states. Then, what changes in the interatomic distances and bond angles will be brought about by the electronic excitation in this molecule?

We have calculated four α_g skeleton-vibration frequencies of *p*-dichlorobenzene in the two states, assuming the simple valence-force field, in which the benzene ring is considered as a six-particle system. The α_{1g} (992 cm^{-1} in the ground state and 923 cm^{-1} in the excited state) and the ϵ_g^+-(606 cm^{-1} in the ground state and 521 cm^{-1} in the excited state) benzene frequencies are used to determine the stretching and inplane-deformation-force constants of the ring. These constants are carried over into *p*-dichlorobenzene and the equation for determining the four α_g skeleton frequencies is set up including the C—Cl stretching-force constant as a parameter. Putting into this equation two sets of observed totally symmetrical vibration frequencies, ν_2 (1102 cm^{-1} in the ground state and 1051 cm^{-1} in the excited state) and ν_3 (755 cm^{-1} in the ground state and 725 cm^{-1} in the excited state), the C—Cl stretching force constant is obtained as given in Table III. While calculated values in the two columns agree fairly well for the ground state, the agreement is very poor for the excited state, but we may say at least that the C—Cl stretching-force constant increases in the upper state. The disagreement for the excited state is not due merely to the assumption of the simple valence-force field, since the values for the ground state agree fairly well. In the valence-bond language, the resonance contributions from parts of the molecule other than the benzene ring become much more important in the excited state than in the ground state. From this argument we see that the carrying over of the benzene force constants into *p*-dichlorobenzene is not a good approximation for the excited state, though it is fair for the ground state.

Badger's relation[14] with these values of the force constant would give the change of the C—Cl distance in this molecule, but a quantitative conclusion cannot be reached owing to the unreliability of the change of the force constant. We can only say that the C—Cl distance decreases by the electronic excitation. With regard to the change of the C—C bond length by the electronic excitation, it is assumed to be the same as in the case of benzene. This amounts to the assumption that the benzene force constant can be carried over to the *p*-dichlorobenzene molecule, since the bond length is uniquely determined by the bond stretching force constant for a particular pair of atoms.[14,15]

TABLE III. Calculated values of C—Cl stretching-force constant (in 10^5 dyne/cm).

	from ν_2	from ν_3
Ground state	2.76	2.90
Excited state	3.00	4.26

Let us now consider the possibility of determining the molecular structure of *p*-dichlorobenzene in the excited state by Craig's method.[16] The totally symmetrical deformation of the molecule, assuming single mass points for the CH-groups, may be expressed by four q's (q is the difference of normal-coordinate origins in the ground- and in the excited-electronic states) corresponding to four totally symmetrical skeleton vibrations. According to Craig's formula[17] the intensity distribution does not depend upon the sign of q,[18] so that the number of possible models for the excited molecule consistent with the experimental intensity distribution is $2^4=16$. But it makes no difference as to which of these 16 models should be used. Therefore Craig's method is not helpful for determining the structure of this molecule in the excited state. However, the fact that the only progression-forming frequency is 1051 cm^{-1} suggests that the difference between the molecular structures in the two electronic states is mainly determined by the difference of the normal-coordinate origins of this vibration. The calculated mode of this vibration is shown in Fig. 3. It is interesting to see in this figure that when the benzene ring expands (elongations of C—C bonds are not all equal) the C—Cl bonds contract. Therefore, if the C—C bonds stretch by the electronic excitation as in the case of the benzene molecule, the C—Cl bonds must contract in the upper state. This is in agreement with the conclusion reached from the change of the force constant.

The authors express their hearty thanks to Professor S. Imanishi and Dr. Y. Kanda for reading the manuscript and for many valuable suggestions and discussions.

[14] R. M. Badger, J. Chem. Phys. **2**, 128 (1934) and **3**, 710 (1935).

[15] C. H. Douglas Clark, Phil. Mag. **18**, 459 (1934) and H. S. Allen and A. K. Longair, Nature **135**, 764 (1935).

[16] D. P. Craig, J. Chem. Soc. **1950**, 2146.

[17] See Eq. (6) in reference 16.

[18] It is not clearly shown in Craig's paper that the change of q should be considered as the ring expansion.

THE JOURNAL OF CHEMICAL PHYSICS VOLUME 23, NUMBER 5 MAY, 1955

Nuclear Magnetic Resonance in Concentrated Aqueous Electrolytes

JAMES N. SHOOLERY, *Varian Associates, Palo Alto, California*

AND

BERNI J. ALDER, *Department of Chemistry and Chemical Engineering, University of California, Berkeley, California*

(Received August 9, 1954)

The proton magnetic resonance of water has been examined in the presence of various concentrations of different diamagnetic salts. The observed shifts of the resonance frequency relative to that of pure water are interpreted in terms of the breakdown of the hydrogen-bonded structure of water and the ability of the ions to polarize the water molecules. The concentration dependence of the shifts for the multivalent electrolytes indicates cation-anion interactions at higher concentrations. The quite narrow single line observed for all but the Al^{+++}, Be^{++}, and the very concentrated $ZnCl_2$ solutions shows that in most cases the proton exchanges faster than 10^4 times per second. The magnetic field dependence of the line width in the $AlCl_3$ solution indicates that a rate of exchange of the proton of about 10^2 times per second is responsible for the broadening, while in the $ZnCl_2$ and $BeCl_2$ solutions the high viscosity appears mainly to be responsible for the increased line width. The fluorine magnetic resonance studied at several concentrations in KF solutions provides further information about the solvent-ion interaction.

INTRODUCTION

IT has by now been well established[1,2] that the nuclear magnetic resonance frequencies depend on the electronic environment of the nucleus due to the magnetic shielding by the electron cloud. The distribution of electrons around a given element changes from one compound to another depending upon the nature of the bonding to the rest of the molecule, and this change in electron density varies the effective magnetic field at the nucleus. Since the nuclear-precession frequencies are proportional to the effective field at the nucleus, shifts in the resonances are found.

The electron distribution around a given nucleus can, however, also be changed by external forces which perturb the molecule. These forces must be reasonably strong before their effect can be detected by present methods as a shift in the resonance frequency. Examples of such relatively strong perturbations are the dipole-dipole interactions which manifest themselves in the formation of hydrogen bonds, and the large electrostatic fields in the neighborhood of ions which polarize the surrounding dipoles. The former case has previously been discussed by several investigators[3,4] and the present paper is concerned with the effect of various ions on the magnetic shielding of protons in water molecules.

The ions in aqueous-electrolyte solutions not only polarize the surrounding medium but also, in the process of being solvated, break down the hydrogen-bonded network of water molecules. The shift which is observed should therefore be the result of the combined effect of these two factors. However, the polarization effect by its strong dependence on the size and charge of the ion ought to be differentiable from the hydrogen-bond-breaking effect, which probably depends to a small degree only on the size of the ion.

The attraction between the solvent and the electrolyte for some ions is strong enough so that a complex can be identified in solution. A well-known example is that of the Cr^{+++} ion where it has been possible to measure the exchange rate of the complexed water molecules in the solution. Since nuclear magnetic-resonance experiments also allow life times of molecules to be determined for times which are shorter than has been accessible by previous techniques, less stable complexes should be identifiable.

EXPERIMENTAL

The proton magnetic-resonance shifts relative to pure water were measured for a number of salt solutions at a frequency of 30 megacycles in a field of approximately 7050 gauss. The instrument used was a Varian Associates V-4300 high-resolution spectrometer in conjunction with a 12-in. electromagnet system. With this instrument, it was possible to obtain line widths of only a few cycles except in a few cases where the "natural" line width was greater. Consequently, it was possible to measure the shift relative to pure water for most of the samples to within one cycle, as evidenced by the statistics. Possible systematic errors which might have influenced the results are random-field fluctuations and slow-field drift, both of which were eliminated by the procedure described in the following.

Both of the aforementioned systematic errors can be eliminated by comparing the resonances for the electrolyte solutions and pure water, (1) at the same instant and (2) in essentially the same magnetic field. The second condition can be met by separating the sample and the reference substance by a thin-glass membrane across the 5-mm pyrex-glass tubing used as a cell in the

[1] N. F. Ramsey, Phys. Rev. **78**, 699 (1950); **76**, 243 (1952).
[2] L. H. Meyer and H. S. Gutowsky, J. Phys. Chem. **57**, 481 (1953).
[3] J. T. Arnold and M. E. Packard, J. Chem. Phys. **19**, 1608 (1951).
[4] R. A. Ogg, J. Chem. Phys. **22**, 560 (1954).

receiver coil of the sensing head, or "probe," of the spectrometer. Two resonances are observed which are separated in time on the oscilloscope trace as the magnetic field is swept slowly through the region of resonance. The problem is to observe a response from both samples at the same instant. This is done by introducing an audio-frequency oscillating component to the sweep field at exactly the frequency separation of the two resonances. The oscillating field behaves as if it were a frequency modulation of the Larmor-precession frequency of the nuclei, resulting in a central resonance and a symmetrical group of evenly spaced "sideband" resonances. When the carefully calibrated oscillator is adjusted to the exact frequency separation of the two resonances, the sideband of each resonance superimposes upon the fundamental of the other and a pair of lines of maximum height and sharpness results. Using this criterion one can reset the oscillator within a few tenths of a cycle when the resonances are narrow.

The glass in or near the membrane can distort the magnetic-flux pattern which, in the case of an imperfectly-symmetrical sample cell, results in a dependence of the observed shift on the orientation of the cell. This difficulty was resolved by rotating the cell in a Teflon bearing at a speed great enough to average out the inhomogeneity due to the cell asymmetry.[5]

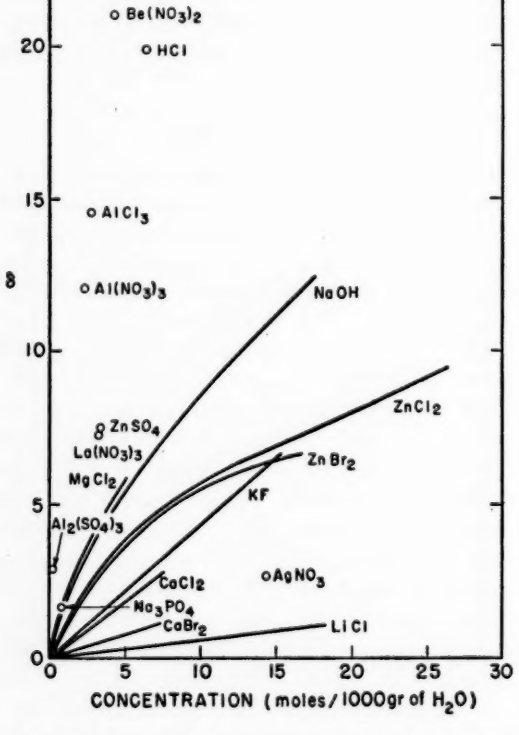

FIG. 1. Positive proton shifts in aqueous electrolyte solutions as a function of concentration.

[5] F. Bloch, Phys. Rev. 94, 496 (1954).

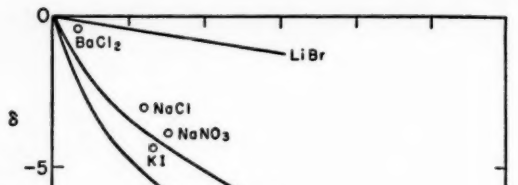

FIG. 2. Negative proton shifts in aqueous electrolyte solutions as a function of concentration.

A speed of several hundred rpm was adequate and could be attained with a small air turbine.

Two samples located on opposite sides of a partition cannot be regarded as being in exactly the same field if gradients exist in the magnetic field. To minimize this effect, a slightly more complex procedure was followed. A third substance, acetone, was chosen as a reference compound and was sealed in the lower half of the cell. Measurements of the shift of the proton resonance relative to this standard were made for pure water. The cell was then rinsed and filled with the electrolyte solution being studied and the shift measured again. Subtracting the two measured values gave the shift of the electrolyte relative to pure water, and any effect due to the difference in field on opposite sides of the membrane was cancelled out.

Line widths were measured at both 30 megacycles and 3 megacycles for several of the solutions. In each case, the measurements were made by recording with a Sanborn fast-writing recorder the envelope of the absorption lines as the field was swept slowly through them. The sweep rate was calibrated by introducing a 60-cycle modulation frequency and recording the carrier and first sideband resonances of a sample of pure water. The separation of consecutive peaks on the trace was then exactly 60 cycles, and the sweep rate in milligauss per inch on the chart could be determined.

The salts used were of commercial cp grade. They were dissolved in water and their concentrations were determined by standard microchemical analysis to an accuracy of 0.1 mole per liter.

RESULTS

The shifts δ of the proton resonances for the various electrolyte solutions are presented in Figs. 1 and 2, and are also recorded in Table I, where δ is defined here as:

$$\delta = 10^7 \times (H_{H_2O} - H_{sample})/H_{H_2O}.$$

The shifts reported correspond to the displacement of the observed proton peak from that of pure water at

room temperature. Both positive and negative shifts are found.

In all cases a single line is observed near 30 megacycles with a field of about 7050 gauss. For all solutions except the 27 M $ZnCl_2$, the Al^{+++}, and the Be^{++} solutions, the line widths were not noticeably broader than the one for pure water. In Table II the line widths of these three exceptional solutions are recorded at 30 and 3 megacycles and included also are their viscosities.

The only ion whose nuclear magnetic resonance was studied was fluoride ion. The δ value of the fluoride ion in a 12 MKF was found to be -16.7 relative to a 4-MFK solution.

DISCUSSION

Effects Contributing to Proton Shifts

An instantaneous picture of water in which a salt has been dissolved would yield at least three types of protons experiencing different interactions. There would be protons in the neighborhood of positive ions, protons near negative ions, and protons relatively far away from any ion and therefore nearly in the same state as in pure water. A water molecule near a positive ion would have, on the average, the oxygen pointed toward the ion. Considering the water molecule as a polarizable charge distribution, the electrons would be shifted to make it less probable to find them on the hydrogen atoms and more probable to find them on the oxygen. On the other hand, the proton would be attracted to an anion and the electrons would be repelled so that again they would more likely be found on the oxygen atom. Thus, in the neighborhood of both types of ions the water molecule is polarized such that, on the average, fewer electrons will be found on the protons and, therefore, less shielding of the nucleus from an external magnetic field is expected if this mechanism is valid.

TABLE I. Shift of proton resonance in water with addition of electrolyte.

Compound	Conc (moles/1)	Conc (moles/1000 g H_2O)	δ[a]
$NaClO_4$	4.0	4.9	−4.7
$NaClO_4$	8.0	13.2	−7.7
KI	5.0	6.6	−4.3
NaI	4.1	4.8	−3.3
NaI	8.0	11.9	−5.7
$NaNO_3$	6.1	7.6	−3.8
NaCl	5.3	6.0	−3.0
$BaCl_2$	1.5	1.6	−0.4
LiBr	8.0	10.2	−0.9
LiBr	10.0	13.8	−1.1
LiCl	4.0	4.4	0.2
LiCl	12.0	16.4	1.0
$CaBr_2$	4.0	4.9	0.8
$CaBr_2$	5.0	6.5	1.0
$AgNO_3$	9.4	14.3	2.7
$CaCl_2$	2.2	2.3	0.9
$CaCl_2$	5.0	6.0	2.3
KF	4.0	4.2	2.0
KF	8.0	9.2	3.9
KF	12.0	15.6	6.6
$ZnBr_2$	3.6	4.3	3.4
$ZnBr_2$	8.2	14.4	6.4
$ZnCl_2$	5.0	6.1	4.3
$ZnCl_2$	9.6	15.6	7.0
$ZnCl_2$	12.5	26.5	9.4
Na_3PO_4	0.7	0.8	1.7
NaOH	6.0	6.1	6.4
NaOH	15.9	17.3	12.3
$MgCl_2$	3.0	3.3	4.4
$MgCl_2$	4.0	4.5	5.6
$La(NO_3)_3$	1.3	1.4	2.2
$La(NO_3)_3$	2.8	3.3	7.3
$ZnSO_4$	3.3	3.4	7.5
HCl	5.6	6.3	19.9
HCl	10.2	13.0	36.5
$Al_2(SO_4)_3$	0.2	0.2	2.9
$Al(NO_3)_3$	2.1	2.4	12.1
$AlCl_3$	2.5	2.8	14.1
$Be(NO_3)_2$	3.5	4.3	21.0
$BeCl_2$	3.8	4.7	22.1
$HgCl_2$	concentrated		0

[a] The δ's reported are the average of at least 3 different measurements.

TABLE II. Half-width of absorption lines at room temperature at two different frequencies; also, the viscosity of the solutions.

Solution	3 mc	30 mc	Viscosity
pure H_2O	12 cycles	12 cycles	1.0 cp
2.5 M $AlCl_3$	15 cycles	27 cycles	8.3 cp
12.5 M $ZnCl_2$	24 cycles	25 cycles	1100 cp
3.8 M $BeCl_2$	35 cycles	37 cycles	240 cp

In addition to polarizing the water molecule, the ions also break down the hydrogen-bonded structure of water. If the picture in the previous paragraph is adopted, an approximately tetrahedrally-coordinated water molecule has at least one hydrogen bond broken when it comes into contact with an ion. Since each ion is surrounded by approximately six water molecules, a considerable number of hydrogen bonds are ruptured in a one-molar salt solution, and this effect on the electron distribution must be taken into account. The effect might be estimated from an experiment in which the shift in the proton resonance of steam relative to that of water is measured. The result of breaking hydrogen bonds is to shield the proton more thoroughly from the external magnetic field. This effect is opposite to the polarization induced by the ions and can qualitatively be explained as follows: In separating two water molecules the mutually induced dipoles are removed. Thus, the electron density in the neighborhood of the proton is increased. In addition, a change in the asymmetry of the electron distribution around the proton nucleus could also contribute to the greater shielding. However, effects of the latter type were not found necessary to introduce to explain the results of this paper.

Application to the Experimental Results

The uni-univalent electrolytes consisting of relatively large ions mainly break down the hydrogen-bonded network of water and their polarization of the water molecules is less important as indicated by their negative shifts. On the other hand, the multivalent ions predominantly polarize the water and hence show positive shifts. It can further be observed that the smaller

the ion and the higher its charge, the larger the polarization or positive shift becomes. Thus, NaI has a more positive shift than KI and similarly NaCl with respect to NaI. The introduction of the smaller Li^+ and especially of F^- in the alkali-halide series causes a very significant increase in the polarization. The resonances from the doubly-charged alkali-earth ions Be^{++}, Mg^{++}, Ca^{++}, and Ba^{++} are in the order one would expect from their relative diameters. The triply valent, small Al^{+++} ion gives a larger positive shift than the bigger La^{+++} ion. All of this suggests that it is possible to assign to each ion a value representing its contribution to the shift in the proton resonance.

The HCl and NaOH solutions are special cases since these hydrogen containing ions can exchange with the protons of the water. The acid was studied to determine that hydrolysis of the ions has a negligible effect on any of the measurements made. The acid and base results were also compared with previous values.[6] The shifts for HCl were found to be slightly larger while the NaOH data agreed within experimental error. It is interesting to note that for the alkali-metal bases the order of the shift is reversed from the ones found for their salts just as in the case of the activity coefficients.

$HgCl_2$ was studied to determine that a weak salt would not show a measurable shift.

Concentration Dependence

The concentration dependence of the shift of the univalent electrolytes indicates that as the concentration of the electrolyte is increased a smaller number of hydrogen bonds will be ruptured per ion added. This phenomenon should begin to occur when the concentration of salt is so high that there are, on the average, only 6 to 8 water molecules per ion. A further addition of salt would require that some water already partially freed from its hydrogen-bonded neighbors and attached to ions would solvate the newly added salt. This sharing of water molecules between ions should start for uni-univalent electrolytes somewhere around 4 M and up to that point the shift should be linear with concentration. It is unfortunate that due to the small magnitude of the shifts, they could not be determined with sufficient accuracy in that concentration region. However, both for NaI and $NaClO_4$ above 5 M, the concentration dependence of the shift becomes markedly smaller.

The concentration dependence of the shift due to the polarization part alone can also be considered to be linear up to about 4 M for uni-univalent electrolytes and up to 1 M for all the salts studied. In order to explain a linear concentration dependence the polarization effect cannot extend appreciably beyond the first layer of water molecules around an ion. If there were a large overlapping of the polarizing effect of ions, the shift would be nonlinear at low concentrations. Again the experimental evidence for the behavior of the shift at low concentrations is difficult to obtain. However, in the KF solutions the shift is linear within experimental error up to the highest concentration studied and in the $CaCl_2$ and $CaBr_2$ solutions the concentration dependence of the proton shift is almost linear up to quite high concentrations. There is a small downward curvature of the shift *versus* concentration which could be explained by polarization of water molecules beyond the first layer or by the formation of ion pairs, the latter probably having the more pronounced effect. In the $MgCl_2$, $ZnBr_2$, and $ZnCl_2$ solutions, the effect is considerably magnified. In the 27-M solutions of the latter, where there are almost as many ions as there are water molecules, cation-anion contacts contribute to the saturation effect of the shift with concentration. Equilibrium constants for the formation of ion pairs have been determined for the zinc halides.[7] When the probability of ion-ion collisions becomes quite high such ion pairs, or higher clusters of ions, can be considered as dipoles and higher multipoles which do not have as strong a perturbing effect on the electron cloud of a water molecule as the separate ions would. The polarization per water molecule must always increase with concentration but less rapidly so in these cases at higher concentrations.

Superimposed on the shift due to the polarization is the shift due to hydrogen-bond breaking which changes oppositely with concentration. Thus, for example, the linear dependence obtained for KF does suggest the possibility of some small amount of ion-pair formation at the highest concentrations. The LiCl solution curves slightly upward suggesting that there is less ion-pair formation. Other factors which could cause a decreasing shift with concentration are (1) the nonlinearity of the polarizability of a water molecule with the increased electric field it experiences as the concentration increases and (2) the increase in the bulk diamagnetic susceptability of the solutions with concentration.

It is difficult to disentangle all these effects; however, it seems reasonable to conclude that ion-cluster formation accounts, at least partially, for the concentration dependence of the shift. Precise measurements of the index of refraction of aqueous electrolytes[8] also give an indication of ion pair formation at higher concentrations in those cases where it is also expected from nuclear magnetic resonance experiments. The constancy of the polarizability of an ion with concentration can be used as a criterion for normal behavior where an ion is mainly surrounded by water molecules. When ion-ion collision frequencies become high, deviations of the effective polarizability of an ion from a constant value must be expected due to the largely different perturbing forces. Of those solutions which show a positive shift, only the KF and $CaCl_2$ solutions can be compared, and both show deviation from a constant polarizability,

[6] H. S. Gutowsky and A. Saika, J. Chem. Phys. **21**, 1688 (1953).

[7] Sillen and Liljequist, Svensk Kem. Tidskr **56**, 85 (1944).

[8] C. J. F. Böttcher, Rec. Trav. Chem. **39**, 65 (1940).

while all the other solutions have a comparatively constant value. For $CaCl_2$, Böttcher's calculated polarizability shows the largest deviation from constancy, the deviations beginning appreciably at about 4 M. This is an indication that ion pair formation has to be taken into consideration in the theory. For the KF solutions the deviations are smaller and the apparent experimental uncertainties large enough so that it is not meaningful to draw such conclusions.

CALCULATIONS

From the discussion of the preceding section, it appears possible to assign to each ion a molar shift, δ^+ or δ^-, which in the proper combinations for a given salt reproduce the data reported in Table I. Since the behavior in concentrated solution, as discussed, is not characteristic of each ion, values of δ^+ or δ^- can be computed only for interpolated shifts at 1-M concentration. A line of appropriate curvature has been drawn between 0.0 M and the points taken at higher concentrations for each salt. The values for each ion are given in Table III. In order to establish a reference shift with which to compare all other molar shifts, the large, singly-charged ClO_4^- ion was arbitrarily assumed to have a shift per mole of -0.85. As will be seen later, this value for that ion makes the shifts due to the polarization effect alone a small positive quantity.

In dilute solution, the shift of the proton resonance in any of the electrolyte solutions in Table I is given by the following expression:

$$\delta = m(n^+\delta^+ + n^-\delta^-),$$

where δ^+ and δ^- are the relative molar shifts by the positively and negatively charged ions, respectively, and n^+ and n^- are the number of moles of cations and anions formed in the dissociation of one mole of salt. The concentration in moles per 1000 grams of water is m. With this expression it is possible to reproduce the shifts to within the uncertainties of the extrapolation and experimental errors, that is, to within about 0.1δ unit. It can be observed that charge and size have a pronounced effect on the shift. It seems unprofitable at the moment to make any detailed correlation of the shift with charge and size of the ion due to the complicated nature of the phenomena and the general uncertainties involved in deriving these values. The correlation in any case is not simple, since a knowledge of the effective electric field in the neighborhood of a proton must be evaluated, which is dependent not only on the field of the ion itself but also on the field of the surrounding dipoles. Furthermore, the effect of this field on the shift requires a perturbation calculation with the wave function of the water molecules. However, it can be seen that the negative ions have a larger effect on the proton resonance than the positive ions regardless of how the arbitrary scale is set up. The Cl^- and Na^+ ions, both of which have about the same ionic entropies and the same effective radius in solution,[9] are a good example. The Cl^- has the larger ion radius, and yet its shift is considerably larger. The explanation lies undoubtedly in the fact that the proton is much nearer to the negative ion and is therefore directly influenced by it, while near a positive ion the field the proton experiences is screened by the oxygens.

TABLE III. Relative molar shifts of the proton resonance for each ion.

Ion		Ion		Ion	
I^-	−0.35	K^+	−0.71	Ba^{++}	−0.23
Br^-	−0.21	Na^+	−0.57	Ca^{++}	0.45
Cl^-	−0.01	Li^+	0.09	Mg^{++}	2.08
F^-	1.20			Be^{++}	4.89
		Ag^+	0.28		
ClO_4^-	−0.85[a]			Zn^{++}	1.24
NO_3^-	−0.09				
$SO_4^=$	1.17			La^{+++}	2.39
$PO_4^{\equiv}$	3.83			Al^{+++}	5.19

[a] Assumed to establish relative scale.

The values given in Table III reflect the combined effect of the hydrogen-bond-breaking action of an ion and the polarization contribution. The relative magnitude of these two factors can be roughly estimated if the number of hydrogen bonds broken per ion is assumed. The shift per broken bond might be obtained from measurements for steam. A shift of approximately $\delta = 21$ has been found[10] which corresponds roughly to a shift of $0.4\ \delta$ for a mole of bonds ruptured in 55.5 moles of water. It has been assumed in this calculation that approximately 55 moles of hydrogen bonds exist per 1000 grams of liquid water[11] and that all of them have been broken in the process of vaporization. On the basis that 5 to 6 bonds are broken by each ion, a mole of ions in a liter of solution will give a negative shift of about 2.0 in δ. Thus, by adding 2.0 to each value in Table III, it is possible to assign a value due to the polarization alone for each ion.

FLUORINE RESONANCE

Further information about the interaction of the solvent and ions could be gathered if the nuclear magnetic resonances of the anions and cations and also the oxygen were studied. It can be predicted from a purely electrostatic point of view, that the positive ions would be less shielded at higher concentrations while the negative ions would be more shielded. This effect can only be observed at rather high concentrations when most of the water molecules have been tied up by the ions. A further introduction of ions would then take already bound water molecules away from the ions. Thus, a positive ion would no longer have as many oxygen atoms surrounding it. Those oxygens which are

[9] L. Pauling, *Nature of the Chemical Bond* (Cornell University Press, Ithaca, New York, 1948), p. 346.
[10] Unpublished results at Varian Associates.
[11] Cross, Burnham, and Leighton, J. A. C. S. **59, 1134 (1937).**

the negative ends of the dipoles of water molecules have the effect of repelling the electrons of the positive ion towards its center, thus in effect increasing the shielding of the nucleus. When the number of bound water molecules per positive ion are decreased, the effect is then to reduce the shielding, while for anions the exact opposite occurs. It should be emphasized that when further interactions between any of the species in the solution can occur such as covalent complex formation or ion pair formation these conclusions are invalidated.

For positive ions the qualitative picture is confirmed by results obtained by Gutowsky and McGarvey[12] for Cs^+. A shift corresponding approximately to a δ of 300 has been found for a saturated solution of CsCl relative to a half-saturated solution, where the more concentrated solution was less shielded.

For the negative fluoride ions the predicted qualitative trend was found also. The resonance of the 8-M and 12-M KF solutions was measured relative to the 4-M KF solution. The shielding was found to be greater in the more concentrated solutions and the resonance did not vary linearly with concentration. The 8-M solution had a very small negative shift while the 12-M solution had a shift of -16.7 in δ relative to the 4-M solution.

Fluoride ion interacts strongly with the protons of the water molecules. The relatively high value of the molar shift assigned to it in Table III indicates this. Further evidence is found in the measurements of the activity coefficients, where a high value of the effective radius must be assigned to this ion to account for the data. If this is not done, a reversal of the usual cationic effect is observed from that of other alkali halides.[13] Furthermore, fluoride ion does not have the largest shielding of any fluorine compound as one might have expected.[14] As was pointed out, the effect of hydration is to spread out the electron cloud toward the surrounding protons.

This strong interaction between water and fluoride ion makes it reasonable that ion-pair formation is energetically not favorable, as was also indicated by the linear concentration dependence of the proton shift. The concentration dependence of the fluorine resonance shift confirms this also, since ion-pair formation would denude the fluoride ion of electrons through the attraction of the positive ion, which would decrease the shielding in concentrated solutions opposite to what was found. However, to prove the last statement, one would have to demonstrate that the potassium ion polarizes the fluoride ion more than the dipoles of water which it displaces.

[12] H. S. Gutowsky and B. R. McGarvey, Phys. Rev. **91**, 81 (1953).

[13] H. Harned and B. Owen, *The Physical Chemistry of Electrolyte Solutions* (Reinhold Publishing Corporation, 1950), p. 394.

[14] H. S. Gutowsky and C. F. Hoffman, J. Chem. Phys. **19**, 1259 (1951).

Line Widths and Proton Exchange Rates

The possibility of exchange of protons among the various kinds of environments previously discussed must also be taken into account. If all the protons exchange rapidly relative to the times determined by the frequency separation of the possible states of the proton, a single sharp line will be observed which is characteristic of the number average of the various resonance frequencies. In this case, a lower limit on the rate of exchange can be set. If several different resonance frequencies were observed, an upper limit to the exchange rate could be set. If a broadening of the line is noted it is necessary to make sure that it is due to an interchange of protons in a time intermediate between the two previous situations rather than to other causes. The most likely other factor which can cause broadening of the resonance line in this case is the existence of low-frequency terms in the magnetic fields due to other nuclear moments. These can become important when the viscosities of the solutions become high. This broadening can be differentiated from exchange broadening by the different dependence of the line width on the external magnetic field.

As already pointed out, a single line is observed for the proton resonance in each electrolyte solution at room temperature and 7050 gauss. With the exception of the Al^{+++}, Be^{++}, and the most concentrated $ZnCl_2$ solutions, the line was not noticeably broadened over and above the broadening observed for pure water. This means that the time of exchange of protons is fast enough so that only the average proton resonance is observed and furthermore that all internal-relaxation mechanisms are such that the broadening of the line is determined by the inhomogeneity in the external field. Therefore, the proton exchange in these solutions is faster than 10^{-4} sec.[6]

In order to understand the nature of the broadening in the other solutions and their dependence on the external magnetic field, the various relaxation mechanisms described by Bloembergen, Purcell, and Pound[15] must be studied. They distinguish between two main types of relaxation: those due to spin-lattice and spin-spin interactions. Interactions of the spins with the lattice permit energy to be exchanged with the magnetic field. A characteristic relaxation time, called T_1, is associated with this process. The interactions between nuclear spins on the other hand, are independent of the magnitude of the magnetic field and represent the loss of phase coherence of the nuclear precession frequencies during a characteristic time T_2. Measurements of the line breadth yield T_2 through the relation $T_2=2/\gamma\Delta H$, where γ is the gyromagnetic ratio and ΔH is the width of the absorption curve. The theory of Bloembergen, Purcell, and Pound predicts a dependence of the relaxation times T_1 and T_2 on the ratio of viscosity to absolute

[15] Bloembergen, Purcell, and Pound, Phys. Rev. **73**, 679 (1948).

temperature. Both viscosity and temperature influence T_2, since it depends on the characteristic time, τ_c, during which molecular orientation persists. For the solutions investigated in this study, the relation $2\pi\nu\tau_c \ll 1$ between the precession frequency, ν, and the correlation time, τ_c, is satisfied. Then T_1 and T_2 are approximately equal and both are independent of the applied magnetic field.

The studies of line widths recorded in Table II at the frequencies 30 mc and 3 mc show clearly a difference in the behavior of the $AlCl_3$ solutions from the $BeCl_2$ and $ZnCl_2$ solutions. Of the three, only the $ZnCl_2$ solution fits the theory of Bloembergen, Purcell, and Pound reasonably well. This solution has about the same viscosity of pure glycerine, but its line width is a hundred times narrower, probably because of dilution of the spin system by the spinless Zn ion. Even here, the measured value of T_2 is not independent of the precession frequency. However, the major contribution to the line width does appear to be due to the viscosity of the solution. This is also the case for the $BeCl_2$ solution. The higher proton density explains the fact that this solution, in spite of its lower viscosity, shows a larger line width than the $ZnCl_2$ solution. The $AlCl_3$ solution shows an entirely different behavior, however, since the line width decreases by more than a factor of 5 in going from a precession frequency of 30 mc to 3 mc. This dependence of line width on precession frequency can be explained by postulating that in the 2.5-M $AlCl_3$ solution there exist states for water molecules in which they are either bound by Al^{+++} ions or essentially free, but that there are not a significant number of water molecules in intermediate states. Exchange between the bound and free states takes place with an exchange correlation time, τ_e. Gutowsky and Saika[6] have discussed the effect of τ_e on the shape of nuclear magnetic resonance lines. A single, sharp, resonance line appears if τ_e is very short, so that $2\tau_e\delta\omega \ll 1$, where $\delta\omega$ is the difference in angular frequency of precession for the two states of the proton between which exchange occurs. If τ_e is so long that $2\tau_e\delta\omega \gg 1$, the two states behave essentially as noninteracting species and two sharp resonances spaced $\delta\omega$ apart are observed. Furthermore, $2\tau_e\delta\omega \approx 1$ represents a transition region in which the width of the line is determined by the values of τ_e and $\delta\omega$. Since $\delta\omega$ is linearly field dependent, the line width becomes a function of the precession frequency.

For the $AlCl_3$ solution $\delta\omega$ cannot be measured exactly, but is certainly of the order of twice the shift of the proton resonance found for this system relative to pure H_2O. If the variation in line width observed in going from 30 mc to 3 mc is interpreted as making $2\tau_e\delta\omega \approx 1$, then τ_e for this solution is about 8 milliseconds.

The picture adopted above for purposes of calculations is certainly oversimplified. The anion was observed to have some effect. The $Al(NO_3)_3$ solution had a slightly narrower line than the $AlCl_3$ solution, indicative of the fact that the NO_3^- does not hold the proton as tightly as the Cl^- as confirmed by the δ values in Table III. Furthermore, lowering the temperature to slow down the proton exchange resulted only in a broadening of the line rather than a splitting of the line which would correspond to an actual separation of the frequencies of the proton states. Thus, a more realistic picture would probably be that in these solutions not two definite states for the proton exist, but rather a variety of closely similar states near a positive ion and similarly such states near a negative ion and relatively few protons in intermediate states at the concentrations used.

On First-Order Phase Transitions in Canonical and Grand Ensembles

TERRELL L. HILL
Naval Medical Research Institute, Bethesda, Maryland

(Received August 3, 1954)

S. Katsura has found evidence from exact calculations on finite systems that has led him to suggest that, contrary to the generally accepted view, a van der Waals type loop will be found in an exact application of the canonical ensemble to a first-order phase transition. It is shown here that Katsura's results can be understood in terms of interfacial free energy in the two-phase region. A loop is indeed obtained, but it is not of the van der Waals type. In particular, the loop vanishes in the limit of an infinite system. The well-known argument of van Hove showing that a loop does not exist in an infinite system (canonical ensemble) is discussed in this connection.

I. INTRODUCTION

THIS paper is concerned with the question of whether or not a "loop" should be expected in $\mu-N/V$ or $p-V/N$ curves for an exact theory of a first-order phase transition, using the canonical ensemble. Hill[1] and Katsura[2] have recently discussed this question, and its relation to the grand ensemble, in papers which come to the same conclusions (insofar as they overlap) with respect to approximate theories[3] but to different conclusions with respect to exact theories.[4]

Let us use the Ising model of a lattice gas to be specific. Much of the following notation is the same as that in reference 1. There are B equivalent sites in the lattice and the partition function for the motion of a molecule at a site is j. Let w be the nearest neighbor interaction energy and z the number of nearest neighbor sites to a given site. Then the canonical ensemble partition function in the Bragg-Williams approximation is[1]

$$Q(N,B,T)=\frac{B!j^N}{N!(B-N)!}\exp\left(-\frac{\alpha N^2}{B}\right),\qquad \alpha\equiv zw/2kT. \tag{1}$$

The exact partition function is

$$Q(N,B,T)=\sum_{\mathfrak{N}} g(N,\mathfrak{N},B)j^N\exp(-w\mathfrak{N}/kT), \tag{2}$$

where $g(N,\mathfrak{N},B)$ is the number of configurations with $\mathfrak{N}$ nearest neighbor pairs.

In the grand ensemble define

$$P(N)=Q(N,B,T)\lambda^N,\qquad \lambda\equiv e^{\mu/kT}. \tag{3}$$

Then $P(N)$ is proportional to the probability that a given system in the grand ensemble contains exactly N molecules. Let $\lambda_0=\exp(\mu_0/kT)$ be the value of λ for which $\bar{N}=B/2$ in the grand ensemble,[5] and $P_0\equiv Q\lambda_0{}^N$. Then, in the Ising model, $P_0(N)$ is symmetrical about $N=B/2$. Hill[1] and Katsura[2] agree that below the critical temperature, using an approximate theory, $P_0(N)$ has the form shown in Fig. 1. Figure 1 in the grand ensemble is the equivalent[6] of a loop in the $\mu-N/B$ curve in the canonical ensemble.

For the exact theory, Hill[1] assumed that $P_0(N)$ has the form shown[7] in Fig. 2. The equivalent of this in the canonical ensemble is a $\mu-N/B$ curve with a flat region instead of a loop. On the other hand, Katsura[2] conjectures that an exact theory will give the same qualitative behavior as an approximate theory: $P_0(N)$ as in Fig. 1, and a loop of the van der Waals type in the $\mu-N/B$ (or pressure-volume) curve. The only evidence that he cites [but this is almost conclusive for the form of $P_0(N)$ in the author's opinion], pertaining to an exact treatment, is that, at low temperatures, he has found maxima[8] as in Fig. 1, in an exact evaluation of a finite system, which become sharper as B increases.

In Sec. III it will be shown by a simple argument that a compromise between the two conflicting points of view above appears to be called for: interfacial effects between the two phases present are sufficient to give a $P_0(N)$ as in Fig. 1 and as found by Katsura[2] and Hill[8] for finite systems, but the corresponding canonical ensemble loop, unlike that in an approximate theory, disappears in the limit $B\to\infty$. This limiting behavior is in agreement with the earlier work of van Hove,[9] which we digress to discuss briefly in the next section.

II. THE ARGUMENT OF VAN HOVE

A careful argument has been given by van Hove[9] showing that no loop is obtained from the complete evaluation of the canonical ensemble partition function

[1] T. L. Hill, J. Phys. Chem. **57**, 324 (1953).
[2] S. Katsura, J. Chem. Phys. **22**, 1277 (1954). *Note added in proof.*—See also S. Katsura, Progr. Theoret. Phys. (Japan) **11**, 476 (1954).
[3] E.g., Bragg-Williams, van der Waals, quasi-chemical, etc.
[4] E.g., Mayer's imperfect gas theory, the two- or three-dimensional Ising model, etc.
[5] This value, for both Eqs. (1) and (2), is given by $j\lambda_0=\exp(zw/2kT)$.
[6] See Eqs. (8) and (10) of reference 1.
[7] This is correct only if the interface between the two phases is ignored. See Eq. (13) below.
[8] The present author has confirmed this for a set of 12 sites on a sphere using the table published by R. Peierls, Proc. Roy. Soc. (London) **154A**, 207 (1936); and M. F. Morales and J. Botts, J. Chem. Phys. **16**, 587 (1948). See the Appendix.
[9] L. van Hove, Physica **15**, 951 (1949). See also S. Katsura and H. Fujita, Progr. Theoret. Phys. (Japan) **5**, 997 (1950).

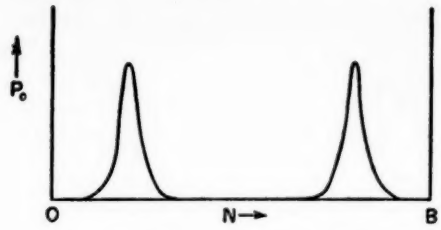

FIG. 1. P_0 as a function of N (schematic).

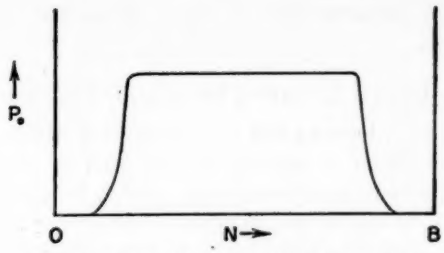

FIG. 2. P_0 as a function of N (schematic).

of an infinite fluid. The argument is based on the division of the system into sufficiently large cells, and neglect (which is shown to be justified) of molecular interactions between cells in the limit of an infinite system. Katsura's conjecture concerning a van der Waals loop, mentioned in Section I, contradicts the above result of van Hove, and hence Katsura[2] questions the validity of van Hove's reasoning. In the next section we shall try to show that it is not necessary for Katsura to invoke a van der Waals type of loop in order to explain his $P_0(N)$ curves, and hence his reason for questioning van Hove's argument is eliminated.

It may, however, be helpful here to supplement van Hove's discussion by the following alternative but essentially equivalent considerations. Let Q be the canonical ensemble partition function for a system of N molecules and volume V. Divide V into M cells of equal volume. Following van Hove, we take V/M large enough so that molecular interactions between molecules in different cells can be neglected. Then

$$Q=\sum \frac{M!Q_1^{n_1}Q_2^{n_2}\cdots}{n_1!n_2!\cdots}, \tag{4}$$

where $Q_m(V/M,T)$ is the canonical ensemble partition function for a system of m molecules and volume V/M, and n_m is the number of cells containing m molecules. The sum is over all distributions of the N molecules among cells such that

$$\sum_m n_m=M, \qquad \sum_m mn_m=N. \tag{5}$$

The most probable distribution [maximize the summand in Eq. (4) subject to Eqs. (5)] is easily found by Lagrange's method to be

$$\frac{n_m}{M}=\frac{e^{-\beta m}Q_m}{\sum_m e^{-\beta m}Q_m}, \tag{6}$$

where β is an undetermined multiplier, If we replace $\ln Q$ by the logarithm of the largest term in Eq. (4) and use Eq. (6) to eliminate the n_m, we obtain

$$\ln Q=M\ln\sum_m e^{-\beta m}Q_m+\beta N. \tag{7}$$

Now we know that

$$\left(\frac{\partial \ln Q}{\partial N}\right)_{V,T}=-\frac{\mu}{kT}. \tag{8}$$

Taking this same derivative in Eq. (7), keeping M constant, we find

$$\left(\frac{\partial \ln Q}{\partial N}\right)_{V,T,M}=\frac{-M\dfrac{\partial\beta}{\partial N}\sum_m e^{-\beta m}mQ_m}{\sum_m e^{-\beta m}Q_m}+\beta+N\frac{\partial\beta}{\partial N}=\beta. \tag{9}$$

From Eqs. (8) and (9) we conclude that

$$\beta=-\mu/kT. \tag{10}$$

Equations (7) and (10) yield

$$A=\mu N-pV=-kT\ln Q$$
$$=-kTM\ln\sum_m e^{\mu m/kT}Q_m+\mu N,$$

or

$$p\left(\frac{V}{M}\right)=kT\ln\sum_m e^{\mu m/kT}Q_m(V/M,T),$$
$$=kT\ln\Xi, \tag{11}$$

where Ξ is the grand partition function for a system of volume V/M. Equation (11) is the conventional relationship for the pressure using a grand ensemble.

Now a pressure-volume loop can never be obtained from a grand partition function,[1] so we can conclude from Eq. (11) that whenever the canonical ensemble partition function Q can be written in the form of Eq. (4), a loop will not be found. It should be noted that Eq. (4) will be valid for any theory (regardless of how exactly the Q_m are evaluated): (a) which allows all possible fluctuations in the number of molecules in each cell, and (b) with cells chosen large enough (infinite system, strictly) so that interactions between molecules in different cells can be neglected (see van Hove[9]). Approximate theories of the van der Waals, Bragg-Williams, etc., type, which contain the implicit or explicit restriction of the same fixed density in every cell, are excluded because of condition (a) above,[10] and,

[10] The author is indebted to Dr. L. van Hove for this observation.

as is well known, lead to loops from the canonical ensemble.

III. LOOPS IN THE CANONICAL ENSEMBLE

We return here to the Ising problem. All configurations, for given N and B, are included in the sum in Eq. (2). The conventional view (which is supported by the work of van Hove) is that, below the critical temperature and for a value of N in the two-phase region, configurations with separated phases will predominate in the sum relative to, for example, configurations with an essentially uniform macroscopic density throughout V. If we accept this point of view, we can write (ignoring interfacial effects temporarily)

$$\begin{aligned} A&=A_1+A_2=(N_1\mu_0-pV_1)+(N_2\mu_0-pV_2)\\ Q(N,V,T)&=Ce^{-(N_1\mu_0-pV_1)/kT}e^{-(N_2\mu_0-pV_2)/kT}\\ &=Ce^{-(N\mu_0-pV)/kT}, \end{aligned} \tag{12}$$

where A, Q, N, and V refer to the complete system, while A_1, Q_1, N_1, V_1, and A_2, Q_2, N_2, V_2 refer to the separate phases. V is proportional to B. The constant[11] $\ln C$ may be of order $\ln B$, but is thermodynamically negligible. From Eq. (12),

$$P_0(N)=Q(N)\lambda_0{}^N=Ce^{pV/kT}, \tag{13}$$

which is independent of N (see reference 7 and Fig. 2). No canonical ensemble loop will be found in this case, as already remarked in Sec. I.

On the other hand, if we should restrict the sum in Eq. (2) to configurations with only one phase throughout V, we would obtain $P_0(N)$ as in Fig. 1, and, in the canonical ensemble, metastable states and a van der Waals type of loop.[12]

Katsura,[2] with good evidence for $P_0(N)$ as in Fig. 1, conjectures that a van der Waals type of loop will also follow from an exact theory. The conventional view, again, is that such a loop could only follow from the restraint of one phase or uniform density in V; the complete sum in Eq. (2) is not subject to this restraint and should not give a van der Waals loop. In place of Katsura's suggestion, the author presents the argument below showing that interfacial effects will account for $P_0(N)$ as in Fig. 1 and will lead to a corresponding loop which, however, unlike a van der Waals loop, vanishes as $B\to\infty$. Interfacial contributions are automatically taken care of, of course, in Eq. (2); the object here is to estimate their order of magnitude.

Let N_1' be the number of molecules in V when phase 1 (the less dense phase) occupies the entire volume, and similarly for $N_2'=B-N_1'$ (phase 2, the more dense phase). For simplicity, instead of considering all values of N between N_1' and N_2', let us discuss first $N=N_1'$, $B/2$, and N_2'. At N_1' and N_2' a single phase exists and

$$\begin{aligned} P_0(N_1')=P_0(N_2')&=Q(N_1')\lambda_0{}^{N_1'}=Q(N_2')\lambda_0{}^{N_2'}\\ &=Ce^{-(N_1'\mu_0-pV)/kT}\lambda_0{}^{N_1'}\\ &=Ce^{pV/kT}\equiv C'. \end{aligned} \tag{14}$$

At $N=B/2$, two phases exist but A is not quite additive as assumed in Eq. (12). There will be of the order of $B^{\frac{1}{2}}$ molecules at the interface, which will result in of the order of $B^{\frac{1}{2}}$ "missing" nearest neighbor interactions. The total surface free energy, to be added to A, will then be of the order $kTB^{\frac{1}{2}}$. Thus

$$Q(B/2)=C\exp\left[-\left(\frac{B}{2}\mu_0-pV\right)\Big/kT\right]\times\exp(-aB^{\frac{1}{2}}) \tag{15}$$

$$P_0(B/2)=C'\exp(-aB^{\frac{1}{2}}), \tag{16}$$

where a is a positive constant of order unity. The term in $B^{\frac{1}{2}}$ in Eq. (15) is negligible thermodynamically (i.e., in A) but is not negligible in Eq. (16). In fact, from Eqs. (14) and (16) and the symmetry of $P_0(N)$, it is clear that $P_0(N)$ has maxima at N_1' and N_2' and a minimum at $B/2$. The ratio

$$\frac{P_0(N_1')}{P_0(B/2)}=\exp(aB^{\frac{1}{2}}) \tag{17}$$

is very large for large B and increases as B increases. Thus the behavior found in Fig. 1 by Katsura[2] and Hill[8] can be accounted for as a surface phenomenon.[13] In two dimensions, the ratio in Eq. (17) is $\exp(aB^{\frac{1}{2}})$; in a theory with the restraint of uniform density (including Bragg-Williams, etc.), it is rather obviously $\exp(aB)$.

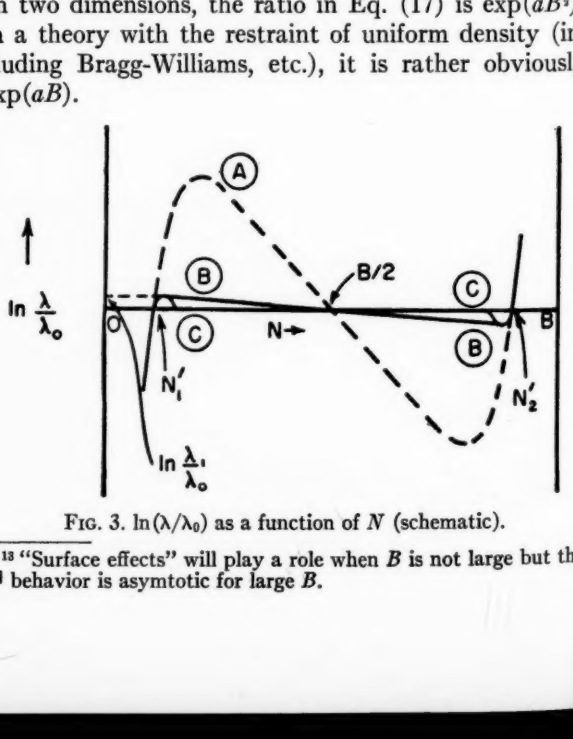

FIG. 3. $\ln(\lambda/\lambda_0)$ as a function of N (schematic).

[11] For simplicity we treat C as a constant. Actually, it may vary slowly with N, for example, $C(N)\sim N^n$ where n is of order unity. In this case $C(N)$ must be symmetrical about $N=B/2$. For reference below, we remark that a corresponding loop could result from the canonical ensemble but that it would vanish as $B\to\infty$ according to $\ln(\lambda_1/\lambda_0)=O(B^{-1})$. This contribution to a loop would therefore disappear faster (as $B\to\infty$) than the interfacial contribution of Eq. (20) which is $O(B^{-\frac{1}{2}})$ or $O(B^{-\frac{1}{3}})$.

[12] It is the uniform macroscopic density throughout V, implicit in the Bragg-Williams and most other approximations, which gives rise to metastable states and a loop.

[13] "Surface effects" will play a role when B is not large but the $B^{\frac{1}{2}}$ behavior is asymtotic for large B.

We now wish to consider the extent of the loop to be expected in a $\mu-N/B$ curve (from the canonical ensemble), as compared to the loop in an approximate theory (see Fig. 3). As pointed out in reference 1, a loop in Fig. 3 for the canonical ensemble is the locus of the two maxima and one minimum in Fig. 1 for the grand ensemble. The value of $\ln(\lambda_1/\lambda_0)$ (which locates the extent of the loop—see Fig. 3) can thus be determined as the value of $\ln(\lambda/\lambda_0)$ at which the maximum at $N=N_1'$ disappears. This will occur essentially when

$$\ln P(N_1')=\ln P(B/2). \tag{18}$$

Now we have

$$\begin{aligned} P(N)&=Q(N)\lambda^N \\ &=P_0(N)(\lambda/\lambda_0)^N \\ \ln P&=\ln P_0+N\ln(\lambda/\lambda_0). \end{aligned} \tag{19}$$

Then $\ln(\lambda_1/\lambda_0)$ is given by

$$\begin{aligned} \ln P(N_1')&=\ln C'+N_1'\ln(\lambda_1/\lambda_0) \\ &=\ln P(B/2) \\ &=\ln C'-aB^{\frac{1}{2}}+(B/2)\ln(\lambda_1/\lambda_0), \end{aligned}$$

or

$$\ln\frac{\lambda_1}{\lambda_0}=\frac{aB^{\frac{1}{2}}}{(B/2)-N_1'}=O(B^{-\frac{1}{2}}). \tag{20}$$

As $B\to\infty$, $\ln(\lambda_1/\lambda_0)\to 0$. Thus the canonical ensemble loop (solid curves B and C in Fig. 3) vanishes as $B\to\infty$ in an exact theory. In two dimensions, $\ln(\lambda_1/\lambda_0)=O(B^{-\frac{1}{2}})$. In an approximate theory (or with the restraint of uniform density), $\ln(\lambda_1/\lambda_0)=O(1)=$ constant as $B\to\infty$; the loop (dotted curve A in Fig. 3) in this case does *not* vanish as $B\to\infty$.

Whether an exact theory will give a loop of type B or C in Fig. 3 depends on the geometry of the system. For example, suppose the sites of a two-dimensional system are arranged on the surface of a torus of inner radius r_i and outer radius r_0. If $(r_0-r_i)/r_i$ is small, the interfacial regions will tend to occur in planes perpendicular to the plane of the torus and passing through its center, since this will minimize the interfacial area. In this case the surface correction in $P_0(N)$ (see[14] Eq. (16) for $N=B/2$) will be practically independent of N between N_1' and N_2', because the interfacial area is independent of the proportion of the two phases present. One can then see from Eq. (19) that a curve of type C in Fig. 3 will result. On the other hand, suppose the sites are distributed on the surface of a sphere. Then the interfacial area increases between N_1' and $B/2$ and decreases between $B/2$ and N_2'. Except near N_1', $B/2$, and N_2', $B^{\frac{1}{2}}$ in Eq. (16)[14] will be replaced approximately by $(N-N_1')^{\frac{1}{2}}$ for $N_1'\lesssim N<B/2$ and $(N_2'-N)^{\frac{1}{2}}$ for $B/2<N<N_2'$. The result will be a curve of type B in Fig. 3.

Figure 1 and Eq. (17) imply that an open system at λ_0 will practically always be found to have $N=N_1'$ or N_2' but not intermediate values of N (except for very small fluctuations in the neighborhood of N_1' and N_2'). We should expect this result from the grand ensemble point of view, for the total free energy (see Sec. II) of an ensemble of open systems will be lower if (a) half of the systems have $N=N_1'$ and half $N=N_2'$ rather than if (b) the systems have all values of N from N_1' to N_2' with an average N of $B/2$. This follows because there will be an interface with an extra surface free energy in the systems of (b) but there will be no surface contributions in (a) since molecular interactions between systems of the ensemble are not counted. These remarks apply to idealized systems without "edges" (e.g., the surface of a torus or a sphere, mentioned above) or interacting containing walls, such as are usually employed for theoretical calculations. Of course in a *closed* system (canonical ensemble), both phases will in general be present at $\lambda=\lambda_0$. The interface cannot be avoided as in an open system.

APPENDIX

We consider here the special case $B=12$, $z=4$ with sites arranged on the surface of a sphere[8] (cubic close packing). From Eqs. (2) and (3),

$$P(N)=\sum_{\mathfrak{N}} g(N,\mathfrak{N},B)(j\lambda)^N\exp(-w\mathfrak{N}/kT). \tag{21}$$

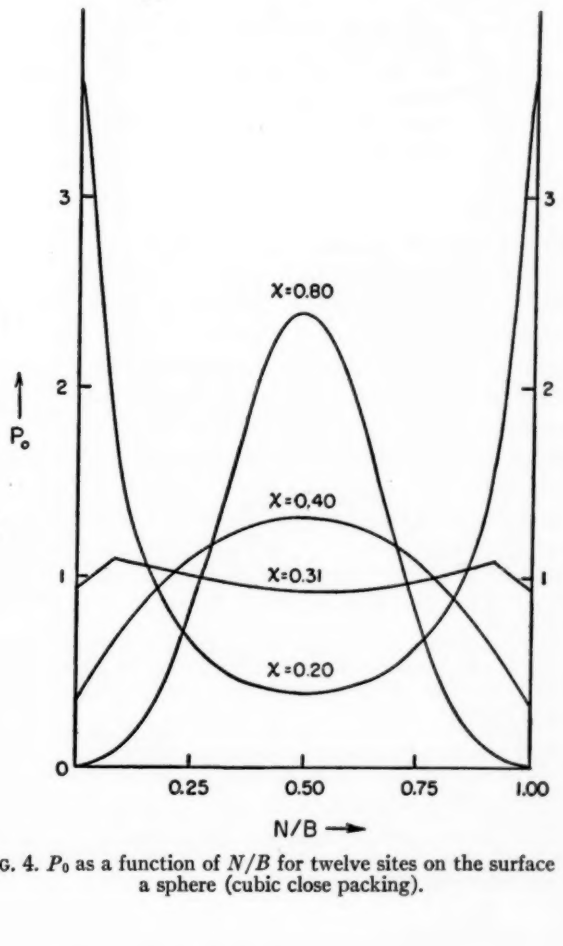

FIG. 4. P_0 as a function of N/B for twelve sites on the surface of a sphere (cubic close packing).

[14] Replace $\frac{2}{3}$ by $\frac{1}{2}$ for a two-dimensional system.

To obtain $P_0(N)$ we put[5] $j\lambda=\exp(2w/kT)$. Then

$$P_0(N)=\sum_M g(N,M,B)x^{2N-M}, \qquad (22)$$

$$x\equiv e^{w/kT}$$

where we have replaced $\mathfrak{N}$ by M for typographical reasons.

Specifically,[8] we have

$$P_0(0)=P_0(12)=1$$

$$P_0(1)=P_0(11)=12x^2$$

$$P_0(2)=P_0(10)=42x^4+24x^3$$

$$P_0(3)=P_0(9)=44x^6+120x^5+48x^4+8x^3 \qquad (23)$$

$$P_0(4)=P_0(8)=9x^8+96x^7+240x^6+96x^5+54x^4$$

$$P_0(5)=P_0(7)=108x^8+264x^7+264x^6+120x^5+36x^4$$

$$P_0(6)=216x^8+240x^7+336x^6+96x^5+36x^4.$$

Figure 4 shows $P_0(N)$ with $w<0$ for various values of x, normalized to unity. At high temperatures (x near unity) a single peak ("one phase") is obtained while at low temperatures (x near zero) two peaks appear ("phase splitting"). The critical value of x for the infinite system ($z=4$) has been shown by Kramers and Wannier and by Onsager to be $x_c=0.172$. The apparent higher "critical temperature" in Fig. 4 ($x_c\cong 0.32$) is probably due to the fact that "cooperation" between molecules is enhanced by the closer proximity (neighborwise) of sites to each other here, as compared to an infinite plane lattice.

THE JOURNAL OF CHEMICAL PHYSICS VOLUME 23, NUMBER 5 MAY, 1955

Experimental Determination of the Thickness of Weak Shock Fronts in Liquids*

W. M. Flook, Jr.,† and D. F. Hornig
Metcalf Research Laboratory, Brown University, Providence, Rhode Island

(Received August 23, 1954)

The thickness of weak shock fronts, across which the pressure difference was in the vicinity of ten atmospheres, was measured by the reflectivity method in acetone, ethyl alcohol, and ethyl ether. They are all of the order of 10^{-4} cm thick. Lower limits to the thickness were established in water, carbon tetrachloride, benzene, and ethylene glycol. A theoretical expression for the thickness is derived. Comparison between theory and experiment suggests that the effective viscosity in the shock front is several times the ordinary shear viscosity in ethyl ether and acetone but agrees well in ethyl alcohol.

INTRODUCTION

It has proved possible to investigate the transition region in shock fronts in gases by making use of the fact that under suitable conditions of shock strength and initial gas pressure the thickness of the transition region is of the same order of magnitude as the wavelength of visible light; because of this circumstance the optical reflectivity is sensitive to the thickness and density profile of the shock front. From their reflectivity the thickness of shock fronts has been measured in argon, nitrogen, oxygen, and hydrogen, and rotational heat capacity lags have been studied in the latter three molecules.[1–3] Very little has been published relating to the thickness of shock fronts in liquids. Cole[4] has published a summary of the work in underwater explosions, and in it he states: "A number of writers have made such estimates [of the thickness of intense shock fronts, based on hydrodynamic theory] . . . the common result is . . . that they predict thicknesses of the order of 10^{-5} or 10^{-6} cm . . . ." No detailed theoretical work has been done to date on this subject, and there has been no experimental evidence as to the thickness of any shock in a liquid. In the present paper, the thicknesses of weak shocks in liquids will be calculated from the hydrodynamic equations and an equation of state. An apparatus to measure these thicknesses will be described, and experimental results in a variety of liquids will be presented.

SHOCK FRONT THICKNESS IN LIQUIDS

The three hydrodynamic equations representing the conservation of mass, momentum, and energy across a plane shock front progressing in the positive X direction in a homogeneous compressible fluid may be written, respectively,

* This paper is based on a thesis submitted in partial fulfillment of the requirements for the degree of Doctor of Philosophy at Brown University, 1952. The work was supported by the Office of Naval Research.

† Present address: E. I. duPont de Nemours Company, Engineering Research Laboratory, Wilmington, Delaware.

[1] G. R. Cowan and D. F. Hornig, J. Chem. Phys. **18**, 1008 (1950).

[2] Greene, Cowan, and Hornig, J. Chem. Phys. **19**, 427 (1951).

[3] E. F. Greene and D. F. Hornig, J. Chem. Phys. **21**, 617 (1953).

[4] R. H. Cole, *Underwater Explosions* (Princeton University Press, Princeton, 1948), p. 46.

$$\rho u = a, \tag{1}$$

$$\frac{4}{3}\mu\frac{du}{dx} = au + p - b, \tag{2}$$

$$K\frac{dT}{dx} = uE + ub - \tfrac{1}{2}au^2 - c, \tag{3}$$

where ρ is the density at any point in the fluid, u the particle velocity with respect to the shock front, μ the shear viscosity, p the pressure, E the internal energy per unit volume, K the coefficient of thermal conductivity, and T the absolute temperature; a, b, and c are constants defined by the initial and final conditions. A convenient equation of state is obtained by expanding the pressure as a function of the density and the entropy as follows:

$$\delta p = \left(\frac{\partial p}{\partial \rho}\right)_S \delta\rho + \left(\frac{\partial p}{\partial S}\right)_\rho \delta S + \tfrac{1}{2}\left[\left(\frac{\partial^2 p}{\partial \rho^2}\right)_S \delta\rho^2 + 2\left(\frac{\partial^2 p}{\partial \rho \partial S}\right)_{S,\rho} \delta\rho\delta S + \left(\frac{\partial^2 p}{\partial S^2}\right)_\rho \delta S^2\right]. \tag{4}$$

Weak shock fronts in liquids, across which the pressure difference Δp is of the order of ten atmospheres, are to a good approximation isentropic. Therefore, the terms in δS in Eq. (4) may be dropped and only those in $\delta\rho$ and $\delta\rho^2$ used. This approximation is equivalent to replacing Eq. (3) by

$$dS/dx = 0. \tag{5}$$

The thickness of the shock front is defined by the expression

$$L = \frac{\rho_2 - \rho_1}{(d\rho/dx)_{\max}}, \tag{6}$$

where the subscripts 1 and 2 refer to the limiting regions ahead of and behind the shock front. Equations (1), (2), and (4) may be solved for $d\rho/dx$ to yield, in the case of weak shocks,

$$-\frac{4}{3}\mu\frac{du}{dx} = \frac{c_0^2\rho_1}{a}\left[1 + \frac{\rho_1}{2c_0^2}\left(\frac{\partial^2 p}{\partial \rho^2}\right)_S - \Delta p\left\{\frac{2}{c_0^2\rho_1} + \frac{\rho_1}{2c_0^4}\left(\frac{\partial^2 \rho}{\partial \rho^2}\right)_S\right\}\right]\delta\rho^2 - \frac{\rho_1\Delta p}{a}\left[1 + \frac{\rho_1}{2c_0^2}\left(\frac{\partial^2 p}{\partial \rho^2}\right)_S\right]\delta\rho. \tag{7}$$

In deriving this equation use has been made of the fact that $au_1 + p_1 - b = 0$ in the limiting region before the front, and that u_1, the velocity of the shock front, differs from the sound velocity c_0 by less than one part in one hundred. Use was also made of the relations

$$\left(\frac{\partial p}{\partial \rho}\right)_S = \frac{c_p}{c_v}\left(\frac{\partial p}{\partial \rho}\right)_T = c_0^2, \tag{8}$$

and

$$u_1^2 = \frac{\rho_2}{\rho_1}\frac{\Delta p}{\Delta \rho}. \tag{9}$$

The last two terms in $\delta\rho^2$ in Eq. (7) are actually third order as a consequence of Eq. (9). For example, for a 10 atmosphere shock in ethyl alcohol, they amount to less than one part in 700 of the complete term in $\delta\rho^2$, if the coefficients are taken from the data of Amagat.[5]

Consequently, to second order Eq. (7) becomes

$$-\frac{4}{3}\mu\frac{du}{dx} = \frac{\rho_1}{a}\left[1 + \frac{\rho_1}{2c_0^2}\left(\frac{\partial^2 p}{\partial \rho^2}\right)_S\right][c_0^2\delta\rho^2 - \Delta p\delta\rho], \tag{10}$$

so that

$$L = \frac{16\mu c_0}{3\Delta p\left[1 + \frac{\rho_1}{2c_0^2}\left(\frac{\partial^2 p}{\partial \rho^2}\right)_S\right]}. \tag{11}$$

The coefficient $(\partial^2 p/\partial\rho^2)_S$ has not been determined for any of the substances studied. It could best be obtained from a study of the variation of the velocity of sound with pressure and temperature, or with density and temperature, since it is given by either of the following two relations:

$$\frac{\rho_1}{2c_0^2}\left(\frac{\partial^2 p}{\partial \rho^2}\right)_S = \rho_1 c_0\left(\frac{\partial c_0}{\partial p}\right)_T + \frac{1}{\rho_1 c_0 c_v}\left(p - \frac{T\alpha}{\beta}\right)\left(\frac{\partial c_0}{\partial T}\right)_p \tag{12}$$

$$= \frac{\rho_1}{c_0}\left(\frac{\partial c_0}{\partial \rho}\right)_T + \frac{1}{\rho_1 c_0 c_v}\left(p - \frac{T\alpha}{\beta}\right)\left(\frac{\partial c_0}{\partial T}\right)_\rho, \tag{13}$$

where in addition to the symbols previously defined, α is the coefficient of thermal expansion and β is the compressibility. For any real liquid the last term is negligible to a very good approximation so that

$$\left(\frac{\partial^2 p}{\partial \rho^2}\right)_S = 2c_0^3\left(\frac{\partial c_0}{\partial p}\right)_T \tag{14}$$

$$= 2c_0\left(\frac{\partial c_0}{\partial \rho}\right)_T. \tag{15}$$

Except for water, very little information is available on the dependence of sound velocity on pressure. As an

[5] E. H. Amagat, Ann. chim. et phys. **29**, 505 (1893).

TABLE I. Theoretical shock thickness.

Material	c_0[a] cm sec^{-1}	μ[b] (centipoise)	ρ_1 g cm^{-3}	$(\partial^2 p/\partial\rho^2)_T$ dyne cm^4 g^{-2} Reference 5	Reference d	$L\Delta p$ atmos×cm
Ethyl ether	1.00×10^5	0.232	0.713	14.6×10^{10}	24.8×10^{10}	1.3×10^{-4}
Acetone	1.27×10^5	0.30	0.791	$11.9^c\times10^{10}$	19.9×10^{10}	3.5×10^{-4}
Ethyl alcohol	1.17×10^5	1.72	0.789	19.0×10^{10}	15.2×10^{10}	19.9×10^{-4}
Water	1.40×10^5	1.00	0.998	···	9.7×10^{10}	23.4×10^{-4}

[a] Freyer, Hubbard and Andrews, J. Am. Chem. Soc. **51**, 759 (1929).
[b] Thorpe and Roger, Phil. Trans. **A185**, 397 (1895).
[c] At 0°C.
[d] P. W. Bridgman, *International Critical Tables* (McGraw-Hill Book Company, Inc., New York, 1928), Vol. III, p. 41.

approximation to $(\partial^2 p/\partial\rho^2)_S$ one may use $(\partial^2 p/\partial\rho^2)_T$, which is available from the compressibility measurements of Bridgman and Amagat. Bridgman's values are presumably the more accurate but the points are taken at widely spaced pressure intervals (500 atmospheres) so that it is not certain that the average curvature of the p *vs* ρ curve is equal to that at one atmosphere. Amagat's data were taken at lower pressures, but the value of the second differences depend on the last decimal place of his measurements. The values of $(d^2p/d\rho^2)_T$ from both sources, together with the expected shock front thickness based on the Bridgman value, are given for several substances in Table I. For water, in which Eq. (14) can be used, the correct value of $(d^2p/d\rho^2)_S$ is 9.2×10^{10}, in good agreement with that obtained from Bridgman.[6] In interpreting Table I we must realize that in using the ordinary shear viscosities it has been assumed that μ does not depend on the rate of shear. Because compression in the shock is equivalent to sonic processes of the order of 300 Mc/sec, this is not necessarily a safe assumption. All of the values listed in Table I were taken at 20°C except where noted.

THE EFFECT OF BULK VISCOSITY ON THE THICKNESS

In recent work in the field of ultrasonic absorption the validity of using only the shear viscosity μ to describe the dissipative forces in a dynamic system has been questioned.[7–10] Tisza has proposed that in addition to μ, a bulk viscosity may be effective under dynamic conditions. If k is the bulk viscosity, Eq. (11) becomes

$$L'=\left(\frac{4}{3}\mu+k\right)\frac{4c_0}{\Delta p\left[1+\dfrac{\rho_1}{2c_0^2}\left(\dfrac{\partial^2 p}{\partial\rho^2}\right)_S\right]}. \tag{16}$$

If the value of k/μ is of the order of 3, as has been reported[8] for some liquids, L' would be about $3L$. Accurate experimental measurements of L combined with a well-established value of $(\partial^2 p/\partial\rho^2)_S$ should yield information as to the bulk viscosity forces acting in the shock process.

[6] A. H. Smith and A. W. Lawson, J. Chem. Phys. **22**, 351 (1954).
[7] L. Tisza, Phys. Rev. **61**, 531 (1948).
[8] Carl Eckart, Phys. Rev. **73**, 68 (1948).
[9] Markham, Beyer, and Lindsay, Revs. Modern Phys. **23**, 353 (1951).
[10] L. Hall, Phys. Rev. **73**, 775 (1948).

Experimental Method

In order to apply the reflectivity method, a knowledge of the variation of index of refraction, n, with distance through the shock front is necessary. This may be obtained by integrating Eq. (10) to obtain

$$\rho(x)=\rho_1+\frac{\Delta\rho}{1+e^{-4x/L}}, \tag{17}$$

and since $\delta n(x)$ is a linear function of $\delta\rho(x)$

$$n(x)=n_1+\frac{\Delta n}{1+e^{-4x/L}}. \tag{18}$$

It is interesting to note that this is exactly the expression used by Cowan and Hornig[1] as their "Model II" function. The reflectivity equation is therefore the same as that of Cowan and Hornig

$$R=\frac{\Delta n^2}{4{n_1}^2}(1+\tan^4\theta)\left[\frac{\left(\dfrac{\pi^2 L\cos\theta}{\lambda}\right)^2}{\sinh^2\left(\dfrac{\pi^2 L\cos\theta}{\lambda}\right)}\right]. \tag{19}$$

In the above equation R is the reflectivity, λ the wavelength of the incident light, θ the angle of incidence and n_1 the index of refraction of the medium. The total change in index of refraction across the shock front is Δn. The part of the equation enclosed in square brackets is plotted as a function of $\lambda/L\cos\theta$ in Fig. 1.

Two essentially different methods of determining L from Eq. (19) suggest themselves. First, following Cowan and Hornig, we find the parameter $L\cos\theta/\lambda$ may be varied by changing either λ or θ, and the slope of the reflectivity function determined. The value of L may then be determined from Fig. 1. Alternately, the apparatus may be calibrated in terms of absolute reflectivity and Eq. (19) solved for L. In this case Δn is given by the Lorentz-Lorenz formula which is, for

sufficiently weak shocks,

$$\Delta n=\frac{\Delta\rho}{2n_1\rho_1}(n_1^2-1). \tag{20}$$

APPARATUS

A schematic diagram of the apparatus used is shown in Fig. 2. The apparatus was a modification of that used by Cowan and Hornig. A shock wave was generated in nitrogen by means of a bursting diaphragm in a vertically mounted, $2\frac{7}{8}$ in. diameter shock tube. Copper diaphragms, 0.008 in. thick, were used to produce shocks with a pressure difference of 10 atmospheres. The shock wave travelled down the tube until it impinged at normal incidence on the surface of the liquid in the bottom of the tube. A 0.001-in. membrane of duPont "Mylar" film was located about a centimeter below the surface of the liquid and served to separate contaminated liquid above from the carefully filtered clean sample in a cell at the base of the tube. The 3-cm layer of liquid above the cell tended to slow down copper fragments and to protect the membrane. Windows in opposite sides of the cell allowed the collimated light beam from a carbon arc to enter the liquid at a known angle to the vertical; a type 931 A photomultiplier in conjunction with an optical system received the reflected light pulse as the shock travelled past the window. Suspended matter in the sample had to be carefully eliminated since it caused intolerable light noise; in fact, the reduction of scattered light was one of the major experimental problems in this work. Samples were filtered through three fine sintered glass filters directly into the cell, which was constructed entirely of stainless steel, to eliminate suspended particles as far as possible.

The shock tube was adjusted to within 2 minutes of arc of the vertical by means of a plumb bob, and the optical zero was fixed within 30 seconds of horizontal using surveying instruments. Accurate angle settings were imperative since the angles of incidence used were close to grazing, where the $(1+\tan^4\theta)$ factor in Eq. (10) changes rapidly with angle. Shock pressures were computed from the measured pressures in the compression and expansion chambers, using previously published relations.[11] A correction was made for the 7 percent decrease in shock strength, resulting from nonideal bursting conditions, reported by Bleakney *et al.*,[12] as well as for the more than two-fold increase[13] in shock pressure caused by reflection at the liquid-gas interface.

An image of the carbon arc light source was cast on a horizontal slit, which then became the effective light source for the rest of the system. The slit was designed so that the divergence of the beam in the vertical plane was limited to plus or minus 30 minutes of arc. The optical system was arranged so that the direct light beam passed through the cell and left through the exit window; it was absorbed on a black paper mask outside the tube. This arrangement was found to materially reduce the background of scattered light. A lens and mask in the exit system permitted only nearly parallel light to reach the photomultiplier, still further reducing the unwanted scattered rays. The entire optical system

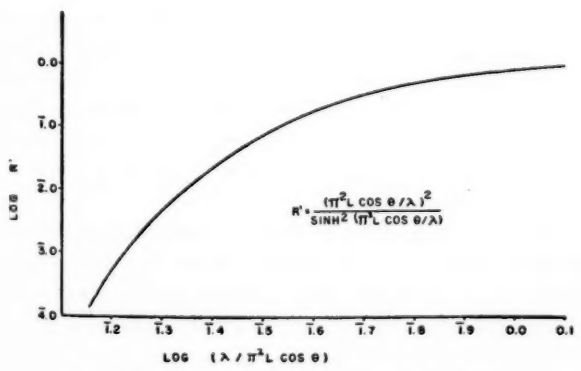

FIG. 1. Theoretical reflectivity of a shock front.

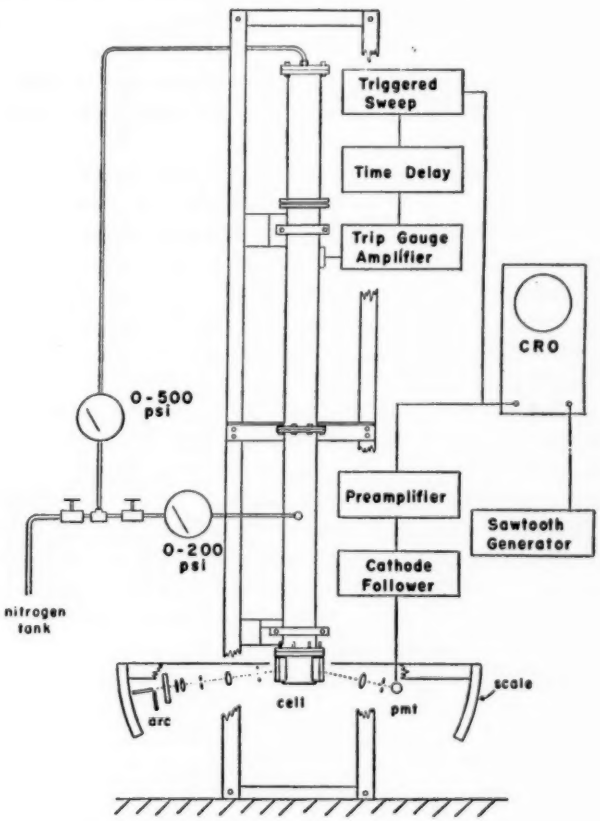

FIG. 2. Apparatus used to measure shock front reflectivities in liquids.

[11] F. W. Geiger and C. W. Mautz, "The Shock Tube as an Instrument for the Investigation of Transonic and Supersonic Flow Patterns," U. S. Navy Department of Naval Research Contract No. N6-ONR-232 Task Order IV, Engineering Research Institute, University of Michigan, June, 1949, p. 12.

[12] Bleakney, Weimer, and Fletcher, Rev. Sci. Instr. **20**, 807 (1949).

[13] R. Courant and K. O. Friedrichs, *Supersonic Flow and Shock Waves* (Interscience Publishers, Inc., New York, 1948), p. 153.

TABLE II. Experimental shock thicknesses at 26°C.

Liquid	Shock strength (atmospheres)	Method	Thickness (cm $\times 10^4$)	Av. thickness (cm $\times 10^4$)	$L\Delta P$
Acetone	9.3	Angle dep. Absolute mag. Wavelength dep.	1.37±0.2 1.20±0.08 1.54±0.2	1.40	13×10^{-4}
	13.1	Angle dep. Absolute mag. Wavelength dep.	0.72±0.15 0.86±0.07 0.85±0.12	0.80	10.5×10^{-4}
Ethyl alcohol	13.1	Wavelength dep. Absolute mag.	1.00±0.15 1.32[a]	1.16	15.2
	16.7	Angle dep. Absolute mag.	0.90±0.2 1.21±0.09	1.11	18.5
Ethyl ether	9.3	Wavelength dep. Angle dep. Absolute mag.	0.90±0.15 1.04±0.08 0.75±0.09	0.85	7.9
Water	16.7	Absolute mag.	>1.1		>18.3
Carbon tetrachloride	16.7	Absolute mag.	>2		>33.4
Benzene	16.7	Absolute mag.	>1.9		>31.8
Ethylene glycol	16.7	Absolute mag.	>1.6		>27

[a] One record.

was mounted on a 500-lb concrete block, entirely separate from the shock tube, to prevent vibrations from reaching the detection system.

The scattering level in the cell was measured before each shot by setting the angle of incidence at a standard value, and measuring the signal obtained when the arc beam was "chopped" by a rotating sector. Whenever the scattering level increased following a shot, a pin hole was found in the membrane. High scattering levels gave rise not only to random "light" noise but also to well defined spurious signals.

Effective angles of incidence in the liquid were computed by using the known divergence of the light beam in connection with the reflectivity equation to obtain a properly weighted average, after allowance had been made for refraction at the windows. The external angles of incidence used were 80° and 82°, corresponding to actual effective values, in acetone and ethyl alcohol, of 82°45′ and 84°15′. In ethyl ether the effective values were 82°37′ and 84°05′.

Wavelengths were isolated at two points in the visible spectrum by Wratten filters; effective wavelength values were fixed by combining filter transmissions (measured using a carbon arc source in connection with a recording spectrograph) with the theoretical reflectivity curve to obtain a weighted average value. The detector in the spectrograph was a type 1P21 photomultiplier, which has the same spectral sensitivity as the 931-A. Wratten filter No. 35 yielded a weighted average wavelength of 4300 A, based on a shock thickness of 10^{-4} cm. Wratten No. 21 yielded an average value of 5700 A. These two filters, as well as the white light average of 4750 A, were used in all the experimental work.

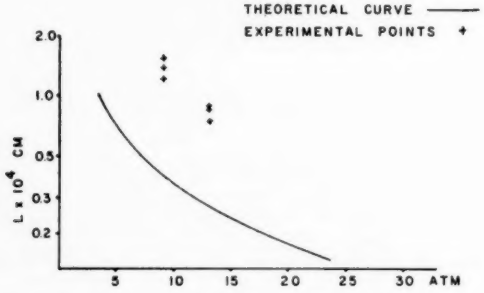

FIG. 3. Thickness of shock fronts in acetone.

Output signals were displayed on a cathode-ray oscilloscope and recorded photographically. An expanded sweep allowed accurate timing measurements to be made. The frequency response of the electronic system was constant to 100 kc, falling off to 50 percent at 400 kc.

A signal was observed in some liquids upon passage of the primary shock wave. A second signal was observed as the shock was reflected from the bottom plate of the cell and again traversed the light beam. These signals were identified as true reflections by their timing, their shape, their duration, and especially by their wavelength dependence. The signals were observed to be stronger at longer wavelengths, eliminating any possibility that they might be caused by any spurious scattering phenomenon.

The recording system was calibrated in terms of absolute reflectivity by using a shock front of known thickness in nitrogen as a reference. A shock wave which had been thoroughly studied by Greene *et al.*[2] was generated in the tube by duplicating their conditions. The thickness of this shock was known to be

1.63×10^{-5} cm plus or minus 15 percent; its reflectivity was established through the use of the Rankine-Hugeniot relation in conjunction with Eqs. (19) and (20). For this shock $\lambda/\pi^2 L\cos\theta$ falls to the right on Fig. 1, where the reflectivity varies slowly with thickness, thus enhancing the accuracy of the calibration. The thicknesses observed in liquids, on the other hand, correspond to points on the left of Fig. 1, in a region of rapidly varying reflectivity, which tends to increase the reliability of the results.

The scatter of reflectivity values obtained from gas calibration shocks was considerably less than that observed in the liquid; this was originally attributed to the complications introduced by the passage of the shock through the liquid-gas interface as well as the factors mentioned in the preceding paragraph. However, the condition of this interface at the instant of arrival of the shock wave was investigated by totally reflecting a light beam from the surface and observing any deflections. No disturbances were observed in the central portion of the surface prior to the arrival of the shock, although there was some evidence of deformations near the edges.

EXPERIMENTAL RESULTS

The experimental results at 26 ± 3°C are listed in Table II. Shock-wave thicknesses were successfully measured in acetone, ethyl alcohol, and ethyl ether, but no reflections could be observed in water, carbon tetrachloride, benzene, or ethylene glycol, even from the strongest shock waves ($\Delta p=16.7$ atmospheres) available. The minimum reflectivity observable with this apparatus was about $R=10^{-7}$; this fact establishes a lower limit on the shock front thickness in these liquids, as indicated in the table. The thickness values listed in Table II represent the average of 4 or 5 reflectivity measurements at each of the angle or wavelength settings, except as noted. Probable limits were computed from the scatter in experimental values. This scatter was relatively large, possibly reflecting uncertain conditions at the liquid-gas interface at the instant of arrival of the shock. The probable errors of the reflectivity values ranged from 11 percent to 35 percent, with an average value of 15 percent. The scatter in gas calibration reflectivities yielded a probable error of only 1.6 percent. It will be noted that while there appears to be some discrepancy between the results of the various methods of measuring L, in most cases the limits of error overlap for identical shocks. The experimental results are plotted in Figs. 3, 4, and 5, together with the corresponding theoretical curves computed from Eq. (11).

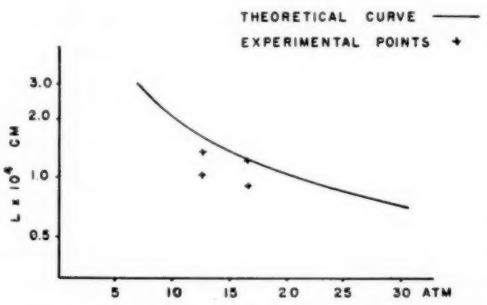

FIG. 4. Thickness of shock fronts in ethyl alcohol.

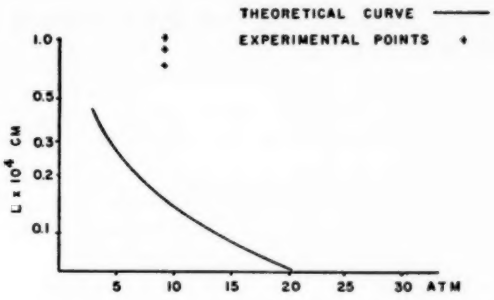

FIG. 5. Thickness of shock fronts in ethyl ether.

CONCLUSIONS

The comparison between the experimental and theoretical results for acetone and ethyl ether suggests that either the shear viscosity is markedly greater under these conditions or that a bulk viscosity effect is present, since the measured values of L all lie significantly above the predicted values. The values of $(\partial^2 p/\partial\rho^2)_S$ used in the theoretical computations are so questionable, however, that no clear-cut conclusions may be drawn regarding the magnitude of the effect. The potentiality of the method for gaining information about the viscous behavior of liquids has, however, been demonstrated; an expression for shock thickness in liquids, valid for weak shocks, has been derived from hydrodynamic theory, and an apparatus to measure the thickness of such shock waves has been described.

The authors wish to thank Edward F. Greene for valuable help and suggestions throughout the experimental work and Thomas L. Dawson for help in designing and constructing the apparatus.

Reactions of $Hg(^3P_1)$ with Toluene*

A. H. SEHON† AND B. DEB. DARWENT‡
National Research Laboratories, Ottawa, Canada
(Received September 21, 1954)

The reactions between $Hg(^3P_1)$ and toluene have been investigated between 150° and 400°C at pressures from 0.4 to 30.5 mm Hg. The gaseous products are H_2, CH_4, and C_2H_6. The quantum yield for H_2 is 5×10^{-4} at 150°C and increases to about 10^{-1} at 400°C. A mechanism based on two types of excited toluene molecules is proposed.

I. INTRODUCTION

THE mechanisms of the reactions of excited mercury atoms with alkanes and alkenes have been fairly well established. Thus the alkanes have been shown to react by a simple carbon-hydrogen split and the alkenes generally by the formation of excited molecules. In contrast, very little is known about the reactions of excited mercury atoms with aromatic hydrocarbons. Two papers on those reactions have been published recently by Scott and Steacie[1] on benzene, and Hentz and Burton[2] on toluene. The quantum yields of both reactions were very small at room temperature and even at the more elevated temperatures at which the reactions were investigated. The reaction of $Hg(^3P_1)$ with toluene[2] was investigated only incidentally to a more general survey of the photochemistry and radiation chemistry of substituted benzenes and little can be said about the details of the reaction. The results of a more detailed study of the reaction between $Hg(^3P_1)$ and toluene are reported in this communication.

II. EXPERIMENTAL

The toluene and propane were Phillips Research Grade Products and were further purified by simple bulb-to-bulb distillations.

The apparatus was similar to that used for investigating other mercury photosensitized reactions in this laboratory. A cyclindrical quartz reaction cell (5 cm diameter, 10 cm long) was placed concentrically in a cylindrical aluminum furnace, the ends of which were closed by quartz plates. The temperature along the cell did not vary by more than 2°C and, in any one experiment, the temperature at the center of the cell did not fluctuate by more than 2 degrees. The reaction vessel was connected through a mercury cutoff to the main vacuum line and an analytical system consisting of a Ward[3] still, a mercury diffusion pump, and a combined Toepler pump and gas burette. Unreversed resonance radiation of λ2537 was obtained from a low-pressure mercury lamp filled with neon to 3 mm pressure and run at 100 ma from a stabilized power source. The light was roughly collimated by a quartz lens and filled the whole of the reaction vessel. The intensity of light was determined by measuring the rate of formation of hydrogen in the mercury photosensitized decomposition of propane at 300 mm pressure and room temperature. The quantum yield[4] for the decomposition of propane was taken to be 0.5.

Before an experiment, toluene was admitted to the reaction system from a storage vessel and further degassed by repeated freezing and melting in vacuo. After a measured period of illumination the toluene was frozen out at −80°C and the hydrogen, methane, and other volatile hydrocarbons were removed by the mercury diffusion and Toepler pumps and collected and measured in the gas burette. The products were further separated into fractions by distillation in the Ward still. The gases uncondensable at −196°C were analyzed either by combustion over copper oxide or mass spectrometrically. The other products were analyzed mass spectrometrically and found to consist largely of C_2 hydrocarbons and, occasionally, traces of C_3 hydrocarbons; they have been regarded as C_2H_6 in this work.

III. RESULTS

Preliminary investigation showed that there was no observable reaction after 48-hours exposure at room temperature and subsequent experiments were performed at temperatures which were high enough for reasonable rates to be obtained but low enough for the thermal reaction to be insignificant. The reaction was investigated in fair detail at 295°C and less intensively at 150° and 400°C.

The results obtained at 295°C, presented in Table I, provide information about the effect of pressure on the rates of production of H_2, CH_4, and C_2H_6 and on the composition of the gaseous products. The rates of production of H_2, CH_4, and C_2H_6 are shown as functions of the pressure of toluene in Fig. 1. The rapid increase in R_{H_2} with increasing pressure between zero and about 2 mm can be explained most easily by assuming that the quenching is incomplete in this region and increases with increasing pressure. The rate of

* Contribution No. 3595 from the National Research Council, Ottawa, Canada.

† Present address: Department of Experimental Medicine, McGill University, Montreal, P.Q. Canada.

‡ Present address: Olin Mathieson Chemical Corporation, General Research Laboratories, New Haven, Connecticut.

[1] E. J. Y. Scott and E. W. R. Steacie, Can. J. Chem. **29**, 233 (1951).

[2] R. R. Hentz and M. Burton, J. Am. Chem. Soc. **73**, 532 (1951).

[3] E. C. Ward, Ind. Eng. Chem. (Anal. Ed.) **10**, 169 (1938).

[4] S. Bywater and E. W. R. Steacie, J. Chem. Phys. **19**, 172 (1951).

production of hydrogen (R_{H_2}) then decreases with a further increase in pressure between 2 and 15 mm after which it appears to be independent of pressure. The rate of production of methane also increases with increasing pressure in the low-pressure region; it does not attain a maximum as did R_{H_2} but becomes either independent of or increases very slowly with increasing pressure between about 10 mm and 30 mm. In contrast to the effect of pressure on R_{H_2} and R_{CH_4}, the rate of production of C_2H_6 is independent of pressure over a wide range and appears to increase slightly with decreasing pressure below about 2 mm.

Based on the assumption that the H_2 arose from the reaction of H atoms with toluene, the CH_4 from CH_3+toluene and the C_2H_6 from the combination of CH_3 radicals, we have attempted to investigate the effect of pressure on the relative rates of production of CH_3 and H by plotting the ratio $(CH_4+2C_2H_6)/H_2$ as a function of pressure (Fig. 2). The points on this graph are rather widely scattered but it does seem very probable that the extrapolation of the data to zero pressure leads to a positive intercept of between 0.2 and 0.3.

Subsequent experiments were performed at about 150° and 400°C (Table II). In general, the results are similar to those obtained at 295°; the rate of production of hydrogen also goes through a maximum and then becomes approximately constant as the pressure is increased. The rate of the reaction appears to be moderately sensitive to temperature but the ratio of hydrogen to methane does not appear to be significantly effected by changes in temperature.

The quantum yield for the production of hydrogen was measured in the high-pressure region, at the three temperatures investigated, by comparing the rates of production of hydrogen from toluene at those temperatures with that from propane at room temperature and 300 mm pressure. The following values were obtained: 150°, $\phi_{H_2}=5\times10^{-4}$; 295°, $\phi_{H_2}=5\times10^{-2}$; 400°C, $\phi_{H_2}\approx10^{-1}$. Hentz and Burton[2] did not report quantum yields for the photosensitized reaction but obtained a value of 6×10^{-5} at 150°C in the direct photolysis of toluene. The quantum yield found in this work is of the same order as that found by Scott and Steacie[1] for the mercury photosensitized decomposition of benzene.

TABLE I. The reaction of $Hg(^3P_1)$ with toluene at 295°C.

Expt. no.	p (mm Hg)	10^4 rate (CH_4+H_2) cc N.T.P./min	$\frac{CH_4}{(CH_4+H_2)}$	$\frac{C_xH_y}{(CH_4+H_2)}$
27	0.4	4.33	0.09	0.12
30	0.6	4.7	0.08	0.09
26	2.0	5.7	0.18	0.06
29	3.3	4.97	0.17	0.05
21	5.0	4.8	0.22	0.05
22	5.0	4.75	0.29	0.05
24	6.7	4.17	0.39	0.04
25	8.2	3.41	0.27	0.10
23	12.0	3.37	0.33	0.04
28	15.0	3.08	0.35	0.08
14	25.0	3.34	0.34	···
9	26	3.19	0.41	···
10	26	3.59	0.38	···
11	26	3.21	0.41	0.06
15	29	3.36	0.45	···
16	30.5	3.74	0.52	···
17	30.5	3.72	0.40	···

IV. DISCUSSION

The nature of the products indicates that H atoms are produced in the initial step of the reaction between $Hg(^3P_1)$ and toluene and the fact that the ratio CH_3/H, as measured by the ratio $(CH_4+2C_2H_6)/H_2$ (Fig. 2), extrapolates to a finite value of 0.2 to 0.3 shows that methyl radicals are probably also produced in the initial reaction. The fact that R_{H_2}, when plotted (Fig. 1) as a function of pressure, passes through a maximum is not inconsistent with the suggestion that an excited molecule is formed in the reaction of $Hg(^3P_1)$ with toluene,

$$Hg(^3P_1)+C_6H_5\cdot CH_3\rightarrow C_6H_5\cdot CH_3{}^*+Hg(^1S_0), \quad (1)$$

and that the excited molecule can either be deactivated,

$$C_6H_5\cdot CH_3{}^*+M\rightarrow C_6H_5\cdot CH_3+M, \quad (2)$$

or decompose. Since H and CH_3 are probably formed initially the decomposition may then occur by the following two processes:

$$C_6H_5\cdot CH_3{}^*\rightarrow C_6H_5\cdot CH_2\cdot+H \quad (3)$$

$$\rightarrow C_6H_5\cdot+\cdot CH_3. \quad (4)$$

Because of the high temperatures in this investigation the ultimate products probably arise by reaction of H atoms and CH_3 radicals with toluene:

$$CH_3+C_6H_5CH_3\rightarrow C_6H_5CH_2+CH_4 \quad (5)$$

$$H+C_6H_5CH_3\rightarrow C_6H_5CH_2+H_2 \quad (6)$$

as well as by combination of methyls to form ethane:

$$2CH_3\rightarrow C_2H_6. \quad (7)$$

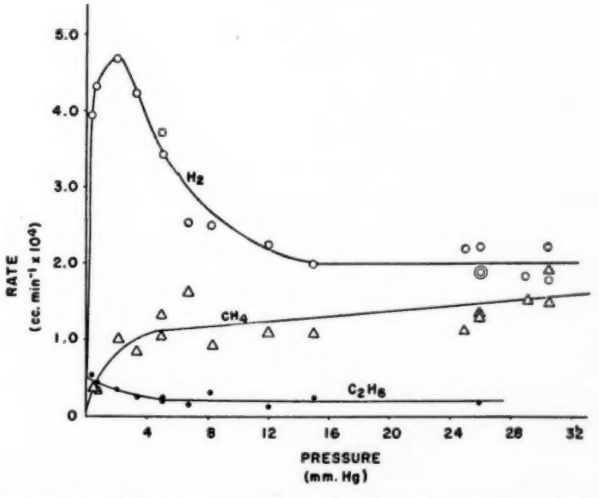

FIG. 1. The effect of pressure on the rates of production of H_2, CH_4, and C_2H_6 at 295°C.

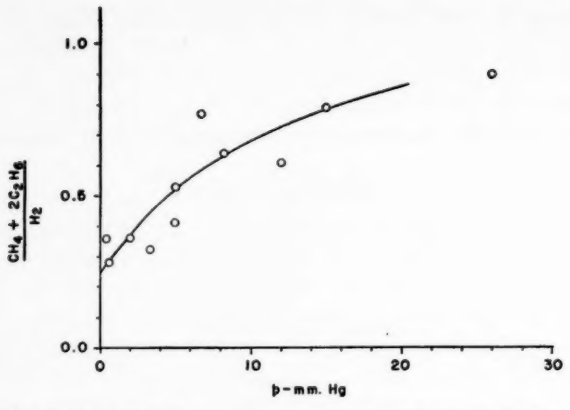

FIG. 2. The effect of pressure on the ratio CH_3/H_2 at 295°C.

This mechanism certainly accounts for the products observed in this investigation and the suggestion that an excited molecule is formed is consistent with the claim[1] that an excited molecule is formed in the analogous reaction with benzene. However the usual assumptions of a stationary state show that the rate of decomposition, taken as $(k_3+k_4)T^*$, where T^* represents the concentration of excited toluene, is given by the equation:

$$R_D=(k_3+k_4)T^*=\frac{(k_3+k_4)\cdot k_1\cdot I_a}{(k_3+k_4)+k_2p}, \qquad (A)$$

where p represents the concentration of toluene. Equation (A) demands that $R_D\rightarrow 0$ as $p\rightarrow\infty$, which is contrary to the observation (Fig. 1) that the rate becomes essentially independent of pressure between 15 and 30 mm.

Furthermore, the mechanism requires CH_3 and H to be formed in similar processes, (3) and (4) and, since R_{H_2} was shown to have a maximum value at 2 mm, R_{CH_3} should also have had a maximum value at that pressure. No such maximum has been found.

Although the mechanism involving an excited molecule does not appear to be adequate it does seem to be a reasonable suggestion in view of the past work on benzene[1] and on other compounds involving carbon-to-carbon double bonds. If such a mechanism is to be retained then one is forced to suggest that more than one excited species is formed and that at least one of those species is so short lived that it is essentially never deactivated and always decomposes:

$$Hg(^3P_1)+C_6H_5\cdot CH_3\rightarrow C_6H_5\cdot CH_3^+ + Hg(^1S_0) \qquad (1')$$

$$C_6H_5\cdot CH_3^+\rightarrow C_6H_5\cdot CH_2\cdot + H \qquad (3')$$

$$\rightarrow C_6H_5\cdot + \cdot CH_3. \qquad (4')$$

The rate of decomposition is then given by the equation

$$R_D=\frac{k_1(k_3+k_4)I_a}{k_3+k_4+k_2p}+k_1'I_a \qquad (B)$$

which allows R_D to attain a finite value $(k_1'I_a)$ as $p\rightarrow\infty$.

TABLE II. The reaction of $Hg(^3P_1)$ with toluene at 152° and 403°C.

A. 152(±2)°C

Expt. no.	p (mm Hg)	10^4 rate (CH_4+H_2) cc N.T.P./min	$\frac{CH_4}{(CH_4+H_2)}$	$\frac{C_xH_y}{(CH_4+H_2)}$
36	0.6	7.82	0.50	0.24
33	1.0	10.12	0.50	0.25
35	3.0	7.66	0.29	0.06
32	5.0	7.40	0.33	0.12
34	17.0	3.64	0.50	0.10
37	30.5	3.16	0.54	0.20

B. 403(±4)°C

Expt. no.	p (mm Hg)	10^4 rate (CH_4+H_2) cc N.T.P./min	$\frac{CH_4}{(CH_4+H_2)}$	$\frac{C_xH_y}{(CH_4+H_2)}$
42	0.2	2.41	0.16	0.10
41	1.2	8.06	0.26	0.04
44	3.0	8.0	···	0.02
40	6.0	9.58	···	0.02
45	10.0	7.83	0.45	0.03
43	15.0	7.85	0.42	0.01
39	30.0	7.95	···	0.02
38	30.0	7.55	0.43	0.03

To reconcile this mechanism with the fact that R_{CH_3} does not have a well-defined maximum, it then becomes necessary to postulate that CH_3 is produced only from $C_6H_5\cdot CH_3^+$ [reaction (4')] and not from $C_6H_5\cdot CH_3^*$ as suggested by reaction (4).

The suggested mechanism thus accounts qualitatively for the effect of pressure on the rate of decomposition of toluene. It may now be examined in relationship to the effect of pressure on the rates of production of the individual products.

The rate of production of hydrogen, in the region of complete quenching is given by the equation

$$R_{H_2}=k_5[H]p=k_3T^*+k_{3'}T'$$

$$=I_a\left(\frac{k_1k_3}{k_2p+k_3}+\frac{k_{1'}}{k_{3'}+k_{4'}}\right) \qquad (C)$$

which is of the same type as Eq. (B) and is consistent with our observations on the effect of pressure on R_{H_2}.

Making the usual stationary state assumptions we find the concentration of CH_3 to be

$$[CH_3]=\frac{1}{2k_7}\left[\left(k_5^2p^2+\frac{4k_{1'}k_4k_7I_a}{k_{3'}+k_{4'}}\right)^{\frac{1}{2}}-k_5p\right]. \qquad (D)$$

The fact that $R_{C_2H_6}$ appears to be independent of pressure between 5 and 30 mm indicates that $[CH_3]$ is also independent of pressure in that region. This is in accordance with Eq. (D) if $4k_{1'}k_4k_7I_a/(k_{3'}+k_{4'})\gg k_5^2p^2$ since Eq. (D) may then be simplified to

$$[CH_3]=\left[\frac{k_{1'}k_4I_a}{k_7(k_{3'}+k_{4'})}\right]^{\frac{1}{2}}=\alpha \qquad (D')$$

i.e., that $[CH_3]$ is independent of pressure. This leads to the equation

$$R_{CH_4}=k_5[CH_3]p=k_5\alpha p,$$

requiring R_{CH_4} to be a linear function of pressure. The results shown in Fig. 1 are not in disagreement with this requirement.

This mechanism is certainly oversimplified, since no attention was paid to reactions of H and CH_3 with the heavier radicals produced, which were tacitly assumed to disappear entirely by combination processes not involving H or CH_3. Also the following reactions of H and toluene

$$H+C_6H_5\cdot CH_3\rightarrow C_6H_6+CH_3 \qquad (6')$$

$$\rightarrow\cdot C_6H_6\cdot CH_3 \qquad (6'')$$

the first of which was suggested by Szwarc[5] and the second of which appears to be a very probable process, have not been included specifically in the mechanism. All of these reactions doubtless occur and reactions such as (6″) and

$$H+C_6H_5\cdot CH_2\cdot\rightarrow C_6H_5CH_3 \qquad (8)$$

could be responsible for the low-quantum yield. However, further discussion would be largely speculative and would require much more detailed experimental results and a complete kinetic treatment of the data.

[5] M. Szwarc, J. Chem. Phys. **16**, 128 (1948).

THE JOURNAL OF CHEMICAL PHYSICS VOLUME 23, NUMBER 5 MAY, 1955

Photochemical Decomposition of Aqueous Permanganate Ion

GEORGE ZIMMERMAN*
Department of Chemistry, Bryn Mawr College, Bryn Mawr, Pennsylvania
(Received August 20, 1954)

Quantum yields for the photochemical decomposition of aqueous MnO_4^- have been measured under a variety of conditions using a sensitive method for measuring O_2 production, first developed by Pringsheim and co-workers. The quantum yield was found to depend strongly on the wavelength of the light, slightly on temperature at the longer wavelengths, and not at all on the composition of the solution or on light intensity. Additional experiments were carried out which showed that the isotopic composition of photochemically produced O_2 was independent of the O-isotopic composition of the solvent water. These results lead to the conclusion that the radiant energy absorbed by the MnO_4^- ion is converted with high probability into vibrational energy of the ground state, after which the ion dissociates thermally into MnO_2 and O_2 (in a single act) or cools down without dissociation (the position of the extra electron is uncertain). A possible quantitative theory which predicts fairly successfully the dependence of the quantum yield on wavelength is outlined.

I. INTRODUCTION

FOR some time it has been known that neutral or alkaline-aqueous solutions of permanganates are photochemically decomposed[1] to give $O_2(g)$ and either $MnO_2(s)$ or $MnO_4^=(aq)$, the final product depending on the pH of the solution. Several studies[2,3] of this photochemical reaction have been made but do not seem to allow for more than an order-of-magnitude estimate of a quantum yield. The present work consists of measurements of quantum yields for the reaction under a variety of conditions, together with some tracer experiments using the isotope, O^{18}; from the experimental results a reasonably detailed mechanism for the primary photochemical process can be constructed.

Although MnO_4^- is thermodynamically unstable with respect to oxidizing water at all pH's, the rate of the reaction for neutral and moderately alkaline solutions is too small to detect at room temperature.[4] In highly alkaline solutions and acid solutions of $<$pH 3[5–7] the thermal decomposition increases considerably; therefore, because of this decreasing stability and also in order to preserve the identity of the light-absorbing species,[8] the experimental solutions were restricted to a pH range of 6.8 to 13.

It is possible that MnO_4^- could photosensitize the decomposition of H_2O into H_2 and O_2 as has been shown to be the case with BrO_3^-;[9] however, it has been found (in connection with the tracer experiments described below) that the gas produced photochemically was pure O_2 (100.0±0.5 percent).

* This work was carried out as a Lindsay Light and Chemical Company pre-doctoral fellow in the department of chemistry of the University of Chicago, and was presented there in partial fulfilment of the Ph.D. degree.

[1] J. H. Mathews and L. H. Dewey, J. Phys. Chem. **17**, 211 (1913).

[2] E. K. Rideal and R. G. W. Norrish, Proc. Roy. Soc. (London) **A103**, 342 (1923).

[3] A. L. Sundara Rao, Proc. Indian Acad. Sci. **6A**, 293 (1937).

[4] For example, over a period of nearly a year, no significant change could be found in the concentration of a neutral 0.004 m $KMnO_4$ solution, rigorously shielded from light. Also the same solution in a sealed tube heated to 300°C, held there for about 1 minute and cooled, showed only slight decomposition and that because of a heterogeneous reaction at the wall.

[5] J. Holluta, Z. physik. Chem. **115**, 143 (1925).

[6] F. R. Duke, J. Am. Chem. Soc. **70**, 3975 (1948).

[7] M. C. R. Symons, J. Chem. Soc. 3956 (1953); 3676 (1954).

[8] In acid solutions the molecules $HMnO_4$, $H_2MnO_4^+$, Mn_2O_7 begin to appear.

[9] L. Farkas and F. S. Klein, J. Chem. Phys. **16**, 886 (1943).

II. EXPERIMENTAL PROCEDURE

A. Measurement of the Photochemical Reaction Rate

In all experiments to be described, the rate of O_2 production was measured with the type of apparatus developed by Pringsheim, *et al.*[10,11] The method is based on the great sensitivity and the reproducibility of the reversible quenching of phosphorescence of the dye, trypaflavine (acriflavine), adsorbed on silica gel, by O_2 gas.[12] A typical quenching curve is shown in Fig. 1. Note that reasonable precision requirements limit one to O_2 partial pressures below about 15×10^{-5} mm Hg, as the quenching becomes quite insensitive to O_2 pressure at higher values.

The apparatus shown schematically in Fig. 2, is designed to record continuously the quenching caused by O_2 gas contained in a stream of N_2 gas at one atmosphere. Following the N_2 in its journey through the apparatus, we find [1] capillary flowmeter, [2] heated column containing finely divided copper to remove traces of O_2,[13] [3] test solution contained in a cell [Fig. 2(b)] with a sintered glass-gas bubbler to provide for rapid exchange of O_2 from solution to N_2 gas stream, [4] liquid N_2 cooled trap to remove water vapor from the gas stream, [5] trypaflavine phosphor, and [6] bubbler. Stopcocks are arranged so that different parts may be separately evacuated or flushed with pure N_2. The phosphorescence intensity is measured with a 931 A photomultiplier tube in conjunction with a Bequerel rotating sector phosphoroscope[14] with a period of 0.03 sec. The current from the photomultiplier tube is of the order of one μa and is amplified by a General Radio Company type 715 A, dc amplifier to around 5 ma and recorded on an Esteline-Angus recording dc milliammeter.

Figure 3 shows two examples of original records, (A) being a set of calibration measurements, and (B) being several measurements of photochemical production of O_2 from 0.004 m $KMnO_4$ solution.[15] The calibration is effected by introducing [from reservoir 7 in Fig. 2(a)] to part of the system, including the phosphor and initially evacuated, a small quantity of air; then measuring the pressure with a McLeod gauge while the quenching is recorded as in the figure. The sample of air is then pumped out and the procedure repeated to give a number of points. A total pressure of $<10^{-6}$ mm Hg is taken as the standard for "no oxygen" and gives to within 1 percent the same "base line" as carefully purified N_2 gas. Figure 3(A) shows that the quenching is completely and rapidly reversible, the only lag being a result of the finite speed of pumping out the gas. The small instability is typical and entirely due to electronic causes. A separate calibration was made before each run with a given solution; the calibration curves differ significantly but not greatly. In practice the test solution was flushed (to remove dissolved O_2) through a by-pass [Fig. 2 (A)], the phosphor remaining in vacuo. After sufficient flushing the gas stream was diverted into the phosphor section until the pressure therein had reached 1 atmosphere, whereupon the by-pass was closed and the gas stream caused to flow over the phosphor. With care this operation could be managed so that conditions in the cell remained constant throughout. The shape of the curves immediately after the illumination is started [Fig. 3(B); 1, 3, 5] or cut off [Fig. 3(B); 2, 4, 8] is due to (a) a 30-sec lag, representing the time for an element of the

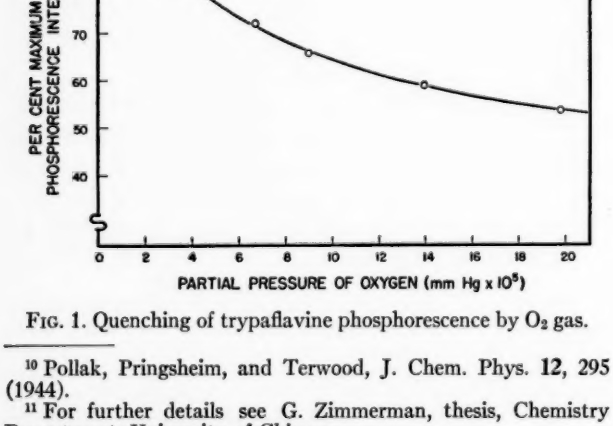

FIG. 1. Quenching of trypaflavine phosphorescence by O_2 gas.

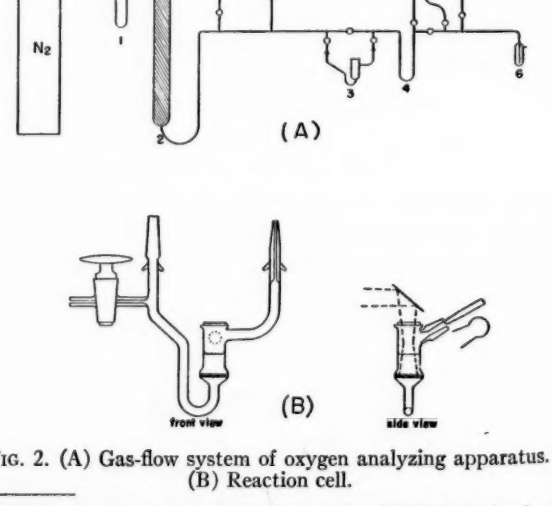

FIG. 2. (A) Gas-flow system of oxygen analyzing apparatus. (B) Reaction cell.

[10] Pollak, Pringsheim, and Terwood, J. Chem. Phys. **12**, 295 (1944).

[11] For further details see G. Zimmerman, thesis, Chemistry Department, University of Chicago.

[12] H. Kautsky and A. Hirsh, Z. anorg. u. allgem. Chem. **222**, 126 (1935).

[13] F. B. Meyer and G. Ronge, Z. angew. Chem. **52**, 63 (1939).

[14] P. Pringsheim, *Fluorescence and Phosphorescence* (Interscience Publishers, Inc., New York, 1949).

[15] All permanganate solutions were made with Baker's Analyzed Reagent grade $KMnO_4$.

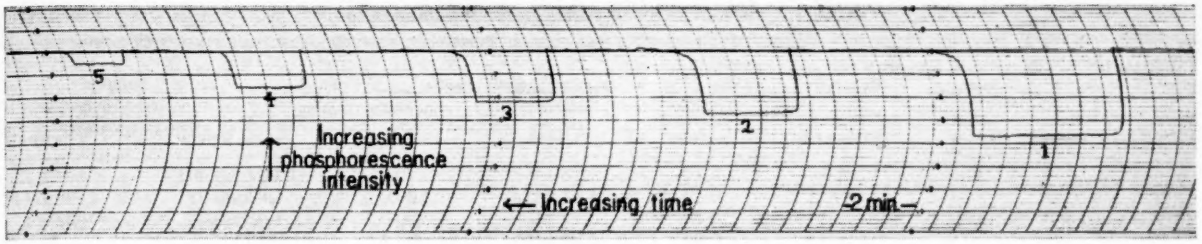

(A)

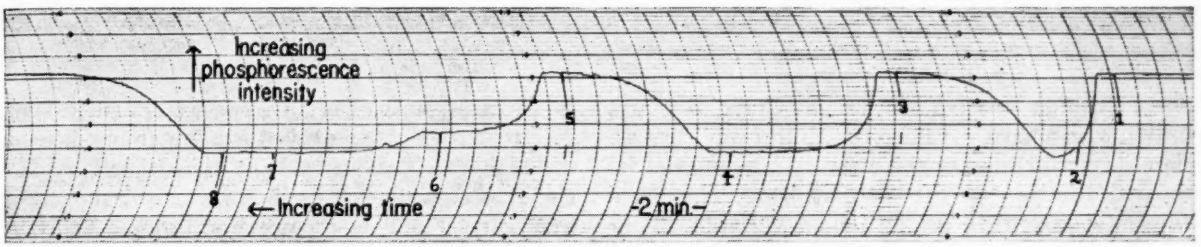

(B)

FIG. 3. (A) Record of calibration of the oxygen apparatus. (B) Record of photochemical oxygen production.

gas stream to travel from the cell to the phosphor (b) the saturation of the solution with O_2 and sweeping out of dissolved O_2. Measurements were made by adjusting the light intensity so that a steady state of photochemical O_2 production was reached [as at 4, 7, and 8 in Fig. 3(A)] within the range of calibration. Thus, knowing the carrier gas (N_2) flow rate and the quenching curve, the rate of O_2 production could be obtained. The small "background" quenchings often found were due to incomplete removal of traces of O_2 from the N_2 gas and not to any dark chemical reaction in the cell (see Table I for numerical examples). Since the total amount of reaction for a given run never exceeded 0.1 percent of the amount of reactant present, *initial rates* were measured, uncomplicated by the accumulation of significant amounts of products.

B. Measurements of Light Intensity

In studying quantum yields (nearly) monochromatic light was obtained by the use of mercury arcs and appropriate filters (to isolate lines).[16] For convenience single wavelengths will be written although in some cases the radiation actually consisted of several close lines. Speaking thus, the wavelengths used were (in A) 2537, 3130, 3650, 4050, 4360, and 5790. The 2357 A light came from a low-pressure mercury-arc lamp (G.E. 4-watt germicidal) and that of the other wavelengths from a high pressure mercury arc (usually G.E. AH4) with the glass envelope removed. In all cases the ac or dc power came from special voltage stabilizers. The optics used quartz lenses arranged so that there was a parallel portion of the beam within which could be mounted calibrated screens or filters and so that a slightly divergent pencil of light entered the reaction cell [Fig. 2(B)] through a quartz window at the top, having been reflected downwards by a front-surface aluminized diagonal mirror. For all solutions and wavelengths, light absorption in the reaction cell was complete or very nearly so, and thus was independent of small variations of the geometry of the solution, which was constantly stirred by streams of gas bubbles.

For all but the two longest wavelengths absolute quantum fluxes were measured actinometrically with uranyl-oxalate solution[17] irradiated in the reaction cell under the same conditions used with permanganate solutions. It was found that, after the sintered glass disk was wet with solution, 3 cc portions could be put into or taken out of the cell surprisingly reproducibly with a long hypodermic needle. To avoid volume changes in the solutions during long exposures, the N_2 gas was saturated with water vapor before it reached the cell. Relative quantum fluxes for the same wavelengths were checked periodically with the fluorescence photometer devised by Bowen[18]; relative quantum fluxes for the four longest wavelengths were measured with a Weston Type 1 photronic cell, using spectral sensitivity data supplied by the manufacturers. The uncertainty in the absolute quantum fluxes calculated for the two longest wavelengths was estimated to be ± 5 percent and for the other wavelengths ± 2 percent. The radiation from any given lamp was monitored at all times with the same type Weston Cell, refitted with a quartz window and placed so as to receive the radiation from either the mercury lamp or a standard carbon-filament lamp (U. S. Bureau of Standards) mounted in

[16] E. J. Bowen, *The Chemical Aspects of Light* (Oxford University Press, London, 1946), second edition.

[17] G. S. Forbes and L. J. Heidt, J. Am. Chem. Soc. **52**, 2363 (1934).

[18] E. J. Bowen, Proc. Roy. Soc. (London) **A154**, 349 (1936).

TABLE I. Quantum yields of permanganate decomposition.[a]

Wavelength	O_2 pressure, mm Hg $\times 10^5$ Background	Photochemical steady state	Corrected for background	N_2 flow rate cc per sec	O_2 molecules produced per sec $\times 10^{-11}$	Percent incident light absorbed	Photons absorbed per sec $\times 10^{-14}$	Quantum yield $\times 10^{-4}$
2537	0.8	12.9	11.9±0.1	6.79	4.78±0.5	100.0	0.087±0.003	550±25
3130	0.8	13.4	12.6±0.1	6.59	4.91±0.5	100.0	1.03±0.03	48±2
3650	0.4	10.2	9.8±0.1	6.53	3.78±0.5	100.0	1.65±0.03	23±1
4050	0.7	8.6	7.9±0.1	6.53	3.05±0.5	97.4	2.76±0.06	11.0±0.5
4360	0.5	6.1	5.6±0.1	6.53	2.16±0.5	95.6	13.4±0.3	1.61±0.07
5460	0.4	6.9	6.5±0.1	6.53	2.51±0.5	100.0	183±9	0.14±0.01
5780	0.4	2.2	1.8±0.1	6.53	0.69±0.5	100.0	69±4	0.10±0.01

[a] All data refer to a 0.01 m solution of $KMnO_4$, pH =6.8–7.0, 25–30°C; estimated uncertainties given.

a fixed position relative to the photronic cell and operated with a fixed voltage drop. In this way changes of intensity with time of the mercury lamps could be compared directly with the standard lamp. The measurements showed that the maximum variation of intensity over a period of several hours rarely exceeded 5 percent; however, from day to day, the maximum variation was about 10 percent. Intensities used to calculate quantum yields were corrected for these variations. The responses of the photronic cells were found to be strictly linearly dependent on the light intensity within the intensity ranges used.

C. Tracer Experiments with O^{18}

The principal experiment consisted of photochemically decomposing a solution of $KMnO_4$ of known O-isotopic composition in water also of known and different (about 2-fold enriched in O^{18}) 0-isotopic composition and comparing the isotopic composition of the O_2 gas formed with that of the $KMnO_4$ and the water. In addition the small (but not insignificant) rate of exchange of O atoms between MnO_4^- and H_2O at room temperature was measured, in order to be able properly to correct the results of the photochemical experiments.

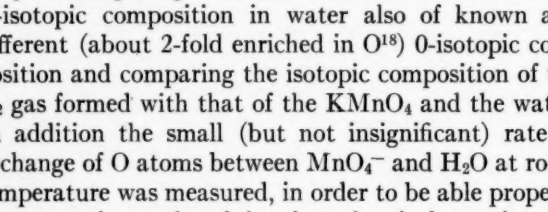

FIG. 4. Apparatus for tracer experiments.

In all cases samples of CO_2 gas were analyzed mass-spectrometrically for oxygen isotope abundances with the high precision instrument constructed by H. C. Urey and co-workers.[19] Preliminary chemical operations were carried out as follows: for isotopic analysis of water, the sample (about 6 cc of liquid) was equilibrated for a period of six days at a fixed temperature (28.1°C in this work) with about 20 cc of CO_2 gas at 1 atmosphere pressure. Since the amount of water is very much greater than the amount of CO_2, one can neglect the change in isotopic composition of the H_2O and assume safely that (after correcting for the equilibrium fractionation)[20] the composition of the CO_2 and H_2O are the same; for isotopic analysis of O_2, it was quantitatively converted to CO_2 by combination with the exactly equivalent amount of pure CO gas.[21] The apparatus for carrying out this conversion (Fig. 4) was designed to handle small amounts of gas (5 cc at 1 atmos) quantitatively. Starting with a sample of pure O_2 in a vessel connected at the ground joint, 7, the gas was expanded slowly into volume 2 of the Toepler pump through the liquid N_2 cooled trap, 6, to remove H_2O vapor present, then compressed into the calibrated volume, 4, and its volume and pressure carefully measured. This O_2 sample was then temporarily "stored" in the catalyst vessel (5). A sample of CO gas from the reservoir was then admitted to volumes 2, 3, and 4, and its pressure carefully adjusted so that the amount left in 4 would be equivalent to the amount of O_2. After the residual CO in volumes 2 and 3 was pumped out, that in 4 plus the O_2 in 5 were expanded into volume 2, and then alternately expanded and compressed on to the catalyst three or four times. The sample was transferred back to volume 4 in order to measure the amount carefully and then condensed in the trap with liquid N_2. The amount of residual noncondensible gas provided a sensitive test of completeness of the reaction, and showed that the average deviation from the correct stoichiometry in carrying out the conversion of O_2 to CO_2 was ±1 percent. The CO_2 sample condensed in the trap was pumped free of traces of noncondensible gas and

[19] H. C. Urey, Science **108**, 489 (1948).
[20] H. C. Urey, J. Chem. Soc. **562** (1947).
[21] Prepared by adding slowly (in vacuo) carefully purified sodium formate to pure, degassed, concentrated H_2SO_4.

TABLE II. Oxygen isotope analyses.

	Compound	Description of sample	Preparation for analysis	Isotopic composition[a]
1	$H_2O(l)$	Normal	CO_2 equilibrium	0.940
2		Enriched No. 1	CO_2 equilibrium	1.790
3		Enriched No. 2	CO_2 equilibrium	1.468
4		From HgO	CO_2 equilibrium	0.973
5	$CO_2(g)$	Reservoir	None	0.981
6	$CO(g)$	Reservoir	—	0.999 (calc)
7	$KMnO_4(s)$	Baker's analyzed reagent and the same recrystallized from normal H_2O	Thermal decomp., react O_2 with CO	0.940±0.004
8		Equilibrated in solution with enriched H_2O No. 1 for 20 hours, 25°C	Thermal decomp., react O_2 with CO	1.028
9	$O_2(g)$	From photochemical decomposition of solution of $KMnO_4$ in normal H_2O for 4 hours, 25°C	React with CO	0.923
10		From photochemical decomposition of solution of $KMnO_4$ in enriched H_2O for 4 hours, 25°C	React with CO	0.943

[a] Expressed as a fraction of percentage composition of an arbitrary standard.

distilled into the container, (*C*), now attached to the system at 7. For convenience in analysis, some of the CO_2 samples prepared as described were isotopically diluted with a measured amount of CO_2 of "normal" isotopic composition taken from the reservoir shown. In order to compare isotopic analyses of O_2 with those of H_2O, the isotopic composition of the CO gas was determined indirectly by splitting a portion of pure HgO into two parts, of which one was completely converted to Hg and O_2 by heating, and the other to Hg and H_2O by reduction with H_2 gas. The H_2O and O_2 of identical isotopic composition thus obtained were analyzed as described and the CO composition calculated (see Table II below for numerical examples).

Oxygen gas was obtained by either thermally decomposing dry $KMnO_4$ crystals or photochemically decomposing a solution. The thermal decomposition was carried out in the vessel (*B*) (Fig. 4) by rapid immersion in an oil bath at 290°C; at this temperature the decomposition reaction reached completion in less than one minute. Photochemically produced O_2 was collected in the vessel (*D*). The Pyrex heat filter, (*E*), fits into the space, (*D*), and the mercury lamp into the space, (*E*), so that nearly all the light is utilized for the photochemistry. An air-bubble lift pump, (*F*), circulated copper-sulfate solution through (*E*) and through the condenser, thus keeping the solution in (*D*) close to 25°C. In carrying out a photochemical decomposition, the vessel (*D*) was filled up to the bulb with $KMnO_4$ solution and sealed to the system at 7 with Apiezon W wax. The dissolved air was pumped out and the O_2 gas produced photochemically, collected as described. To test for the O exchange between MnO_4^- and H_2O, solutions were equilibrated in the vessel shown in (*B*), Fig. 4, and water was rapidly pumped off, the solid $KMnO_4$ thoroughly pumped and then decomposed as described. All solutions were made with reagent grade $KMnO_4$ and normal or enriched water,[22] and along with each photochemical experiment was run a dark and illuminated exchange control.[23,24]

III. EXPERIMENTAL RESULTS

The quantum yield, ϕ, of O_2 production[25] was found to be independent of steady and varying light intensity to an estimated precision of 1 percent. Figure 3(B) shows one of several experiments (wavelength = 3650 A) with flashing light. The flat portion of the curve immediately before point 7 represents a steady O_2 production under illumination produced by interrupting the light of a dc mercury arc 240 times a second with a rotating sector which diminished by exactly one-half the intensity of the arc. At point 7 the sector was quickly stopped in the "open" position and a screen (which also halved the intensity) inserted in the parallel portion of the light beam; as can be seen, the O_2 production, and hence the quantum yield, remained constant. At point 6 both screen and rotating sector were serving to quarter the average intensity and the calculated O_2 pressure for this plateau is 6.3×10^{-5} mm Hg, as compared with 12.7 for the plateau at 7, demonstrating no dependence on intensity. This sort of result established the independence on intensity over about a ten-fold range of variation for each wavelength. The flashing light experiments suggest the absence of any not-too-rapid competing dark-back reactions of chemical inter-

[22] About seven-fold enriched (about 1.5 percent O^{18}) D_2O (Stewart Oxygen Company, authorized by the U. S. Atomic Energy Commission) was the starting material; for all the experiments portions of this were diluted with normal H_2O to give an approximately two-fold enriched sample. The small deuterium error introduced in the calculation of the H_2O-CO_2 equilibrium constants by the presence of deuterium is insignificant here.

[23] J. P. Hunt and H. Taube, J. Chem. Phys. **19**, 602 (1951).

[24] H. Taube and J. P. Hunt, J. Am. Chem. Soc. **74**, 5999 (1952).

[25] Defined as $\dfrac{O_2 \text{ molecules produced per second}}{\text{photons absorbed per second}}$.

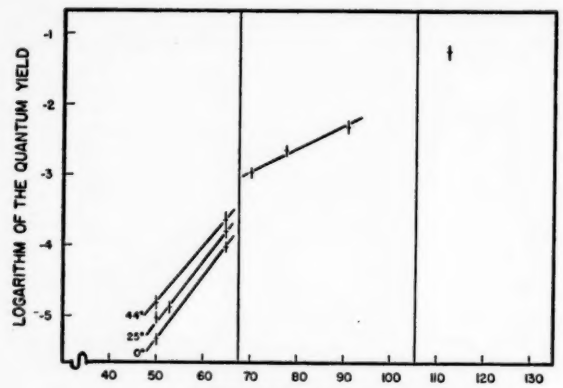

FIG. 5. Quantum yield of permanganate ion decomposition as a function of wavelength.

mediates[26] and made it possible to use 60-cycle-ac or dc mercury arcs interchangeably.

The dependence of ϕ on wavelength is shown in Table I and Fig. 5. The basic measurements needed for the calculation of ϕ are included in the table as a sample of the magnitudes involved. In Fig. 5 the estimated accuracy for each point is given by the length of the vertical line; the vertical lines dividing the graph represent the position of the minima between the three-electronic absorption bands of the MnO_4^- spectrum (see Fig. 6). Irradiation with red light (45 kcal) resulted in a definite photochemical reaction for which ϕ would fall roughly on the line in Fig. 5. This result is omitted because of its poor precision.

Table III summarizes some typical evidence for concluding that, within the experimental uncertainty, ϕ is independent of the concentration of MnO_4^-, pH (within the limits set), and the presence in the solution of Cl^- or $MnO_4^{=}$. It was thought that Cl^- or $MnO_4^{=}$ might act as inhibitors by reaction with unstable intermediates.

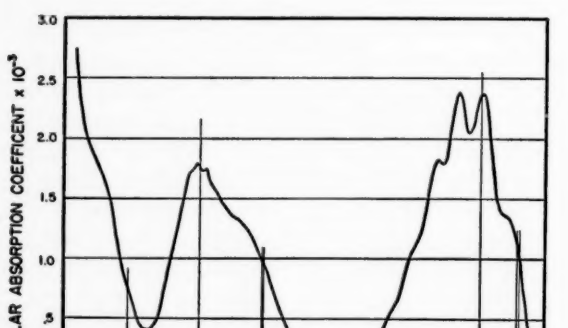

FIG. 6. Absorption spectrum of aqueous permanganate ion.

[26] W. A. Noyes, Jr. and P. A. Leighton, *The Photochemistry of Gases* (Reinhold Publishing Corporation, New York, 1941), pp. 202–209.

Only with light of wavelengths 4360 A or greater was ϕ found to be significantly temperature dependent (see Fig. 5). The strongest temperature dependence was found with light of the longest wavelength (5780 A); an Arrhenius plot for the wavelength yielded an apparent "activation energy" of 4 kcal/mole. The temperature dependence decreased slightly with decreasing wavelength.

The MnO_4^-—H_2O oxygen exchange rate has been previously studied by Mills[27] and by Hall and Alexander,[28] in both cases at 100°C only, with concentrated solutions, and by analyzing the water through density differences. Their results show that exchange in neutral solution at 100°C is practically complete in 4–12 hrs, there being no significant difference within wide limits of error for alkaline solutions. Present results (e.g., 8, Table II) yield an average initial rate of 0.5 percent exchange per hour for dilute, neutral solutions[29] at 25°C±2° (precision not high because of poor temperature control). Table II shows typical results for thermal and photochemical decomposition of MnO_4^-; the small difference between 7 and 9 is no doubt due to different fractionations. If 10 is corrected for the small amount of exchange[30] taking place during the irradiation, agreement with 9 is better than 0.5 percent (similarly with two duplicate experiments). From this one can conclude unambiguously that all the O_2 gas produced comes from the MnO_4^- ions.[24]

IV. DISCUSSION OF THE MECHANISM

The experimental facts can be summarized as follows: (1) The quantum yield, ϕ, is small compared with unity and decreases monotonically with increasing wavelength from 0.05 at 2537 to 10^{-5} at 5790 A (Fig. 5); (2) ϕ is independent of pH, concentrations of reactant, products, and possible inhibitors (there is no indication of thermal back reactions); (3) at the longer wavelengths only, there is a small positive-temperature coefficient of ϕ, decreasing with decreasing wavelength; (4) All of the atoms of the photochemically produced O_2 came from the MnO_4^- ions. These results show that the primary photochemical reaction[31] must be a simple dissociation of the MnO_4^- into two fragments and that no appreciable electron exchange between the dissociation fragment destined to become O_2 and H_2O or OH^- can occur. Table IV gives the reasonable possibilities and estimated values of ΔH^0 for each. One might guess that the energy for a single dissociation into MnO_2 and O_2 (neglecting for the moment the position of the

[27] G. A. Mills, J. Am. Chem. Soc. **62**, 2833 (1940).

[28] N. F. Hall and O. R. Alexander, J. Am. Chem. Soc. **62**, 3455 (1940).

[29] In solutions of pH near 1 exchange was complete in 20 minutes.

[30] Irradiation did not have any noticeable effect on the rate of exchange.

[31] The course of the thermal reactions subsequent to the primary photochemical process to give chemically stable final products will not be considered; the possibilities are restricted, however, by the tracer result.

TABLE III. Dependence of quantum yield on composition of solution.[a]

	pH[e]→	6.8	7.0	7.0	6.9	10	12.6	14	13[b]	14[e]	
	MnO_4^-→molarity	0.01	0.004	0.001	0.0004	0.004	0.01	0.005	0.004	0.005	Average[d]
Quantum yield for	λ=2537→	5.5	5.4	5.1	5.6	—	5.6	5.1	—	5.4	$5.4\pm0.2\times10^{-2}$
	λ=3650→	2.3	2.0	2.0	1.9	2.1	2.1	2.0	2.0	2.2	$2.1\pm0.1\times10^{-3}$
	λ=5640→	1.4	1.4	1.3	1.3	1.3	1.5	1.5	—	—	$1.4\pm0.1\times10^{-5}$

[a] All quantum yields in any row should be multiplied by the power of ten given in the last column.
[b] 0.1 m KCl added.
[c] 0.0005 m K_2MnO_4 added.
[d] Mean deviations given.
[e] Measured with a glass electrode.

electron) would be smaller than for dissociation into MnO_3 and O. A mode of vibration of the tetrahedral MnO_4^- consisting of the proper superposition of two nondegenerate normal modes (of class F_2) could lead to a dissociation where simultaneously two Mn−O bonds are broken and an O−O bond formed. Roughly speaking, if the O−O bond energy (118 kcal/mole) is larger than the average Mn−O bond energy, our guess might be correct. This qualitative feeling is confirmed by the ΔH^0 values in Table IV; the height of the energy barrier for dissociation would certainly be larger than these ΔH^0's, which refer to final equilibrium states, i.e., to physically though not chemically stable intermediates. From the observed photochemistry, it seems as though the first two possibilities in Table IV must be ruled out; for, taking radiation of the lowest energy which still gives rise to photochemistry, 45 kcal, and adding 5–10 kcal as the maximum thermal energy which is available for the dissociation, one obtains 50–55 kcal as the upper limit for ΔH^0 of any possible dissociation reaction. If, as there is reason to believe from similar photochemical behavior at other wavelengths, the primary reaction is the same for all wavelengths, we can conclude that MnO_4 dissociates into MnO_2 and O_2, where the position of the extra electron is left uncertain. Additional evidence against the presence of O^- or O as an intermediate is provided by the failure of Cl^- or $MnO_4^=$ to inhibit, and the lack of exchange of O mentioned before.[32]

The absorption spectrum of MnO_4^- (see Fig. 6)[33] consists of three distinct bands representing electronic excited states. The two longer wavelength bands show traces of vibrational structure which become sharp lines for solid solutions of MnO_4^- at −253°C;[34] these bands have been explained and analyzed successfully in terms of a molecular orbital treatment by Wolfsberg and Helmholz.[35] The short wavelength band shows no structure under any conditions (so far), and may represent an electron transfer spectrum involving the neighboring solvent molecules.[36,37] Most probably the short wavelength band, and certainly, the other two represent transitions to stable-electronic excited states; hence, the absence of fluorescence of MnO_4^- solutions implies, roughly, that the half-life of the excited state is $\sim10^{-12}$ seconds, and that within this time interval predissociation or internal conversion must occur with a high

TABLE IV. Heats of reaction.

Oxidation number of Mn in product	Products[g] of decomposition	Estimated ΔH^0 for MnO_4^-→products (kcal/mole)
6	MnO_3 $+O^-$ −79[a] +20[b]	+71±10
5	MnO_3^- $+O$ −75[a] +56[c]	+111±10
4	$MnO_2(c)+O_2^-$ −124 +3[d]	+9[f]
3	MnO_2^- $+O_2$ −115[e] −4	+11±5

[a] Estimated as follows: from the series, $MnO_3+H_2O\xrightarrow{1}H_2MnO_4\xrightarrow{2}MnO_4^{--}+2H^+$ the ΔH^0 of formation of MnO_3 may be related to that of MnO_4^{--} if ΔH^0's for 1 and 2 are known. Assume that ΔH^0 for 1 is small and negative; for 2, ΔF^0 and ΔS^0 come from guessing the ionization constants and entropies from the semiempirical generalizations discussed in W. M. Latimer [*Oxidation Potential* (Prentice-Hall, Inc., New York, 1952), second edition]; R. E. Connick and R. E. Powell, [J. Chem. Phys. **21**, 2206 (1953)] and E. L. King [J. Chem. Educ. **30**, 71 (1953) (see also references in bibliography)]. There is perhaps as much as 10 kcal uncertainty, probably less. These values (hence those in the third column) are lower limits because of the assumption regarding step 1. The ΔH^0 for MnO_4^{--} comes from the ΔF^0 given in Latimer, plus an entropy estimated according to Connick and Powell. The procedure is similar for MnO_3^-; here ΔF^0 for the ion, MnO_4^{---} [see H. Lux, Z. Naturforsch. **1**, 281 (1946)] is estimated by considering that (from semiquantitative observations) about equal concentrations (10^{-2} m) of MnO_4^{---} and MnO_4^{--} exist in equilibrium with $MnO_2(c)$ and with $a_{OH^-}=10$.

[b] Calculated from the sequence, $O(g)\xrightarrow{1}O^-(g)\xrightarrow{2}O^-(aq)$; the value for 1 is from M. Metlay and G. E. Kimball, J. Chem. Phys. **16**, 774 (1948), that in Latimer being from older data and probably less reliable. For 2 the hydration energy of O^- relative to Cl^- is estimated from a plot against $1/r$ (r = ionic radius).

[c] The heat of solution was assumed to be about the same as for argon [see also N. Uri, Chem. Revs. **50**, 375 (1952)].

[d] ΔF^0 is taken from Latimer; S^0 is guessed to be 10±10 eu (see also Uri).

[e] ΔF^0 obtained from estimated solubility of $Mn(OH)_3$ in concentrated NaOH; S^0 taken from Connick and Powell.

[f] What is really wanted would involve molecularly dissolved MnO_2, hence this value would need to be increased by 10 or 20 kcal.

[g] The numbers under the molecules are estimated ΔH^0's of formation from the elements; except where noted all values are for dilute aqueous solutions. Where not explicitly noted thermodynamic values come from Latimer.

[32] There is evidence for exchange between OH (or O^-) and H_2O in Forshheimer and Taube, J. Am. Chem. Soc. **74**, 3705 (1952).

[33] Measured with a Beckman spectrophotometer (Model DU).

[34] J. Teltow, Z. physik. Chem. **B40**, 397 (1938); **B43**, 198 (1939).

[35] M. Wolfsberg and L. Helmholz, J. Chem. Phys. **20**, 837 (1952).

[36] E. Rabinowitch, Revs. Modern Phys. **14**, 112 (1942).

[37] J. Franck and R. L. Platzman, *L. Farkas Memorial Volume. Research Council of Israel Special Publication No. 1* (Interscience Publishers, Inc., New York, 1952).

TABLE V. Theoretical and observed quantum yields.

Wavelength A	$\phi_{obs} \times 10^4$	$\phi_{calc} \times 10^4$
2537	550	282
3130	48	70
3650	23	22
4050	11	6
4360	1.6	1.4

probability.[38] The latter alternative seems preferable; i.e., that the molecule undergoes a radiationless transition to a high vibrational level of the ground state. If, however, predissociation occurs, the small quantum yields would have to be ascribed to primary recombination of the two fragments remaining in the same solvent "cage" and the dependence of yield on wavelength to a greater probability of escape of the more energetic fragments. It seems more likely that internal conversion produces "hot" (i.e., containing excess vibrational energy) MnO_4^- ions which dissociate thermally with a certain probability within the interval of "cooling off." Thus, one would expect the probability of dissociation (hence the quantum yield) to increase with decreasing wavelength since the molecule has available more energy and a longer time interval for dissociation. One might expect also that when the excitation energy differs only slightly from the threshold energy (for dissociation) the amount of equilibrium thermal energy contained in the molecule before excitation would begin to influence the dissociation probability and hence give rise to the temperature dependence found at the longer wavelengths.

A quantitative theory for the dependence of quantum yield on wavelength based on the above picture and following the ideas of Eyring, *et al.*,[39] Magee,[40] and others[41] can be constructed as follows: Assume that all excess electronic energy of a molecule which has just absorbed a photon becomes vibrational energy (of the ground state) and becomes randomly distributed among the various modes within a time interval short compared to the cooling time. The "hot" molecule cools according to the solution of the heat-conduction equation for a point source in an infinite medium. If the initial ($t=0$) electronic energy is E, the energy at any time, t, thereafter is e, and the equilibrium thermal energy is e_{Av}, then $e=e_{Av}+(E-e_{Av})e^{-bt}$, where b is a constant depending on the solvent. Let the probability that a hot molecule decompose within a time interval, dt, be $P(t)dt$; since e and t are functionally related, $P(t)dt=p(e)dt$. Assume that $p(e)=k_1(1-e^0/e)^{n-1}$ for $e>e^0$ and 0 for $e<e^0$; for a given type of molecule k_1 is a constant, and e^0 is a threshold energy below which no dissociation can occur. This relationship has been derived by Kassel[42] and others[41] for the case of n weakly coupled classical oscillators and applies to one particular mode of dissociation (which may be degenerate). The quantum yield, ϕ, being the total probability that the molecule will dissociate at some time, becomes for the above assumptions (and neglecting e_{Av} compared to the values of e in which we are interested)

$$\phi=k_2\int_{e^0/E}^{1}\frac{(1-x)^{n-1}}{x}dx,$$

where $x=e^0/e$. The function $1/x$ varies with e so weakly compared to the rest of the integrand that it can be considered constant, giving

$$\phi=k_3(1-e^0/E)^n.$$

For very large E, ϕ should approach 1, hence $k_3=1$. Assuming, as before that $e^0=50$ kcal/mole, the best fit with the experimental data is found for $n=6$ (see Table V). In view of the rather drastic assumptions made, it is not surprising that n is less than 9, and it seems reasonable to conclude that the experimental data is quantitatively consistent with the mechanism described.

ACKNOWLEDGMENT

The author wishes to express his appreciation to Professor James Franck for his advice and encouragement at all stages of this work, and to Professor H. C. Urey and co-workers for the mass-spectrographic analyses.

[38] J. Franck and H. Sponer, *Contribution to the Study of Molecular Structure* (Maison Desoer, Liege, 1947–1948).

[39] Rosenstock, Wallenstein, Wahrhaftig, and Eyring, Proc. Natl. Acad. Sci. U. S. **38**, 667 (1952).

[40] J. L. Magee, Proc. Natl. Acad. Sci. U. S. **38**, 764 (1952).

[41] See bibliographies in references 39 and 40.

[42] L. S. Kassel, J. Phys. Chem. **32**, 225 (1928).

Substituted Methanes. XXVI. Raman and Infrared Spectral Data, Assignments, Potential Constants, and Thermodynamic Properties for $CHBrCl_2$ and $CDBrCl_2$*

SANTIAGO R. POLO,† ANN PALM, FRED L. VOELZ, FORREST F. CLEVELAND, AND ARNOLD G. MEISTER,
Spectroscopy Laboratory,‡ Department of Physics

AND

RICHARD B. BERNSTEIN§ AND ROBERT H. SHERMAN, *Department of Chemistry,*
Illinois Institute of Technology, Chicago 16, Illinois

(Received August 30, 1954)

Raman displacements, semiquantitative relative intensities, and quantitative depolarization factors for liquid bromodichloromethane and deuterobromodichloromethane, as well as infrared wave numbers and percent transmission curves for both the liquid and gas in the region 400–4000K (K = kaysers = cm^{-1}), were obtained and compared with previous data. Assignments were made for both molecules and a reasonable set of potential constants was determined by use of Wilson's FG matrix method. The heat content, free energy, entropy, and heat capacity were calculated for 12 temperatures from 100° to 1000°K.

INTRODUCTION

RAMAN displacements and estimated relative intensities for liquid $CHBrCl_2$ have been obtained in three investigations.[1–3] One determination[4] of the depolarization factors has been made, but this did not yield any definite conclusions as to the polarization state of four of the lines (fundamentals).

Infrared spectral data for $CHBrCl_2$ also have been

TABLE I. Raman spectral data for liquid bromodichloromethane ($CHBrCl_2$).[a]

Bonino, Brüll		Kohlrausch, Köppl		Delwaulle, Francois		Glockler, Leader		Present results			Probable values			
$\Delta\sigma$	I_e	$\Delta\sigma$	I_e	$\Delta\sigma$	PS	$\Delta\sigma$	I_e	$\Delta\sigma$	I	ρ	$\Delta\sigma$	I	ρ	PS
225	5	218	10	218	···	214.6 220.4	9 10	219	100	0.65	215 220	100	0.65	P
330	4	329	7	329	P	329.6	8	329	74	0.24	330	74	0.24	P
···	···	···	···	···	···	···	···	384	vvw	···	384	vvw	···	···
···	···	···	···	···	···	···	···	437	vvw	···	437	vvw	···	···
···	···	···	···	···	···	···	···	549	vw	···	549	vw	···	···
606	5	600	8	600	P	601.7	9	602	82	0.14	602	82	0.14	P
···	···	···	···	···	···	···	···	663	vw	···	663	vw	···	···
720	3	716	4b	716	···	718.8	4b	719	20	0.77	719	20	0.77	P
760	2	760	3	760	···	760.0	3d	763	8	0.83	761	8	0.83	D
···	···	···	···	···	···	···	···	(821)	vvw	···	(821)	vvw	···	···
···	···	···	···	···	···	···	···	939	vvw	···	939	vvw	···	···
···	···	···	···	···	···	···	···	1047	vvw	···	1047	vvw	···	···
1181	1.5	1165	2	1166	P	1170.8	2	1171	6	0.64	1171	6	0.64	P
···	···	1204	1	1204	D	1214.3	1	1214	4	0.82	1214	4	0.82	D
···	···	···	···	···	···	···	···	(1319)	vvw	···	(1319)	vvw	···	···
···	···	···	···	···	···	···	···	(1364)	vvw	···	(1364)	vvw	···	···
···	···	···	···	···	···	···	···	(1389)	vvw	···	(1389)	vvw	···	···
···	···	···	···	···	···	···	···	(1432)	vw	···	(1432)	vw	···	···
···	···	···	···	···	···	···	···	(1472)	vvw	···	(1472)	vvw	···	···
···	···	···	···	···	···	···	···	1515	vw	···	1515	vw	···	···
···	···	···	···	···	···	···	···	(1777)	vvw	···	(1777)	vvw	···	···
···	···	···	···	···	···	···	···	(1886)	vvw	···	(1886)	vvw	···	···
···	···	···	···	···	···	···	···	(2331)	vvw	···	(2331)	vvw	···	···
···	···	···	···	···	···	···	···	(2390)	vvw	···	(2390)	vvw	···	···
···	···	···	···	···	···	···	···	(2418)	vvw	···	(2418)	vvw	···	···
3025	3	3017	4b	3017	P	3020.5	5	3022	22	0.25	3021	22	0.25	P
···	···	···	···	···	···	···	···	(3462)	vvw	···	(3462)	vvw	···	···

[a] $\Delta\sigma$ = Raman displacement in K; I_e = estimated relative intensity (b = broad, d = diffuse); I = relative intensity obtained with a microdensitometer or microphotometer (w = weak, v = very); ρ = depolarization factor; PS = polarization state (P = polarized, D = depolarized); and uncertain values are enclosed in parentheses.

* Presented in part at the Chicago meeting of the American Physical Society, November, 1950 [Phys. Rev. **81**, 300 (1951)] and at the Columbus meeting of the Division of Chemical Physics of the American Physical Society, June, 1951.

† Present address: Department of Chemistry, Harvard University, Cambridge, Massachusetts.

‡ Publication No. 110.

§ Present address: Department of Chemistry, University of Michigan, Ann Arbor, Michigan.

[1] G. B. Bonino and L. Brüll, Atti accad. nazl. Lincei **13**, 789 (1931); Chem. Absts. **26**, 1189 (1932).

[2] K. W. F. Kohlrausch and F. Köppl, Sitzber. Akad. Wiss. Math-naturw. K. IIb, **143**, 537 (1935); Monatsh. Chem. **65**, 185 (1935).

[3] G. Glockler and G. L. Leader, J. Chem. Phys. **8**, 699 (1940).

[4] M. L. Delwaulle and F. Francois, J. phys. radium **7**, 15 (1946).

TABLE II. Infrared spectral data for bromodichloromethane ($CHBrCl_2$).[a]

Plyler, Benedict		Liquid Present results		Probable values		Gas Present results	
σ	I	σ	I	σ	I	σ	I
330[b]	m			330	m		
383	w			383	w		
437	w	435[c]	w	436	w	...	...
495	w	495	w	495	w	494	w
552	w	546	w	549	w	545	w
604	s	600	s	602	s	602	s
643	m	658	m	658	m	666	m
719	vs	719	vs	719	vs	731 737	s s
760	vs	759	vs	759	vs	768 777	s s
795	m	...	...	795	m	...	...
814	w	812	s	813	s	...	...
843	vw	842	m	842	m	...	...
858	w	...	...	858	w	...	...
884	w	881	w	883	w	...	...
916	w	914	w	915	w	...	...
924 942	w w	932	w	932	w	...	...
...	...	976	w	976	w	...	...
1004	vw	...	...	1004	vw	...	...
1052	w	1055	w	1054	w	...	...
1066 1114	w w	1074	m	1074	m	...	...
1168	s	1169	vs	1169	vs	1172 1181	vs vs
1189	m	...	...	1189	m	...	...
1211	s	1214	vs	1213	vs	1212 1221	vs vs
1312	w	1316	m	1314	m	(1333)	w
1385	vw	1386	m	1386	m	1391	m
1414	vw	1417	vw	1416	vw	...	...
...	...	1446	m	1446	m	...	...
...	...	1472	m	1472	m	1493	m
1506	w	1506	m	1506	m	...	...
...	...	1515	m	1515	m	1533	w
1592	w	1601	m	1601	m	...	...
...	...	1732	w	1732	w	...	...
...	...	1775	m	1775	m	...	...
...	...	2326	m	2326	m	...	...
2421	w	2420	m	2420	m	2422	vw
3040	s	3022	vs	3022	vs	3028	m
3077	vw	...	...	3077	vw	...	...
...	...	3615	m	3615	m	...	...
3802	vw	...	...	3802	vw	...	...
4237	m	...	...	4237	m	...	...
4291	w	...	...	4291	w	...	...
4504	vw	...	...	4504	vw	...	...

[a] σ = wave number in K at the point of maximum absorption, and I = intensity (w = weak, m = medium, s = strong, v = very).
[b] Not investigated below 263 K. Plyler (reference 5) obtained 330, 381, and 437 K for the first three bands.
[c] Not investigated below 400 K.

reported.[5,6] However, no Raman or infrared data for $CDBrCl_2$ were found in the literature.

The present paper reports for both molecules Raman and infrared spectral data, assignments, quadratic potential constants, and calculated thermodynamic properties.

EXPERIMENTAL PROCEDURES

The method of preparation has been described.[7] The samples were purified by fractional distillation in an all-glass system and the Raman spectra were obtained with the samples sealed *in vacuo*. Samples contained 100, 85, and 60 percent $CHBrCl_2$, the remainder being $CDBrCl_2$.

The Raman spectra were obtained as described in previous papers of this series. The infrared spectra were obtained with the spectrometers: Beckman IR-2 (KBr optics) and Perkin-Elmer 12C single-beam and 21 double-beam (NaCl optics). With the Beckman, the gas and liquid cells were 10 cm and 0.11 mm in thickness, respectively; with the Perkin-Elmer, gas cells of 5 and 10 cm thickness and liquid cells of 0.05 and 0.11 mm were used.

SPECTRAL DATA

$CHBrCl_2$

The Raman spectral data for $CHBrCl_2$ are summarized in Table I. The infrared spectral data are given in Table II, and the percent transmission curves are shown in Figs. 1(a) and 1(b). In Table III, the probable Raman and infrared spectral data are given, together with the assignments and calculated wave numbers.

$CDBrCl_2$

The present Raman and infrared spectral data for $CDBrCl_2$, obtained in the presence of $CHBrCl_2$, are given in Table IV, along with the assignments and calculated wave numbers. The infrared percent transmission curves for the $CDBrCl_2$, $CHBrCl_2$ mixture are shown in Figs. 2, 3(a), 3(b), and 4.

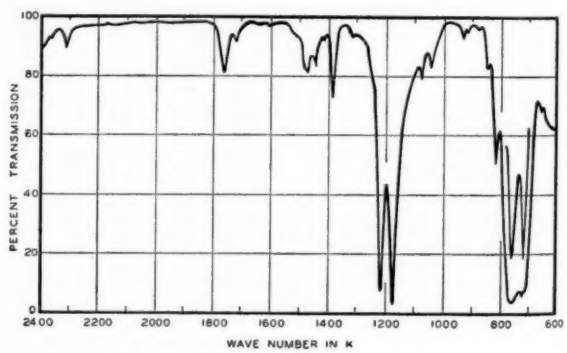

(a)

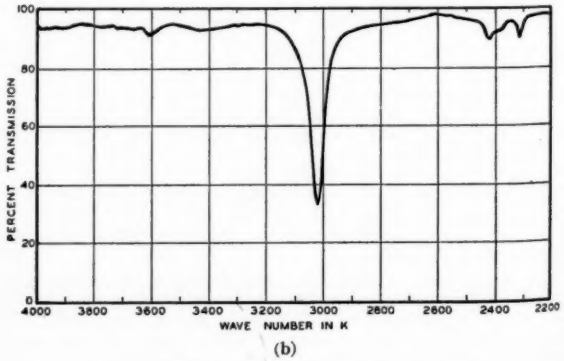

(b)

FIG. 1. Infrared absorption bands for liquid $CHBrCl_2$ (NaCl optics).

[5] E. K. Plyler, J. Chem. Phys. **17**, 218 (1949).
[6] E. K. Plyler and W. S. Benedict, J. Research Natl. Bur. Standards **47**, 202 (1951).
[7] R. H. Sherman and R. B. Bernstein, J. Am. Chem. Soc. **73**, 1376 (1951).

The line at 219 K was unresolved. However, its measured displacement is the same as that measured for the corresponding line in $CHBrCl_2$, which indicates no shift in displacement from $CHBrCl_2$ to $CDBrCl_2$. It is therefore reasonable to assume that this line corresponds to the unresolved doublet 215, 220 K, as observed by Glockler and Leader for $CHBrCl_2$ (see Table I).

NORMAL COORDINATE TREATMENT

As a check on the assignments and to establish a set of potential constants, a normal coordinate treatment (FG-matrix method[8]) was carried out for each molecule with the most general quadratic potential energy function. The notations for the potential constants[9] and the F- and G-matrix elements[10] have been given previously.

Values for some of the potential constants were transferred from structurally related molecules, with subsequent modification. The revised set of potential constants is given in Table V. This set is the result of

TABLE III. Probable values for the Raman and infrared spectral data, calculated wave numbers, and assignments for liquid $CHBrCl_2$.[a]

Raman $\Delta\sigma$	Raman I	PS	Infrared σ	Infrared I	σ_c	Theoretical assignment	Type
215 / 220	100	P	Not investigated below 263K		**215**[b] / **226**	σ_9 / σ_6	a'' / a'
330	74	P	330	m	**322**	σ_5	a'
384	vvw	···	383	w	*382*	$\sigma_4-\sigma_6$	A'
437	vvw	···	436	w	*440*	$2\sigma_6$	A'
···	···	···	495	w	*495*	$\sigma_7-\sigma_3$	A''
549	vw	···	549	w	*550*	$\sigma_5+\sigma_6$	A'
602	82	P	602	s	**595**	σ_4	a'
663	vw	···	658	m	*660*	$2\sigma_5$	A'
719	20	P	719	vs	**708**	σ_3	a'
761	8	D	759	vs	**761**	σ_8	a''
···	···	···	795[c]	m	*784*	$\sigma_7-2\sigma_9$?	A''
(821)	vvw	···	813	s	*817*	$\sigma_4+\sigma_9$	A''
···	···	···	842	m	*840*	$\sigma_2-\sigma_5$	A'
···	···	···	858[c]	w	*875*	$2\sigma_5+\sigma_9$?	A''
···	···	···	883	w	*884*	$\sigma_7-\sigma_5$	A''
···	···	···	915	w	*932*	$\sigma_4+\sigma_5$	A'
939	vvw	···	932	w	*939*	$\sigma_3+\sigma_6$	A'
···	···	···	976	w	*980*	$\sigma_6+\sigma_8$	A''
···	···	···	1004	vw	*999*	$\sigma_7-\sigma_9$	A'
1047	vvw	···	1054	w	*1049*	$\sigma_3+\sigma_5$	A'
···	···	···	1074	m	*1090*	$\sigma_5+\sigma_8$	A''
1171	6	P	1169	vs	**1167**	σ_2	a'
···	···	···	1189[c]	m	*1190*	$2\sigma_8-\sigma_5$?	A'
1214	4	D	1213	vs	**1214**	σ_7	a''
(1319)	vvw	···	1314	m	*1321*	$\sigma_3+\sigma_4$	A'
(1364)	vvw	···	···	···	*1362*	$\sigma_4+\sigma_8$	A''
(1389)	vvw	···	1386	m	*1390*	$\sigma_2+\sigma_6$	A'
(1432)	vw	···	1416	vw	*1429*	$\sigma_7+\sigma_9$	A'
···	···	···	1446	m	*1438*	$2\sigma_3$	A'
(1472)	vvw	···	1472	m	*1479*	$\sigma_3+\sigma_8$	A''
···	···	···	1506	m	*1500*	$\sigma_2+\sigma_5$	A'
1515	vw	···	1515	m	*1520*	$2\sigma_8$	A'
···	···	···	1601	m	*1600*	$\sigma_2+2\sigma_9$	A'
···	···	···	1732	w	*1740*	$\sigma_6+2\sigma_8$	A'
(1777)	vvw	···	1775	m	*1772*	$\sigma_2+\sigma_4$	A'
(1886)	vvw	···	···	···	*1889*	$\sigma_2+\sigma_3$	A'
(2331)	vvw	···	2326	m	*2340*	$2\sigma_2$	A'
(2390)	vvw	···	···	···	*2384*	$\sigma_2+\sigma_7$	A''
(2418)	vvw	···	2420	m	*2419*	$\sigma_1-\sigma_4$	A'
3021	22	P	3022	vs	**3041**	σ_1	a'
···	···	···	3077	vw	*3100*	$\sigma_8+2\sigma_2$	A''
(3462)	vvw	···	···	···	*3461*	$\sigma_1+2\sigma_6$	A'
···	···	···	3615	m	*3623*	$\sigma_1+\sigma_4$	A'
···	···	···	3802	vw	*3781*	$\sigma_1+\sigma_8$	A''
···	···	···	4237	m	*4235*	$\sigma_1+\sigma_7$	A''
···	···	···	4291	w	*4342*	$\sigma_1+\sigma_3+\sigma_4$	A'
···	···	···	4504	vw	*4541*	$\sigma_1+2\sigma_8$	A'

[a] Symbols have the same meaning as in Tables I and II.
[b] Normal coordinate values (bold face); combinations and overtones (italics) calculated from observed wave numbers for the liquid. See Table VI.
[c] Observed only by Plyler and Benedict, not in the present investigation.

TABLE IV. Raman and infrared spectral data, calculated wave numbers, and assignments for $CDBrCl_2$.[a]

Raman $\Delta\sigma$	Raman I	Raman ρ	PS	Infrared Liquid σ	Infrared Liquid I	Infrared Gas σ	Infrared Gas I	Theoretical σ_c	Theoretical assignment	Type
219[b]	100	0.65	P	Not investigated below 400K				**216**	σ_9	a''
								223	σ_6	a'
329	74	0.24	P					**316**	σ_5	a'
579	71	0.18	P	578	s	584	m	**575**	σ_4	a'
699	15	0.57	P	699	s	709 s / 716 s		**704**	σ_3	a'
735	6	0.87	D	741	vvs	750	m	**735**	σ_8	a''
872	3	0.58	P	872	vvs	878 m / 883 m		**875**	σ_2	a'
904	3	0.83	D	904	vvs	904 m / 913 m		**905**	σ_7	a''
···	···	···	···	1055	m	···	···	*1064*	$\sigma_5+\sigma_8$	A''
···	···	···	···	1084	w	···	···	*1092*	$\sigma_2+\sigma_6$	A'
···	···	···	···	1274	m	1289	w	*1278*	$\sigma_3+\sigma_4$	A'
···	···	···	···	1347	vw	···	···	*1349*	$\sigma_1-\sigma_7$?	A''
···	···	···	···	1430	m	1449	m	*1434*	$\sigma_3+\sigma_8$	A''
···	···	···	···	(1507)	m	···	···	*1518*	$\sigma_1-\sigma_8$?	A''
···	···	···	···	1556	vw	···	···	*1554*	$\sigma_1-\sigma_3$	A'
···	···	···	···	1635	w	···	···	*1639*	$\sigma_7+\sigma_8$	A'
···	···	···	···	1676	w	···	···	*1674*	$\sigma_1-\sigma_4$	A'
···	···	···	···	(1719)	m	···	···	*1744*	$2\sigma_2$	A'
···	···	···	···	1801	w	···	···	*1808*	$2\sigma_7$	A'
···	···	···	···	(1931)	vw	···	···	*1924*	$\sigma_1-\sigma_5$	A'
2253	15	0.47	P	2254	s	2264	vw	**2243**	σ_1	a'
···	···	···	···	2827	w	···	···	*2832*	$\sigma_1+\sigma_4$	A'
···	···	···	···	(3110)	m	···	···	*3125*	$\sigma_1+\sigma_2$	A'
···	···	···	···	(3143)	m	···	···	*3157*	$\sigma_1+\sigma_7$	A''

[a] Symbols have the same meaning as in Tables I and II.
[b] Believed to be the unresolved doublet 215, 220 K (see text).

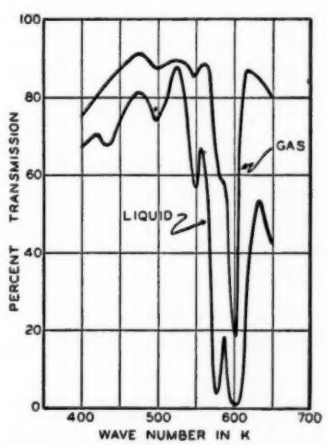

FIG. 2. Infrared absorption bands for liquid and gaseous $CHBrCl_2$, $CDBrCl_2$ mixture (KBr optics).

[8] E. B. Wilson, Jr., J. Chem. Phys. **7**, 1047 (1939); **9**, 76 (1941).
[9] Davis, Cleveland, and Meister, J. Chem. Phys. **20**, 454 (1952).
[10] Weber, Meister, and Cleveland, J. Chem. Phys. **21**, 930 (1953).

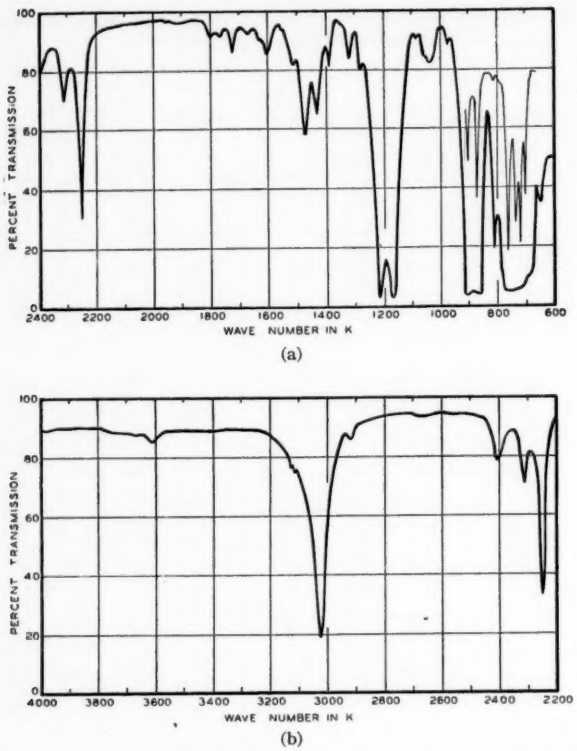

FIG. 3. Infrared absorption bands for liquid $CHBrCl_2$, $CDBrCl_2$ mixture (NaCl optics).

attempting to fit equally well the observed fundamentals for both $CHBrCl_2$ and $CDBrCl_2$. It was desired to reproduce the fundamentals observed for the liquid state since not all of the fundamentals for the gas could be observed. For some of the fundamentals, a close agreement with the observed wave numbers for one molecule could not be attained without a simultaneous divergence from the observed values for the other molecule. Therefore, the potential constants given in Table V were chosen to split these differences, as may be seen in the calculated sets of wave numbers for the fundamentals given in Table VI.

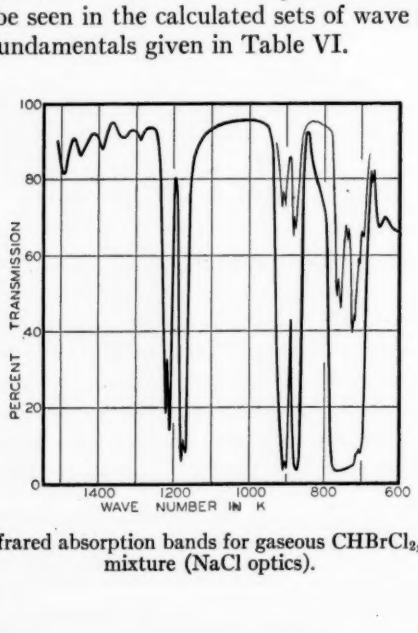

FIG. 4. Infrared absorption bands for gaseous $CHBrCl_2$, $CDBrCl_2$ mixture (NaCl optics).

TABLE V. Potential constants for $CHBrCl_2$ and $CDBrCl_2$.

Bond-Bond (md/A)		Bond-Angle (md/rad)		Angle-Angle (md A/rad²)	
Constant	Value	Constant	Value	Constant	Value
f_b	2.7000[a]	f_b^{bc}	0.36345	f_{bc}	1.1798
f_c	3.4204	f_b^{bh}	0.25970	f_{bh}	0.59044
f_h	5.0099	f_b^{cc}	−0.16258	f_{cc}	1.1360
f_b^c	0.39000	f_b^{ch}	−0.16400	f_{ch}	0.69700
f_b^h	0.06000	f_c^{bc}	0.33700	$f_{bc}^{bc'}$	0.1198
f_c^h	0.09000	$f_c^{bc'}$	−0.21300	f_{bc}^{ch}	−0.01415
f_c^c	0.41040	f_c^{bh}	−0.15200	$f_{bc}^{c'h}$	−0.11415
		f_c^{ch}	0.25000	f_{bc}^{cc}	0.02623
		$f_c^{c'h}$	−0.19000	f_{bc}^{bh}	0.07781
		f_c^{cc}	0.36022	f_{bh}^{ch}	0.02935
		f_h^{bc}	0.45000	f_{bh}^{cc}	−0.04166
		f_h^{bh}	0.23000	f_{cc}^{ch}	0.02573
		f_h^{cc}	0.48000	$f_{ch}^{c'h}$	0.04000
		f_h^{ch}	0.26000		

[a] The retention of five significant figures is not justifiable, but is necessary to secure internal consistency in the calculations.

TABLE VI. Observed and calculated fundamentals for $CHBrCl_2$ and $CDBrCl_2$.

		Wave numbers in kaysers					
		$CHBrCl_2$			$CDBrCl_2$		
			Observed			Observed	
Fundamental[a]	Type	Calculated	Liquid	Gas	Calculated	Liquid	Gas
σ_1	a'	3041	3021	3028	2243	2253	2264
σ_2	a'	1167	1170	1177	875	872	881
σ_3	a'	708	719	734	704	699	713
σ_4	a'	595	602	597	575	579	···
σ_5	a'	322	330	···	316	329	···
σ_6	a'	226	220	···	223	220	···
σ_7	a''	1214	1214	1217	905	904	909
σ_8	a''	761	760	773	735	735	750
σ_9	a''	215	215	···	216	215	···

[a] All the fundamentals are nondegenerate (degeneracy = 1).

TABLE VII. Molecular constants for $CHBrCl_2$ and $CDBrCl_2$.

Quantity	Value	Quantity	Value	Quantity	Value
m_H	1.00785 awu	C−H	1.093 A	Symmetry No.	1
m_D	2.01418 awu	C−D	1.093 A	$I_AI_BI_C$ for $CHBrCl_2$	$1.702 \cdot 10^7$ (awu A²)³
m_{Br}	79.91050 awu	C−Br	1.910 A		
m_{Cl}	35.44959 awu	C−Cl	1.760 A	$I_AI_BI_C$ for $CDBrCl_2$	$1.752 \cdot 10^7$ (awu A²)³
m_C	12.01139 awu	Angles	109°28′		

TABLE VIII. Heat content, free energy, entropy, and heat capacity of $CHBrCl_2$ and $CDBrCl_2$ for the ideal gaseous state at 1 atmos pressure.[a]

	$(H^0-E_0^0)/T$		$-(F^0-E_0^0)/T$		S^0		C_p^0	
T(°K)	H[b]	D	H	D	H	D	H	D
100	8.60	8.60	52.87	52.92	61.48	61.53	10.24	10.25
200	9.12	10.36	59.36	59.42	69.66	69.78	13.56	13.87
273.16	11.44	11.61	62.74	62.84	74.18	74.45	15.51	16.15
298.16	11.81	12.02	63.76	63.87	75.56	75.90	16.10	16.83
300	11.83	12.05	63.83	63.95	75.66	76.00	16.15	16.88
400	13.17	13.55	67.43	67.63	80.60	81.17	18.12	19.02
500	14.31	14.80	70.49	70.78	84.80	85.58	19.56	20.48
600	15.28	15.83	73.19	73.58	88.46	89.41	20.61	21.52
700	16.10	16.70	75.61	76.09	91.71	92.79	21.40	22.27
800	16.80	17.44	77.80	78.36	94.60	95.80	22.02	22.86
900	17.41	18.07	79.85	80.49	97.26	98.56	22.52	23.32
1000	17.94	18.61	81.68	82.39	99.62	101.00	22.93	23.68

[a] The units are cal deg^{-1} mole^{-1}.
[b] H = $CHBrCl_2$, D = $CDBrCl_2$.

THERMODYNAMIC PROPERTIES

The heat content, free energy, entropy, and heat capacity at 1 atmos pressure were computed for 12 temperatures for the ideal gaseous state and with the rigid rotator, harmonic oscillator approximation. The observed wave numbers and molecular constants used are listed in Tables VI and VII. The wave numbers for the gaseous state were used when available. The results are given in Table VIII. For $CHBrCl_2$, the agreement with the values of Gelles and Pitzer[11] is rather close. For example, their values for S^0 and C_p^0 both average 0.03 cal deg^{-1} $mole^{-1}$ greater than our values. Apparently no previous thermodynamic properties have been calculated for $CDBrCl_2$.

[11] E. Gelles and K. S. Pitzer, J. Am. Chem. Soc. **75**, 5259 (1953). It should be noted that the values for the heat content of $CHBrCl_2$ on page 5263 are interchanged with those for $CFBrCl_2$.

ACKNOWLEDGMENTS

This investigation was part of a research program which has been aided by a contract with the Office of Ordnance Research (U. S. Army) and by grants from the Research Corporation, the Socony-Vacuum Laboratories, and the American Academy of Arts and Sciences. The authors are grateful for this assistance.

THE JOURNAL OF CHEMICAL PHYSICS VOLUME 23, NUMBER 5 MAY, 1955

Counter-Ion Distribution in Dilute Solutions of Rigid Spherical Macromolecular Ions in the Absence of Added Salt

HIROSHI FUJITA*
Department of Fisheries, Faculty of Agriculture, Kyoto University, Maizuru, Japan
(Received August 3, 1954)

The electrostatic potential field and the accompanying counter-ion distribution in dilute solutions of rigid spherical-polyelectrolyte ions in the absence of added salt is calculated on the basis of an approximate Poisson-Boltzmann equation. The exact Poisson-Boltzmann equation is approximated so that its characteristic nonlinearity is conserved properly, and the nonlinear equation thus obtained is solved rigorously under relevant boundary conditions. The calculated results reveal a strong tendency of the counter-ions to cluster near the macro-ion, and this occurs even at such extremely low concentrations of the solution as would be beyond the limit of experimental investigation. It is shown that the zeroth-order approximation (in which the basic equation is linear) gives unexpectedly good solutions for the potential distribution even at a fairly high degree of ionization of the macro-ion, but leads to incorrect results for the counter-ion distribution except at a very low degree of ionization.

INTRODUCTION

ONE of the basic problems concerning the characteristic behavior of dilute polyelectrolyte solutions is the nature of the electrostatic potential field and the accompanying counter-ion distribution around a macro-ion as functions of various physico-chemical parameters such as the polymer concentration, the concentration of added simple salts, the degree of ionization, and the dielectric constant of the medium. Many attempts have been made recently to solve this problem on the basis of the Poisson-Boltzmann equation, but a general and rigorous solution relating to the macromolecular electrostatic field has been presented only in one case, namely for rodlike molecules, by Fuoss, Katchalsky, and Lifson,[1] and, independently, by Alfrey, Berg, and Morawetz,[2] and by Imai and Ōsawa.[3] The special case treated by these authors is a salt-free solution consisting of rodlike molecules of infinite length arranged parallel to each other at equal intervals. Although this solution appears to be useful at a sufficiently high degree of ionization, it is clear that the assumption of cylindrical symmetry of the solute molecule is untenable at a lower degree of ionization, and thus the solution fails to hold. At a sufficiently low degree of ionization, we may assume spherical symmetry for macro-ions and treat the problem by means of either the Debye-Hückel or the Donnan approximation. Such cases of low degree of ionization were extensively investigated by many authors,[4–7] notably by Hermans and Overbeek.[4] These investigations led to a number of important and useful conclusions; some of which may be compared with experimental data. Of practical interest is the intermediate case of medium degree of ionization, where not only does the macro-ion assume an intermediate shape between the rod and the sphere, but also the

* Present address: Department of Chemistry, University of Wisconsin, Madison, Wisconsin.

[1] Fuoss, Katchalsky, and Lifson, Proc. Natl. Acad. Sci. U. S. **37**, 579 (1951).

[2] Alfrey, Berg, and Morawetz, J. Polymer Sci. **7**, 543 (1951).

[3] N. Imai and F. Ōsawa, Busseiron Kenkyu No. **46**, 14; **47**, 49 (1952).

[4] J. J. Hermans and J. Th. G. Overbeek, Rec. trav. chim. **67**, 761 (1948).

[5] Kimball, Cutler, and Samelson, J. Phys. Chem. **56**, 57 (1952).

[6] F. Ōsawa and N. Imai, Busseiron Kenkyu No. **35**, 98 (1951); Ōsawa, Imai, and Kagawa, J. Polymer Sci. **13**, 93 (1954).

[7] P. J. Flory, J. Chem. Phys. **21**, 162 (1953).

approximations of Debye or Donnan probably cease to be applicable. As a first approach to this intermediate region, Hill[8] has presented recently a solution for elliptical symmetry, employing, however, the Debye approximation. In contrast to this, Imai and Ōsawa[9–11] have given a series of approximate solutions in which spherical symmetry is assumed but no such linearizations as those involved in Debye's approximation are employed. Quite recently, Imai[12] has extended a similar approach to the case of coiling macro-ions.

The purpose of the present paper is to approach this problem by solving the Poisson-Boltzmann equation for dilute solutions of rigid spherical macro-ions containing no extraneous salt, with the aid of an approximate method which is different essentially from that of Imai and Ōsawa. The method, however, contains two serious limitations: first, it is applicable only to solutions containing no added electrolytes, and secondly, quantitatively, the degree of approximation becomes worse even at such relatively small electrostatic energies as several times kT (k is Boltzmann's constant and T is the absolute temperature). This second condition, however, is compatible with the assumption of a spherical model, and for high enough electrostatic energies the cylindrical model is certainly more practical.

MATHEMATICAL DEVELOPMENT

1. Physical Model of the Solution and Basic Equations

The physical model of the solution used for the present calculation is essentially the same as that used by Künzle,[13] and by Imai and Ōsawa for their theoretical treatment of solutions of spherical polyelectrolyte molecules. Each solute macro-ion, which is assumed to be a uniform rigid sphere of radius a, is located at the center of a spherical region containing all counter-ions dissociated from it. This region is conveniently referred to as the "free volume" of the given macro-ion. The entire solution is closely packed with a set of such free volumes. The charges of the macro-ion are assumed to be spread uniformly over its surface. It is then clear that the time-average counter-ion (or potential) distribution around a particular macro-ion is spherically symmetrical about the center of the free volume. It is, moreover, assumed that the solution is so dilute that neighboring interactions between macro-ions may be neglected.

Let us consider that n counter-ions, each assumed to be univalent, are dissociated in a single free volume. If $\rho(r)$ is the local density at distance r from the center of the macro-ion, the electrostatic potential $\psi(r)$ of a test ion placed there is determined by the Poisson-Boltzmann equation in the form:

$$\frac{d^2\psi}{dr^2}+\frac{2}{r}\frac{d\psi}{dr}=\frac{4\pi\epsilon}{D}\rho(r), \tag{1}$$

where $\rho(r)$ is given by

$$\rho(r)=ne^{\epsilon\psi(r)/kT}\left(\int_a^R 4\pi r^2 e^{\epsilon\psi(r)/kT}dr\right)^{-1}, \tag{2}$$

where ϵ is the elementary charge, and D is the dielectric constant of the solvent.

The electric field vanishes at the boundary of the free volume owing to the time-average spherical symmetry of neighboring macro-ions and their counter-ions. Thus, denoting the radius of the free volume by R,

$$(d\psi/dr)_{r=R}=0. \tag{3}$$

For the same reason, the boundary of the free volume, considered on a time-average basis, should be an equipotential surface

$$(\psi)_{r=R}=\text{const.} \tag{4}$$

Equations (1), (2), (3), and (4) are invariant for the substitution $\psi\rightarrow\psi+\text{constant}$. Therefore, we may assume, without loss of generality, that

$$(\psi)_{r=R}=0. \tag{5}$$

Equations (3) and (5) give the boundary conditions for the differential equation for ψ which can be derived from Eqs. (1) and (2) by eliminating ρ. It is shown easily that the condition of electrical neutrality of the solution is fulfilled automatically in terms of the normalizing factor introduced in Eq. (2).

Introducing the dimensionless variables defined by

$$x=\kappa r,\quad y=\epsilon\psi/kT,\quad \alpha=\kappa a,\qquad \beta=\kappa R,\quad \lambda=n\epsilon^2/DkTa, \tag{6}$$

with

$$\kappa^2=(n\epsilon^2/DkT)\left(\int_a^R r^2 e^{\epsilon\psi/kT}dr\right)^{-1}, \tag{7}$$

gives for the potential distribution a differential equation of the form:

$$\frac{d^2y}{dx^2}+\frac{2}{x}\frac{dy}{dx}=e^y, \tag{8}$$

and the boundary conditions (3) and (5) reduce to

$$(dy/dx)_{x=\beta}=0, \tag{9}$$

$$(y)_{x=\beta}=0. \tag{10}$$

The principal aim of the present calculation is to solve Eq. (8) subject to conditions (9) and (10) without recourse to such linearization approximations as are used in Debye's treatment.

[8] T. L. Hill, J. Chem. Phys. **20**, 1173 (1952).
[9] N. Imai and F. Ōsawa, Busseiron Kenkyu No. **52**, 42 (1952).
[10] N. Imai, Busseiron Kenkyu No. **59**, 99 (1953).
[11] N. Imai, Busseiron Kenkyu No. **62**, 16 (1953).
[12] N. Imai, Busseiron Kenkyu No. **67**, 63 (1953).
[13] O. Künzle, Rec. trav. chim. **68**, 699 (1949).

2. Approximation

It appears impossible to obtain the exact analytical solution of Eq. (8) subject to Eqs. (9) and (10). On the other hand, use of the Debye-Hückel approximation in which it is assumed that $0 \leqslant y \ll 1$ is not of interest in evaluating the electrostatic potential field at medium degrees of ionization. The usual method of successive approximations is not very hopeful for the significant range y greater than unity. As Imai has stressed frequently, the most essential point in the mathematics of this kind of problem is how successfully one can manage the strongly nonlinear term e^y in the basic equation (8).

It is proposed that e^y be approximated by an algebraic function Y of the form:

$$Y=\left(1+\frac{y}{5}\right)^5. \tag{11}$$

Since, by definition,

$$e^y=\lim_{N\to\infty}\left(1+\frac{y}{N}\right)^N,$$

the substitution (11) may be considered a reasonable approximation, not only qualitatively but also quantitatively, insofar as values of y are limited to the order of 3 or 4. In Fig. 1, the true function e^y is compared with the approximate function Y over the range of y from 0 to 4. It is seen from the figure that, although the quantitative agreement of Y with e^y is never very satisfactory even at these relatively low values of y, the nonlinear behavior of Y resembles rather closely that of the true function. This resemblance leads us to expect that the solution to be derived on the basis of this approximation would reveal, at least qualitatively, the characteristic features involved in the original Poisson-Boltzmann equation. A further reason for the above approximation, despite its quantitatively unsatisfactory nature, is that it permits integration of Eq. (8) in terms of known functions.

After making the above-mentioned approximation, and setting

$$z=1+\frac{y}{5}, \tag{12}$$

Eq. (8) reduces to the form:

$$\frac{d^2z}{dx^2}+\frac{2}{x}\frac{dz}{dx}=\frac{1}{5}z^5. \tag{13}$$

This is a special case of the Emden-type equation, which is known to be integrable analytically. Integration once gives

$$\left(x\frac{dZ}{dx}\right)^2=\frac{1}{4}Z^2+\frac{1}{15}Z^6+B, \tag{14}$$

where

$$Z=x^{\frac{1}{2}}z, \tag{15}$$

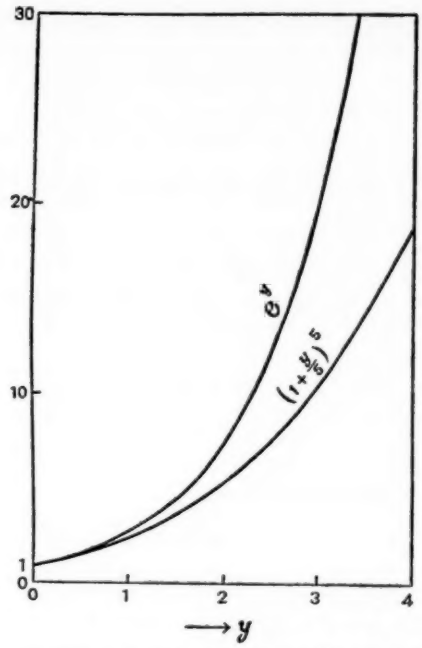

FIG. 1. Comparison of $Y=[1+(y/5)]^5$ with the true function e^y.

and B is an integration constant. Equations (9) and (10) in terms of Z become:

$$\left(\frac{dZ}{dx}\right)_{x=\beta}=\frac{1}{2}(\beta)^{-\frac{1}{2}}, \tag{16}$$

and

$$(Z)_{x=\beta}=(\beta)^{\frac{1}{2}}. \tag{17}$$

Substitution of these into Eq. (14) determines the constant B, leading to

$$\left(x\frac{dZ}{dx}\right)^2=\frac{1}{4}\left[Z^2+\frac{4}{15}(Z^6-\beta^3)\right].$$

By introducing the new variables

$$Z=(\beta)^{\frac{1}{2}}\cdot\theta, \quad (x/\alpha)^{\frac{1}{2}}=\xi, \quad \frac{4}{15}\beta^2=b, \tag{18}$$

this equation can be put into the form:

$$\left(\xi\frac{d\theta}{d\xi}\right)^2=\theta^2+b(\theta^6-1). \tag{19}$$

Here we note that $b>0$.

Now, consider the cubic equation in

$$\eta^3+(\eta/b)-1=0, \tag{20}$$

with $b>0$. It is shown readily that this equation possesses only one real root, η, such that $0<\eta<b$, and hence, the other two roots are complex and conjugate. It follows then that the quantity m defined by

$$m=\left(3-\frac{2\eta}{b}\right)^{\frac{1}{2}} \tag{21}$$

satisfies the condition: $1<m<3^{\frac{1}{2}}$.

On making the transformation from θ to w by the relation:

$$w=\left\{1-\left[\frac{(m-1)\theta^2+\eta}{(m+1)\theta^2-\eta}\right]^2\right\}^{\frac{1}{2}}, \tag{22}$$

it is found, after simple but lengthy calculations, that Eq. (19) becomes

$$\left(\xi\frac{dw}{d\xi}\right)^2=\left(\frac{8m}{3-m^2}\right)(1-w^2)(1-h^2w^2), \tag{23}$$

where

$$h^2=\frac{m^2+4m+3}{8m}. \tag{24}$$

A further transformation by

$$w=sn(u,h), \tag{25}$$

where $sn(u,h)$ is the Jacobian elliptic "sn" function whose variable is u and whose modulus is h, gives for Eq. (23)

$$\left(\xi\frac{du}{d\xi}\right)^2=\frac{8m}{3-m^2}, \tag{26}$$

which can be integrated to give

$$u=\pm\left(\frac{8m}{3-m^2}\right)^{\frac{1}{2}}\ln\xi+A, \tag{27}$$

where A is an integration constant. If we denote by ξ_* the value of ξ corresponding to the θ value at which the right-hand side of Eq. (19) vanishes, it is shown easily that A is given by

$$A=\mp\left(\frac{8m}{3-m^2}\right)^{\frac{1}{2}}\ln\xi_*.$$

Hence, Eq. (27) becomes

$$u=\pm\left(\frac{8m}{3-m^2}\right)^{\frac{1}{2}}\ln(\xi/\xi_*). \tag{28}$$

Combining Eqs. (28), (25), (22), and (21), the resulting equation for θ in terms of ξ is

$$\theta^2=\frac{b(3-m^2)}{2}\cdot\frac{1+cn[(8m/3-m^2)^{\frac{1}{2}}\ln(\xi/\xi_*),\,h]}{1-m+(1+m)cn[(8m/3-m^2)^{\frac{1}{2}}\ln(\xi/\xi_*),\,h]}. \tag{29}$$

From Eq. (17) it follows that

$$(\theta)_{\xi=(\beta/\alpha)^{\frac{1}{2}}}=1, \tag{30}$$

and, therefore, from Eq. (29),

$$\frac{b(3-m^2)}{2}\cdot\frac{1+cn[(8m/3-m^2)^{\frac{1}{2}}\ln(1/\sigma\xi_*),\,h]}{1-m+(1+m)cn[(8m/3-m^2)^{\frac{1}{2}}\ln(1/\sigma\xi_*),\,h]}=1, \tag{31}$$

where

$$\sigma=\left(\frac{\alpha}{\beta}\right)^{\frac{1}{2}}. \tag{32}$$

If the values of w and u corresponding to $\theta=1$ are denoted by w_1 and u_1, respectively, then from Eqs. (22) and (25)

$$w_1=\frac{2\{2m[2-b(3-m^2)]\}^{\frac{1}{2}}}{2(m+1)-b(3-m^2)}, \tag{33}$$

$$u_1=\int_0^{w_1}[(1-w^2)(1-h^2w^2)]^{-\frac{1}{2}}dw. \tag{34}$$

By combining Eqs. (31), (33), and (34) properly, it can be shown that the relation

$$\left(\frac{8m}{3-m^2}\right)^{\frac{1}{2}}\ln\frac{1}{\sigma\xi_*}=u_1 \tag{35}$$

must be satisfied. This is the equation for the determination of unknown parameter ξ_*, knowledge of which permits determination of the integration constant, A.

Elimination of ξ_* from Eq. (29) by Eq. (35) then gives the final expression for θ^2 as:

$$\theta^2=\frac{b(3-m^2)}{2}\cdot\frac{1+cn[(8m/3-m^2)^{\frac{1}{2}}\ln\sigma\xi+u_1,\,h]}{1-m+(1+m)cn[(8m/3-m^2)^{\frac{1}{2}}\ln\sigma\xi+u_1,\,h]}. \tag{36}$$

Multiplication of Eq. (13) by x^2 and integration from $x=\alpha$ to $x=\beta$ gives

$$-\alpha^2\left(\frac{dz}{dx}\right)_{x=\alpha}=\frac{1}{5}\int_\alpha^\beta x^2z^5dx. \tag{37}$$

On the other hand, Eq. (7), expressed in terms of the dimensionless quantities defined by Eq. (6), reduces to

$$\alpha\lambda=\int_\alpha^\beta x^2e^vdx. \tag{38}$$

For the sake of consistency, it is necessary to replace e^v in the integrand of Eq. (38) by the approximation function Y defined by Eq. (11). Thus,

$$\alpha\lambda=\int_\alpha^\beta x^2z^5dx. \tag{39}$$

Comparison of Eqs. (37) and (39) yields

$$\left(\frac{dz}{dx}\right)_{x=\alpha}=-\frac{\lambda}{5\alpha}, \tag{40}$$

which may be combined with Eq. (15) to give

$$\left(x\frac{dZ}{dx}\right)_{x=\alpha}=\frac{Z_\alpha}{2}-\frac{\alpha^{\frac{1}{2}}}{5}, \tag{41}$$

where Z_α is the value of Z at $x=\alpha$. This equation may be written in terms of θ and ξ as

$$\left(\xi\frac{d\theta}{d\xi}\right)_{x=\alpha}=\theta_\alpha-\frac{2}{5}\sigma\lambda, \tag{42}$$

where θ_α is the value of θ at $x=\alpha$. Putting $x=\alpha$ in Eq. (19), and eliminating $(\xi d\theta/d\xi)_{x=\alpha}$ from the resultant equation using Eq. (42), it is found that

$$\theta_\alpha{}^6+\frac{4\sigma\lambda}{5b}\theta_\alpha-\left(1+\frac{4\sigma^2\lambda^2}{25b}\right)=0. \tag{43}$$

The value of θ_α obtained from Eq. (36) is

$$\theta_\alpha{}^2=\frac{b(3-m^2)}{2}\cdot\frac{1+cn[(8m^2/3-m^2)^{\frac{1}{2}}\ln\sigma+u_1, h]}{1-m+(1+m)cn[(8m^2/3-m^2)^{\frac{1}{2}}\ln\sigma+u_1, h]}, \tag{44}$$

since, by Eq. (18), $x=\alpha$ corresponds to $\xi=1$.

Inspection of the mathematical process described above shows that the parameters η, m, h, w_1, and u_1 all are functions of a single parameter b, and therefore, if we eliminate θ_α from Eqs. (43) and (44), there will be obtained a transcendental equation which involves b, σ, and λ as variables. It is supposed that this equation has been solved for b to give $b=b(\sigma,\lambda)$. Then, m, h, and u_1 are evaluated as functions of σ and λ, and the relation between θ and ξ can be computed numerically with σ and λ as independent parameters.

It can be shown that

$$y=\frac{\epsilon\psi}{kT}=5\left(\frac{\theta}{\sigma\xi}-1\right), \tag{45}$$

and

$$r/a=\xi^2. \tag{46}$$

Hence, when θ has been found in this way as a function of ξ with the independent parameters σ and λ, y may be plotted readily against r/a; i.e., the required potential distribution around the macro-ion under consideration is determined. The corresponding counter-ion distribution is then calculated from Eq. (2) using the potential distribution thus obtained. However, in order to see the extent to which the counter-ions are crowded around the macro-ion, it is convenient to plot the ratio of the actual distribution density ρ to the uniform density $\bar{\rho}$ in such a hypothetical state of the solution that all the charges, on the macro-ions as well as on the counter-ions, are discharged. The choice of the "discharged" solution as the reference state has been employed recently by Lifson and Katchalsky[14] in the calculation of the electrostatic free energy of solutions of rodlike polyelectrolytes. The hypothetical density $\bar{\rho}$ is obviously

$$\bar{\rho}=n\Big/\frac{4\pi}{3}(R^3-a^3).$$

It may be shown easily that the ratio $\rho/\bar{\rho}$ can be calculated from

$$\frac{\rho}{\bar{\rho}}=\frac{5b}{4\lambda}\left(\frac{1-\sigma^6}{\sigma^2}\right)\left(\frac{\theta}{\sigma\xi}\right)^5 \tag{47}$$

as a function of r/a.

Now consider the physical meanings of the quantities σ and λ involved in these final equations as parameters. From Eq. (32) and the definitions of α and β,

$$\sigma=(a/R)^{\frac{1}{2}}.$$

If the over-all polymer concentration of the given solution, the molecular weight of the macro-ion and Avogadro's number are denoted by c (g/100 ml), M and N_A, respectively, then

$$R=(75M/\pi cN_A)^{\frac{1}{3}},$$

and

$$c=\frac{75M}{\pi N_A a^3}\sigma^6.$$

Hence, for a given rigid spherical macro-ion the concentration c of the solution is proportional to the sixth power of σ; i.e., σ is a measure of the polymer concentration.

The quantity λ is directly proportional to n, the number of counter-ions dissociated from a single macro-ion, and therefore, it is a measure of the degree of ionization of the macro-ion.

In view of these physical interpretations, σ and λ are referred to as the "concentration parameter" and the "ionization parameter," respectively.

3. Modification of the Solutions

The mathematical solutions derived in the preceding section are analytically exact, but are so complicated that it is not easy to examine them numerically in their original forms. The numerical evaluation of the cn function is particularly difficult for reasons which are mentioned below.

As already noted, m varies between 1 and $3^{\frac{1}{2}}$. In Fig. 2, h is plotted as a function of m for this range

[14] S. Lifson and A. Katchalsky, J. Polymer Sci. 13, 43 (1954).

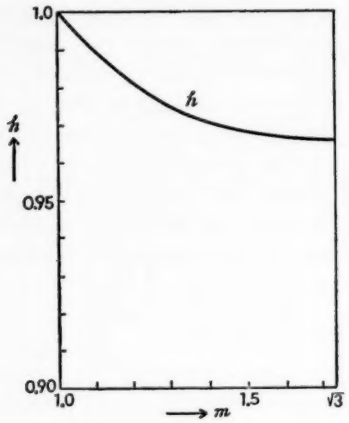

FIG. 2. h as a function of m.

[see Eq. (24)]. It is seen that h is very near unity in this range of m, which indicates that numerical values of a *cn* function whose modulus is close to unity must be computed. It is well known that evaluation of the Jacobian elliptic functions is very tedious for such moduli. This is the first difficulty in numerical work. It can be shown without difficulty that the value of w_1 tends to unity as h approaches unity. Hence, it follows from Eq. (34) that u_1 diverges to infinity in the limit when m tends to unity. This suggests that the argument of the *cn* function in question becomes very large for values of m near unity, thus making it almost impossible to compute the corresponding *cn* values by means of such conventional methods as the series expansion formula. This presents a second difficulty.

Although, for these reasons, the general solutions are very inconvenient in their original forms for numerical calculations, it can be shown that they may be put into a form in which the numerical computation may be performed rather easily, if use is made of the condition that h is very near unity.

Introduce the Riemann *theta*† functions whose parameter is determined by the equation:

$$h^2=\left[\frac{\vartheta_2(0|\tau)}{\vartheta_3(0|\tau)}\right]^4 \tag{48}$$

and put, for convenience,

$$v=\frac{u_1+(8m/3-m^2)^{\frac{1}{2}}\ln\sigma\xi}{\pi[\vartheta_3(0|\tau)]^2}. \tag{49}$$

Then it can be shown that the *cn* function in question may be written in terms of *theta* functions as follows:

$$L\equiv cn[(8m/3-m^2)^{\frac{1}{2}}\ln\sigma\xi+u_1, h]=\frac{\vartheta_4(0|\tau)\vartheta_2(v|\tau)}{\vartheta_2(0|\tau)\vartheta_4(v|\tau)}. \tag{50}$$

† The notation and representation of the *theta* functions used herein follow S. Tomotika, *Theory of Elliptic Functions* (Kawade Book Company, Tokyo, 1942).

It follows from Eq. (48) that absolute values of τ are close to zero for h close to unity; here it should be noted that τ is an imaginary quantity such that the imaginary part of $\tau>0$. In accordance with the theory of *theta* functions, it is advantageous in such a case to transform the system to another one in which the parameter is $-1/\tau$ with the aid of Jacobi's imaginary transformations. Application of such transformations to Eq. (50) yields

$$L=\frac{\vartheta_2\left(0\middle|-\frac{1}{\tau}\right)\vartheta_4\left(\frac{v}{\tau}\middle|-\frac{1}{\tau}\right)}{\vartheta_4\left(0\middle|-\frac{1}{\tau}\right)\vartheta_2\left(\frac{v}{\tau}\middle|-\frac{1}{\tau}\right)}. \tag{51}$$

For small τ the quantity q defined as $\exp(-\pi i/\tau)$ is very small. In fact, as shown later, $0<q<0.0044$ for $1<m<3^{\frac{1}{2}}$. It may be expected, therefore, that sufficiently good approximations can be obtained by retaining only terms up to the order of q and neglecting all higher terms in comparison with unity.

The equation for L is then approximately

$$L=2q^{\frac{1}{4}}(1+2q)\frac{\vartheta_4\left(\frac{v}{\tau}\middle|-\frac{1}{\tau}\right)}{\vartheta_2\left(\frac{v}{\tau}\middle|-\frac{1}{\tau}\right)}. \tag{52}$$

The ratio of the two *theta* functions involving the independent variable v cannot be approximated in such a way, but must be represented in terms of their defining equations as follows:

$$\frac{\vartheta_4\left(\frac{v}{\tau}\middle|-\frac{1}{\tau}\right)}{\vartheta_2\left(\frac{v}{\tau}\middle|-\frac{1}{\tau}\right)}=q^{v-\frac{1}{4}}\frac{1+\sum_{n=1}^{\infty}(-1)^n q^{n^2}(q^{2nv}+q^{-2nv})}{1+\sum_{n=1}^{\infty}q^{n^2}[q^{2n(v-\frac{1}{2})}+q^{-2n(v-\frac{1}{2})}]}. \tag{53}$$

Now, define U and V such that

$$U=u_1/\pi[\vartheta_3(0|\tau)]^2, \tag{54}$$

$$V=[8m/(3-m^2)]^{\frac{1}{2}}/\pi[\vartheta_3(0|\tau)]^2. \tag{55}$$

Equation (34) then may be written in terms of *theta* functions,

$$w_1=\frac{\vartheta_3(0|\tau)\vartheta_1(U|\tau)}{\vartheta_2(0|\tau)\vartheta_4(U|\tau)},$$

which is transformed to

$$w_1=i\frac{\vartheta_3\left(0\middle|-\frac{1}{\tau}\right)\vartheta_1\left(\frac{U}{\tau}\middle|-\frac{1}{\tau}\right)}{\vartheta_4\left(0\middle|-\frac{1}{\tau}\right)\vartheta_2\left(\frac{U}{\tau}\middle|-\frac{1}{\tau}\right)}.$$

The right-hand side of this equation may be approximated as before, leading to

$$w_1=(1+4q)\frac{\sum_{n=-\infty}^{\infty}(-1)^n\exp\left[-\frac{\pi i}{\tau}(U+n-\frac{1}{2})^2\right]}{\sum_{n=-\infty}^{\infty}\exp\left[-\frac{\pi i}{\tau}(U+n-\frac{1}{2})^2\right]}. \quad (56)$$

It is shown in the next section that, when $b>0$, U satisfies the following inequality:

$$0<U<\tfrac{1}{3}. \quad (57)$$

Accepting for the moment that this is the case, Eq. (56) gives, to the degree of approximation mentioned above,

$$w_1=(1+4q)\left(\frac{1-q^{2U}}{1+q^{2U}}\right), \quad (58)$$

from which, to the same degree of approximation,

$$q^{2U}=\frac{1-w_1(1-4q)}{1+w_1(1-4q)}. \quad (59)$$

Then, since

$$\pi[\vartheta_3(0|\tau)]^2=\frac{\pi i}{\tau}\left[\vartheta_3\left(0\middle|-\frac{1}{\tau}\right)\right]^2$$

$$=-(\ln q)\times[1+4q+0(q^2)],$$

V (defined by Eq. (55)) may be written

$$V=-\frac{[8m/(3-m^2)]^{\frac{1}{2}}}{\ln q}[1-4q+0(q^2)],$$

from which, approximately,

$$q^{2V\ln\sigma\xi}=\sigma\xi^{-2(1-4q)[8m/(3-m^2)]^{\frac{1}{2}}}. \quad (60)$$

Thus, it follows that

$$q^{2v}=q^{2U+2V\ln\sigma\xi} \quad (61)$$

with

$$\mu=\frac{1-w_1(1-4q)}{1+w_1(1-4q)}, \quad (62)$$

and

$$\nu=2(1-4q)\left(\frac{8m}{3-m^2}\right)^{\frac{1}{2}}. \quad (63)$$

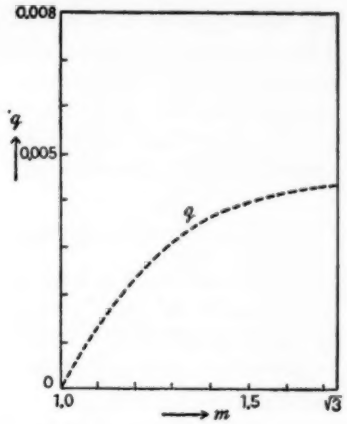

FIG. 3. q as a function of m.

If Eq. (61) is substituted in Eq. (53) and the resultant equation is combined with Eq. (52), the final expression for L is obtained in the form:

$$L=2(1+2q)[\mu(\sigma\xi)^{-\nu}]^{\frac{1}{2}}\cdot\frac{1+\sum_{n=1}^{\infty}(-1)^n q^{n^2}[\mu^n(\sigma\xi)^{-\nu n}+\mu^{-n}(\sigma\xi)^{\nu n}]}{1+\sum_{n=1}^{\infty}q^{n^2}\left[\left(\frac{\mu}{q}\right)^n(\sigma\xi)^{-\nu n}+\left(\frac{\mu}{q}\right)^{-n}(\sigma\xi)^{\nu n}\right]}, \quad (64)$$

which is correct to the approximation that terms higher than $0(q)$ may be neglected in comparison with unity.

Applying Jacobi's imaginary transformations for Eq. (48), and expanding in q,

$$h^2=1-16q+128q^2+0(q^3), \quad (65)$$

which confirms that $q\cong 0$ when $h\cong 1$. Solving this for q, and recalling Eq. (24) gives

$$q=\left(\frac{4m-3-m^2}{128m}\right)+8\left(\frac{4m-3-m^2}{128m}\right)^2+0\left[\left(\frac{4m-3-m^2}{128m}\right)^3\right]. \quad (66)$$

q is plotted as a function of m in Fig. 3, from which it is seen that q is very small over the range of m plotted, justifying the validity of the approximate analysis presented above.

The numerical process of calculating L as a function of $\sigma\xi$ for any given value of b is briefly as follows. For given b the real root η of Eq. (20) is sought first. Then, the corresponding m value is obtained from Eq. (21), substitution of which into Eq. (66) determines the q value. The ν value is then computed from Eq. (63). Also, the w_1 value is obtained from Eq. (33) with the m value determined. Then, the μ value follows at once from Eq. (62). In this way, all parameters contained in Eq. (64) with the exception of the concentration parameter σ may be determined, thus making possible

the evaluation of L as a function of the argument $\sigma\xi$. The numerical computation of L may be performed readily because both series involved converge very rapidly for $q \ll 1$. The first two terms are sufficient for obtaining accurate values in either series, within the range treated in this research.

4. The Special Case $\lambda \to 0$

In this section, the limiting behavior of the general solutions for the case in which the degree of ionization becomes infinitesimally small, while the polymer concentration is finite, is of interest. This is realized by making $\lambda \to 0$ with $\sigma \neq 0$.

Assume that b approaches zero when λ tends to zero with $\sigma \neq 0$. (This condition can be deduced in a general way without resorting to detailed calculation.) For small b, Eq. (20) gives

$$\eta = b[1 - b^3 + 0(b^6)]. \tag{67}$$

Equation (21) then becomes

$$m = 1 + b^3 + 0(b^6). \tag{68}$$

Thus, it follows from Eq. (66) that

$$q = \frac{b^3}{64}[1 + 0(b^3)]. \tag{69}$$

Substituting Eq. (68) in Eq. (33) leads to

$$w_1 = 1 - \frac{b^2}{8} - \frac{b^3}{8} + 0(b^4). \tag{70}$$

With these results, Eqs. (62) and (63) yield

$$\mu = \frac{b^2}{16}[1 + \tfrac{3}{2}b + 0(b^2)], \tag{71}$$

$$\nu = 4[1 + 0(b^3)]. \tag{72}$$

Inserting Eqs. (69), (71), and (72) into Eq. (64), and

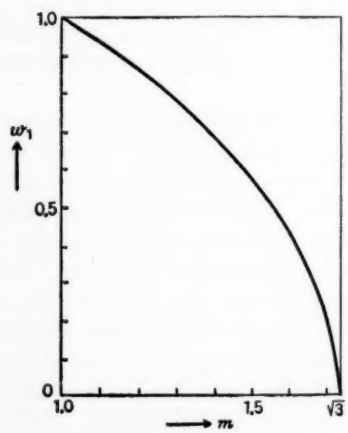

FIG. 4. w_1 as a function of m.

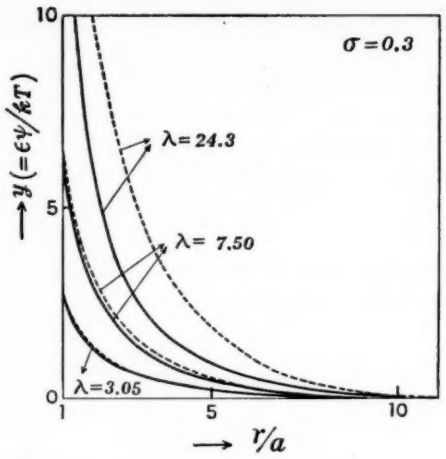

FIG. 5. Potential distributions for different values of λ at a fixed value of σ. (Effect of degree of ionization.)

expanding in powers of b,

$$L = \frac{b}{2(\sigma\xi)^2}\left\{1 + \frac{b}{4}[3 - (\sigma\xi)^4] + 0(b^2)\right\}. \tag{73}$$

This is substituted in Eq. (36), to give the following series expansion of θ in b:

$$\theta = \sigma\xi\left\{1 + \frac{b}{8}\left[(\sigma\xi)^4 + \frac{2}{(\sigma\xi)^2} - 3\right] + 0(b^2)\right\}. \tag{74}$$

Hence,

$$\theta_a = \sigma\left\{1 + \frac{b}{8}\left(\sigma^4 + \frac{2}{\sigma^2} - 3\right) + 0(b^2)\right\}. \tag{75}$$

If this is substituted in Eq. (43) and the resultant equation is solved for b, there results

$$b = \frac{4\lambda\sigma^2}{5(1 - \sigma^6)}[1 + 0(\lambda)], \tag{76}$$

which indicates that $b \to 0$ as $\lambda \to 0$, thus confirming the starting assumption for the above limiting calculation.

On combining Eqs. (74), (76), (45), and (46), the required solution for the potential distribution at a very low degree of ionization is found to be

$$y = \frac{e\psi}{kT} = \frac{\lambda(a/R)}{2[1 - (a/R)^3]}\left[\left(\frac{r}{R}\right)^2 + 2\frac{R}{r} - 3\right]. \tag{77}$$

The corresponding solution for counter-ion distribution becomes

$$\frac{\rho}{\bar{\rho}} = 1 + \frac{\lambda(a/R)}{2[1 - (a/R)^3]}\left[\left(\frac{r}{R}\right)^2 + 2\frac{R}{r} - 3\right]. \tag{78}$$

These equations are in complete agreement with those which have been derived by Imai and Ōsawa[9] using a method essentially different from the one presented

here, and, in addition, are shown to be obtained directly from the original Poisson-Boltzmann equation by setting e^{y} approximately equal to unity.

In Section 3, the analysis was advanced assuming that

$$0<U<\tfrac{1}{3} \quad (b>0),$$

a proof of which, though not analytically rigorous, is given below.

In Fig. 4, w_1 is plotted as a function of m over the range of interest here, from which it is seen that $0<w_1<1$ for $b>0$. It then follows from Eq. (34) that $u_1>0$, and from Eq. (54),

$$U>0.$$

Next, using the fact that $0<w_1<1$, it is found that

$$U<\frac{\int_0^1 [(1-w^2)(1-h^2w^2)]^{-\frac{1}{2}}dw}{\pi[\vartheta_3(0|\tau)]^2}=\frac{\frac{\pi}{2}[\vartheta_3(0|\tau)]^2}{\pi[\vartheta_3(0|\tau)]^2}=\frac{1}{2}.$$

Thus, as a rough estimate,

$$0<U<\tfrac{1}{2}.$$

Under this condition, Eq. (56) may be put in the form:

$$w_1=[1+4q+0(q^2)]\left[\frac{1-q^{2U}-q^{2(1-U)}+0(q^{2k_1})}{1+q^{2U}+q^{2(1-U)}+0(q^{2k_1})}\right],$$

where k_1 is a quantity which is larger than unity if $0<U<\frac{1}{2}$. Solving for q and neglecting terms higher than $0(q^2)$ in comparison with unity,

$$q^{2U}=\frac{1}{2}\left[\frac{1-w_1(1-4q)}{1+w_1(1-4q)}\right]\cdot\left[1\pm\left\{1-4q^2\left[\frac{1+w_1(1-4q)}{1-w_1(1-4q)}\right]^2\right\}^{\frac{1}{2}}\right].$$

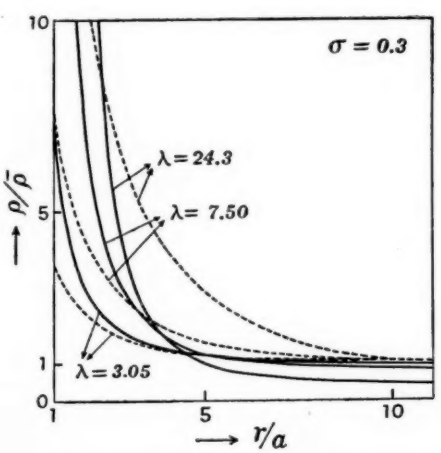

FIG. 6. Counter-ion distribution for different values of λ at a fixed value of σ. (Effect of degree of ionization.)

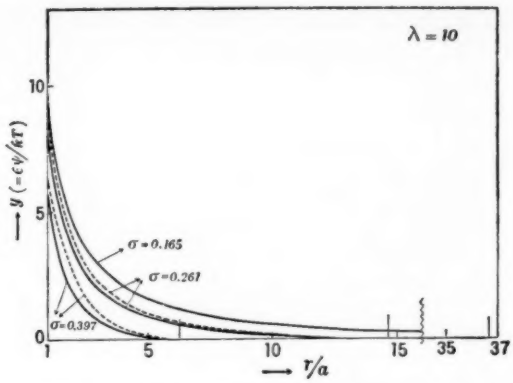

FIG. 7. Potential distributions for different values of σ at a fixed value of λ. (Effect of polymer concentration.)

Figure 4 shows that $w_1\to 0$, hence $U\to 0$, as $m\to 3^{\frac{1}{2}}$, while Fig. 3 shows that q remains finite when $m\to 3^{\frac{1}{2}}$. Therefore, the above equation leads, when $m\to 3^{\frac{1}{2}}$, to

$$1=\tfrac{1}{2}[1\pm(1-4q^2)^{\frac{1}{2}}].$$

In order that this relation may be satisfied to the approximation of neglecting $0(q^2)$ in comparison with unity, the plus sign must be taken. Thus,

$$q^{2U}=\frac{1}{2}\left[\frac{1-w_1(1-4q)}{1+w_1(1-4q)}\right]\cdot\left[1+\left\{1-4q^2\left[\frac{1+w_1(1-4q)}{1-w_1(1-4q)}\right]^2\right\}^{\frac{1}{2}}\right], \quad (79)$$

from which U can be plotted as a function of m for $1<m<3^{\frac{1}{2}}$. The graph (not shown here) indicates that U starts with a finite value (say U_1) at $m=1$, decreases monotonously with increasing m, and vanishes at $m=3^{\frac{1}{2}}$. The value of U_1 can be determined analytically by going to the limit $b\to 0$ with the aid of the b-expansions for q and w_1 derived previously. The result is $U_1=\frac{1}{3}$. Thus, it has been proved that $0<U<\frac{1}{3}$ for $b>0$, which is the inequality required.

NUMERICAL RESULTS

Evaluation of the general equations presented above was performed (1) for different values of λ with a fixed value of σ, and (2) for different values of σ with a fixed value of λ. The case (1) is concerned with the effect produced by the change in degree of ionization, while the case (2) treats the concentration effect at constant degree of ionization. The corresponding problems for rodlike molecules were investigated by Alfrey *et al.*[2] using the rigorous solution.

The numerical results obtained are shown graphically in Figs. 5, 6, 7, and 8, wherein the first two illustrate the potential and counter-ion distributions in case (1), and the last two are the corresponding distributions in case (2). In these figures, the dotted curves were

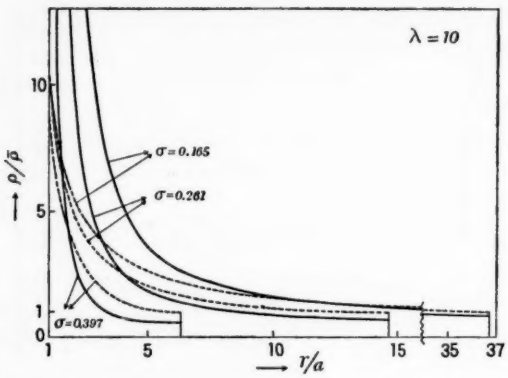

FIG. 8. Counter-ion distributions for different values of σ at a fixed value of λ. (Effect of polymer concentration.)

calculated from Eqs. (77) and (78) and are included for comparison.

As an illustration, consider an aqueous solution of rigid spherical macro-ions whose radius and molecular weight are $A=200$ A and $M=100\,000$. Then, $\sigma=0.3$ represents a solution as dilute as $c=0.00036$ g/100 ml. Let N^* be the total number of ionizable groups per macro-ion, which are assumed, in the present model, to be distributed uniformly over the surface of the polymer ion. The degree of ionization γ of the macro-ion in the state where n counter-ions are liberated in each free volume is given by

$$\gamma = DkTa\lambda/N_*\epsilon.$$

Taking, for example, $T=300°$K and $N_*=100$, $\lambda=24.3$ is found to correspond to $\gamma=0.7$. The γ values for other λ values indicated in the figures are found readily.

Figures 6 and 8 reveal the strong tendency of the counter-ions to cluster near the macro-ion, a condition which obtains even at such extremely low concentrations as would be beyond the limit of experimental investigation. In particular, Fig. 8 suggests that it is practically impossible to reach, in experimental work, the ideal state as assumed in the calculation of Katchalsky, Künzle, and Kuhn,[15] where counter-ions are sufficiently removed from the macromolecules that they do not interfere with the interaction of the fixed charges. These results agree with those demonstrated by Alfrey *et al.*[2] for rodlike molecules, and in part confirm the phenomenon which has been called by Kagawa[16] "fixation of counter-ions."

[15] Katchalsky, Künzle, and Kuhn, J. Polymer Sci. **5**, 283 (1950).
[16] I. Kagawa and K. Katsuura, J. Polymer Sci. **9**, 405 (1952).

Figures 5 and 7 indicate unexpectedly good agreement of the zeroth-order approximate solution for the potential, Eq. (77), with the present solution, except for the case $\lambda=24.3$, for which Eq. (77) gives too large a value. It appears that the degree of approximation of Eq. (77) becomes better for lower values of either λ or σ. From the agreements demonstrated, we may infer that for a set of values of σ and λ such that $0<\sigma<0.3$ and $0<\lambda<10$, Eq. (77) may be used with fair reliability for calculating the electrostatic potential around each rigid spherical macro-ion in a solution containing no added salt. In contrast to such good agreement for the potential functions, the counter-ion distributions calculated from the corresponding zeroth-order approximation, Eq. (78), differ greatly from the present more correct solution, as shown in Figs. 6 and 8. It must be kept in mind, however, that the present solution is probably not very reliable as regards the counter-ion distribution, because this distribution is very sensitive, and hence erroneously estimated by the approximation $e^y \cong [1+(y/5)]^5$. Nevertheless, it seems to be of interest that the approximate solution manifests the characteristic association of the counter-ions to the highly charged macro-ion, in accordance with the concept of "ion-fixation" reached by Kagawa and his co-workers through a number of experimental investigations. This is probably because of the nonlinear character of the approximated Poisson-Boltzmann equation, though its nonlinearity is far less than that of the original equation.

Finally, mention must be made of the reliability of the plotted curves in the vicinity of $r/a=1$. In all cases examined, the y values (hence, $\rho/\bar{\rho}$) in this region far exceed the limit of applicability of the present approximation. Accordingly, no quantitative reliability may be attached to the plotted curves in the neighborhood of the macro-ion. Probably, the true curves rise more steeply near the macro-ion, and thus result in a more marked association of the counter-ions.

ACKNOWLEDGMENTS

It is a pleasure to acknowledge the helpful suggestions and encouragement rendered by Mr. Nobuhisa Imai of the Department of Physics, Faculty of Science, Nagoya University. Thanks are also due to Mr. Akira Kishimoto of this Department for his help in the numerical calculations, and to Dr. J. W. Lorimer, University of Leiden, for aid in preparation of the manuscript.

Interrelation of Gaseous Viscosity, Self-Diffusion, and Isotopic Thermal Diffusion*

EUGENE M. HOLLERAN
St. John's University, Brooklyn 6, New York
(Received August 30, 1954)

The general interrelation of the theoretical first approximations to viscosity, self-diffusion, and thermal diffusion previously derived is modified to conform with a simpler and more accurate approximation for the thermal diffusion ratio due to Kihara. The accuracy and limitations of this interrelation are discussed, with particular regard to the effect of considering higher approximations to the transport properties. With the recently published results for the modified Buckingham potential as a guide, the relation is further simplified, leading in particular to an approximate relation between viscosity and thermal diffusion which is shown to be in good agreement with the experimental data for argon.

INTRODUCTION

WHEN a binary mixture of gases is confined in a vessel consisting of two bulbs, one at a temperature T_2 and the other at a lower temperature T_1, the composition of the mixture differs in the two regions. According to the kinetic theory[1]

$$\Delta x=\int_{T_1}^{T_2}\frac{k_T}{T}dT, \tag{1}$$

where Δx is the difference in the mole fraction of one of the components in one bulb compared to the other bulb. The quantity k_T, known as the thermal diffusion ratio, is a function of the temperature. According to the mean value theorem

$$k_T(\bar{T})=\Delta x\cdot(\ln T_2/T_1)^{-1}, \tag{2}$$

where $\bar{T}$ is some temperature between T_1 and T_2. The value of $\bar{T}$ to be assigned to a value of k_T determined experimentally by the right side of Eq. (2) depends, according to Eq. (1), on the exact temperature dependence of k_T.

The thermal diffusion ratio also depends on the molecular weights, M_A and M_B, of the two components, and on their mole fractions, x_A and x_B. For the special case of heavy isotopes k_T is proportional to $x_Ax_B(M_A-M_B)/(M_A+M_B)$. Two quantities, R_T and k_T^*, have been defined to be independent of this factor. R_T expresses the thermal diffusion ratio in units of the theoretical first approximation to k_T for molecules behaving as hard spheres. Even experimental values of R_T thus depend on the choice of the hard sphere value, for which two different theoretical approximations are available. To avoid this ambiguity Mason[2] has recently proposed the use of

$$k_T^*=\frac{k_T(M_A+M_B)}{x_Ax_B(M_A-M_B)}, \tag{3}$$

which is adopted here.

The two different first approximations to k_T^* are derived from the very involved exact theoretical result by the method of Chapman and Cowling,[3] and the method of Kihara.[4] These are designated by $[k_T^*]_1^{CC}$ and $[k_T^*]_1^K$.

$$[k_T^*]_1^{CC}=\frac{15(2A^*+5)(6C^*-5)}{2A^*(16A^*-12B^*+55)} \tag{4}$$

$$[k_T^*]_1^K=\frac{15(6C^*-5)}{16A^*}. \tag{5}$$

The quantities A^*, B^*, and C^* are ratios of collision cross section integrals and for a given gas are functions of the temperature only.†

The complicated second approximation according to the method of Chapman and Cowling has been evaluated by Mason[2] for the realistic modified Buckingham potential and compared with the two first approximations. He concludes that $(k_T^*)_1^K$ is generally more accurate than the more cumbersome $[k_T^*]_1^{CC}$. One purpose of the present paper is to present in terms of Kihara's approximation the interrelation of isotopic thermal diffusion, viscosity, and self-diffusion previously derived on the basis of Chapman and Cowling's expression.

THE GENERAL INTERRELATION OF k_T^*, D, AND n

In combination with the relations

$$B^*=C^*(4-3C^*-d\ln C^*/d\ln T), \tag{6}$$

and

$$(6C^*-5)=2(2-n), \tag{7}$$

where n is the constant pressure derivative of the logarithm of the self-diffusion coefficient D with respect

* This work was supported by a St. John's University Summer Research Grant.

[1] Hirschfelder, Curtiss, and Bird, *Molecular Theory of Gases and Liquids* (John Wiley and Sons, Inc., New York, 1954).

[2] E. A. Mason, J. Chem. Phys. 22, 169 (1954).

[3] S. Chapman and T. G. Cowling, *The Mathematical Theory of Non-Uniform Gases* (Cambridge University Press, Teddington, England, 1952).

[4] T. Kihara, *Imperfect Gases* (Asakusa Bookstore, Tokyo, Japan, 1949). Translated into English by the U. S. Office of Air Research, Wright-Patterson Air Force Base.

† These are the quantities used by Mason and by Hirschfelder, Curtiss and Bird (see reference 1). They are related to the A, B, and C of Chapman and Cowling as follows: $5A=2A^*$; $5B=3B^*$; $5C=6C^*$.

to $\ln T$,‡ Chapman and Cowling's first approximation leads to[5]

$$k_T^*=\frac{15(2A^*+5)(2-n)}{4A^*[4A^*+16-n(5-n)-q]} \tag{8}$$

where q is $dn/d\ln T$. According to the first approximations of the theory to the coefficients of viscosity, η, and self-diffusion at one atmosphere, both coefficients referring to the same isotope of molecular weight M,

$$A^*=MD/98.45\eta T \tag{9}$$

so that Eq. (8) interrelates the three transport properties, k_T^*, D, and η.

The corresponding relationship derived from Kihara's more accurate expression is considerably simpler, and can be written as

$$MDk_T^*=184.6\eta T(2-n). \tag{10}$$

Equation (10) is subject to the following limitations:

(1) It is based on the results of the Enskog-Chapman kinetic theory which assumes[1]: (a) The temperature is not so low that quantum effects become important. This point is about 200°K for the lightest gases,[6] lower for others. (b) The temperature is not so high that excited energy states become important (causing inelastic collisions). This restriction appears to be severe only for thermal conductivity. (c) The density is not so high that triple collisions become important. (d) The density is not so low that either the dimensions of the vessel are large compared to the mean free path, or the gradient of any physical property is appreciable compared to the inverse of the mean free path. (e) The molecules are spherically symmetric. Although spherically symmetric potentials can account for single properties of unsymmetric molecules, different sets of parameters appear necessary for different properties.[7] The restriction to symmetric molecules may therefore be necessary for interrelations such as Eq. (10).

(2) Equation (10) is valid only for isotopes for which $(M_A-M_B)/(M_A+M_B)$ is less than about 0.15, since at larger values the dependence of k_T^* on this quantity becomes appreciable.[8] This restriction affects hydrogen and helium.

(3) Only the first approximations for η, D, n, and k_T^* have been considered. Higher approximations are considered in Appendix I, where it is shown that errors due to the first approximations largely cancel.

(4) Equation (7) is based on the assumption that the intermolecular potential is temperature independent.[5] For actual potentials, this appears to be equivalent to limitation (1*b*). An artificially temperature dependent potential is discussed in Appendix II.

(5) The most severe limitation at the present time to the practical application of Eq. (10) is the scarcity of experimental data. Viscosity measurements appear to be adequate, but self-diffusion and thermal diffusion data are too sparse in most cases. The greatest difficulty is encountered in the evaluation of the factor $(2-n)$, first because n is difficult to determine accurately from the diffusion measurements, and second because its value is always close to two.

THE CASE OF CONSTANT A^*

Equation (10) can be simplified by taking A^* to be constant. This appears justified on the basis of the best theoretical results. Table I includes Mason's values of A^* for the modified Buckingham potential as a function of $T^*=kT/\epsilon$ for $\alpha=14$. (ϵ/k and α are adjustable parameters of this potential.) From this it is seen that A^* is nearly constant over a considerable range of T^*. Similar results are shown by this potential with other values of α, and also by the Lennard-Jones 12, 6 potential,[9] A^* being constant within about two percent from $T^*=0.5$ in all cases to 13 for $\alpha=12$ (the worst case), 27 for $\alpha=15$, and 100 for the Lennard-Jones model. For most gases ϵ/k is over 100 (exceptions[6,7]: He, 9.16; H_2, 37.3; Ne, 38.0), and the approximate constancy of A^* thus extends over a very wide range of temperature. For example, argon ($\alpha=14$; $\epsilon/k=123.2$) has $A^*=1.12$ within 1 percent between about 125°K and 1470°K, and within 2 percent between 55°K and 2300°K.

From smoothed experimental data for viscosity and self-diffusion A^* for argon appears to be 1.105 ± 2 percent between about 120°K and at least 350°K, but falling off below this to a value 7 percent lower at 78°K.[10] A similar drop appears to occur for neon in the same temperature range (but different T^* range). This sort of behavior implies one or more of the following: (1) Eq. (9) is incorrect or inapplicable. (2) Neither the modified Buckingham nor the Lennard-Jones potential can account for the two properties, viscosity and diffusion, with the same set of parameters for the same gas. (3) The experimental data are inaccurate. The third possibility seems the most likely, especially since the apparent falling off of A^* is based on only two low temperature experimental values for argon, and only one for neon. We will therefore assume in what follows that the theoretically predicted behavior of A^* is more reliable than present experimental results.

Equation (10) can be written in the form

$$k_T^*=z^*(2-n), \tag{11}$$

where z^*, which is $15/8A^*$, can be considered constant. A similar conclusion was reached[10] concerning Eq. (8) even though the factor corresponding to z^* is much

‡ The constant density derivative, s_D, used by Mason is $n-1$.

[5] E. M. Holleran and H. M. Hulburt, J. Phys. Chem. **56**, 1034 (1952).

[6] E. A. Mason and W. E. Rice, J. Chem. Phys. **22**, 522 (1954).

[7] E. A. Mason and W. E. Rice, J. Chem. Phys. **22**, 843 (1954).

[8] E. R. S. Winter, Trans. Faraday Soc. **46**, 81 (1950).

[9] Hirschfelder, Bird, and Spotz, J. Chem. Phys. **16**, 968 (1948).

[10] E. M. Holleran, J. Chem. Phys. **21**, 2184 (1953).

TABLE I. Pertinent quantities for the modified Buckingham potential with $\alpha=14$ (see reference 2).

Col. 1	2	3	4	5	6	7	8	9	10	11	12
T^*	A^*	$10^3 s_A$	$\frac{100 s_A}{s_0-1}$	$[k_T^*]_1^K$	$\frac{dk_T^*}{d\ln T}$	$10^4\Delta$	$10^4(\gamma-\Delta)$	$10^4 d\Delta/d\ln T$	$10^3\epsilon$	$10^3\kappa$	$10^3(\epsilon+\kappa+\epsilon\kappa)$
0.0	1.0065	0	0.0	0.3105	0.00	20	−3	0	0.00	0.90	0.90
0.2	1.0374	52	−40.0	0.2341	−0.16	13	7	−17	−1.34	2.56	1.19
0.4	1.0932	62	−240	0.0451	−0.26	1	5	−6	−2.14	7.32	5.03
0.5	1.1070	39	1300	−0.0042	−0.17	0	2	0	−1.40	−12.00	−13.25
0.6	1.1128	18	120	−0.0254	−0.06	0	0	1	−0.50	0.78	0.28
0.8	1.1142	−8	−80	−0.0163	0.12	0	0	−1	1.01	−0.61	0.39
1.0	1.1106	−18	120	0.0252	0.24	0	0	3	1.98	−3.17	−1.25
1.2	1.1067	−20	44	0.0756	0.31	2	−1	11	2.54	−2.91	−0.44
1.4	1.1037	−18	24	0.1267	0.34	4	−1	21	2.80	−3.24	−0.53
1.6	1.1013	−14	14	0.1735	0.35	7	−2	29	2.86	−3.17	−0.40
1.8	1.0999	−10	7.9	0.2146	0.34	11	−3	36	2.83	−2.94	−0.19
2.0	1.0990	−5	3.4	0.2506	0.33	15	−3	40	2.75	−2.71	−0.03
2.5	1.0987	5	−2.7	0.3213	0.29	24	−2	46	2.42	−2.12	+0.25
3.0	1.1002	11	−5.0	0.3710	0.26	32	−1	46	2.10	−1.40	0.64
3.5	1.1026	15	−6.3	0.4069	0.22	39	0	43	1.78	−0.84	0.93
4.0	1.1050	19	−7.5	0.4325	0.19	45	1	39	1.53	−0.38	1.15
5	1.1101	23	−8.3	0.4660	0.14	53	2	32	1.16	0.41	1.57
6	1.1147	24	−8.3	0.4868	0.10	59	2	24	0.82	0.88	1.70
8	1.1224	23	−7.6	0.5055	0.05	65	2	13	0.44	1.50	1.94
10	1.1281	22	−7.1	0.5114	0.03	67	2	7	0.23	1.84	2.07
20	1.1449	20	−6.5	0.5074	−0.02	68	0	−4	−0.13	2.29	2.16
30	1.1542	20	−6.5	0.4994	−0.01	67	1	−2	−0.07	2.24	2.17
50	1.1668	22	−7.2	0.4930	0.01	67	1	3	0.09	2.13	2.22
100	1.1858	25	−7.9	0.4998	0.03	70	3	8	0.26	1.94	2.20
200	1.2068	27	−8.1	0.5182	0.05	77	4	14	0.43	1.83	2.26

more complicated, and involves n and q.§ An inspection of Mason's tabulations shows that, in the absence of prior information concerning a given gas, but assuming that the modified Buckingham potential will apply, A^* can be taken as 1.11 with an uncertainty of only two or three percent over very wide ranges of T^* for any reasonable α. The relation then becomes

$$k_T^*=1.69(2-n). \tag{12}$$

A knowledge of α, or accurate experimental values of A^*, may produce a slightly improved value for z^*, but in most cases, except at very high or low temperatures, the inherent error of Eq. (12) is less than the usual experimental error of thermal diffusion measurements.

The accurate experimental determination of n from self-diffusion measurements remains the most difficult problem, however. The simplest procedure is to evaluate $\Delta\ln D/\Delta\ln T$, the increment of $\ln D$ divided by the corresponding increment in $\ln T$ for two experimental determinations of $D(T)$. As will be seen, this procedure is practical only for fairly large increments. $\Delta\ln D/\Delta\ln T$ is then equal to n at some unknown intermediate temperature. Fortunately, the constancy of A^* leads to the result that the temperature appropriate to n determined in this way from two self-diffusion measurements at T_1 and T_2 is the same as $\bar{T}$, the temperature to be assigned to the thermal diffusion ratio measured between the same two temperatures. Thus

$$k_T^*(\bar{T})=1.69(2-\Delta\ln D/\Delta\ln T), \tag{13}$$

irrespective of the temperature dependence of k_T^* or n, that is, no matter what (unknown) value $\bar{T}$ assumes between T_1 and T_2. An equivalent expression is obtained from Eqs. (2) and (3):

$$\Delta x(T_1,T_2)=1.69Q\ln(D_1T_2^2/D_2T_1^2), \tag{14}$$

where $\Delta x(T_1,T_2)$ is the difference in mole fraction of either isotope between the two regions at T_1 and T_2. Q is $x_Ax_B(M_A-M_B)/(M_A+M_B)$. It might be noted that while k_T^* is constant for constant $\bar{T}$, Δx is not.

In these equations small errors in D lead to relatively large errors in k_T^* and Δx. The ratio of the percentage error in k_T^* as calculated from Eq. (13) to the experimental percentage error in D_2/D_1 is equal to $1.69/k_T^*\Delta\ln T$, assuming a negligible error in T_2/T_1. Thus even for the rather high k_T^* value of 0.6 this ratio is 5 for $T_2=1.76T_1$, and 10 for $T_2=1.33T_1$.

When more than two values of D are available, the utility of the measurements is greatly improved by smoothing. It is then possible to calculate $\bar{T}$ as a function of T_1 and T_2, and to estimate n and k_T^* for any given temperature in the range of the data. The accuracy of such results depends of course on the accuracy of the data, but it is also appreciably sensitive to the method of smoothing, since many curves differing considerably in slope at various points can reasonably fit the data if they are sparse. It is therefore very helpful

§ z^* differs from z of reference 10 in two respects: (1) it is based on Kihara's approximation rather than Chapman and Cowling's, and (2) it refers to k_T^* rather than R_T.

to know the appropriate form of empirical equation to employ. One fairly simple form is implied by the results of experimental measurements of the thermal diffusion ratio by Stier.[11]

THE CASE OF k_T^* LINEAR IN $\ln T$

Stier's data for argon and neon isotopes obey the empirical equation

$$k_T^* = a^* \ln(T/b), \tag{15}$$

where a^* and b are constants.|| This behavior is in limited qualitative agreement with the predictions of the modified Buckingham and Lennard-Jones potentials, according to which the curves k_T^* *versus* $\ln T$, while obviously not linear (see Table I, columns 5 and 6), can be approximated by straight lines within 5 percent (Stier's experimental error) for T^* between about 1 and 5. The neon measurements, however, are for temperatures well beyond this (T^* between about 3.5 and 19), and the reported values are much too high to be consistent with viscosity measurements, according to these models. The steep repulsive potential implied by these high values is also inconsistent[7] with the results of high velocity atomic beam scattering experiments.[12] For these reasons the thermal diffusion data for neon are doubtful and will not be considered further here. For argon, the temperature range is about right, and the numerical values are in fair agreement with the modified Buckingham potential.[7] We will therefore assume that Eq. (15) can represent thermal diffusion measurements within the rather large experimental error over an important part of the temperature range.

When Eq. (15) is valid $\bar{T}$ is $(T_1T_2)^{\frac{1}{2}}$, and D should obey the empirical equation[10]

$$\ln D = \ln\alpha_D + \beta_D(\ln T) + \gamma_D(\ln T)^2, \tag{16}$$

where α_D, β_D, γ_D are constants. β_D and γ_D are related to a^* and b as follows:

$$a^* = -2z^*\gamma_D; \quad \ln b = (2-\beta_D)/2\gamma_D. \tag{17}$$

For argon, the observed k_T^* values give $a^*=0.228$, $b=91.0$°K.[13] With $z^*=1.69$ these lead to $\beta_D=2.610$ and $\gamma_D=-0.0676$ which with $\ln\alpha_D=-14.382$¶ reproduce Winn's diffusion data[14] within 1.5 percent which is also within the reported experimental error. Assuming Stier's thermal diffusion data for argon to be correct up to the highest temperature (729°K), Eq. (16) with the constants just given should be useful for extrapolating the diffusion data beyond the present experimental temperature range. The calculated D values (for 1 atmos pressure) at 400°, 500°, 600°, and 700°K are 0.310, 0.461, 0.636, and 0.831 cm^2 sec^{-1}.

The results of the reverse procedure of finding β_D, γ_D, and thence a^*, b, and k_T^* from diffusion measurements are not so good at present. A least squares fit of Eq. (16) to Winn's six measured values for argon give $\beta_D=2.860$, $\gamma_D=-0.09094$. These lead to $a^*=0.303$ and $b=113$°K which differ from the observed values by more than the experimental error.[10]

Presumably, trustworthy values of n and k_T^* can be found from more abundant experimental diffusion data when these become available. Until then it may be useful to estimate n and k_T^* from the more extensive and accurate viscosity data. The practicality of this depends on exactly how constant A^* is.

VISCOSITY AND THERMAL DIFFUSION

From Eq. (9) it is seen that $n=1+s_\eta+s_A$, where s_η is $d\ln\eta/d\ln T$ and s_A is $d\ln A^*/d\ln T$. Since A^* is nearly constant, s_A can be expected to be small. If it can be neglected, we have

$$k_T^* = 1.69(1-s_\eta), \tag{18}$$

which would be more useful than Eq. (12) at the present time because of the better viscosity data. However, omitting s_A from the parenthesis of Eq. (18) assumes a much stricter constancy for A^* than has been assumed heretofore. Table I includes s_A as a function of T^* for the modified Buckingham potential with $\alpha=14$, s_A having been found as the difference between the s_D and s_η which are tabulated by Mason. From this it is seen that the absolute error in k_T^*, which is $1.69s_A$, lies between the limits of ±0.05 for T^* above about 0.55. Column 4 of Table I lists $100s_A/(s_D-1)$ which is the percentage error in k_T^*, according to this molecular model, caused by using Eq. (18) rather than Eq. (12). The error is less than 8.5 percent for T^* above 1.8, much smaller near $T^*=2.26$ where it vanishes, and much larger near the inversion temperatures. Other values of α show similar results, except that for small α the error becomes larger at very high temperatures. Even for $\alpha=12$, however, the error is less than 10 percent for T^* between 1.6 and 13.

Thus Eq. (18), although subject to this inherent error which is on the average much greater than that of Eq. (12), is to be preferred in many cases at the present time as a means of estimating the thermal diffusion ratio. This also applies to the relation corresponding to Eq. (14):

$$\Delta x = 1.69Q\ln(\eta_1T_2/\eta_2T_1). \tag{19}$$

An error arises here from neglecting A_1^*/A_2^* in the argument of the logarithm. As has been seen, according to the modified Buckingham potential, A_1^* and A_2^* may differ by a few percent in the temperature range under consideration, again leading to appreciable error. However, A_1^* and A_2^* may be practically equal, and the error quite small, if T_1 and T_2 happen to straddle

[11] L. G. Stier, Phys. Rev. **62**, 548 (1942).

|| a^* is smaller than the a of references 10, 11, and 13 by the factor 105/118.

[12] I. Amdur and E. A. Mason (to be published).

[13] E. M. Holleran, J. Chem. Phys. **21**, 1901 (L) (1953).

¶ These values differ somewhat from the values found (see reference 10) on the basis of Chapman and Cowling's approximation.

[14] E. B. Winn, Phys. Rev. **80**, 1024 (1950).

the point at which s_A vanishes, so that $\bar{T}$ is near this point.

For the temperature range in which k_T^* can be considered linear in $\ln T$ the approximation of constant A^* gives

$$\ln\eta=\ln\alpha_\eta+\beta_\eta(\ln T)+\gamma_\eta(\ln T)^2 \qquad (20)$$

as an empirical equation for the temperature dependence of viscosity, with the constants β_η and γ_η determinable from thermal diffusion. These constants are related to those of Eqs. (16) and (17) as follows for $A^*=1.11$:

$$\alpha_\eta=M\alpha_D/109.3;\quad \beta_\eta=\beta_D-1;\quad \gamma_\eta=\gamma_D. \qquad (21)$$

The values of a^* and b found from Stier's thermal diffusion data for argon give $\beta_\eta=1.610$, $\gamma_\eta=-0.0676$. Using these constants in Eq. (20), together with Johnson and Grilly's 17 experimental viscosity values between 77.9°K and 296°K,[15] gives calculated values of $\ln\alpha_\eta$ equal to -15.3754 ± 0.0040 except for the two lowest temperatures (77.9° and 90.3°K) where appreciable deviation occurs. Equation (20) with this constant value of $\ln\alpha_\eta$ and the thermal diffusion values of β_η and γ_η just given can therefore reproduce the 15 experimental viscosity values above the two lowest within four-tenths of one percent.

The reverse procedure of calculating k_T^* from viscosity measurements is also successful in this case. The least squares fit of Eq. (20) to the data of Johnson and Grilly (omitting the two lowest points which do not fit well even when included) reproduces the viscosity data within 0.36 percent with the constants: $\ln\alpha_\eta=-15.3823$, $\beta_\eta=1.6075$, $\gamma_\eta=-0.06687$. These yield $k_T^*=0.226\ln(T/93.9)$ as the predicted behavior of the reduced thermal diffusion ratio. The constants of this equation are so close to the experimentally determined values that a rather good reproduction of the thermal diffusion data results. Table II shows that the agreement is excellent except at the two lowest temperatures. Discrepancies can be expected at these temperatures because (1) T_1 is below the temperature region in which Eq. (20) is valid; (2) Eq. (15) fails for the lowest k_T^* value; and (3) according to the modified Buckingham potential, the neglect of s_A by Eq. (18) should cause considerable error below about 200°K for argon. A relation similar to Eq. (18) was derived[16,17] on the basis of the inverse power model (see Appendix II) and was shown by Stier to give fairly good agreement with his data.

The experimental viscosity constants of Eq. (20) can also be used to calculate the self-diffusion coefficient. Substitution of the viscosity constants in Eqs. (21) with $M=40$ gives $\ln\alpha_D=-14.3771$, $\beta_D=2.6075$, $\gamma_D=-0.06687$. Values of the self-diffusion coefficient calculated from Eq. (16) with these constants agree with Winn's results within the experimental error except at the two lowest temperatures 77.7°K and 90.2°K, where the errors are still only 1.8 percent and 2.4 percent in spite of the fact that the viscosity constants are invalid for temperatures this low.

TABLE II. Thermal diffusion ratios for argon, observed, and calculated from viscosity.

T_1	T_2	$(T_1T_2)^{\frac{1}{2}}$	k_T^*(obs)	$k_T^*(\eta)$
90	195	132	0.060	0.078
90	296	163	0.134	0.126
195	296	240	0.221	0.214
195	495	311	0.278	0.274
273	623	412	0.346	0.338
455	685	558	0.415	0.408
638	833	729	0.475	0.469

It has thus been seen that in the case of argon Johnson and Grilly's experimental viscosity data, Winn's self-diffusion data, and Stier's thermal diffusion data can be represented rather well by the three empirical equations, (20), (16), and (15), with only three independent arbitrary constants among them. The experimental quantity $Dk_T^*/\eta T(2-n)$ is therefore easily seen to be constant at 4.62 as required by Eq. (10) with $M=40$.

These particular empirical equations cannot be expected to be so successful generally. More elaborate empirical equations may be needed in many cases when extensive data are available. Occasionally, however, especially for limited temperature ranges, even simpler equations may be useful. For example, Sutherland's equation may sometimes be valid for viscosity or diffusion, in which case Eq. (12) reduces to $k_T^*=0.84(T-C)/(T+C)$, where Sutherland's constant, C, is preferably determined from diffusion data. A similar relation, $k_T^*=0.89(T-0.98C)/(T+0.92C)$, was given by Jones[16] on the basis of the high temperature results of Sutherland's intermolecular potential. Unfortunately, the Sutherland equation is frequently incapable of representing correctly the slope of $\ln D$ or $\ln\eta$ *versus* $\ln T$ except over very limited temperature intervals. It is not adequate, for example, in the case of the argon viscosity data discussed above.

More promising is the possibility that, as predicted by the modified Buckingham and Lennard-Jones potentials, at very high temperatures k_T^* may be nearly constant, and $\ln D$ and $\ln\eta$ approximately linear in $\ln T$.

APPENDIX I. THE EFFECT OF CONSIDERING HIGHER APPROXIMATIONS TO THE TRANSPORT PROPERTIES

The kinetic theory expressions for the transport properties can be written as

$$\eta=[\eta]_1(1+\gamma);\quad D=[D]_1(1+\Delta);$$
$$k_T^*=[k_T^*]_1(1+\kappa) \qquad (22)$$

where $[\eta]_1$, $[D]_1$, $[k_T^*]_1$, represent the first nonzero approximation expressions of the theory for η, D, and k_T^*, to which Eqs. (22) reduce upon insertion of the

[15] H. L. Johnston and E. R. Grilly, J. Phys. Chem. **46**, 948 (1942).
[16] R. C. Jones, Phys. Rev. **58**, 111 (1940).
[17] H. Brown, Phys. Rev. **57**, 242(L) (1940).

first approximations to γ, Δ, and κ which are zero. Higher approximation expressions for γ, Δ, and κ rapidly become very complicated, but these quantities, especially γ and Δ, are so small compared to unity that the second approximations are probably sufficient for many purposes. However, the third approximations to γ and Δ are available for the modified Buckingham potential,[2] and these values will be used here. (Δ for $\alpha=14$ is included in Table I, column 7.)

One source of error in Eq. (10) is the fact that Eq. (9) relating A^*, D, and η is derived on the basis of the first approximations to D and η. When actual values of these coefficients are used A^* is therefore not strictly given by Eq. (9), but more exactly by

$$A^*=MD(1+\gamma-\Delta)/98.45\eta T. \tag{23}$$

Table I, column 8, lists $\gamma-\Delta$ to the third approximation according to the modified Buckingham potential with $\alpha=14$. Other values of α give similar results. Due to a remarkably close parallelism between Δ and γ, the error caused by using actual values of D and η in Eqs. (9) and (10) is seen to be quite unimportant.

Another source of error in Eq. (10) and subsequent relations is the fact that Eq. (7) is derived from the expression for $[D]_1$. The actual value of n is therefore not strictly equal to $9/2-3C^*$ as stated in Eq. (7), but is given by

$$n=9/2-3C^*+d\Delta/d\ln T. \tag{24}$$

Because k_T^* is very sensitively related to the value of n, neglect of the term $d\Delta/d\ln T$ may lead to appreciable error. To estimate the size of this error according to the modified Buckingham potential Kihara's second approximation expression for Δ will be used:

$$\Delta=(6C^*-5)^2/(16A^*+40). \tag{25}$$

This gives

$$\frac{d\Delta}{d\ln T}=\frac{12\Delta dC^*/d\ln T}{(6C^*-5)}$$

$$=\frac{3(6C^*-5)(4C^*-3C^{*2}-B^*)}{(4A^*+10)}, \tag{26}$$

assuming constant A^*. This assumption is equivalent to neglecting the term $s_A A^*\Delta/(A^*+2.5)$ which is always less than 10^{-4} according to the modified Buckingham potential. The rightmost member in Eqs. (26) was obtained with the help of Eq. (6). Table I, column 9, lists $d\Delta/d\ln T$ for $\alpha=14$. Omission of this quantity is seen to produce an error ($\sim 1.69 d\Delta/d\ln T$) in calculated k_T^* which is at most 0.008 in absolute magnitude. Column 10 lists ϵ, defined as $2(d\Delta/d\ln T)/(6C^*-5)$ so that 100ϵ is the percentage error in k_T^* from this source, and the factor $(2-n)$ in Eqs. (7), (10), etc. should be replaced by $(2-n)(1+\epsilon)$. The error is seen to be about two or three percent over an important part of the temperature range.

It should be noted that the quantities Δ, $d\Delta/d\ln T$, and ϵ can in principle be determined from experimental data for k_T^*, a procedure which would be preferable if sufficiently accurate data were available. Thus, Eqs. (5) and (25) with $A^*=1.11$ give $\Delta\approx 0.024\ k_T^{*2}$; $d\Delta/d\ln T \approx 0.049\ k_T^*(dk_T^*/d\ln T)$; $\epsilon\approx 0.082\ (dk_T^*/d\ln T)$. When Eq. (15) holds, $dk_T^*/d\ln T$ is constant at the value a^* (compare Table I, column 6). For argon this would give ϵ constant at about 0.019 between about 150°K and 700°K.

The final source of error in Eqs. (10) ff. is the fact that they are based on Kihara's first approximation to k_T^*. Higher approximations have not been worked out by Kihara's method. Probably the best estimate at present for the κ appropriate to $[k_T^*]_1^K$ is given by $(1+\kappa)=[k_T^*]_2^{CC}/[k_T^*]_1^K$, since Chapman and Cowling's second approximation is presumably the most accurate expression for k_T^* now available. Table I, column II, lists κ determined in this way for the modified Buckingham potential with $\alpha=14$. It is seen that errors from this source are also two or three percent over a large range of temperature. Fortunately, ϵ and κ are of opposite sign and comparable magnitude in the temperature range in which ϵ is largest. Column 12 shows that the combined error is quite small in this important temperature range, which includes room temperature for most gases. However, future evaluation of κ on the basis of higher approximations to k_T^* may revise these figures somewhat.

APPENDIX II. RELATIONS ACCORDING TO SIMPLE POTENTIAL MODELS

Relations between viscosity and thermal diffusion have been derived in the past on the basis of simple intermolecular potentials. Two such relations have been mentioned: one based on the Sutherland potential, and another, which can be written as $k_T^*\sim 1.5(1-s_\eta)$, given by Brown[17] and Jones[16] on the basis of the inverse power model. Relations such as these were properly treated with caution, since they were based on crude potential models, and there was no theoretical justification for assuming their general validity.

It can now be seen that these relations are roughly correct under certain conditions. In fact, the above equation of Brown and Jones differs from the approximate relation (18) only in the constant factor. It may at first seem surprising that such simple potentials should yield relations so near the general truth. The basic reason for this is that the results of any spherically symmetric, temperature independent intermolecular potential must obey Eqs. (6) and (7), and therefore (within the limitations previously mentioned) also the transport property interrelations (10), etc. For the most realistic potentials these relations are not immediately apparent because of the complexity of the results. Simpler potentials have the advantage that relations among the various quantities are apparent almost upon inspection. But of course such unrealistic

potentials also have the disadvantages that (1) some of the obvious relations will not be true for actual potentials, and (2) generally true relations, like Eqs. (6) and (7), though obeyed, may be hidden by trivialities.

A good illustration of this is the inverse power model, for which the intermolecular potential equals ar^{-m}, where a and m are constants, and r is the intermolecular separation. This model gives[3] $B^*=(3m-2)(m+2)/3m^2$ and $C^*=(3m-2)/3m$. The general relation (6) is of course obeyed by these equations, but it cannot be deduced from them, and the obvious relation, $B^*=C^*(4-3C^*)$, is not generally true.

According to the first approximations to the transport properties the inverse power model also gives:

$$\eta=cT^{(m+4)/2m};\ D=c'T^{(3m+4)/2m};\ k_T^*=z^*(m-4)/2m, \quad (27)$$

where c and c' are constants depending on a and m. z^* equals $15/8A^*$ which is approximately equal to 1.5 for common values of m. Because m is constant, the exponent $(m+4)/2m$ is equal to s_η, and the relation of Brown and Jones follows directly. The more correct relation, $k_T^*=z^*(1-s_\eta-s_A)$, is also obeyed, but is not apparent because s_A is zero. However, this same equation in the form, $k_T^*=z^*(2-n)$, does follow from Eqs. (27). This relation seems to have been ignored, doubtless because it could not compare in immediate usefulness with the viscosity relation.

Application of these relations to actual cases requires that s_η, n, k_T^*, and therefore m vary with temperature. This violates the assumption of temperature independent potential required for the general validity of Eqs. (6) and (7), and it can be seen that Eq. (6) cannot possibly hold when m varies with T. Fortunately, however, an *ad hoc* choice of $a(T)$ permits conformity with Eq. (7). Acceptance of the relation, $k_T^*=z^*(2-n)$, tacitly assumes the correct $a(T)$, and use of the somewhat incorrect $k_T^*=z^*(1-s_\eta)$, automatically assumes an $a(T)$ leading to some deviation from Eq. (7).

THE JOURNAL OF CHEMICAL PHYSICS VOLUME 23, NUMBER 5 MAY, 1955

Spectra and Electronic Structure of Fluorochromate Ion, Chromyl Chloride, and Some Related Compounds*†

LINDSAY HELMHOLZ AND HARRY BRENNAN, *Chemistry Department, Washington University, St. Louis, Missouri*

AND

MAX WOLFSBERG, *Chemistry Department, Brookhaven National Laboratory, Upton, Long Island, New York*

(Received June 11, 1954)

A semiempirical treatment, which gives satisfactory agreement between calculated and observed spectra for chromate and permanganate ions, has been employed to calculate the excited state energies and transition moments for the related molecules of the chemical formulas CrO_3X^- and CrO_2X_2. The results show agreement with experimental data which unfortunately are not extensive for these molecules. The calculations indicate an absorption for SO_2Cl_2 in the farther ultraviolet in agreement with experiment. The qualitative significance of the results, so far as the relative importance of σ and π bonding, is discussed.

INTRODUCTION

IN a previous report[1] a semiempirical method was employed to calculate the energies of the ground state and first few excited orbitals for the inorganic ions, chromate ($CrO_4^=$), permanganate (MnO_4^-), and perchlorate (ClO_4^-). The results showed qualitative agreement between calculated and observed spectra and a greater measure of quantitative agreement than might have been anticipated. We have applied the same simple approximate method to the ions (and molecules) CrO_3F^-, CrO_3Cl^-, CrO_2F_2, CrO_2Cl_2, and SO_2Cl_2 to test the usefulness of the method and to try to gain some insight into the electronic structure of these molecules. Unfortunately no detailed spectral data exist for these molecules, but the qualitative agreement with observations both with regard to energies of excitation and intensities is found to be good. The calculations yield the observed modification of the spectra which result from the substitution of first one and then two halogen atoms for oxygen, and also the observed shifts resulting from the substitution of fluorine for chlorine.

Some qualitative suggestions concerning the relative importance of π and σ bonding seem justified in view of the agreement obtained.

PROCEDURE

The calculation of the orbital energies was carried out by the method outlined in the previous paper. Some simplifications have been introduced. The tetrahedral angle has been assumed for all bond angles in

* Abstracted from a thesis submitted by Harry Brennan in partial fulfillment of the requirements for the Degree of Doctor of Philosophy at Washington University.

† Research carried out in part under the auspices of the U. S. Atomic Energy Commission.

[1] M. Wolfsberg and L. Helmholz, J. Chem. Phys. **20**, 837 (1952).

TABLE I.

Representation	Cr	Halogen	Oxygen
		$C_{3v}-CrO_3X^-$	
A_1	s, $(\frac{1}{3})^{\frac{1}{2}}(d_{xy}+d_{xz}+d_{yz})$, $(\frac{1}{3})^{\frac{1}{2}}(p_x+p_y+p_z)$	σ_1	$(\frac{1}{3})^{\frac{1}{2}}(\sigma_2+\sigma_3+\sigma_4)$, $(\frac{1}{3})^{\frac{1}{2}}(\pi x_2+\pi x_3+\pi x_4)$
A_2			$(\frac{1}{3})^{\frac{1}{2}}(\pi y_2+\pi y_3+\pi y_4)$
E	$(\frac{1}{6})^{\frac{1}{2}}(d_{xz}+d_{yz}-2d_{xy})$, $(\frac{1}{6})^{\frac{1}{2}}(2p_z-p_x-p_y)$, d_z^2	πx_1	$(\frac{1}{6})^{\frac{1}{2}}(\sigma_3+\sigma_4-2\sigma_2)$, $(\frac{1}{6})^{\frac{1}{2}}(\pi x_3+\pi x_4-2\pi x_2)$, $(\frac{1}{2})^{\frac{1}{2}}(\pi y_4-\pi y_3)$
	$(\frac{1}{2})^{\frac{1}{2}}(d_{xz}-d_{yz})$, $(\frac{1}{2})^{\frac{1}{2}}(p_x-p_y)$, $d_{x^2-y^2}$	πy_1	$(\frac{1}{2})^{\frac{1}{2}}(\sigma_3-\sigma_4)$, $(\frac{1}{2})^{\frac{1}{2}}(\pi x_4-\pi x_3)$, $(\frac{1}{6})^{\frac{1}{2}}(2\pi y_2-\pi y_3-\pi y_4)$
		$C_{2v}-CrO_2X_2$	
A_1	s, d_{z^2}, d_{xy}	$(\frac{1}{2})^{\frac{1}{2}}(\sigma_3+\sigma_4)$, $(\frac{1}{2})^{\frac{1}{2}}(\pi y_3+\pi y_4)$	$(\frac{1}{2})^{\frac{1}{2}}(\sigma_1+\sigma_2)$, $(\frac{1}{2})^{\frac{1}{2}}(\pi y_1+\pi y_2)$
A_2	$d_{x^2-y^2}$	$(\frac{1}{2})^{\frac{1}{2}}(\pi x_3+\pi x_4)$	$(\frac{1}{2})^{\frac{1}{2}}(\pi x_1+\pi x_2)$
B_1	$(\frac{1}{2})^{\frac{1}{2}}(d_{xz}+d_{yz})$	$(\frac{1}{2})^{\frac{1}{2}}(\pi x_3-\pi x_4)$	$(\frac{1}{2})^{\frac{1}{2}}(\sigma_1-\sigma_2)$, $(\frac{1}{2})^{\frac{1}{2}}(\pi y_1-\pi y_2)$
B_2	$(\frac{1}{2})^{\frac{1}{2}}(d_{xz}-d_{yz})$	$(\frac{1}{2})^{\frac{1}{2}}(\sigma_3-\sigma_4)$, $(\frac{1}{2})^{\frac{1}{2}}(\pi y_3-\pi y_4)$	$(\frac{1}{2})^{\frac{1}{2}}(\pi x_3-\pi x_2)$

spite of the fact that electron diffraction[2] and x-ray[3] results indicate deviations from 109°28′ by as much as five degrees. The $4p$ orbitals of chromium have not been considered in the chromyl compounds, since it was found in previous calculations on $CrO_4^=$ that neglect of these orbitals caused only minor differences in the molecular orbital energies. Finally the orientation of the oxygen and halogen p orbitals have been taken so as to give the simplest form for the combinations belonging to the irreducible representations of the symmetry group in question. Since the form of the wave functions depends on this choice, the orientations are given in Fig. 1 in terms of the direction cosines of the orbitals relative to the axial system indicated on the central atom. The atomic orbitals and combinations of equivalent orbitals belonging to the indicated irreducible representations are given in Table I.

The empirical method, discussed in some detail in the presentation of the calculation on MnO_4^- and $CrO_4^=$, involves the solution of secular determinants of the form $|H_{ij}-G_{ij}\epsilon|=0$ by means of the approximation $H_{ij}=K_{\sigma,\pi}[(H_{ii}+H_{jj})/2]G_{ij}$. The H_{ii}'s for chromium were employed in previous calculations as adjustable parameters, but set very nearly equal to the valence state ionization potentials.[4] In the present calculation the values have been taken equal to the values used in the $CrO_4^=$ case minus 0.5 ev for each decrease in negative charge on the molecule, for example H_{dd} Cr (in $CrO_4^=$) $=-8.5$ ev, H_{dd} Cr (in CrO_3F^-) $=-9.0$ ev, and H_{dd} Cr (in CrO_2Cl_2) $=-9.5$ ev. We felt that the correction would take into account the effect of decreasing negative charge on the atoms as the negative charge on the molecule as a whole decreased; however, the energies of the low-lying transitions are relatively insensitive to these shifts, and in the absence of ionization data we are unable to check the correctness of the magnitude of the changes. The value of H_{ii} Cl was taken as equal to that for oxygen, and that for fluorine 1 ev lower than the oxygen values. The empirical constants, K_σ for σ overlaps and K_π for π overlaps, were taken to be 1.67 and 2.00, respectively, the same values used previously. The $G(i,j)$ are the group overlap integrals, for example:

$$\int d_{z^2}\cdot[(\tfrac{1}{6})^{\frac{1}{2}}](\sigma_3+\sigma_4-2\sigma_2)d\tau=G_E[d_{z^2},\sigma(\text{oxygen})]$$

(see Table I).

The experimental spectra are shown in Fig. 2 and the results of calculations for CrO_3F^- and CrO_2Cl_2, in Fig. 3 with the $CrO_4^=$ results for comparison. With the assumption that the energies of transition correspond to the difference between the initial and final orbital energies, it will be seen that the qualitative changes in the observed energies of transition are given by the calculation. For example: in going from $CrO_4^=$ to CrO_3F^- an absorption appears at lower energies than the first maximum in $CrO_4^=$ and a more intense absorption appears at higher energies. Further calculation and discussion needed for a comparison of calculations and experiment are given in the following.

Fluorochromate, CrO_3F^-, and chloro-chromate, CrO_3Cl^-: The first transition in these ions, according to

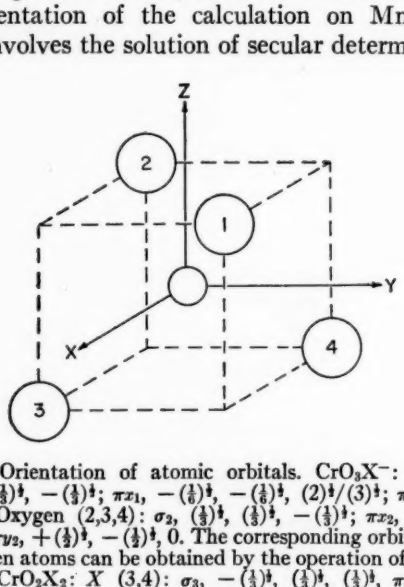

FIG. 1. Orientation of atomic orbitals. CrO_3X^-: $X(1)$: σ_1, $-(\frac{1}{3})^{\frac{1}{2}}$, $-(\frac{1}{3})^{\frac{1}{2}}$, $-(\frac{1}{3})^{\frac{1}{2}}$; πx_1, $-(\frac{1}{6})^{\frac{1}{2}}$, $-(\frac{1}{6})^{\frac{1}{2}}$, $(2)^{\frac{1}{2}}/(3)^{\frac{1}{2}}$; πy_1, $-(\frac{1}{2})^{\frac{1}{2}}$, $+(\frac{1}{2})^{\frac{1}{2}}$, 0. Oxygen (2,3,4): σ_2, $(\frac{1}{3})^{\frac{1}{2}}$, $(\frac{1}{3})^{\frac{1}{2}}$, $-(\frac{1}{3})^{\frac{1}{2}}$; πx_2, $(\frac{1}{6})^{\frac{1}{2}}$, $(\frac{1}{6})^{\frac{1}{2}}$, $(2)^{\frac{1}{2}}/(3)^{\frac{1}{2}}$; πy_2, $+(\frac{1}{2})^{\frac{1}{2}}$, $-(\frac{1}{2})^{\frac{1}{2}}$, 0. The corresponding orbitals on the other oxygen atoms can be obtained by the operation of the three-fold axis. CrO_2X_2: X (3,4): σ_3, $-(\frac{1}{3})^{\frac{1}{2}}$, $(\frac{1}{3})^{\frac{1}{2}}$, $(\frac{1}{3})^{\frac{1}{2}}$, πx_3, $+(\frac{1}{2})^{\frac{1}{2}}$, $+(\frac{1}{2})^{\frac{1}{2}}$, 0; πy_3, $-(\frac{1}{6})^{\frac{1}{2}}$, $+(\frac{1}{6})^{\frac{1}{2}}$, $-2^{\frac{1}{2}}/3^{\frac{1}{2}}$. Oxygen (1,2): σ_1, $-(\frac{1}{3})^{\frac{1}{2}}$, $-(\frac{1}{3})^{\frac{1}{2}}$, $-(\frac{1}{3})^{\frac{1}{2}}$; πx_1, $+(\frac{1}{2})^{\frac{1}{2}}$, $-(\frac{1}{2})^{\frac{1}{2}}$, 0; πy_1, $-(\frac{1}{6})^{\frac{1}{2}}$, $-(\frac{1}{6})^{\frac{1}{2}}$, $+(2)^{\frac{1}{2}}/(3)^{\frac{1}{2}}$. The corresponding orbitals on atoms 2 and 4 may be obtained by the operations of the twofold axis (Z-axis) of C_{2v}.

[2] K. J. Palmer, J. Am. Chem. Soc. **60**, 2360 (1938).
[3] L. Helmholz and W. R. Foster, J. Am. Chem. Soc. **72**, 4971 (1950).
[4] R. S. Mulliken, J. Chem. Phys. **2**, 782 (1934).

our calculations, involves the excitation of an a_2 nonbonding electron to the antibonding $5e$ orbital, the resulting state having the symmetry E. The data on the dichroism of the substance $KCrO_3Cl$[3] indicate that this lowest-energy absorption is due (principally at least) to a transition from the A_1 ground state to an excited E state. This information concerning the symmetry of the excited states is all that exists at present.

The excitation of a $4e$ electron to the $5e$ orbital gives rise to three excited states of symmetries A_1, A_2, and E. Since dipole transitions are allowed to both A_1 and E states, a calculation of the absorption spectrum must include a calculation of the energies of the A_1 and E states belonging to the $(4e)^{-1}$ $5e$ configuration. The expressions for the energies of transition to these states are given in Appendix I in terms of the indicated Coulomb and exchange integrals and the orbital energies. We have attempted to evaluate these integrals in

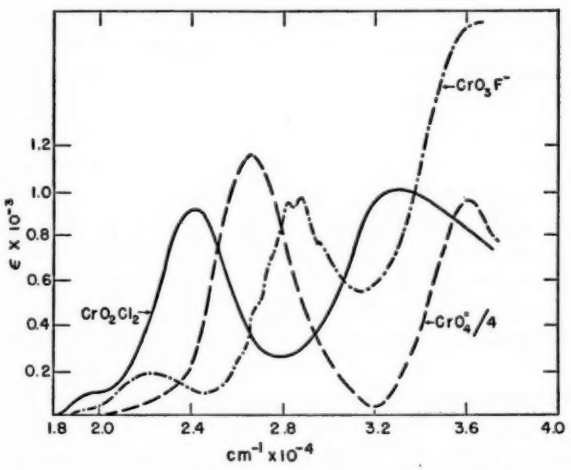

FIG. 2. Observed absorption of $CrO_4^=$, CrO_3F^-, and CrO_2Cl_2. The values of the extinction coefficients of $CrO_4^=$ have been divided by 4 as indicated. The vibrational structure in the case of CrO_3F^- appear in less polar solvents, not in water solutions.

the following manner. All integrals except those over the same atom have been neglected. The resulting expressions for the energies of excitation contain the coefficients of the atomic orbitals in the normalized molecular orbitals and Coulomb and exchange integrals for these atoms. The separation between the $^1T_2$, ^1E, and $^1T_1$ excited states can be calculated for chromate ion in terms of similar integrals and the atomic orbital coefficients, and experimental values for these separations can be obtained from the spectrum of $CrO_4^=$ dissolved in nonabsorbing solids. The atomic exchange and Coulomb integrals have been evaluated from a comparison of calculations and observations for the chromate case, and the same empirically derived values used for both oxygen and fluorine atoms in the CrO_3F^- calculations.

The f-values have been calculated in the same manner as in the permanganate calculations, with neglect of all

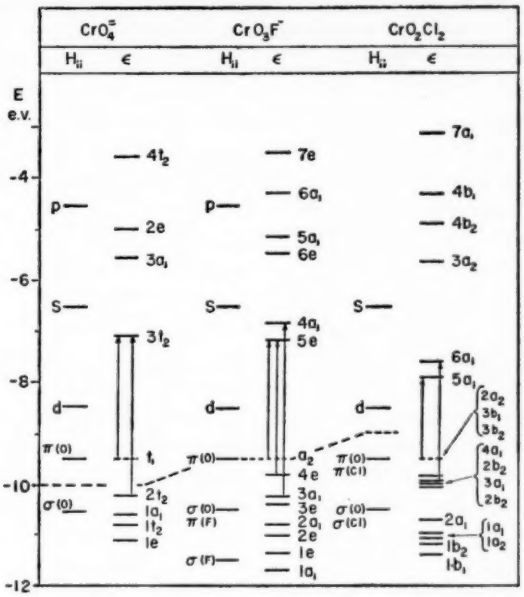

FIG. 3. Orbital energy level diagram for $CrO_4^=$, CrO_3F^-, and CrO_2Cl_2.

integrals except those over the same atom. The energies and f-values are shown in Fig. 4. The height of the lines indicates the magnitude of the f-values relative to $f(^1A_1 \rightarrow {}^1T_2)$ for the first transition in chromate as shown in the lower part of the figure. The dotted lines indicate the experimental position of the $^1T_2$ level (longer line) and the approximate position of the ^1E level (shorter line) for chromate ion. The $^1E - {}^1T_2$ separation was used in evaluating the integrals as discussed in the previous paragraph. The results of these calculations are given in Table II. The discrepancy between calculated f-values and those observed is somewhat greater (a factor of 4 to 5) than was the case for the first allowed chromate transition where the factor was 2.5.

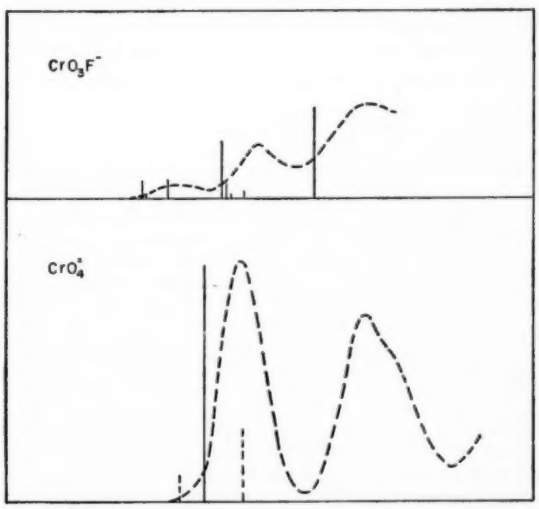

FIG. 4. Comparison of observed and calculated spectra for $CrO_4^=$ and CrO_3F^-.

TABLE II. Calculated energies of transition and f-values for visible and near ultraviolet absorption of CrO_3F^-.

Final state	Configuration	E(calc) cm^{-1}	E(obs)	f-value calc	f-value obs
^1E	$(a_2)^{-1}5e$	19 500	22 500	0.013	0.003
^1E	$(4e)^{-1}5e$	19 500		0.00001	
^1E	$(3a)^{-1}5e$	23 000	28 500	0.012	0.016
^1E	$(4e)^{-1}4a_1$	26 400		0.042	
$^1A_1$	$(4e)^{-1}5e$	27 600		0.016	
^1E	$(3e)^{-1}5e$	28 000		0.004	
$^1A_1$	$(3e)^{-1}5e$	28 300		0.005	
$^1A_1$	$(3a_1)^{-1}4a_1$	35 600		0.063	

The calculated energies seem to be too small by two to three thousand wave numbers. This discrepancy could be removed in increasing K_σ and K_π, but it is doubtful that better agreement would be of much significance in view of the approximate character of the calculation.

The spectrum of CrO_3Cl^- is almost the same as that of CrO_3F^- except that it is shifted somewhat toward the red. This shift is indicated by the calculation. The calculated shift of the second peak is 2000 cm^{-1}, the observed 1000 cm^{-1}.[5]

Chromyl chloride (CrO_2Cl_2), chromyl fluoride (CrO_2F_2), and sulfuryl chloride (SO_2Cl_2): For these molecules with symmetry C_{2V}, no degenerate orbitals exist and no refinements in the calculations of absorption energies have been made. The absorption energies have been set equal to the difference between the orbital energies.[6]

The results are given in Table III and indicate essential agreement with experiment: a low-energy absorption with relatively small f-value and a more intense absorption displaced toward the violet, but at longer wavelength than the first chromate absorption. The calculated energies are too small in this case, and the f-values too large particularly for the low-energy absorption. The overestimation of the f-values may be due, in part at least, to the neglect of the Cr $4p$ function which was found in the previous calculations to produce only a slight effect on the orbital energies but a considerable influence (decrease) in the f-value of the first transition.

The spectra show a shift toward the ultraviolet amounting to 1000 cm^{-1} for the first absorption with substitution of fluorine for chlorine. The calculations give very closely the same energy for the first transition and a shift of approximately 2000 cm^{-1} toward the violet for the second.

Considerable discussion has been given the first absorption in CrO_2Cl_2 and CrO_2F_2, which apparently leads to dissociation. Spectra taken at low temperatures, however, indicate the existence of two excited states lying in this region one of which has a potential minimum.[7] The $5a_1$ orbital which is the excited final orbital in both these transitions is strongly Cr—Cl antibonding and probably slightly bonding with respect to Cr—O. The $3b_2 \rightarrow 5a_1$ transition, furthermore, involves the transfer of considerable charge from the chlorine to chromium. For these two reasons the $3b_2 \rightarrow 5a_1$ transition might be associated with the repulsive state which would have the symmetry B_2 and leads to dissociation $CrO_2Cl_2 \rightarrow CrO_2 + Cl_2$.

The fact that the substitution of halogen atoms for oxygen atoms in $CrO_4^=$ produces absorption at longer wavelengths suggests that the same substitution in $SO_4^=$ might produce absorption in the relatively near ultraviolet. Calculations similar to those above in which only sulfur $3s$ and $3p$ orbitals were considered show that this should be so. With neglect of the sulfur $3d$ orbitals, the a_2 orbitals are nonbonding and the first

TABLE III. Calculated energies of transition and f-value for visible and near ultraviolet absorption of CrO_2Cl_2.

Transition	E(calc)	E(obs)	f-value[a] relative calc	f-value[a] relative obs
$3b_2-5a_1$	13 000	18 000	0.1	0.035
$3b_1-5a_1$			0.017	
$4a_1-5a_1$	15 000		0.065	
$3b_2-6a_1$	16 000		0.082	
$3b_1-6a_1$			0.010	
$2b_2-5a_1$	16 700		0.055	
$2b_1-5a_1$	17 200	24 000	0.002	
$3a_2-5a_1$	17 300		0.003	0.20
$4a_1-6a_1$	17 700		0.075	
$2b_2-6a_1$	19 400		0.030	
$2b_1-6a_1$	19 900		0.127	
$3a_1-6a_1$	20 100		0.120	

[a] f-value relative calc $= \dfrac{f\text{-value calc } CrO_2Cl_2}{f\text{-value calc } CrO_4^=[(t_1)^{-1}(3t_2)]} = \dfrac{f\text{-value calc } CrO_2Cl_2}{0.22}$.

f-value relative obs $= \dfrac{f\text{-value obs } CrO_2Cl_2}{f\text{-value } CrO_4^=[(t_1)^{-1}(3t_2)]\text{obs}} = \dfrac{f\text{-value obs } CrO_2Cl_2}{0.089}$.

[5] Two experimental facts are worth noting in connection with these compounds. The spectrum of chromate ion in dilute solution (0.0005M) with 0.1M acid is almost identical with that of CrO_3F^- so far as the first three maxima are concerned. In such a solution nearly all the chromate should exist as $HCrO_4^-$ according to existing equilibrium data [W. H. Latimer, *Oxidation Potentials* (Prentice Hall, Inc., New York, 1952)]. This effect indicates the approximate equivalence of the effects of OH and F on the spectrum. The spectrum of MnO_4^- in concentrated sulfuric acid (a green solution) bears the same relation to the MnO_4^- spectrum that $HCrO_4^-$ bears to the $CrO_4^=$ spectrum and we would predict that the green compound, MnO_3F [K. Weichert, Z. anorg. Chem. **261**, 310 (1950)], would show the same effect, namely, a weak maximum deplaced toward the red from the permanganate peak (5200 A) and a more intense absorption at shorter wavelength.

[6] The contribution due to Coulomb and exchange integrals would tend to lower the excitation energies (by less than 0.5 ev) and thus increase the difference between calculation and experiment. Taking the contribution due to these integrals into account would have been somewhat more consistent with the previous calculations.

[7] G. Shapenko, J. chim. phys. **47**, 22 (1950). This paper contains reference to other experimental and theoretical work with these molecules.

absorption should correspond to a $(2a_2)^{-1}\,4b_1$ transition. The orbital energy diagram is quite different in this case largely because of the difference in the overlap integrals, the σ overlaps being larger than the π overlaps in this case whereas the reverse is true for the chromium compounds.

The observed spectra[8] show three bands in the ultraviolet, the first about 33 000 cm^{-1}, the second at 36 000 cm^{-1}, and the third less intense, at 37 000 cm^{-1}. The calculated energy for the first absorption is 37 000 cm^{-1}. We attach no more than qualitative significance to these calculations. The alteration in the sulfate spectrum is given correctly and the energy of absorption has the correct relationship to the first absorption in $SO_4^=$ and $CrO_4^=$.

DISCUSSION

The qualitative features of the spectra of halogen substituted $CrO_4^=$ have been obtained from the same approximate method of calculation employed for chromate, permanganate, and perchlorate ions with the introduction of no new parameters (if the slight changes in the H_{ii} are not considered to be important). The adjustable parameters introduced into the original calculations are (1) the relative positions of the H_{ii} for chromium and oxygen. (2) The relative positions of $H_{\sigma\sigma}$ and $H_{\pi\pi}$. (3) and (4) The values of K_σ and K_π, the proportionality constants relating H_{ij} to the σ and π group overlaps.

One requirement placed on our calculations is that the charge distribution should be chemically "reasonable," and roughly self-consistent, i.e., the formal charges on the atoms should not be too different from the charges assumed in arriving at the value of H_{ii} and the overlap integrals. Table IV gives the formal charges calculated from the final wave functions attributing the shared charge‡ to the central atom. It is seen that the assumption mentioned earlier that the formal charges would become less negative as the negative charge on the molecule decrease is born out.

It appears, however, that the ionic contribution is overestimated. This would seem to be the case as judged by the f-values for the transitions which are calculated too high, and the fact that a simple calculation of the dipole moment of CrO_2Cl_2 gives a value approximately three times too large.

TABLE IV. Charge distribution.

	Cr	O	Cl
$CrO_4^=$	+1.06	−0.765	...
CrO_2Cl_2	+1.20	−0.50	−0.10

[8] H. N. Thompson, Nature **132**, 896 (1933).

‡ The following example will illustrate the meaning of "shared charge." For the a_2 orbital of C_{2v} (see Table I), $a_1d+b_1\pi_x+c_1\pi_0$, the normalization factor is $[a_1^2+b_1^2+c_1^2+2a_1b_1GA_2(d,\pi(x))+2a_1c_1GA_2\ (d,\ \pi(\text{oxygen})]^{-\frac{1}{2}}$. The shared charge referred to is $2a_1b_1GA_2[d,\pi(x)]+2a_1c_1GA_2\ [d,\pi(\text{oxygen})]$ times the square of the normalization factor, multiplied by the number of electrons occupying the orbital.

In comparing the energy states of CrO_3F^- and CrO_3Cl^- with those of $CrO_4^=$, it becomes attractive to think of the halogenated molecules as slightly perturbed $CrO_4^=$ molecules, since it appears as though the first permitted transition in $CrO_4^=$ (to the lowest lying T_2 state) is split into two transitions when one passes to CrO_3F^- and CrO_3Cl^-. This is exactly the behavior which one would expect for a slight perturbation which splits the T_2 state into an E state and an A_1 state in the lower symmetry. The interpretation becomes completely untenable, however, when one realizes that the sum of the oscillator strengths of the first two transitions in CrO_3Cl^- (and CrO_3F^-) is only about one-third the oscillator strength of the $CrO_4^=$ transition. The consideration of the lowering of the symmetry as a perturbation brings up a difficulty with the empirical method which we discuss in Appendix II.

The coefficients of the atomic orbitals in the molecular orbitals permit a rough calculation to be made of the relative importance of π and σ bonding. The products of the orbital coefficients multiplied by the corresponding overlap integrals were added, and the ratio of these sums for σ and π bonding considered to give a measure of their relative importance. For chromyl chloride the ratio is $\sigma/\pi=1.5$ for chlorine, and $\sigma/\pi=0.73$ for oxygen. While the magnitude of these ratios may be without significance, we feel that the decreased importance of π bonding for chlorine relative to oxygen is significant. For SO_2Cl_2 the σ bonding is more important than π bonding for both oxygen and chlorine. This effect arises, in our calculations, from the greater relative magnitude of the σ overlap integrals.

APPENDIX I

The transition energies from the A_1 ground state to the indicated states is given below in terms of the orbital energies and the exchange and Coulomb integrals between molecular orbitals.

$(a_2)^{-1}$ 5e Configuration

$$E(^1E)-E\ (^1A_1 \text{ ground state})=\epsilon_{5e}-\epsilon_{a_2}-J+2K,$$

$$J=\int\phi_{5e}(1)\phi_{a_2}(2)\frac{e^2}{r_{12}}\phi_{5e}(1)\phi_{a_2}(2)d\tau,$$

$$K=\int\phi_{5e}(1)\phi_{a_2}(2)\frac{e^2}{r_{12}}\phi_{5e}(2)\phi_{a_2}(1)d\tau.$$

$(4_e)^{-1}$ 5e Configuration

$$E(^1A_1)-E\ (\text{ground state})$$
$$=\epsilon_{5e}-\epsilon_{4e}-J_{11}+2K_{11}-(J_{12}-2K_{12}),$$

$$E(^1E)-E \text{ (ground state)}$$
$$=\epsilon_{5e}-\epsilon_{4e}-J_{11}+2K_{11}+(J_{12}-2K_{12}),$$
$$J_{11}=\int \phi_{4e}{}^1(1)\phi_{5e}{}^1(2)\frac{e^2}{r_{12}}\phi_{4e}{}^1(1)\phi_{5e}{}^1(2)d\tau,$$
$$K_{11}=\int \phi_{4e}{}^1(1)\phi_{5e}{}^1(2)\frac{e^2}{r_{12}}\phi_{4e}{}^1(2)\phi_{5e}{}^1(1)d\tau,$$
$$J_{12}=\int \phi_{4e}{}^1(1)\phi_{5e}{}^2(2)\frac{e^2}{r_{12}}\phi_{4e}{}^2(2)\phi_{5e}{}^1(2)d\tau,$$
$$K_{12}=\int \phi_{4e}{}^1(1)\phi_{5e}{}^2(2)\frac{e^2}{r_{12}}\phi_{4e}{}^2(2)\phi_{5e}{}^1(1)d\tau.$$

The terms $\phi_e{}^1$ and $\phi_e{}^2$ are the two wave functions of the degenerate e orbital.

APPENDIX II

Comparison of the completely antisymmetrized wave functions of a symmetrical molecule, resulting from a configuration having one electron missing from a degenerate orbital shell and having one extra electron in another degenerate orbital, with the wave function of a similar molecule perturbed to a lower symmetry in which these degeneracies are reduced, shows, in general, that the lower symmetry state wave functions do not go smoothly into a corresponding higher symmetry state wave function.

As an example consider MO_4 (symmetry T_d) and MO_3X (symmetry C_{3V}). Consider molecular orbitals $1t_2$ and $2t_2$ of MO_4. The configuration $(1t_2)^5(2t_2)$ gives rise to four states in symmetry T_d, A_1, E, T_1, T_2. In symmetry C_{3V}, $1t_2$ and $2t_2$ become $1e$, $1a_1$, $2e$, $2a_1$. As the perturbation goes to zero, the three orbitals $1e$, $1a_1$ become identical to the three orbitals $1t_2$, etc. One finds, however, that the A_1 state in symmetry C_{3V}, resulting from the configuration $1a_1{}^1\ 2a_1$, ψ_{A_1} $(a_1{}^1a_1)$ becomes equal to a linear combination of two states of symmetry T_d, and likewise for $\psi_{A_1}(e^1e)$. Thus

$$\psi_{A_1}(a_1{}^1a_1)=(\tfrac{1}{3})^{\frac{1}{2}}\psi_{A_1}(t_2{}^1t_2,T_dA_1)+(\tfrac{2}{3})^{\frac{1}{2}}\psi_{A_1}(t_2{}^1t_2,T_dT_2),$$
$$\psi_{A_1}(e^1e)=(\tfrac{2}{3})^{\frac{1}{2}}\psi_{A_1}(t_2{}^1t_2,T_dA_1)-(\tfrac{1}{3})^{\frac{1}{2}}\psi_{A_1}(t_2{}^1t_2,T_dT_2).$$

Here $\psi_{A_1}(t_2{}^1t_2,T_dA_1)$ stands for the A_1 state in symmetry T_d resulting from the configuration $(1t_2)^5(2t_2)$, which also belongs to symmetry A_1 in C_{3V}. Likewise, $\psi_{A_1}(t_2{}^1t_2,T_dT_2)$ refers to that T_2 wave function in symmetry T_d resulting from the configuration $(1t_2)^5(2t_2)$ which transforms according to the representation A_1 under the C_{3V} symmetry operations.

When the perturbation goes to zero, the energies of the orbitals $1t_2$, $1a_1$, and $1e$ become the same, likewise $2t_2$, $2a_1$, and $2e$. Therefore in the semiempirical molecular orbital theory, which takes for the difference in energy between states only the difference in the ϵ's of the molecular orbitals involved in the transition, we find at zero perturbation that the T_d states $^{1,3}E$, $^{1,3}T_2$, which all have the same energy in this approximation, all have exactly the same energy as the corresponding states in symmetry C_{3V}, which also all have the same energy. Thus, although there is apparently a configuration interaction of the states $\psi(t_2{}^1t_2,T_dA_1)$ and $\psi(t_2{}^1t_2,T_dT_2)$ necessary in order to correspond to the single configuration state $\psi A_1(a_1{}^1a_1)$, the energies of all of these states become the same at zero perturbation in this approximation. If, however, one tries to improve the expression for the energy differences between states by adding other terms, in addition to the differences of the ϵ's [see Appendix I], which then serve to separate the eight above states in symmetry T_d, one will no longer find that the symmetry C_{3V} states correspond in energy exactly to symmetry T_d states at zero perturbation unless one introduces configuration interaction into the calculation.

This configuration interaction also upsets the intensities at zero perturbation. If the ground state is $^1A_1$, then the only permitted transition in T_d is $^1A_1\rightarrow{}^1T_2$, which in symmetry C_{3V} should break up into two transitions $^1A_1\rightarrow{}^1E$ and $^1A_1\rightarrow{}^1A_1$, with the first having twice the intensity of the second. In the zero perturbation case in symmetry C_{3V}, we find however, since $\psi_{A_1}(t_2{}^1,T_dT_2)$ mixed into both the wave functions $\psi_{A_1}(a_1{}^1a_1)$ and $\psi_{A_1}(e^1e)$, that transitions are permitted to two excited A_1 states as well as to other E states.

Since the question of configuration interaction thus arises very seriously at or near zero perturbation in the intensities, one may seriously ask whether one must not also worry about it when the perturbation becomes larger.

Nitrogen Afterglow in a Magnetic Field

WALTER R. KANE* AND K. C. CLARK
Department of Physics, University of Washington, Seattle, Washington
(Received September 13, 1954)

The effect of a magnetic field on the simple exponential decay of a nitrogen afterglow at 0.017 mm pressure is reported. During the afterglow a magnetic field of 850 gauss parallel to the tube axis was alternately present and absent in 95 successive tests; the effect of the field was to slow the decay rate of 0.061 millisecond, as recorded by photomultiplier and oscillograph, by 2.9±0.5 percent. Kinetic theory calculations of the effect, based on plausible assumptions concerning ambipolar diffusion, thermalization of electrons, and electron attachment, are in approximate agreement with the observation, if one considers that ionic recombination provides much of the excitation energy for this short afterglow. An absence of the magnetic effect would be expected if ions played no role in the optical excitation.

INTRODUCTION

WHILE it seems probable that the long-lived Lewis-Rayleigh afterglow of active nitrogen is sustained by the recombination of neutral atoms,[1–4] the presence of ions is also an established feature of the process. The large value of the ionic recombination coefficient ($\alpha \approx 10^{-6}$ cm^3/sec)[5] clearly requires that in the long afterglows the ion population must be continually replenished by collision processes. The emission of light, however, may be in part initiated by ionic recombination even in the long afterglows as well as in the shorter-lived afterglows of Kaplan (auroral)[6] and of Herman and Herman.[7] To test the dependence of light emission on ion concentration, an experiment was performed which utilized the effect of a magnetic field upon the diffusion rate of ions. Only a short-lived afterglow could be studied because of the conditions of experimental detection. However, a small but definite effect was observed.

THEORY

With certain simplifying assumptions, one can estimate the size of the magnetic effect on the gas kinetic processes. For a charged particle the coefficient of diffusion D' transverse to the magnetic field is related to the zero-field value D by the equation,[8]

$$\frac{D'}{D}=\frac{1}{1+(\omega/\nu)^2} \tag{1}$$

where ω is the cyclotron frequency of the charged particle and ν is its collision frequency. The diffusion coefficients D_p, D_n, and D_e of positive ions, negative ions, and electrons, respectively, can be combined to give a coefficient of ambipolar diffusion D_a, as discussed subsequently; in a magnetic field the coefficients D_p', D_n', and D_e', similarly give the ambipolar coefficient D_a'.

Since experimental conditions were so chosen that the afterglow intensity decayed exponentially with time, one can consider the population of positive ions n to be limited by wall deactivation. For a long, cylindrical tube the solution of the diffusion equation yields the result,

$$n(r,t)=\sum_i A_i J_0[r(m_i/D_a)^{\frac{1}{2}}]e^{-m_i t} \tag{2}$$

where r is the radial distance from the tube axis. Since the initial ion distribution was probably rather uniform and the decay was observed to follow a simple exponential law, only the leading term in Eq. (2) is considered. The dependence of the decay constant m upon D_a can be obtained through the boundary condition involving destruction at the wall: if c is the mean speed of the ion and g the probability that a wall collision will destroy it, then the ion flux at the wall, where $r=R$, is

$$-D_a\frac{\partial n(R,t)}{\partial r}=\frac{cgn(R,t)}{4} \tag{3}$$

or

$$\frac{cgR}{4D_a}J_0(x)=xJ_1(x) \tag{4}$$

where

$$x\equiv R(m/D_a)^{\frac{1}{2}}.$$

The constant cg is evaluated from Eq. (4) under zero-field conditions. When a magnetic field is present parallel to the tube axis, D_a' replaces D_a, and Eq. (4) then yields the modified decay constant m'. Since the change in D_a must be large to produce an appreciable change in m, it is advantageous to use low pressures and poisoned walls in order to enhance the effect of a given magnetic field.

---

* Now at Los Alamos Scientific Laboratory, University of California, Los Alamos, New Mexico.

[1] S. K. Mitra, Phys. Rev. **90**, 516 (1953).
[2] O. Oldenberg, Phys. Rev. **90**, 727 (1953).
[3] M. Brook, Sci. Rept. No. 2, Inst. of Geophys., University of California, Los Angeles, March, 1953.
[4] G. Cario and L. H. Reinecke, Abhandl. braunschweig. wiss. Ges. **1**, 8 (1949).
[5] R. B. Byran, Doctoral thesis, 1951, Harvard University, Cambridge, Massachusetts.
[6] J. Kaplan, Rept. Gassiot Comm. Roy. Soc., *Emission Spectra of the Night Sky and Aurorae* (Physical Society, London, 1948), p. 118.
[7] R. Herman and L. Herman, Trans. Am. Geophys. Union **33**, 489 (1952).
[8] Lax, Allis, and Brown, J. Appl. Phys. **21**, 1297 (1950).

EXPERIMENT

The afterglow was produced by a pulsed electrodeless discharge in a closed Pyrex tube of 8 cm diameter and 80 cm length, located within a uniform field customarily used for a beta-ray spectrograph.[9] Light from the discharge tube was reflected out to a distant, magnetically shielded, 1P22 photomultiplier tube, and the afterglow transient was photographed on a calibrated oscilloscope. Intensity modulation by a 60-cps square wave was used to avoid possible effects of sweep nonlinearity. A sequencing system turned on the magnetic field and the photomultiplier at the termination of the discharge, the magnetic field reaching 90 percent of its full value of 850 gauss in about 100 milliseconds.

The discharge tube contained nitrogen with a trace of oxygen at a pressure of 0.017 mm. To obtain a sufficiently rapid decay, it was necessary to poison the walls of the tube with silicone pump oil. Under these conditions the decay was closely exponential, with a time constant of about 0.061 sec, indicating destruction of the active particles on the walls with an efficiency $g \approx 1/740$. In all, 95 decay transients were photographed with the magnetic field alternately present and absent.

The effect of the magnetic field was to reduce the decay rate of the afterglow by 2.9 ± 0.5 percent. The effect was insignificant during the early stage of the afterglow, when the magnetic field was still appreciably below its maximum value, and the above figure applies to decay rates measured between about 100 and 350 milliseconds after the discharge.

DISCUSSION

The magnetic field must be considered to affect only the diffusion process, and not the efficiency g of destruction at the wall or the rate of release of stored energy in the afterglow. A direct theoretical prediction of the reported result is not possible, since the volume density of the ions and the degree of electron attachment to oxygen are not known. It is plausible to assume that the ion density is sufficient to create conditions of ambipolar diffusion and that elastic collisions have equalized ionic and electronic temperatures. The coefficient of ambipolar diffusion D_a is then related to the diffusion coefficients D_p, D_n, and D_e for N_2^+, O_2^-, and electrons, respectively, and to the fraction χ of free electrons in the total negative population by the equation,[10]

$$D_a = \frac{2\chi D_p D_e + 2(1-\chi) D_p D_n}{D_p + \chi D_e + (1-\chi) D_n}. \tag{5}$$

The degree of attachment $(1-\chi)$ may be considerable and undoubtedly varies during the observed decay. One may assume that the high electron energy during discharge has been largely dissipated in collisions prior to the observations and that the attachment cross section is high at 3–6 volt as well as thermal energies.[11,12]

Taking as an example the choice of $\chi = 0.7$ and the values $D_p = 1340$, $D_n = 1880$, and $D_e = 2.4 \times 10^7$ cm²/sec,[10] one obtains $D_a = 2680$ cm²/sec at zero field and $D_a' = 570$ cm²/sec at 850 gauss. These values, substituted in Eq. (4), give as the decay constants of positive ion density $m = 8.200$ sec^{-1} and $m' = 8.016$ sec^{-1} without and with the magnetic field, respectively. This 2.2 percent change in m applies equally to the change in decay rate of the afterglow, provided that the afterglow is the result largely of ionic recombination.

Close agreement of the prediction with experiment is not to be expected because of the assumptions discussed above. The assumed degree of electron attachment $(1-\chi)$, however, is not critical except where its value is low. The effect of a wide choice in χ is illustrated in Fig. 1, where the calculated percent change in m is plotted as a function of χ. It is seen that for values of χ above 0.2, as may be the experimental case, the percent change is considerably enhanced.

The observed magnetic effect indicates that energy released in ionic recombination contributes appreciably to the excitation of this short-lived afterglow. In view of the care taken to avoid systematic errors in the data and their interpretation, it is felt that the experimental result here reported is clearly significant. It is to be hoped that the experiment will be repeated, using a much higher magnetic field.

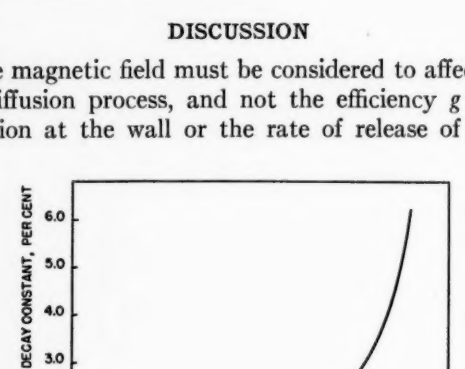

FIG. 1. Percent change in decay constant as a function of the fraction of free electrons.

[9] F. H. Schmidt, Rev. Sci. Instr. **23**, 361 (1952).

[10] A. von Engel and M. Steenbeck, *Electrische Gasentladungen* (Verlag Julius Springer, Berlin, Germany, 1932), Vol. I, Table 26, abb. 89.

[11] M. A. Harrison and R. Geballe, Phys. Rev. **91**, 1 (1953).

[12] N. Bradbury, Phys. Rev. **44**, 883 (1933).

THE JOURNAL OF CHEMICAL PHYSICS VOLUME 23, NUMBER 5 MAY, 1955

Thermal Accommodation Coefficient of Helium on a Bare Tungsten Surface

LLOYD B. THOMAS AND E. B. SCHOFIELD
Chemical Laboratory, University of Missouri, Columbia, Missouri

(Received September 7, 1954)

The accommodation coefficient of helium on a presumably clean tungsten surface is determined from 83° to 303°K. A getter technique is applied in which, after thorough baking of the tube and vacuum system, aluminum is evaporated in vacuum over the inner walls of the measuring tube. The technique appears to be superior to the circulation over charcoal used by Roberts. Clean surface values of the accommodation coefficient, found by linear extrapolation to time of flashing the filament, lie between 0.0151 and 0.0172 (with small positive corrections probably to be applied). The variation with temperature is small and the values themselves are much lower than any heretofore reported.

IN a great preponderance of the work on accommodation coefficients (hereafter denoted as A.C.) presented in the literature, no serious attempt has been made to create or maintain a clean surface of the solid. It may be possible to maintain a strictly bare metal surface only in the presence of a limited number of gases, helium and neon for example, but the initial statement applies also to work with these. J. K. Roberts[1] found that the extent of molecular attachment, presumably of impurity gases, to a tungsten surface had a profound influence upon the observed thermal A.C. values of He and Ne. Roberts' findings, substantiated by several investigations of others,[2,3] were questioned by Bremner[4] then confirmed again by Eggleton, Tompkins, and Wanford.[5] Work in this laboratory extending from a time previous to references 4 and 5 confirms emphatically the existence of the low A.C. values on clean tungsten, as observed by Roberts, and also on clean platinum. J. W. Faust, working in this laboratory with inert gases on evaporated aluminum surfaces, found that low A.C. values were often observed and maintained, with slow rates of increase, on platinum and tungsten filament surfaces which were kept hot in the tube while aluminum was evaporated from other filaments to the walls. The aluminum acts as a getter to perform the same clean-up function as the circulation over charcoal used by Roberts, and its effectiveness appears to be superior to the circulation over charcoal. The present paper reports an attempt to exploit this technique to check and extend the existing measurements of the A.C. of helium on clean tungsten over the range $-190°$ to $+30°$C. In view of the fact that theoretical work on the A.C. leans heavily on the three points given for He over this temperature range by Roberts and in view of the precarious nature of such measurements we have undertaken the work reported here, and expect to extend it over the first five inert gases.

[1] J. K. Roberts, Proc. Roy. Soc. (London) **A142**, 518 (1953).
[2] Mann, Proc. Roy. Soc. (London) **A146**, 776 (1934).
[3] Van Cleave, Trans. Faraday Soc. **34**, 1174 (1938).
[4] Bremner, Proc. Roy. Soc. (London) **A201**, 305 and 321 (1950).
[5] Eggleton, Tompkins, and Wanford, Proc. Roy. Soc. (London) **A213**, 266 (1952).

EXPERIMENTAL

The principal apparatus used consists of the experimental tube; a cryostat; a vacuum system with gas purifying and admitting equipment and an accurate McLeod gauge; and the electrical system.

The tube used is shown in Fig. 1. It was kept quite simple in order to minimize sources of impurity, yet was of a design which we hoped would give quite accurate values of the A.C. without recourse to extensive correction, since the necessary data for correction (thermal conductivity and emissivity) are not known with certainty over the temperature range needed. A 0.003-in. tungsten filament, unpolished, 28.98 cm in length, with a single potential lead of 0.002-in. tungsten 4.0 cm in length attached 7.01 cm from the upper end of the filament was used. The purpose of this design is to allow subtraction of the appropriate measurements, taken on the shorter upper section, from those on the lower section to obtain net measurements which apply to a middle section, which is relatively free from changing end losses as one passes from vacuum to the gas filled condition. Two springs, as nearly identical in dimensions as we could make them, of 6.2 cm of 0.007-in. diameter tungsten held the filament taut. An aluminum evaporator filament of two twisted strands of 0.007-in. tungsten runs the full length of the main filament. This has, at 0.5-cm intervals, pieces of 0.012-in. aluminum wire, 0.5 cm long, inserted between the strands and then wrapped around them. The two filament systems are held by glass insulated tungsten supports attached to a 0.045-in. nickel wire frame, and the electrical connections are made through a four lead uranium glass press as illustrated. The tube envelope is of 3.0 cm i.d. Pyrex and keeps the full diameter through the temperature gradient region from cryostat to room conditions to minimize the thermomolecular pressure correction.

The cryostat followed the general pattern of that described by Scott and Brickwedde,[6] with an outer insulating can holding an outer permanently evacuated glass Dewar, and an inner Dewar with pressure vari-

[6] Scott and Brickwedde, J. Research Natl. Bur. Standards **6**, 401 (1931).

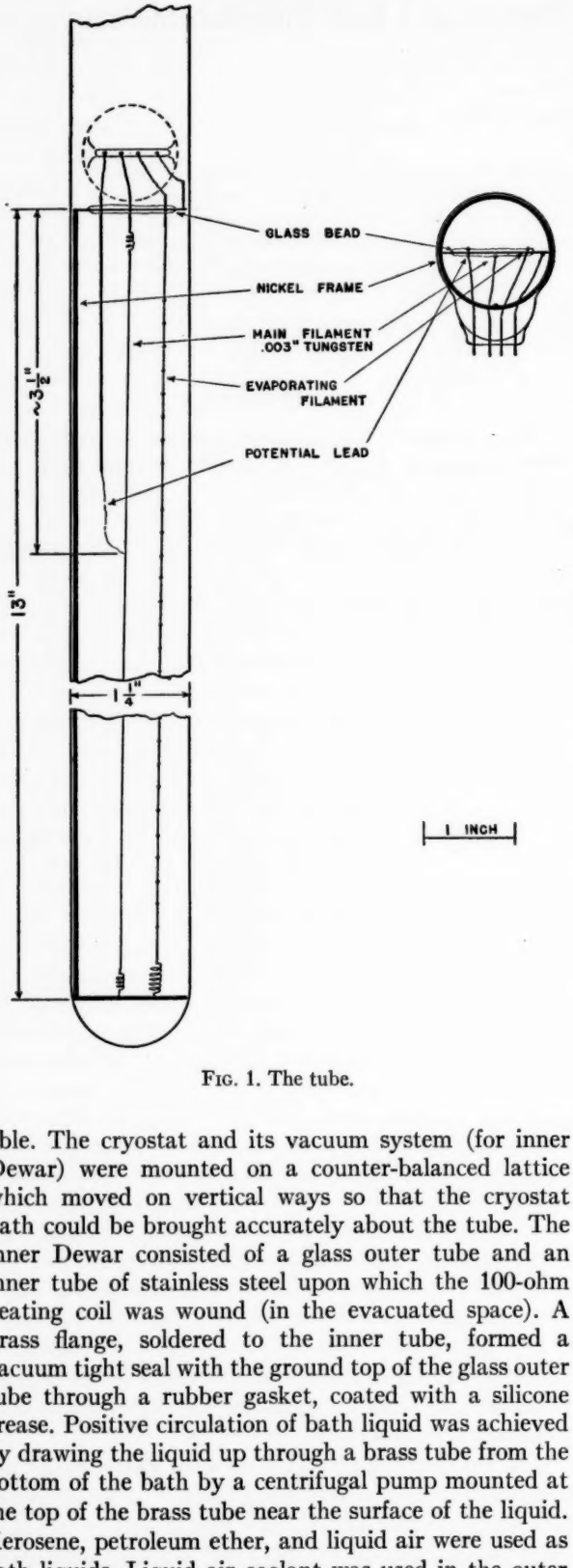

FIG. 1. The tube.

able. The cryostat and its vacuum system (for inner Dewar) were mounted on a counter-balanced lattice which moved on vertical ways so that the cryostat bath could be brought accurately about the tube. The inner Dewar consisted of a glass outer tube and an inner tube of stainless steel upon which the 100-ohm heating coil was wound (in the evacuated space). A brass flange, soldered to the inner tube, formed a vacuum tight seal with the ground top of the glass outer tube through a rubber gasket, coated with a silicone grease. Positive circulation of bath liquid was achieved by drawing the liquid up through a brass tube from the bottom of the bath by a centrifugal pump mounted at the top of the brass tube near the surface of the liquid. Kerosene, petroleum ether, and liquid air were used as bath liquids. Liquid air coolant was used in the outer Dewar and its level was maintained by periodic manual addition. The cryostat temperature was set and controlled by two copper constantan thermo-couples in series in a potentiometer circuit and was maintained by the bath heater current controlled through a thyratron circuit by the degree of off-balance of the galvanometer in the thermocouple circuit. A separate bath thermocouple and potentiometer was used to measure the temperature and to serve as the standard, after calibration, for the work. Temperatures were maintained within $\pm 0.02°$ of the original setting over long periods of time.

It is necessary to mention the vacuum system and procedure since the results cannot be observed without a certain standard of vacuum usage. The system was all Pyrex with two mercury condensation pumps in tandem, with no stopcocks in the high vacuum line, but with several special grind mercury seal stopcocks in the gas supply and purifying system, which was separated from the main system at all times by a mercury cutoff except during preliminary evacuation and admission of gas. A carefully calibrated McLeod gauge was used at room temperature to determine the gas pressures and this gauge was checked against two others, independently calibrated, placed on the line temporarily for comparison. Pressure measurements are probably good within 0.5 percent in the range used. A double "U" tube (two passes through liquid air) separates the mercury containing parts of the system from the tube and was kept immersed in liquid air except during part of the bake-out period. The gas storage, purifying, and admitting system uses highest purity "Airco" helium in Pyrex, opened to mercury seal stopcocks by "break-offsky" procedure, and then, after standing over

TABLE I. A sample set of data for one A.C. value.

(a)	Potential fall across long section of filament	0.026010 volt
(b)	Potential fall across short section of filament	0.009225 volt
(c)	Potential fall across center section of filament, (a)–(b)	0.016785 volt
(d)	Potential fall over taps of calibrated resistance in series with filament (4.0379 ohms)	0.085565 volt
(e)	Current through filament	0.021190 amp
(f)	Resistance of filament (center section), (c)/(e)	0.7921 ohm
(g)	R_0 of filament for this temperature range	1.6765 ohms
(h)	Average temperature of filament from (f), (g), and $R=R_0(1+0.00448t)$	−117.72°C
(i)	Bath temperature (calibrated Cu. Const. T.C.)	−134.97°C
(j)	$\Delta T=T_f-T_b$, (h)–(i)	17.25°C
(k)	Total power loss from center section (c)×(e)	0.00035567 watt
(l)	Power loss in vacuum (center section)	0.00021250 watt
(m)	Power loss assigned to gas conduction	0.00014317 watt
(n)	Area of filament (center section)	0.34966 cm²
(o)	Pressure of gas by McLeod	0.0335 mm
(p)	Calculated gas conduction from filament area for unit ΔT and unit P assuming A.C.=1	0.014558 watt
(q)	Possible gas conduction at existing ΔT and P, (p)×(o)×(j)	0.0084127 watt
(r)	Accommodation coefficient (m)/(q)	0.01702

thoroughly outgassed charcoal at liquid air temperature, admitted to the A.C. measuring system by means of a lock arrangement between mercury seal stopcocks (Apiezon "N" grease).

Electrical measurements were made with a Type K-2 potentiometer and suitable standard resistors. Tube and potentiometers were supplied by lead storage cells. The evaporating filament was supplied by a variable transformer and the filament was flashed by rectified current controlled also by a "Variac."

EXPERIMENTAL PROCEDURE

Extreme cleanness of the vacuum system is essential, so the preparation is rather rigorous. With the system open to the pumps, the aluminum evaporator filament is heated nearly to incipient evaporation and held for an extended period. The main filament is flashed at 1800°C also for an extended period during which its electrical resistance reaches a stable value for any given temperature (unless the filament is inadvertantly mistreated later, such as by heating it during bake out and not having the system open to the pumps). Ovens are then placed about the tube, charcoal trap on the gas supply manifold, and liquid air trap. These are baked at about 400°C for several hours, open to the pumps. With the ovens hot, the rest of the system is then heated repeatedly with a large brush gas-air flame for two to three hours, almost to the softening point of the glass, with special attention devoted to the region between the liquid air trap and the tube. After cessation of flaming, the ovens are turned off, liquid air is put on the single U-tube on the mercury side of the trap, and the filament is heated to flashing temperature. Resistances of the filament over the desired range of temperature are then determined by introducing a few tenths of a millimeter of helium, cutting the flashing current and setting the desired bath temperatures. At each bath temperature, resistances are taken at a series of small currents and plotted against power input. These give linear plots which, when extrapolated to zero power input, give the resistance of the filament at the bath temperature. Such measurements form the basis for fixing the average filament temperatures for the A.C. runs through evaluation of R_0 and α over limited ranges and using $R=R_0(1+\alpha t)$ to evaluate "t" from the filament resistance, "R," within the range. The gas is then evacuated and, with the filament too hot to accept a deposit, aluminum is evaporated to give a partially transparent coat on the glass walls. With one such preparation it was practicable to work three to six days, after which baking and aluminum evaporation were repeated. Once the tube was in a clean condition measurements were taken continuously over the several days period. At each operating bath temperature a set of power-loss-in-vacuum points was taken over the needed range of filament temperatures—apparently the radiation losses from the filament are unaffected by the changing surface conditions which affect the A.C. values so markedly.

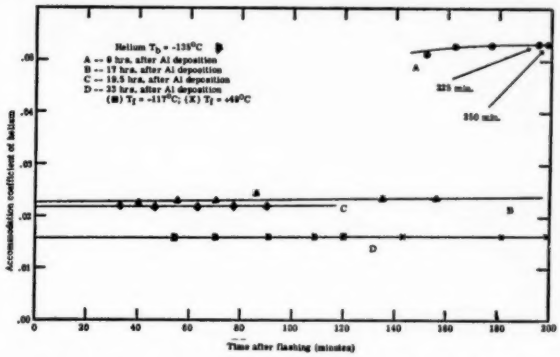
Helium T_b = -135°C
A -- 9 hrs. after Al deposition
B -- 17 hrs. after Al deposition
C -- 19.5 hrs. after Al deposition
D -- 33 hrs. after Al deposition
(●) T_f = -117°C; (X) T_f = +48°C
Accommodation coefficient of helium
Time after flashing (minutes)
325 min.
350 min.

FIG. 2. The approach toward a clean surface following evaporation of aluminum.

For an A.C. run the filament is first flashed and about 0.035 mm of helium is admitted. Ten minutes after gas admission the flashing current is cut to the predetermined measuring current and the clock started with this time of cessation of flashing as zero. A.C. measurements are then taken at about 10-minute intervals for several hours until the course of the values becomes definitely set. The early values are low because the filament is at an abnormally high temperature from flashing but the 30-minute or 40-minute values usually appear free from this effect, and, from these on, a definite linear course in the values with time is set. The values are plotted against time and extrapolated back to zero time as illustrated later. A set of data and derived quantities for one typical A.C. value, as given in Table I, serves to indicate the detail of a measurement and the extent of care taken.

The set of data above (Table I) determined the A.C. 83 minutes after shutting off the flashing current and is one set of ten taken for this run. The results reported in the next section are taken from over 50 runs on helium in four tubes over bath temperatures ranging from −190°C to +30°C.

EXPERIMENTAL RESULTS AND DISCUSSION

The four tubes used are so nearly identical that they will not be distinguished in the following. Typical time runs, including some at each bath temperature, are given in the following graphs and characteristic behavior observed is pointed out with reference to specific curves.

To obtain the low A.C. values reported, a period of aging following aluminum evaporation was necessary. Progress toward the low (clean) values is shown in Fig. 2, Curves A to D, which were taken in that order at 9, 17, 19.5, and 33 hours after evaporation of aluminum. Helium was admitted just following evaporation and this sample used for Curves A, B, and C. A new sample was used for Curve D. As in all our time runs the filament was flashed before each run and the flash-

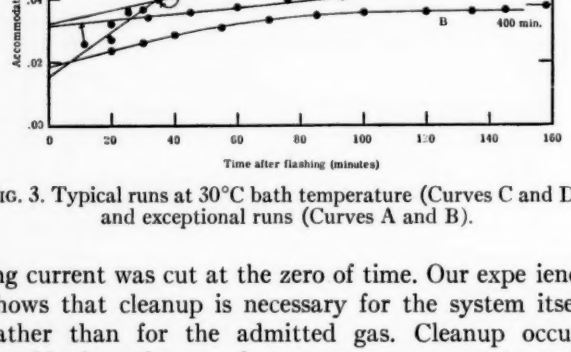

FIG. 3. Typical runs at 30°C bath temperature (Curves C and D), and exceptional runs (Curves A and B).

ing current was cut at the zero of time. Our expe ience shows that cleanup is necessary for the system itself rather than for the admitted gas. Cleanup occurs roughly four times as fast at room temperature as in the case illustrated with tube at −135°C and was usually accomplished by letting the tube stand at room temperature overnight following evaporation.

Curve D, Fig. 2, also illustrates a remarkable characteristic of the work, found repeatedly. The first five points were taken with filament at −117°C (ΔT=18°) and the last three with filament at 49°C (ΔT=184°). There is no noticeable break in the A.C. values yielded. This was entirely unexpected from previous experience with ordinary (gas saturated) A.C. measurements or from the "clean" surface work of others. This behavior was found at a variety of pressures, ΔT values, and bath temperatures, and was also found with neon and could hardly result from any consistent sizable error just compensating for a real temperature effect.

Figure 3 shows four runs with bath temperature at +30°C. Curves C and D are typical of some twelve runs at this bath temperature in that they give linear plots above about 30 minutes and the lines extrapolate to give A.C. values between 0.028 and 0.035 at zero time. Curves A and B are exceptional at this bath temperature in that they definitely extrapolate to values well below the group mentioned above, in this case to 0.016 and 0.0185. On evidence brought out below, which is independent of the occasional runs as A and B, we credit the exceptional low values as representing the true clean surface values at +30°. The difficulty at this temperature in our work (and in previous work) no

FIG. 4. Three time runs at bath temperature −30°C.

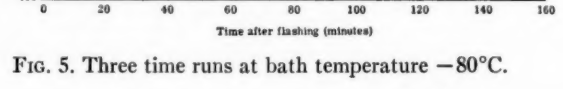

FIG. 5. Three time runs at bath temperature −80°C.

doubt arises from the fact that impurities arise more readily and are less completely removed on the walls at this temperature than at lower bath temperatures, as will be indicated by following curves.

Figure 4 gives plots of three runs with the bath at −30°C. These curves show small slopes, are quite linear, and yield "clean" A.C. values closely grouped about 0.0175. Note that the points for T_f=−14.5°C and +88°C fall very closely on the same line, which again emphasizes the apparent independence of the clean surface A.C. values from the ΔT of the measurement. Some runs at this bath temperature gave extrapolated A.C. values around 0.03 (refer to preceding paragraph) but the lower values were more readily attained than at T_b=+30°C.

Figure 5 is a plot of three runs, representing two filament temperatures at bath temperature −80°C. These extrapolate to "clean" values closely about 0.0165 and are quite uniform. Figure 6 shows a set of three runs with bath at −135°C. The curves are very similar to those at −80°C, and extrapolate closely about 0.0165. Both of these sets show practically identical time curves with widely differing ΔT values.

Figure 7 is a plot of two time runs with bath temperature −190°C. At intervals shown on the plot, the filament temperature was varied from −170°C to +20°C and then after 200 minutes (circle designated points) was returned to −170°C. The final points, after 200 minutes, are slightly lower (about 2 percent) than the initial ones at the same ΔT. The set of points illustrates the practically zero slope which, taken with previous curves, indicates the relative ease of maintaining a clean filament surface with the tube walls at this low temperature. The apparent rise of the A.C. with ΔT in both curves of Fig. 7 probably indicates that we are getting the A.C. value characteristic of the filament tempera-

FIG. 6. Three time runs at bath temperature −135°C.

ture and this is not modified by the large ΔT at which the A.C. is observed at the upper filament temperatures.

The extrapolated A.C. values at each bath temperature are summarized in Table II, giving the filament temperature, number of runs included, and the average deviation from the mean of the included runs. Except for the first entry, we have included only runs of ΔT about 18°. Since the A.C. approaches a minimum value as the surface becomes clean, the value itself serves as an indicator of surface conditions and there seems no point in reporting the higher values obtained. When the low values were not obtained, there is a definite preference for values about 0.03 found for all bath temperatures except −190°C, while values between 0.018 and 0.028 very rarely occurred. At each of the bath temperatures except +30° the low values were found within narrow limits (only about half of them are represented in Table II because of the ΔT limitation imposed) often enough that they definitely indicate a lower limit to the A.C. for the technique used.

Figure 8 brings together the results of this investigation with those of Roberts, which appear to be generally credited. The A.C. values over the same temperature range are much lower by our getter technique than by

TABLE II. Summary of limiting clean surface A.C. values.

Bath temp.	Fil. temp.	Runs averaged	A.C. value
30° to −190°C	47°C (approx.)	8	0.0169(±0.0007)
30° (only)	47°	2	0.0167(±0.0015)
−30°	−14°	1	0.0172
−80°	−62°	2	0.0162(±0.0003)
−135°	−117°	3	0.0162(±0.0003)
−190°	−170°	2	0.0151(±0.0002)

the gas circulation method used by Roberts and others. Furthermore the increase in the A.C. with temperature over the range, according to our results, is quite small. From our experience with the increasing difficulty of getting and holding clean surface values at the high bath temperatures we offer the suggestion that the large temperature coefficient obtained by Roberts is a manifestation of this difficulty, i.e., he was unable to obtain and hold as clean a surface at 300°K as at 83°K. Had we not obtained the A.C. value about 0.017 with the filament at 47°C from the lower bath temperatures we would probably have discounted the two runs of the second line of the table in favor of the much more prevalent value about 0.03. However, we have no reasonable doubt that the lower values are real and the higher values are due to experimental inadequacies.[7]

[7] In support of the validity of the low values about room temperature, we mention here unpublished work from this laboratory by Miss F. E. Becker. Using extreme baking and flashing preparation in a simple tube similar to Roberts', with no getter, she obtained repeatedly A.C. values for helium on tungsten about 0.020 (without end loss correction, which lowers the A.C. value when applied). Upon successive additions of trace quantities of oxygen (by magnetic breaking device) the A.C. values of helium, plotted against time, rose stepwise to a limiting value of 0.18 from the 0.02 value. Hydrogen, admitted in like manner, gave a limiting value of 0.07 for the helium A.C.

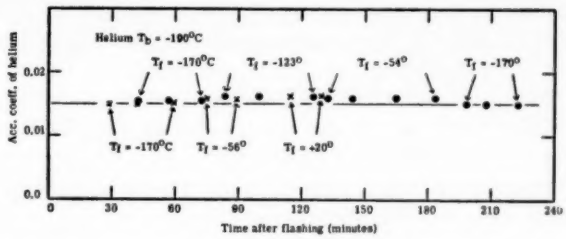

FIG. 7. Two time runs with bath temperature −190°C and with filament temperatures from −170° to 20°C. The line drawn in is of zero slope at 0.015.

Two possible sources of appreciable error in the reported values are the thermomolecular pressure difference between the McLeod reading and the pressure in the cryostat, and failure of the single potential lead tube to compensate for end losses adequately. The first was calculated from the equation of Weber and Schmidt with appropriate constants for helium.[8] The correction to be added to our A.C. value at −190°C is 3.8 percent and at −80°C is 2.2 percent for the typical pressure 0.033 mm and 1.5-cm radius of the tube through the temperature gradient region. For the second type of correction Mr. R. E. Brown of this laboratory has developed a method of calculation of the temperature distribution in the filament system of the single potential lead tube and of the error involved. The principal error arises from the fact that the potential lead, in carrying away heat, lowers the temperature along the short end of the filament so that, when its resistance is subtracted from that of the long end, too much resistance is assigned to the center section. This results in assigning too large a ΔT value which results in too small an A.C. as calculated. Mr. Brown's calculations at a typical set of conditions ($T_b = -135°$, $\Delta T = 18°$, $p = 0.033$ mm He) show the A.C. value calculated as reported in this work to be 6 percent too low. This error is affected very little by varying the pressure ±50 percent and is little affected by changing the bath temperature. (Experimental work with the same design tube with a much finer potential lead, done since com-

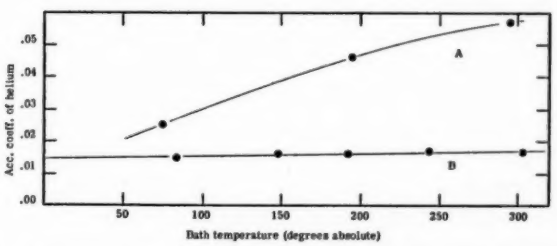

FIG. 8. The accommodation coefficients of helium on clean tungsten: Curve A, Robert's values; Curve B, this work.

[8] Van Itterbeek and de Grande, Physica 13, 292 (1947). (The coefficient given as 0.15283 should be 0.15823, p. 292.)

pletion of the work reported here, confirms that this error is minor.) The corrections mentioned above have not been applied in the results presented.

In conclusion, the A.C. values presented here are quite radically lower and the temperature coefficient of the A.C. is lower than previously reported, which suggests at least that a reapplication of existing theory to these data may be in order to yield revised force function constants for the interaction of helium atoms with a tungsten surface. The results also suggest that the classical mechanical theory of Baule is not as poor a description of the A.C. as has been supposed. Following the work reported here, investigation has been undertaken in this laboratory which we hope will give a view of the A.C. of all the inert gases on clean tungsten. Discussion with regard to theory can, with profit, be left till this view is available.

We acknowledge with thanks the support of this investigation by the Office of Ordnance Research. We also wish to express appreciation for the help of Dr. Walter L. Silvernail who has shared in the building and operation of the equipment and to Mr. Robert E. Brown for help with the cryostat control and the heat flow problem.

THE JOURNAL OF CHEMICAL PHYSICS VOLUME 23, NUMBER 5 MAY, 1955

Reactions of Nitrogen Activated by Electric Discharge

R. N. VARNEY*
The Research Laboratory of Linde Air Products Company, A Division of Union Carbide and Carbon Corporation, Tonawanda, New York

(Received September 27, 1954)

For gaseous reactions of nitrogen with hydrogen or with oxygen, it was necessary to pass only the nitrogen through a glow discharge, the other gas being admitted at a later point in the flow line. Ammonia, nitrous oxide, and dinitrogen trioxide were formed, respectively. By suitable control of fields it was established that nitrogen ions were playing no direct role in the reactions but rather a neutral form of activated nitrogen in every case. Passing the hydrogen or oxygen alone through the discharge and then admixing nitrogen yielded no reaction product at all. Several further results indicated that ionic processes on the whole are not active in gas discharge reactions.

THE present work describes experiments designed to test the roles of excitation and of ionization of nitrogen in "activating" it. The term "activating" is used here to mean rendering the nitrogen capable of reacting directly with gases like hydrogen, oxygen, or methane without further external influences such as heat, electrical potentials, or catalysts. Previous work[1,2] has indicated that under selected circumstances, nitrogen passing through an electric discharge may contain N^+, N_2^+, N_3^+, and N_4^+ ions, to mention only the singly-charged varieties. One possibility envisaged for the present experiment was to determine the influence of these various ions on the chemical activity of nitrogen.

The apparatus used is shown schematically in Fig. 1. At inlet 1, nitrogen was admitted after first having flowed through a narrow, liquid-nitrogen chilled trap, primarily for removal of water vapor. The pressure of nitrogen within the upper chamber was varied over a range from 2 to 12 mm Hg. Between electrodes 1 and 2 a potential difference of approximately 250 volts was applied causing a glow discharge to appear, regulated to 5 to 10 milliamp by suitable resistors. The potential was obtained from a rectified and filtered supply and was thus dc with a negligible ripple. Electrode 2 was normally made the cathode, and the perforations in it permitted positive ions to pass through and on down the tube.

Between electrodes 2 and 3 a potential difference was established both of variable magnitude and variable direction. If electrode 3 was more negative, the positive ions were drawn to it and through its apertures into the next field region. If it was more positive, ions from 2 were repelled and driven back to 2. The drift velocity of ions may be computed[3] from the equation

$$v=\mu E\times(760/p).$$

Here μ is the mobility, E the field strength in volts/cm, and p the pressure in mm Hg. In all the work above, μ was of the order of 2 cm^2/volt sec, E of about 50 volts/cm, and p of about 10 mm, making v of the order of magnitude of 0.5 to 1.0×10^4 cm/sec. The flow of gas through the tube between electrodes 2 and 3 occurred at a rate not exceeding 5×10^2 cm/sec. Hence if a reverse field was applied, tending to hold back ions to electrode 2, the drift velocity was adequate by a factor of 10 to 20 to exceed the flow rate. The fractional number of ions diffusing against a drift velocity v for a distance x with a diffusion coefficient D is given by

* Now at Physics Department, Washington University, St. Louis 5, Missouri.

[1] O. Luhr, Phys. Rev. 44, 459 (1933).

[2] R. Varney, Phys. Rev. 89, 708 (1953).

[3] L. B. Loeb, *Fundamental Processes of Electrical Discharge in Gases* (John Wiley and Sons, Inc., New York, 1939), p. 35.

$\exp(-vx/D)$. In the least favorable condition listed here, this factor has the fantastically small value of 10^{-200}. This is, in fact, what is meant by statements that ions have unique mobilities.

At inlet 2, a second gas was admitted, the principal ones of interest in this report being hydrogen and oxygen. As for inlet 1, the entering gas passed first through a liquid-nitrogen chilled trap primarily to remove water vapor. A field between electrodes 3 and 4 could be utilized to regulate the energy of impact with which such ions of nitrogen as reached this region collided with molecules of the newly admixed gas. *A discharge was not allowed to occur between electrodes 2 and 3 or between 3 and 4.*

The mixture of gases together with any products of reaction passed on through still another trap chilled with liquid nitrogen and finally out through a vacuum pump. The last trap was fitted with a glass ball joint to permit its removal for subsequent analysis of trapped products. No greased joint or stop cock was located anywhere in the path of the flowing gases except prior to one of the incoming liquid-nitrogen traps or subsequently to the last trap.

Runs were made for periods of one to four hours. In cases where visible reaction products were formed, they could be seen qualitatively to increase in amount as the time progressed.

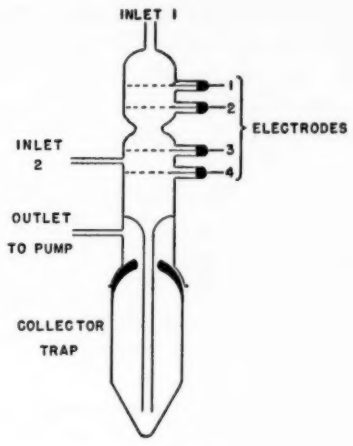

FIG. 1. Schematic diagram of the apparatus. The diameter of the principal sections of the tube was $\frac{3}{4}$ in.

RESULTS OF N_2+H_2 TESTS

With hydrogen admitted at inlet 2, a dark brown crystalline material appeared in the collector trap. The material was apparently unstable at room temperature; it could be preserved indefinitely at the low temperature, and the collector trap could even be removed, re-evacuated, and sealed off. But if the trap was ever allowed to warm appreciably, even though still below the ice point, the material evaporated and could never be recondensed as a visible, brown crystal.

Extensive mass spectrographic analysis showed no product except NH_3, and the characteristic ammonia odor was always readily recognizable. Both mass spectrographic and indicator tests were made for hydrazine but results were negative.

The following control tests were made, all with essentially negative results, by way of establishing the nature of the process observed.

(a) Potentials between electrodes 2 and 3 were set either to aid or to prevent the motion of positive ions from the upper to the lower tube. No difference in end product was ever observed. It is thus clear that the primary reaction occurring was *not* ionic in character, but depended essentially on a nonionized condition of the nitrogen when it reached the hydrogen. Whether this was atomic nitrogen or a metastable, excited molecular state was not established.

(b) With the discharge off between electrodes 1 and 2, no product appeared in the collector trap.

(c) With the gases reversed, H_2 entering at inlet 1 and passing through the discharge, and N_2 being admixed at inlet 2, no product, visible or mass spectrographic, was found in the collector. (It may be specifically mentioned that water was not found in the collector although small amounts were trapped in the inlet traps.)

(d) With only N_2 admitted at inlet 1, the discharge in operation, and inlet 2 closed off, no product was found in the trap.

(e) In an effort to establish whether the hydrogen was diffusing against the flow of nitrogen and being activated in the discharge simultaneously with the nitrogen, various flow rates and pressures were used. At a pressure of 1 mm of N_2 and 1 mm of H_2 there was visible evidence of hydrogen in the color and spectrum of the glow discharge. Even at 2 mm of N_2 and 1 mm of H_2 this effect disappeared. Runs were made at pressures as high as 10 mm of N_2 with only 1 mm of H_2, and while NH_3 still was collected in the trap, no evidence of H_2 in the discharge was found. The steady-state solution of the diffusion equation indicates that the concentration of H_2 in the N_2 stream a distance x above the H_2 inlet should satisfy the equation

$$n=n_0e^{-vx/D},$$

where n_0 is the concentration at the inlet point, v is the streaming speed, and D the coefficient of diffusion. To reach the discharge, the hydrogen needed to diffuse a distance x equal to 3 cm. The value of D for H_2 in N_2 is approximately $0.265\times(760/p$ mm). Thus if the pressure was as low as 1 mm and v 100 cm/sec, n/n_0 could be as high as 0.24. However, with p of 10 mm and v of 500 cm/sec, n/n_0 was only $\sim10^{-32}$, confirming the qualitative experimental observations.

(f) Tests were made both with and without the constriction in the tube walls shown in Fig. 1 between electrode 2 and 3. The function of the constriction was to increase the flow velocity and diminish the chance of backward diffusion. No difference was observed however, except that at the very lowest pressures, some back diffusion still seemed to occur.

It seems fair to conclude from these observations that the formation of NH_3 depends *only* on activating the N_2, not the H_2, that the "activated nitrogen" has a life of at least several milliseconds, and that ionized nitrogen is *not* essential to the formation of NH_3.

RESULTS OF N_2 AND O_2 TESTS

With O_2 admitted at inlet 2, a similar series of tests was conducted to those with H_2. With N_2 pressures of approximately 3 mm Hg and O_2 of 1 mm, a product was found in the trap identified as N_2O by mass spectrographic test. At pressures of 10 mm and 4 mm respectively of N_2 and O_2, while some N_2O was still identified, the mass spectrometer disclosed a "nitric oxide."† Opened to the air, the collector trap emitted the odor commonly associated with NO_2. During operation, a pure blue crystalline material collected in the trap which on evaporation became a brown gas and which could be refrozen into the blue crystalline form. It is believed that N_2O_3 satisfies these characteristics and that neither NO, NO_2, nor N_2O_4 alone do. The belief is supported by the general picture of formation of a product under the given conditions, and by the additional observation that if air was admitted to the sealed-off collector bottle, only a white crystal could thereafter be condensed from the brown gas, presumably now N_2O_4, thanks to the additional oxygen supplied.

Again, as for the tests with H_2, all of the control tests were tried with O_2 with essentially the same form of results. The direction of the field between electrodes 2 and 3 had no influence. No product at all was obtained if any feature of the process was omitted, nor was any product found if the O_2 and the N_2 were interchanged. Oxygen was found to diffuse even less readily than H_2 against the stream of N_2 as might be expected from the values of the diffusion coefficients.

The possibility that radiation from the upper discharge could influence the results is greatest in the case of the nitrogen-oxygen[4] combination used here, and is not completely ruled out. The reference cited and much additional work on behavior of Geiger-Mueller counters establishes that N_2 is very poorly ionized by its own radiation. This fact, coupled with the small apertures in the electrodes, makes the chance of a secondary source of N_2 ions by such a process negligibly small. Oxygen does become ionized by the radiation from a nitrogen discharge. It is shown, however, by the negative result obtained on interchanging the N_2 and O_2, that the N_2 must be activated, so if the O_2 must also be activated or ionized by the radiation, a second order process is called for, wherein an activated N_2 meets an activated O_2 molecule, and this is indeed unlikely.

The combination of the several observations seems to rule out strongly any conclusions other than that the activation of N_2 does not call for an ion in the active state, and that activation of the O_2 is not needed at all. An additional indication from the selective formation of nitrous and nitric oxide under varying conditions is that there must be several "active" states of N_2 and that whether the nitrogen is atomic or molecular, excitation to several levels must occur.

NITROGEN-METHANE REACTIONS

Only a cursory examination of this combination was undertaken as the complexity of the results threatened to exceed the capacities of the simple apparatus used. Methane was never used as the discharge gas, the nitrogen being exclusively used for that purpose. A product was formed only at the lower pressure range (2–4 mm) identified by mass spectrograph and by odor as containing trimethyl-dimethyl, and methylamine, and some oily polymers in addition. Ions of nitrogen again seemed not to be involved as judged by the independence of the results on the ion-extraction field.

CARBON MONOXIDE DISCHARGES

This gas was tested in a static, nonflow system to investigate a suggestion that at field-strength-to-pressure ratios of 90–240 volts/cm per mm Hg pressure, a cluster ion, probably $(CO)_2^+$, could break up into either CO and CO^+ or CO_2 and C^+. If the conjecture is correct it was *not* confirmed in the present work at any field-strength-to-pressure values from 20 to 200 volts/cm per mm Hg. On the contrary the reactions bore a great similarity to the nitrogen reactions described above in being apparently nonionic. The gas pressure dropped; CO_2 collected in the chilled trap, but a feather of sooty carbon grew on the *anode* implying that a reduction of carbon

$$CO = C + O$$

was occurring directly at the anode. Neither CO^+, $(CO)_2^+$, nor C^+ would be expected under any mechanism to be involved in the deposit of carbon on the *anode*.

It is concluded that several of the simple chemical processes involving nitrogen in discharge reactions depend only on activation of some non-ionized state of nitrogen, not on nitrogen ions, and not on direct excitation of the other reacting member. Similarly, the decomposition of CO in a discharge to C and CO_2 is not characterized by an ionic process but by a direct reaction at the anode surface.

† We are advised by the operators of the mass spectrometer that NO, NO_2, N_2O_4, and probably N_2O_3 all show essentially a peak at mass 30 and cannot be reliably distinguished from one another.

[4] E. L. Huber, "Breakdown processes in N_2, O_2, and mixtures," Seventh Annual Gaseous Electronics Conference, October 14–16, 1954, paper C-5.

High-Speed Machine Computation of Ideal Gas Thermodynamic Functions. II. The Diatomic Free Radicals of the Isotopic Hydrides of Oxygen and Sulfur*

LESTER HAAR† AND A. S. FRIEDMAN
National Bureau of Standards, Washington 25, D. C.

(Received September 7, 1954)

The partition functions for the free radicals are obtained in closed form. They include terms to account for the special low-temperature effects arising with these molecules. The splitting of the $^2\pi$ ground state is complicated by the uncoupling of the electronic spin from the nuclear axis. In addition to this effect the partition function includes first-order corrections for rotation-vibration coupling, rotational stretching, and vibrational anharmonicity. Tables of thermal functions are computed on the NBS Eastern Automatic Computer—SEAC—from 50° to 5000°K for OH, OD, OT, SH, SD, and ST.

INTRODUCTION

As part of a program in progress at the National Bureau of Standards to investigate the isotope effects on thermodynamic properties of hydrides, the ideal gas thermal functions of a large number of substances containing hydrogen and its isotopes are being calculated. The calculations have been greatly facilitated by programming the problem for automatic machine computation on the National Bureau of Standards Eastern Automatic Computer—SEAC. The procedure has been previously applied to the calculation of the thermodynamic functions of the six hydrogen, deuterium, and tritium substituted isotopes of water.[1]

The ideal gas thermal functions of OH, OD, OT, SH, SD, and ST are presented here. These molecules have $^2\pi$ electronic ground states. The procedure employed takes into account the low-temperature effects of the uncoupling of the electronic spin from the internuclear axis and the nonclassical nuclear rotation, in addition to first-order corrections for the high-temperature effects of anharmonicity, rotation-vibration coupling, and rotational stretching. Tables of thermal functions are tabulated from 50° to 5000°K.

THE PARTITION FUNCTION

The contribution of the ground electronic state to the internal partition function can be written.

$$Q=\sum_v\{e^{-\epsilon_v/kT}\sum_J P_J e^{-\epsilon_J/kT}\}. \quad (1)$$

In this expression P_J is the degeneracy of the rotational level having energy ϵ_J; J and v are the rotational and vibrational quantum numbers, respectively.

For the multiplet electronic states of some of the lighter molecules, the simple approximation procedure for including the effect of the multiplicity by an electronic factor to the partition function is not valid. Hill and Van Vleck[2] have derived expressions for the rotational energies for these molecules. For a $^2\pi$ state,

$$H_1(J)=B_v\left\{(J+\tfrac{1}{2})^2-1-\left[(J+\tfrac{1}{2})^2+\left(\frac{A}{2B_v}\right)^2-\frac{A}{B_v}\right]^{\frac{1}{2}}\right\}-D_vJ^4, \quad (2)$$

$$H_2(J)=B_v\left\{(J+\tfrac{1}{2})^2-1+\left[(J+\tfrac{1}{2})^2+\left(\frac{A}{2B_v}\right)^2-\frac{A}{B_v}\right]^{\frac{1}{2}}\right\}-D_v(J+1)^4. \quad (3)$$

B_v is the rotational function and A is the separation of the minima of the potential energy curves. The rotational quantum number J can assume only half integral values. D_v is a function of the rotational stretching. To refer the potential functions to the lowest molecular energy level as the zero of energy, the lowest molecular energy β must be subtracted from $H_1(J)$ and $H_2(J)$. For the molecules treated here $\beta=H_1(\frac{3}{2})$.

The rotational partition function can be expressed‡ as

$$Q_{\rm rot}=2\exp\left[\frac{hc}{kT}\beta+(\tfrac{3}{4})\sigma\right]\times\left\{\sum_{\frac{1}{2},\frac{3}{2},\cdots}^{\infty J}(2J+1)\exp\left[\left(-\sigma J(J+1)+X^{\frac{1}{2}}+\frac{hc}{kT}D_vJ^2(J+1)^2\right)\right]+\sum_{\frac{1}{2},\frac{3}{2},\cdots}^{\infty J}(2J+1)\exp\left[\left(-\sigma J(J+1)-X^{\frac{1}{2}}+\frac{hc}{kT}D_vJ^2(J+1)^2\right)\right]-2e^{-\gamma\sigma}\right\}, \quad (4)$$

where

$$\sigma=\frac{hc}{kT}B_v;\quad X=\sigma^2\left[J(J+1)+\left(\frac{A}{2B_v}\right)^2-\frac{A}{B_v}+\frac{1}{4}\right].$$

* Sponsored in part by the U. S. Atomic Energy Commission Division of Research.

† Present address: Johns Hopkins University, Applied Physics Laboratory, Baltimore, Maryland.

[1] A. S. Friedman and L. Haar, J. Chem. Phys. **22**, 2051 (1954).

[2] E. L. Hill and J. H. Van Vleck, Phys. Rev. **32**, 250 (1923).

‡ The change in notation from $(J+\frac{1}{2})^2$ to $J(J+1)$ permits a more convenient representation.

The term $2e^{-\gamma\sigma}$ must be included to account for the fact that only one level with $J=\frac{1}{2}$ exists; $\gamma=(A/2B_v)-\frac{1}{4}$. The entire expression contains the factor 2 to account for the electronic degeneracy.

The two summations over J may be combined, and upon expansion§ of the hyperbolic factor $\exp(+X^{\frac{1}{2}})+\exp(-X^{\frac{1}{2}})$, and the factor $\exp[(hc/kT)D_vJ^2(J+1)^2]$, the rotational partition function becomes:

$$Q_{\text{rot}}=4\exp\left[\frac{hc}{kT}\beta+(\tfrac{3}{4})\sigma\right]\times\left[\sum_{\frac{1}{2},\frac{3}{2},\cdots}^{\infty J}\left\{(2J+1)e^{-\sigma J(J+1)}\times\left[1+\frac{hc}{kT}D_vJ^2(J+1)^2\right]\sum_0^{\infty n}\frac{X^n}{(2n)!}\right\}-e^{-\gamma\sigma}\right]. \quad (5)$$

Expanding and rearranging the X^n in powers of $J(J+1)$, the following relation is obtained:

$$\sum_{\frac{1}{2},\frac{3}{2},\cdots}^{\infty J}\left\{(2J+1)e^{-\sigma J(J+1)}\times\left[1+\frac{hc}{kT}D_vJ^2(J+1)^2\right]\sum_0^{\infty n}\frac{X^n}{(2n)!}\right\}=\sum_0^{\infty k}\bar{g}_k\sum_{\frac{1}{2},\frac{3}{2},\cdots}^{\infty J}J^k(J+1)^k(2J+1)e^{-\sigma J(J+1)}\times\left[1+\frac{hc}{kT}D_vJ^2(J+1)^2\right]. \quad (6)$$

The $\bar{g}_k$ are polynomials in σ which can be generated from the relation

$$\bar{g}_k=\frac{\sigma^{2k}}{k!}\sum_0^{\infty n}\frac{(n+k)!}{(2n+2_k)!}\frac{(\sigma^2a)^n}{n!},$$

where

$$a\equiv\left(\frac{A}{2B_v}\right)^2-\frac{A}{B_v}+\frac{1}{4}.$$

Note that the $\bar{g}_k$ are very small for large k. Also note that the $\bar{g}_k$ all converge.

With the aid of the identity

$$J^k(J+1)^k(2J+1)e^{-\sigma J(J+1)}\equiv(-1)^k\frac{d^k}{d\sigma^k}(2J+1)e^{-\sigma J(J+1)}$$

the relation

$$\sum_{0,1,2,\cdots}^{\infty k}\bar{g}_k\sum_{\frac{1}{2},\frac{3}{2},\cdots}^{\infty J}J^k(J+1)^k\times(2J+1)e^{-\sigma J(J+1)}\left[1+\frac{hc}{kT}D_vJ^2(J+1)^2\right]=\sum_{0,1,\cdots}^{\infty k}g_k\frac{d^k}{d\sigma^k}\left\{\left[1+\frac{hc}{kT}D_v\frac{d^2}{d\sigma^2}\right]\times\sum_{\frac{1}{2},\frac{3}{2},\cdots}^{\infty J}(2J+1)e^{-\sigma J(J+1)}\right\} \quad (7)$$

is obtained. $g_k=\bar{g}_k(-1)^k$.

As the low-temperature contribution of the D_v term is very small, it is valid to employ the relations

$$\frac{hc}{kT}D_v\frac{d^2}{d\sigma^2}\sum_{\frac{1}{2},\frac{3}{2},\cdots}^{\infty J}(2J+1)e^{-\sigma J(J+1)}\cong\frac{hc}{kT}D_v\frac{d^2}{d\sigma^2}\frac{1}{\sigma},$$

and

$$\frac{hc}{kT}D_v\frac{d^2}{d\sigma^2}\frac{1}{\sigma}\cong\frac{hc}{kT}\frac{2D_v}{\sigma^2}\sum_{\frac{1}{2},\frac{3}{2},\cdots}^{\infty J}(2J+1)e^{-\sigma J(J+1)}.$$

The right-hand side of Eq. (7) then expands to

$$\left[1+\frac{hc}{kT}\frac{2D_v}{\sigma^2}\right]\sum_0^{\infty k}g_k\frac{d^k}{d\sigma^k}\sum_{\frac{1}{2},\frac{3}{2},\cdots}^{\infty J}(2J+1)e^{-\sigma J(J+1)}+\sum_{\frac{1}{2},\frac{3}{2},\cdots}^{\infty J}(2J+1)e^{-\sigma J(J+1)}\sum_1^{\infty k}g_k\frac{d^k}{d\sigma^k}\frac{hc}{kT}\frac{2D_v}{\sigma^2}.$$

The second series of terms is small compared with the first and can be neglected.‖

The expression for the rotational partition function can then be written

$$Q_{\text{rot}}=4\exp\left[\frac{hc}{kT}\beta+(\tfrac{3}{4})\sigma\right]\left[1+\frac{hc}{kT}\frac{2D_v}{\sigma^2}\right]\times\left\{\sum_0^{\infty k}\left(g_k\frac{d^k}{d\sigma^k}\sum_{\frac{1}{2},\frac{3}{2},\cdots}^{\infty J}(2J+1)e^{-\sigma J(J+1)}\right)-e^{-\gamma\sigma}\right\}, \quad (8)$$

where the approximation

$$\frac{e^{-\gamma\sigma}}{1+\dfrac{2D_v}{\sigma^2}\dfrac{hc}{kT}}\cong e^{-\gamma\sigma}$$

leads to negligible error.

§ The expression for the partition function is summed from $J=0$ to $J=\infty$. However, the molecular states actually contributing to Q have an upper limit for J. After these expansions the Q summation may be performed over all J to $J=\infty$ with negligible error at all but the highest temperatures considered. The upper limit for J is such that the approximation

$$\exp[(hc/kT)D_vJ^2(J+1)^2]\cong1+(hc/kT)D_vJ^2(J+1)^2$$

may be employed.

‖ g_k is of the order $\sigma^{2k}/(2k)!$ and $(d^k/d\sigma^k)2/\sigma^2$ is of the order $(k+2)!/\sigma^{k+2}$; hence $g_k(d^k/d\sigma^k)2/\sigma^2$ is of the order $[\sigma^{2k}/(2k)!]\times[(2+k)!/\sigma^{k+2}]\to0$ for k large, since $\sigma<1$. The largest contribution to the second term arises from the $k=1$ term and is approximately $(1/\sigma)(3D_v/B_0)$. Since the first series of terms is of the order of $1/\sigma$ and $3D_v/B_0$ is of the order 10^{-5}, the second series of terms is completely negligible.

TABLE I. Ground state molecular constants used in the calculation of ideal gas thermal properties.

	Units	OH	OD	OT	SH	SD	ST
ν	cm^{-1}	3569.6	2632.5	2221	2582	1878	1567
$X_e\omega_e/\nu$	dimensionless	0.0232	0.0168	0.014	0.0232	0.017	0.014
δ	dimensionless	0.0384	0.0304	0.023	0.0317	0.0225	0.019
B_0	cm^{-1}	18.514	9.868	6.97	9.461	4.900	3.40
ρ	$°K^{-1}$	7.59×10^{-6}	7.59×10^{-6}	7.59×10^{-6}	7.5×10^{-6}	7.5×10^{-6}	7.5×10^{-6}
A	cm^{-1}	−139.7	−139.7	−139.7	−376.96	−376.96	−376.96

A convenient expression for

$$\sum_{\frac{1}{2},\frac{3}{2},\cdots}^{\infty}{}_J\ (2J+1)e^{-\sigma J(J+1)}$$

is obtained by using the identity

$$\sum_{\frac{1}{2},\frac{3}{2},\cdots}^{\infty}{}_J f(J)\equiv \sum_{0,\frac{1}{2},1,\frac{3}{2},\cdots}^{\infty}{}_J f(J)-\sum_{0,1,2,\cdots}^{\infty}{}_J f(J).$$

The Euler expansion for this quantity can be put in the form

$$\sum_{0,\frac{1}{2},1,\frac{3}{2},\cdots}^{\infty}{}_J f(J)-\sum_{0,1,2,\cdots}^{\infty}{}_J f(J)\cong\int_0^{\infty} f(J)dJ - \sum_{1,3,5,\cdots}^{n}{}_r \frac{B_{(r+1)}}{(r+1)!}f^r(0)[(\tfrac{1}{2})^r-1],$$

where $f(J)=(2J+1)e^{-\sigma J(J+1)}$ and $f^r(0)$ is the rth derivative of $f(J)$ evaluated at $J=0$. $B_{(r+1)}$ are the Bernoulli coefficients. In this way is obtained

$$\sum_{\frac{1}{2},\frac{3}{2},\cdots}^{\infty}{}_J\ (2J+1)e^{-\sigma J(J+1)} =\frac{1}{\sigma}(1+0.0833\sigma-0.0271\sigma^2-0.0107\sigma^3-0.0032\sigma^4). \quad (9)$$

Since the terms

$$g_k\frac{d^k}{d\sigma^k}\sum_{\frac{1}{2},\frac{3}{2},\cdots}^{\infty}{}_J\ (2J+1)e^{-\sigma J(J+1)}$$

rapidly diminish for increasing values of k, it is not necessary to include any $k>3$. The summation over the k numbers can then be written as a polynomial in σ. This is combined with the power series expansion of $e^{-\gamma\sigma}$ to yield the expression for the rotational partition function,

$$Q_{\rm rot}=4\left(1+\frac{hc}{kT}\frac{2D_v}{\sigma^2}\right)\exp\left[\frac{hc}{kT}\beta+(\tfrac{3}{4})\sigma\right]\frac{1}{\sigma}\sum C_n\sigma^n. \quad (10)$$

The polynomial was summed from $n=0$ to $n=12$; the C_n are constants.

The complete internal partition function is obtained by summing Eq. (1) over the vibrational coordinates using Eq. (10) for $Q_{\rm rot}$.

A two-constant energy level expression for $G(v)$ is used; $G(v)=\nu v+\omega_e x_e v-\omega_e x_e v^2$, where ν is the observed fundamental and $\omega_e x_e$ is the first anharmonicity coefficient. The sum over the vibrational coordinates yields the partition function expression

$$Q=\left[\frac{4}{\sigma_0}\left(\sum_0^{12}{}_n C_n\sigma_0{}^n\right)(1-e^{-u})^{-1}\left(1+\frac{\delta}{e^u-1}\right)\times\left(1+\frac{\left[\frac{2X_e\omega_e}{\nu}\right]}{(e^u-1)^2}\right)(1+\rho T)\right]\exp\left[\frac{hc}{kT}\beta+(\tfrac{3}{4})\sigma_0\right]. \quad (11)$$

The constants σ_0 and δ are defined by the relation $\sigma=\sigma_0(1+\delta v)$;

$$u\equiv\frac{hc}{kT}\nu;\quad \rho\equiv 2\left(\frac{hc}{k}\frac{D_0}{T^2\sigma_0{}^2}\right),$$

where $D_0\equiv D_v$ for $v=0$.

The factors in the large square brackets and also the translational factor were evaluated and their contributions to the thermodynamic functions were computed on the SEAC.[1] The contributions of the remaining exponential term $\exp[(hc/kT)\beta+(\frac{3}{4})\sigma]$ were then added to the values obtained on the SEAC.

For the thermodynamic properties of SH, SD, and ST below 150°K a different expression was employed. The large ratio of A/B_v for these molecules requires a polynomial higher than the 12th degree for an accurate calculation below 150°K. However, for large A/B_v the formulas given in Eqs. (2) and (3) may be replaced by a modified Hund's case a representation.[3] The expressions for the energy levels, referring to the lowest rotational state as zero, are

$$F_1(J)=B_1J(J+1)-\beta_1;\quad F_2(J)=B_2J(J+1)-\beta_2;$$
$$B_1=B_v/k_1\quad\text{and}\quad B_2=B_v/k_2,$$

where

$$k_1=\left(1+\frac{B_v}{A}\right)^{-1}\quad\text{and}\quad k_2=\left(1-\frac{B_v}{A}\right)^{-1},$$

[3] G. Herzberg, *Molecular Spectra and Molecular Structure. I. Spectra of Diatomic Molecules* (D. Van Nostrand Company, Inc., New York, 1951), second edition.

TABLE II. Ideal gas thermodynamic functions for OH.

°K	$\frac{C_p^0}{R}$	$\frac{(H^0-E_0^0)}{RT}$	$\frac{-(F^0-E_0^0)}{RT}$	$\frac{S^0}{R}$
50	3.50050	2.87580	12.59278	15.46858
70	3.73237	3.09296	13.59680	16.68976
90	3.80047	3.24458	14.39361	17.63819
110	3.79879	3.34611	15.05523	18.40134
130	3.77249	3.41389	15.62010	19.03399
150	3.74051	3.45958	16.11202	19.57160
170	3.70993	3.49080	16.54706	20.03786
190	3.68295	3.51241	16.93658	20.44899
210	3.65993	3.52753	17.28891	20.81644
230	3.64053	3.53817	17.61033	21.14850
250	3.62424	3.54568	17.90567	21.45135
300	3.59395	3.55608	18.55318	22.10926
350	3.57393	3.55997	19.10164	22.66161
400	3.56053	3.56081	19.57714	23.13795
450	3.55189	3.56027	19.99653	23.55680
500	3.54721	3.55916	20.37158	23.93074
600	3.54912	3.55712	21.02029	24.57741
700	3.56602	3.55700	21.56859	25.12559
800	3.59683	3.55992	22.04372	25.60364
900	3.63880	3.56627	22.46334	26.02961
1000	3.68844	3.57596	22.83956	26.41552
1100	3.74245	3.58861	23.18096	26.76957
1200	3.79811	3.60375	23.49384	27.09759
1300	3.85345	3.62083	23.78296	27.40379
1400	3.90711	3.63938	24.05197	27.69135
1500	3.95832	3.65895	24.30372	27.96267
1600	4.00660	3.67918	24.54050	28.21968
1700	4.05179	3.69979	24.76417	28.46396
1800	4.09386	3.72052	24.97623	28.69675
1900	4.13294	3.74121	25.17794	28.91915
2000	4.16916	3.76172	25.37037	29.13209
2200	4.23382	3.80177	25.73079	29.53256
2400	4.28949	3.84015	26.06324	29.90339
2600	4.33769	3.87661	26.37207	30.24868
2800	4.37974	3.91108	26.66063	30.57171
3000	4.41674	3.94359	26.93159	30.87518
3200	4.44962	3.97420	27.18709	31.16129
3400	4.47905	4.00305	27.42890	31.43195
3600	4.50564	4.03025	27.65849	31.68874
3800	4.52985	4.05592	27.87708	31.93300
4000	4.55208	4.08017	28.08574	32.16591
4200	4.57262	4.10314	28.28538	32.38852
4400	4.59173	4.12492	28.47676	32.60168
4600	4.60962	4.14561	28.66058	32.80619
4800	4.62645	4.16529	28.83744	33.00273
5000	4.64238	4.18406	29.00786	33.19192

respectively.

$$\beta_1=\frac{B_v}{k_1}\frac{15}{4};\quad \beta_2=\frac{B_v}{k_2}\frac{3}{4}-H_2(\tfrac{1}{2})+H_1(\tfrac{3}{2}),$$

where H_1 and H_2 are the functions given in Eqs. (2) and (3).

The rotational partition function with these relations is

$$Q_{\rm rot}=2\exp\left(\frac{hc}{kT}\beta_1\right)\left\{\sum_{\frac{1}{2},\frac{3}{2},\cdots}^{\infty J}(2J+1)e^{-\sigma_1 J(J+1)}-2e^{-(\frac{1}{2})\sigma_1}\right\}$$
$$+\exp\left(\frac{hc}{kT}\beta_2\right)\sum_{\frac{1}{2},\frac{3}{2},\cdots}^{\infty J}(2J+1)e^{-\sigma_2 J(J+1)},\quad(12)$$

where $\sigma_1=(hc/kT)B_1$, $\sigma_2=(hc/kT)B_2$. The term $2e^{-(\frac{1}{2})\sigma_1}$ is included to account for the fact that only one level with $J=\frac{1}{2}$ exists.

Using the expansion for

$$\sum_{\frac{1}{2},\frac{3}{2},\cdots}^{\infty J}(2J+1)e^{-\sigma J(J+1)},$$

Eq. (9), and expanding $e^{-(\frac{1}{2})\sigma_1}$, the rotational expression applicable to large A/B_v is obtained,

$$Q_{\rm rot}=\frac{2}{\sigma}\exp\left(\frac{hc}{kT}\beta_1\right)\left\{k_1-\frac{23}{12}\sigma+\frac{1.473}{k_1}\sigma^2-\frac{0.5625}{k_1^2}\sigma^3\right.$$
$$\left.+\exp\left(\frac{hc}{kT}\beta_3\right)\left[k_2+\frac{\sigma}{12}-\frac{0.027}{k_2}\sigma^2\right]\right\},\quad(13)$$

where $\beta_3=\beta_2-\beta_1$.

TABLE III. Ideal gas thermodynamic functions for OD.

°K	$\frac{C_p^0}{R}$	$\frac{(H^0-E_0^0)}{RT}$	$\frac{-(F^0-E_0^0)}{RT}$	$\frac{S^0}{R}$
50	3.68420	3.13107	12.94356	16.07463
70	3.84240	3.31558	14.02836	17.34394
90	3.87567	3.43794	14.87746	18.31540
110	3.85244	3.51589	15.57553	19.09142
130	3.81171	3.56462	16.16713	19.73175
150	3.76978	3.59474	16.67951	20.27425
170	3.73221	3.61306	17.13067	20.74373
190	3.70024	3.62388	17.53319	21.15707
210	3.67360	3.62985	17.89619	21.52604
230	3.65153	3.63266	18.22656	21.85922
250	3.63325	3.63341	18.52949	22.16290
300	3.60014	3.63041	19.19175	22.82216
350	3.58007	3.62453	19.75095	23.37548
400	3.56994	3.61824	20.23454	23.85278
450	3.56856	3.61272	20.66038	24.27310
500	3.57536	3.60858	21.04079	24.64937
600	3.61036	3.60560	21.69832	25.30392
700	3.66664	3.61011	22.25438	25.86449
800	3.73487	3.62135	22.73711	26.35846
900	3.80736	3.63798	23.16456	26.80254
1000	3.87899	3.65852	23.54889	27.20741
1100	3.94686	3.68169	23.89866	27.58035
1200	4.00957	3.70644	24.22006	27.92650
1300	4.06663	3.73199	24.51774	28.24973
1400	4.11816	3.75776	24.79525	28.55301
1500	4.16451	3.78336	25.05539	28.83875
1600	4.20615	3.80851	25.30036	29.10887
1700	4.24360	3.83302	25.53199	29.36501
1800	4.27734	3.85678	25.75176	29.60854
1900	4.30784	3.87973	25.96090	29.84063
2000	4.33549	3.90184	26.16048	30.06232
2200	4.38365	3.94351	26.53434	30.47785
2400	4.42419	3.98193	26.87914	30.86107
2600	4.45883	4.01731	27.19929	31.21660
2800	4.48892	4.04995	27.49821	31.54816
3000	4.51542	4.08011	27.77867	31.85878
3200	4.53907	4.10807	28.04290	32.15097
3400	4.56043	4.13407	28.29274	32.42681
3600	4.57994	4.15830	28.52972	32.68802
3800	4.59793	4.18098	28.75518	32.93616
4000	4.61466	4.20225	28.97017	33.17242
4200	4.63035	4.22226	29.17570	33.39796
4400	4.64516	4.24115	29.37254	33.61369
4600	4.65920	4.25902	29.56147	33.82049
4800	4.67261	4.27597	29.74310	34.01907
5000	4.68548	4.29211	29.91799	34.21010

TABLE IV. Ideal gas thermodynamic functions for OT.

°K	$\frac{C_p^0}{R}$	$\frac{(H^0-E_0^0)}{RT}$	$\frac{-(F^0-E_0^0)}{RT}$	$\frac{S^0}{R}$
50	3.72686	3.24159	13.23305	16.47464
70	3.87087	3.40436	14.35131	17.75567
90	3.89672	3.51244	15.22089	18.73333
110	3.86809	3.58015	15.93286	19.51301
130	3.82340	3.62108	16.53455	20.15563
150	3.77861	3.64503	17.05456	20.69959
170	3.73897	3.65835	17.51170	21.17005
190	3.70553	3.66503	17.91902	21.58405
210	3.67781	3.66753	18.28597	21.95350
230	3.65504	3.66739	18.61963	22.28702
250	3.63639	3.66564	18.92535	22.59099
300	3.60407	3.65781	19.59303	23.25084
350	3.58807	3.64882	20.15621	23.80503
400	3.58579	3.64095	20.64290	24.28385
450	3.59563	3.63526	21.07140	24.70666
500	3.61579	3.63223	21.45423	25.08646
600	3.67869	3.63439	22.11650	25.75089
700	3.75808	3.64628	22.67751	26.32379
800	3.84162	3.66549	23.16560	26.83109
900	3.92209	3.68957	23.59869	27.28826
1000	3.99601	3.71658	23.98880	27.70538
1100	4.06224	3.74506	24.34435	28.08941
1200	4.12082	3.77398	24.67146	28.44544
1300	4.17236	3.80268	24.97467	28.77735
1400	4.21767	3.83074	25.25752	29.08826
1500	4.25754	3.85790	25.52274	29.38064
1600	4.29277	3.88399	25.77256	29.65655
1700	4.32403	3.90897	26.00879	29.91776
1800	4.35191	3.93283	26.23289	30.16572
1900	4.37689	3.95555	26.44614	30.40169
2000	4.39942	3.97719	26.64960	30.62679
2200	4.43846	4.01740	27.03059	31.04799
2400	4.47121	4.05389	27.38173	31.43562
2600	4.49925	4.08709	27.70756	31.79465
2800	4.52369	4.11742	28.01157	32.12899
3000	4.54533	4.14525	28.29660	32.44185
3200	4.56480	4.17087	28.56496	32.73583
3400	4.58253	4.19457	28.81854	33.01311
3600	4.59884	4.21659	29.05892	33.27551
3800	4.61403	4.23710	29.28746	33.52456
4000	4.62828	4.25632	29.50528	33.76160
4200	4.64174	4.27435	29.71340	33.98775
4400	4.65456	4.29134	29.91263	34.20397
4600	4.66681	4.30740	30.10374	34.41114
4800	4.67859	4.32263	30.28739	34.61002
5000	4.68996	4.33709	30.46415	34.80124

The rotational stretching correction, omitted in the energy expression given above, can be treated as a factor to the partition function.

The summation over the vibrational energy states then gives the ground state contribution to the internal partition function.

$$Q=\left\{\frac{2}{\sigma_0}(1-e^{-u})^{-1}\left(1+\frac{\delta}{e^u-1}\right)\left[1+\frac{\left[\frac{2X_e\omega_e}{\nu}\right]}{(e^u-1)^2}\right](1+\rho T)\right\}$$
$$\times\exp\left(\frac{hc}{kT}\beta_1\right)\left[k_1-\frac{23}{12}\sigma_0+\frac{1.473}{k_1}\sigma_0^2-\frac{0.5625}{k_1^2}\sigma_0^3\right.$$
$$\left.+\exp\left(\frac{hc}{kT}\beta_3\right)\left(k_2+\frac{\sigma_0}{12}-\frac{0.027}{k_2}\sigma_0^2\right)\right]. \quad (14)$$

This expression was used only for SH, SD, and ST below 150°K. At higher temperatures it was easier to use the partition function expression obtained previously, Eq. (11). The contributions of the quantity in curly brackets were computed on the SEAC.[1] The contributions of the remaining factors were then added to these after hand computation.

MOLECULAR CONSTANTS

The ground state molecular data for OH and OD were taken from the selected list reported by Herzberg.[3] The molecular data for OT were calculated with the aid of the isotope relations from the OH data. The molecular data for SH and SD are the values re-

TABLE V. Ideal gas thermodynamic functions for SH.

°K	$\frac{C_p^0}{R}$	$\frac{(H^0-E_0^0)}{RT}$	$\frac{-(F^0-E_0^0)}{RT}$	$\frac{S^0}{R}$
50	3.42596	3.07447	13.84212	16.91659
70	3.49225	3.18495	14.89561	18.08056
90	3.56468	3.26090	15.70560	18.96650
110	3.65267	3.32402	16.36621	19.69023
130	3.73955	3.38137	16.92620	20.30757
150	3.81216	3.43417	17.41385	20.84802
170	3.86524	3.48197	17.84667	21.32864
190	3.89915	3.52425	18.23631	21.76056
210	3.91700	3.56094	18.59015	22.15109
230	3.92266	3.59224	18.91493	22.50717
250	3.91876	3.61857	19.21558	22.83415
300	3.88685	3.66624	19.87989	23.54613
350	3.84457	3.69475	20.44738	24.14213
400	3.80599	3.71099	20.94191	24.65290
450	3.77690	3.71983	21.37957	25.09940
500	3.75911	3.72455	21.77177	25.49632
600	3.75551	3.72947	22.45129	26.18076
700	3.78465	3.73496	23.02658	26.76154
800	3.83346	3.74408	23.52586	27.26994
900	3.89168	3.75720	23.96758	27.72478
1000	3.95250	3.77369	24.36426	28.13795
1100	4.01198	3.79266	24.72481	28.51747
1200	4.06806	3.81329	25.05568	28.86897
1300	4.11986	3.83492	25.36176	29.19668
1400	4.16714	3.85699	25.64677	29.50376
1500	4.21007	3.87912	25.91362	29.79274
1600	4.24893	3.90104	26.16468	30.06572
1700	4.28412	3.92255	26.40183	30.32438
1800	4.31603	3.94354	26.62663	30.57017
1900	4.34504	3.96393	26.84039	30.80432
2000	4.37151	3.98365	27.04423	31.02788
2200	4.41798	4.02109	27.42568	31.44677
2400	4.45751	4.05585	27.77707	31.83292
2600	4.49166	4.08809	28.10301	32.19110
2800	4.52163	4.11800	28.40708	32.52508
3000	4.54828	4.14582	28.69216	32.83798
3200	4.57229	4.17173	28.96056	33.13229
3400	4.59418	4.19595	29.21420	33.41015
3600	4.61433	4.21864	29.45469	33.67333
3800	4.63306	4.23996	29.68336	33.92332
4000	4.65061	4.26006	29.90135	34.16141
4200	4.66716	4.27905	30.10967	34.38872
4400	4.68288	4.29706	30.30914	34.60620
4600	4.69789	4.31416	30.50054	34.81470
4800	4.71228	4.33045	30.68449	35.01494
5000	4.72613	4.34601	30.86159	35.20760

TABLE VI. Ideal gas thermodynamic functions for SD.

°K	$\frac{C_p^0}{R}$	$\frac{(H^0-E_0^0)}{RT}$	$\frac{-(F^0-E_0^0)}{RT}$	$\frac{S^0}{R}$
50	3.48664	3.26071	14.32377	17.58448
70	3.51771	3.32913	15.43278	18.76191
90	3.58009	3.37736	16.27543	19.65279
110	3.66486	3.42176	16.95749	20.37925
130	3.75097	3.46588	17.53266	20.99854
150	3.82360	3.50894	18.03169	21.54063
170	3.87679	3.54928	18.47339	22.02267
190	3.91073	3.58568	18.87019	22.45587
210	3.92844	3.61788	19.23055	22.84843
230	3.93377	3.64566	19.56083	23.20649
250	3.93034	3.66853	19.86578	23.53431
300	3.90366	3.71015	20.53861	24.24876
350	3.87446	3.73562	21.11262	24.84824
400	3.85665	3.75172	21.61257	25.36429
450	3.85359	3.76307	22.05514	25.81821
500	3.86384	3.77253	22.45211	26.22464
600	3.91185	3.79136	23.14156	26.93292
700	3.97770	3.81317	23.72759	27.54076
800	4.04682	3.83808	24.23837	28.07645
900	4.11213	3.86495	24.69197	28.55692
1000	4.17099	3.89267	25.10061	28.99328
1100	4.22289	3.92038	25.47293	29.39331
1200	4.26824	3.94752	25.81521	29.76273
1300	4.30782	3.97374	26.13223	30.10597
1400	4.34246	3.99888	26.42764	30.42652
1500	4.37291	4.02282	26.70437	30.72719
1600	4.39985	4.04556	26.96471	31.01027
1700	4.42383	4.06711	27.21064	31.27775
1800	4.44534	4.08754	27.44368	31.53122
1900	4.46477	4.10689	27.66520	31.77209
2000	4.48242	4.12524	27.87634	32.00158
2200	4.51348	4.15915	28.27113	32.43028
2400	4.54012	4.18982	28.63437	32.82419
2600	4.56347	4.21769	28.97082	33.18851
2800	4.58433	4.24313	29.28435	33.52748
3000	4.60328	4.26653	29.57791	33.84444
3200	4.62072	4.28812	29.85398	34.14210
3400	4.63697	4.30818	30.11454	34.42272
3600	4.65225	4.32688	30.36132	34.68820
3800	4.66674	4.34438	30.59575	34.94013
4000	4.68056	4.36084	30.81901	35.17985
4200	4.69386	4.37639	31.03215	35.40854
4400	4.70667	4.39111	31.23609	35.62720
4600	4.71909	4.40510	31.43158	35.83668
4800	4.73117	4.41843	31.61935	36.03778
5000	4.74294	4.43119	31.79997	36.23116

ported by Ramsay.[4] It should be noted that the vibrational fundamentals for SH and SD were not directly observed. The observed electronic transitions include the (0,0) and (1,0) bands for both SH and SD which yield vibrational data for the $^2\Sigma$ states. The ground state data were obtained from the solutions of four equations, two involving the theoretical relation for the (0,0) transition of the two isotopes and two equations involving the Morse relation for the rotation-vibration coupling constants. Recently, Leach, in a preliminary note,[5] reported an experimental value for the force constant of SH: $k_e=4.1929\times10^5$ dynes/cm. The value obtained from the Ramsey data, $k_e=4.201\times10^5$ dynes/cm, agrees to within 0.2 percent. The data for ST were calculated from the SH data. The spin coupling constant A used in the OH, OD, and OT calculations was the value reported for OH. Similarly, the value used for A for SH, SD, and ST was the SH value. Though the value changes slightly for the three isotopes, the properties calculated are not sensitive to these small changes.

The chemical atomic weights used in the calculations of the translational contributions to the thermal functions were obtained from the values listed by Wichers.[6] The atomic weights used in the calculation

TABLE VII. Ideal gas thermodynamic functions for ST.

°K	$\frac{C_p^0}{R}$	$\frac{(H^0-E_0^0)}{RT}$	$\frac{-(F^0-E_0^0)}{RT}$	$\frac{S^0}{R}$
50	3.49544	3.32989	14.65352	17.98341
70	3.52224	3.38031	15.78265	19.16296
90	3.58359	3.41804	16.63681	20.05485
110	3.66840	3.45567	17.32637	20.78204
130	3.75473	3.49512	17.90691	21.40203
150	3.82752	3.53478	18.40994	21.94472
170	3.88086	3.57254	18.85483	22.42737
190	3.91513	3.60692	19.25426	22.86118
210	3.93388	3.63743	19.61629	23.25372
230	3.94115	3.66377	19.94742	23.61119
250	3.94094	3.68599	20.25444	23.94043
300	3.92745	3.72747	20.93021	24.65768
350	3.91718	3.75517	21.50702	25.26219
400	3.92035	3.77547	22.00983	25.78530
450	3.93692	3.79238	22.45551	26.24789
500	3.96340	3.80809	22.85590	26.66399
600	4.03161	3.83949	23.55296	27.39245
700	4.10387	3.87213	24.14727	28.01940
800	4.17065	3.90535	24.66647	28.57182
900	4.22912	3.93816	25.12836	29.06652
1000	4.27916	3.96982	25.54494	29.51476
1100	4.32179	3.99994	25.92472	29.92466
1200	4.35816	4.02831	26.27399	30.30230
1300	4.38943	4.05492	26.59750	30.65242
1400	4.41686	4.07944	26.89893	30.97837
1500	4.44020	4.10305	27.18121	31.28426
1600	4.46140	4.12452	27.44671	31.57123
1700	4.47977	4.14513	27.69738	31.84251
1800	4.49656	4.16419	27.93487	32.09906
1900	4.51179	4.18210	28.16050	32.34260
2000	4.52572	4.19893	28.37545	32.57438
2200	4.55050	4.22980	28.77712	33.00692
2400	4.57213	4.25746	29.14636	33.40382
2600	4.59144	4.28240	29.48815	33.77055
2800	4.60900	4.30511	29.80635	34.11146
3000	4.62524	4.32592	30.10410	34.43002
3200	4.64042	4.34510	30.38391	34.72901
3400	4.65477	4.36290	30.64788	35.01078
3600	4.66845	4.37950	30.89772	35.27722
3800	4.68157	4.39505	31.13493	35.52998
4000	4.69424	4.40968	31.36075	35.77043
4200	4.70653	4.42355	31.57623	35.99978
4400	4.71847	4.43668	31.78232	36.21900
4600	4.73014	4.44924	31.97982	36.42906
4800	4.74156	4.46112	32.16943	36.63055
5000	4.75275	4.47257	32.35176	36.82433

[4] D. A. Ramsay, J. Chem. Phys. **20**, 1920 (1952).
[5] S. Leach, J. Chem. Phys. **22**, 1261 (1954).
[6] E. Wichers, J. Am. Chem. Soc. **74**, 2447 (1952).

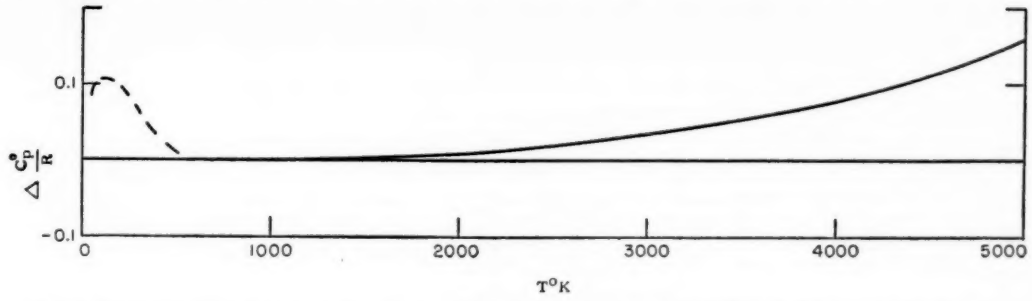

FIG. 1. Comparison of heat capacity values of OH. Base line: this calculation. Solid curve: direct summation calculation minus this calculation. Dashed curve: Hund's case *a*, with electronic contribution as separate factor, minus this calculation.

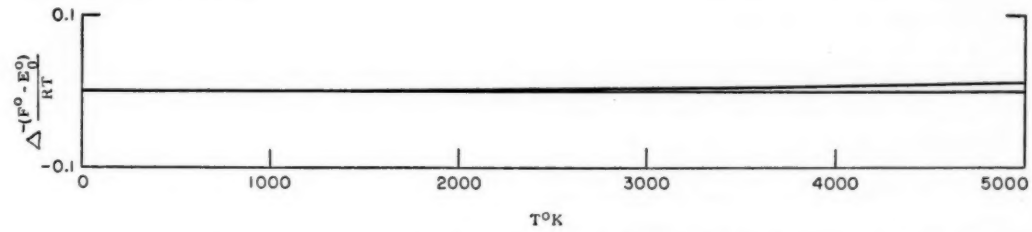

FIG. 2. Comparison of free energy functions of OH. Base line: this calculation. Solid curve: direct summation calculation minus this calculation.

of the molecular data for OT and ST are the values listed by Mattauch.[7]

The molecular constants are listed in Table I.

THERMAL PROPERTIES

The dimensionless heat capacity, enthalpy, free energy, and entropy for OH, OD, OT, and SH, SD, ST are tabulated in Tables II to VII. These tabulated functions include only the contribution of the ground electronic state; the contributions of excited electronic states are insignificant at all but the highest temperatures. The tabulated thermal properties were calculated using the molecular constants for the oxygen and sulfur isotopes O^{16} and S^{32}, the predominant species. The molecular constants obtained by substitution of the other isotopes of oxygen and sulfur do not differ appreciably from those of the predominant species. This, together with the very large relative abundance of the predominant species, results in completely negligible difference between the values of the properties tabulated here and those referring to the naturally occurring mixtures. The entropy of nuclear spin and the entropy of isotopic mixing have been omitted.

The reliability of the tables up to temperatures of approximately 1000°K depends primarily on the accuracy of the rotational and vibrational fundamentals and the spin-coupling constants. At the higher temperatures the reliability depends on the accuracy of the molecular constants used in the first-order corrections for anharmonicity, rotational stretching, and rotation-vibration coupling; but it is even more sensitive to the effect of the omission of higher order corrections for these effects and the neglect of rotational cutoff.

It is thought that the uncertainties in the tabulated heat capacity functions, the most sensitive of the functions are less than 0.1 percent below 1000°K, but increase to 0.3 percent at 5000°K. Although the thermodynamic functions are not accurate to the number of decimal places given in these tables, their differences between isotopes (used in chemical equilibrium calculations) are.

The SEAC calculations for OH are compared in Fig. 1 and 2 with a direct term by term summation of the unexpanded partition function for OH performed at the Ohio State University Cryogenic Laboratory.[8] The very small differences in the heat capacity and free energy below 1000°K (<0.1 percent) can be ascribed to the use of slightly different molecular data. For purposes of comparison a calculation based on the assumption that the electronic multiplicity can be accounted for by an independent factor to the partition function is also included in Fig. 1.

The SEAC performed its part of the calculations in less than five minutes per molecule.

A denser set of thermodynamic functions have been punched on I.B.M. cards. These will be used to tabulate equilibrium data for various isotope exchange reactions involving hydrogen, deuterium, and tritium.

ACKNOWLEDGMENT

The authors are greatly indebted to Ethel C. Marden of the NBS Mathematics Division coding staff for her assistance.

[7] J. Mattauch, *Nuclear Physics Tables* (Springer-Verlag OHG., 1942).

[8] Johnston, Belzer, and Savedoff, O.S.U. Research Foundation Tech. Report No. 316-5.

Ultrasonic Absorption in Sugar Solutions

G. S. VERMA
Department of Physics, University of Allahabad, Allahabad, India
(Received June 8, 1954)

Ultrasonic absorption and the frequency at which maximum absorption is to be expected have been calculated in solutions of sucrose, glucose, and lactose at various concentrations and temperatures on the basis of structural changes in the quasi-crystalline structure of the liquid medium. The relaxation frequencies for sugar solutions lie just beyond the ordinary experimental range (~100 Mcs).

INTRODUCTION

IT has been pointed out by the author in one of his previous papers[1] that structural changes in the quasi-crystalline state of the liquid play a very important part in the ultrasonic absorption and that the phenomenon of absorption and viscosity, which are related ones, can be described in terms of "hole" theory of viscosity of liquid. The maximum absorption ($2\mu_m$) and the frequency (N_m) at which maximum absorption is to be expected were calculated in a number of unassociated liquids for which ultrasonic absorption has been measured.[2] Next the calculations were applied to acetic acid[3] whose maximum absorption frequency lies in the frequency range experimentally approachable. It was shown that variation of maximum absorption frequency (N_m) in the case of acetic acid with variation of temperature (20°C to 65°C) as observed by Lamb and Pinkerton[4] can be explained by this theory. In the present paper similar calculations have been performed in the case of sugar solutions.

BRIEF OUTLINE OF THE THEORY

Liquids, like crystals, have short-distance order arrangement and geometrical regularity. In this lattice arrangement there are certain sites which are unoccupied by molecules. These vacant sites are called "holes." These unoccupied places are filled by molecules from outside. Similarly in the lattice arrangement when a molecule jumps out, a vacancy is caused, i.e. a "hole" is created. At a given temperature a statistical equilibrium is maintained.

In the case of ultrasonic waves it is suggested that the statistical equilibrium at a particular temperature is disturbed and the number of holes increases. The required energy to increase the number of holes is taken from the incident sound waves. If during the cycle the sound wave completes one period, the holes return to their equilibrium value and no absorption will result. If, on the other hand, there is a lag, then the energy taken away by the holes will not be given back to the sound waves, and this will amount to loss of energy from the sound waves.

The required energy (A) cal/mole, i.e., the work function for the holes per gram molecule of liquid, can be known from the relation given by Furth[5] in connection with the hole theory of viscosity of liquid medium.

$$A=R\frac{TT'}{T'-T}\log\frac{\eta T'}{\eta' T} \tag{1}$$

where R is the gas constant, η and η' are the viscosities at two temperatures T and T'. The corresponding structural specific heat Ci is known from

$$C_i=R\left(\frac{A}{RT}\right)^2 e^{-A/RT}. \tag{2}$$

The maximum absorption ($2\mu_m$) is given by

$$2\mu_m=\pi\frac{\chi}{\chi'}\frac{\chi'-1}{C_p}C_i. \tag{3}$$

where χ represents the ratio of specific heats, χ' the same when ultrasonic absorption takes place, and C_p the specific heat at constant pressure. The maximum absorption frequency (N_m) is determined from

$$N_m=\frac{2\mu_m}{V}[1/(\alpha/N^2)]N\ll N_m, \tag{4}$$

where V represents the velocity of ultrasonic waves and α the ultrasonic absorption coefficient at frequency N.

TABLE I. Showing the values of viscosity of sugar solutions at different temperatures and concentrations.

Substance	Temperature	η(cp)
Sucrose	20°C	6.20
40 percent	40°C	3.25
	60°C	1.98
Glucose	20°C	3.90
35 percent	40°C	2.16
Lactose	25°C	2.14
23.4 percent	21°C	2.34

[1] R. N. Ghosh and G. S. Verma, J. Sci. Ind. Res. (India) **8**, 192 (1949).
[2] G. S. Verma, J. Chem. Phys. **18**, 1352 (1950).
[3] R. N. Ghosh and G. S. Verma, Ind. J. Phys. **24**, 125 (1950).
[4] J. Lamb and J. M. M. Pinkerton, Proc. Roy. Soc. (London) **199**, 114 (1949).
[5] R. Furth, Proc. Cambridge Phil. Soc. **37**, 252 (1941).

The last two relations are exactly similar to those given by Bauer.[6]

CALCULATIONS FOR SUGAR SOLUTIONS

Table I gives the values of viscosity at different temperatures for the various sugar solutions at different concentrations. Values of viscosity for sucrose solutions are based upon the measurements of Bingham and Jackson,[7] and for glucose solutions viscosity measurements of Powell[8] have been consulted. Viscosity for lactose solution at 23.4 percent concentration and at 25°C has been taken from Proyor and Roscoe's[9] measurements. Viscosity at the same concentration but at temperature 21°C has been extrapolated.

Table II gives the values of "A" and structural specific heat "C_i" for the different sugar solutions at different concentrations and temperatures.

TABLE II. Showing the values of work function A and structural specific heat C_i.

Substance	Temperature	A (cals/mole)	Ci (cal deg^{-1} mole^{-1})
Sucrose 40 percent	20°C 40°C	5800	0.0094 0.0160
Glucose 35 percent	20°C	5973	0.0074
Lactose 23.4 percent	25°C	4631	0.0440

Table III gives the values of maximum absorption ($2\mu_m$) and the absorption frequencies (N_m) for different sugar solutions. Values of ultrasonic velocity and absorption $\alpha/N^2\times10^{15}$ sec^2 cm^{-1} have been taken from Pryor and Roscoe's measurements of ultrasonic absorption (6–25 Mc) in solutions of sucrose, glucose, and lactose at various concentrations and temperatures. Specific heats C_p for different sugar crystals and water are known from International Critical Tables. Value of specific heat of the solution is computed from them on a percentage basis.

TABLE III. Showing the values of max absorption $2\mu_m$ and max absorption frequency N_m.

Substance	Temperature	V meters/sec	$\alpha/N^2\times10^{15}$ sec^2 cm^{-1}	$2\mu_m$ 10^{-4}	N_m(Mcs)
Sucrose 40 percent	20°C 40°C	1650 1674	0.97 0.49	148 251	95 306
Glucose 35 percent	20°C	1654	0.77	121.6	95.5
Lactose 23.4 percent	25°C	1582	0.36	412	724

It may be observed from Table III that the frequencies at which maximum absorption is to be expected lie in the range of 95–724 Mc. But this method of calculation fails in those cases where viscosity variation is very large with respect to temperature variation. In that case "A" comes out to be a large quantity with the result that "C_i" becomes very small, and the corresponding absorption and absorption frequency does too, which seems absurd.

From the measurements of Pryor and Roscoe it is evident that the experimentally observed absorption is almost three times the classical absorption which is to be expected on the basis of Stokes law. This is true in the case of associated liquids such as water and alcohols which have been classified into Class II liquids by Pinkerton as well as the author. In this class of liquids structural changes play a very important part in ultrasonic absorption, and it is to be expected that they play the similar role in sugar solutions. The negative temperature coefficient of absorption too justifies the above stand.

ACKNOWLEDGMENT

The author is grateful to Dr. K. Bannerjee D.Sc., F.N.I., for his interest and helpful advice.

[6] E. Bauer, Proc. Phys. Soc. (London) **62**, 141 (1949).
[7] E. C. Bingham and R. F. Jackson, Bull. U. S. Bur. Standards **14**, 59 (1918–1919).
[8] C. W. R. Powell, J. Chem. Soc. **105**, 1 (1914).
[9] A. W. Pryor and R. Roscoe, Proc. Phys. Soc. (London) **B67**, 70 (1954).

Proton Magnetic Resonance in Liquid Crystals—Orientation Effects*

P. L. JAIN, J. C. LEE, AND R. D. SPENCE
Department of Physics, Michigan State College, East Lansing, Michigan
(Received September 10, 1954)

This communication reports a study of the proton magnetic resonance signal from the liquid crystal phase of 4-4′ methoxyazoxybenzene, 4-4′ methoxy D_3 azoxybenzene, and 4-4′ ethyoxyazoxybenzene in an effort to obtain information concerning the temperature dependence and relative extent of the molecular orientation in such phases. The experimental results lead to a qualitative picture of the distribution of molecular orientations for the first two compounds and show that the extent of orientation in the last compound is greater than in the first two.

INTRODUCTION

THE liquid crystal phase is a true phase in that it is separated from both the crystalline phase at lower temperatures and the normal liquid phase at higher temperatures by first-order transitions.[1,2] In the absence of an external magnetic field the viscosity of the liquid crystal phases of the compounds considered in this report exhibit a viscosity[3] only slightly greater than that of water. However in the presence of an external field the viscosity as well as other physical properties such as the dielectric constant[4] becomes anisotropic and the substance behaves much like a crystal.

The work reported in this paper was initiated as a result of the observation[5] that the liquid crystal phase of p-azoxyanisole yields a proton magnetic-resonance signal with a structure quite unlike that found in either its solid or liquid phases [see Fig. 1(a)]. The structure has been shown to be field independent and has been tentatively explained[6] on the basis of the dipole-dipole interaction between the protons. The present communication reports a comparative examination of the structure and temperature dependence of the proton resonance lines found in PAA (p-azoxyanisole=4-4′ methyoxyazoxy-benzene), DPAA(4-4′ methoxyD_3-azoxybenzene), and PAP (p-azoxyphenetol=4-4′ ethyoxyazoxybenzene). Structural models for these compounds are given in Table I. These rod-like molecules yield a *nematic* liquid crystal phase which is characterized by an anisotropic distribution of orientations of the longest molecular axis and a uniform density in space in contrast to the *smectic* liquid crystal phase in which the density is periodic in one dimension. Proton magnetic resonance in smectic liquid crystals will be mentioned briefly in another section of this paper.

EXPERIMENTAL ARRANGEMENT

The proton resonance signals were detected by a twin-T bridge followed by a preamplifier and a Hallicrafters–Sx 62 receiver. Signals were displayed on an oscilloscope and recorded photographically along with a time-base signal which served to calibrate the sweep in gauss. The dc magnetic field was provided by an electromagnet powered by marine storage batteries. Most of the data were taken at fields of 7280 gauss corresponding to a proton resonance frequency of 31 mc. The modulating field was of a frequency of either 30 or 60 cycles.

The samples were heated by placing the sample coil in a fiber tube through which hot air was passed from an external heater. This simple device was capable of producing readily variable temperatures up to 270°C, and at the same time appeared to have none of the difficulties associated with trying to mount an electric heater directly between the pole pieces of the electromagnet. The temperature was determined with a copper-constantan thermocouple placed directly in the sample. The samples were held in small test tubes and ranged from 0.1 cc to 1.0 cc in volume.

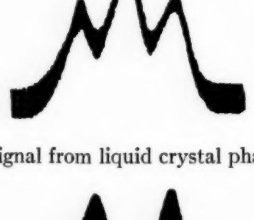

FIG. 1(a). Signal from liquid crystal phase of PAA.

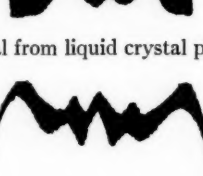

FIG. 1(b). Signal from liquid crystal phase of DPAA.

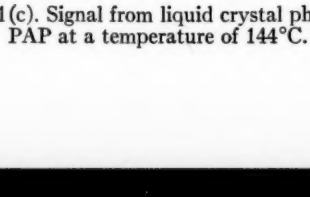

FIG. 1(c). Signal from liquid crystal phase of PAP at a temperature of 144°C.

* Portions of this paper are taken from a dissertation submitted by P. L. Jain in partial fulfilment of the requirements for the Ph.D. degree at Michigan State College.

[1] R. Schenck, *Kristallinische Flussigkeiten* (Leipzig, 1905).
[2] C. Kreutzer, Ann. Physik **33**, 192 (1938).
[3] M. Miesowicz, Bull. Acad. polon. d Sciences et Lettres (Ser. A) 228 (1936).
[4] See for example M. Jezewski, J. phys. radium **6**, 59 (1924); W. Kast, Ann. Physik **73**, 145 (1924); W. Maier, Z. Naturforsch. **2a**, 458 (1947).
[5] Spence, Moses, and Jain, J. Chem. Phys. **21**, 380 (1953).
[6] Spence, Gutowsky, and Holm, J. Chem. Phys. **21**, 1891 (1953).

EXPERIMENTAL RESULTS

On passing from the normal liquid phase to the liquid crystal phase, the proton resonance line in each of the three compounds previously mentioned changes abruptly from a single narrow line into a rather wide line showing a definite structure.

In the case of PAA the liquid crystal line is a triplet as shown in Fig. 1(a). Except for a gradual decrease of satellite separation as the temperature is increased the line shape remains essentially the same throughout the liquid crystal phase.

The compound DPAA is the same compound except that the end groups have been deuterated and therefore the only sources of signal are the protons on the benzene rings. The signal in the liquid crystal phase consists of a strong doublet [see Fig. 1(b)] together with a very weak central component. As in the compound with the undeuterated end groups the general shape of the signal remains unchanged throughout most of the liquid crystal phase except for a gradual decrease of the doublet separation as the temperature is increased. However at about $\frac{1}{2}$ degree below the liquid crystal-liquid transition point, the central component begins to grow very rapidly. This continues until at the liquid crystal-liquid transition point the central component is about $\frac{3}{2}$ as strong as the satellites. At this point the satellites, which have grown progressively weaker, suddenly disappear and only a single narrow line is observed.

In contrast to the previous two cases, the structure of the signal from the liquid crystal phase of PAP shows a considerable variation with temperature. At the highest temperatures in the liquid crystal phase, the line appears to be a triplet much like that shown in Fig. 1(a) for PAA. As the temperature is reduced, the central peak shrinks and two additional small symmetrically located satellite peaks appear. As the temperature is further reduced, the entire signal broadens rapidly and at the lowest temperatures in the liquid crystal phase it consists of five peaks of nearly the same amplitude on a rather broad base as shown in Fig. 1(c).

TABLE I. Structural formulas of the compounds investigated.

PAA p-azoxyanisole 4-4′ methyoxyazoxy-benzene	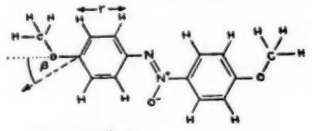
DPAA 4-4′ methyoxy D_3-azoxybenzene	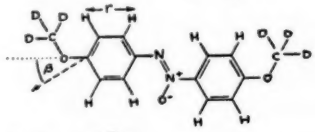
PAP p-azoxy phenetole 4-4′ ethyoxyazoxy benzene	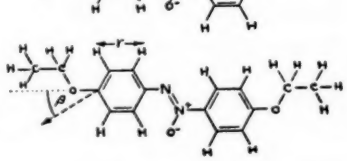

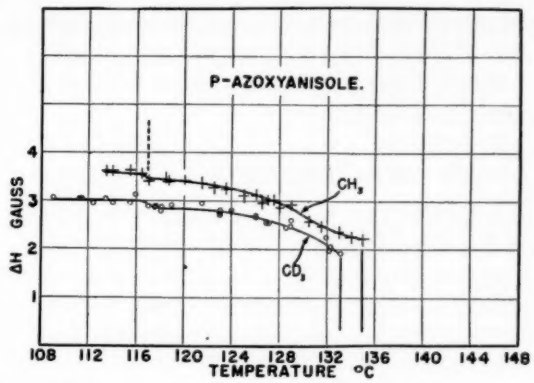

FIG. 2. Temperature dependence of the satellite separation for the two forms of p-azoxyanisole. Top curve PAA (CH_3 groups) bottom curve DPAA (CD_3 groups).

The temperature dependence of the separation in gauss between the outermost satellites of the liquid crystal signal of these three compounds is shown in Figs. 2 and 3. Both PAA and DPAA tend to "supercool" if the temperature is gradually reduced to below the melting point. This effect has been observed by several other workers.[7] This appears to be very much like an ordinary supercooled state in that if the sample is shaken, it quickly passes over into the crystalline phase. On the other hand, it appears from Fig. 2 that as the sample passes into the supercooled state, Δh, the separation between the satellites changes abruptly by a small amount at the temperature corresponding to liquid crystal-crystal transition point. The transition from the crystalline to the liquid crystal phase on heating is very sharp. The signal from the crystalline phase is very broad[6] with a central spike (if the end group contains protons). As the transition temperature is passed, the broad line is suddenly replaced by the somewhat narrower structured line characteristic of the liquid

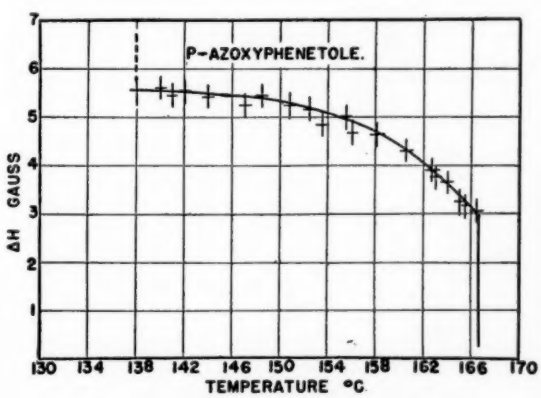

FIG. 3. Temperature dependence of outer satellite separation in PAP.

[7] See for example Föex and Royer, Compt. rend. **180**, 1912 (1925).

crystal phase. No supercooling effects were observed in the case of PAP. The transition between liquid-crystal and crystalline phases was well defined for both cooling and heating of the sample.

DISCUSSION

Since in DPAA we have only to consider the protons on the benzene rings, we shall discuss the line structure expected for this case first. The protons on opposite sides of the benzene rings may be considered as isolated proton pairs and should, therefore, yield a doublet given by[8]

$$h=(H-H_0)=\pm\alpha(3\cos^2\beta-1) \tag{1}$$

where H_0 is the resonance field in the absence of the dipole-dipole interaction,

$$\alpha=\tfrac{3}{2}\mu r_1^{-3}=1.44 \text{ gauss} \tag{2}$$

and β is the angle between axis of the molecule and the magnetic field (see Table I). We visualize the molecules of the liquid crystal phase as lying in rather shallow potential wells whose directions vary from point to point throughout the sample. The number of such wells whose directions with respect to the magnetic field lie between θ and $\theta+d\theta$ will be $dn_w=\frac{1}{2}n_w f(\theta)\sin\theta d\theta$. Orientation of the liquid crystal implies that $f(\theta)$ has a maximum at $\theta=0$. Of the total number of molecules N only N_b may be considered as having energies low enough to be effectively bound by the wells. The remainder $N_u=N-N_b$ which have energies above the well will be able to rotate above it. If on escaping from the well such molecules have complete freedom, they will contribute a single line at $h=0$. One expects such lines to be rather weak except at temperatures near the liquid crystal-liquid transition point.

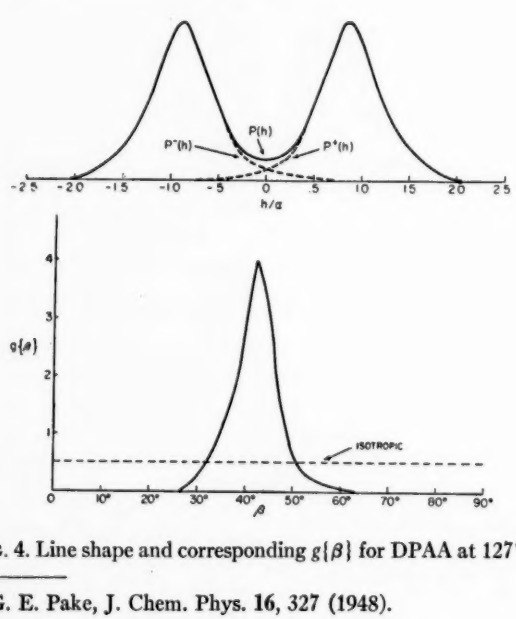

FIG. 4. Line shape and corresponding $g\{\beta\}$ for DPAA at 127°C.

[8] G. E. Pake, J. Chem. Phys. 16, 327 (1948).

Let the fraction of the number of bound molecules N_b whose axes lie in the cone between β and $\beta+d\beta$ be

$$\frac{dN_b}{N_b}=g\{\beta,T\}\sin\beta d\beta \tag{3}$$

where T is the temperature and

$$\int_0^\pi g\{\beta,T\}\sin\beta d\beta=1. \tag{4}$$

The line shape consists of the sum of two overlapping branches

$$P(h,T)=P^+(h,T)+P^-(h,T) \tag{5a}$$

$$P^+(h,T)=\frac{g\{\cos^{-1}[\frac{1}{3}(1+h/\alpha)]^{\frac{1}{2}},T\}}{4(3)^{\frac{1}{2}}(1+h/\alpha)^{\frac{1}{2}}}\quad -\alpha\leq h\leq 2\alpha \tag{5b}$$

$$P^-(h,T)=\frac{g\{\cos^{-1}[\frac{1}{3}(1-h/\alpha)]^{\frac{1}{2}},T\}}{4(3)^{\frac{1}{2}}(1-h/\alpha)^{\frac{1}{2}}}\quad -2\alpha\leq h\leq \alpha \tag{5c}$$

where P^+ and P^- have been normalized such that

$$\int_{-2\alpha}^{+2\alpha} P(h,T)dh=1. \tag{5d}$$

The distribution function $g\{\beta,T\}$ is not known[9] for the liquid crystal phase and therefore one of the most important results which we may hope to obtain from our experiment is a qualitative picture of the shape of this function. Since the maxima in the line shape $P(h)$ are temperature dependent, they cannot arise from the zeros at $h=\pm\alpha$ in the denominators of Eqs. (5b) and (5c). It appears that the numerators of Eqs. (5b) and (5c) must vanish at least as fast as $(1\pm h/\alpha)^{\frac{1}{2}}$ as $h\to\pm\alpha$. This restriction can be understood physically by noting that $h=\pm\alpha$ corresponds to $\beta=\pi/2$. Molecules having energies high enough to reach this angle are essentially free to rotate and therefore do not belong to the class of bound molecules whose angular distribution is given by $g\{\beta,T\}$. The intermolecular broadening prevents the experimental line shapes from faithfully reproducing the theoretical shape of Eqs. (5). However, rotation about the molecular axis probably tends to minimize this effect. If we assume that the intermolecular broadening has a negligible effect, we may deduce $g\{\beta,T\}$ from the observed lines from which the central component has been subtracted. Typical results are shown in Fig. 4.

An examination of our experimental line shapes indicates that the distribution functions $P^+(h)$ and $P^-(h)$ satisfy an approximate relation between their mode

[9] Our previous remarks imply that $g\{\beta,T\}$ should be of the form $g\{\beta,T\}\sim C(T)\int_0^\pi \exp[-\gamma(T)V(\beta-\theta)]f(\theta)\sin\theta d\theta$ where $V(\beta-\theta)$ is the potential of a well oriented along θ.

and mean of the form

$$2\int_{-\alpha}^{+2\alpha} hP^{+}(h,T)dh \simeq h_m(T)+\epsilon \qquad (6a)$$

$$2\int_{-2\alpha}^{\alpha} hP^{-}(h,T)dh \simeq -h_m(T)-\epsilon, \qquad (6b)$$

where $h_m(T)$ is the position of the maxima of the line shape and ϵ is parameter which is assumed to be independent of temperature. These equations lead to the result

$$\alpha\langle 3\cos^2\beta-1\rangle_{Av} \simeq h_m(T)+\epsilon \qquad (7a)$$

$$\Delta h = 2h_m \simeq 2\alpha\langle 3\cos^2\beta-1\rangle_{Av}-2\epsilon. \qquad (7b)$$

Unfortunately we have no way of checking this result directly for DPAA. However, in the case of the corresponding undeuterated compound, the values of $\langle 3\cos^2\beta-1\rangle_{Av}$ have been calculated by Zwetkoff[10] from experimental data on the diamagnetic susceptibility and the indices of refraction. If we assume that the signal from the CH_3 group in PAA does not appreciably modify the position of the satellites from the benzene ring then we should expect that Eqs. (7a) and (7b) should also be approximately correct in this case. Figure 5 shows Δh plotted as a function of $\langle 3\cos^2\beta-1\rangle_{Av}$ at corresponding temperatures for this case. As expected from Eq. (7b) the relation between the two variables is linear except at temperatures near the clear point. The slope is 2.93 gauss rather than 2.88 gauss as indicated by Eq. (7b). The value of ϵ is 0.21 gauss.

The separation between the outermost satellites in PAP near the liquid crystal-crystal transition temperature is 5.5 gauss which is almost as large as the value of 5.8 gauss expected for a *complete* orientation of molecules of the liquid crystal phase. Comparing this with the value 3.5 gauss found for PAA at corresponding temperatures we see it appears that replacing CH_3 groups with C_2H_5 groups leads to a somewhat more completely oriented liquid crystal phase. Deuterated methyl groups give the smallest amount of orientation since for this case the satellite separation at the liquid crystal-crystal transition is only 3.0 gauss. Even at the other extreme of the liquid crystal phase, i.e., the liquid crystal-liquid transition, the amount of orientation still appears to be greatest with C_2H_5 groups, next largest with CH_3 groups, and least with CD_3. If we associate the latent heat of the liquid crystal-liquid transition with the energy required to raise the molecules from oriented to rotating states, the fact that this latent heat is 0.90 cal/M for PAP and 0.46 cal/M for PAA is at least qualitatively reasonable. One expects that the latent heat for the deuterated compound should be less than either of these values.

We now consider the origin of the central portion of the line structure of each of the three compounds. The central component in the compound with the deuterated end groups probably arises from molecules with incompletely deuterated end groups (the deuteration was estimated as about 95 percent complete) and from molecules in unbound or rotating states. The fact that the central component is not completely due to incomplete deuteration is demonstrated by the rapid growth of the central component with temperature as the liquid crystal-liquid transition is approached.

The central component in PAA probably arises from the protons in the CH_3 groups and from all the protons on molecules in unbound states. It is difficult to say exactly what the exact shape of the signal from the CH_3 groups on molecules in the bound states will be since it is not known to what extent the potential wells are effective in restricting the motion of these groups. The amplitude and width of the central line[6] are such that it is plausible to assume that the motion plus intermolecular broadening are sufficient to narrow the signal into a single structureless line.

Similar remarks appear to apply to the signal from the C_2H_5 group in PAP in the higher temperature portions of the liquid crystal phase. However as the temperature is decreased a structure begins to appear in the central portion of the line as we have previously indicated in the experimental section. If we assume rotation about the C—O, O—C, and C—C bonds we should expect an additional pair of satellites whose spacing would approximate 0.3 the spacing between the satellites due to the protons on the benzene rings. The additional pair of satellites arise from the superposition of a doublet from the two protons around one carbon in the C_2H_5 group on the outer wings of a triplet

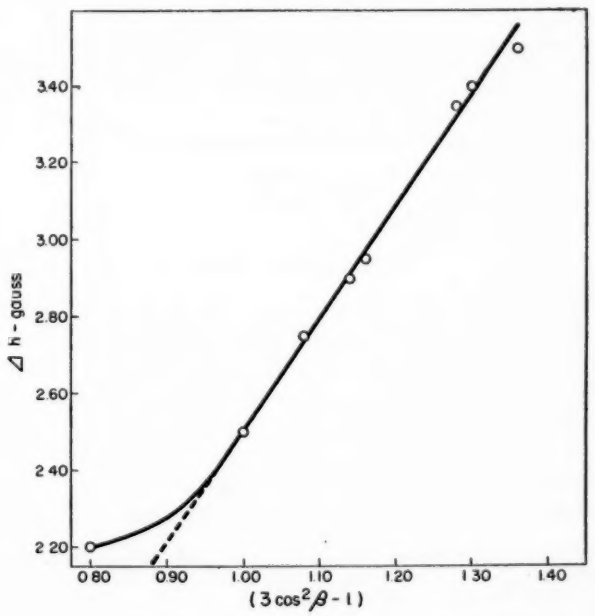

FIG. 5. For PAA Δh *vs* $\langle 3\cos^2\beta-1\rangle_{Av}$.

[10] W. Zwetkoff, Acta Physicochim. U.R.S.S. **16**, 132 (1942).

from the three protons[11] around the other carbon in the group. The spacing predicted on this model is in good agreement with that actually observed. The existence of such structure in the lower-temperature portion of liquid crystal phase of this compound can be construed as further supporting our previous argument of fairly complete orientation in this temperature range.

RESULTS ON OTHER LIQUID CRYSTALS

Exploratory experiments on compounds such as 4-4′ propyloxyazoxybenzene and anisaldazine which are similar in structure to those we have discussed show that the proton resonance signal from their liquid crystal phase exhibits a structure similar to that found for PAA. On the other hand, the signal from smectic liquid crystal phases[12] such as exist in sodium oleate and sodium stearate appears to be a single structureless line with a width intermediate between that of the liquid and crystalline phases. Work is also underway on compounds which exhibit more than one liquid crystal phase.

The authors wish to thank Dr. G. S. Gutowsky of the University of Illinois for the help derived from several discussions of this problem. We gratefully acknowledge the fact that the present work was made possible by several grants-in-aid from the All College Research Committee of Michigan State College.

[11] Andrews and Bersohn, J. Chem. Phys. **18**, 159 (1950).

[12] H. A. Moses, M. S. thesis, Michigan State College (1953).

THE JOURNAL OF CHEMICAL PHYSICS VOLUME 23, NUMBER 5 MAY, 1955

Vacuum Photolysis of Silver Bromide and Silver Chloride*

GEORGE W. LUCKEY
Research Laboratories, Eastman Kodak Company, Rochester 4, New York

(Received September 27, 1954)

The quantum yields of halogen production in the vacuum photolysis of silver bromide and silver chloride have been measured at various temperatures, wavelengths, and light intensities. Silver-bromide crystals containing small amounts of copper and cadmium bromide have also been studied. At room temperature, the yields of thick crystals follow the equation,

$$\phi = Q(1-e^{-ka}),$$

where Q is the surface efficiency, k is the absorption coefficient, and a is a parameter which is defined below. At room temperature, in the halogen evolution range studied, the value of a for silver bromide is about 0.4 micron and that for silver chloride is about 0.24 micron. The values of Q are usually between 0.5 and 1.0.

The quantum yield of halogen production at room temperature is similar to the yield of a fast wall reaction. Both depend on the diffusion of reactants to the surface. The parameter a is related to the thickness of the diffusion layer. A numerical solution of the diffusion equation by C. A. Duboc has shown that

$$a = \frac{1.154 D^{\frac{1}{2}}}{k^{\frac{1}{2}} k_1^{\frac{1}{2}} I_o^{\frac{1}{2}}},$$

where D is the diffusion coefficient of positive holes and electrons, k_1 is the recombination coefficient of positive holes and electrons in the silver halide, and I_o is the incident intensity of light.

Above a certain temperature, the quantum yields decrease with increasing temperature, the long-wavelength yields increase relative to those at short wavelength and the yields increase with increasing light intensity. These effects are inhibited by the addition of copper bromide to silver-bromide crystals. The decrease in yield at high temperatures is probably caused by the decreased effectiveness of traps. The cadmium results indicate that this decrease is also affected by the ionic conductivity of the crystals. The addition of copper or cadmium ion does not have a large effect on the quantum yields at room temperature. This indicates that positive-ion vacancies in the silver halides are not good positive hole-traps at room temperature. The data and the solution of the diffusion equation indicate that the quantum yield of photoconductivity and photolysis are closely related. Additional measurements of photoconductivity and light-absorption coefficients are needed before the results can be completely interpreted.

I. INTRODUCTION

THE quantum yields of bromine production in the vacuum photolysis of silver bromide have been measured.[1] The yields of thick crystals increased with decreasing wavelength, reaching values near unity at short wavelengths. When thin crystals were used, the long-wavelength yields increased. These facts were explained by assuming that the light absorption which produces gaseous bromine occurs within a thin surface layer of the crystal. As the wavelength decreases, more of the incident radiation is absorbed in the surface layer, and the quantum yield increases. In thin crystals or emulsion grains, the thickness is comparable with that of the active layer, and the yield is large at long wavelengths.

The first measurements of silver-chloride photolysis efficiency were reported by Eggert and Noddack[2] in 1925. The quantum yields of silver production in the room-temperature photolysis of silver chloride–gelatin emulsions were measured at 365 mμ and were between 0.87 and 0.81 in the intensity range between 1.15×10^{15}

* Communication No. 1691 from the Kodak Research Laboratories.

[1] G. W. Luckey, J. Phys. Chem. **57**, 791 (1953). A bibliography of the work on the photolysis of silver bromide is given in this article.

[2] J. Eggert and W. Noddack, Z. Physik **31**, 922 (1925).

and 147×10^{15} quanta/cm^2/sec. These emulsion studies were recently resumed by Meidinger[3] who showed that the quantum yield of silver production at 366 mμ and 20°C was 0.45, with or without chemical halogen acceptors present. At 100°C the yield was 0.53 in the absence of a halogen acceptor and 0.92 in the presence of a one percent solution of sodium nitrite.

The photolysis of gelatin-free silver chloride precipitates was studied by Feldmann and co-workers.[4–6] The quantum yield of chlorine production in the photolysis of water suspensions of silver chloride was 0.45 at 365 mμ and room temperature. In the presence of nitrite ion, the yields were close to unity at both 365 and 313 mμ. These results were criticized by Plotnikow,[7] but the error caused by the light absorption of the nitrite ion was probably less than 25 percent.[6]

Hilsch and Pohl[8] measured the quantum yield of silver formation in the photolysis of thick, dry, silver-chloride crystals. The yield was about 0.4 at 405 mμ. Later work showed that this result was caused by mechanical deformation of the crystals.[9] Stasiw and Teltow[10] showed that thick silver-chloride crystals were very insensitive and that print-out occurred only on the surface of pure crystals. No quantitative data were reported by these investigators.

The present work was undertaken to extend the study of the vacuum photolysis of silver bromide and to measure the quantum yields of chlorine production in the vacuum photolysis of silver chloride.

II. EXPERIMENTAL

Preparation of Silver Halides

The silver halides were prepared from Eastman Kodak Company C.P. silver nitrate and redistilled hydrobromic or hydrochloric acid. Several types of silver halide were used: films fused between two Vycor plates, slabs fused in an atmosphere of nitrogen or halogen, halogenated silver, and crystals prepared by isothermal distillation of water into a solution of silver halide in the corresponding halogen acid.

In preparing the fused samples, the precipitate was melted and the corresponding halogen and hydrogen–halide gases were bubbled through the melt. The molten material was filtered through a fine glass capillary and collected in a vessel maintained at ice temperature. The halide was then remelted on one of the Vycor plates[11] and the corresponding halogen and hydrogen halide were again bubbled through the melt. If this treatment was continued, the halide coalesced into a droplet which did not wet Vycor. In this form, the low interfacial tension prevented easy spreading between the plates. This difficulty was removed when a small amount of oxygen was present.[12] As a result, almost all of the fused crystals used in this work may have contained minute traces of silver oxide. Experiments with crystals prepared from the completely halogenated melt showed that these traces did not affect the quantum yields of photolysis. The use of the hydrogen halide was suggested by J. W. Mitchell.[13] Hedges and Mitchell[14] have recently published additional details about the preparation of crystals of this type. Spectroscopic analysis of these crystals[15] showed that trace quantities of aluminum, calcium, copper, chromium, iron, magnesium, nickel, silicon, sodium, and zinc were present. These impurities are also present in the silver nitrate used in emulsion manufacture.

Several samples of rolled and unrolled silver chloride were obtained from the Harshaw Chemical Company. The impurities in these crystals were similar to those reported in a preceding paragraph. The Harshaw crystals contained some silver, which could be removed by chlorination.

Some of the fused samples of silver halide were suspended in a saturated solution of silver halide in the corresponding distilled halogen acid. The solution was magnetically stirred and slowly diluted by isothermal distillation.[16] The surfaces of most of the fused crystals had a (100) orientation as described by Hedges and Mitchell.[14] The silver halide from the solution was deposited on the (111) faces of the fused crystal, producing long needles of silver halide at the edge and square-based pyramids on the (100) faces. The surface of the resultant crystal was (111) oriented. The orientation of the crystals was determined by development as described by Keith and Mitchell.[17]

The fused slabs used in these experiments were similar to those described previously.[1]

Preparation of Mixed Crystals

The mixed crystals were prepared by adding the desired impurity halide to the melt. The homogeneous mixture was then pressed between the glass plates and crystallized as previously described.

Preparation of Halogen

The bromine was prepared by the method used before.[1] Large quantities of chlorine gas were not purified and stored because of its high vapor pressure at room temperature. In these experiments, Matheson chlorine

[3] W. Meidinger, Z. wiss. Phot. **44**, 1 (1949).
[4] P. Feldmann, Z. physik. Chem. **B12**, 449 (1931).
[5] P. Feldmann and A. Stern, Z. physik. Chem. **B12**, 467 (1931).
[6] P. Feldmann and A. Stern, Z. physik. Chem. **B26**, 45 (1934).
[7] J. Plotnikow, Phot. Korr. **67**, 199 (1931).
[8] R. Hilsch and R. W. Pohl, Z. Physik **64**, 606 (1930).
[9] H. Pick and R. W. Pohl, Z. Naturforsch. **6a**, 360 (1951).
[10] O. Stasiw and J. Teltow, Nachr. Akad. Wiss. Göttingen, Math.-physik. Kl. **IIa**, 93 (1941).
[11] Obtainable from Corning Glass Works, Corning, New York.
[12] O. Stasiw and J. Teltow, Z. anorg. Chem. **257**, 109 (1948).
[13] J. W. Mitchell, private communication (1953).
[14] J. M. Hedges and J. W. Mitchell, Phil. Mag. **44**, 357 (1953).
[15] The crystals were analyzed by J. Moore, of these Laboratories.
[16] The method of isothermal distillation was suggested by R. H. Lambert, of these Laboratories.
[17] H. D. Keith and J. W. Mitchell, Phil. Mag. **44**, 877 (1953).

TABLE I. Typical quantum yields of bromine production at various wavelengths and temperatures.

Sample description	Temp. in °C	Surface efficiency	Corrected quantum yield at 280 mμ	313 mμ	365 mμ	405 mμ	436 mμ
(1) Pure, no etch, 0.13 mm thick	25	0.69	0.93	0.79	0.267	0.101	0.038
	66	0.44	1.0	1.0	0.42	0.22	0.10
	92	0.26	1.0	1.0	0.55	0.37	0.25
	134	0.06	1.0	1.0	1.00		
(2) Pure, NH_3 and HBr etch, fused slab 3 mm thick	25	0.60	0.93	0.87	0.282	0.114	0.044
	71	0.23	1.0	1.0	0.47	0.24	0.10
	97	0.049	1.0	1.0	0.58	0.37	0.16
(3) Solution grown	25	0.51	0.93	0.79	0.292	0.098	0.047
	71	0.17	1.00	0.82	0.36	0.20	0.11
(4) Pure, NH_3 and HBr etch, same as (1)	25	0.68	0.93	0.91	0.224	0.090	0.023
(5) Pure, KCN and HBr etch, 0.13 mm	25	0.66	0.93	0.85	0.168	0.068	0.024
(6) Brominated Johnson-Matthey Silver (28 ppm Cu)	25	0.81	0.93	0.93	0.28	0.103	0.041
	92	0.30	1.00	0.87	0.43	0.16	
(7) Brominated Silver, Fine (221 ppm Cu)	25	0.60	0.93	0.93	0.30	0.095	0.035
	90	0.69	1.00	0.91	0.33	0.14	0.058
	138	0.73	1.00	0.91	0.34	0.18	0.075
(8) Fused, 0.14% Cu, 0.13 mm thick	25	0.89	0.93	0.80	0.220	0.054	0.017
	92	0.90	1.00	1.00	0.25	0.11	0.035
	146	0.68	1.00	1.00	0.35	0.16	0.063
	174	0.15	1.0	1.0	0.52	0.23	
(9) Fused, 0.023% Cu, 0.13 mm thick	25	1.0	0.93	0.77	0.220	0.064	0.022
	89	0.89	1.00	0.89	0.40	0.17	0.075
	139	0.45	1.00	0.89	0.42	0.13	0.060
	170	0.070	1.0	0.83	0.56	0.22	
(10) Fused, 0.003% Cu, 0.13 mm thick	25	1.0	0.93	0.81	0.155	0.056	0.022
	92	0.71	1.00	0.90	0.30	0.11	0.037
	113	0.24	1.0	0.92	0.39	0.20	
(11) Fused, 0.019% Cd, 0.13 mm thick	25	1.0	0.93	0.78	0.150	0.065	0.022
	89	0.21	1.0	0.94	0.23	0.066	0.02
	120	0.15	1.0	0.81	0.26		
	158	0.12	1.0	1.0	0.37	0.12	
(12) Fused, 0.003% Cd, 0.13 mm thick	25	0.73	0.93	0.90	0.25	0.094	0.033
	70	0.48	1.00	1.00	0.47	0.20	0.075
	100	0.14	1.0	1.0	0.68	0.27	0.10
(13) Fused, 0.0001% Cd, 0.13 mm thick	25	0.79	0.93	0.83	0.25	0.076	0.026
	76	0.52	1.00	1.00	0.49	0.19	0.043
	105	0.086	1.0	1.0	0.82	0.37	0.18

was admitted to the vacuum system and condensed with liquid nitrogen. After degassing, the chlorine was warmed to the temperature of solid carbon dioxide and distilled into the reaction system. The excess chlorine was removed by evacuation.

Apparatus

The apparatus was similar to that described previously.[1] It was calibrated chemically and gasometrically in the range used in these experiments. The light absorption of the samples was measured with a Model 11 MS Cary Recording Spectrophotometer.[18] The light source was a General Electric Type AH-6 water-cooled mercury arc. The light from this arc passed through a Bausch and Lomb 500-mm focal-length grating monochromator. Two gratings were used. One produced a band of transmitted wavelengths about 10 mμ wide; the other produced a band about 5 mμ wide. This change in band width did not affect the results. The light intensity was measured with a calibrated thermopile, as described previously.

[18] The author is indebted to A. Johnson and E. E. Richardson, of these Laboratories, for these measurements.

Procedure

The procedure used in these experiments was similar to that described before.[1] It has been found[19] that silver halides adsorb appreciable amounts of water. This adsorbed layer decreases the quantum yield of halogen production and prevents accurate measurements. Therefore, all of the samples were heated to 200°C in a vacuum for at least six hours before they were irradiated. At higher temperatures, some of the silver halide evaporated, but no evaporation was observed at 200°C.

Errors

As mentioned before,[11] the experimental error of most of the short-wavelength quantum-yield measurements at room temperature is less than 15 percent. In some cases, particularly with the less effective wavelengths of light, the errors are larger than this. The usual error of the high-temperature results is less than 30 percent. This increase in error is caused by the increased rate of recombination of photolytic silver and halogen and the smaller yields.

The poor precision of the results obtained with different samples is probably caused by small amounts of

[19] G. W. Luckey and W. West (to be published).

TABLE II. Comparison of theory and experiment at 25°C.

Item description	Wavelength in mμ 280	302	313	334	365	405	436
(1) Average corrected yield, surface efficiency unity, silver chloride	0.57	0.27	0.186	0.122	0.041		
(2) Average deviation of data in (1) in percent	0	10	10	14	13		
(3) Absorption coefficients k, in units of 10^4 cm^{-1} (Milliman)	4.00	1.30	0.91	0.45	0.18		
(4) Calculated value of a in $(1-e^{-ka})$ in units of 10^{-5} cm	2.1	2.4	2.3	2.9	2.3		
(5) Average corrected yield, surface efficiency unity, silver bromide	0.93	0.89	0.83	0.51	0.225	0.086	0.032
(6) Average deviation of data in (5) in percent	0	3	3	11	18	20	22
(7) Absorption coefficients k, in units of 10^4 cm^{-1} (Slade and Toy; Fesefeldt and Gyulai)	4.2	2.9	2.7	1.3	0.61	0.172	0.0505
(8) Calculated value of a in $(1-e^{-ka})$ in units of 10^{-5} cm	6.3	7.6	6.6	5.5	4.2	5.2	6.4

impurities in the samples. The level of impurity in the silver halide is about one part in one million. This concentration has an appreciable effect on the quantum yield.

III. EXPERIMENTAL RESULTS

A. Silver Bromide

The quantum yields of bromine production in the vacuum photolysis of silver bromide crystals are summarized in Tables I and II. The measured yields are equal to the corrected yields multiplied by the surface efficiency given in the table.

This surface efficiency was chosen so that the quotient of the measured yield at 280 mμ and the efficiency was 0.93 for silver bromide and 0.57 for silver chloride. At high temperatures, the corrected quantum yield at 280 mμ was assumed to be 1.0. This assumption is probably valid for silver bromide, but may not be valid for silver chloride at the temperatures tested. This concept of surface efficiency separates the effects of wavelength variation from those of intrinsic crystal sensitivity. It is necessary because not all of the halogen escapes from the crystal surface. The quantum yields in these and the other tables are the yields of halogen-atom production, and are twice the yields of halogen-molecule production. As will be shown, the quantum yields depend on the rate of absorption of light in the element of crystal volume under consideration. In order to remove this dependence, the wavelength-variation data were measured at equal rates of halogen evolution wherever possible. The bromine evolution rate was usually about 1×10^{16} atoms/cm²/min at room temperature. At high temperatures, the decrease in surface efficiency decreased this rate. The yields of crystals from the same silver bromide preparation are reproducible. The yields vary when different preparations are used. Some of the crystals were etched in 28 percent Eastman Kodak ammonia water, 10 percent Baker and Adamson Reagent Grade potassium cyanide solution, or constant-boiling hydrobromic acid. Treatment with cyanide alone suppresses the evolution of bromine. If the cyanide etch is followed by a hydrobromic acid treatment, high yields are obtained. A 10-μ thickness of silver halide was usually removed by the etch treatments. Etching with volatile agents has little effect on the quantum yield of silver bromide.

The gaseous bromine produced by photolysis recombines with the photolytic silver. Prolonged exposure to light and increased temperature accelerate the rate of this regression. Addition of cadmium to the crystals decreases the rate of regression.

The effect of temperature on the efficiency of silver bromide photolysis is shown in Fig. 1. In this figure, the negative logarithm of the surface efficiency is plotted against reciprocal absolute temperature at constant light intensity. Some typical high-temperature results at various wavelengths are given in Table I. The data in Fig. 1 were obtained with several different crystals. As described in succeeding sections, the scatter of the points is probably caused by small amounts of impurities in the crystals.

B. Silver Chloride

Some of the quantum yields of chlorine formation in the vacuum photolysis of silver chloride at room temperature are given in Table III. Table II summarizes all the data. The chlorine evolution rate was usually 5×10^{15} atoms/cm²/min at room temperature. Etch treatments of silver chloride crystals with a 28 percent ammonia solution or with Baker and Adamson C. P. concentrated hydrochloric acid improved the sensitivity as shown in Table III. An etch treatment with a 10 percent potassium-cyanide solution again suppresses the evolution of halogen, but this suppression is removed by a subsequent treatment with dilute hydrochloric acid.

The rate of regression in silver-chloride photolysis is

TABLE III. Typical quantum yields of chlorine production at various wavelengths and temperatures.

Sample description	Temp. in °C	Surface efficiency	Corrected quantum yield at 280 mμ	302 mμ	313 mμ	334 mμ	365 mμ
(1) Harshaw, 0.27 mm thick, rolled, no etch	25	0.35	0.57	0.25	0.160	0.11	0.034
(2) Harshaw, 0.27 mm thick, rolled, NH_3 and HCl etch	25	0.74	0.57	0.29	0.20	0.13	0.043
	74	0.36	1.00		0.70		0.17
	100	0.18	1.0		0.75		0.23
	139	0.07	1.0		0.9		0.3
(3) Fused, 0.1 mm thick, no etch	25	0.20	0.57	0.24	0.15		
(4) Fused, 0.1 mm thick, NH_3 and HCl etch	25	0.65	0.57	0.28	0.21	0.138	0.040
	66	0.56	1.00		0.53		0.121
	96	0.24	1.0		0.61		0.19
	118	0.08	1.0		0.86		0.21
(5) Fused slab, 3 mm no etch	25	0.29	0.57	0.26	0.176	0.11	0.041
(6) Fused slab, 3 mm NH_3 etch	25	0.87	0.57	0.27	0.181	0.147	0.043
(7) Harshaw, 1 mm not rolled, KCN and HCl etch	25	0.78	0.57	0.28	0.180	0.115	0.040
(8) Chlorinated Johnson-Matthey Silver	25	0.75	0.57	0.34	0.22	0.103	0.028

much slower than that in silver-bromide photolysis, but also increases with increasing temperature and decomposition.

The effect of temperature on the efficiency of silver-chloride photolysis is shown in Fig. 2. Some typical high-temperature results at various wavelengths are given in Table III.

C. Effect of Exposure

The quantum yields of the fused crystals increase rapidly with exposure and become constant after about 2×10^{16} atoms/cm^2 of halogen have been evolved. The usual increase is about a factor of two. After reaching this level, the yields are unchanged until about 10^{18}–10^{19} atoms/cm^2 of halogen have been liberated. Above this exposure, the yields decrease slowly with increasing irradiation. The initial increase may not be significant because some absorption of halogen by dust particles and the walls may occur. The yields reported in Tables I, II, III, and IV are those in the constant-yield region.

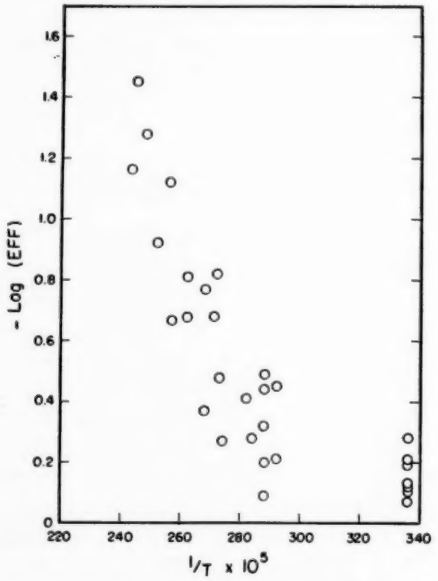

FIG. 1. $-\text{Log(EFF)}$ *vs* $1/T$ "pure" silver-bromide constant intensity ($I_{313}=1.0\times10^{17}$ quanta/minute).

D. Effect of Light Intensity

The effect of light intensity on the quantum yields of the evolution of halogen from some of the crystals is shown in Tables IV and V. At room temperature, a decrease in intensity usually increases the quantum yield of silver chloride. The silver-bromide yields are usually unaffected. At high temperature, a decrease in intensity decreases the quantum yield of both silver chloride and silver bromide. As already mentioned, most of the yields in Tables I, II, and III were measured at constant rates of evolution of halogen. Where this was not possible, the results were corrected by use of the measured variation of yield with the light intensity. This correction did not exceed 20 percent.

E. Effect of Copper and Cadmium Impurities

As shown in Table I, addition of copper or cadmium ion to silver-bromide crystals does not have a large effect on the quantum yields at room temperature. These impurities do affect the yields and the intensity-dependence of high temperature, as shown in Tables I and IV. Copper ion, in particular, is a very effective photolytic sensitizer at high temperature.

The experimental results obtained with brominated silver are also listed in Tables I and IV. Chemical analysis[20] showed that the fine silver contained about 220 parts per million of copper and that the Johnson-Matthey spectroscopically-pure silver contained 28 parts per million. The tables show that this copper is probably responsible for the large quantum yields of brominated silver at high temperatures.

Cadmium ion also increases the quantum yields at high temperature. At temperatures where the electrical conductivity is known to be due to silver-ion vacancies produced by the cadmium,[19] the quantum yields are

[20] The author is indebted to T. Carroll, of these Laboratories, for these analyses.

TABLE IV. Effect of intensity on the quantum yield of silver bromide.

Sample description	Temp. in °C	Wavelength in mμ	I_o	Quantum yield at 0.192 I_o	0.111 I_o	0.062 I_o
(1) Fused, pure, 0.13 mm	25	313	0.37			0.42
(2) Fused, pure, no etch, 0.13 mm	25	313	0.37	0.37	0.36	
	87	313	0.27	0.22		
	106	313	0.08	0.04		
(3) Solution grown	25	313	0.66	0.82		
	71	313	0.22	0.15		
(4) Fused, pure, 0.13 mm thick	25	313	0.29	0.37		
	55	313	0.20	0.13		
(5) Brominated Johnson-Matthey Silver (28 ppm Cu)	25	302	0.56	0.59		
	92	313	0.23	0.19		
(6) Brominated silver 1000 Fine (221 ppm Cu)	25	302	0.53	0.65		
	64	313	0.56	0.62		
	90	302	0.67	0.58		
	138	313	0.53	0.66		
(7) Same as (5), 0.14% Cu	25	365	0.112	0.109		
	92	365	0.181	0.176		
	146	365	0.18	0.24		
(8) Same as (6), 0.023% Cu	25	313	0.62	0.62		
	89	302	0.79	0.75		
	139	313	0.39	0.42		
(9) Same as (6), 0.003% Cu	25	302	0.61	0.67		
	92	365	0.21	0.20		
(10) Same as (6), 0.019% Cd	25	365	0.10	0.13		
	90	313	0.18	0.20		
	139	313	0.13	0.10		

appreciable. In the intrinsic conductivity region, the quantum yield decreases rapidly with increasing temperature. Copper ion in the concentrations tested does not have an appreciable effect on the dark conductivity of silver bromide at the temperatures used for these experiments.

IV. DISCUSSION OF RESULTS

The wavelength-dependence of the quantum yield at room temperature has been explained by the assumption that positive holes which are formed in a thin surface layer of the halide crystal diffuse to the crystal surface and form halogen molecules.[1] If the thickness of this surface layer is a cm and the crystal thickness is z cm, the rate of production of halogen, from both surface layers, is

$$\frac{dX}{dt}=I_o[1-e^{-ka}+e^{-kz}(e^{ka}-1)]. \quad (1)$$

In this expression, I_o is the incident intensity in quanta/cm²/sec, and k is the absorption coefficient of the silver halide in cm⁻¹. The quantum yield of halogen production is the rate of production divided by the absorbed intensity, or

$$\phi=\frac{1-e^{-ka}+e^{-kz}(e^{ka}-1)}{(1-e^{-kz})}. \quad (2)$$

If the crystal thickness is much larger than that of the surface layer,

$$\phi=1-e^{-ka}. \quad (3)$$

The absorption coefficients of silver chloride at various wavelengths have been recently determined by Milliman[21] and by Kaiser.[22] The absorption coefficients of silver bromide have been determined by Slade and Toy[23] and by Fesefeldt and Gyulai.[24] The data of Slade

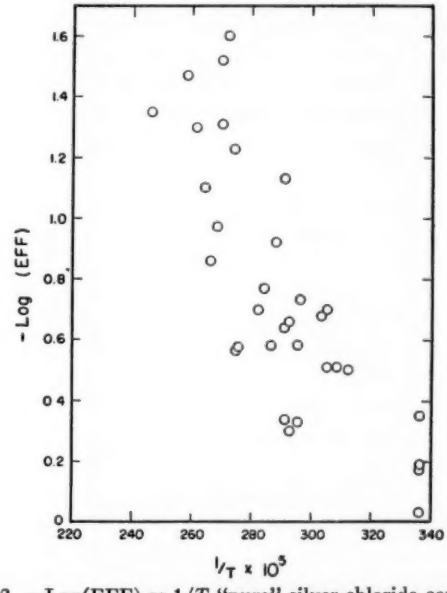

FIG. 2. $-\text{Log}(\text{EFF})$ *vs* $1/T$ "pure" silver-chloride constant intensity ($I_{280}=2\times10^{16}$ quanta/minute).

[21] P. D. Milliman, Master of Science thesis, Cornell University, Ithaca, New York, September, 1953.
[22] W. Kaiser, Z. Physik **132**, 497 (1952).
[23] R. E. Slade and F. C. Toy, Proc. Roy. Soc. (London) **A97**, 181 (1920).
[24] H. Fesefeldt and Z. Gyulai, Nachr. Ges. Wiss. Göttingen, Math.-physik. Kl. **IIa**, 226 (1929).

TABLE V. Effect of intensity on the quantum yield of silver chloride.

Sample description	Temp. in °C	Wavelength in mμ	I_o	Quantum yield at 0.192 I_o	0.111 I_o
(1) Fused slab, no etch 3 mm thick	25	313	0.051	0.079	
(2) Harshaw, 2 mm NH_3 and HCl etch	25	313	0.083	0.151	
	82	313	0.176	0.173	
	115	313	0.216	0.159	
(3) Fused, 0.1 mm NH_3 and HCl etch	25	313	0.148		0.220
	66	313	0.290		0.250
	96	313	0.200	0.143	0.115
	118	313	0.080		0.038
(4) Harshaw, 0.27 mm NH_3 and HCl etch	25	313	0.166		0.244
	74	313	0.294		0.221
	100	313	0.219		0.104

and Toy are absolute, but these authors did not measure absorption coefficients at wavelengths shorter than 360 mμ. Consequently, it is necessary to normalize the relative data of Fesefeldt and Gyulai so that the coefficients at 365 and 405 mμ agree with those of Slade and Toy.

These absorption coefficients and the average corrected quantum yields of silver bromide and silver chloride photolysis are summarized in Table II. As in Eqs. (1)–(3), the surface efficiency is assumed to be unity. Since the crystals used in this study were thick, the values of a calculated from Eq. (3) should be constant at all wavelengths. As shown in Table II, the silver-chloride data agree with the equation within the limits of experimental error. The silver-bromide values indicate that the short-wavelength absorption coefficients used in the calculation are too small.[25] This error is not surprising, because the Fesefeldt and Gyulai results are probably too large at long wavelengths[21] and it is difficult to correct them for light reflection and scatter. There is a great need for accurate measurements of the absorption coefficients of silver bromide at short wavelengths.

The absorption of light by the silver halide produces mobile positive holes and electrons in the crystal at room temperature.[26–28] The electrons are trapped or recombine with positive holes. The positive holes also combine at the crystal surface, forming halogen molecules. These processes may be summarized as follows:

$$X^- + h_\nu = X^o + e \qquad kI_o \qquad (4)$$

$$X^o + e = X^- \qquad k_1 pn \qquad (5)$$

$$2Ag_i^+ + X^o + X^o = X_2 + 2Ag_i^+ \qquad k_2 p^2 \qquad (6)$$

$$Ag_i^+ + e + M = M'. \qquad k_3(M)n(i). \qquad (7)$$

In these equations, I_o is the light intensity incident on the crystal volume in quanta/cm²/sec, p, n, M, and i are the positive-hole, electron, trap, and mobile silver-ion concentrations in particles per cm³. As earlier in the paper, k is the absorption coefficient in cm⁻¹ and k_1, k_2, k_3 are rate constants for the processes shown. The symbols X^-, X^o, Ag_i^+, Ag_i^+, and X_2 represent halogen ions, positive holes, lattice silver ion, interstitial or surface silver ion, and halogen gas, respectively. This mechanism is certainly not complete. Impurities and disorder in the crystal undoubtedly trap both positive holes and electrons[29,30] and affect the rate of recombination. However, at the high intensities and long exposures used in these experiments, some simplification may be justified and Eqs. (4)–(7) may describe the total reaction. The rate constants probably represent the summation of a number of detailed processes rather than the specific ones shown here.

Inside the crystal at long wavelengths and high light intensities, the concentration of positive holes and electrons in the steady state is probably determined by processes (4) and (5). The vacuum photolysis data show that, near the crystal surface, a large fraction of the positive holes leave the crystal as halogen gas. This evolution of halogen will decrease the surface concentration of positive holes. Since long exposures do not decrease the quantum yield greatly, the electrons near the surface must react with silver ions or traps and the surface electron concentration will also be low. Putseĭko and Meĭklyar[27] have shown that the photoconductivity of silver halide crystals is small at short wavelengths, where most of the light is absorbed near the crystal surface. Measurements of the quantum efficiency of photoconduction in these Laboratories[31] also indicate that the surface concentrations of positive holes and electrons are low.

If the concentration of holes and electrons is large inside the crystal and small near the surface, the holes and electrons will diffuse from the interior to the surface. The system is similar to a photochemical decomposition in which an efficient wall reaction removes reactants formed near the surface and the remaining reactants are removed by homogeneous recombination.

[25] Unpublished preliminary results by the late Dr. M. Biltz support this conclusion.
[26] W. West and B. H. Carroll, J. Chem. Phys. **15**, 529 (1947).
[27] E. K. Putseĭko and P. V. Meĭklyar, Zhur. Eksptl. Teoret. Fiz. U.S.S.R. **21**, 341 (1951).
[28] W. West, *Fundamental Mechanisms of Photographic Sensitivity*, J. W. Mitchell, editor (Butterworths Scientific Publications Ltd., London, 1951), p. 99.
[29] J. W. Mitchell, J. Phot. Sci. **1**, 110 (1953).
[30] F. Seitz, Revs. Modern Phys. **23**, 328 (1951).
[31] W. West, private communication.

Such a system has been considered by R. M. Noyes.[32] He approximated the steady-state conditions by stating that the concentration of reactant atoms in a uniformly illuminated vessel is $(kI_o/k_1)^{\frac{1}{2}}$ in most parts of the system but is zero in a shell which goes in from the wall a distance of 0.9 $(D^2/kI_ok_1)^{\frac{1}{4}}$ cm, where D is the diffusion coefficient of the reactant and k, I_o, and k_1 have meanings similar to those just given. The situation in silver halide photolysis is more complex than that considered by Noyes, because the distribution of light in the crystal is not uniform in the wavelength region studied. Duboc[33] has solved the diffusion equation for this case and has shown that the corrected yield of halogen production is approximated by the equation,

$$\phi=1-\exp\left(-\frac{1.154kD^{\frac{1}{2}}}{k^{\frac{1}{2}}k_1^{\frac{1}{2}}I_o^{\frac{1}{2}}}\right), \tag{8}$$

and consequently,

$$a=\frac{1.154D^{\frac{1}{2}}}{k^{\frac{1}{2}}k_1^{\frac{1}{2}}I_o^{\frac{1}{2}}}. \tag{9}$$

These equations predict that a decrease in the incident intensity will increase the value of the parameter a and consequently the quantum yield. Tables IV and V show that this increase is observed at room temperature in some cases. The equations also give a relation between the photochemical and photoelectric properties of the silver halides. The details of this relation are given in Duboe's work.[33]

As the temperature of photolysis increases above a certain value, the quantum yields at long wavelengths increase relative to those at short wavelengths, the surface efficiency decreases, and the quantum yields decrease with decreasing intensity. This increase in relative yield at long wavelengths is related to the large values of the silver-bromide parameter calculated at long wavelengths, and the absence of an intensity dependence of quantum yield at room temperature. As shown in Figs. 1 and 2, the silver bromide results at room temperature are probably affected by these changes with increasing temperature, while the silver chloride results are not. For a reliable test of the Duboc equation, the silver bromide crystals should be photolyzed at temperatures near zero degrees C, where the surface efficiency is large.

Since the quantum yields do not decrease with increasing intensity at high temperatures, the decrease in surface efficiency is not caused by the increase in positive-hole and electron concentration described previously.[1] The results obtained with silver-bromide crystals containing copper ion provide a clue to the mechanism of this decrease. The copper additions do not affect the dark conductivity of the silver bromide in the temperature range studied, but do cause a large increase in the high-temperature surface efficiency. This increase is approximately proportional to the copper concentration in the crystal in the concentration range tested. The copper also removes the usual increase in the relative quantum yields at long wavelength and the decrease in yield with decreasing intensity. Since the evolution of bromine is increased, it is reasonable to assume that the copper additions prevent recombination of positive holes and electrons. The decrease in surface efficiency at high temperature is probably caused by the decreased effectiveness of traps in the silver-halide crystal.

Katz[34] and Webb[35] have shown that low-intensity reciprocity failure in silver-halide emulsions is probably caused by the instability of trapped electrons. This instability increases with increasing temperature, and Webb concluded that the activation energy in emulsions is about 0.77 electron-volt at the grain surface and 0.65 electron-volt inside the grain. The same analysis may be applied to the present data. The time necessary to form a given amount of photolytic silver is inversely proportional to the quantum yield at constant absorbed intensity. Consequently, following Webb,

$$\log t_2/t_1=\log 1/\phi_2=\frac{0.434E}{k}\left[\frac{1}{T_1}-\frac{1}{T_2}\right]. \tag{10}$$

The value of E for the pure silver bromide crystals are between 0.5 and 0.6 electron-volt. The addition of copper increases this energy to between 0.8 and 0.9 electron-volt. The silver-chloride crystals have E-values of about 0.5 electron-volt. This value may be somewhat larger if the corrected yield at 280 mμ is not 1.0 in the temperature range above 60°C.

It is possible to write a mechanism for the high-temperature reaction. However, consideration of the mechanism shows that the quantum yield depends on variables which are not known at present. Measurements of the efficiency of photoconduction and the light-absorption coefficients of the silver halides at various wavelengths and temperatures are needed to test the mechanism.

The experimental results do show the great importance of impurities in determining the photolytic properties of the silver halides. The results with brominated silver should serve as a warning to those who use this material for fundamental studies. The effect of etch treatments of silver chloride with volatile reagents on the surface efficiency of photolysis may be due to the removal of impurities from the surface. The silver chloride crystals are prepared at high temperatures and may be contaminated by impurities from the Vycor plates. The Harshaw crystals could be contaminated during handling and shipment.

It is interesting that large amounts of cadmium ion do not decrease the quantum yield of evolution of halogen. This observation supports a suggestion made

[32] R. M. Noyes, J. Am. Chem. Soc. **73**, 3039 (1951).
[33] C. A. Duboc, private communication.
[34] E. Katz, J. Chem. Phys. **17**, 1132 (1949).
[35] J. H. Webb, J. Opt. Soc. Am. **40**, 3 (1950).

by Seitz[36] that positive-ion vacancies in the silver halides are not good positive-hole traps at room temperature.

The rate of regression of photolysis is apparently related to the interstitial silver-ion concentration of the crystals. The addition of cadmium bromide to silver bromide decreases the rate, and the rate in silver chloride photolysis is much slower than that in silver bromide photolysis. This agrees with the work of Hauffe and Gensch[37] which showed that cadmium additions decrease the rate of corrosion of silver by gaseous bromine. Earlier work by Wagner[38] showed that the rate of corrosion of silver by chlorine was much slower than the rate of corrosion by bromine.

V. CONCLUSIONS

At room temperature and constant halogen evolution, the quantum yields of halogen production in the vacuum photolysis of the silver halides follow the equation,

$$\phi = Q(1-e^{-ka}),$$

where Q is the surface efficiency, k is the absorption coefficient, and a is a parameter. The value of a for silver bromide is about 0.4 micron at room temperature. The a value for silver chloride is about 0.24 micron. The values of Q are usually between 0.5 and 1.0. The quantum yield of halogen production at room temperature is similar to the quantum yield of a fast wall reaction. Both depend on the diffusion of reactants to the surface. The parameter a is related to the thickness of a diffusion layer near the crystal surface. The solution of the diffusion equation by Duboc has shown that

$$a = \frac{1.154 D^{\frac{1}{2}}}{k^{\frac{1}{2}} k_1^{\frac{1}{2}} I_o^{\frac{1}{2}}},$$

where D is the diffusion coefficient of positive holes and electrons, k is the absorption coefficient of the silver halide, k_1 is the recombination rate constant for positive holes and electrons, and I_o is the intensity of the incident light.

Above a certain temperature, the quantum yields decrease with increasing temperature, the long-wavelength yields increase relative to those at short wavelengths, and the quantum yields increase with increasing light intensity. These effects are inhibited by small amounts of copper ion in silver bromide. The decrease in yield is probably caused mainly by the decreased effectiveness of traps, although the results obtained when small amounts of cadmium were added to the crystals indicated that ionic conductivity may also have some effect. The photolysis of silver bromide at room temperature is probably affected by these high-temperature changes. Consequently, the quantum yields are independent of absorbed light-intensity and the long wavelength yields are larger than those predicted by theory. Similar behavior is observed in silver chloride photolysis at temperatures between 60° and 70°C.

Measurements of the silver-halide light-absorption coefficients and photoconductivity efficiencies are necessary before the high-temperature photolysis mechanism can be established.

The addition of cadmium ion does not decrease the quantum yields at room temperature. This supports a suggestion by Seitz that positive-ion vacancies in the silver halides are not good positive hole traps at room temperature.

VI. ACKNOWLEDGMENT

The author is indebted to C. A. Duboc, T. H. James, J. A. Leermakers, F. Urbach, W. Vanselow, and W. West, of these Laboratories, for their interest, encouragement, and helpful suggestions.

[36] F. Seitz, private communication.
[37] K. Hauffe and C. Gensch, Z. physik. Chem. **A195**, 116 (1950).
[38] C. Wagner, Z. physik. Chem. **B32**, 447 (1936).

Selection Rules for Normal Modes of Chain Molecules*

MARVIN C. TOBIN
Olin Industries, New Haven, Connecticut
(Received August 25, 1954)

The selection rules for chain molecules are derived on the basis of the theory of one-dimensional space groups. The selection rules for crystals of polymer chains are discussed and correlated with those of isolated chains. The polyethylene molecule is analyzed in detail by these methods and the predictions of the theory compared with experiment. The effects of perturbations on the spectra are discussed.

THE current revival of activity in the study of the spectra of crystals is in no small part due to the development of theoretical tools for the interpretation of such spectra.[1,2] Such tools have in main been lacking so far as chain molecules go, although selection rules for these may be readily derived. In this paper, the spectra of isolated chain molecules and crystals of chain molecules will be treated from the point of view of group theory. The possible effect of coiling of polymer chains will be discussed.

LINE GROUPS AND THEIR REPRESENTATIONS

Let us consider an isolated, infinite chain molecule, such as Nylon or cellulose. If the molecule is fully extended, its symmetry may be described by a one-dimensional space group. We call this group a line group. It will contain, in addition to the familiar point covering operations, translations and possibly glide planes and screw axes.[3]

The translations plus the identity constitute an invariant subgroup of the line group. The translational subgroup plus its cosets constitute a factor group of the line group. This factor group describes the symmetry of a single repeat unit, since the elements of a given coset of the translational group are all equivalent operations.[3]

Like factor groups of space groups, the factor groups of line groups are isomorphous with one of the point groups.

Part of the full body of line-group representation is given by the representations of the factor group. In these particular representations, the matrices corresponding to pure translations are unit matrices. Therefore, any normal mode of a chain molecule which belongs to a factor group representation will be totally symmetric under translation. These are the only normal modes for which this is so.

Winston and Halford[2] have given an expression for the entries in the character table of a space group. They point out that an irreducible representation of a space group may be characterized by two quantities. The first of these is a set of wave-number vectors $\{\kappa\}$, which are sent into each other by the point group underlying the space group. One each of a set of isomorphous subgroups of this point group will leave one of the vectors of $\{\kappa\}$ invariant. A representation of the subgroup is the second quantity characterizing an irreducible representation of a space group.

We may use this character table for line groups by noting that (1) the translation vectors now all lie in the same direction, and (2) the vectors in the reciprocal lattice all lie in the same direction, which is the direction of the space lattice. These two points are a consequence of the fact that our lattice is one-dimensional, even though it has a three-dimensional motive superposed upon it.

Theory shows that the normal modes of a chain fall into frequency branches, where the frequency is a periodic function of the wave number.[4] There will be three of these branches for each atom found in a repeat unit. The normal modes corresponding to factor group representations of the line group are found at zero wave number. To each branch may be ascribed a symmetry species of the factor group. The symmetries of the non-factor group modes may be characterized as follows. First, we select a wave-number vector, and generate the set of vectors to which it gives rise under the operations of the point group underlying the line group. Second, we collect those elements of this point group which leave any one of these vectors invariant. Third, we reduce the representations of the full point group among those of its subgroup. This last operation is equivalent to reducing the factor-group representations among those of the subgroup. This is so because the factor group of a line group will be isomorphous with the point group underlying the line group.

Now, the symmetry of our chosen normal mode will be given by the set of wave-number vectors and the subgroup representation into which the factor-group representation of its frequency branch reduces.

This method of characterizing the symmetries of normal modes of chain molecules is equivalent to that given by Boukaert, Smoluchowski, and Wigner[5] for crystals.

* Part of the material in this paper was presented at the Symposium on Molecular Structure and Spectroscopy, Columbus, Ohio, 1954.

[1] D. F. Hornig, J. Chem. Phys. **16**, 1063 (1948).

[2] H. Winston and R. S. Halford, J. Chem. Phys. **17**, 607 (1949).

[3] S. Bhagavantam and T. Venkatarayudu, *The Theory of Groups and its Application to Physical Problems* (Andhra University Press, Waltair, India, 1951).

[4] F. Seitz, *The Modern Theory of Solids* (McGraw-Hill Book Company, Inc., New York, 1940).

[5] Boukaert, Smoluchowski, and Wigner, Phys. Rev. **50**, 58 (1936).

We conclude the discussion of line-group representations with a few remarks on the subject of degeneracy. The line group cannot contain more than one screw axis or greater-than-twofold rotation axis. Therefore, no factor-group normal mode can have a degeneracy greater than two. Likewise, the set $\{\kappa\}$ for any chain lattice will never contain more than two members, corresponding to the two directions along the line lattice. It is readily shown from this that[2] the possible symmetry-caused degeneracies of nonfactor-group normal modes are 1, 2, or 4 only.

Besides the symmetry-caused degeneracy, there is the degeneracy caused by "time reversal" symmetry.[5] This arises from the symmetry properties of the Hamiltonian, and has the effect of making the eigenlevels corresponding to κ the same as those corresponding to $-\kappa$. This need not concern us further.

SELECTION RULES FOR FUNDAMENTALS

We may now, given the preceding discussion, proceed to derive selection rules for fundamental modes of chain molecules. A given transition will have spectral activity only if one of the matrix elements

$$\int \psi_j^* M \psi_i d\tau \tag{1}$$

is nonvanishing. Here M is the dipole moment or polarizability. Since we are considering fundamentals, we may use the harmonic oscillator approximation, for which the condition for the nonvanishing of (1) is[6]

$$\Gamma(\psi_j^*)_{\text{line}} = \Gamma(x_M)_{\text{line}}. \tag{2}$$

Here x_M is a component of the dipole moment or polarizability, and Γ is a line-group representation. Now, vectors and tensors are totally symmetric under translation. They therefore generate only factor-group representations under the line-group covering operations. We see immediately that only those normal modes of a chain molecule which are totally symmetric under translation, and therefore generate factor-group representations, can give rise to spectral activity. In addition, of these only those modes which belong to the same representation as a component of the dipole moment or polarizability will give rise to spectral activity.

The nonfactor-group normal modes, which constitute the vast majority of normal modes of a chain, are totally inactive as fundamentals.

It may be worthwhile to consider this from another point of view. Since the factor-group modes are totally symmetric under translation, the phase change in going from repeat unit to repeat unit is zero. For the nonfactor group modes, there is a constant phase shift. In these, the contributions to the dipole moment or polarizability change from the various parts of the chain cancel each other out.

[6] Eyring, Walter, and Kimball, *Quantum Chemistry* (John Wiley and Sons, Inc., New York, 1948), p. 276.

Once the factor-group character table is available, the activities of the various symmetry species may be obtained either by inspection, or by the usual formulas.[2,3]

ENUMERATION OF FACTOR GROUP NORMAL MODES

We wish to derive the number of normal modes of a polymer chain, which belongs to each symmetry species of the factor group. As stated earlier, if there are n atoms in a repeat unit, there will be $3n$ factor-group normal modes.

The number of normal modes in each species is given by[3]

$$N_i = \frac{1}{h} \sum_R \omega_R (\pm 1 + 2\cos\phi(R)) \chi'(R). \tag{3}$$

The symbol ω_R requires some explanation. This quantity is the number of atoms of a repeat unit left invariant under the operation R. An atom is considered as invariant if it either remains in its original position, or is carried into an identical position in a neighboring repeat unit. This latter is true because the operation in question has the same effect on this atom as a simple translation. Under the factor group, all translations are identity operations.

The values of N_i given in (3) include "translations" and "rotations" of the repeat unit as a whole. The former are translations of the molecule as a whole, and may be subtracted from (3) to give

$$N_i = \frac{1}{h} \sum_R (\omega_R - 1)(\pm 1 + 2\cos\phi(R)) \chi'(R). \tag{4}$$

The "rotations" of the repeat unit require closer scrutiny. A rotation of the repeat unit around the chain axis is, except for totally linear molecules, a rotation of the molecule as a whole. However rotations of the repeat unit perpendicular to the chain axis are stretchings and bendings of the chain skeleton. There will thus be $3n-4$ vibrational branches for a chain whose repeat unit contains n atoms. The symmetry species of the rotation must be determined for each line group. Once this has been done, the mode corresponding to the factor-group pure rotations may be subtracted from the enumeration given by Eq. (4). The remaining two rotations correspond to nonfactor-group modes where the wavelength equals the chain length.

SELECTION RULES FOR OVERTONES AND COMBINATION TONES

In a crystal, as shown by Winston and Halford,[2] the vast majority of wave-number vectors is left invariant by the identity operation only. As a consequence of this, the only restriction on combination or overtone nonfactor-group normal modes is that both components must have the same wave-number vector. This latter restriction is active for chain molecules, but there are, in addition, further restrictions. These are a conse-

quence of the fact that in a chain, the space lattice and reciprocal lattice lie in the same direction. The wave-number vectors will often be left invariant under some operation other than identity, especially for chains of high symmetry.

The selection rule for combinations is given by Eq. (18) of Winston and Halford's paper

$$a_i^{f.g.}=\frac{1}{k}\sum_{R \text{ in } \{K\}} \chi_j^{*\{K\}}\chi_1^{\{K\}}\chi_i^{f.g.}(R). \qquad (5)$$

Here $\chi_i^{f.g.}$ is a factor-group character and $\chi_j^{\{K\}}$ is a character characteristic of the point group leaving a wave-number vector invariant. The R are the elements of the point group underlying the space group which are contained in the group $\{K\}$.

The content of this equation is as follows. Two non-factor-group normal modes having the same wave-number vectors may be assigned line-group symmetries as described in the section on line groups and their representations. If the direct product of their characters in the group $\{K\}$ contains a factor-group representation, then the corresponding combination tone will have the activity of that factor-group representation.

In obtaining the characters $\chi_i^{f.g.}(R)$, of course, we take advantage of the isomorphism of the factor group and the point group underlying the line group.

One immediate consequence of this treatment is that all first overtones will have the activity of the totally symmetric factor-group mode. For line groups having centers of inversion, first overtones are infrared inactive.

CRYSTALS OF CHAIN MOLECULES

Most polymeric substances crystallize to a greater or lesser extent, and the crystal structures of a number have been determined. The methods for setting up selection rules for crystals cannot be applied to crystals of polymers without some modification.

We approach the problem first from the site group point of view of Halford.[2,7] Halford has pointed out that if the center of gravity of a molecule lies on a crystallographic special position, some of the point operations of the space group leave the molecular center of gravity invariant. These point operations constitute a group which is a subgroup of both the space group and free molecular group. The molecule is treated as if it had the symmetry of the site group and selection rules are derived on this basis.

When we pass to a chain molecule, the center of gravity is replaced by an "axis of gravity," and some nonpoint operations will leave this invariant. The collection of these operations is a line group, which we will refer to as the site-group line group. We may derive selection rules for the site group from those of its factor group, just as was done for free molecules. The site-group factor group will, as before, be isomorphous with one of the point groups.

[7] R. S. Halford, J. Chem. Phys. **14**, 8 (1946).

The discussion of the selection rules under the space group is identical with that for molecular crystals[1,2,8] if we recall that the dimension of the crystallographic unit cell in the direction of a chain axis is precisely the length of a chain repeat unit. The one difference will be that some of the modes which would be lattice modes in a molecular crystal will be internal modes in a polymer crystal. The selection rules may be derived either by using the method of Hornig[1] and the site-group factor group, or by using the method of Bhagavantam and Venkatarayudu.[3,8]

It seems worthwhile to compare the vibrations of a polymer crystal with those of an ordinary crystal. As was just mentioned, under the space group, the two are not particularly different. This is not true under the site group. As will be seen below, in a crystal of polyethylene, the methylene groups lie on crystallographic special positions of symmetry C_s. If we imagine a crystal of polyethylene in which the C—C bonds are dissolved, the spectrum will, in the site-group approximation, be that of a single methylene group. The coupling of the CH_2 groups introduces new elements of site symmetry, including, among others, translations. The site symmetry is now that of a chain having a line-group symmetry with a factor group isomorphous to C_{2h}.

We might expect that the spectrum of a molecular crystal having a particularly strong lattice bond, such as a hydrogen bond, in one direction, might be treated as if the system had a line-group type symmetry. That is to say, we might characterize the effect of hydrogen bonding by reducing the representations of the site-group factor group among those of the crystallographic site-point groups.

On the matter of overtones and combination tones, crystals of chain molecules will behave exactly like molecular crystals under the space group. This is to say that almost no symmetry restrictions will be operative. However in cases where the site-group selection rules predominate, we expect rather stringent selection rules for combinations and overtones. This would be the case in a mixed crystal of a hydrogen and a deuterium compound.

APPLICATION TO POLYETHYLENE

As an illustration of the theory the selection rules for polyethylene will be completely analyzed. If we consider an extended zigzag chain, the covering operations are the following:

(1) identity (E),
(2) a mirror plane in the plane of the carbon chain (σ_h),
(3) mirror planes in the planes of the methylene groups (σ_v),
(4) twofold axes bisecting the methylene groups (C_2),
(5) twofold axes bisecting the C—C bonds and perpendicular to σ_h (C_2'),

[8] J. Mathieu, *Spectres de Vibration et Symetrie des Molecules et des Cristaux* (Hermann & Cie., Paris, 1945).

TABLE I. Multiplication table for V_h (line).

	E	σ_v	σ_h	$\bar{\sigma}_h$	i	$\bar{C}_2$	C_2'	C_2
E	E	σ_v	σ_h	$\bar{\sigma}_h$	i	$\bar{C}_2$	C_2'	C_2
σ_v	σ_v	E	C_2	C_2'	$\bar{C}_2$	i	$\bar{\sigma}_h$	σ_h
σ_h	σ_h	C_2	E	$\bar{C}_2$	C_2'	$\bar{\sigma}_h$	i	σ_v
$\bar{\sigma}_h$	$\bar{\sigma}_h$	C_2'	$\bar{C}_2$	E	C_2	σ_h	σ_v	i
i	i	$\bar{C}_2$	C_2'	C_2	E	σ_v	σ_h	$\bar{\sigma}_h$
$\bar{C}_2$	$\bar{C}_2$	i	$\bar{\sigma}_h$	σ_h	σ_v	E	C_2	C_2'
C_2'	C_2'	$\bar{\sigma}_h$	i	σ_v	σ_h	C_2	E	$\bar{C}_2$
C_2	C_2	σ_h	σ_v	i	$\bar{\sigma}_h$	C_2'	$\bar{C}_2$	E

(6) centers of inversion at the midpoints of the C−C bonds (i),
(7) a twofold screw axis lying along the chain axis ($\bar{C}_2$),
(8) a glide plane containing the chain axis, and perpendicular to σ_v and σ_h ($\bar{\sigma}_h$),
(9) pure translations along the chain axis.

The multiplication table for the factor group of this line group is shown in Table I. This table was obtained by carrying out typical line-group operations on a single repeat unit. Any operation which had the effect of translating a repeat unit completely into the next was taken as identity. It is easily shown from the multiplication table that the factor group for polyethylene is isomorphous with point group V_h. The character table is shown in Table II.

Even at this point the analysis has given the useful result, that for an infinite polyethylene chain, the mutual exclusion rule must hold. Using the character table, the symmetry species of the translations, rotations, and components of the dipole moment and polarizability were obtained. These are shown in Table II.

Applying Eq. (3), we find the enumeration of factor-group normal modes given in Table III. The translations and rotations have been left in. In determining the vibrational modes, they may be subtracted by using Table II and Eq. (4).

The classification of the vibrational factor group modes is shown in Table IV. A similar classification has been given before,[9] but this is the first derived by rigorous group theoretical methods.

For the treatment of combination tones we easily find that each set $\{\kappa\}$ consists of a wave-number vector and its negative. The only exception is the wave-number vector whose terminus is at the end of the first Brillouin zone.[4] This vector is left invariant by the full factor group.[5]

For all but this last vector, a group isomorphous with C_{2v} leaves each wave-number vector invariant. The correlation chart connecting the species of V_h with those of C_{2v} is shown in Fig. 1.

From this chart and Eq. (5), we quickly find that combinations between, for example, the A_u twisting branch and the B_{2u} translational branch will give rise to both infrared and Raman activity. This is because direct products between line-group representations of these branches contain factor-group representations B_{2g} and B_{3u}. This completes the treatment of the isolated polyethylene molecule.

Passing to the crystal, Bunn[10] has shown that polyethylene has the space group Pnam-V_h^{16}, with two chains passing through each unit cell. The factor-group operations of this space group are identity, three twofold screw axes, two glide planes, one mirror plane, and a center of inversion. The factor group is isomorphous with V_h.

Of the factor-group operations, the mirror plane, a screw axis, the center of inversion and identity leave the axis of gravity of any particular chain invariant. These operations constitute the factor group of a site group, this factor group being isomorphous with C_{2h}. The site-group subgroup which leaves any given wave-number vector invariant is isomorphous with C_2.

The enumeration of normal modes under the site group and space group is shown in Table III. The correlation chart between the species of the factor groups of the line, site, and space groups is shown in Fig. 2. We see from Table III and Fig. 2 that each factor-group mode of the line group will split into two under the space group. Both components arising from perpendicular vibrations will be infrared active. Only one component arising from parallel vibrations will be infrared active.

TABLE II. Character table for V_h (line).

	E	σ_v	σ_h	$\bar{\sigma}_h$	i	$\bar{C}_2$	C_2'	C_2	Activity	Translations and rotations
A_g	+1	+1	+1	+1	+1	+1	+1	+1	$\alpha_{\bar{C}_2}^2$, $\alpha_{C_2'}^2$, $\alpha_{C_2}^2$	${}^RC_2$
A_u	+1	−1	−1	−1	−1	+1	+1	+1		
B_{1g}	+1	+1	−1	−1	+1	+1	−1	−1	$\alpha_{C_2'C_2}$	${}^R\bar{C}_2$
B_{1u}	+1	−1	+1	+1	−1	+1	−1	−1	${}^M\bar{C}_2$	${}^T\bar{C}_2$
B_{2g}	+1	−1	+1	−1	+1	−1	+1	−1	$\alpha_{\bar{C}_2C_2}$	${}^RC_2'$
B_{2u}	+1	+1	−1	+1	−1	−1	+1	−1	${}^MC_2'$	${}^TC_2'$
B_{3g}	+1	−1	−1	+1	+1	−1	−1	+1	$\alpha_{\bar{C}_2C_2'}$	
B_{3u}	+1	+1	+1	−1	−1	−1	−1	+1	${}^MC_2$	${}^TC_2$

[9] L. Kellner, Proc. Roy. Soc. (London) **A64**, 521 (1951).
[10] C. Bunn, Trans. Faraday Soc. **35**, 482 (1939).

The 36 frequency branches of the crystal may be classified as follows:

(1) three acoustic translational modes,
(2) three translational lattice modes,
(3) two rotational lattice modes,
(4) twenty-eight internal vibrational modes.

COMPARISON WITH EXPERIMENT

The cause of the splitting of certain bands in going from molten to crystalline polymers has long been a source of puzzlement. The outstanding example is the 13.9-micron band in long-chain hydrocarbons.[11] In the crystal, this band splits into a doublet at 13.7 and 13.9 microns. It has been established that these two have opposite polarizations, along the crystal a and b axes.[12] In dilute solutions of hydrocarbon in deutero-hydrocarbon, the band again appears as a singlet.[13] These phenomena are in exact accord with the theoretical analysis. The 13.9-micron band, which arises from a perpendicular rocking of the methylene group, splits into two components in the crystal, according to the space-group selection rules. In the solid solution, however, the site-group rules are operative[1] and the band appears as a singlet.

The other perpendicular bands are found to split in the same manner.

Likewise, only one band arising from a parallel vibration is found in the infrared spectrum.[13]

TABLE III. Enumeration of factor-group normal modes. for polyethylene under the various groups.

Line	A_g 3	A_u 1	B_{1g} 3	B_{1u} 2	B_{2g} 2	B_{2u} 3	B_{3g} 1	B_{3u} 3
Site			A_g 6	A_u 3	B_g 3	B_u 6		
Space	A_g 6	A_u 3	B_{1g} 6	B_{1u} 3	B_{2g} 3	B_{2u} 6	B_{3g} 3	B_{3u} 6

TABLE IV. Classification of the factor-group normal modes for polyethylene.

CH stretch A_g, B_{1g}, B_{2u}, B_{3u}
CH_2 bend A_g, B_{3u}
CH_2 rock B_{1g}, B_{2u}
CH_2 twist A_u, B_{3g}
CH_2 wag B_{1u}, B_{2g}
CC stretch B_{2g}
C_3 bend A_g

EFFECT OF PERTURBATIONS

The analysis presented in this paper was predicated on a completely oriented polymer chain of infinite extent. In actuality, the chains are liable to contain a thousand or fewer repeat units, and are found in random crumpled configurations.

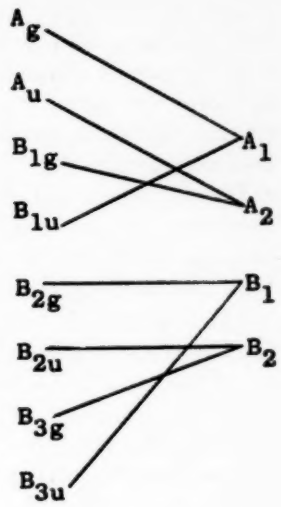

FIG. 1. Correlation chart between V_h and C_{2v}.

The finite chain length may be taken into account by assuming the Born-Karman boundary conditions to hold.[2,4] On the basis of this approximation, one would predict that the factor-group frequencies would not be affected by changes in chain length, but that the non-factor-group frequencies would shift slightly. End effects might cause some breakdown of selection rules in relatively short chains.[9]

The effect of disordering of the chains is more difficult to predict theoretically. However, it is found upon examining the spectra of molten chain hydrocarbons, that the number of bands assigned to methylene motions is not greater than that predicted by the factor-

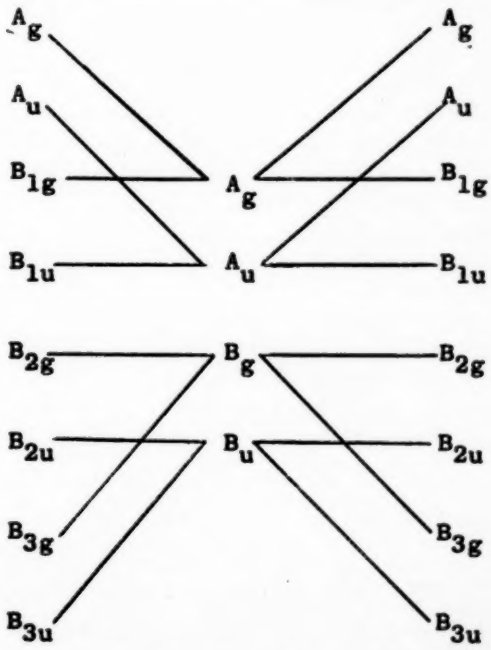

FIG. 2. Correlation chart for the various groups of polyethylene

[11] Rugg, Smith, and Wartman, J. Polymer Sci. 11, 1 (1953).
[12] S. Krimm, Pittsburgh Conference on Analytical Chemistry and Applied Spectroscopy, 1954.
[13] S. Krimm, private communication.

group analysis, and that, furthermore, about the correct numbers of parallel and perpendicular bands appear.[11] Bands appear in the infrared spectrum which are forbidden under the factor-group analysis. In the crystal, the space-group selection rules are found to hold very well.[13]

We may thus conclude tentatively that the effect of the disordering is to break down the factor group selection rules without introducing new frequencies other than possibly nonfactor-group ones.

The final perturbation of interest is that arising from combinations of nonfactor-group modes in the translational and rotational branches with those in vibrational branches. It was indicated earlier that some of these are permitted by the line group selection rules.

Whitcomb, Nielsen, and Thomas[14] have carried out a normal coordinate analysis of an infinite hydrocarbon chain, using a central-force potential. Their analysis indicates that the translational and rotational branches cover frequency ranges 250 cm^{-1} to 450 cm^{-1} wide. Combinations with a higher fundamental might cover twice this range. Actually, the bands in the polyethylene spectrum are relatively narrow, and no bands of this breadth occur. We conclude that combinations of this type are of very low intensity in polyethylene.

A band 200 cm^{-1} wide has, however, been observed in a Nylon type polymer.[15]

Note added in proof.—The author wishes to thank Dr. Harvey Winston for pointing out that the Winston-Halford character table may fail at the Brillouin zone boundary for space groups having glide planes or screw axes. It will always fail for such line groups. In this case the characters may be obtained by other methods. One such method will be described by the author in a forthcoming paper, "Irreducible Representations of the Line Groups."

[14] Whitcomb, Nielsen, and Thomas, J. Chem. Phys. **8**, 143 (1940).

[15] M. C. Tobin, unpublished research.

THE JOURNAL OF CHEMICAL PHYSICS VOLUME 23, NUMBER 5 MAY, 1955

Infrared Intensity of the C−D Stretch of Chloroform-*d* in Various Solvents*

CHARLES M. HUGGINS AND GEORGE C. PIMENTEL
Department of Chemistry and Chemical Engineering, University of California, Berkeley, California

(Received August 30, 1954)

Infrared measurements of the frequency and intensity of the C−D stretching and bending motions of $CDCl_3$ in various solvents are presented. The expected relationship between heat of solution and lowered stretching frequency is shown not to extend to $CDCl_3$. There is, however, a correlation between apparent integrated intensity of this band and the extent of interaction in the same solvent. The band is over thirty times as intense in triethylamine as in carbon tetrachloride solution. No large change in the intensity of the bending motion was observed. The infrared spectral properties of chloroform-*d* are interpreted to indicate molecular interactions similar to hydrogen bonding interactions.

INTRODUCTION

VARIOUS chemical evidence has indicated that the fairly strong interactions of chloroform with basic solvents are not simply van der Waals interactions.[1] It has been generally accepted that the interaction involves hydrogen bonding, in which the major attractive force is associated with the C−H ··· X configuration. For the particular case of chloroform-acetone, a C−H ··· O=C binding energy of 4.1 kcal was calculated[2] by the application of the van't Hoff equation to the vapor pressure data of Schulze.[3]

Hydrogen bonds involving O−H or N−H groups have long been characterized by the lowered stretching frequency of the O−H or N−H bond.[4] Correspondingly, infrared studies of solutions of chloroform offer a possible criterion to aid in identifying C−H hydrogen bonding. Indirect studies of this type have been made. Whiffen[5] has investigated the influence of solvents on the frequency, half-width, and intensity of the degenerate C−Cl stretch of chloroform (at 670 cm^{-1}). He found no significant frequency or intensity changes. Tamres[6] obtained a correlation between the integral heat of solution of chloroform in various organic solvents and the frequency shift of the O−D stretch of methanol-*d* in these same solvents. Klemperer, Cronyn, Maki, and Pimentel[7] have interpreted the infrared spectra of amides in chloroform and other solvents as evidence for a chloroform hydrogen bond to the carbonyl of the amide. It is the intent of this

* The results given in this paper were presented at the Symposium on Spectroscopy and Molecular Structure, The Ohio State University, Columbus, Ohio, in June, 1954.

[1] For discussion of the experimental and theoretical arguments related to essentially chemical observations, see J. H. Hildebrand and R. L. Scott, *Solubility of Nonelectrolytes* (Reinhold Publishing Corporation, New York, 1950).

[2] E. A. Moelwyn-Hughes and A. Sherman, J. Chem. Soc. **1936**, 101 (1936).

[3] A. Schulze, Z. physik. Chem. **93**, 370 (1919).

[4] Hendricks, Wulf, Hilbert, and Liddel, J. Am. Chem. Soc. **58**, 1991 (1936).

[5] D. A. Whiffen, Trans. Faraday Soc. **49**, 878 (1953).

[6] M. Tamres, J. Am. Chem. Soc. **74**, 3375–8 (1952).

[7] Klemperer, Cronyn, Maki, and Pimentel, J. Am. Chem. Soc. **76**, 5846 (1954).

work to investigate the solvent environmental influence on the C—D stretch of chloroform-*d*.

EXPERIMENTAL

All spectra were obtained using a Perkin-Elmer Model 21 Spectrophotometer with CaF_2 and/or NaCl optics. The cell temperature was found to be 32.5±2°C. The frequency calibration was checked against the known spectra of CO, HBr, CO_2, and H_2O. The zero and total transmissions were checked periodically over the frequency range of interest to preclude any instrument drift. A sealed liquid cell of 0.0095-cm thickness (calibrated by comparison to a cell of similar thickness known from optical interference patterns) and with NaCl windows was used. No evaporation of volatile solvents from the cell was noticed in periods as long as four hours.

Chloroform-*d* was prepared by the reaction of anhydrous chloral with 6N NaOD in D_2O. The product was distilled and a fraction with boiling range 61.5–62.5°C was accepted. The resulting chloroform-*d* was analyzed with the aid of its infrared spectrum and found to contain, in addition to $CDCl_3$, 24 percent $CHCl_3$, and an impurity of unknown origin containing carbonyl (estimated concentration, less than 0.05 molar). No attempt was made to purify the product further. Suitable corrections were made for the $CHCl_3/CDCl_3$ ratio in the intensity measurements.

Acetone: Commercial solvent-grade acetone was distilled twice from anhydrous $CaCl_2$ in a thirty-plate, bubble-cap column and a center fraction boiling at 56.0±0.1°C was chosen.

Benzene: Merck cp benzene was redistilled from anhydrous $CaCl_2$ in the same multiplate column and a center fraction boiling at 81.1±0.1°C was chosen.

Carbon tetrachloride: Baker's Analyzed carbon tetrachloride was redistilled from P_2O_5 in a single-stage still.

Mesitylene: Eastman Kodak White Label mesitylene was purified by distillation and successive recrystallizations.

Nitrobenzene: Eastman Kodak White Label nitrobenzene was redistilled from anhydrous $CaCl_2$ in a single-stage still.

Triethylamine: Eastman Kodak White Label triethylamine was refluxed and redistilled from KOH in the same multiplate column; a center fraction boiling at 89.5±0.5°C was chosen.

In addition, all materials were examined for spurious infrared absorption with particular attention to the carbonyl and O—H stretching regions.

All solutions were prepared quantitatively with Misco micropipettes to a total volume of not less than 0.25 ml. By weighing experiments, it was found that the precision of delivery was ±8 percent. For each solvent, at least two solutions were prepared and the spectrum of each was obtained.

Solutions were prepared in the concentration range necessary for optimum measurements of intensity in a 0.0095-cm liquid cell. In no case did the concentration exceed 20 percent by volume and in some solvents the concentration was less than 10 percent by volume. The band intensities were determined by integration over a frequency range extending five times the half-width on each side of the band maximum. Small corrections were necessary because of solvent absorption. No attempt was made to extrapolate the apparent absorption coefficient to infinite dilution.

It is felt that the frequency shifts are reliable to within 3 cm^{-1} for CaF_2 optics and to within 5 cm^{-1} for NaCl optics. The intensities reported are reproducible to within 10 percent and are considered reliable to within 15 percent.

TABLE I. Spectral characteristics of the C—D stretch of $CDCl_3$ in various solvents.

Solvent	$\Delta\nu$ (cm^{-1})	Half-width (cm^{-1})	B (liters $mole^{-1}$ cm^{-2})	ΔH (sol'n)[a] (cal/mole sol'n)
Carbon tetrachloride	0	12	50	+20
Chloroform-*d*	0	11	62	···
Benzene	5	11	310	−90
Nitrobenzene[b]	4	13	300	−118
Mesitylene	5	11	340	−216
Acetone[b]	0	15	540	−495
N-ethylacetamide[b]	0	25	1700	···[c]
Triethylamine[b]	84	42	1800	∼−1200[d]

[a] Equimolar mixture.
[b] NaCl prism, otherwise CaF_2.
[c] Data not available.
[d] Estimated by comparison to other trialkylamines.

RESULTS

The observations are listed in Table I. The column labeled $\Delta\nu$ is given by $\nu_0-\nu'$, where ν_0 is the frequency of maximum absorption of the C—D stretch in pure liquid chloroform-*d* and ν' is the frequency of maximum absorption of the same band in the solvent listed. The value of ν_0 was found to be 2258±4 cm^{-1}. It is readily apparent from the data in Table I that there is no useful correlation between the quantitative frequency shift and the heat of solution. Studies by Badger[8] indicate a correlation between the frequency shift of the O—H stretching mode and the energy of the hydrogen bond. Assuming the same relation,[8] and an energy of interaction between 2 and 4 kcal, a shift of about 50 to 100 cm^{-1} is expected for the C—D stretching in acetone solution. Thus the principal spectral evidence of hydrogen bonding has failed, except in the case of triethylamine, to provide corroborativee vidence of hydrogen bonding involving chloroform.

Another spectral property generally associated with the formation of a hydrogen bond is an increase in the half-width of the absorption ascribed to the stretching motion. Table I lists the half-widths observed for the C—D stretch in the several solvents. There is an

[8] R. M. Badger and S. H. Bauer, J. Chem. Phys. **5**, 839 (1937); R. M. Badger, J. Chem. Phys. **8**, 288 (1940).

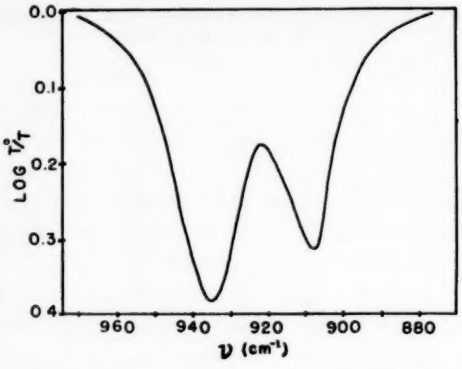

FIG. 1. The absorption near 908 cm^{-1} of $CDCl_3$ in triethylamine solution after correction for triethylamine absorption. (Concentration: 4 percent $CDCl_3$ by volume.)

apparent trend among the stronger bases but none among the bases weaker than acetone.

A third spectral characteristic which was studied is the apparent intensity of the absorption at 2258 cm^{-1}. The quantity B is defined $B=(1/CL)\int \log(T_0/T)d\nu$ where C is the concentration in moles liter^{-1}, L is the cell thickness in centimeters, T_0 is the incident light intensity, T is the transmitted light intensity, and ν is the frequency in cm^{-1}. In Table I it is evident that there is not only a systematic correlation between B and the integral heat of solution, but also that the change in B is extremely large over the range of solvents studied. Such intensification has been previously observed in hydrogen bonding systems. For example, Williams and Plyler[9] observed qualitatively the intensification of the O—H stretch of water in acetone solutions. Similarly, Badger and Bauer[8] have observed the intensification of the O—H stretch of alcohols upon forming dimers or higher polymers.

The extreme changes observed in the intensity of the C—D stretching motion lead naturally to an investigation of the intensity of the C—D bending motion at 908 cm^{-1}. The intensity of this band was studied in three solvents, carbon tetrachloride, benzene, and triethylamine. In benzene solution, no new absorption was observed near 908 cm^{-1} and the apparent extinction coefficient of the 908 cm^{-1} band itself was the same, within experimental error, as in carbon tetrachloride (about 4400 liters mole^{-1} cm^{-2}). In triethylamine a new band at 935 cm^{-1} appears which is attributed to the hydrogen-bonded species. This band is shown in Fig. 1 and it is seen to have somewhat greater intensity than the residual absorption at 908 cm^{-1}. In view of the difficulty of separating these two bands, the total area under the two bands was measured. The apparent extinction coefficient based on total area was again found to be the same within a few percent. The experimental uncertainty was higher, possibly 25 percent, because of interference by bands of triethylamine.

With the simple interpretation that the intensity of the C—D bending motion reflects the magnitude of the C—D bond moment, it is necessary to conclude that the interaction between chloroform-*d* and these two solvents does not involve a large net movement of charge. It is inferred that the ionic character of the C—D bond of chloroform-*d* does not change by a large amount upon formation of this bond, considered to be of the hydrogen bond type.

This apparent absence of increase in the bond moment of the C—D bond merely compounds the difficulty of explaining the large change of intensity of the C—D stretching motion. It is evident that any proposed theory of hydrogen bonding can be tested by checking the predicted infrared intensities.

CONCLUSION

The particularly large intensity changes reported here are interpreted to be analogous to those observed in O—H systems. In view of the observations of Whiffen[5] that the degenerate C—Cl stretching motion shows no intensity changes due to solvent interactions, the effects noted here are indicative of a strong and specific interaction of the C—D group. Despite the absence of a systematic frequency shift of the C—D stretch, it seems appropriate to conclude that this interaction is analogous to hydrogen bonding. Hence it is concluded that the apparent intensity of the C—D stretching frequency is an extremely sensitive measure of the hydrogen (or deuterium) bonding of chloroform-*d* and it is expected that this will be true for chloroform also. The approximate constancy of the intensity of the C—D bending frequency of $CDCl_3$ indicates that the large intensity change of the stretch cannot readily be ascribed to an increase in the ionic character of the C—D bond.

The impact of these observations upon the interpretation of band intensities may be considerable. Environmental change of band intensities could be a phenomenon of frequent occurrence, possibly particularly associated with solutions which differ from ideality. In any event, the use of chloroform as a solvent must be appraised with caution in quantitative infrared measurements. It is to be remembered that chloroform is a good solvent for many compounds because it does interact in the same specific way that presumably gives rise to the effects noted here.

[9] D. Williams and E. K. Plyler, J. Chem. Phys. 4, 154 (1936).

Method of Integrating the Rate Equations for Free Radical Initiated Polymerizations

JOHN P. HOWE*
General Electric Research Laboratory, The Knolls, Schenectady, New York
(Received February 12, 1954)

A method is given for integrating the equations for the rate of polymerization reactions without the assumption of steady states for the concentrations of the various free radicals. The main reaction steps used are: free radical production, chain propagation, chain transfer, and chain termination. Explicit expressions are found for the total amount of polymer, the number average, and the weight average as a function of time for the particular case of free radicals produced initially by a pulse of light. Other modes of dependence on time for the primary free radicals may also be treated.

INTRODUCTION

THIS paper presents a method of integrating the equations for the rate of polymerization reactions initiated by free radicals. Since the method does not assume that free radicals attain a steady-state concentration, transient conditions may be analyzed. In particular, expressions for the time dependence of the total amount of polymer, the number average molecular weight and the weight average molecular weight are derived. For the special case of their production by a pulse of light or ionization, or for that matter for any means of establishing an initially determined number of free radicals without subsequent production of any primary radicals, and in the case that the monomer activity is constant, it proves to be simple to give explicit expressions. In principle, any rate of production of primary free radicals may be treated.

A reaction scheme similar to those discussed by other authors[1] is used. No experimental data are compared with the theory. Rather it is hoped that the analysis given will assist in widening the methods for determining rate constants for the various steps in polymerization reactions; for example, by measurements on systems after a pulse of light.

THE REACTION SCHEME

The following series of reactions is considered[2]: (1) free radical production k_d; (2) chain propagation k_p; (3) chain transfer with formation of a product molecule k_{tr}; (4) chain termination by combination k_{tc}; (5) chain termination by disproportionation k_{td}.

The customary assumptions are made concerning the rate constants and rates of reaction. Free radicals result from the dissociation of an activated molecule A^*, the concentration of which may in the general case vary in time. For this discussion the dissociation is considered to be a first-order reaction. In addition the several zero-order free radicals are assumed to have identical properties.

THE GENERAL METHOD

In standard fashion, the rate expressions which are to be integrated may be written

$$\frac{dR_0}{dt}=nk_dA^*-(k_p+k_{tr})MR_0 + k_{tr}M\sum_{j=0}^{\infty}R_j-(k_{tc}+k_{td})R_0\sum_{j=0}^{\infty}R_j, \quad (1a)$$

$$\frac{dR_q}{dt}=k_pMR_{q-1}-(k_p+k_{tr})MR_q - (k_{tc}+k_{td})R_q\sum_{j=0}^{\infty}R_j, \quad (1b)$$

$$\frac{dM}{dt}=-(k_p+k_{tr})M\sum_{j=0}^{\infty}R_j, \quad (1c)$$

$$\frac{dP_q}{dt}=k_{tc}/2\sum_{j=0}^{q}R_jR_{q-j}+k_{td}R_q\sum_{j=0}^{\infty}R_j+k_{tr}MR_q. \quad (1d)$$

In these equations nk_dA^* gives the rate of production of free radicals by the primary initiating reactions, the n giving the number of radicals from A^*.

New equations for generating functions for the R_q's and P_q's are now obtained by multiplying the set of Eqs. (1b) and (1d) by a parameter x^q respectively and summing over q. Also the set (1b) is summed directly. It is convenient at this point to introduce a set of dimensionless variables and define the following quantities:

$$y=M_0(k_{tc}+k_{td})t,$$

$$M_0\phi(x,y)=\sum_{q=0}^{\infty}R_qx^q,$$

$$M_0s(y)=M_0\phi(1,y)=\sum_{q=0}^{\infty}R_q,$$

$$M_0m=M,$$

$$M_0\pi=\sum_{q=0}^{\infty}P_qx^q,$$

* Present address: Nuclear Engineering and Manufacturing, North American Aviation, Inc., P.O. Box 309, Downey, California.

[1] For example: C. H. Bamford and M. J. S. Dewar, Proc. Roy. Soc. (London) **A192**, 309 (1948); H. W. Melville and G. M. Burnett, Proc. Roy. Soc. (London) **A189**, 456 (1947).

[2] The notation used by Paul J. Flory, *Principles of Polymer Chemistry* (Cornell University Press, Ithaca, 1953), is followed partially.

$$M_0^2(k_{tc}+k_{td})g(y)=nk_dA^*,$$

$$\alpha(k_{td}+k_{tc})=k_p,$$

$$\beta(k_{td}+k_{tc})=k_{tr},$$

$$\gamma_1(k_{td}+k_{tc})=k_{tc},$$

$$\gamma_2(k_{td}+k_{tc})=k_{td}.$$

The differential equations for the generating functions now are:

$$\frac{d\phi}{dy}=g+\beta ms+\{[\alpha(x-1)-\beta]m-s\}\phi, \tag{2a}$$

$$\frac{ds}{dy}=g-s^2, \tag{2b}$$

$$\frac{dm}{dy}=-(\alpha+\beta)ms, \tag{2c}$$

$$\frac{d\pi}{dy}=\frac{\gamma_1}{2}\phi^2+\gamma_2 s\phi+\beta m\phi. \tag{2d}$$

From these new functions the concentration of a given species may be obtained. Thus

$$R_j=\frac{M_0}{j!}\left(\frac{\partial}{\partial x}\right)^j\phi\Big|_{x=0},$$

$$P_j=\frac{M_0}{j!}\left(\frac{\partial}{\partial x}\right)^j\pi\Big|_{x=0}.$$

Quantities often determined experimentally are given by the expressions:

$$\text{Total amount of polymer}=\sum_{q=0}^{\infty}P_q=\pi(1,y)M_0. \tag{3a}$$

Number average:

$$\langle q\rangle_n=\frac{\sum_{q=0}^{\infty}qP_q}{\sum_{q=0}^{\infty}P_q}=\frac{x}{\pi}\frac{\partial\pi}{\partial x}\Big|_{x=1}. \tag{3b}$$

Weight average:

$$\langle q\rangle_m=\frac{\sum_{q=0}^{\infty}q^2P_q}{\sum_{q=0}^{\infty}qP_q}=\frac{\dfrac{\partial}{\partial x}\left(x\dfrac{\partial\pi}{\partial x}\right)}{\dfrac{\partial\pi}{\partial x}}\Big|_{x=1}. \tag{3c}$$

The function g is determined by the special conditions attending the reaction, for example production of free radicals by (1) a pulse of light, (2) steady illumination, (3) sector illumination, (4) thermal activation of a molecule, (5) by ionization in the track of a charged particle, and conceivably in other ways. The first case will be treated fully in a following section and a procedure for the second and third outlined. Cases 2 and 4 are formally the same.

Initial conditions for the equations although special for given conditions may be stated in reasonably general terms as follows:

$$\phi(0,0)=\phi(1,0)=s(0)=\frac{R_0^0}{M_0},$$

$$m(0)=1,\ \pi(0,0)=0.$$

These conditions pertain to reactions in which no secondary free radicals or products are present at the start of the reaction. It is necessary to know the concentration of primary free radicals at the start of time measurement. In cases 1, 2, and 3 this information is available if the usual photochemical constants have been determined. The assumption of steady state kinetics for A^* so produced is warranted at least for most photochemical reactions. One may treat cases in which secondary radicals and products are already present provided he can go back to the point $y=0$ at which primary free radicals are first introduced to the monomer and integrate the equations to the point in question. In principle, the rate of production of primary free radicals may be changed arbitrarily at any time as the reaction proceeds.

If, for a given g and appropriate initial conditions, the function ϕ can be expanded in a Taylor's series around the point $x=1$,

$$\phi=A_0+A_1(x-1)+A_2\frac{(x-1)^2}{2!}+,$$

and substituted in Eq. (2d) a similar expansion for π may be obtained. Thus

$$\pi=B_0+B_1(x-1)+B_2\frac{(x-1)^2}{2!}+.$$

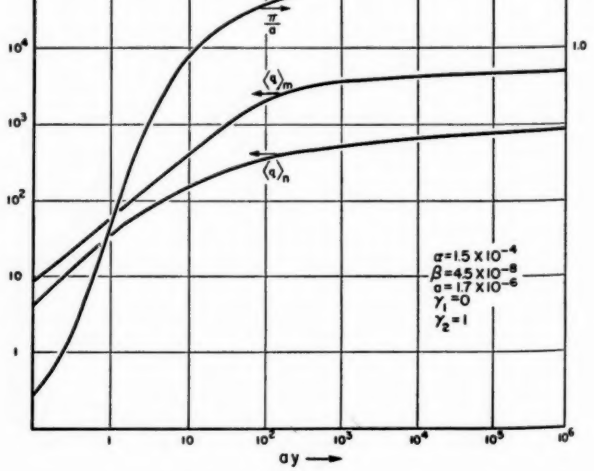

FIG. 1.

These coefficients, upon employing Eqs. (3a), (3b), and (3c), permit the experimentally observed quantities to be written as follows:

$$\pi(1,y)=B_0, \tag{4a}$$

$$\langle q\rangle_n=\frac{B_1}{B_0}, \tag{4b}$$

$$\langle q\rangle_m=1+\frac{B_2}{B_1}, \tag{4c}$$

where, if the above boundary conditions are appropriate and m is constant as explained below,

$$B_0=\int_0^y\left[\left(\frac{\gamma_1}{2}+\gamma_2\right)A_0^2+\beta A_0\right]dy', \tag{5a}$$

$$B_1=\int_0^y(A_0A_1+\beta A_1)dy', \tag{5b}$$

$$B_2=\int_0^y(A_0A_2+\gamma_1A_1^2+\beta A_2)dy'. \tag{5c}$$

Computation of the distribution function $P(q)$ has not been attempted. Rather than the method of Bamford and Tompa[3] inversion of the sum $\pi(x)$ by contour integration would appear to offer a method for such a calculation.

A simplification with respect to Eqs. (2a), (2c), and (2d) is possible in that m may be considered constant in interesting systems because (a) the fraction of monomer disappearing may be small, (b) its effective concentration or activity may tend to stay constant even over an appreciable change in actual concentration,[4] and (c) the value of $(\alpha+\beta)$ may be small as is the case in reference 3.

PRODUCTION OF FREE RADICALS IN A PULSE

If an initial concentration of primary radicals is produced at $y=0$ for example by a pulse of radiation, and no primary radicals are produced subsequently, then $g=0$ and ϕ may be determined from Eqs. (2a) and (2b) subject to the aforementioned initial conditions. Further, if $m=1$, explicit expressions may be obtained for the B's from Eqs. (5a), (5b), and (5c) and in turn used in Eqs. (4a), (4b), and (4c). The expressions for the B's are:

$$B_0=a\left(\frac{\gamma_1}{2}+\gamma_2\right)[1-(1+ay)^{-1}]+\beta\ln(1+ay),$$

$$B_1=\alpha\ln(1+ay)-\frac{\alpha a}{\beta}(1+ay)^{-1}(1-e^{-\beta y}),$$

$$B_2=\frac{2\alpha^2a}{\beta^2}\Big\{(1+ay)^{-1}(\beta ye^{-\beta y}+e^{-\beta y}-1)$$

$$-\frac{\gamma_1}{2}(1+ay)^{-1}(1-2e^{-\beta y}+e^{-2\beta y})+\beta/a\ln(1+ay)$$

$$+(\gamma_1-1)\beta\frac{e^{\beta/a}}{a}[Ei[-(\beta/a)(1+ay)]-Ei(-\beta/a)]$$

$$-\gamma_1\beta\frac{e^{2\beta/a}}{a}\left[Ei[-(2\beta/a)(1+ay)]-Ei(-2\beta/a)\right]\Big\}.$$ [5]

The observables $\pi(1,y)$, $\langle q\rangle_n$ and $\langle q\rangle_m$ are plotted in Fig. 1 for purposes of illustration.

An abbreviation $M_0a=R_0^0$ has been introduced. For the case of a typical photochemical reaction for which k_a gives the quanta absorbed per unit concentration of molecules A, I represents the flux of quanta, k_f the constant for monomolecular deactivation of A^*, k_d is as previously defined, and Δt is an irradiation time short with respect to free radical lives but long compared to the life of A^*,

$$M_0a=\frac{nk_ak_dI\Delta t}{k_a+k_f}.$$

If Δt is shorter than the half-life of A^*, an unlikely circumstance, the denominator tends to two and the square of the time interval enters. If a second pulse of primary radicals, a_1 is introduced at a value, y_1, of the time variable, the boundary conditions given above are extended simply by noting that

$$s(y_1+0)=s(y_1-0)+a_1=\phi(1,y_1+0).$$

DISCUSSION OF OTHER MODES OF PRODUCTION OF PRIMARY FREE RADICALS

Free radicals may be produced at a constant rate photochemically or thermally. In this case g is constant, a may be zero thus s and ϕ may be determined and hence the coefficients A_0, A_1, and A_2 may be calculated. The coefficients B_0, B_1, and B_2 have not been determined, consequently, the incomplete analysis is not repeated here.

Sector illumination is represented by a steady rate of primary radical production say, g_1 from 0 to y_1 another steady rate, g_2 from y_1 to y_2, g_1 from y_2 to y_3 and so on, where usually the alternate intervals are equal in length, but adjacent intervals may be unequal. It is clear how to determine ϕ within each interval and that the ϕ's

[3] C. H. Bamford and H. J. Tompa, J. Polymer Sci. **10**, 345 (1953).

[4] Private discussion with Bruno Zimm, General Electric Research Laboratory, Schenectady, New York.

[5] The definition of the exponential integral used, *Ei*, is given in E. Jahnke and F. Emde, *Tables of Functions* (Dover Publications, New York, 1943).

for adjacent intervals should be joined. In turn the integrals for π or its expansion coefficients will be broken up into a sum of integrals each over the respective intervals. For short intervals, approximations to the necessary integrals may be used, however, the tractability of the summations which result has not been investigated. A method for the case wherein g is constant is suggested in the appendix.

The author wishes to acknowledge helpful discussions with Dr. Bruno Zimm of the Chemistry Department, Research Laboratory, General Electric Company. Computations by Melba Nead and checking of equations by R. Sehnert of the Nuclear Engineering and Manufacturing, North American Aviation, Inc., are also gratefully acknowledged. Thanks are due Serge Gratch for useful criticisms and suggestions.

APPENDIX. SOLUTION WHEN g IS CONSTANT

Equation (2b) being Ricattian may be rewritten

$$du^2/dy^2=gu,$$

where

$$du/udy=S.$$

If m is constant Eq. (2a) may be written in integral form for the interval 0 to y

$$\phi=-\frac{1}{u}\frac{du}{dy}+\frac{\alpha(x-1)}{u}e^{-[\beta-\alpha(x-1)]y}\int_0^y\frac{du}{dy'}e^{[\beta-\alpha(x-1)]y'}dy'.$$

From this equation the expansion around the point $x=1$ is simple. In any case for which the solution of the second-order differential equation is available this method is useful.

THE JOURNAL OF CHEMICAL PHYSICS VOLUME 23, NUMBER 5 MAY, 1955

Decomposition of Carbon Dioxide by Ionizing Radiation.*† Part I

P. Harteck and S. Dondes
Chemistry Department, Rensselaer Polytechnic Institute, Troy, New York
(Received August 29, 1954)

The irradiation of gaseous carbon dioxide with radon or in a nuclear reactor, produces about 0.1 percent decomposition of primarily dissociated carbon dioxide, correlating with previous results in the literature. The irradiation of solid carbon dioxide with radon produces carbon monoxide and oxygen with a G value of 9 to 10. The irradiation of gaseous carbon dioxide, containing a small amount of nitrogen dioxide, by radon or in a nuclear reactor, produced carbon monoxide and oxygen, with a G value of 9 to 10. Percentages as small as 0.5 percent of nitrogen dioxide are sufficient to stop the back reaction to carbon dioxide. A new mechanism has therefore been proposed for the ineffectual decomposition of carbon dioxide by ionizing radiation, and the effective decomposition when nitrogen dioxide is present. With the proposed mechanisms, the classical experiments of Lind, the carbon monoxide oxidation and the carbon monoxide decomposition, are quantitatively explained.

INTRODUCTION

With the development of modern reactor technology radiation effects on carbon dioxide become of increasing interest, since the carbon dioxide is a favorable coolant and can be considered a moderator In the classical literature, Lind[1] and Hirschfelder and Taylor[2] have shown that carbon dioxide at room temperature is slightly decomposed by ionizing radiation (about 0.1 percent of the expected decomposition). We have confirmed these results experimentally. The mechanism, in part, proposed by Hirschfelder and Taylor to describe the ineffectual decomposition, is:

$$CO+O_3=CO_2+O_2+103\text{ kcal.} \quad (1)$$

Our experimental investigation on reaction (1) indicate that this reaction has a heat of activation of over 28 kcal.[3] Therefore reaction (1) would proceed very slowly at room temperature and cannot be responsible for the reformation of carbon dioxide.

In another group of experiments, decomposition of carbon dioxide into carbon monoxide and oxygen was achieved by introduction of a small amount of nitrogen dioxide. The nitrogen dioxide acts as an inhibitor of recombination of radicals and atoms (produced during irradiation) to form carbon dioxide. The results obtained led to formulation of new mechanisms for the ineffectual decomposition of pure carbon dioxide and for the effectual decomposition when nitrogen dioxide was present. These mechanisms may also explain some of the discrepancies of the photochemical decomposition of carbon dioxide in the literature.

* Based in part on a thesis by S. Dondes in partial fulfillment for the requirements for the degree of doctor of philosophy at Rensselaer Polytechnic Institute.

† This work was supported by the U. S. Atomic Energy Commission under Contract At(30–3)32.

[1] S. C. Lind and D. C. Bardwell, J. Am. Chem. Soc. **47**, 2675 (1925); E. E. Wourtzel, Le Radium **11**, 346 (1919).

[2] J. C. Hirschfelder and H. S. Taylor, J. Chem. Phys. **6**, 783 (1938).

[3] To be published and similar to the work of Garvin, J. Am. Chem. Soc. **76**, 1523 (1954).

EXPERIMENTAL

A. Utilizing Radon as the Source of Ionizing Radiation

1. Reagents

Carbon dioxide and nitrogen dioxide, purchased from the Matheson Company were purified by fractional distillation at low temperatures. A radium carbonate source (100 mg) was supplied by the U. S. Atomic Energy Commission and specifically manufactured for us according to the method of Hahn and Heidenhain.[4]

2. Equipment

a. *Chemical.*—The system for use with radon as the ionizing source is shown in Fig. 1. For work at room temperature, the ionization chamber was used also as a reaction chamber and an analytical vessel. A Pirani gauge, manufactured by the Consolidated Vacuum Company was used to measure the pressures.

For work at higher temperatures, a double-walled Pyrex reaction vessel was used. The gases in the inner flask were heated by boiling water or o-dichlorobenzene in the outer jacket. Two small traps, one for condensation of carbon dioxide, nitrogen dioxide, and radon, and the other for condensation of carbon monoxide and oxygen on silica gel at 77°K, were attached to the reaction vessel. The inner vessel containing the gases had a small condenser at its uppermost section to keep the ground glass joint and its grease cold.

b. *Electrical.*—Saturation current measurements were made using a model 3417 galvanometer and its associated model 1290 Ayrton shunt, products of the Rubicon Company. The high voltage for the ionization chamber was provided by a Nuclear Instrument and Chemical Company model 1090A power supply.

3. Reaction

For room temperature operation, the experiments were conducted as follows: (a) purified carbon dioxide was condensed at 77°K into the ionization chamber; (b) purified radon was condensed into the ionization chamber; (c) the radon and carbon dioxide were permitted to expand and react; (d) at predetermined time intervals, the gases were again condensed at 77°K and the pressure of the noncondensibles measured. When nitrogen dioxide was introduced, a known amount was added to the condensed carbon dioxide and radon, and the gases were permitted to expand.

When operating at higher temperatures, i.e., at 100° and 180°C, the gases were similarly condensed into the large reaction vessel, permitted to expand and react, and analyzed according to the procedure described below.

[4] O. Hahn and J. Heidenhain, Ber. deut. chem. Ges. **59**, 291 (1926).

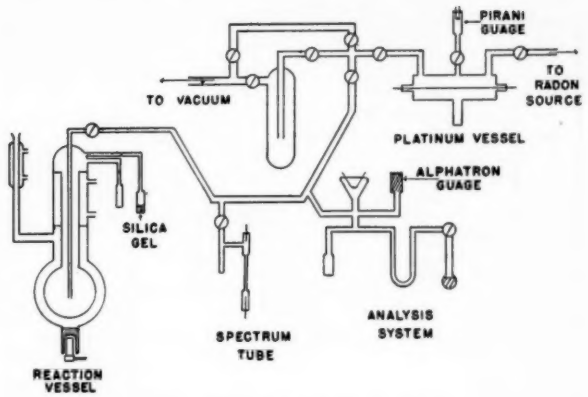

FIG. 1. Modified radon assembly.

4. Analysis

For room temperature irradiation of carbon dioxide by radon, the analysis consisted of condensing the carbon dioxide plus radon at 77°K and measuring the noncondensibles with a Pirani gauge. Almost no carbon and oxygen was absorbed by the carbon dioxide crystals.

At higher temperatures, the analysis system consisted of a small 50-cc bulb containing a No. 40 platinum wire, a "U" tube, and a silica gel trap with stopcock. An alphatron gauge, capable of measuring from 0.1 microns to 1000 millimeters with a 2 percent error, was attached to this system. A spectrum tube was also included for gas identification. The analysis method involved: (a) condensing the carbon dioxide, radon, and nitrogen dioxide (if used) in the large reaction vessel at 77°K; (b) absorbing the uncondensed gases on the silica gel in the analysis system at 77°K; (c) releasing the gases from the silica gel by removal of the liquid nitrogen bath; (d) measuring the pressure of the gases released; (e) combining these gases under the influence of a glowing platinum wire and condensing the products formed in the "U" tube at 77°K. By this method, one part of carbon monoxide in one-hundred thousand of carbon dioxide could be readily detected.

B. Utilizing a Nuclear Reactor as the Source of Ionizing Radiation

1. Reagents

The nitrogen dioxide and carbon dioxide were both fractionally distilled prior to the filling process. The gases were condensed in the quartz reaction vessel (Fig. 2), at 77°K and the vessel sealed.

2. Surface Area

In one group of experiments, the exposed surface area, in contact with the gases, was increased about 100 times by the addition of about two grams of clean quartz wool to the reaction vessel.

3. Equipment

Figure 2 shows a typical quartz vessel such as in these experiments. They were manufactured by the

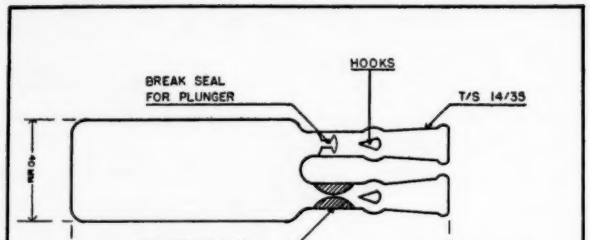

FIG. 2. Reactor vessel.

Amersil Company of New Jersey. The seal was broken after irradiation with an iron plunger by the usual magnet techniques.

4. Reaction

In a typical experiment the quartz vessel was evacuated to 0.5 micron (alphatron gauge measurement to include mercury vapor) and about $\frac{3}{4}$ of an atmosphere of pure carbon dioxide was added. When nitrogen dioxide was used, 0.1, 0.5, and 2 percent quantities were introduced together with $\frac{3}{4}$ of an atmosphere of carbon dioxide. When pure nitrogen dioxide was irradiated, $\frac{3}{4}$ of an atmosphere was utilized. As a control, a blank vessel was sealed under the same set of conditions.

Upon completion of the filling process, the vessels were brought to the Brookhaven National Laboratories, wrapped in pure aluminum foil, and placed [six at a time in a three-foot aluminum (2S, >99 percent purity)] for simultaneous irradiation. The aluminum tube was placed in an experimental hole in the pile, parallel to the fuel, and irradiated for a period extending from 7 to 10 days. Upon the removal of the aluminum tube from the pile, it was placed in a lead tunnel and permitted to "cool." About seven to fourteen days later, when the radiation intensity was low enough for handling, the quartz vessels were removed from the aluminum tube, placed in lead containers and returned to Rensselear Polytechnic Institute for analysis.

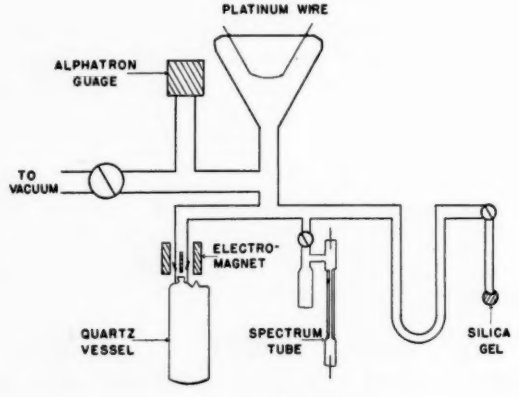

FIG. 3. Analysis system.

5. Analysis

The analysis system (Fig. 3) is similar to the type used in the radon work. The quartz vessel was attached to this evacuated system and immersed in a liquid nitrogen bath. The seal was then broken and the pressure of the gases noncondensible at 77°K was measured. The noncondensible gases (i.e., carbon monoxide and oxygen) were combined under the influence of a glowing platinum wire and the carbon dioxide was condensed. The residual pressure was then measured and the emission spectrum of the residual gas identified. Upon completion of this portion of the analysis, the vessels were evacuated of all gases, to less than a micron, and strongly heated. The material evolved was then similarly analyzed.

6. Neutron Flux and Pile Temperature

The neutron flux in the experimental hole, was about 3.3×10^{12} neutrons per cm^2 per second, and the temperature about 140°C. The epi-cadmium neutrons were approximately 3 percent of the total neutron flux.[5]

7. Relative Intensities of the Absorbed Energy

In the reactor, the following particles and radiations are present for interaction with carbon dioxide: (a) "thermal" neutrons; (b) "fast" neutrons; (c) beta particles; (d) gamma rays. The "thermal" neutrons have almost no effect on the decomposition of carbon dioxide, since the capture cross section is very small for oxygen and carbon. Of the "fast" neutrons, (3 percent of the total flux), only a third would have energies of 10^4 electron volts or more. The beta particles derived from the fission fragments and the aluminum wrappings, would probably not penetrate the thick quartz wall. However, the beta particles derived from the silicon in the quartz would add to the ionizing radiation, but this is small compared to the total intensity (about 5 percent). The dominant contribution to the dissociation of the carbon dioxide thus is due to the gamma rays, primarily derived from the fission process, fission fragments, and thermal neutron absorption by materials within the pile.

RESULTS

A. Radon and Carbon Dioxide

The work of Lind[1] shows that the interaction of radon with carbon dioxide produces but a small decomposition of carbon dioxide. Since radon and carbon dioxide have little or no vapor pressure at 77°K, any

[5] Values obtained are from pile personnel and our own measurements.

decomposition involving the formation of carbon monoxide and oxygen (not condensible at this temperature) could readily be measured. From Fig. 4, the yield of carbon monoxide and oxygen during the initial hours of the irradiation was 10 microns per hour. Actually the yield is much smaller since a slight production of carbon monoxide and oxygen occurs in the irradiation of condensed carbon dioxide during the mensuration period. Thus, in another group of experiments, when solid carbon dioxide was irradiated for a longer period than used in mensuration, the apparent yield was about 3 to 3.5 molecules of carbon dioxide decomposed per each ion pair, a G value of 9 to 10. The typical blue color of ozone, readily observable if formed in stoichiometric ratio during the decomposition of solid carbon dioxide at 77°K, was not found.

B. Radon, Carbon Dioxide, and Nitrogen Dioxide

The effect of using nitrogen dioxide as an inhibitor (3.8 and 6.3 percent nitrogen dioxide) is shown in Fig. 5.

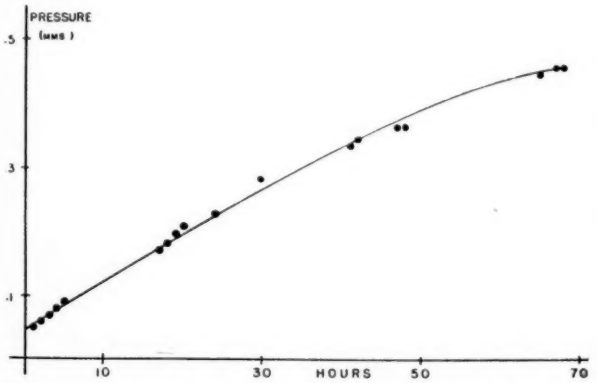

FIG. 4. Formation of CO_2+O_2 (27°C) from $Rn+CO_2$ in 380 cc.

Note that increasing the concentration of the inhibitor did not radically change the production of carbon monoxide and oxygen. This fact was further verified in the pile irradiation experiments.

C. Higher Temperatures

The irradiation of pure carbon dioxide utilizing a small amount of radon at 100°C produced results similar to those obtained at room temperature. Figure 6 indicates the effect of increase in percentage of nitrogen dioxide in the system on production of carbon monoxide and oxygen. Increase in concentration of inhibitor does not radically change the production of carbon monoxide and oxygen. The indicated yield was approximately 3.3 ± 0.2 molecules of carbon dioxide decomposed per ion pair, a G value of 10.

D. Pile Irradiation

Table I summarizes the results of the pile irradiation experiments. The blank vessel indicated 7 microns of

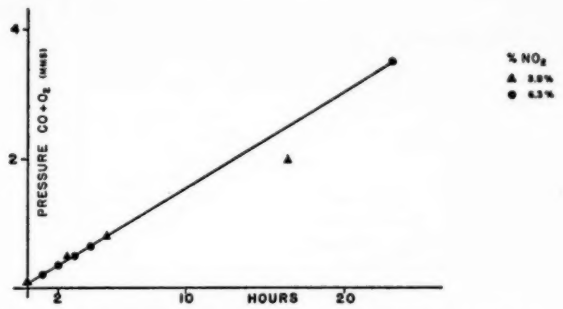

FIG. 5. Formation $CO+O_2$ from $Rn+CO_2+NO_2$ (27°C).

gaseous materials, reflecting the purity of the quartz vessels. In the case of pure carbon dioxide, pile irradiation yielded results similar to those obtained by Lind[1] and ourselves utilizing radon. When nitrogen dioxide was added as an inhibitor, approximately 0.5 percent was sufficient to stop the back reaction to carbon dioxide. From Fig. 7 addition of nitrogen dioxide in concentrations greater than 0.5 percent did not materially increase the decomposition. As an example of the purity of the carbon monoxide and oxygen obtained, the recombination of the mixture under the influence of a glowing platinum wire reached over 99.4 percent. Decomposition of nitrogen dioxide alone yielded nitrogen, oxygen, and nitrous oxide. On strong heating of the quartz vessels after evacuation of all the gases, polymerization products were found in the case of pure carbon dioxide and none in the case where nitrogen dioxide was used. Increase of surface area by a factor of approximately 100 produced no notable radical effect. Thus surface catalysis plays no major part in the formation of carbon monoxide and oxygen when nitrogen dioxide is present. The exact explanation of this surface phenomena is extremely complex and omitted here since it is not of major importance. However, it should be noted from Table I that on irradiation of pure carbon dioxide, oxygen was found when no quartz wool was present, whereas only carbon monoxide was found when the wool was present. With nitrogen dioxide alone, much nitrous oxide was found in addition to some nitrogen when no quartz wool was used, whereas, when quartz wool was used, only a smaller amount of gas was

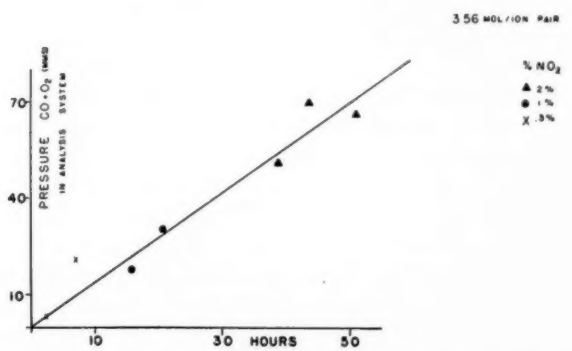

FIG. 6. Formation $CO+O_2$ from $Rn+CO_2+NO_2$ (180°C).

TABLE I. Pile irradiation (at 140°C).

Material irradiated	Sample	Yields as pressure (mm)	
Blank	0	7×10^{-3}	noncondensibles in liquid nitrogen
Nitrogen dioxide	1	26.6	
	2	26.75	as oxygen plus nitrogen
	3	25.5	
	1	16.1	
	2	12.3	as nitrous oxide
	3	11.0	
Carbon dioxide	4	0.125	as oxygen
	5	0.129	
	4	0.113	as carbon monoxide from polymerized products
		0.113	
Carbon dioxide plus (%) nitrogen dioxide	6(0.1 percent)	29.6	as carbon monoxide and oxygen
	7(0.5 percent)	61.4	
	8(2 percent)	66.8	
	(Quartz wool added)		
Carbon dioxide	9	8.2	as carbon monoxide (no O_2)
	9	4.7	as carbon monoxide from polymerized product
Carbon dioxide plus 2 percent nitrogen dioxide	10	79.5	as carbon monoxide and oxygen
Nitrogen dioxide	11	5.1	as nitrogen and oxygen
	11	21.8	as nitrous oxide

obtained (predominantly nitrogen and nitrous oxide). In either case, the oxygen was used up when quartz wool was present. At present we do not know the mechanism of oxygen consumption; however, it seems not to be attributable to the oxidation of possible organic contaminants on the quartz wool.

DISCUSSION

A. Mechanism of Decomposition of Carbon Dioxide

Since the back reaction of carbon monoxide and oxygen proceeds almost quantitatively during the irradiation, a chain type reaction is presupposed. Upon heating the quartz vessels, after the removal of the carbon dioxide, we obtained carbon monoxide from the

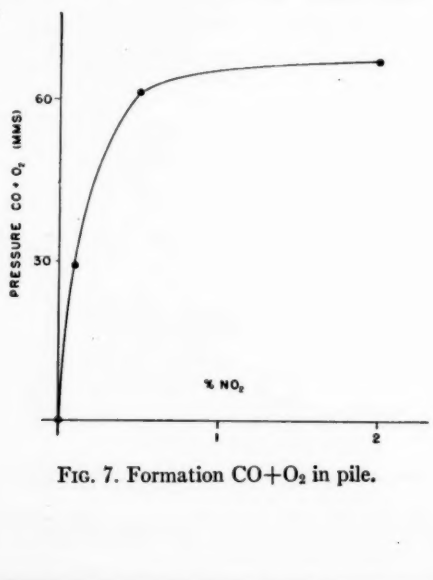

FIG. 7. Formation $CO+O_2$ in pile.

decomposition of the carbon suboxide polymer, $(C_3O_2)_n$, one of the products formed in the irradiation of carbon dioxide by radon.[1] The layer of the polymer on the surface of the quartz was so thin as to be invisible.

The mechanism in Table II, treating only the chemical aspects, seems to explain the principle features of the reaction.[6] This scheme fulfills all the requirements indicated. It has the characteristics of a chain reaction which is initiated as soon as a small amount of carbon monoxide and carbon atoms are present; ensuant formation of C_2O, C_3O_2, (and O_3) thus becomes possible. The C_2O molecules in reactions (6), (6a), and (6b) act as a catalyzer for the reaction of carbon monoxide with oxygen atoms or ozone. The products C_2O and C_3O_2 diffuse partly to the walls and form polymerization products. Thus, a surplus of oxygen should remain in the vessel on irradiation; this result was found experimentally.

The mechanism also indicates that, if carbon dioxide becomes photochemically dissociated into carbon monoxide and oxygen atoms, there will be almost no back reaction.[7] However, if the carbon monoxide produced photochemically also becomes dissociated into carbon and oxygen atoms, then a catalyzed back reaction may take place according to reactions (3) to (7).[8] Reaction (7) is known to be hindered by a small heat of activa-

[6] Hirschfelder and Taylor (see reference 2) and our experimentation indicate that ions are not responsible for the catalytic back reaction. The theoretical aspects of molecular excitation, dissociation, and the behavior of ions, will be published upon conclusion of experimentation in process.

[7] W. Groth, Z. physik. Chem. **B37**, 307 (1937).

[8] Watson, Vanpee, and Lind, J. Phys. & Colloid Chem. 54 391 (1950).

tion, about 2 kcal,[9] as compared with (5), which has no heat of activation.[10] Therefore, carbon dioxide, if photochemically dissociated only into carbon monoxide and oxygen atoms, should form carbon monoxide and oxygen (and ozone) with a quantum efficiency of almost one.[11]

For the decomposition of carbon monoxide alone, Lind and co-workers[12] have found the products; carbon dioxide, carbon suboxide polymers, and carbon, in agreement with the mechanism indicated. They also found, that about 3 molecules of carbon monoxide were chemically decomposed per ion pair, G value about 9. With the energy required per ion pair in carbon monoxide being about 35 electron volts, and with the dissociation energy of carbon monoxide into carbon and oxygen atoms being 11.11 electron volts,[13] three molecules of carbon monoxide could not be primarily dissociated. Their yield can be explained and correlated by the similar mechanisms:

$$CO \rightarrow C+O, \tag{2c}$$

$$C+CO+M=C_2O+M, \tag{3}$$

$$C_2O+CO+M=C_3O_2+M, \tag{4}$$

$$C_3O_2+O=C_2O+CO_2, \tag{6b}$$

$$C \xrightarrow[\text{wall}]{} \text{graphite}, \tag{8a}$$

$$C_2O,\ C_3O_2 \xrightarrow[\text{wall}]{} \text{polymerization products}. \tag{8b}$$

From this mechanism, further consumption of carbon monoxide is required for each carbon monoxide molecule primarily dissociated. Thus, three additional carbon monoxide molecules are consumed by reactions (3), (4), and (6b), or one, by reactions (6b) and (8a).

TABLE II.

	Heat of activation[a] (lower limit)	Coefficients of rates of reactions (particles per cm³)	
$CO_2 \rightarrow$ (a) $CO+O$			(2a)
(b) $C+O+O$			(2b)
$CO+C+M=C_2O+M$	2 kcal	$k_3=5\times10^{-36}$	(3)
$C_2O+CO+M=C_3O_2+M$	2 kcal	$k_4=5\times10^{-36}$	(4)
$O_2+O+M=O_3+M$	0 kcal	$k_5=5\times10^{-34}$	(5)
$C_3O_2+O_3=CO_2+O_2+C_2O$[b]	3 kcal	$k_{6a}=10^{-3}$	(6a)
$C_3O_2+O=CO_2+C_2O$[b]	3 kcal	$k_{6b}=10^{-13}$	(6b)
$CO+O+M=CO_2+M$	2 kcal	$k_7=5\times10^{-36}$	(7)

[a] The values used in reactions (5) and (7) are known; the others are approximated from our results.

[b] It is difficult to perceive whether C_2O or C_3O_2 reacts with ozone or with oxygen atoms.

[9] B. Lewis and G. von Elbe, *Combustion, Flames and Explosions of Gases* (Academic Press, Inc., New York, 1951).

[10] The question of whether a steric factor or a small heat of activation is involved in reaction (7) will be discussed shortly in a forthcoming publication.

[11] See also the discussion of this problem in the paper of Zelikoff and Aschenbrand, J. Chem. Phys. **22**, 1680 (1954).

[12] S. C. Lind, *The Chemical Effects of Alpha Particles and Electrons* (Reinhold Publishing Corporation, New York, 1928).

[13] A. G. Gaydon, *Dissociation Energies* (Dover Publications, New York, 1950).

TABLE III.

Reaction	Heat of activation	
$CO_2 \rightarrow CO_2^+ + e$; 14.4 ev		
$CO_2 \rightarrow$ (a) $CO+O$; 5.57 ev		(2a)
(b) $C+O+O$; 15.00 to 16.68 ev[a]		(2b)
$NO_2+O=NO+O_2$	2 to 4 kcal	(9)
$NO_2+C=NO+CO$	about 5 kcal	(10)
$2NO+O_2=2NO_2$	negative temperature coefficient	(11)

[a] From the heats of dissociation and the ionization energy, more than one molecule of carbon dioxide should be dissociated per ion pair for reaction (2a), and less than one for (2b).

If about one (0.8 to 1.5) molecule of carbon monoxide is primarily dissociated per ion pair,[14] and for one primarily dissociated carbon monoxide molecule, one or three molecules of carbon monoxide are consumed in additional reactions, the results obtained by Lind of 3 molecules of carbon monoxide decomposed per ion pair, are readily explained. This result can be further correlated with Lind's work on the effect of radon on a mixture of carbon monoxide and oxygen.[12]

The effects of radon on condensed carbon dioxide with or without the inhibitor were also interesting. The products produced in both cases were similar to those obtained using one percent nitrogen dioxide in the gas phase irradiation at high temperature. From the above mechanism, only reactions (2a) and (2b) proceed, without occurrence of ensuant reactions (3) to (6b). Reaction (7) may be suppressed by steric hindrance and a small heat of activation. Therefore, the oxygen atoms recombine among themselves to form oxygen molecules or with the carbon atoms to form carbon monoxide. Thus, almost the total amount of previously decomposed carbon dioxide will remain as carbon monoxide and oxygen. A slight amount of condensation product, carbon suboxides was also found. Thus, in the condensed phase at 77°K, about 3 to 3.5 molecules of carbon dioxide became decomposed per 34 electron volts, a G value of 9 to 10.

B. Mechanism when Nitrogen Dioxide is Used as Inhibitor

In utilizing nitrogen dioxide to prevent reforming of carbon dioxide from radicals and atoms, the mechanism in Table III, which treats only the chemical aspects seems to explain the reaction.

Physico-chemical analysis for the products were made approximately two weeks after the samples were removed from the pile, indicating that the gases could remain together at room temperatures for long periods without recombining. This result is normal for a mixture of carbon monoxide, oxygen, carbon dioxide, and nitrogen dioxide and seems to be in agreement with the mechanism shown. Another indication, that of heating

[14] Note that primarily produced excited molecules can contribute to primary decomposition.

the quartz vessels after the evacuation of all gases, failed to show the presence of carbon suboxide polymers on the walls of the vessel. All pile experiments were conducted at about 140°C.[15]

After we used nitrogen dioxide as an inhibitor, the kinetics of the nitrogen dioxide decomposition were investigated. The work is the subject of another paper.[16]

The heat of formation of carbon dioxide from carbon monoxide and oxygen is 2.9 ev. With about 34 ev of energy consumed per ion pair, the limiting M/N values at 140°C lie between three irreversible decomposed molecules for one ion pair (25 percent of the expended energy transformed into chemical energy) and 3.5 decomposed carbon dioxide molecules (30 percent) assuming a homogeneous reactor. A more exact evaluation of the number of molecules decomposed per ion pair is presently being undertaken. It seems to the authors that at the present time this is the largest transformation of radiation energy into chemical energy known.

C. Contributions of Various Ionizing Radiations in the BNL Pile to Chemical Effects

The distribution of fission energy in the pile is[17]: (a) kinetic energy of fission fragments—162 Mev; (b) beta energy—5 Mev; (c) gamma decay energy—5 Mev; (d) neutrino energy—11 Mev; (e) energy of fission neutrons—6 Mev; (f) instantaneous gamma-ray energy —6 Mev. Further gamma energy is derived from the capture of neutrons by all substances within the pile. Of these, in our experimental arrangement, the gamma radiations are predominantly responsible for the ionization and decomposition of the carbon dioxide (see page 904). Other contributors include the "fast" neutrons, which by their elastic collision with carbon dioxide molecules may contribute 10 percent to the ionizing radiation, and beta particles derived from thermal neutron bombardment of the quartz (Si-30), which may contribute a small percentage.

The Brookhaven National Laboratory reactor consists of 60 tons of uranium metal and 700 tons of graphite.[18] It operated at 24 megawatts of power during our experiment. The amount of gamma energy absorbed in the pile by one mole of carbon dioxide is (assuming 10 percent of the total energy developed in the pile is gamma energy)

$$\frac{\text{mass } CO_2}{\text{mass of the reactor}} \times \frac{\text{energy of reactor}}{760\times10^6} \times \text{gamma radiation} = \frac{44}{760\times10^6} \times 24\times10^6 \times 10\times10^{-2}$$

$$= 13.8\times10^{-2} \text{ watt/sec/mole } CO_2.$$

Therefore, the following percentage of the carbon dioxide should be decomposed in 6.7×10^5 seconds, (duration of the experiment) assuming 3 molecules of carbon dioxide decomposed per ion pair:

$$\frac{\text{watt/sec/mole } CO_2}{\text{volts per ion pair}} \times \frac{\text{seconds}}{\text{coulombs per Faraday}} \times \text{No. of molecules dissociated/ion pair} = \frac{13.8\times10^{-2}}{34} \times \frac{6.7\times10^5}{0.964\times10^5} \times 3$$

$$= 8.5 \text{ percent decomposed.}$$

Experimentally, 8.1 percent was found. This result is in fair agreement with our value of 3 carbon dioxide molecules decomposed per ion pair.

Thus, from the power output and the mass of the pile, together with the mass of the sample, it seems possible to reasonably compute the radiation intensity absorbed by the sample without further dosimetry.

This work is being continued.

ACKNOWLEDGMENTS

We would like to thank L. G. Bassett and H. M. Clark for their friendly help and discussions. We would also like to extend thanks to R. F. Van Wye of the Schenectady Office of the U. S. Atomic Energy Commission for assisting in the administrative burdens and especially to M. Fox, R. Powell, J. Floyd, and F. Reeve of the Brookhaven National Laboratory for their invaluable advice and cooperation in the pile experiments.

[15] The effect of the nitrogen dioxide inhibitor in quantitative removal of the oxygen atoms and carbon atoms should not be temperature, intensity, or concentration dependent. This independence was proved in the pile experiments where more than 0.5 percent nitrogen dioxide was present at a temperature of 140°C. However, at room temperature, the effect of nitrogen dioxide is more complex since reaction (10) seems to have a reasonable heat of activation, causing the formation of carbon suboxides and lowering the amount of carbon monoxide and oxygen formed per ion pair. The latter information is from a private communication of A. J. Hogan, Renssalear Polytechnic Institute.

[16] P. Harteck and S. Dondes, J. Chem. Phys. **22**, 953 (1954).

[17] S. Glasstone and W. C. Edlund, *The Elements of Nuclear Reactor Theory* (D. Van Nostrand Company, Inc., New York, 1952).

[18] J. A. Lane, Nucleonics **12**, 4, 12 (1954).

O—O Bond Dissociation Energies in Propionyl and Butyryl Peroxides

A. REMBAUM AND M. SZWARC
Chemistry Department, State University of New York, College of Forestry, Syracuse 10, New York
(Received September 7, 1954)

The kinetics of the decomposition of gaseous propionyl and butyryl peroxides was studied in a flow system. It was found that both compounds decompose in a unimolecular manner. The rate constant for the decomposition of propionyl peroxide is given by the equation

$$k=2.5\cdot10^{14}\cdot\exp(-30\,000/RT),$$

and that for butyryl peroxide by the equation

$$k=1.9\cdot10^{14}\cdot\exp(-29\,600/RT).$$

It is concluded that

$$D(C_2H_5\cdot CO\cdot O-O\cdot CO\cdot C_2H_5)\simeq D(C_3H_7\cdot CO\cdot O-O\cdot CO\cdot C_3H_7)\simeq 30\cdot\text{kcal/mole}.$$

The fates of the ethyl and propyl radicals produced in the decomposition are discussed.

WHILE acetyl peroxide is a notoriously explosive compound, its homologues like propionyl or butyryl peroxide appear to be relatively stable substances. Since the thermal decomposition of all these peroxides is initiated by the O—O bond breaking reaction

$$R\cdot CO\cdot O\cdot O\cdot CO\cdot R\rightarrow 2R\cdot CO_2,$$

one might conclude that the O—O bond dissociation energies in propionyl and butyryl peroxides are higher than that in acetyl peroxide. The latter bond dissociation energy has been determined recently[1] at 29.5 kcal/mole. It was decided, therefore, to extend this work and to determine $D(C_2H_5\cdot CO\cdot O-O\cdot CO\cdot C_2H_5)$ and $D(C_3H_7\cdot CO\cdot O-O\cdot CO\cdot C_3H_7)$ in order to prove or disprove the above assertion.

The results, reported below in this paper, show that within experimental error $D(CH_3\cdot CO\cdot O-O\cdot CO\cdot CH_3)=D(C_2H_5\cdot CO\cdot O-O\cdot CO\cdot C_2H_5)=D(C_3H_7\cdot CO\cdot O-O\cdot CO\cdot C_3H_7)$. Furthermore, it is found that the rate of decomposition of gaseous propionyl peroxide is the same as that of acetyl peroxide while the decomposition of gaseous butyryl peroxide actually proceeds at a slightly higher rate than the decompositions of the former peroxides. Hence, the explosive character of crystalline acetyl peroxide should probably be attributed to the efficiency of the chain reaction initiated by the primary dissociation process, rather than to a lower O—O dissociation energy.

EXPERIMENTAL

Propionyl and butyryl peroxides were prepared by the method described previously[1] for the preparation of acetyl peroxide, starting with propionic anhydride and butyric anhydride respectively. Since these peroxides could not be crystalized from ether solutions, even at −80°C, they were purified by distillation at room temperature in high vacuum. The finally purified compounds crystallized easily when cooled to −80°C, and by titration of weighed samples they were found to be at least 99 percent pure.

The kinetic studies were carried out in an apparatus shown in Fig. 1. One or two cc of a 0.3M solution of the peroxide in toluene were pipetted into tube U. The solution was then frozen by surrounding tube U with a liquid-air bath, and the apparatus was evacuated to a pressure lower than 10^{-4} mm Hg. After evacuation the liquid-air bath was replaced by a water bath kept at a constant temperature, and simultaneously the stopcock 1 was opened. By choosing different temperatures of the water bath,* it was possible to vary at will the partial pressure of the peroxide in the reaction vessel.

The experiment was initiated by opening stopcock 1. By this operation flask H, containing previously deaerated toluene or benzene, was connected with the pumping system and the carrier gas (i.e., toluene or benzene vapor) began to flow through the apparatus. The flow was continued until the solution in tube U had completely evaporated.

The peroxide vapor, picked up by the carrier gas, flowed through the reaction vessel maintained at a temperature constant within ±0.1°C. The variation of temperature along the reaction vessel was not greater than ±0.75°C, and a special correction was introduced to take care of this nonhomogeneous temperature distribution. The temperature was measured to an accuracy better than 0.1°C by means of a thermocouple and a potentiometer. The reading of the latter was standardized with the help of a precision thermometer calibrated by the National Bureau of Standards.

The vapor of the undecomposed peroxide and of the carrier gas was condensed in trap T_1, cooled to −80°C, while the gaseous products of the decomposition were pumped into a storage volume by means of two mercury vapor pumps (I and II). The rate of decomposition was measured by the rate of formation of carbon dioxide, 2 moles of which are formed for each mole of peroxide

[1] A. Rembaum and M. Szwarc, J. Am. Chem. Soc. **76**, 5975 (1954).

* The temperature of the water bath was never higher than 40°C in order to prevent the decomposition of the solution during the evaporation process.

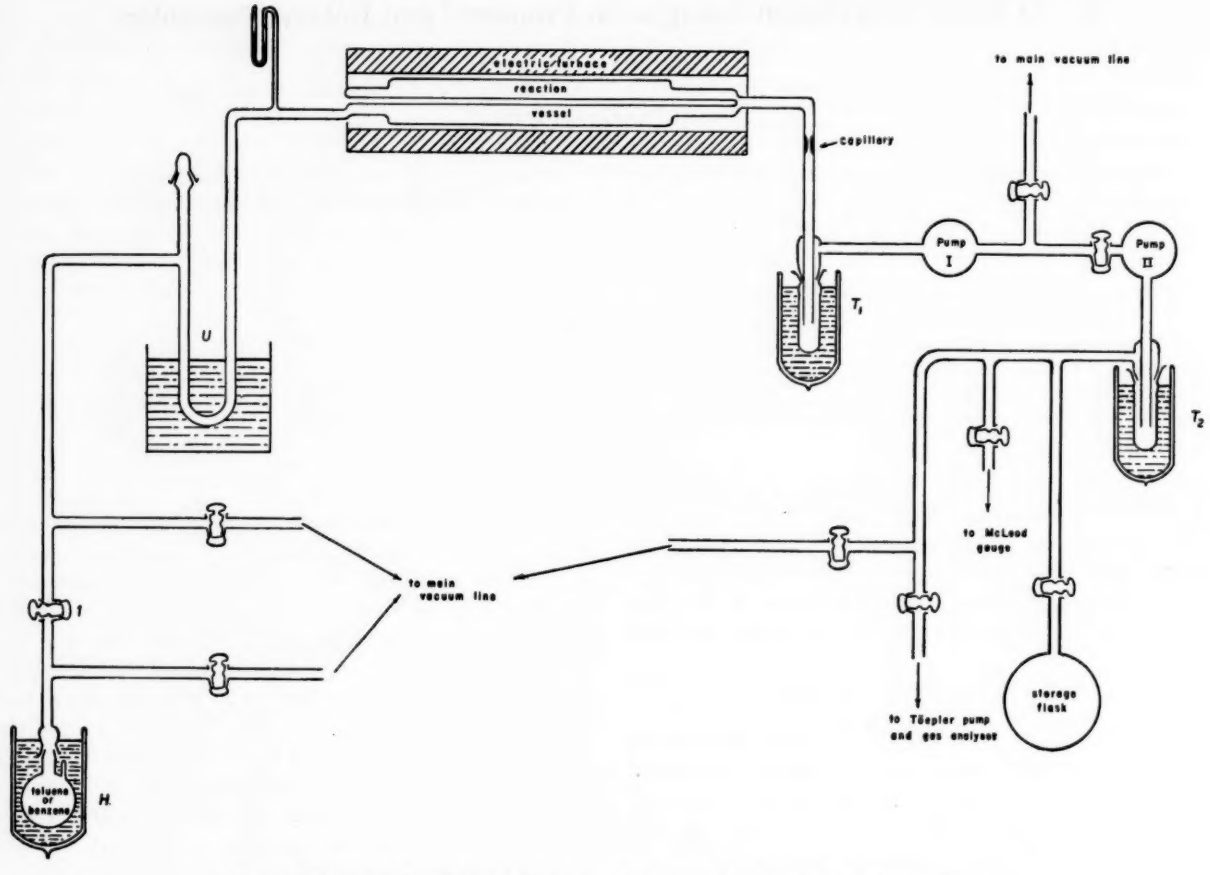

FIG. 1. The O—O bond dissociation energies in propionyl and butyryl peroxides.

decomposed. This stoichiometric relation was proved for each peroxide, by carrying the decomposition of a known amount of the compound to completion and determining the amount of carbon dioxide formed. Typical results of such experiments are given in Table I. To obtain further confirmation for this relationship, the percentage of decomposition was determined by titrating the amount of the undecomposed peroxide collected in trap T_1. This result was then compared with the value obtained on the basis of the amount of carbon dioxide produced. The relevant data are listed in Table II.

RESULTS

The decomposition of propionyl and butyryl peroxide was studied over the temperature range 130°–250°C. It was shown that butane and carbon dioxide are the products of decomposition of propionyl peroxide, and that hexane† and carbon dioxide are the main products of decomposition of butyryl peroxide. Analysis of the gases condensable at liquid-air temperature, showed that the decomposition of propionyl peroxide yields a mixture containing 66–70 percent‡ of carbon dioxide, while the decomposition of butyryl peroxides yields a mixture containing about 90 percent of carbon dioxide. The condensable gases collected in the pyrolysis of propionyl peroxide, after being freed from CO_2, were analyzed by means of a mass-spectrograph and their composition was found as follows: C_2H_4—8.4 percent, C_2H_6—8.6 percent, n-C_4H_{10}—80.9 percent. It follows from this observation that about 90 percent of ethyl radicals, produced by the decarboxylation of $C_2H_5 \cdot CO_2$ radicals§ dimerise, the remaining 10 percent undergoing disproportionation. On the other hand, since hexane produced in the pyrolysis of butyryl peroxide is condensed completely in trap T_1, the condensable gas should contain carbon dioxide only if no disproportionation takes place. The presence of 10 percent of

TABLE I.

Compound	T°C	Peroxide introduced millimoles	CO_2 collected millimoles	CO_2 / peroxide
Propionyl peroxide	241	0.136	0.280	2.06
Propionyl peroxide	253	0.136	0.278	2.04
Butyryl peroxide	235	0.142	0.286	2.02

† Hexane was isolated and identified in separate experiments, in which CO_2 was used as a carrier gas.

‡ Small amounts of butane were probably condensed in trap T_1. This is presumably the reason for finding in some cases a slightly higher percent of CO_2 than 66.7 percent.

§ It is not possible to refute the suggestion that butane results from the reaction $2C_2H_5 \cdot CO_2 \rightarrow C_4H_{10} + 2CO_2$.

other gases indicates, therefore, that some disproportionation actually takes place, and it is found again that the probability of the latter is about $\frac{1}{9}$ of the probability of dimerization. Since no permanent gases (noncondensable in liquid-air trap) are formed in the pyrolysis of butyryl peroxide, it may be concluded that the reaction

$$C_3H_7 \rightarrow C_2H_4 + CH_3$$

is much slower than the dimerization. Approximate calculation shows that this conclusion is plausible.

The rate of the decomposition was measured by the rate of formation of carbon dioxide. It was found that this method is more reliable than the alternative method based on the titration of the undecomposed peroxide; moreover, the latter method fails entirely when one tries to determine low percentages of decomposition.

The kinetic studies showed that the decomposition of both propionyl and butyryl peroxide are first-order reactions. The relevant data are collected in Tables III and IV, inspection of which shows that the first-order rate constants are not affected either by the variation

TABLE II.

Compound	Percent decomposition based on titration	Percent decomposition based on CO_2
Propionyl peroxide	40.5	42.6
Propionyl peroxide	53.6	54.9
Propionyl peroxide	59.0	58.6
Propionyl peroxide	55.3	54.1
Propionyl peroxide	62.3	63.3
Propionyl peroxide	54.7	56.1
Butyryl peroxide	58.6	59.0
Butyryl peroxide	27.6	30.4
Butyryl peroxide	57.0	56.0
Butyryl peroxide	60.4	58.7

of the partial pressure of the peroxide or by the change of time of contact.‖ The plots of log of the rate constants against reciprocals of temperature are presented in Fig. 2, and for the sake of comparison we plotted the results obtained for acetyl peroxide on the same graph. These graphs show the high reproducibility of the results and confirm again the first-order character of the reaction.

TABLE III. Decomposition of propionyl peroxide.

$T°K$	P_{total} mm Hg	$P_{peroxide}$ mm Hg	Time of contact sec	Percent decomp.	k sec^{-1}
372.7	20.6	0.270	39.4	3.2	0.0008
373.7	20.1	0.274	35.7	3.5	0.0010
381.2	19.0	0.298	41.0	7.2	0.0018
407.7	13.4	0.065	0.79	2.0	0.026
408.7	12.6	0.063	0.70	2.3	0.030
409.2	13.3	0.064	0.74	2.4	0.031
410.9	22.3	0.305	21.6	51.1	0.033
411.0	13.3	0.068	0.78	2.9	0.038
411.5	13.2	0.067	0.78	2.8	0.037
416.7	13.5	0.047	0.74	4.2	0.058
425.5	13.1	0.071	0.75	8.1	0.113
425.5	13.2	0.072	0.76	8.8	0.122
429.0	13.4	0.072	0.76	11.5	0.160
430.0	12.5	0.067	0.71	12.0	0.180
443.2	13.0	0.068	0.72	27.1	0.454
449.0	13.4	0.055	0.73	43.5	0.78
449.7	12.5	0.052	0.70	42.6	0.80
449.9	13.1	0.054	0.73	45.1	0.82
451.5	10.5	0.134	0.94	55.2	0.85
451.7	14.0	0.055	0.73	54.9	1.09
452.0	10.2	0.143	0.91	58.6	1.08
452.4	13.6	0.066	0.71	54.1	1.10
452.5	13.0	0.041	0.65	50.8	1.09
454.0	8.8	0.105	0.94	63.3	1.16
454.2	13.3	0.047	0.69	56.1	1.20
454.3	7.6	0.054	0.27	27.7	1.13
455.5	13.2	0.052	0.68	58.0	1.34
464.2	13.8	0.088	0.76	83.0	2.33

TABLE IV. Decomposition of butyryl peroxide.

$T°K$	P_{total} mm Hg	$P_{peroxide}$ mm Hg	Time of contact sec	Percent decomp.	k sec^{-1}
370.0	20.9	0.210	41.2	3.5	0.00086
370.0	19.9	0.128	36.8	3.3	0.00091
371.1	20.0	0.146	34.5	3.2	0.00094
395.5	21.0	0.015	22.42	24.7	0.013
398.0	20.1	0.016	24.0	26.2	0.013
400.7	19.8	0.023	29.9	37.6	0.015
406.2	8.5	0.054	1.02	3.0	0.030
407.2	8.6	0.058	1.04	3.1	0.031
409.2	7.9	0.050	0.94	3.6	0.039
417.1	12.0	0.026	0.71	5.4	0.079
432.2	13.1	0.027	0.71	19.2	0.300
440.1	13.6	0.029	0.75	30.4	0.480
441.0	12.7	0.027	0.70	31.6	0.540
448.7	8.5	0.061	0.93	58.7	0.95
449.0	8.5	0.061	0.92	58.8	0.96
450.5	8.3	0.048	0.90	63.7	1.13
451.1	12.9	0.027	0.70	56.0	1.17
451.2	13.1	0.030	0.71	55.6	1.14
451.3	12.6	0.027	0.68	56.6	1.22
452.2	12.8	0.030	0.69	58.7	1.27

‖ We have to discuss at some length the methods used in calculation of the first-order rate constants from experimental data. In experiments in which the time of contact is short (less than 1 sec), and the rate of flow is rapid, the diffusion processes are of minor importance. In such cases, the flow can be considered as essentially laminary and the rate constant k would be computed from the experimentally observed fraction of decomposition f by applying the formulas

$$k=\frac{1}{t}\ln(1-f)^{-1},$$

t—denoting the time of contact. However, if the time of contact is very long (20–30 sec), the diffusion processes might affect considerably the rate of reaction. In the extreme case, one should consider the reaction vessel as a stirred reactor which is supplied continuously with the substrate and from which the products are continuously removed. If this is the case, then the unimolecular rate constants should be computed by means of the formulas

$$k=\frac{1}{t}\cdot f.$$

One may easily verify that both formulas give essentially the same numerical answers for $f<0.03$ (i.e., for a decomposition not exceeding 3 percent), however, a substantial discrepancy arises for higher fraction of decomposition. In order to obtain some idea about the magnitude of this discrepancy, we used both formulas in computing the rate constants derived from two experiments carried out with butyryl peroxide at very low temperature and long time of contact. The results are denoted in Fig. 2 by pairs of squares connected by a solid line. Those two experiments are the only ones for which the problem of computation is essential.

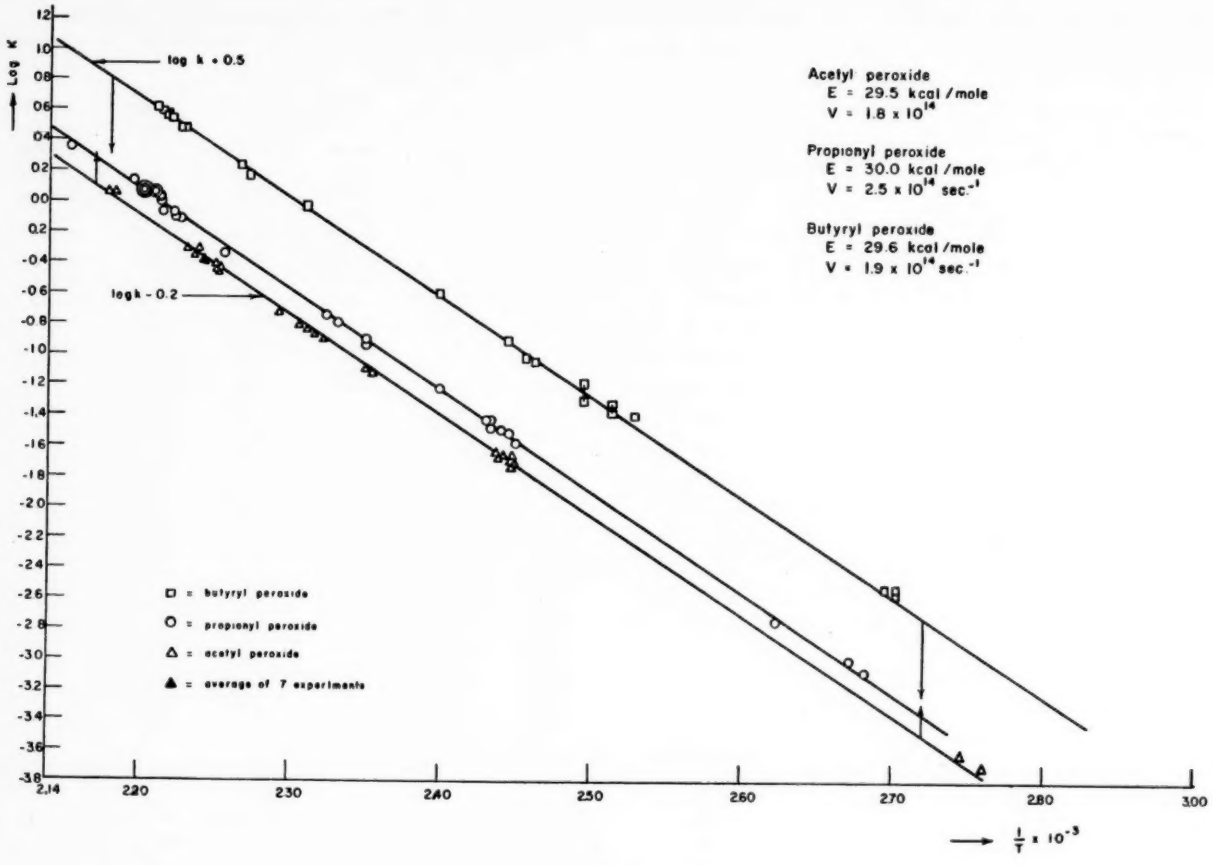

FIG. 2.

From the Arrhenius plots we calculate by the least-square method the activation energies for the decompositions of propionyl and butyryl peroxides at 30.0 and 29.6 kcal/mole respectively. These values are uncertain within experimental errors lower than ±0.5 kcal/mole. The frequency factors are $2.5 \cdot 10^{14}$ sec^{-1} and $1.9 \cdot 10^{14}$ sec^{-1} respectively.

DISCUSSION

The mechanism of decomposition of acyl-peroxides is well established. It involves the following three elementary reactions:

$$R \cdot CO \cdot O \cdot O \cdot CO \cdot R \rightarrow 2R \cdot CO_2 \quad (1)$$

$$R \cdot CO_2 \rightarrow R + CO_2 \quad (2)$$

$$R + R \rightarrow \text{products} \quad (3)$$

of which the first one is rate determining. Our present observations provide us with the activation energies and frequency factors of reaction (1) for $R = C_2H_5$ and $R = C_3H_7$. Introducing the usual assumption that the reverse of reaction (1) does not require any activation energy, we conclude that $D(C_2H_5 \cdot CO \cdot O \cdot O - O \cdot CO \cdot C_2H_5) \approx D(C_3H_7 \cdot CO \cdot O - O \cdot CO \cdot C_3H_7) \approx 30$ kcal/mole. This value should be compared with

$$D(CH_3 \cdot CO \cdot O - O \cdot CO \cdot CH_3) = 29.5 \text{ kcal/mole}$$

found in previous studies.[1] Hence, we conclude that the O—O bond dissociation energy is essentially independent of the length of the hydrocarbon chain R. This result is plausible, since the structural changes in the peroxides investigated involve centers which are separated at least by two atoms from the site of reaction.

The fact that 2 moles of CO_2 are obtained from each mole of peroxide decomposed proves that the reaction

$$(R \cdot CO_2)_2 \rightarrow R \cdot CO \cdot O \cdot R + CO_2$$

does not take place in the gaseous phase. Similar observations lead to the same conclusions with respect to the decomposition of gaseous acetyl peroxide.[1]

Comparison of kinetics of decomposition of acetyl peroxide in gaseous phase and in solutions[2] lead to the conclusion that the effect of a solvent on the activation energy of the process originates most probably from the different probabilities of the cage recombination at various temperatures. It is argued that the activation energy of a *homolytic* bond rupture is not significantly affected by the presence of a solvent, since the molecules

[2] Levy, Steinberg, and Szwarc, J. Am. Chem. Soc. **76**, 5978 (1954).

of the latter are too far from the site of the reaction (i.e., from the O—O group). Our present results offer further support to this argument, showing that even a modification of the molecule does not affect considerably the activation of the homolytic process, provided that the constitutional changes take place sufficiently far from the reacting center.

In conclusion, we would like to thank the National Science Foundation for the financial support of this investigation.

THE JOURNAL OF CHEMICAL PHYSICS VOLUME 23, NUMBER 5 MAY, 1955

Statistical Computation of Mean Dimensions of Macromolecules. II*

F. T. WALL, L. A. HILLER, JR., AND W. F. ATCHISON
Noyes Chemical Laboratory, University of Illinois, Urbana, Illinois
(Received September 10, 1954)

Random walks subject to the excluded volume effect have been generated by means of a high-speed electronic digital computer for four different two-dimensional lattices. A semiempirical theory has also been developed for interpreting the statistical data. From the results obtained it is possible to show for several two-dimensional lattices that the quotient, $\langle r_n^2\rangle_{Av}/n$, diverges as $n\rightarrow\infty$, where $\langle r_n^2\rangle_{Av}$ is the mean square length of permissible walks of n steps. This conclusion was reached by using an appropriate difference equation in conjunction with data on the mean square lengths of successful walks and the mean square lengths of failures resulting from ring closures. Integration of that difference equation indicates that if n is sufficiently large, $\langle r_n^2\rangle_{Av}$ is proportional to n^A, where A depends upon the lattice system.

INTRODUCTION

IN a previous publication from this laboratory,[1] there was described the generation of restricted random walks by means of a high-speed electronic digital computer. Similar work has been reported by Rosenbluth and Rosenbluth[2] with results in agreement with our own. Earlier, G. W. King[3] used IBM punched-card methods in an attack upon this problem. Teramoto and Kurata[4] have also investigated the statistical problem by hand calculations, which work was necessarily restricted to relatively short chains.

A restricted random walk is defined as a walk in a given lattice that does not involve double occupancy of any lattice site; hence, these walks are said to be subject to the "excluded volume effect." Since no two chain units of a flexible long-chain polymer molecule can occupy the same volume element in space, a restricted random walk provides a convenient model for describing the mean dimensions of polymers. It is our ultimate objective to establish a relationship between the mean-square end-to-end separation of a polymer chain and the number of links in the chain. This mean-square length will be denoted by $\langle r_n^2\rangle_{Av}$, where n is the number of steps or links in the chain.

A question still unanswered concerns the behavior of the quotient $\langle r_n^2\rangle_{Av}/n$ as $n\rightarrow\infty$. Both convergence and divergence of this ratio have been predicted for three dimensions, but there is a general feeling that it diverges in two and converges in four dimensions, although we shall see later that the number of dimensions alone may not be determinative.

We have now generated restricted random walks for a variety of lattice systems in two, three, and four dimensions to investigate both the effect of the number of dimensions and of the lattice system on the behavior of the above mentioned quotient. In the present article we shall discuss our results for several two-dimensional lattices and will formulate theoretical considerations for their interpretation. The results for three and four dimensions will be published in a future article.

It was shown previously[1] that the fraction of the starting number of samples remaining after n-steps, N_n, decreases exponentially with increasing n. This attrition of samples is so large that it is virtually impossible to obtain reliable data for n greater than about 80 for most lattices. Consequently, the direct examination of the functional dependence of $\langle r_n^2\rangle_{Av}/n$ on n is not practical.

The two-dimensional lattices which we have treated are the following: (a) the two-choice 90° lattice, (b) the three-choice 90° lattice, where the step angle may be either 90° or 180°, (c) the two-choice 120° lattice, and (d) the five-choice 60° lattice, where the step angle may be 60°, 120°, or 180°. These are shown in Fig. 1. The last three lattices are really equivalent to four-choice, three-choice, and six-choice systems, respectively, since the mathematical analysis of the results is simplified by making the average of the trial vectors equal to zero,

* The work discussed herein was supported in part by the research project sponsored by the Reconstruction Finance Corporation in connection with the Government Synthetic Rubber Program.

[1] Wall, Hiller, and Wheeler, J. Chem. Phys. **22**, 1036 (1954).

[2] M. N. Rosenbluth and A. W. Rosenbluth, J. Chem. Phys. **23**, 356 (1955).

[3] G. W. King, Natl. Bur. Standards, Appl. Math. Ser. AMS 12 (June 11, 1951).

[4] E. Teramoto and M. Kurata, Kyoto University, private communication.

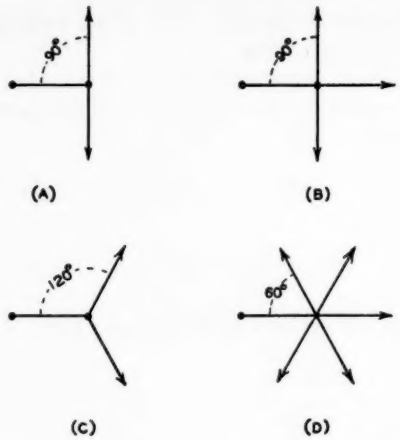

FIG. 1. Representation of experimental two-dimensional lattices: (a) two-choice 90° lattice, (b) three-choice 90° lattice, (c) two-choice 120° lattice, (d) five-choice 60° lattice.

thus implying the possibility of trying to step backwards. Since a backward step is certain to fail, it can be directly eliminated from the machine computations without effect on mean-square distance data. However, the effect of a backward step on attrition and ring-closure probabilities can be easily calculated and incorporated into the theoretical analysis.

The restricted random walks were generated using the ILLIAC electronic digital computer by methods already described.[1] The computation code was altered for each lattice to insure the desired number of choices and the proper angular relationships between successive vectors. The following data were obtained: (a) the total number of samples, N_n, remaining at step n, (b) the mean-square lengths of allowable walks, $\langle r_n^2\rangle_{Av}$, at step n, (c) the number of single-ring closures of each possible size, k, at each step n, and (d) the mean-square distances of these ring closures from the point of closure back to the origin. The last were desired since a knowledge of the relationship between the mean-square distances of successful walks and of ring closures is necessary for solving a significant difference equation to be derived later.

Because of the limitations of the memory capacity of the computer, all random walks in our present group of lattices were terminated at $n=50$. At least 200 000 walks were generated for each lattice; because of the high attrition in the two-choice square lattice, 650 000 walks were generated in this case.

In addition to the above, the randomness of the successive vector selection was examined. To select successive vectors, a random number such as 0.1π rounded off to 39 binary digits is stored in the computer. This number is multiplied by 7 to obtain a new number. If the integral part of this new number is 0, 1, 2, or 3 (for example, in a four-choice lattice), it is used to choose the next vector in a walk. If the integer is 4, 5, or 6 (in the same example), it is rejected. To obtain a new integer, the integral part of the previous product is rejected and the remainder is multiplied by 7. On each machine run a different random 39 binary digit number is used at the start.

To examine the randomness of this process, a selection of numbers was carried out on the computer using the method described above for a total of 840 000 trials, which is greater than the total number of trials made in any run. At each step the nonintegral part of the product was compared to the original number to see whether a cycle had been set up. The original number never recurred in the test. In addition, the integers, 0, 1, 2, and 3 each occurred about 120 000 times as expected since the probability for obtaining any one of these numbers is one-seventh.

ATTRITION

The attrition in a restricted random walk can be expressed as follows[1]:

$$N_n = N_0 \exp(-\lambda n). \tag{1}$$

Since Eq. (1) does not fit the data for low values of n, N_0 is an extrapolated value for $n=0$ and is greater than N_{initial}, the actual number of starting samples used. The parameter, λ, is called the attrition constant. Graphs of $\log(N_n/N_{\text{initial}})$ *versus* n for the several lattices are shown in Fig. 2.

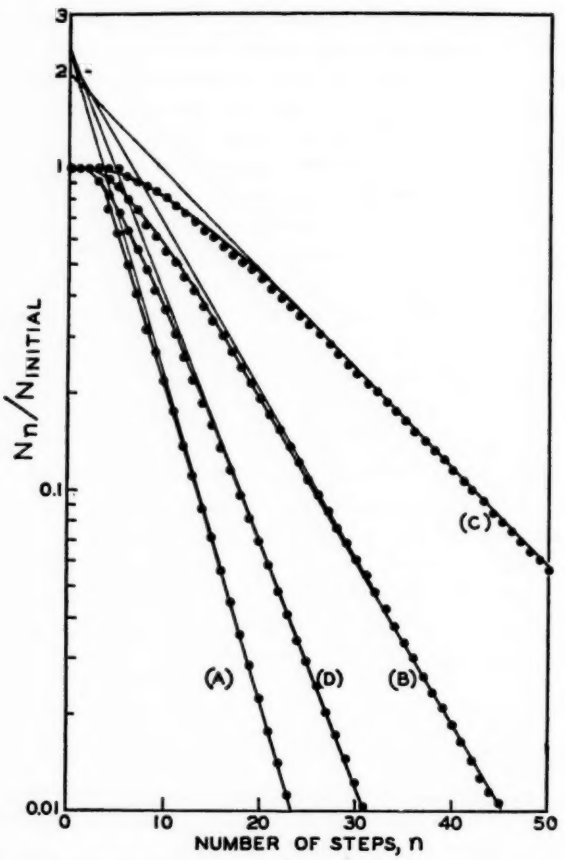

FIG. 2. Attrition in two-dimensional lattices: (a) two-choice 90° lattice, (b) three-choice 90° lattice, (c) two-choice 120° lattice, (d) five-choice 60° lattice.

TABLE I. Attrition in two-dimensional lattices.

Lattice	λ	$1-\exp(-\lambda)$	$n_{\frac{1}{2}}$	N_0/N_{initial}
Experimental Lattices				
(a) 2-choice 90°	0.226	0.202	3.07	2.20
(b) 3-choice 90°	0.119	0.112	5.83	2.17
(c) 2-choice 120°	0.071	0.069	9.76	2.00
(d) 5-choice 60°	0.174	0.160	3.98	2.23
Lattices Corrected for Backward Step				
Lattice	λ^*	$1-\exp(-\lambda^*)$	$n_{\frac{1}{2}}^*$	N_0^*/N_{initial}
(a) 2-choice 90°	0.226	0.202	3.07	2.20
(b) 4-choice 90°	0.408	0.334	1.71	2.50
(c) 3-choice 120°	0.477	0.379	1.44	2.33
(d) 6-choice 60°	0.357	0.300	1.96	2.75

Except for small values of n, straight-line relationships are obtained for each lattice when $\log(N_n/N_{\text{initial}})$ is plotted *versus* n. Thus the form of Eq. (1) appears to be unaffected by lattice structure. The constants for Eq. (1) are given in Table I. The values for $1-\exp(-\lambda)$ represent the fractions of samples lost at each step. The "half-walk," $n_{\frac{1}{2}}$, is the number of steps required to reduce the samples by one-half. N_0/N_{initial} was obtained by extrapolation to $n=0$.

As mentioned previously, for all lattices except the two-choice 90° system, the backward step must be included if angular symmetry is to exist. This backward step increases the true attrition considerably because the probability for terminating a walk by a backward step will be $\frac{1}{4}$, $\frac{1}{3}$, and $\frac{1}{6}$ for lattices (b), (c), and (d). The attrition arising by inclusion of this backward step is readily calculated as follows.

Since $1-\exp(-\lambda)$ is the probability for failure, then

$$1-\exp(-\lambda^*)=p_2^*+(1-p_2^*)[1-\exp(-\lambda)] \quad (2)$$

where λ^* is the corrected attrition parameter for the complete lattice, and p_2^* the probability for selecting the backward step. The attrition parameters (λ^*) for what we shall call the four-choice 90° lattice, the three-choice 120° lattice and the six-choice 60° lattice are also given in Table I.

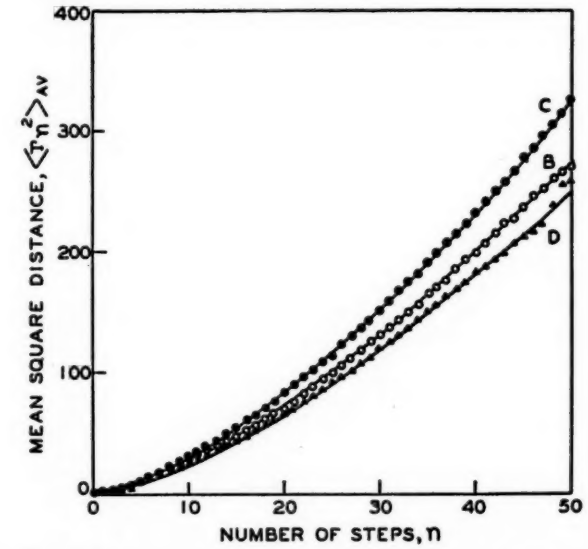

FIG. 3. Mean-square end-to-end distances in two-dimensional lattices: (b) three-choice 90° lattice, (c) two-choice 120° lattice, (d) five-choice 60° lattice. The two-choice 90° lattice, (a), is not shown since it very closely resembles the plot of the 60° lattice, (d).

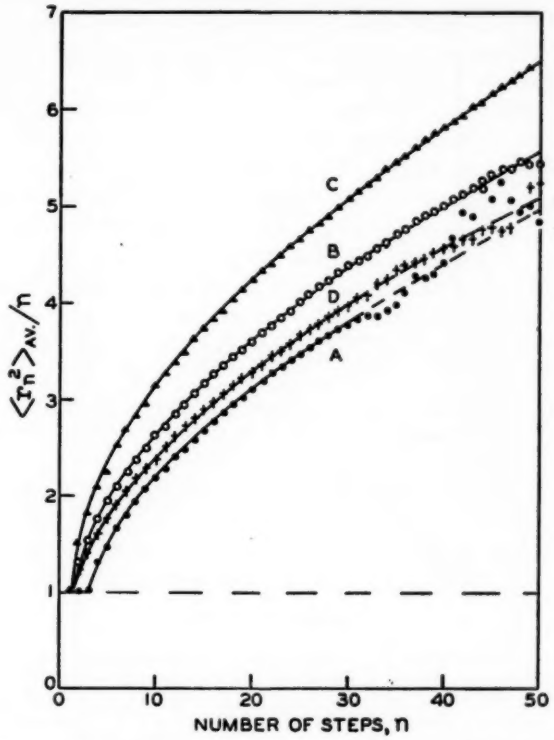

FIG. 4. Plot of $\langle r_n^2\rangle_{AV}/n$ *versus* n for two-dimensional lattices: (a) two-choice 90° lattice, (b) three-choice 90° lattice, (c) two-choice 120° lattice, (d) five-choice 60° lattice.

MEAN-SQUARE DISTANCES OF PERMISSIBLE RESTRICTED RANDOM WALKS

The mean-square distances of permissible restricted random walks are plotted *versus* n in Fig. 3. These experimental data are also plotted in the form of $\langle r_n^2\rangle_{AV}/n$ *versus* n in Fig. 4. It is observed that the deviation of the ratio from unity, i.e., from that predicted for an unrestricted random walk, begins with the steps at which failures first become possible, that is, at $n=2$ except for the orthogonal two-choice lattice, for which the departure begins at $n=4$.

It was shown previously,[1,2] that when the log of the mean-square distances of successful walks are plotted against log n, one obtains straight lines over a wide range of the experimental data. Therefore an equation of the form

$$\langle r_n^2\rangle_{AV}=an^b \quad (3)$$

can be used to fit the data. For three-dimensional lattices, $b=1.22$ with a depending on the lattice structure. It was also pointed out[1] that Eq. (3) cannot be relied upon for describing $\langle r_n^2\rangle_{AV}$ as $n\to\infty$.

Log-log plots of the kind described above can also be made for the two-dimensional lattices with similar

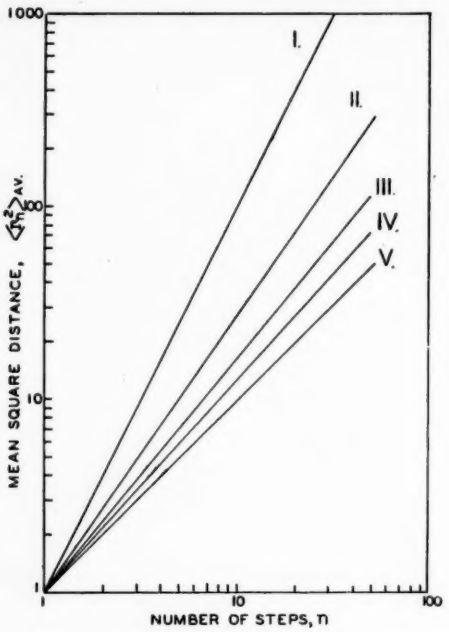

FIG. 5. Plot of log $\langle r_n^2 \rangle_{Av}$ *versus* log n. I. One-dimensional linear lattice (slope=2.00). II. Typical two-dimensional lattice (slope =1.45). III. Typical three-dimensional lattice (slope=1.22). IV. Typical four-dimensional lattice (slope=1.11). V. Unrestricted random walk (slope=1.00).

results (Fig. 5). Values of b for the different lattices are shown in Table II. The exponent b ranges from 1.42 to 1.49 with an average of 1.45 for the four two-dimensional lattices investigated. For comparison, graphs corresponding to the two-choice linear one-dimensional lattice, a three-dimensional and a four-dimensional lattice and an unrestricted random walk have also been included in Fig. 5. (The three- and four-dimensional data will be discussed in a subsequent paper.) It is observed that the slope decreases with the number of dimensions, thus indicating an approach toward the unrestricted random walk.

MEAN-SQUARE LENGTHS OF RING CLOSURES

As mentioned previously, each time a random walk was found to have returned to a lattice site previously occupied during the walk, the particular step on which this occurred was recorded as a failure and the walk was terminated. These failures gave rise to loop closures, the size and frequency of which depend upon the lattice structure. In addition to studying the frequency with which these loop closures occurred, the mean-square distance from the point of closure to the origin was determined. The mean-square length of failures resulting from ring closures of k-steps occurring at the nth step, will be denoted by $\langle {}_kR_n^2 \rangle_{Av}$. This quantity will bear some resemblance to the mean-square length between the origin and the points corresponding to $n-k$ as shown in Fig. 6. However, $\langle {}_kR_n^2 \rangle_{Av}$ will not generally equal $\langle r^2{}_{n-k} \rangle$. In Fig. 7, the mean-square lengths of successful walks and of failures resulting from ring closures are plotted *versus* n for the three-choice square lattice. The results obtained for the other lattices are quite similar to these and will not be considered separately. It is observed that the failure distances follow the same general pattern as the successful walk distances, except that the failure distances are always shorter for a given value of n. Sample losses cause these data to become more scattered as both n and k increase.

It might be assumed that the mean-square lengths of ring closures, $\langle {}_kR_n^2 \rangle_{Av}$ would be equal to the mean-square lengths of permissible walks to step $n-k$, namely $\langle r^2{}_{n-k} \rangle_{Av}$. This hypothesis can be tested by plotting $\langle r_n^2 \rangle_{Av}/n$ *versus* n for the successful walks and $\langle {}_kR_n^2 \rangle_{Av}/(n-k)$ *versus* $n-k$ for the failures, as shown in Fig. 8. The data so plotted refer to the three-choice square lattice and the failures all correspond to rings of size $k=4$. Plots for larger rings are similar but have been omitted to avoid confusion. It is observed that values for $\langle {}_4R_n^2 \rangle_{Av}/(n-4)$ clearly exceed those for $\langle r_{n-4}^2 \rangle/(n-4)$ demonstrating that the mean-square lengths of permissible walks at the $(n-k)$th step cannot be substituted for $\langle {}_kR_n^2 \rangle_{Av}$. This conclusion appears entirely reasonable since the curled-up short configurations fail more frequently than the extended configurations as the number of steps is increased from $n-k$ to n. This means that the failures at n should on the average be longer than the successes at $n-k$.

The most useful plot of the mean-square lengths of ring closures is shown in Fig. 9, in which $\langle {}_kR_n^2 \rangle_{Av}$ is plotted against k, for constant values of n. It is observed that essentially linear plots are obtained except for

TABLE II. Parameters for log-log plot of $\langle r_n^2 \rangle$ *vs* n.

Lattice	Intercept	Slope	Average slope
(a) 2-choice 90°	0.7	1.49	1.45
(b) 3-choice 90°	1.0	1.45	
(c) 2-choice 120°	1.1	1.45	
(d) 5-choice 60°	0.9	1.42	

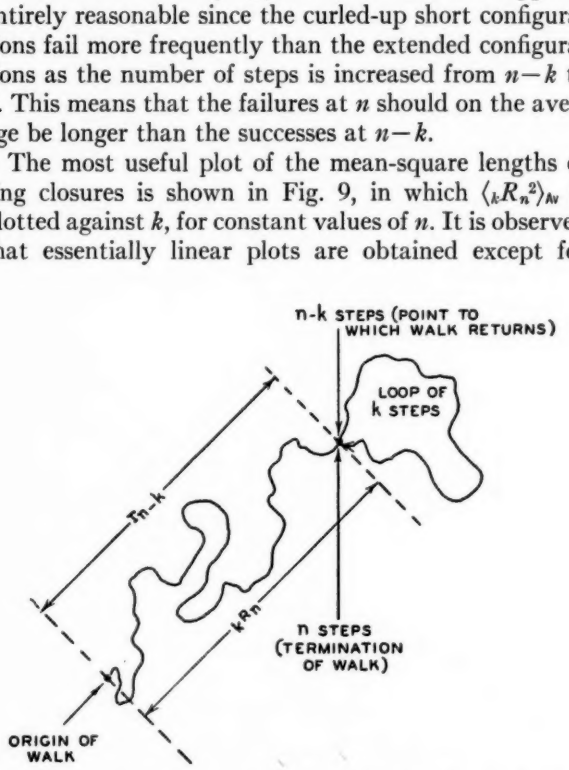

FIG. 6. Schematic representation of a restricted random walk of n-steps closing a loop of k-steps.

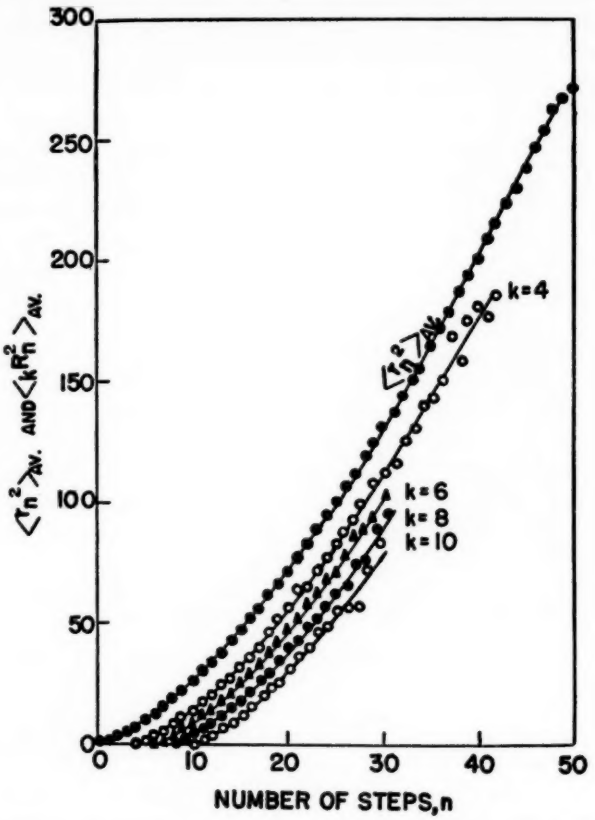

FIG. 7. Plots of mean-square distances of successful walks $\langle r_n^2\rangle_{Av}$ and of ring closures $\langle {}_kR_n^2\rangle_{Av}$ for $k=4$ to 10 *versus* number of steps. All data apply to three-choice 90° lattice.

departures when k becomes nearly equal to n. The deviation in this region is not surprising since ring closures at the origin are atypical. If these graphs are extrapolated to $k=0$, the limiting values so obtained agree well with the mean-square lengths of successful walks; hence, it appears that a simple relationship between $\langle {}_kR_n^2\rangle_{Av}$ and $\langle r_n^2\rangle_{Av}$ exists. Since a straight line can be drawn connecting $\langle r_n^2\rangle_{Av}$ to the point $n=k$ with ordinate values never less than $\langle {}_kR_n^2\rangle_{Av}$, aside from random scatter, we can write that

$$\langle {}_kR_n^2\rangle_{Av} \leqslant \langle r_n^2\rangle_{Av}\left[1-\frac{k}{n}\right]. \tag{4}$$

If it is further assumed that the straight lines in Fig. 9 extrapolate to a value $n-\delta$ on the horizontal axis, then Eq. (4) can be written more precisely in the form:

$$\langle {}_kR_n^2\rangle_{Av}=\langle r_n^2\rangle_{Av}\left[1-\frac{k}{n-\delta}\right]. \tag{5}$$

Equation (5) is quite accurate except, of course, for values of k nearly equal to n.

DIFFERENCE EQUATION FOR RESTRICTED RANDOM WALKS

Consider any distribution of vectors, each vector obtained by successive addition of a set of $n-1$ unit vectors to form a sequential random walk. If we now add unit vectors in every possible direction to the growing ends of all the vectors in this distribution, then the mean-square over-all length of the vectors will be increased by unity, provided the average of all the vectors added to equal is zero. This will be shown in the case of a four-choice orthogonal planar lattice, but the proof is easily extended to other lattices.

If any given vector terminates at position (x,y) in this lattice, then the four new possible positions are $(x\pm1, y)$ and $(x, y\pm1)$. The four new possible square lengths are $x^2\pm2x+1+y^2$ and $x^2+y^2\pm2y+1$, whose average is x^2+y^2+1. This happens for every position; hence, the mean-square length of the walks is increased by unity. We can now apply this proposition to restricted random walks. Thus, if p is the probability for a walk failing at step n and $\langle R_n^2\rangle_{Av}$ is the mean-square length of all failures and $\langle r_n^2\rangle_{Av}$ is the mean-square length of all successful walks, we have the following exact difference equation:

$$p\langle R_n^2\rangle_{Av}+(1-p)\langle r_n^2\rangle_{Av}=\langle r_{n-1}^2\rangle_{Av}+1. \tag{6}$$

The probability, p, of a failure is the sum of the probabilities of ring closures of all possible sizes, k, and can be expressed as:

$$p=\sum_k p_k. \tag{7}$$

If we now assume that the individual probabilities are mutually independent and also independent of n, we

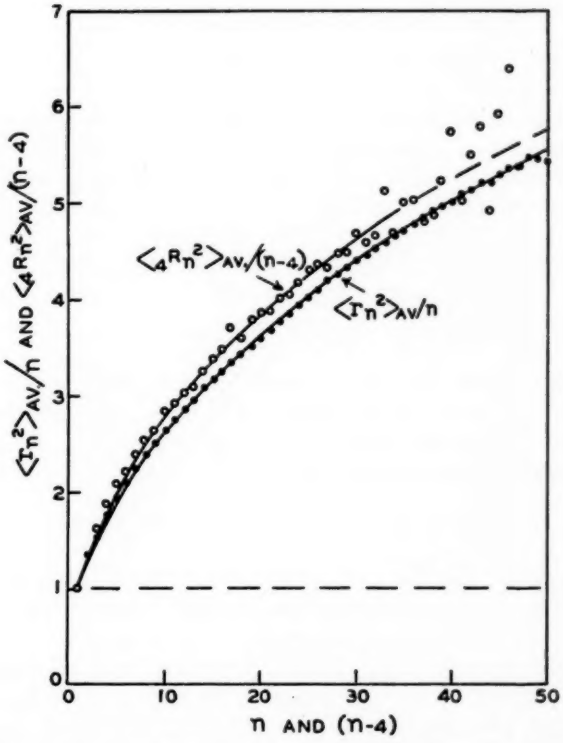

FIG. 8. Plot of $\langle r_n^2\rangle_{Av}/n$ *versus* n and of $\langle {}_4R_n^2\rangle_{Av}/(n-4)$ *vs* $(n-4)$. Data apply to three-choice 90° lattice.

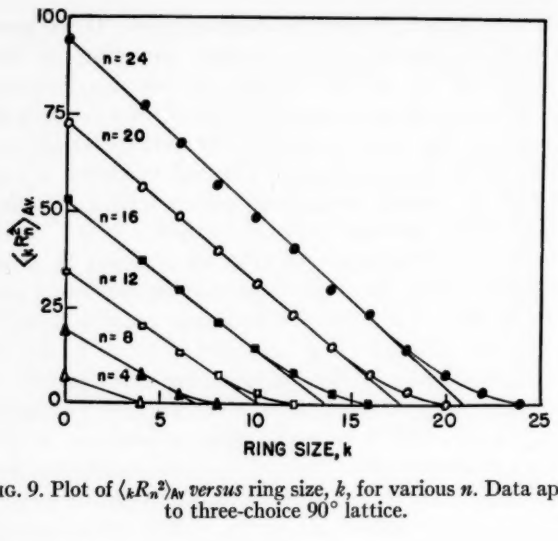

FIG. 9. Plot of $\langle {}_kR_n^2\rangle_{Av}$ *versus* ring size, k, for various n. Data apply to three-choice 90° lattice.

conclude that:

$$p\langle R_n^2\rangle_{Av}=\sum_k p_k\langle {}_kR_n^2\rangle_{Av}. \tag{8}$$

Substitution into Eq. (8) of the relationship between the mean-square distances of ring closures and successful walks, Eq. (4), then yields:

$$p\langle R_n^2\rangle_{Av}\leqslant\sum_k p_k\langle r_n^2\rangle_{Av}(1-k/n). \tag{9}$$

Or:

$$p\langle R_n^2\rangle_{Av}\leqslant\langle r_n^2\rangle_{Av}[\textstyle\sum_k p_k-(1/n)\sum_k kp_k]. \tag{10}$$

Substitution of Eqs. (7) and (10) into Eq. (6) and rearrangement gives

$$\langle r_n^2\rangle_{Av}\geqslant\langle r_{n-1}^2\rangle_{Av}+1+(\langle r_n^2\rangle_{Av}/n)\sum_k kp_k. \tag{11}$$

The term, $(\langle r_n^2\rangle_{Av}/n)\sum kp_k$, represents a perturbation of the unrestricted random walk attributable to the excluded volume effect. An expression valid for the unrestricted random walk is, of course, obtained if this term is set equal to zero. The inequality in Eq. (11) actually exaggerates the effect of the perturbation; thus the approximation given by Eq. (4) is quite safe to use if the effect of the excluded volume is such that the quotient, $\langle r_n^2\rangle_{Av}/n$, tends to diverge. Replacing the inequality of (11) by an equality then gives a lower limit to $\langle r_n^2\rangle_{Av}$. If the more exact form expressed by Eq. (5) had been used in deriving (11) instead of the inequality (4), we would obtain

$$\langle r_n^2\rangle_{Av}=\langle r_{n-1}^2\rangle_{Av}+1+[\langle r_n^2\rangle_{Av}/(n-\delta)]\sum_k kp_k. \tag{12}$$

However, since $(n-\delta)/n\rightarrow 1$ in the limit, we have some justification for dropping the δ, which is equivalent to making (11) an equation instead of an inequality.

The solution of Eq. (12) with $\delta=0$ will depend upon the nature of the summation term, $\sum kp_k$. It will be shown that this term must approach a finite limit and that the quotient, $\langle r_n^2\rangle_{Av}/n$ may or may not reach a limit as $n\rightarrow\infty$, depending on the limiting magnitude of that summation. For large values of n, Eq. (12) can be treated as a differential equation and integrated to obtain an expression relating $\langle r_n^2\rangle_{Av}$ to n. This can be done by setting $d\langle r_n^2\rangle_{Av}/dn$ equal to $\langle r_n^2\rangle_{Av}-\langle r_{n-1}^2\rangle_{Av}$, and assuming that $\sum kp_k$ has an upper bound of finite value, A. Equation (12) then becomes a simple linear first-order differential equation with a solution of the following form:

$$\langle r_n^2\rangle_{Av}=n/(1-A)+Cn^A, \tag{13}$$

where C is the integration constant. It can be seen that A, or $\lim_{n\rightarrow\infty}\sum kp_k$, can never exceed the value 2 since this would mean that $\langle r_n^2\rangle_{Av}$ would exceed n^2 for sufficiently large n. This is physically impossible since n^2 is the maximum square length of any chain. If $1<A\leqslant 2$, then $\langle r_n^2\rangle_{Av}$ is proportional to n^A at large n, under which conditions the quotient $\langle r_n^2\rangle_{Av}/n$ diverges as $n\rightarrow\infty$. On the other hand, if $A<1$, $\langle r_n^2\rangle_{Av}$ is proportional to n at large n, and the quotient converges to a limiting value. Finally, if A is equal to 1, the solution of the differential equation assumes the form:

$$\langle r_n^2\rangle_{Av}=n\ln n+Cn, \tag{14}$$

for which the quotient $\langle r_n^2\rangle_{Av}/n$ is again divergent. It was assumed in the foregoing that $\sum kp_k$ has an upper bound A. Since kp_k can never be negative, the summation must be a monotonically increasing function assuming, of course, that p_k is independent of n. Therefore it must have an upper bound, for if it did not, then A would ultimately exceed 2, a situation that has already been shown to be impossible.

PROBABILITIES FOR SINGLE-RING CLOSURES

From the foregoing treatment it is evident that if Eq. (5) is valid, the solution to our problem of mean-square lengths rests upon the nature of the summation $\sum kp_k$. This suggests, therefore, that it would be profitable to examine the probabilities of ring closures with the hope of establishing an appropriate function that might be used in obtaining the solution to our problem. In the previous article from this laboratory,[1] it was reported for the four-choice three-dimensional cubic lattice that the probability of ring closure varies inversely as the square of the ring size. It was noted, however, that the probability of closing a ring at the origin ($k=n$) was uniquely greater than that for closing a ring of an equal number of steps but not ending at the origin ($k<n$). Accordingly, two probabilities were distinguished from each other, namely p_k^0, which was called the initial ring closure probability, and p_k, which was called the limiting closure probability. Upon plotting the statistically observed probabilities *versus* ring size on log-log paper, straight lines were obtained with slopes very nearly equal to -2, thus suggesting the following expressions, valid for $k\gtrsim 8$,

$$p_k^0=\frac{c^0}{k^2}, \tag{15a}$$

and

$$p_k = \frac{c}{k^2}. \tag{15b}$$

Since an inverse square relationship seemed not unreasonable, no effort was made to force the exponent to have a value different from 2.

For the two-dimensional lattices, results rather similar to those described above have been obtained. Thus for each lattice it was found that the initial and limiting probabilities were different. Moreover, upon plotting p_k^0 and p_k *versus* k on log-log paper, straight lines with slopes near -2 were obtained. Some of the best data of this type are shown in Fig. 10. In the case of lattice d, which actually provided the most reliable data with respect to ring closures, the slope was numerically larger, being more nearly equal to -2.2, but the other lattices, as far as we can tell, have slopes of -2.0 with uncertainty in the next decimal place. However, the log-log lines cannot be safely extrapolated for reasons set forth in the next paragraph.

The first thing we must reckon with in connection with ring-closure probabilities is the effect of the exponent on the summation $\sum kp_k$. Obviously if the ring-closure probabilities vary inversely as the square of the ring size, then the above mentioned sum will diverge as the summation index increases indefinitely. However, this is impossible, according to our previous argument, if we assume the validity of Eqs. (5) and (12). It is interesting to note that if the inverse power dependence on ring size should be changed from 2 to $2+\epsilon$ where $\epsilon>0$, then the summation will converge, although possibly to an upper bound greater than 2,

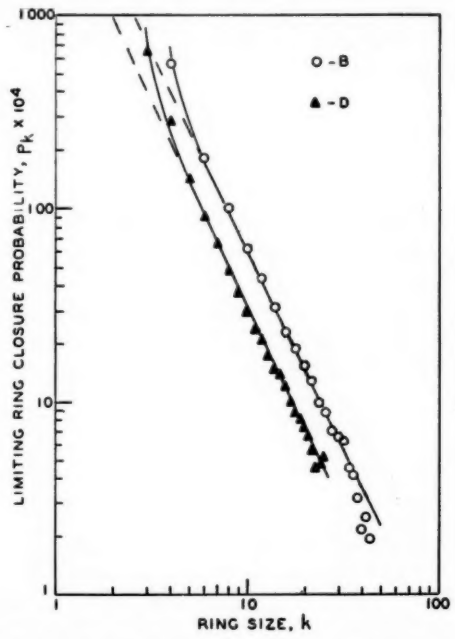

FIG. 10. Log-log plot of limiting probabilities of single-ring closures *versus* ring size: (b) three-choice 90° lattice; (d) five-choice 60° lattice.

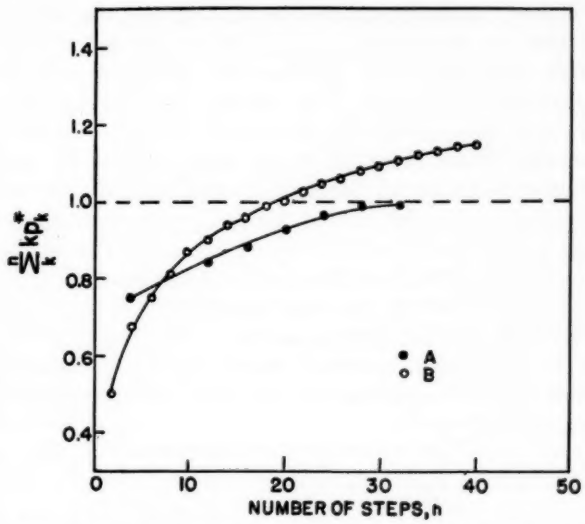

FIG. 11. Plot of $\Sigma\, kp_k^*$ *vs* n. (a) Two-choice 90° lattice; (b) four-choice 90° lattice. Curves for lattices (c) and (d) would closely superimpose on that of (b). Smooth curves have been plotted through points at which the indicated function assumes increments in value.

which would still be physically impossible as far as our problem is concerned. Therefore, if our theory is to have any meaning, we must require that the summation converge to an upper bound less than 2, and to that end we must investigate new means for ascertaining its limiting value. In all of these calculations we must, of course, make an adjustment for the probability of closing a ring with $k=2$, except for lattice (a) which involves only 90° bond angles. This is necessary to make the average of the trial vectors equal to zero, thus justifying Eq. (6). Since the probabilities of closing rings of 2 steps are equal to $\frac{1}{4}$, $\frac{1}{3}$, and $\frac{1}{6}$ respectively for lattices (b), (c), and (d), the probabilities for the larger rings must consequently be reduced, from those apparently observed, by the factors $\frac{3}{4}$, $\frac{2}{3}$, and $\frac{5}{6}$ respectively. These corrected probabilities will be denoted by p_k^{0*} and p_k^*. With this understanding the summation $\sum kp_k$ appearing in Eq. (12) should really be $\sum kp_k^*$.

CALCULATION OF SUMMATION Σkp_k^*

Several methods can be used for estimating the summation, $\sum kp_k^*$, but we shall here describe only three of them, of which the first two have only qualitative significance. Obviously if one knew the precise dependence of p_k^* upon k, one could simply evaluate the summation by numerical or analytical methods. Since most of the evidence concerning functional form suggests an inverse square function, the analytical procedure must be discarded since it would give rise to divergence of the sum and hence to an impossible answer. However, we can take the empirically determined limiting ring-closure probabilities and sum them up as far as the data are reliable. Although this will not give the upper bound to the sum, the results may be significant with respect to qualitative trends. When this procedure is

followed, we find, as shown in Fig. 11, that the sum for lattice (a) very nearly approaches unity in less than 40 steps. For lattice (b), the sum has definitely exceeded unity after 20 steps. This means that the quotient $\langle r_n^2\rangle_{Av}/n$ should diverge for lattice (b) as n becomes infinite. Some uncertainty on this score exists with respect to lattice (a), for we cannot rule out the distinct possibility that the uncomputed ring-closure probabilities will carry the sum over the unity mark. For lattices (c) and (d), results quite similar to lattice (b) are obtained, and for all practical purposes, their graphs in Fig. 11 would be superimposable on that for (b).

An indirect method for getting at the summation involves rearrangement of Eq. (12) to the following form:

$$\sum_k kp_k^* = \frac{\langle r_n^2\rangle_{Av} - \langle r_{n-1}^2\rangle_{Av} - 1}{\langle r_n^2\rangle_{Av}/(n-\delta)}. \tag{16}$$

By putting empirical data into Eq. (16), values of the sum for various n can be calculated from mean-square distance data without explicit utilization of loop-closure probabilities. It will, however, require use of the correction term, δ, which is obtained from the mean-square lengths of the closures. Because of the difference between p_k^{0*} and p_k^*, values of the expression given by Eq. (16) will jump upwards sharply each time a new size ring can form, after which it will fall back to a "normal" value. Except for these jumps, the summation can be regarded as a monotonically increasing function. Hence, we can infer that if the "normal" values of the expression on the right-hand side of Eq. (16) ever exceed unity, then the quotient $\langle r_n^2\rangle_{Av}/n$ must diverge. Direct substitution of mean-square lengths into Eq. (16) gives rise to values of the summation agreeing very well with those shown in Fig. 11, except for the above mentioned zig-zags attributable to the abnormal initial ring-closure probabilities. Hence, the qualitative conclusions appear to be warranted.

Although the above demonstration gives fairly conclusive proof of the divergence of $\langle r_n^2\rangle_{Av}/n$ for certain two-dimensional lattices, a more precise quantitative expression can be obtained by evaluating the summation $\sum kp_k$ by use of attrition data. This can be done in at least two ways, but the best method appears to be the following.

For simplicity, let us assume lattice (b), namely, the three-choice orthogonal two-dimensional system. If p_k^0 and p_k are the observed, uncorrected initial and limiting ring-closure probabilities, and if N_n is the actual number of samples left after n steps, then assuming n to be even we can write that

$$\begin{aligned}\sum_{i=1}^{n+1} N_i/N_{i-1} &= N_1/N_0+N_2/N_1+N_3/N_2 \\ &\quad +N_4/N_3\cdots+N_{n+1}/N_n \\ &= 3+(1-p_4^0)+(1-p_4)+(1-p_4-p_6^0) \\ &\quad +(1-p_4-p_6)+\cdots(1-p_4-p_6\cdots-p_n^0) \\ &\quad +(1-p_4-p_6\cdots p_n). \end{aligned}\tag{17}$$

Upon rearrangement we obtain:

$$\sum_{i=1}^{n+1} N_i/N_{i-1} = n+1-\sum_{k=4}^{n} p_k^0 - (n-3)p_4\cdots-3p_{n-2}-p_n. \tag{18}$$

Solving for $\sum kp_k$, we find that

$$\sum_{k=4}^{n} kp_k = \sum_{i=1}^{n+1} N_i/N_{i-1} - (n+1) + (n+1)\sum_{k=4}^{n} p_k + \sum_{k=4}^{n} p_k^0. \tag{19}$$

But if n is made large enough, N_{n+1}/N_n approaches $1-\sum p_k$ which has as its limit $\exp(-\lambda)$; in other words the attrition curves approach the straight lines of Fig. 2. Assuming that the asymptotic approach of $\ln N_n$ to the straight line takes place rapidly enough, we can assert that

$$\begin{aligned}\lim_{n\to\infty}\sum_{k=4}^{n} kp_k &= \lim_{n\to\infty}\{\sum_{i=1}^{n+1} N_i/N_{i-1} - (n+1)\exp(-\lambda)\} \\ &\quad +\lim_{n\to\infty}\sum_{k=4}^{n} p_k^0. \end{aligned}\tag{20}$$

The first limit on the right-hand side of Eq. (20) can be evaluated by direct count from $n=1$ to some point along the appropriate straight line of Fig. 2. Once the straight-line portion is reached, further terms will contribute nothing to the expression within the braces. To evaluate the limit of $\sum p_k^0$, we shall assume it to be given by

$$\sum_k p_k^0 = \frac{c^0}{c}\sum_k p_k = \frac{c^0}{c}[1-\exp(-\lambda)], \tag{21}$$

where λ is the attrition parameter and c^0/c is the ratio of initial to limiting probabilities of ring closures for rings of specified size. In this case we do not assume any particular power relationship for p_k as a function of k, but we do retain the distinction between p_k^0 and p_k and assume that their ratios are independent of k. Hence

$$\begin{aligned}\lim_{n\to\infty}\sum_{k=4}^{n} kp_k &= \lim_{n\to\infty}\{\sum_{i=1}^{n+1} N_i/N_{i-1} - (n+1)\exp(-\lambda)\} \\ &\quad +\frac{c^0}{c}\left[1-\exp(-\lambda)\right]. \end{aligned}\tag{22}$$

To convert Eq. (22) to corrected probabilities, we

further note that

$$A=\sum_{k=2}^{\infty} kp_k^*=2p_2^*+(1-p_2^*)\sum_{k=4}^{\infty} kp_k. \qquad (23)$$

Equations identical to Eq. (22) can be derived for other lattices as well; care must be exercised, of course, in adjusting the probabilities of ring closures to take care of backward steps when necessary.

Results of calculations using Eqs. (22) and (23) are shown in Table III. It will be observed that except for lattice (a) all of the A values exceed unity thus implying divergence of $\langle r_n^2\rangle_{Av}/n$. For lattice (a), it was found by use of Eq. (22) that $A=0.95$ which is near the threshold value. If the value 0.95 can be accepted as correct, then we would predict convergence of the ratio $\langle r_n^2\rangle_{Av}/n$ for the two-choice orthogonal two-dimensional lattice.

TABLE III. $\lim_{n\to\infty}\sum_k kp_k$ from attrition data.

Lattice	$\lim_{n\to\infty}\sum_k kp_k$	$\lim_{n\to\infty}\sum_k kp_k^*$
(a) 2-choice 90°	0.950	0.950
(b) 3-choice 90°	0.872	1.154
(c) 2-choice 120°	0.810	1.206
(d) 5-choice 60°	0.939	1.116

DISCUSSION

According to Eq. (13), $\langle r_n^2\rangle_{Av}$ is proportional to n^A for large n with $A<1.2$, for the two-dimensional lattices investigated. The results summarized in Table III also indicate that the ratio $\langle r_n^2\rangle_{Av}/n$ is closest to convergence for the 2-choice orthogonal lattice and most divergent for the 120° lattice. This is the order to be expected since the least attrition, and hence, the smallest excluded volume effect exists in the orthogonal lattice and the most attrition and hence, the greatest excluded volume effect occurs in the 120° lattice (including, of course, the backward step).

The fact that the two-choice 90° lattice is close to convergence, if not actually convergent, brings out the point that it is not necessarily the number of dimensions, *per se*, which is the controlling factor in determining the possible convergence of $\lim_{n\to\infty}\langle r_n^2\rangle_{Av}/n$. It appears quite possible that this ratio will converge in some lattices for a given number of dimensions and will diverge in others. This must be considered carefully in the examination of three-dimensional restricted random walks, especially in the orthogonal four-choice cubic system, which would be among the least affected by the excluded volume.

Approximate values of the integration constant, C, in Eq. (13) can be calculated using the values of A given in Table III together with one value of $\langle r_n^2\rangle_{Av}$. Unfortunately, this calculation requires the use of experimental values for $\langle r^2\rangle_{Av}$ which are available only for relatively small values of n. In this experimental range, Eq. (13) is really not applicable because A is not constant for small n.

The question will naturally be raised as to why the exponent A shown in Table III is less than the slope, b, of Table II. The reason is that the function represented by Eq. (13) is of such character that when plotted *vs* n on log-log paper it will give a pseudo-straight line of slope greater than A, at least when C is in the neighborhood of $A/(A-1)$, which is the value of C determined at the point $n=1$.

An extension of the treatment of this paper to three- and four-dimensional lattices will be published in the near future.

Infrared Spectrum of Trideuterosilane and the Structure of the Silane Molecule

D. R. J. Boyd*
Division of Physics, National Research Council, Ottawa, Canada
(Received August 27, 1954)

SiD_3H has been prepared by the action of lithium aluminum deuteride on $SiCl_3H$. A parallel type absorption band has been studied with a high-resolution infrared spectrometer. Analysis of the rotational fine structure of the band gave $B_0=1.7755\pm0.0008$ cm^{-1}. If the assumption is made that the structural parameters of the ground state of SiH_4 are unaltered by the substitution of D for H, the Si-H internuclear distance is found to be 1.4798 ± 0.0004 A. This is appreciably greater than 1.45_6 A which is accepted at present.

INTRODUCTION

FROM valence theory it is predicted that the SiH_4 molecule should have tetrahedral symmetry, point group T_d, similar to that of CH_4. This expectation is confirmed in detail by the infrared spectrum, which has been studied under high dispersion by Tindal, Straley, and Nielsen.[1] These authors derived a value for B_0 of SiH_4 from the fine structure of the ν_3 and ν_4 fundamental modes, which are the only 2 infrared active fundamentals and which are both triply degenerate modes. The bands are perturbed by first and higher orders of the Coriolis interaction. While the first-order interactions may be taken into consideration by the application of a sum rule, it is not possible to deal with the interactions of higher order by a simple procedure. For this reason, the determination of B_0 for SiH_4 is liable to error.

For CH_4, a better procedure[2] for determining the rotational constants of the ground state, and the molecular parameters, is to destroy partially the symmetry of the molecule by the substitution of D for some of the H atoms. It is then always possible to find nondegenerate fundamental vibrations in which there are no first-order Coriolis interactions, and from which the rotational constants of the ground state may be determined by direct methods.

In the present work, a sample of SiD_3H has been prepared. This molecule has the symmetry C_{3v} and hence 6 fundamental frequencies, 3 nondegenerate, 3 doubly degenerate, and all are infrared active. The first overtone of the nondegenerate Si-H stretching frequency has been studied with a high-resolution spectometer. From this study, B_0 has been determined.

To derive a value for the Si-H distance from the B_0 of SiD_3H, it is necessary to make assumptions about the effect of D substitution on the mean internuclear distances in the ground state. However, the errors arising from this uncertainty are probably small compared with those which arise in determining the Si-H distance from the spectrum of SiH_4.

EXPERIMENTAL

SiD_3H was prepared by the action of $LiAlD_4$ in etheral solution on $SiCl_3H$. The $LiAlD_4$ was kindly supplied by Dr. L. C. Leitch of the Division of Pure Chemistry of the National Research Council. The $SiCl_3H$ was obtained from Anderson Laboratories, Inc., (Weston, Michigan) and was stated to be 98 percent pure; however, before use it was fractionated.

An ethereal solution of $LiAlD_4$ is slightly more than the stoichiometric proportion required for the reaction was frozen in a bath of liquid N_2. The $SiCl_3H$ was distilled *in vacuo* onto the top of the solid. On allowing the containing vessel to warm to room temperature, SiD_3H was evolved. The gas was passed through a succession of traps at -95°C to remove the ether and was then condensed with liquid N_2. Finally, the SiD_3H was distilled into a storage bulb from a trap at -95°C. It was found that the sample still contained a slight trace of ether, but since this did not materially affect the analysis of the band, no further purification was attempted. About 1 l of gas at 1 atmos pressure was prepared.

For measurement of the spectrum, a pressure of 2–3 cm Hg of gas was employed in a 1-m multiple reflection cell which was adjusted to give an optical path of 8 or 16 m. The spectrometer and the method of calibration by fringes of a Fabry-Perot interferometer have been described.[3] In the present work, it was not possible to measure the whole band against the interferometer fringes in a single order of the grating. In order to match the fringes in the 2 grating orders, the absolute orders of the interferometer fringes were determined. Application of the grating formula then enabled a match between the two calibrations to be made. It is possible, on account of this, that there is a small systematic error between the measurements of the P and R branches of the band. In order to allow for such an error, the effect of a systematic error of 0.05 cm^{-1} between the P and R branches was included in the errors ascribed to the derived constants. The actual error is believed to be much smaller than this.

* National Research Laboratories Postdoctorate Fellow.
[1] Tindal, Straley, and Nielsen, Phys. Rev. **62**, 151 (1942).
[2] G. Herzberg, *Infrared and Raman Spectra of Polyatomic Molecules* (D. Van Nostrand Company, Inc., New York, 1945).
[3] A. E. Douglas and D. Sharma, J. Chem. Phys. **21**, 448 (1953).

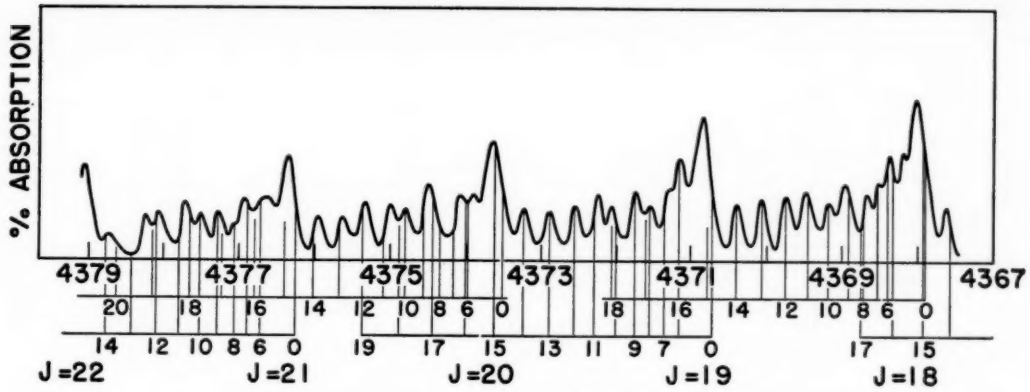

FIG. 1. A portion of the R branch of the $2\nu_1$ band of SiD_3H.

ANALYSIS OF THE ROTATIONAL FINE STRUCTURE

The appearance of the band is very similar to that of the parallel bands of CH_3D[4,5] and CD_3H[6] which have been studied recently with comparable dispersion. Figure 1 shows a portion of the R branch together with the positions of the lines computed from the constants obtained from the analysis. In general, the K structure has been resolved for $K \geqslant 6$, although in some instances the $K=5$ line could be resolved sufficiently for measurement. In the R branch, where the groups with different J converge, the K structure of one J overlaps that of the next J at higher frequency. This makes measurement somewhat inaccurate for a number of the K lines of higher J.

The assignments follow from the first appearance of the K structure with increasing J. Since $K \leqslant J$, there are $J-1$ components of the K structure for a given J in the P branch, and J components in the R branch. A second criterion is the fit of the lines in the analysis. Finally, a third criterion is provided by the intensities of the lines. Theory predicts that there should be a characteristic alternation of intensities of the K structure, lines with $K=0, 3, 6, 9, 12, \cdots$ having a statistical weight of 11, whereas the remaining lines have a statistical weight of 8. In some cases, this alternation of intensities can be clearly seen, thus providing confirmation of the assignment. However, the overlapping of the lines at high J values largely obscures the effect. In fact, for the lines with very high J, the overlapping is so severe that it has not been possible to assign the lines with confidence. It is also possible that perturbations occur for high J in the upper state. The lines that have been assigned are listed in Table I.

A definite perturbation occurs in the upper state of the band at $J'=13$ and $J'=14$. Some of the other lines are affected by this perturbation, but not sufficiently to affect the assignment. Such perturbations are eliminated in taking combination differences and hence do not affect the validity of the results for the ground state. The effect of this perturbation on the P branch of the band is shown in Fig. 2. The effect on the R branch is entirely similar. The rotational constants were evaluated as by Bovey[6] for CD_3H. The rotational energy levels, neglecting perturbations, are given by

$$F(J,K)=BJ(J+1)+(A-B)K^2-D^JJ^2(J+1)^2 - D^{JK}J(J+1)K^2-D^KK^4. \quad (1)$$

For a parallel type band, the selection rules are

$$\Delta J=0, \quad \pm 1; \quad \Delta K=0. \quad (2)$$

The combination differences between lines of the same K in the P and R branches are

$$\Delta_2F(J,K)/J+\tfrac{1}{2} =[4B-6D^J-4D^{JK}K^2]-8D^J(J+\tfrac{1}{2})^2, \quad (3)$$

where $\Delta_2F(J,K)$ is given by $[R(J-1,K)-P(J+1,K)]$ for the lower state, and by $[R(J,K)-P(J,K)]$ for the upper state. Finally, the combination sums are

$$R(J-1,K)+P(J,K) =2\nu_0+2(B_2-B_0)J^2+2[(A_2-A_0)-(B_2-B_0)]K^2 -2(D_2^J-D_0^J)J^2(J+1)^2 -2(D_2^{JK}-D_0^{JK})J^2K^2-2(D_2^K-D_0^K)K^4. \quad (4)$$

The value of D_0^J was determined from the wave numbers of the peaks formed by the unresolved lines with $K \geqslant 6$, using Eq. (3) for the ground state, and putting $K=0$. This gives a better value for D_0^J than could be obtained from the resolved K lines, since the data are more extensive and the positions of the peaks are less liable to be disturbed by overlapping lines than are the relatively weak resolved K lines. Similar curves were then plotted for the ground-state combination differences for the other K values, but making D_0^J in each case equal to that found from the plot of the unresolved peaks. From these graphs, values of $4B_0-6D_0^J-4D_0^{JK}K^2$ were obtained from the intercepts at $(J+\frac{1}{2})^2=0$. By plotting these intercepts against K^2, the quantity $[4B_0-6D_0^J]$ was found as the intercept $K=0$, while the slope of the plot gave $4D_0^{JK}$. In this

[4] D. R. J. Boyd and H. W. Thompson, Proc. Roy. Soc. (London) A216, 143 (1952).
[5] D. R. J. Boyd and H. W. Thompson, Trans. Faraday Soc. 49, 1281 (1953).
[6] L. F. H. Bovey, J. Chem. Phys. 21, 830 (1953).

TABLE I. Wave numbers of the identified lines of the $2\nu_1$ band of $Si^{28}D_3H$.

J	K	$R(J)$ cm^{-1}, vac	$P(J)$
0	...	4310.66	
1	...	4314.17	
2	...	4317.64	4299.97
3	...	4321.07	4296.39
4	...	4324.45	4292.76
5	...	4327.80	4289.10
6	...	4331.12	4285.37
6	5?	4331.50	
6	6	4331.67	
7	...	4334.39	4281.62
7	6	4334.77	4282.01
7	7	4334.96	
8	...	4337.63	4277.86[ether
8	6	4338.02	impurity
8	7	4338.19	band]
8	8	4338.41	
9	...	4340.83	4274.08
9	5	4341.07	
9	6	4341.20	4274.45
9	7	4341.41	4274.61
9	8	4341.61	4274.81
9	9	4341.78	
10	...	4343.99	4270.24
10	6		4270.62
10	7	4344.50	4270.78
10	8	4344.78	4270.98
10	9	4344.94	4271.07
10	10	4345.19	
11	...	4347.18	4266.39
11	5	4347.38	4266.61
11	6	4347.46	4266.78
11	7	4347.68	4266.93
11	8	4347.86	4367.11
11	9	4348.08	4267.33
11	10	4348.34	4267.55
11	11	4348.62	
12	...	Perturbed	4262.51
12	6	strongest line:	4262.88
12	7	4350.18	4263.04
12	8		4263.23
12	9		4263.44
12	10		4263.67
12	11		4263.94
13	...	Perturbed	4258.64
13	6	strongest line:	4258.92
13	7	4353.52	4259.12
13	8		4259.31
13	9		4259.52
13	10		4259.77
13	11		4260.01
13	12		(4260.29)
14	...	4356.39	Perturbed
14	6	4356.69	strongest line:
14	7	4356.90	4254.61
14	8	4357.07	
15	...	4359.32	Perturbed
15	5	4359.56	strongest line:
15	6	4359.65	4250.92
15	7	4359.85	
15	8	4360.02	
15	9	4360.26	
15	10	4360.48	
15	11	4360.81	
15	12	4361.09	
15	13	4361.44	
15	14	4361.84	
16	...	4362.28	4246.79
16	6	4362.64	
16	7	4362.78	
16	8	4362.99	
16	9	4363.20	
16	10	4363.45	
16	11	4363.73	
17	...	4365.15	4242.72
17	6		4243.03
17	7	4365.69	4243.21
17	8	4365.81	4245.39
17	9	4366.08	4243.60
17	10	4366.33	4243.82
17	11	4366.59	4244.07
17	12	4366.88	4244.40
17	13	4367.23	4244.71
17	14	4367.61	4245.11
17	15		4245.35
17	16		(4255.77)
18	...	4367.99	4238.69
18	5	4368.18	
18	6	4368.37	4239.05
18	7	4368.52	4239.15
18	8	4368.72	4239.35
18	9	4368.97	4239.56
18	10	4369.18	4239.79
18	11	4369.47	4240.07
18	12	4369.74	4240.64
18	13		4240.98
18	14		4241.36
18	15		4241.60
19	...	4370.84	4234.59
19	6	4371.16	4234.88
19	7	4371.31	4235.06
19	8	4371.54	4235.26
19	9	4371.74	4235.45
19	10	4372.07	4235.70
19	11	4372.23	4235.94
19	12	4372.56	4236.22
19	13	4372.88	4236.51
19	14	4373.24	4236.88
19	15		4237.25
19	16		4237.59
20	...	4373.64	4230.46
20	5		4230.68
20	6		4230.83
20	7		4230.95
20	8		4231.15
20	9	4374.50	4231.37
20	10	4374.80	4231.60
20	11	4375.01	4231.88
20	12	4375.34	4232.13
20	13	4375.65	4232.41
20	14	4375.97	4232.73
20	15		4233.14
20	16		4233.47
20	17		4233.92
21	...	4376.35	4226.37
21	6		4226.62
21	7		4226.82
21	8	4377.07	4227.02
21	9	4377.29	4227.23
21	10	4377.53	4227.46
21	11	4378.08	4227.70
21	12		4227.99
21	13		4228.28
21	14		4228.58
21	15		4228.94
22	...	4370.05	4222.25
...	...		
22	9		4223.04
22	10		4223.31
22	11		4223.55
22	12		4223.81
22	13		4224.11
22	14		4224.41
22	15		4224.72
22	16		4225.06
22	17		4225.46
23	...	4381.70	4218.05
24	...	4384.40	4213.86
25	...	4386.96	4209.63
26	...	4398.47	4205.40
27	...	Indefinite	4201.18

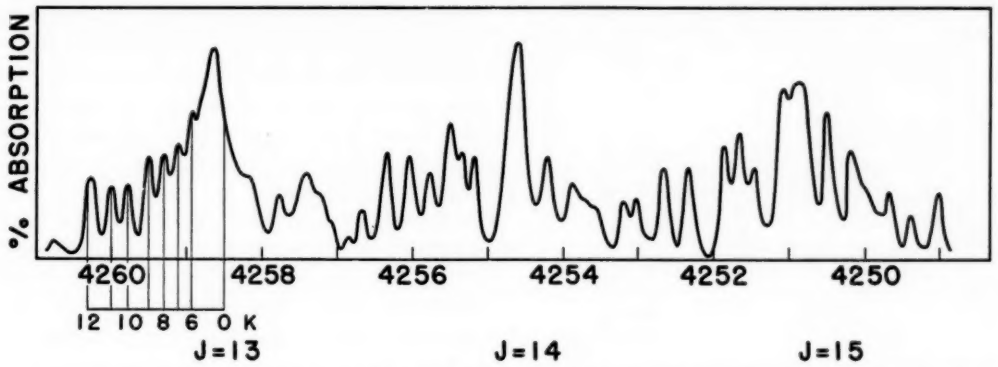

FIG. 2. A portion of the P branch of the $2\nu_1$ band of SiD_3H showing the effect of the perturbation. The effect on the lines of the R branch is similar.

way, it was found that

$$B_0=1.7755\pm0.0008\ \text{cm}^{-1}.$$

The indicated error includes the aforementioned allowance for a possible systematic error in the calibration. D_0^J was found to be $1.67_6\times10^{-5}$ cm^{-1} and D_0^{JK} to be $-(1.26\pm0.2)\times10^{-5}$ cm^{-1}. The negative value for D^{JK} is analogous to the negative value found for this quantity in CD_3H by Bovey.[6]

On account of the perturbation of the upper state, it is not possible to determine the rotational constants of that state with precision. By forming the combination sums, Eq. (4) for $K=0$ with the wave numbers of the unresolved peaks that do not appear to be perturbed greatly, and plotting them against J^2, B_2-B_0 was found to be -0.01628 cm^{-1}. The band center found from this graph needs to be corrected for the influence of the K structure. Again using Eq. (4) and now plotting the combination sums against K^2, for each value of J, values of $(A_2-A_0)-(B_2-B_0)$ are obtained from the slopes. A mean of these values, together with the value obtained above for B_2-B_0, gave $A_2-A_0=-0.0039$ cm^{-1}. From the intercepts of the plots for $(A_2-A_0)-(B_2-B_0)$ and the value of (B_2-B_0) obtained from the unresolved peaks, the band center was found to be 4307.09 cm^{-1}. The random error of this determination was about 0.01 cm^{-1}, but a systematic error of up to 0.1 cm^{-1} over the whole band is possible from differences in the collimation of the calibration and infrared systems. In all the determinations involving Eq. (4), the differences in the centrifugal distortion terms were neglected. The constants derived in this way are collected in Table II.

TABLE II. Constants of SiD_3H.

$B_0=1.7755\pm0.0008$ cm^{-1}	$D_0^J=1.67_6\times10^{-5}$ cm^{-1}
$B_2-B_0=-0.01628$ cm^{-1}	$D_0^{JK}=-(1.26\pm0.20)\times10^{-5}$ cm^{-1}
$A_2-A_0=-0.0039$ cm^{-1}	
$\nu_0(Si^{28}D_3H)=4307.09$ cm$^{-1}\pm0.01$ cm$^{-1}\pm0.1$ cm^{-1}	
$\Delta\nu_0(Si^{29}D_3H)=2.27$ cm^{-1}	
$\Delta\nu_0(Si^{30}D_3H)=4.37$ cm^{-1}	
$I_B=15.764\times10^{-40}$ g cm^2	$r_0=1.4798\pm0.0004$ A

In addition to the principal band attributed to $Si^{28}D_3H$, two weaker satellite bands due to $Si^{29}D_3H$ and $Si^{30}D_3H$ have been observed. The isotopes Si^{29} and Si^{30} occur in natural Si to the extent of 4.67 percent and 3.05 percent, respectively.[7] The rotational isotope effect is very small, since the Si nucleus lies near the center of mass of SiD_3H, and was not detected in the present work. The vibrational isotope effect is small, but still noticeable. It may be estimated roughly by treating SiD_3H as a diatomic molecule with H as one of the atoms and a mass intermediate between that of Si and SiD_3 as the other. It may be shown that the isotope shift $\Delta\nu_i$ is given by

$$\Delta\nu_i=(1-\rho_i)\nu,\quad \rho=\left(\frac{\mu}{\mu_i}\right)^{\frac{1}{2}},$$

where μ is the reduced mass of the "diatomic molecule" $Si^{28}D_3H$, μ_i is the reduced mass of $Si^{29}D_3H$ or $Si^{30}D_3H$, and ν is the wave number of the band. The shift, predicted by this formula for the band center of $Si^{29}D_3H$, lies between 1.8 and 2.6 cm^{-1}, and that of $Si^{30}D_3H$ between 3.4 and 5.0 cm^{-1}. The observed shifts are 2.27 cm^{-1} and 4.37 cm^{-1}, respectively. Since the bands are weak, only the "lines" corresponding to the unresolved structures for low K values were observed. The lines

TABLE III. Identified lines of the $2\nu_1$ band of $Si^{29}D_3H$.

J	$R(J)$	$P(J)$
0	4318.35	
1	4311.87	
2	4315.38	(4297.73)
3	4318.79	4294.12
4	4322.18	4290.47
5	4325.55	4286.81
6	4328.86	4283.11
7	4332.10	4279.38
8	4335.36	4275.64
9	4338.53	4271.82
10	4341.78	4267.98
11		4264.13
12		(4260.29)
13		(4256.35)

[7] M. G. Inghram, Phys. Rev. **70**, 653 (1946).

TABLE IV. Identified lines of the $2\nu_1$ band of $Si^{30}D_2H$.

J	R(J)	P(J)
1	4309.82	
2	4313.28	
3	4316.70	4292.04
4	4320.06	4288.39
5	4323.43	4284.68
6	4326.75	4281.13
7	4330.00	4277.30
8	4333.27	4273.50
9	4336.49	4269.72
10	4339.62	4266.01
11	4342.77	4262.08
12		4258.21

attributed to $Si^{29}D_3H$ are listed in Table III and those attributed to $Si^{30}D_3H$ in Table IV.

DISCUSSION

The moment of inertia in the ground state I_B^0 is given by

$$I_B^0=h/8\pi^2cB_0=\frac{27.989}{B_0}\times10^{-40}\text{ g cm}^2$$
$$=15.764\times10^{-40}\text{ g cm}^2, \quad (5)$$

using the values for the fundamental constants given by Dumond and Cohen[8] and the value for B_0 derived previously. I_B^0 may also be expressed in terms of the structural parameters as follows:

$$I_B^0=m_Hr_H^2+\tfrac{3}{2}(1+\cos^2\phi)m_Dr_D^2$$
$$-(m_Hr_H-3\cos\phi\cdot m_Dr_D)^2/M, \quad (6)$$

where m_H and m_D are the masses of the H and D atoms, M is the total mass of the molecule, ϕ is the angle between a Si-D bond and the symmetry axis of the molecule, and r_H and r_D are the Si-H and Si-D distances in the ground state.

If we make the assumption that the Si-H and Si-D distances are the same in the ground state, and that the angles between the bonds are tetrahedral, the value of the Si-H bond distance is found from Eqs. (5) and (6) to be 1.4798±0.0004 A. The validity of these assumptions may be checked from the results for the analogous case of CH_4 which has been studied more extensively than SiH_4. Bovey,[6] from the spectrum of CHD_3 in the photographic infrared, assuming $r_0(C-H)=r_0(C-D)$, found the C−H distance to be 1.0919 A; Boyd and Thompson,[4,5] from the infrared spectrum of CH_3D, found the C−H distance to be 1.0936 A, while Stoicheff, Cumming, St. John, and Welsh,[9] from the Raman spectrum of CH_4, found the distance to be 1.0927 A. It is therefore expected that the value 1.4798 A for the Si-H distance derived from SiD_3H, assuming $r(SiH)=r(SiD)$, will be close to the true value and probably slightly lower rather than higher.

The only other precise determination of the Si-H distance in the literature was that of Tindal, Straley, and Nielsen[1] who studied the fundamental infrared absorption bands and obtained a value of 1.45_6 A (as corrected by Herzberg[2]). This appears to be somewhat low. The discrepancy between their value and the present result is probably ascribable to the extreme perturbation of the ν_4 band of SiH_4 which makes assignment of the lines difficult. Moreover, since the P and R branches of this band do not have a common upper state, on account of the first-order Coriolis interaction, the perturbation is different in each branch and cannot be treated by the combination principle.

In the course of this work, it was learned that the spectrum of SiH_3D had been studied recently by Polo and Wilson,[10] who obtained a value of 1.477±0.003 A for the Si-H distance. This is in excellent agreement with the present value.

ACKNOWLEDGMENTS

The author wishes to express his thanks to Dr. G. Herzberg who suggested this problem and materially contributed to its solution, to Dr. A. E. Douglas for his invaluable assistance and for many helpful discussions, and to Dr. L. C. Leitch for supplying the lithium aluminium deuteride employed in the synthesis. The author also wishes to thank Dr. S. Polo and Dr. M. K. Wilson of Harvard University for kindly communicating their results on SiH_3D before publication.

[8] J. W. M. Dumond and E. R. Cohen, Revs. Modern Phys. **25**, 691 (1953).

[9] Stoicheff, Cumming, St. John, and Welsh, J. Chem. Phys. **20**, 498 (1952).

[10] S. R. Polo and M. K. Wilson (private communication); J. Chem. Phys. **22**, 1559 (1954).

Ultraviolet Absorption Spectra of Methylnaphthalenes at 77°K

H. M. McConnell and D. D. Tunnicliff
Shell Development Company, Emeryville, California
(Received September 7, 1954)

A simple and reliable apparatus has been developed for the determination of low-temperature ultraviolet absorption spectra in rigid glass media. This apparatus is particularly suitable for the measurement of accurate absorption intensities and has been used for the determination of the ultraviolet absorption spectra of naphthalene, 2-methylnaphthalene, and 2,6-dimethylnaphthalene at the temperature of boiling nitrogen (77°K). A comparison of these low-temperature spectra provides evidence that the electronic transition of naphthalene in the 2900–3200 A range is symmetry allowed.

INTRODUCTION

THE purposes of this paper are (a) to describe an apparatus which is useful for the experimental determination of the ultraviolet absorption spectra of molecules contained in rigid glass media at liquid nitrogen temperatures, and (b) to give the ultraviolet absorption spectra of naphthalene, 2-methylnaphthalene, and 2,6-dimethylnaphthalene in 3-methylpentane rigid glass at 77°K, and (c) to discuss briefly these spectra with regard to current theoretical studies of the electronic states of naphthalene.

Much of the present interest in ultraviolet absorption spectra at liquid-nitrogen temperature stems from the fact that at this temperature the absorption bands of aromatic molecules are generally much sharper than at room temperature. Although experimental techniques for the determination of low-temperature spectra in rigid glass media have been discussed by numerous authors,[1] there have been relatively few attempts to determine accurate absorption intensities at these temperatures.[2–4] The apparatus for the determination of low-temperature spectra described in the present paper has been designed for adaptation to the Cary Model 11 Recording Spectrophotometer and is thought to represent certain improvements over the earlier work referred to in the aforementioned either with regard to the determination of accurate absorption intensities, or simplicity, or both.

It has been pointed out previously that a comparison of the low-temperature absorption spectra of naphthalene and methylnaphthalenes provides strong evidence that the 2900–3200 A transition in naphthalene is an *even-odd* ($g \longrightarrow u$) symmetry allowed electronic transition.[5] The present paper gives the spectra on which this conclusion was based. In addition the present paper compares the low-temperature spectrum of naphthalene reported here with the spectra obtained previously by Kasha and Nauman,[6] and by Clar.[4]

EXPERIMENTAL

Apparatus

The low-temperature apparatus briefly described in the present section was designed for adaptation to a Cary Model 11 Recording Spectrophotometer. Aside from this adaptation, the present design was evolved in an effort to avoid or mitigate some of the characteristic difficulties associated with the experimental determination of low-temperature absorption spectra. Such difficulties include poor reproducibility and accuracy in absorption intensity determinations, absorption cell breakage at reduced temperatures, and long and tedious manipulations required for the repeated preparation and cooling of samples.

As indicated in Fig. 1, the present apparatus consists of a sample cell assembly and a metal-jacketed quartz Dewar having four plane-parallel quartz windows. The sample cell itself is a U-shaped stainless steel form 1-cm thick with two flat quartz windows held in place by means of rubber bands. A thin film of glycerine between the quartz and metal frame acts as a liquid seal for hydrocarbon rigid glass solvents. Quartz plates so attached break only very infrequently; on those infrequent occasions when the plates do break, they are so quickly and inexpensively replaced that this breakage is of little consequence.

The all-quartz Dewar was made by the Hanovia Chemical and Manufacturing Company, but was silvered and evacuated in this Laboratory. The Dewar is mounted in a metal jacket for protection and support. This jacket, in turn, is attached to a cover plate (not shown in Fig. 1) which fits the cell compartment of the spectrophotometer and positions the Dewar so that the light beam passes through the absorption cell.

The absorption cell is supported in the Dewar by means of two $\frac{1}{8}$-inch stainless-steel tubes which in turn are attached to a single $\frac{1}{4}$-inch stainless-steel tube which extends up through the cover of the metal jacket above the Dewar. This cover is sealed in place with an "O" ring and is provided with a vent with a removable cap.

[1] G. N. Lewis and D. Lipkin, J. Am. Chem. Soc. **64**, 2801 (1942); R. N. Beale and E. M. F. Roe, J. Sci. Instr. **28**, 109 (1951); Sinsheimer, Scott, and Loofburrow, J. Biol. Chem. **187**, 299 (1950), describe an apparatus for obtaining low-temperature spectra and review a number of earlier techniques.
[2] W. J. Potts, J. Chem. Phys. **21**, 191 (1953).
[3] R. Passerini and I. G. Ross, J. Sci. Instr. **30**, 274 (1953).
[4] E. Clar, Spectrochemica Acta **4**, 116 (1950).
[5] H. McConnell and D. S. McClure, J. Chem. Phys. **21**, 1296 (1953).
[6] M. Kasha and R. V. Nauman, J. Chem. Phys. **17**, 516 (1949).

A six-volt electrical heater is located beneath the cell with leads up to a plug outlet located on the cover.

Procedure

The spectrum of a sample is obtained as follows. The sample, dissolved in a suitable solvent, is placed in the cell and the cell covered with a Teflon cover. A funnel containing an ordinary folded filter is placed in the top of the Dewar assembly and liquid nitrogen poured through the filter until the quartz Dewar is about $\frac{2}{3}$ full. This filtering very effectively removes ice particles which are often present in laboratory vessels of liquid nitrogen. Then, with the vent cap removed, the cell containing the sample is *slowly* lowered into place. When the bubbling of the liquid nitrogen has nearly ceased, indicating that the sample is entirely cooled, the vent on the cover is closed and the electrical heater is turned on. This vaporizes part of the liquid nitrogen so that the resultant gas pressure in the closed Dewar forces excess liquid nitrogen up the stainless-steel support tube, and out through the cover. As soon as the level of the liquid nitrogen is below the optical light path, the heater is turned off and the absorption spectrum recorded in the usual manner. The observed spectrum is corrected by means of a blank obtained by running the solvent in exactly the same manner.

Performance

This apparatus has been in use for some time with quite satisfactory results. Tests with a thermocouple in the absorption cell showed that the temperature of the absorption cell remains constant for at least thirty minutes after cooling and removing excess liquid nitrogen. This is an adequate time for the recording of a spectrum. Absorbances at wavelengths above 2200 A were found to be reproducible to ± 0.02 absorbancy (optical density) unit. Much of this uncertainty seems to be due to variations in the light scattering by the hydrocarbon glass. Since this error is nearly independent of wavelength, the net error can be reduced to as little as ± 0.005 absorbancy unit by zeroing the instrument at a wavelength where it is known that the sample is transparent. A similar correction for this type of error has been discussed by Potts[2] for a low-temperature absorption cell used with a Beckman Model DU Spectrophotometer.

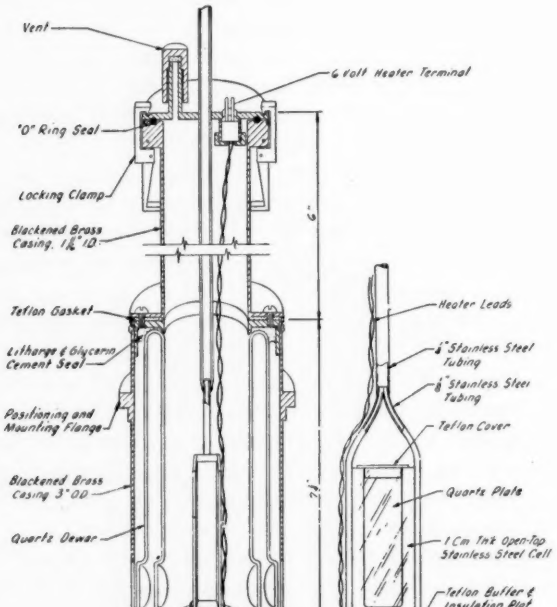

FIG. 1. Apparatus for the determination of low-temperature ultraviolet absorption spectra.

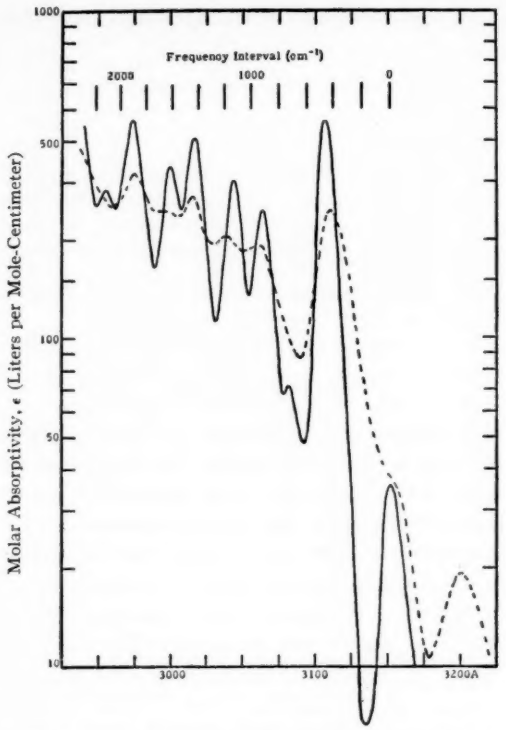

FIG. 2. The absorption spectrum of naphthalene at 25°C in isooctane (----) and at 77°K in 3-methylpentane rigid glass (——).

The low-temperature spectra of a series of samples is readily measured by merely cleaning and drying the sample cell assembly between runs. No special cleaning of the Dewar between runs is necessary provided the top of the Dewar is kept covered to prevent the diffusion of water vapor (air) into the Dewar. The metal extension tube above the Dewar serves to reduce this effect for short periods when the Dewar must be uncovered.

Materials

The rigid glass used for the present work was Phillips 3-methylpentane cooled to 77°K. The 3-methylpentane was purified and dried by passing it through silica gel

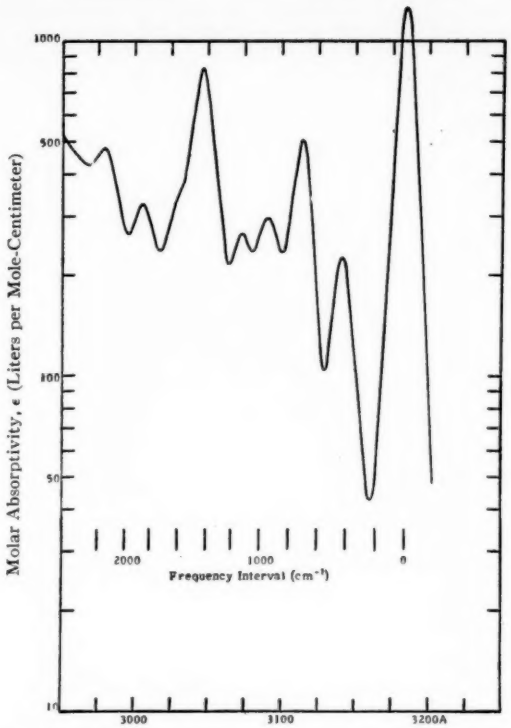

FIG. 3. The absorption spectrum of 2-methylnaphthalene in 3-methylpentane rigid glass at 77°K.

several times.[7] When purified in this manner the hydrocarbon glass does not usually crack even when in contact with boiling nitrogen for periods of several hours and the glass has essentially 100 percent transmission in a one-centimeter cell at wavelengths above 2200 A. (No effort was made to investigate the effects of various modes of purification on the transmission of this glass below 2200 A.) A number of experiments showed the contraction factor of 3-methylpentane in going from room temperature (25°C) to 77°K to be 1.28±0.01. All spectral intensities reported in the present work have been corrected for this contraction.

Bakers *CP* naphthalene was recrystallized four times from ethyl alcohol and then sublimed. The calorimetrically determined purity was 99.92 mole percent.[8]

The 2-methylnaphthalene was a National Bureau of Standards special sample of 99.90±0.05 mole percent purity. The 2,6-dimethylnaphthalene was obtained from the Edcan Laboratories and was recrystallized from ethyl alcohol. The calorimetrically determined purity was 99.8 mole percent.

THE 2900–3200 A ABSORPTION TRANSITION IN NAPHTHALENE

Our hitherto unpublished spectra of naphthalene, 2-methylnaphthalene, and 2,6-dimethylnaphthalene given in Figs. 2, 3, and 4 were used previously by McConnell and McClure[5] as evidence that the 2900–3200 A absorption transition of naphthalene is a symmetry allowed *even-odd electronic* transition. This conclusion regarding the symmetry of this upper state of naphthalene was based on the fact that the intensity of the (0,0) band in the (almost) centrally symmetric 2,6-dimethylnaphthalene molecule is some seventy times higher than the intensity of the (0,0) band in naphthalene. Platt[9] has previously proposed that this transition is even-odd symmetry allowed, both on the basis of over-all intensity changes on opposed disubstitutions and on the basis of a free-electron model for catacondensed polyaromatics in which this transition is called ${}^1A \rightarrow {}^1L_b$. Recent work on the crystal spectrum of naphthalene also indicated this transition to be symmetry allowed.[10] Other attempts to decide whether this electronic transition is $g \rightarrow g$ or $g \rightarrow u$ are reviewed and discussed by Sponer and Nordheim.[11]

The following brief discussion of the 2900–3200 A absorption spectrum of naphthalene is based on the conclusions that this transition is symmetry allowed, and that the upper-state vibrations are totally symmetric.

Since the numerical values of the vibrational intervals in the 2900–3200 A absorption transition of naphthalene play such an important part in theoretical discussions

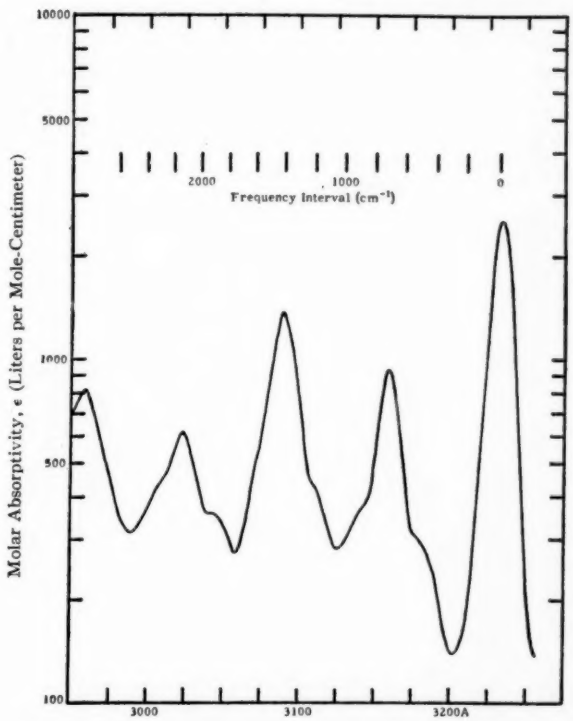

FIG. 4. The absorption spectrum of 2,6-dimethylnaphthalene in 3-methylpentane rigid glass at 77°K.

[7] Similar treatment of the much cheaper Phillips "Commerical Grade Methylpentanes" gives an equally satisfactory glass with the same contraction factor as 3-methylpentane.

[8] D. D. Tunnicliff and H. Stone, Anal. Chem. **27**, 73 (1955).

[9] J. R. Platt, J. Chem. Phys. **17**, 484 (1949); **19**, 1418 (1951).

[10] O. Schnepp, and D. S. McClure, J. Chem. Phys. **21**, 159 (1953).

[11] H. Sponer and G. P. Nordheim, Disc. Faraday Soc. No. 9, **19** (1950).

TABLE I. Absorption frequencies in the 2900–3200A naphthalene transition.

Kasha and Nauman[a] (ν−31 737)	Clar[b] (ν−31 800)	This work[c] (ν−31 730)	Assignments
0	0	0	(0,0)
367	440	430	ν_1
700	700	710	ν_2
859	880	910	ν_3
1073	1120	1130	$\nu_1+\nu_2$
1366	1390	1420	$2\nu_2$
(1891?)	1620	1610	$\nu_2+\nu_3$
(1822?)	1900	1900	$\nu_1+2\nu_2$
	2120	2130	$3\nu_2$
	2390	2400	?

[a] Ether-isopentane-alcohol rigid glass at 77°K.
[b] Ethyl alcohol-methyl alcohol mixture at 103°K.
[c] 3-Methylpentane rigid glass at 77°K.

of the symmetry character of this transition, the vibrational intervals obtained from the data in Fig. 2 are compared in Table I with those obtained by Kasha and Nauman[6] and those calculated from a spectrum obtained by Clar.[4] The spectrum of Kasha and Nauman was obtained in ether-isopentane-alcohol rigid glass at 77°K and the spectrum of Clar was obtained in a mixture of methyl and ethyl alcohols at 103°K.

The absorption frequencies given in Table I are measured relative to the (0,0) band found to be at 31 737 cm^{-1} by Kasha and Nauman, at 31 800 cm^{-1} from the data of Clar, and at 31 730 cm^{-1} (3152 A in Fig. 2) in the present work. The evidence that this band *is* the (0,0) is discussed by Kasha and Nauman,[6] and

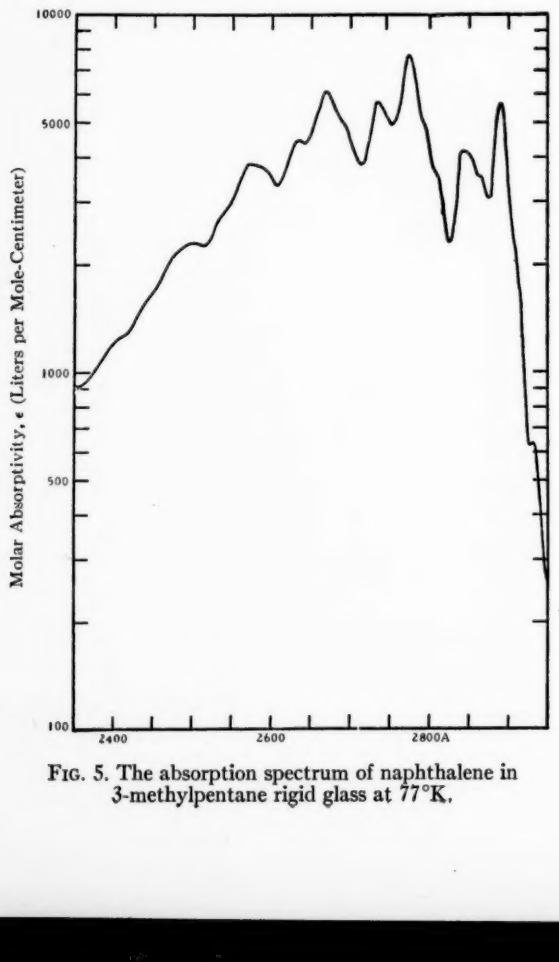

FIG. 5. The absorption spectrum of naphthalene in 3-methylpentane rigid glass at 77°K.

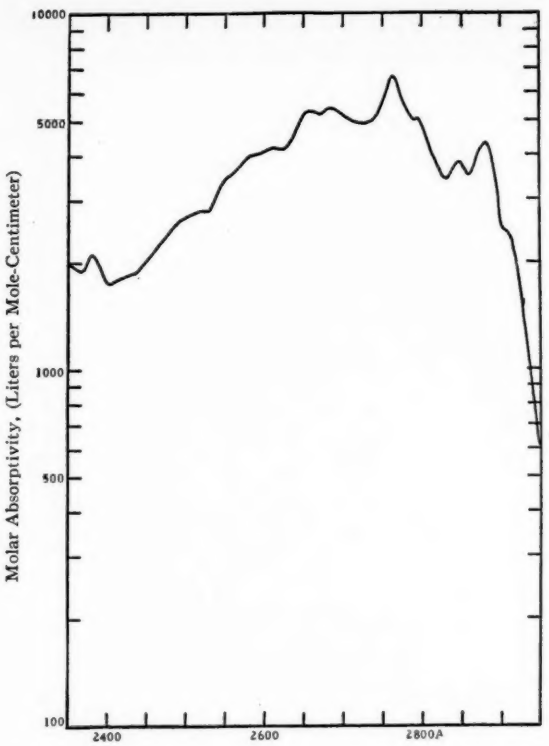

FIG. 6. The absorption spectrum of 2-methylnaphthalene in 3-methylpentane rigid glass at 77°K.

by McConnell and McClure,[5] and by Sponer.[11] The intervals obtained by Kasha and Nauman are generally about 50 cm^{-1} less than the intervals obtained in the present work, whereas the average deviation between the intervals calculated from the data of Clar and the present results is only ±15 cm^{-1}, which is well within the probable experimental errors of ±25 cm^{-1} in our frequency intervals. (It is likely that there is a typographical error in one or both of the frequencies 1891 and 1822 cm^{-1} reported by Kasha and Nauman,[6] see Table I.)

The assignments of the various vibrational bands given in Table I are the same as those proposed earlier except for the 1420-cm^{-1} and the 2400-cm^{-1} bands.[5] The 1420-cm^{-1} vibrational frequency in Table I was previously regarded as the totally symmetric excited-state vibrational mode corresponding to the totally symmetric ground-state Raman frequency of 1380 cm^{-1}. Subsequent work on the low-temperature absorption spectrum of perdeuteronaphthalene has shown this assignment to be incorrect.[12] In Table I the 1420-cm^{-1} band is interpreted as two quanta of the upper-state totally symmetric vibrational frequency, 710 cm^{-1}(ν_2). The corresponding ground-state Raman frequencies are 746 or 764 cm^{-1}, or both.

The band 2400-cm^{-1} away from the (0,0) band was not reported previously and cannot be explained reasonably in terms of combinations of the fundamental

[12] H. McConnell and V. P. Guinn, unpublished experiments.

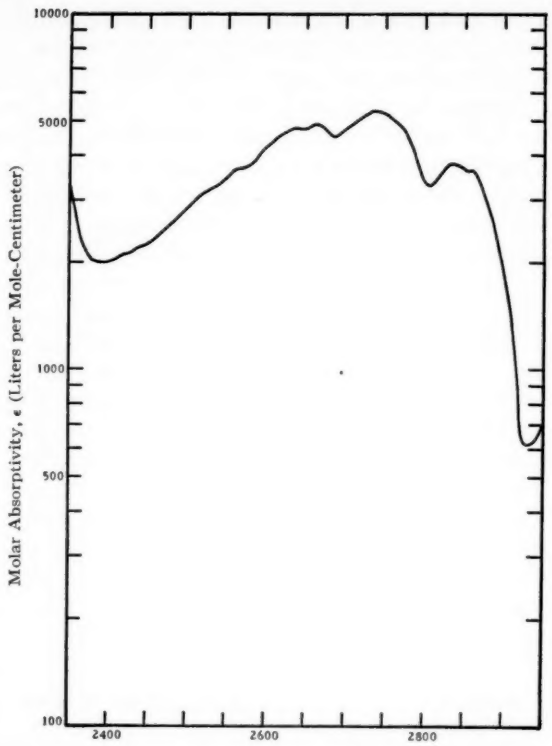

FIG. 7. The absorption spectrum of 2,6-dimethylnaphthalene in 3-methylpentane rigid glass at 77°K.

frequencies ν_1, ν_2, and ν_3. This band may belong to a shorter wavelength electronic transition.

The room-temperature spectrum of naphthalene in isooctane solvent given in Fig. 2 can be used to calculate the separation of the (1,0) and (0,1) bands. The (1,0) band is at 3200 A (one vibrational quantum in the ground state, and no vibrational quanta in the excited state), and the (0,1) band is at 3107 A. The (1,0)–(0,1) separation is 930 cm^{-1}. If the upper-state vibrational frequency of 430 cm^{-1} is interpreted as corresponding to the totally symmetric ground-state Raman frequency of 512 cm^{-1}, then the sum of these two frequencies, 512 +430=942 cm^{-1} must be equal, within the experimental error, to the observed (1,0)–(0,1) separation of 930 cm^{-1}. This is evidently true and is in accordance with the conclusion that the electronic transition is symmetry allowed and the observed upper-state vibrations are totally symmetric. Further evidence for this conclusion is supplied by the data in the next paragraph.

If one assumes that the ratios of the transition intensities of the (0,1) and (1,0) bands are a measure of the ratio of the population of the vibrationless ground electronic state to the population of the ground electronic state having one quantum of 512 cm^{-1} energy, then one can check the observed intensity ratio using Boltzman's law. The observed ratio of the peak absorption intensities is $\epsilon(3107\text{ A})/\epsilon(3200\text{ A})=(245\text{ liter/mole-cm})/(19.2\text{ liter/mole-cm})=13$. The calculated ratio is

$$e^{-hc\nu/kt}=10^{-0.622\nu/T},$$

TABLE II. Absorption frequencies of methylnaphthalenes in the 2900–3200 A range.

2-Methyl ($\nu-31\,412$) cm^{-1}	2,6-Dimethyl ($\nu-30\,950$) cm^{-1}	Assignment
0	0	(0,0)
430	490	ν_1
710	710	ν_2
960	900	ν_3
1140	1190	$\nu_1+\nu_2$
1410	1420	ν_4
...	1630	$\nu_2+\nu_3$
1860	1910	$\nu_1+2\nu_2$
2150	2140	$3\nu_2$
...	2860	$2\nu_4$

and for $\nu=512$ cm^{-1} and $T=300$°K this ratio is 12, in satisfactory agreement with the observed ratio. Essentially similar results have been obtained by Knipe, Sponer, and Cooper in a study of the vapor spectrum of naphthalene as a function of temperature.[13]

THE 2900–3200 A ABSORPTION TRANSITIONS OF 2-METHYLNAPHTHALENE AND 2,6-DIMETHYLNAPTHALENE

The low-temperature absorption spectra of 2-methylnaphthalene and 2,6-dimethylnaphthalene in the 2900–3200 A wavelength range are given in Figs. 3 and 4. Evidence that the (0,0) bands of the monomethyl and the dimethylnaphthalenes are at 31 410 and 30 950 cm^{-1}

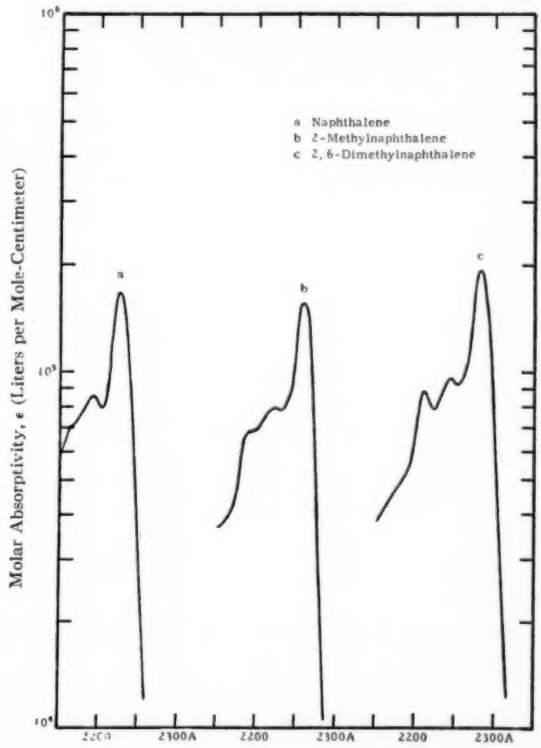

FIG. 8. Absorption spectra in 3-methylpentane rigid glass at 77°K: (a) naphthalene, (b) 2-methylnaphthalene, (c) 2,6-dimethylnaphthalene.

[13] Knipe, Sponer, and Cooper, J. Chem. Phys. **21**, 376 (1953).

TABLE III. Absorption frequencies and intensities of naphthalene and methylnaphthalenes in the 2400–2900 A range.

Naphthalene		2-Methylnaphthalene		2,6-Dimethylnaphthalene	
(cm^{-1})	(l/mole-cm)	(cm^{-1})	(l/mole-cm)	(cm^{-1})	(l/mole-cm)
34 110	[640]	34 410	[2480]	34 950	[3630]
34 590	[5650]	34 700	[4420]	35 250	[3800]
34 920	[3550]	35 130	[3800]	36 070	[4850]
35 160	[4130]	35 760	[5100]	36 460	[5620]
35 600	[3620]	36 170	[6620]	37 520	[4920]
36 040	[7700]	36 260	[5300]	37 890	[4780]
36 520	[5720]	38 250	[4200]		
37 130	[5100]				
37 430	[6100]				
37 940	[4470]				
38 540	[3750]				
38 910	[4850]				

has been discussed previously.[5] Table II gives the analysis of the vibrational bands seen in Figs. 3 and 4.

Note that in Table II the absorption band 1420 cm^{-1} away from the (0,0) band is called ν_4, and is here regarded as a totally symmetric carbon skeletal vibration similar to the 1380 cm^{-1} ground-state Raman frequency of naphthalene. The 1420 cm^{-1} vibration in the upper state of the 2900–3200 A absorption transition of naphthalene is, on the other hand, interpreted as two quanta of the 710 cm^{-1} totally symmetric upper-state frequency. These assignments have been based in part on a comparison of the low-temperature spectra of naphthalene$-d_8$ and 2,6-dimethylnaphthalene$-d_4$.[12]

THE 2400–2900 A ABSORPTION TRANSITIONS OF NAPHTHALENE AND METHYLNAPHTHALENES

The low-temperature absorption spectra of naphthalene, 2-methylnaphthalene and 2,6-dimethylnaphthalene in the 2400–2900 A range are given in Figs. 5, 6, and 7. No detailed analysis of the band systems in these figures will be attempted here because (1) the observed bands are in many cases quite diffuse, (some bank peaks are uncertain by as much as 100 cm^{-1}), (2) the location of the (0,0) bands is not certain, especially in the cases of the methylnaphthalenes, and (3) more than one electronic transition may be responsible for the observed absorptions in the 2400–2900 A range. A tabulation of the absorption frequencies and intensities of the principal absorption bands in Figs. 4, 5, and 6 are given in Table III. The only predominant frequencies found in the spectra in Figs. 5 and 6 are *ca* 1430 cm^{-1} and 500 cm^{-1}. These are probably the upper-state frequencies corresponding to the ground-state Raman frequencies of 1380 and 512 cm^{-1}. Similar frequency intervals have been noted in the crystal spectrum of naphthalene.[10]

It may be mentioned here that further studies on substituted naphthalenes may give much more useful information regarding the excited-state vibrational frequencies for the 2400–2900 A naphthalene absorption transition. Thus, this transition shows much sharper vibrational structure in naphthalene-d_8 and acenaphthene.[12] Such studies may provide a useful supplement to investigations of this transition in crystals.

THE 2200–2300 A ABSORPTION TRANSITIONS IN NAPHTHALENE AND METHYLNAPHTHALENES

The low-temperature absorption transitions of naphthalene, 2-methylnaphthalene, and 2,6-dimethylnaphthalene are given in Fig. 8. The absorption bands of these strong allowed electronic transitions show totally symmetric vibrational frequencies of *ca* 720 and 1400 cm^{-1}.

Infrared Spectra and Structure of NaOH and NaOD*

WILLIAM R. BUSING†
Sterling Chemistry Laboratory,‡ Yale University, New Haven, Connecticut
(Received September 3, 1954)

The infrared spectra of NaOH, NaOD, and mixtures of these compounds have been studied at room and liquid air temperatures. The results at room temperature, taken together with the Raman spectrum of NaOH, are consistent with the x-ray structure and hydrogen positions postulated in the present work. At liquid air temperature the spectrum of NaOD shows an unexpected complexity which cannot be explained at present.

THE x-ray structure of α-NaOH has been reported by Ernst[1] but the positions of the hydrogen atoms have not yet been determined satisfactorily. One question of interest is whether hydrogen bonding occurs between the hydroxide ions of NaOH as it does between the anions of several acid salts.[2] In order to answer this question, as well as for the general purpose of studying the interaction of the vibrations of complex ions in crystals, the infrared spectra of NaOH,[3] NaOD, and mixtures of these compounds have been studied at room and liquid air temperatures. The room temperature results for NaOH will be compared with the corresponding Raman frequency. It will be shown that these spectroscopic data taken together with the x-ray results indicate that hydrogen bonding does not occur in NaOH and that the interaction of the OH stretching vibrations is small.

THE STRUCTURE OF NaOH

Ernst was able to prepare crystals of NaOH for his x-ray study and therefore could obtain Weissenberg and rotation photographs as well as powder patterns. A unit cell of the orthorhombic lattice is shown at the left in Fig. 1. The positions of the sodium and oxygen atoms were determined from the x-ray intensities and they agree very well with known values of the ionic radii. This is a layer structure in which each layer has approximately the NaCl arrangement. These layers are arranged in such a way that displacing alternate ones a distance $a/2$ in the x-direction would give the entire crystal a pseudo-NaCl structure. Ernst has found that the cleavage of sodium hydroxide along the (001) plane (parallel to the layers) is excellent and that cleavage is also good along the (110) planes as is to be expected from this structure.

Basing his argument on the optical properties of the crystal, Ernst has assigned positions to the hydrogen atoms so that the OH dipole is parallel to the y-axis. Such a structure seems unlikely, however, because it requires each hydrogen atom to be very close to two positive sodium ions. The arrangement might be stabilized by a strong hydrogen bond to the neighboring oxygen atom, but the O—H···O distance in this case would be 3.40 A which is much larger than that usually found for this type of hydrogen bond.[4]

If hydrogen bonding is not important, then more reasonable hydrogen positions are those shown in Fig. 1 which could result from the repulsion of the protons for the five sodium ions which surround each oxygen atom. Assuming these hydrogen positions also permits us to interpret the relative placement of successive layers as the result of the repulsion of the positive hydrogens of one layer for the hydrogen atoms and also for the sodium ions of the next. It will be shown that this structure is consistent with the observed infrared and Raman spectra.

In order to predict the selection rules for the vibrational spectrum, we need consider only a primitive unit cell[5] such as that shown at the right on Fig. 1. This cell contains two "molecules" of NaOH related to

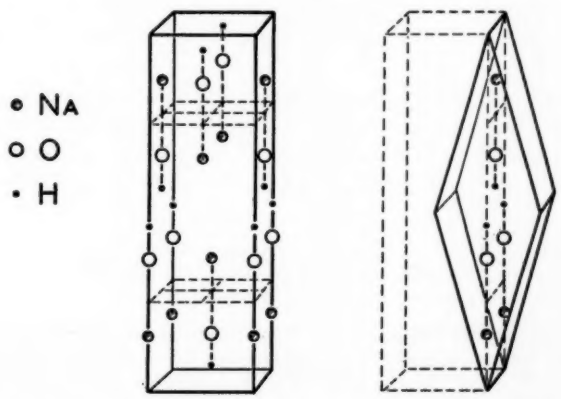

FIG. 1. The crystal structure of NaOH showing the postulated hydrogen positions. At the right is a primitive unit cell which is derived from the larger cell as indicated by the dashed lines.

* This research was supported in part by the U. S. Air Force under contract monitored by the Office of Scientific Research, Air Research and Development Command.
† Present address: Chemistry Division, Oak Ridge National Laboratory, Oak Ridge, Tennessee.
‡ Contribution No. 1249.
[1] T. Ernst, Nachr. Akad. Wiss. Göttingen, Math.-physik. Kl., Math.-physik.-chem. Abt. 76 (1946).
[2] See, for example, L. Pauling, *Nature of the Chemical Bond* (Cornell University Press, Ithaca, New York, 1945), second edition, Chap. IX.
[3] The infrared spectrum of NaOH has previously been reported by Ghosh and Chatterjee, Z. Physik **72**, 542 (1931), but their results were quite different from those of the present study, perhaps because these workers did not protect their sample from atmospheric water vapor.
[4] See reference 2, p. 334.
[5] S. Bhagavantam and T. Venkatarayudu, Proc. Indian Acad. Sci. **9A**, 224 (1939).

each other by centers of symmetry. We will consider only the OH stretching vibrations since no others have been observed to date. The two hydroxide ions can couple with each other to give rise to two normal modes of vibration, one of which is symmetric with respect to the centers of symmetry while the other is antisymmetric. The symmetric vibration will be Raman active while the antisymmetric one will be active in the infrared.[6] The difference between the infrared and Raman frequencies will therefore be a measure of the coupling between hydroxide ions.

EXPERIMENTAL

The cell used for these studies was similar to that described by Wagner and Hornig[7] in which the sample is supported in a vacuum on an infrared window which can be cooled to liquid air temperature. A thermocouple is mounted in this window so that temperature measurements can be made.

The samples were prepared directly in the evacuated cell by condensing a thin film of reagent grade sodium metal on the window from an electrically heated platinum boat. This film was then exposed to gaseous H_2O, D_2O, or mixtures of the two. The pressure of the vapor was carefully controlled in order to prevent the formation of hydrated NaOH. The spectra of some of the hydrates have been observed in other experiments and they are qualitatively quite different from those presented here.

In order to reduce scattering from the films it was necessary to build them up slowly by repeating the aforementioned procedure about two hundred times. Even so, the scattering was such that the samples were nearly opaque to visible light. The transmission at wavelengths longer than 2μ was satisfactory, however. The first twenty or thirty layers of each sample showed interference colors and from these the final thickness was estimated to be 5–6μ.

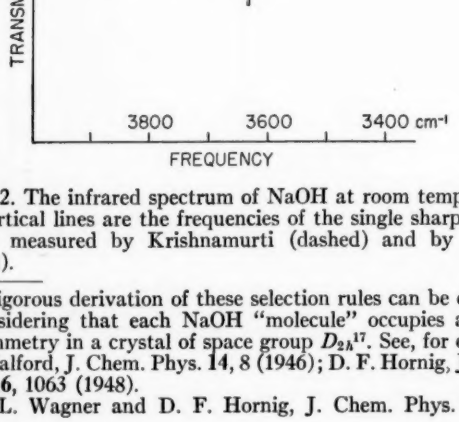

FIG. 2. The infrared spectrum of NaOH at room temperature. The vertical lines are the frequencies of the single sharp Raman line as measured by Krishnamurti (dashed) and by Phillips (dotted).

[6] A rigorous derivation of these selection rules can be obtained by considering that each NaOH "molecule" occupies a site of C_{2v} symmetry in a crystal of space group D_{2h}^{17}. See, for example, R. S. Halford, J. Chem. Phys. **14**, 8 (1946); D. F. Hornig, J. Chem. Phys. **16**, 1063 (1948).

[7] E. L. Wagner and D. F. Hornig, J. Chem. Phys. **18**, 296 (1950).

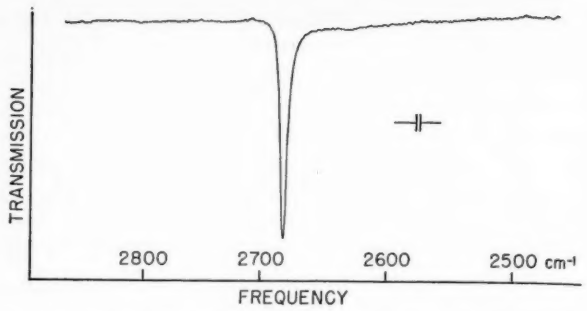

FIG. 3. The infrared spectrum of NaOD at room temperature.

No differences were observed when supporting windows of NaCl, KCl, KBr, and CsBr were used interchangeably and it is therefore believed that orienting effects were absent. One sample was prepared by evaporating NaOH itself and its spectrum did not differ from those of samples made by the other technique.

The spectra were studied using a Perkin-Elmer Model 21 double-beam infrared spectrometer equipped with NaCl and LiF prisms. Although the absorption maximum of NaOH falls in the region of the 3μ water band, atmospheric compensation was good and the background shown in Fig. 2 is typical. Dry nitrogen was blown through the instrument for some measurements, but this produced no significant change in the measured frequencies.

Frequency measurements in the OH and OD regions were made by comparison with a calibration spectrum of atmospheric H_2O or of HCl gas which was superimposed on each sample spectrum. The frequencies assumed for these standards were derived from those reported by Plyler and Sleator[8] and Meyer and Levin.[9] Because the fine structure of the H_2O bands and the isotopic splitting in the HCl spectrum are not resolved by the LiF prism, the frequencies used were weighted averages of the published values. For H_2O, the vacuum correction was also made.

The probable error of the frequency measurements is estimated to be ± 1.3 cm^{-1} and ± 0.5 cm^{-1} in the OH and OD regions, respectively. These figures were derived from the deviations of the individual measurements and from the scatter of the calibrating points about the calibration curves.

RESULTS AT ROOM TEMPERATURE

Except for weak bands which were attributed to traces of stopcock grease or of sodium carbonate, the only absorptions observed in the wavelength range from 1–15μ were those in the OH or OD stretching region of the spectrum. The frequencies measured under various conditions are listed in Table I.

Shown in Fig. 2 is the single sharp absorption of NaOH observed at room temperature with the LiF prism. The spectral slit width of about 8 cm^{-1} is indi-

[8] E. K. Plyler and W. W. Sleator, Phys. Rev. **37**, 1493 (1931).

[9] C. F. Meyer and A. A. Levin, Phys. Rev. **34**, 44 (1929).

cated in the figure. The band width at half-height appears to be about 11 cm^{-1} but the true line width is probably less than this. The observed frequency is 3637.4 cm^{-1}; an average of four measurements on two samples. The band is similar in appearance to that which is found at 3678 cm^{-1} in LiOH.[10]

The vertical dashed line in Fig. 2 indicates the position of the single sharp Raman line at 3630 cm^{-1} which was found by Krishnamurti[11] in his study of NaOH pellets. This frequency has been remeasured in our laboratory by Betty A. Phillips[12] who obtained a value of 3633.1 ± 0.9 cm^{-1}. Her result is indicated by the dotted line in Fig. 2. Without making any assumption as to which value is more nearly correct, it seems fairly certain that there is a real difference of from 4 to 7 cm^{-1} between the frequency of the symmetric Raman vibration and that of the antisymmetric infrared vibration.

Figure 3 shows the absorption peak found for NaOD. A spectral slit width of 3 cm^{-1} was used in this wavelength region, and the band width at half height was about 6 cm^{-1}. The observed frequency was 2681.1 cm^{-1}, an average of six measurements on two samples.

These spectra are consistent with the postulated structure of Fig. 1 in that one strong infrared active OH vibration and one strong Raman active one have been observed. It is probable that the two are of slightly different frequency and therefore represent the antisymmetric and symmetric vibrational modes which were predicted. It should be clear that these observations alone do not rule out other possible structures. They imply only that the two OH^- ions in each unit cell are antiparallel or almost so.

Two more reasons for preferring a structure without hydrogen bonds may now be added to those already cited. First, the absorption bands are much sharper than those usually observed for the stretching vibrations of bonded hydrogens. The line width of the NH stretch in NH_4Cl, for example, is 35 cm^{-1}.[13] Secondly, the small splitting between the infrared and Raman

TABLE I. Infrared absorption frequencies of NaOH and NaOD (cm^{-1} *in vacuo*). The probable errors for the OH and OD bands are ± 1.3 and ± 0.5 cm^{-1}, respectively.

Sample					
Mole percent NaOH	Mole percent NaOD	Room temperature ν_{OH}	Room temperature ν_{OD}	Liquid air temperature ν_{OH}	Liquid air temperature ν_{OD}
~100	~0	3637.4	...	3643.6	...
91	9	3636.3	2680.4	3642.6	2686.0
11	89	3632.0	2680.9	3636.3	2682.6
>1	<99	...	...	3635.9 3622.4	2684.2 2675.4
<1	>99	...	2681.1	...	2683.6 2673.6 2663.1

[10] L. H. Jones, J. Chem. Phys. **22**, 217 (1954).
[11] P. Krishnamurti, Indian J. Phys. **5**, 651 (1930).
[12] B. A. Phillips and W. R. Busing (to be published).
[13] D. F. Hornig, Discussions Faraday Soc. **9**, 115 (1950).

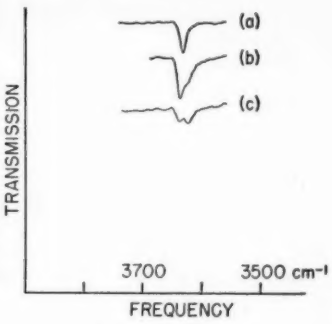

FIG. 4. The OH band in dilute solid solutions of NaOH in NaOD. (a) 11 mole percent NaOH at room temperature. (b) 11 mole percent NaOH at liquid air temperature showing a low frequency sholder similar to that of the OD band [Fig. 5(b)] (c) Still smaller fraction of NaOH at liquid air temperature showing the double band similar in shape to the OD band [Fig. 5(c)].

frequencies means that there is only weak coupling between the hydroxide ions. In a hydrogen bonded structure, however, we would expect this coupling to be strong. For example, in the extreme case of solid HCl[13] the maximum splitting of the components is 131 cm^{-1} as compared with our value of 7 cm^{-1} or less for NaOH.

DILUTE SOLID SOLUTIONS

Hrostowski and Pimentel[14] have suggested that useful information could be obtained by studying the spectra of dilute solid solutions of isotopic substances. For example, we have studied a sample which consisted of 11 mole percent NaOH in 89 mole percent NaOD. The utility of this technique depends upon the fact that although the OH^- ions are in almost the same crystalline field as in pure NaOH, they are unable to couple resonantly with their neighbors because these are, on the average, OD^- ions which have a drastically different natural frequency. Using first-order perturbation theory, Hornig[13] has shown that the frequency of such an isolated ion should be the root mean square of the frequencies which result when coupling is permitted. Thus, if our postulated structure is correct, the sample of NaOH in NaOD should show an OH frequency which is the root mean square of the infrared and Raman frequencies in pure NaOH. This result depends upon the assumption that the force constants are unchanged by isotopic substitution and that higher order perturbations are negligible.

Observations on solid solutions of NaOH and NaOD are included in Table I, and Fig. 4(a) shows the OH absorption in 11 mole percent NaOH at room temperature. The observed frequency is 3632.0 cm^{-1} or about 5 cm^{-1} lower than that found in pure NaOH. This result is significantly different from the value of 3635.2 ± 0.8 cm^{-1} predicted by first-order perturbation theory if Phillips' Raman frequency is taken as correct. If Krishnamurti's measurement is used the agreement is slightly better but still not satisfactory. The discrepancy can probably be attributed to a failure of the assumptions mentioned above.

The OD frequency in 9 mole percent NaOD at room temperature is almost identical with that in pure NaOD. The Raman frequency in NaOD has not been

[14] H. J. Hrostowski and G. C. Pimentel, J. Chem. Phys. **19**, 661 (1951).

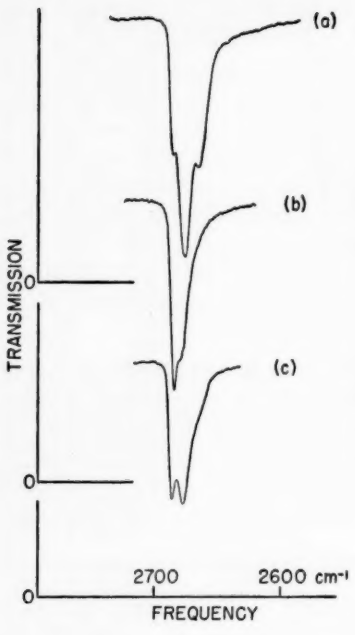

FIG. 5. The infrared spectrum of NaOD at liquid air temperature showing the influence of small amounts of NaOH on the band shape. (a) Substantially pure NaOD. The sample is the same as that shown in Fig. 3. (b) 89 mole percent NaOD with 11 mole percent NaOH. (c) Sample containing something less than 10 mole percent NaOH (see text).

reported but it can be inferred from this result that it is probably very close to the infrared frequency.

At room temperature the frequencies which were due to the major components of these mixtures, i.e., that of the OH band in 91 mole percent NaOH and that of the OD band in 89 mole percent NaOD, were found to be the same as the frequencies in the pure substances within experimental error.

RESULTS AT LIQUID AIR TEMPERATURE

The infrared spectra were also studied at sample temperatures from −165 to −175°C using liquid air as the coolant. Under these conditions the only changes in the spectrum of NaOH were a slight decrease in the band width and a frequency increase of about 6 cm^{-1} (see Table I). This result is not surprising since NaOH has no phase transition between room temperature and 60°K.[15] Under the same conditions the sample of 91 mole percent NaOH with 9 mole percent NaOD showed an OH band essentially identical with that in pure NaOH and a small sharp OD band (see Table I).

Pure NaOD, however, has a very different spectrum at liquid air temperatures in which the single absorption band is replaced by the triple band shown in Fig. 5(a). Table I lists the frequencies of the absorption maxima. The components are separated by about 10 cm^{-1} and the high frequency peak corresponds approximately with the room temperature band. This effect was observed with three samples on supporting windows of NaCl, KCl, and CsBr.

Another sample of NaOD containing 11 mole percent NaOH failed to give the triple absorption but showed instead the single maximum and trailing low frequency shoulder shown in Fig. 5(b). The frequency of greatest absorption (see Table I) corresponded approximately with the room temperature band in NaOD. In order to show that the failure to observe tripling was not the result of insufficient cooling, the sample temperature was lowered to −183°C by pumping on liquid nitrogen. The only effect was to increase the shoulder absorption slightly. It appears, therefore, that it is the presence of NaOH which inhibits the tripling.

This was clearly demonstrated by the following experiment. One of the samples of NaOD in which the low temperature tripling had been observed was examined several days later and found to exhibit only the single band of Fig. 5(b). At the same time a weak OH band appeared in the spectrum indicating that the sample had become contaminated with NaOH, probably by exchanging with traces of H_2O vapor in the vacuum system. An attempt was then made to remove the hydrogen by exchanging several times with D_2O vapor. Apparently this was only partially successful because the low-temperature tripling was not completely restored. Instead, the double band shown in Fig. 5(c) was found. The frequencies of maximum absorption (Table I) corresponded almost exactly with the two high-frequency components of the triplet but the third component appeared only as a trailing shoulder.

For each of these samples the OH band from the small amount of NaOH present was found to have a shape similar to that of the OD band. For example, the OH band in 11 mole percent NaOH has the low frequency shoulder shown in Fig. 4(b) and the sample which showed a double OD band also had the double OH band shown in Fig. 4(c). These OH frequencies are included in Table I. Samples for which the tripling of the OD band was found contained so little NaOH that no OH band could be observed.

The interpretation of these complex band shapes is not clear at present. The possibility of resonance with harmonics of low frequency vibrations of the crystal seems to be ruled out by the observation that in a given sample the change in the OH band parallels that in the OD band. Another suggestion might be that the spectral changes are the result of some phase change which occurs in NaOD in liquid air temperature but which has a much lower transition temperature in NaOH. Solid phase transition temperatures in deuterium containing compounds are usually higher than those in the corresponding hydrogen compounds.[16,17] But this would not explain the fact that a small amount of NaOH inhibits only the lowest frequency band of the OD triplet while a greater amount causes the two low-frequency bands to disappear. The situation would probably be clarified by thermal studies on NaOD.

[15] J. C. R. Kelley and P. E. Snyder, J. Am. Chem. Soc. **73**, 4114 (1951).

[16] A. Eucken, Z. Elektrochem. **45**, 126 (1939).

[17] Stephenson, Corbella, and Russell, J. Chem. Phys. **21**, 1110 (1953).

Calculation of the Dipole Moment of the Carbon-Hydrogen Bond in Methane by the Thomas-Fermi Method*†

HERBERT GLAZER‡ AND HOWARD REISS§
Chemistry Department, Boston University, Boston, Massachusetts

(Received August 30, 1954)

To compute the dipole moment of the CH bond in methane, the pyramids formed by the planes bisecting the HCH bond angles were taken as elements of symmetry. Each pyramid encloses a carbon-hydrogen bond and the four close-pack to form the methane molecule. To symplify the problem, the pyramid was replaced by a cone of equal volume. The Thomas-Fermi equation was solved for the potential within this cone subject to the appropriate boundary conditions, on the IBM Type 701 electronic data processing machines, using the extrapolated Liebmann method. Boundaries were chosen about each nucleus on which the superposition solution was used. The equation was solved for carbon alone and then for carbon-hydrogen within the cone. The dipole moment was taken as the difference between the two in accordance with views recently expressed by Shull and by Coulson. The value obtained was 2.8D C+H−. The large magnitude is attributed to the poor description of the system by the statistical theory.

I. INTRODUCTION

APPLICATION of the Thomas-Fermi model to even the simplest molecules has been limited because in molecules there is no longer spherical symmetry and in the worst cases not even axial symmetry. As a result, the mathematical treatment of the problem becomes very difficult. In fact, it has been possible only in special cases to treat molecules. Recently there has been increased interest in this direction.[1–6] Of particular interest as far as diatomic molecules are concerned is the work of Glazer and Reiss[2] on ICl, of Sheldon and Thomas on the solution of the Thomas-Fermi-Dirac equation for the nitrogen molecule,[5] and the work of Gaspar and Konya[6] who obtained excellent results for the hydrogen-iodide molecule, considering the system as a proton pertubation of the iodide ion.

The derivation of a new Thomas-Fermi equation by Plaskett[7] may lead to interesting applications in the future, although at present it has been possible to validate the new equation in one dimension only. Also of possible future significance is the work of Brinkman,[8] who was able to reproduce the results of Hund[9] by linearizing the Thomas-Fermi equation.

Our interest in computing the electron distribution in methane was stimulated by the successul application of the Thomas-Fermi method to ICl.[2] March[10] had treated methane already using the Thomas-Fermi equation in conjunction with the spherical approximation of Buckingham, Massey, and Tibbs (BMT).[11] We have attempted to apply the Thomas-Fermi equation to methane without invoking the spherical approximation.

Because of its importance there is a great deal of literature on methane and the dipole moment of the CH bond[12,13] whose polarity has been a source of controversy for many years. Smyth[14] accepted the value 0.3D C−H+, as calculated by Hirschfelder. Pauling calculated 0.4D C−H+ from the electronegativity difference between carbon and hydrogen.[15] Coulson using wave functions obtained previously for methane, calculated C−H+0.53D using a method involving effective nuclear charges.[16] Coulson later criticized his own work as well as the concept of effective charges.[17] In a later paper Coulson obtained C+H−0.4D using a molecular orbital approach. He attributed the discrepancy between this result and previous work to the neglect of the atomic dipole term in carbon, i.e., the dipole moment of the atomic orbital out of which the molecular orbital is formed. Coulson's work is open to some criticism suggested by himself. A term has been neglected representing the secondary dipole moment induced in the nonbonding electrons, and the inductive effects between neighboring carbon bonds. Spatial interactions have also been ignored.

Although Coulson calculated that the sense and

* Supported by the Air Force Cambridge Research Center, Geophysics Research Directorate, contract.

† Part of dissertation for the Ph.D degree, Boston University, 1954.

‡ Present address: IBM Watson Laboratory, Columbia University, New York, New York.

§ Present address: Bell Telephone Laboratories, Murray Hill, New Jersey.

[1] H. Reiss and H. Saltsburg, J. Chem. Phys. **18**, 1461 (1950).
[2] H. Glazer and H. Reiss, J. Chem. Phys. **21**, 903 (1953).
[3] W. A. Bowers, J. Chem. Phys. **21**, 1117 (1953).
[4] J. V. Bonet and A. V. Bushkovitch, J. Chem. Phys. **21**, 2199 (1953).
[5] J. W. Sheldon, IBM 701 Staff, New York, New York, private communication.
[6] R. Gasper and A. Konya, Acta. Phys. Acad. Sci. Hung. **3**, 31 (1953).
[7] J. S. Plaskett, Proc. Roy Soc. (London) **A66**, 178 (1953).
[8] H. C. Brinkman, Physica **XX**, 44 (1954).
[9] F. Hund, Z. Physik **77**, 12 (1932).
[10] N. H. March, Proc. Cambridge Phil. Soc. **48**, 665 (1952).
[11] Buckingham, Massey, and Tibbs, Proc. Roy. Soc. (London) **A178**, 119 (1941).
[12] W. L. G. Gent, Quart. Revs. (London) **2**, 383 (1948).
[13] J. W. Smith, Science Progr. **41**, 270 (1953).
[14] C. P. Smyth, J. Phys. Chem. **41**, 209 (1937); "Symposium on the Structure of Molecules and Aggregates of Molecules, Division of Physical and Inorganic Chemistry," American Chemical Society Meeting, Columbia University, New York, December 30, 1940.
[15] L. Pauling, *Nature of the Chemical Bond* (Cornell University Press, Ithaca, New York, 1945), 2nd edition, p. 68.
[16] C. A. Coulson, Trans. Faraday Soc. **33**, 388 (1937).
[17] C. A. Coulson, Trans. Faraday Soc. **38**, 440 (1942).

magnitude of the CH bond moment should remain the same for all normal chemical compounds, i.e., independent of whether the carbon atom is aliphatic, ethylenic, or aromatic, more recent theoretical work[12] leans toward C−H+ in acetylene and approximate neutrality in ethylene. This work also indicates a great sensitivity of the moment to its environment. In general it is now apparent that CH_4 can be treated only as an isolated case, and conclusions drawn from calculations on other molecules are uncertain when applied to methane. To indicate further the confusion in the literature on this point, Pullman and Pullman[18] on pp. 81–83 use Gent's review article[12] to describe the CH bond calculations and then on pp. 112–14 use Smyth's article.[14] The conclusions drawn in these papers are in considerable disagreement.

As far as experimental determinations are concerned, work on the infrared absorption of ethylene[19] indicates a finite CH bond moment, (0.37D), whose sense is taken from Pauling.[15] This is in contradiction to Gent[12] who concludes the CH bond in ethylene should have a zero moment. Because of electronic delocalization Pullman[18] feels that it need not follow that the moment accompanying vibration (infrared) is identical with the static moment.

Mueller and Eyring[20] compromised between the wave mechanical treatment of Coulson[17] in which repulsive terms were omitted and a self-consistent field treatment. In their approach the CH bond was considered as an isolated unit and the effective nuclear charges on carbon and hydrogen taken to be 2.868 a.u. and 1.00 a.u., respectively. The value obtained in this manner was 0.23D C+H−. However the exact value of the effective nuclear charge on carbon is open to question.

The spherical approximation to CH_4 is very attractive because the problem reduces to one involving a central field whose solution is known or can easily be calculated. Hartmann[21] treated CH_4 as a pseudoneon atom, calculating 0.4D C+H− for the CH bond moment. However Coulson[17] in attempting to compute the CH moment using the BMT[11] self-consistent field wave functions could not adapt the spherical model of CH_4 to give any sensible results. The tetrahedral orbitals do not point toward four distinct hydrogen atoms, and the fact that each of the four protons is supposed to be distributed over a part of a spherical surface made the notion of localized bonds untenable.

In closing this section, attention must be called to a basic difficulty which underlies any attempt to define the dipole moment of a CH bond when the latter is part of a molecule. For definiteness, consider methane, and suppose that the electron distrubution is known. At first sight it might seem the logical method for computing the CH moment would involve selecting a quarter section of the molecule whose axis is a line drawn from C to H, and locating the centroid of electron charge in this section. The fallacy in this viewpoint can be highlighted by supposing for the moment that instead of methane we deal with the central carbon atom alone whose electron distribution (at least in the Thomas-Fermi approximation) would be spherical. If we locate the centroid of electron charge in the same quarter section as before, we find that it does not occur at the origin *so that even the isolated carbon atom has a finite dipole moment when the latter is defined as above.* This is not a result of any specially directed atomic orbital either, since we have assumed the electron distribution is spherical.

Actually it is sensible to define a dipole moment only under conditions where the defined quantity has significance in terms of a measurement. For methane no unequivocal measurement exists, and so our interest in computing electron distributions should be directed towards evaluating the direction of polarization in the CH bond rather than its dipole moment. We can (as we have in the following text) define a quantity which measures this polarization and call it a dipole moment, but the quantity has no relation to any particular dipole moment *measurement.*

II. FORMULATION OF THE PROBLEM

For the present treatment of methane, the pyramids formed by the planes bisecting the HCH bond angles, are taken as the elements of symmetry. Each of these pyramids encloses a CH bond, and the four close-pack to form the methane molecule. In analogy with the cell method of solid-state physics,[22] where the atomic polyhedron in a crystal is replaced by a sphere of equal volume, we shall here replace the pyramid by a cone of equal volume. The problem devolves then upon solving the Thomas-Fermi equation for the potential within this cone, subject to appropriate boundary conditions. Replacing the pyramid by a cone reduces to the problem of calculating the apex angle of the isosceles triangle which when rotated 180° about the line bisecting this angle, (the CH bond axis), generates the cone whose volume equals that of the pyramid. From plane geometry, this angle is computed to be 92.80°. Because of symmetry about the bond axis, we may consider only half the triangle.

It is convenient to use spherical polar coordinates[23] with the carbon nucleus as origin. Taking account of cylindrical symmetry, the Thomas-Fermi equation

[18] A. Pullman and B. Pullman, *Les Theories Electroniques de la Chimie Organique* (Mason et Cie, Paris, 1952), p. 83.
[19] Thorndike, Wells, and Wilson, J. Chem. Phys. **15**, 157 (1947).
[20] C. R. Mueller and H. Eyring, J. Chem. Phys. **19**, 193 (1951).
[21] H. Hartmann, Naturforsch. **2A**, 489 (1947).
[22] F. Seitz, *Modern Theory of Solids* (McGraw-Hill Book Company, Inc., New York, 1940), p. 329.
[23] L. Pauling and E. Bright Wilson, Jr., *Introduction to Quantum Mechanics* (McGraw-Hill Book Company, Inc., New York, 1935), Appendix IV.

becomes

$$\frac{1}{r_2}\frac{\partial}{\partial r}\left(r^2\frac{\partial V}{\partial r}\right)+\frac{1}{r^2\sin\theta}\frac{\partial}{\partial\theta}\left(\sin\theta\frac{\partial V}{\partial\theta}\right)=\alpha V^{\frac{1}{2}}, \quad (1)$$

$$\alpha=32\pi^2e(2me)^{\frac{1}{2}}/3h^3, \quad (2)$$

$$0\leq r\leq\infty$$
$$0\leq\theta\leq\theta_m(46.40°). \quad (3)$$

The $\theta=0$ line is taken as the CH bond axis, and the equation is subject to the following boundary conditions:

$$V=0, \quad r=\infty$$
$$\lim_{r\to 0} Vr=Z_C e \quad Z_C=\text{atomic number of carbon},$$
$$\lim_{\substack{r\to r_H\\ \theta\to 0}} Vr=Z_H e \quad Z_H=\text{atomic number of hydrogen}. \quad (4)$$
$$r_H=\text{distance from H atom}.$$

In order that the solution in the cone join smoothly with the solution in other parts of the molecule, the potential was chosen to be stationary at $\theta=0$ and $\theta=\theta_m$, as symmetry requires. Notice that this condition accounts for the effect of other parts of the molecule.

III. METHOD OF SOLUTION

Because this problem was to be solved on a high-speed electronic computer (the IBM Type 701 electronic data processing machines)[24,25] the method of solution chosen was somewhat more routinized than the relaxation method[26] used in a previous calculation.[2] It was an iterative process, "The Extrapolated Liebmann Method"[27] which is related to the Southwell relaxation method in that it involves successively applied local corrections to improve an approximate solution. However, it is routinized in conformity with the requirements of automatic computers, while the relaxation method is flexible and depends in an essential way on the skill of the practitioner. Like the relaxation method it is not directly applicable to partial differential equations (and associated boundary conditions), but only to the finite difference approximations derived in the customary way.

To set the problem up in finite difference form, a net of uniform mesh size, must be constructed with r and θ as coordinate lines. Because the potential changes rapidly in the vicinity of either nucleus, the transformation $r=e^t$ was utilized to reduce the interval near carbon. The further transformation $\phi=\pi e^{t/2}(2V)^{\frac{1}{2}}$ was utilized with V in atomic units. To keep the problem within finite limits, the outer boundary was chosen as defined by $r=6$ a.u. At large distances from the nuclei, the solution approaches the spherical solution for an atom with nucleus of charge equal to the total nuclear charge of the molecule; the larger r is, the smaller the divergence from spherical symmetry.

Accordingly, on the outer boundary, the solution was taken to be the superposition of the spherically symmetric potentials of carbon and hydrogen. The latter was used also along the boundaries enclosing each nucleus, and symmetry conditions were applied at $\theta=0°$, and $\theta=46.40°$. With the above transformations, the Thomas-Fermi equation becomes,

$$\frac{\partial^2\phi^2}{\partial t^2}+\frac{\partial^2\phi^2}{\partial\theta^2}+\operatorname{ctn}\theta\frac{\partial\phi^2}{\partial\theta}=\frac{8}{3\pi^2}e^{3t/2}\phi^3 \quad (5)$$

where we have substituted for α of (2) in atomic units. The difference equation corresponding to (5) is

$$\frac{\phi_{i-1,j}{}^2-2\phi_{ij}{}^2+\phi_{i+1,j}{}^2}{\delta^2}+\frac{\phi_{i,j-1}-2\phi_{ij}{}^2+\phi_{i,j+1}{}^2}{\delta^2}$$
$$+\operatorname{ctn}\theta_i\left(\frac{\phi_{i,j+1}{}^2-\phi_{ij}{}^2}{\delta}\right)=\frac{8}{3\pi^2}e^{3t/2}\phi_{ij}{}^3, \quad (6)$$

where δ is the interval in both the θ and t directions, equal to 0.0578 a.u., and

$$i=1, 2, \cdots, N-1 \qquad N=64,$$
$$j=1, 2, \cdots, M-1 \qquad M=15,$$

the t coordinate thus including 64 points and the θ coordinate, 15.

The iteration method corrects each function value by σ times the "residual".[26] The correction process is applied to each of the lattice points in succession in a regular pattern. The function value so corrected is used in all subsequent operations in the same iteration step. σ is considered a variable and the optimum value of σ is chosen to insure rapid convergence. The optimum value of σ was chosen empirically as the calculation progressed on the machine.

If we have the nth approximation $\phi_{ij}{}^{2(n)}$ to the solution of the difference system, we obtain $\phi_{ij}{}^{2(n+1)}$ by

$$\phi_{ij}{}^{2(n+1)}=\phi_{ij}{}^{2(n)}+\sigma\left[\left\{\frac{\phi_{i-1,j}{}^{2(n+1)}-2\phi_{ij}{}^{2(n)}+\phi_{i+1,j}{}^{2(n)}}{\delta^2}\right\}\right.$$
$$+\left\{\frac{\phi_{i,j-1}{}^{2(n+1)}-2\phi_{ij}{}^{2(n)}+\phi_{i,j+1}{}^{2(n)}}{\delta^2}\right\}$$
$$\left.+\operatorname{ctn}\theta_i\left\{\frac{\phi_{i,j+1}{}^{2(n)}-\phi_{ij}{}^{2(n)}}{\delta}\right\}-\frac{8}{3\pi^2}e^{3t/2}\phi_{ij}{}^{3(n)}\right]. \quad (7)$$

Note that values previously corrected in the iteration process, $\phi_{i-1,j}{}^{2(n+1)}$ and $\phi_{i,j-1}{}^{2(n+1)}$ are used. Values of σ of 1.0 to 1.84 were used as the calculation progressed.

[24] IBM 701 Staff, Principles of Operation Type 701 and Associated Equipment, IBM Corporation, New York, 1953.
[25] J. W. Sheldon and L. H. Thomas, J. Appl. Phys. **24**, 235 (1953).
[26] R. V. Southwell, *Relaxation Methods in Theoretical Physics* (Oxford University Press, London, England, 1946).
[27] S. P. Frankel, Math. Trans. A.C. 4, 65 (1950).

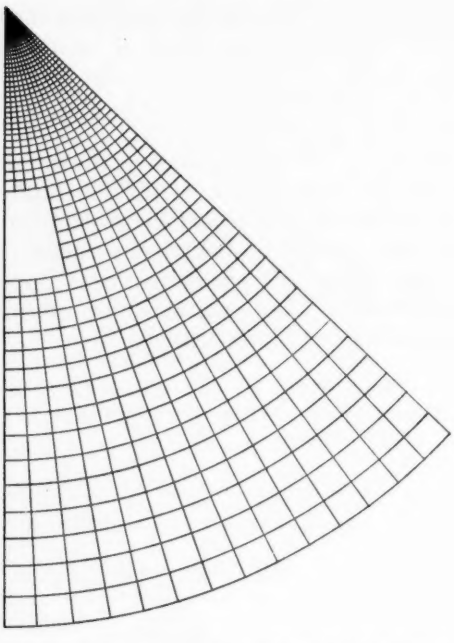

FIG. 1. Iteration net for methane unit cell. Radial lines are lines of constant θ, and arcs are lines of constant t.

(The values were found to have been useful in a similar calculation.)[5] The rate of convergence of this method of solution is treated theoretically by Frankel[27] using an eigenvalue problem analogy. It is necessary to study the "error eigenfunctions" which decrease at definite rates in successive approximations.

The iteration net appears in Fig. 1, where the arcs are values of constant r and the orthogonal slanting lines values of constant θ. Contours of the electron density in the cone appear in Fig. 2.

IV. THE CH BOND MOMENT IN METHANE

The Thomas-Fermi equation was solved for carbon alone and for carbon-hydrogen using the cone approximation. From the potential, the electron distribution in the cone was calculated, permitting the determination of the following charge and moment integrals:

Carbon

$$\text{Electronic Charge}=\int \rho_C d\tau = 1.58 \text{ a.u.}$$

$$\text{Electronic Moment}=\int \rho_C z d\tau = 2.80 \text{ a.u.} = 7.11 \text{ D} \tag{8}$$

Carbon-Hydrogen

$$\text{Electronic Charge}=\int \rho_{CH} d\tau = 2.63 \text{ a.u.}$$

$$\text{Electronic Moment}=\int \rho_{CH} z d\tau = 5.98 \text{ a.u.} = 15.2 \text{ D}, \tag{9}$$

where ρ=electronic charge density, z=z coordinate.

Although it was not possible to determine the charge contained in the cone *a priori*, the pyramid should contain $\frac{1}{4}$ of 10 e or 2.5 e. The charge appears to have been conserved reasonably well in the cone approximation, as indicated above by a value of 2.63 e. Also, the charge conservation has been consistent within the iteration process itself in that a charge of 1.58 e was obtained for carbon, and adding the 1 e for hydrogen gives 2.58 e as compared to the value of 2.63 e actually obtained.

The dipole moment is determined by computing the sum of the products of all charges, positive and negative, times their vector distance from the origin. Because of symmetry all but the z-components cancel. The location of the centroid of positive charge is calculated as follows:

$$\nu_+ = \frac{1.6\times 0 + 1.0\times 2.06}{2.6} \tag{10}$$

with the carbon nucleus as origin. The location of the centroid of negative charge is

$$\nu_- = \frac{5.98}{2.6}. \tag{11}$$

The dipole moment obtained when the expression

$$\mu = 2.6(\nu_- - \nu_+) \tag{12}$$

is evaluated is approximately 10 debyes after conversion from atomic units to esu. So large a value for the CH moment is extremely unlikely and brings up the question of the definition of a bond moment alluded to at the end of Sec. I. The method used above is that used in calculating the moment of any system of charges,[28] and the value obtained is rigorous in this sense. The method leads to reasonable results when applied to diatomic and other molecules, when the entire molecule is treated as a single system. However, when a bond in a molecule is considered as an isolated system, the meaning of the moment is not clear, although the polarity can be defined. The polarity of a bond is intimately associated in most discussions with the *change* from the electron distributions in the isolated atoms, to the distributions in the molecule. This picture of bond polarity is not necessary as far as the strict definition of the dipole moment is concerned. In the case of a diatomic molecule it makes no difference whether we consider the change in the electron distribution on going from the isolated atoms to the molecule or only the distribution in the molecult itself, because the atoms are spherically symmetric and their centers of positive- and negative-charge coincide. However, when we consider a bond in a polyatomic molecule, the situation is different in that the initial atomic distributions are not spherically symmetric. Then the question arises as to which

[28] L. Landau and E. Lifshitz, *The Classical Theory of Fields* (Addison-Wesley Press, Inc., Cambridge, 1951), p. 103.

method of determining the polarity of the bond should be used for the atoms are polar before bond formation. Coulson in the paper[17] mentioned earlier on the CH bond pointed out that such was the case for the carbon-tetrahedral orbital, which had a large dipole moment. It is the large dipole moment of this orbital that leads to the C+H− polarity which he obtains.

V. CONCLUSIONS

Until recently the question of whether the atomic dipoles should be subtracted from the dipole for the bond had not arisen. Recently Shull[29] computed the dipole moment of the CO bond in CO_2 by bisecting the molecule at the carbon atom with the plane perpendicular to the symmetry axis and then considering the semi-infinite region on one side of this plane (molecular orbital calculation). He obtained an extremely large value for the moment which he assumed was due to the large contribution of the asymmetric carbon orbital. When the terms involving this orbital were subtracted, the moment was much more reasonable. This led Shull to conclude that a standard state before bond formation must be chosen with respect to which the polarity of the bond is determined.

It appeared that the ambiguity arose because the method treated a region of space and not an orbital. In connection with Shull's paper, Coulson offered the opinion, that moments resulting from the determination of the asymmetry of charge in any region should be referred to as "volume moments" and that one should be wary about treating them as conventional bond moments. Coulson in this comment refers to a calculation by Orgel in which the CH bond moment was calculated from the BMT data[11] using the volume concept. The electron distribution in methane obtained by BMT was used in the following manner. The solid angle around an isolated carbon atom was divided into four equal tetrahedral parts. The centroid of charge within one of these parts gave a dipole moment of 3.45 D. With a hydrogen atom placed at 2 a.u. from the carbon nucleus and using the BMT methane field, a moment of 4.06 D is obtained. The *difference* is taken to be the dipole moment of the CH bond in methane, 0.6 D C+H−.

If the above concept is used in the present case, and the carbon atomic moment in the cone is subtracted from that of carbon-hydrogen [Eqs. (8) and (9)], then a dipole moment of 2.8 D C+H− is obtained.

[29] H. Shull, Proc. Natl. Acad. Sci. **38**, 400 (1952).

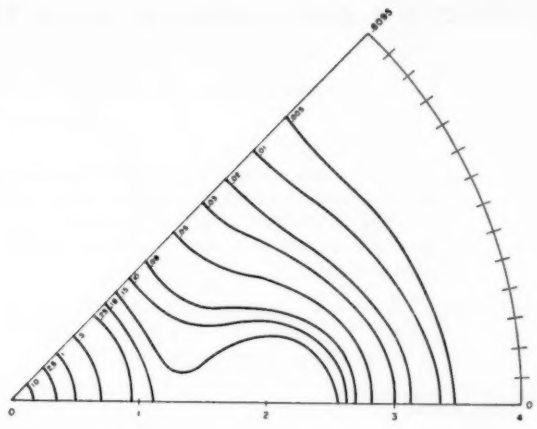

FIG. 2. Map of electron density for methane. The densities listed on the various contour lines are measured in atomic units. Similarly the radial coordinate is in atomic units. The angular coordinate covers the range, 0.8095 radian.

The large value for the carbon atomic moment, Eq. (8), may be attributed to the fact that the number of electrons being considered is small, 1.5 e, and that the statistical method cannot be expected to give an accurate description of the charge distribution of a system with so few electrons. Although the carbon-hydrogen system in the approximation of the cell description of the CH bond, contains a somewhat greater electronic charge, 2.5 e the above criticism is still valid. Certainly the Thomas-Fermi atomic distributions go to zero at large distances much more slowly than those obtained by quantum mechanics, the centroid of charge is located further from the origin leading to a larger moment. The main feature to be emphasized in the present calculation is the polarity C+H− which agrees with Coulson[17] and Mueller and Eyring[20] among others.

VI. ACKNOWLEDGMENTS

The authors wish to acknowledge the aid of Mr. John Sheldon and the 701 staff at the New York office of IBM in the numerical solution of the differential equation. We also wish to thank Mr. Richard Hamming and his group at the Bell Telephone Laboratories for their assistance and the use of their laboratory IBM equipment in preparing the input for the 701 computation.

Thanks are due also Professor Walter Hauser of the Physics Department at Boston University for his valuable comments on this work.

Effect of a High *cis*-Barrier on the Microwave Spectrum of Hydrogen Peroxide*

J. T. Massey and Robert W. Hart
Applied Physics Laboratory, The Johns Hopkins University, Silver Spring, Maryland
(Received September 21, 1954)

The frequency spectrum in the microwave region and the Stark effect are obtained for the case of a potential function with a high *cis*-peak and a low *trans*-peak. Using the presently available experimental data on H_2O_2 it is not possible to determine whether this potential function or the *cis*-peak equal *trans*-peak potential function is correct. It is shown, however, that the microwave data can answer this question if sufficient resolution is obtained.

I. INTRODUCTION

THE available microwave data on H_2O_2 can apparently be satisfactorily explained with the assumption of a sinusoidal hindering potential having a height of only about 113 cm^{-1}.[1] It has been suggested, however, that a high barrier in the *cis*-configuration, combined with a low barrier in the *trans*-position, might also account for the observed splitting in the microwave region.[2,3] Since there is some evidence, both theoretical and experimental, to support this view,[4] we have decided to investigate the effect of such a potential on the microwave spectrum and to determine if the microwave data is sufficient to indicate the form of the hindering potential.

II. THE ENERGY LEVELS AND SELECTION RULES FOR A HIGH *CIS* LOW *TRANS* POTENTIAL FUNCTION

In the previous paper in which the sinusoidal hindering potential function was considered, the hydrogen peroxide molecule was represented by a symmetric top.[1] This resulted in a separable wave equation allowing the effect of hindered rotation to be studied separately and its characteristic energy levels to be superposed on the rotational spectrum of the symmetric top. These same assumptions will be used for this study, and are summarized as follows: (1) The molecule is assumed to be a symmetric top. (Fig. 1). (2) The molecule is assumed to be rigid except for the hindered internal motion. (3) The hindering potential $V(\chi)$ is assumed to be an even periodic function of the general form shown in Fig. 2. These assumptions lead to a wave equation having solutions of the form[5]

$$U(\psi,\theta,\varphi_1,\varphi_2)=\frac{1}{2\pi}\Theta(\theta)P(\chi)\exp(im\psi+iK\varphi),$$

where ψ, θ, φ, are the usual Eulerian angles, φ_1 and φ_2 refer to the two O—H bars (Fig. 1), and where $\varphi=(\varphi_1+\varphi_2)/2$, $\chi=\pi-(\varphi_1-\varphi_2)$. The effect of hindered rotation is described by $P(\chi)$, which satisfies the equation:

$$\frac{d^2P(\chi)}{d\chi^2}+\frac{I_a}{2\hbar^2}[W_2-V(\chi)]P(\chi)=0, \tag{1}$$

where I_a is the small moment of inertia for the hydrogen-peroxide molecule. The boundary conditions on $P(\chi)$ are determined by requiring that the total wave function U be a single-valued function of the coordinates φ_1 and φ_2. Substitution of this condition into the expression for the total wave function leads to $P(\pi)=P(-\pi)$ for even K and $P(\pi)=-P(-\pi)$ for odd K. Therefore,

	for symmetric $P(\chi)$	for antisymmetric $P(\chi)$†
for even K	$\left\{\frac{dP(\chi)}{d\chi}\Big\|_{\chi=-\pi}=\frac{dP(\chi)}{d\chi}\Big\|_{+\pi}\right.=0,$	$P(-\pi)=-P(+\pi)=0,$
for odd K	$\left\{P(-\pi)=+P(+\pi)=0,\right.$	$\frac{dP(\chi)}{d\chi}\Big\|_{-\pi}=-\frac{dP(\chi)}{d\chi}\Big\|_{+\pi}=0.$

(2)

It will now be demonstrated that for the case of a high *cis*- and low *trans*-barrier, those hindered rotation states lying far below the *cis*-peak are dependent on the symmetry of the wave function but independent of the values of K. As a result, the lower states of the spectrum characterizing this model can be constructed without actually specifying the shape and magnitude of the hindering potential. Let $P_{a,b}$ represent the function $P(\chi)$, with the first subscript indicating odd or even K,

* This work was supported by the Bureau of Ordnance, Department of the Navy, under NOrd 7386.
[1] J. T. Massey and D. R. Bianco, J. Chem. Phys. **22**, 442 (1954).
[2] W. S. Benedict (private communication).
[3] N. W. Luft (private communication).
[4] See bibliography of reference 1.
[5] J. S. Koehler and D. M. Dennison, Phys. Rev. **57**, 1006 (1940).
† See Herzberg (Chapter II) for a discussion of the symmetry properties of the vibrational eigenfunctions for a molecule of this type (point group C_2).

and the second indicating symmetric (s) or antisymmetric (a) wave functions. Then

$$\frac{d^2P_{0,s}}{d\chi^2}+\frac{I_a}{2\hbar^2}[W_{0,s}-V(\chi)]P_{0,s}=0 \quad (3)$$

and

$$\frac{d^2P_{e,s}}{d\chi^2}+\frac{I_a}{2\hbar^2}[W_{e,s}-V(\chi)]P_{e,s}=0. \quad (4)$$

Multiply the first equation by $P_{e,s}$, the second by $P_{0,s}$ and subtract to obtain

$$\frac{d}{d\chi}\left\{\frac{dP_{0,s}}{d\chi}P_{e,s}-\frac{dP_{e,s}}{d\chi}P_{0,s}\right\}=\frac{I_a}{2\hbar^2}[W_{0,s}-W_{e,s}]P_{0,s}P_{e,s}. \quad (5)$$

Integrating between $-\pi$ and $+\pi$, we obtain the

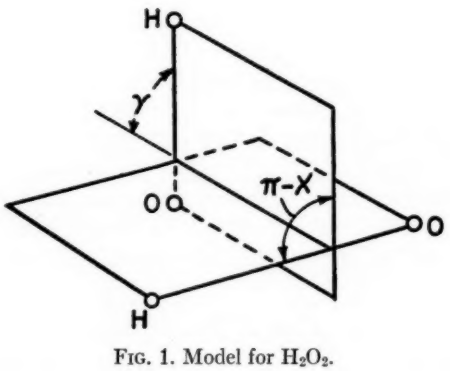

FIG. 1. Model for H_2O_2.

equation

$$\left\{\frac{dP_{0,s}}{d\chi}P_{e,s}-\frac{dP_{e,s}}{d\chi}P_{0,s}\right\}\Bigg|_{-\pi}^{\pi}=\frac{I_a}{2\hbar^2}[W_{0,s}-W_{e,s}]\int_{-\pi}^{\pi}P_{0,s}P_{e,s}d\chi. \quad (6)$$

Note that $dP_{e,s}(\pm\pi)/d\chi$ and $P_{0,s}(\pm\pi)$ are both zero from the boundary conditions [Eq. (2)]‡ so that $P_{0,s}$ and $P_{e,s}$ are not, in general, orthogonal. As the *cis*-barrier is increased in height, however, the wave function $P_{e,s}(\pm\pi)$ approaches zero and $dP_{0,s}(\pm\pi)/d\chi$ must remain finite. The left-hand side of Eq. (6) then approaches zero and since the integral does not, in general, vanish, the two energy levels must approach each other. A similar argument can be applied to the antisymmetric wave functions to establish the independence of the hindered rotation energy levels on K for large *cis*-barriers.

‡ Requiring single valuedness of the total wave function leads to boundary conditions which are not the same for odd K as for even K and eigenfunctions corresponding to an eigenvalue associated with odd K are not, in general, orthogonal to eigenfunctions corresponding to an eigenvalue associated with even K.

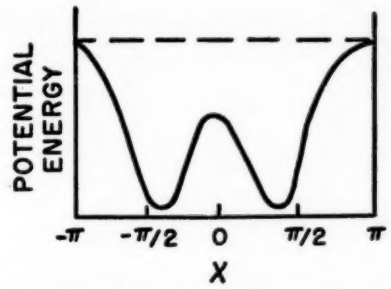

FIG. 2. General form of the variation of potential energy with the angle χ for the model of Fig. 1.

The selection rules for this molecule allow only transitions for which $\Delta J=0, \pm1$, and for which $\Delta K=\pm1$. Since the dipole moment operator is antisymmetric in the angle χ, the selection rules allow only transitions between two hindered rotation states of opposite symmetry.

III. THE SPECTRUM

The spectra predicted by the high *cis* low *trans* and low *cis*=*trans* barriers will now be compared with each other and with the available microwave data. The transitions which are available for comparison are indicated in Table I, and the general method of comparison will be similar to that adopted in the previous paper.[1] It is necessary, in order that the new model be consistent with the data, that it be able to predict the transitions of Table I with reasonable values of the hydrogen-peroxide molecule moments of inertia.

The energy levels characteristic of either the high *cis* low *trans* or the low *cis*=*trans* models are given by[1]

$$W=[BJ(J+1)+AK^2]+W_2, \quad (7)$$

where the terms in the bracket correspond to the symmetric top energy, and where W_2 is one of the appropriate eigenvalues of Eq. (1). The geometry of the hydrogen-peroxide molecule yields approximate values

TABLE I.

Line	Frequency Mc/sec	Remarks
1	14 829.5±0.2	Quadratic Stark effect $J^*=1$
2	37 517.6±0.2	Quadratic Stark effect $J^*=2$
3	22 054.5±0.2	Quadratic Stark effect $J^*\geq7$, $\lvert\Delta J\rvert=1$
4	27 639.6±0.2	Quadratic Stark effect $J^*\geq7$, $\lvert\Delta J\rvert=1$
5	11 072.4±0.5	Quadratic Stark effect "probably high J"
6	35 916±2	Quadratic Stark effect high J, $\lvert\Delta J\rvert=1$
7	39 033±2	Probably high J
8	39 495±2	Probably high J
9	39 760±2	Probably high J
10	16 032±2[a]	

J^* is the larger of the two values of J involved. Lines 5, 6, and 7 are relatively weak.

[a] This line was found by Jen, Beard, and Massey subsequent to the publication of reference 1.

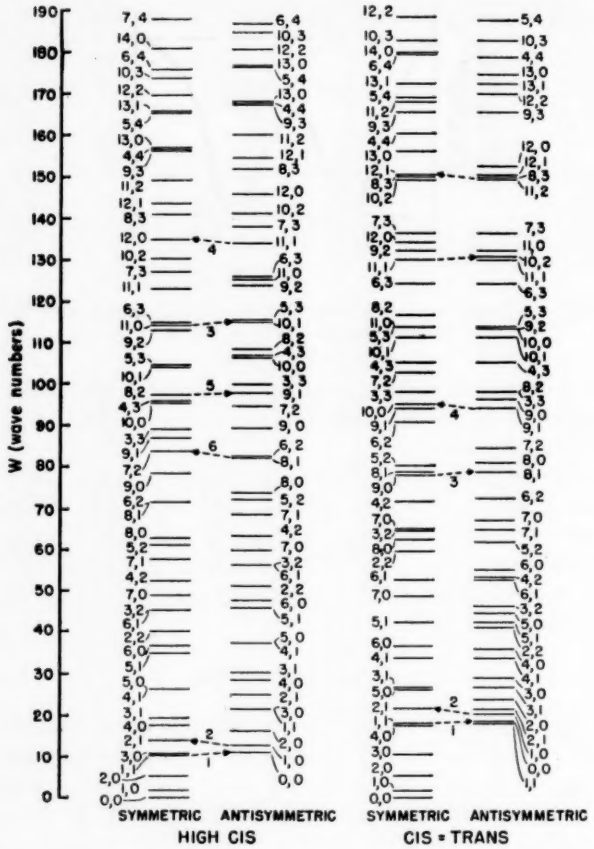

FIG. 3. Energy level diagram for both the low *cis*=*trans* and high *cis* low *trans* potential function (J,K).

of the constants A and B. It is found that[1]

$$B=\frac{\hbar}{4\pi cI_b}\approx 0.83 \text{ cm}^{-1} \text{ to } 0.92 \text{ cm}^{-1}$$

$$A=\frac{\hbar}{4\pi c}\left[\frac{1}{I_a}-\frac{1}{I_b}\right]\approx 8.4 \text{ cm}^{-1} \text{ to } 9.2 \text{ cm}^{-1}$$

[and, therefore, that $I_a/2\hbar^2=1/4(A+B)$ when A, B are in wave numbers and $I_a/2\hbar^2$ is in reciprocal wave numbers].

Consider, first, the two transitions which have been uniquely assigned by experiment (Table I). By writing Eq. (7) with the values of K and J representing these transitions, and then subtracting, it is found that $B=0.8725$ cm^{-1} (for either model). This value of B leads to

$$A-\Delta=2.2394 \text{ cm}^{-1},$$

where Δ is the splitting between the symmetric and antisymmetric hindered rotation levels.

If experiment had been able to assign definite J and K values to one additional pair of lines, it should be possible immediately to test whether the model is consistent with the data. In the absence of this information, we ask whether or not this model will predict such transitions with reasonable values of the molecular parameters B and A. Introduce a small centrifugal distortion coefficient B_1 in order to provide another parameter to fit two more lines. The energy levels are now assumed to be given by

$$W=J(J+1)\{B+B_1J(J+1)\}+AK^2+W_2. \quad (8)$$

The assignment of lines (3) and (4) which yields the most reasonable values of A and B appears to be to the pair 11,0,s→10,1,a; 11,1,a→12,0,s for which it is found that $B=0.8732$ cm^{-1}, $B_1=-0.00005673$ cm^{-1}, and $A=8.7019$ cm^{-1}. The splitting of the lowest hindered rotation state is also determined by this procedure to be $\Delta=10.942$ cm^{-1}.

An energy level diagram obtained by using these values in Eq. (8) is illustrated in Fig. 3. A diagram obtained in a similar way from the low *cis*=*trans* model is also shown. In so far as the number of microwave transitions is concerned, the two models are similar. However, the transitions do not occur between levels of the same quantum numbers.

On the basis of the low *cis*=*trans* model, lines (3) and (4) were assigned to the levels (9,0)→(8,1) and (9,1)→(10,0), respectively, whereas in this model they are assigned to the levels (11,0)→(10,1) and (11,1)→(12,0), respectively. If the J-value could be definitely assigned from experiment, these transitions might provide evidence substantiating one or the other of the models.

The values of the molecular parameters obtained using the high *cis*- low *trans*-barrier are close to those obtained from the low *cis*=*trans* model, and do not appear to form any basis for preferring one model above the other.

IV. THE STARK EFFECT

Examination of the matrix elements for the Stark effect indicates that the influence of hindered internal rotation is the same for both the low *cis*=*trans* case and the high *cis* low *trans* case. The effect of hindered rotation is twofold: (1) The value of the permanent dipole moment to be used is dependent upon the hindered rotation and (2) in the actual evaluation of the matrix elements from the results in the literature[6] one-half the line strength must be used since the inversion degeneracy has been removed. The calculations are made using the values of A, B, B_1, and W_2 from the preceding section to determine the energy differences not available from the experimental data. The results are, for $\Delta m=0$,

Line 1 $\Delta\nu=\mu^2\epsilon^2[5.76-5.68 \text{ m}^2]\times10^{-6}$ Mc/sec

Line 2 $\Delta\nu=\mu^2\epsilon^2[1.29-0.804 \text{ m}^2]\times10^{-6}$ Mc/sec

Line 3 $\Delta\nu=\mu^2\epsilon^2[1.42-0.0117 \text{ m}^2]\times10^{-6}$ Mc/sec

Line 4 $\Delta\nu=\mu^2\epsilon^2[0.980-0.0069 \text{ m}^2]\times10^{-6}$ Mc/sec

Line 5 $\Delta\nu=\mu^2\epsilon^2[0.978-0.0123 \text{ m}^2]\times10^{-6}$ Mc/sec

Line 6 $\Delta\nu=\mu^2\epsilon^2[0.307-0.0045 \text{ m}^2]\times10^{-6}$ Mc/sec.

[6] P. C. Cross and R. M. Hainer, J. Chem. Phys. **12**, 210 (1944); S. Golden and E. B. Wilson, Jr., J. Chem. Phys. **16**, 669 (1948).

It can be seen that the calculated energy differences will be slightly in error for $K>1$ since the correction to A which depends upon J and K was not made in Sec. III. This makes very little difference since the perturbing effect of these levels is small compared to that of the levels involved in the transition.

The calculated results may now be compared with the experimental results. The experimental data available is listed below:

Line 1 $\Delta\nu=29.09\epsilon^2\times10^{-6}$ Mc/sec

Line 2 $\Delta\nu=(6.88-4.25\,m^2)\epsilon^2\times10^{-6}$ Mc/sec

Line 3 $\Delta\nu=(6.07-0.0727\,m^2)\epsilon^2\times10^{-6}$ Mc/sec $(J^*\geqq9)$
$\Delta\nu=(6.47-0.0623\,m^2)\epsilon^2\times10^{-6}$ Mc/sec $(J^*\geqq10)$
$\Delta\nu=(6.95-0.0552\,m^2)\epsilon^2\times10^{-6}$ Mc/sec $(J^*\geqq11)$

Line 4 $\Delta\nu=(4.18-0.0537\,m^2)\epsilon^2\times10^{-6}$ Mc/sec $(J^*\geqq8)$
$\Delta\nu=(4.49-0.0459\,m^2)\epsilon^2\times10^{-6}$ Mc/sec $(J^*\geqq9)$
$\Delta\nu=(5.10-0.0356\,m^2)\epsilon^2\times10^{-6}$ Mc/sec $(J^*\geqq10)$.

It is found that the best fits occur if the following assignment is made. (For lines 1 and 2 there is no question.)

Line 3 $\Delta\nu=(6.95-0.0552\,m^2)\epsilon^2\times10^{-6}$ Mc/sec $(J^*\geqq11)$
Line 4 $\Delta\nu=(5.10-0.0356\,m^2)\epsilon^2\times10^{-6}$ Mc/sec $(J^*\geqq10)$.

Table II indicates the values of dipole moment and comparison of the B/A ratio for both the low *cis*=*trans* and the high *cis* low *trans* case.

V. THE HIGH *CIS* LOW *TRANS* POTENTIAL FUNCTION

Magnitudes of the high *cis*- low *trans*-barriers will now be determined which yield the splitting of 10.9 wave numbers indicated by the microwave data. Since only the lowest state of the hindered rotation part of the wave equation [Eq. (1)] is involved, we will not attempt to use the WKB method, but will calculate the energy levels by selecting hindering potentials for which the solutions of equations of this form are known.

TABLE II. Dipole moments and ratios of B to A in the expression $\Delta\nu=(A-Bm^2)\epsilon^2\times10^{-6}$.

	Low *cis*=*trans* case[a]			High *cis* low*t rans* case		
Line	μ	Exp B/A	Calc B/A	μ	Exp B/A	Calc B/A
1	2.26	···	−1.00	2.25	···	−0.985
2	2.26	−0.618	−0.598	2.31	−0.618	−0.624
3	2.16	−0.0120	−0.0115	2.21	−0.00794	−0.00824
4	2.10	−0.0102	−0.0109	2.28	−0.00698	−0.00704
5				2.31	···	−0.0126[b]
6				2.39	···	−0.0146[b]

[a] The calculated values are slightly different from those of reference 1 partly because in that paper a centrifugal distortion coefficient was not included, and partly because all of the perturbing elements allowed by the symmetry of the hindered rotation wave functions were not used.

[b] In order to obtain a reasonable value for μ, lines (5) and (6) were assigned to the transitions

$8,2,s\rightarrow9,1,a$ and
$8,1,a\rightarrow7,2,s$, respectively.

The measured Stark effect is

Line 5 $\Delta\nu=5.213\ \epsilon^2\times10^{-6}$ Mc/sec
Line 6 $\Delta\nu=1.749\ \epsilon^2\times10^{-6}$ Mc/sec.

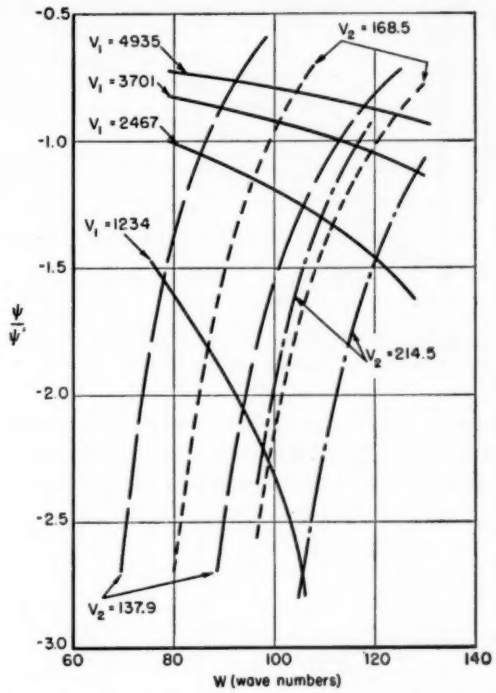

FIG. 4. Reciprocals of the logarithmic derivatives for matching the wave functions (V_1 and V_2 are given in wave numbers).

Let the hindering potential function be represented by

$$V(\chi)=\left(\frac{2}{\pi}\right)^2V_1\left(\chi-\frac{\pi}{2}\right)^2$$
$$+\frac{\pi}{2}\leq\chi\leq+\pi \text{ (region 1)}$$
$$V(\chi)=V_2\left(\frac{1+\cos2\chi}{2}\right)$$
$$-\frac{\pi}{2}\leq\chi\leq+\frac{\pi}{2} \text{ (region 2)} \quad (9)$$
$$V(\chi)=\left(\frac{2}{\pi}\right)^2V_1\left(\chi+\frac{\pi}{2}\right)^2$$
$$-\pi\leq\chi\leq-\frac{\pi}{2} \text{ (region 3)}.$$

The method of solution of problems of this type is well known and will not be reproduced here. Two significant points may be noted, however.

(1) In regions (1) and (3), solutions of Eq. (1) are hypergeometric functions. Because of the fact that $\frac{1}{2}I_a(V_1/\hbar^2)\gg1$, the asymptotic representation[7] for the hypergeometric functions may be used when applying the boundary conditions Eq. (2) at $\chi=\pm\pi$. Only the

[7] Jeffries and Jeffries, *Mathematical Physics* (Cambridge University Press, New York, 1946), p. 578.

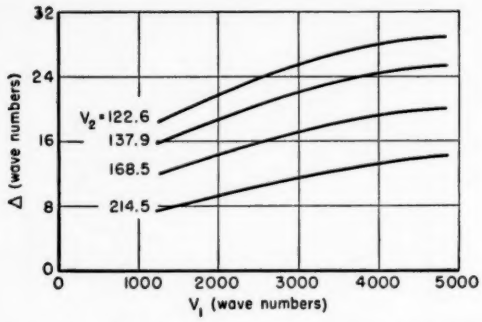

FIG. 5. Variation of the splitting (Δ) with height of the *cis*-barrier (V_2 in wave numbers).

first term of the power series expansion is required at $\chi=\pm\pi/2$. The logarithmic derivative of the wave function in region (1) evaluated at $\pi/2$ is then given by

$$\frac{d}{d\chi}\ln P(\chi)\bigg|_{\pi/2}=-\frac{1}{2}\left(\frac{I_a}{\pi^2\hbar^2}2V_1\right)^{-\frac{1}{4}}\left\{\frac{\Gamma\left[\frac{3}{4}-\frac{WI_a/2\hbar^2}{\left(\frac{2I_aV_1}{\pi^2\hbar^2}\right)^{\frac{1}{4}}}\right]}{\Gamma\left[\frac{1}{4}-\frac{WI_a/2\hbar^2}{\left(\frac{2I_aV_1}{\pi^2\hbar^2}\right)^{\frac{1}{4}}}\right]}\right\} \tag{10}$$

for both symmetric and antisymmetric $P(\chi)$ and for both even and odd K. From Sec. III, $I_a/2\hbar^2=1/4(A+B)=1/38.3$ cm^{-1} in order to yield the observed splitting.

(2) In the central region, solutions of Eq. (1) are Mathieu functions of nonintegral order. Although suitable tables of such functions are not available, computation is relatively simple although lengthy for the low barriers under consideration.[8]

Figure 4 illustrates the behavior of the logarithmic derivatives of $P(\chi)$ at $\pi/2$, and the intersections correspond to the energy levels W_2. Unlike the case for the low *cis*=*trans* sinusoidal potential function where the barrier height is uniquely determined by the splitting, the case under consideration has a continuum of possible values of V_1 and V_2. Approximately 11 cm^{-1} splitting is obtained, for example, for $V_1=2800$ cm^{-1} and $V_2=214.5$ cm^{-1}. It is evident that increasing the *cis*-barrier height tends to raise the energy levels and to increase the splitting. This behavior is illustrated in Fig. 5.

A square well potential function and a triangular potential function were also used to indicate the effect of barrier shape on the values of V_1 and V_2 as well as to give a qualitative check to the analysis. The results indicate that the potential function used gives values of V_1 and V_2 which are intermediate between those for the extreme potential shapes above.

VI. CONCLUSIONS

Evaluation of the expression

$$\frac{\int|P(\chi)|^2\cos\left(\frac{\pi-\chi}{2}\right)d\chi}{\int|P(\chi)|^2d\chi}$$

leads to a result which can be interpreted physically as the average of the cosine of the angle between the two O—H bars. For the case $V_1=2800$ cm^{-1} and $V_2=214.5$ cm^{-1} the value of this expression is 0.58, corresponding to an average $(\pi-\chi)$ of 108°. This, in turn, indicates a value of 1.9 Debye units for the component of OH dipole moment perpendicular to the figure axis of the H_2O_2 molecule.

The results of the analysis of this paper indicate:

(1) With the microwave data now available it is not possible to decide whether the high *cis* low *trans* or the low *cis*=*trans* potential function is correct.

(2) If sufficient resolution to determine uniquely the value of J^* for lines 3, 4, 5, and 6 can be obtained, it should be possible to decide which potential function is correct from the microwave data alone.

(3) The microwave data is not sufficient to assign unique values to V_1 and V_2.

ACKNOWLEDGMENTS

The authors wish to express their appreciation to their colleagues Dr. C. K. Jen, Dr. C. I. Beard, Dr. R. Fristrom, and Mr. D. R. Bianco for helpful discussions. Particular appreciation is due Mrs. Mary Lynam for her computational assistance and Mr. G. C. Weiffenbach for preparation of the figures.

[8] McLachlan, *Theory and Application of Mathieu Functions* (Oxford University Press, New York, 1951), Ch. IV.

Infrared Spectrum, X-Ray Diffraction Pattern, and Structure of Ammonium Fluoride*

ROBERT C. PLUMB† ‡ AND DONALD F. HORNIG
Metcalf Chemical Laboratories, Brown University, Providence, Rhode Island
(Received August 23, 1954)

The infrared spectrum of ammonium fluoride and deutero-ammonium fluoride at −195°C and 25°C is shown to be explicable in terms of "essentially" T_d symmetry requiring that the axial ratio (c/a) be 1.63. New x-ray-lattice parameter measurements show this to be true. A comparison of the spectrum of NH_4F with other ammonium salts indicates that broad bands do not necessarily accompany strong hydrogen bonds.

I. INTRODUCTION

AMMONIUM fluoride is of considerable interest because strong hydrogen bonds can be anticipated and their effect on the spectrum of the ammonium ion determined by comparison with the other ammonium halides. Moreover, the structure of ammonium fluoride is essentially the same as that of ice and the N−F distances are very nearly equal to the O−O distance (2.76 A). The information gained from NH_4F may be useful in interpreting the spectrum of ice which is complicated by disorder in the proton positions.

The crystal structure of ammonium fluoride is hexagonal.[1] The unit cell parameters have been reported as $a=4.39\pm0.04$ A, $c=7.02\pm0.06$ A, and the space group as C_6^6 or C_6v^4. The reported axial ratio (c/a) is 1.60 ±0.03 compared to 1.63 for hexagonal closest packing, requiring that one N−F distance is 2.63 A and the other three are 2.69 A if the parameter u has the value $\frac{3}{8}$ reported by Zachariasen. Such a large distortion from a tetrahedral arrangement of the fluorine ions about each ammonium ion would show up strongly in the infrared spectrum. In ammonium bromide displacement of the bromide ions by 0.09 A from the cubic positions produces a splitting of 25 cm^{-1} in the triply degenerate bending vibrations of the ammonium ion (ν_4),[2] and in ammonium iodide a distortion of only 0.04 A produces a splitting of 19 cm^{-1}.[3,4]

The Raman spectrum of crystalline ammonium fluoride has been reported,[5] and Bovey[4] has recently published the results of infrared absorption and reflection measurements on ammonium fluoride. He found that the triply degenerate bending vibration ν_4 was split by 19 cm^{-1} and that the stretching region was very broad and diffuse. However, since a preliminary investigation in this laboratory[6] had shown that exchange of halogen ions occurs on the sodium-chloride backing used by Bovey, it seemed desirable to undertake a new investigation.

Finally, the existence of a small heat-capacity maximum at −30°C indicates that NH_4F undergoes a phase change.[7] In the other ammonium salts, in which each ammonium ion is surrounded by eight halide ions, similar phase changes have been demonstrated to result from disordering of the equilibrium orientation of the NH_4^+ ions. Since there are only four nearest neighbors in the NH_4F structure, a different explanation must be sought if the phase change is genuine.

II. EXPERIMENTAL

The experimental procedures used in this investigation were similar to those described previously.[2,8] The ammonium fluoride§ was purified by fractional vacuum sublimation. Samples for infrared-absorption studies were prepared by sublimation to a salt window cooled to −78°C. Films thus prepared showed distinct interference fringes. All manipulation of the films was carried out in vacuum or in a stream of dry nitrogen gas. The thicknesses of the films were estimated from the variation of interference color with angle of observation. Because of the high vapor pressure of ammonium fluoride, it was not possible to evacuate the cell before cooling it to liquid-nitrogen temperature. The room-temperature spectrum was obtained with the cell containing 1 cm Hg pressure of nitrogen. The ammonium-fluoride film was then cooled with dry nitrogen blowing on the cell windows to prevent condensation of atmospheric moisture. When the temperature had been reduced to where the vapor pressure of the ammonium fluoride was negligible, the cell was evacuated. Since it was found that ammonium fluoride exchanged halogen ions rapidly with sodium chloride and potassium bromide, films were investigated on silver-chloride backing windows where no exchange was observed. Films were also prepared on a calcium-fluoride backing to see if there were any orientation effects caused by the silver-chloride lattice. No effects were observed.

Deutero-ammonium fluoride was prepared by exchanging ammonium fluoride with D_2O. The cell shown

* Based on a thesis presented by Robert C. Plumb in partial fulfillment of the requirements for the Ph.D. degree, Brown University, 1953.

† Present address, Aluminum Research Laboratories, Aluminum Company of America, New Kensington, Pennsylvania.

‡ E. I. de Pont de Nemours and Company, Inc., Fellow in Chemistry, 1951–52.

[1] W. Zachariasen, Z. physik. Chem. **127**, 218 (1927).

[2] E. L. Wagner and D. F. Hornig, J. Chem. Phys. **18**, 296, 304 (1950).

[3] Dinsmore, Hornig, and Plumb (to be published).

[4] L. F. H. Bovey, J. Opt. Soc. Am. **41**, 836–48 (1951).

[5] R. Ananthakrishnan, Proc. Indian Acad. Sci. **5A**, 76 (1937).

[6] E. L. Wagner (unpublished observation).

[7] F. Simon, Z. physik. Chem. **129**, 339 (1927).

[8] Hornig, Hyde, and Adcock, J. Opt. Soc. Am. **40**, 497 (1950).

§ Baker and Adamson, C.P. Grade.

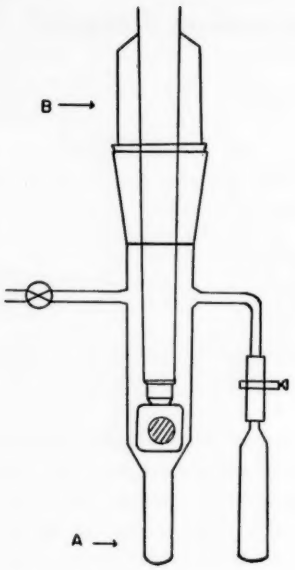

FIG. 1. Cell used for deuterating NH_4F and preparing films of ND_4F.

in Fig. 1 was used for the exchange reaction. The ammonium fluoride was placed in the nipple *A*. The upper part of the cell *B* was the coolant reservoir and block of the absorption cell. The D_2O vial was connected by Tygon tubing to the cell. D_2O was transferred by evaporation, controlled by a Hoffman clamp. The silver-chloride backing window was placed on the block before the exchange process was started so that all steps from the first exchange to the final preparation of the film could be carried out in the same system. The transfer of the upper part of cell *B* to the absorption cell was carried out while blowing nitrogen gas (dried with a liquid nitrogen trap) over the film. The deutero-ammonium fluoride thus prepared was better than 95 percent deuterated as estimated from the relative intensity of bands which are assigned to ND_3HF.

III. EXPERIMENTAL RESULTS

The observed spectra of ammonium fluoride and deutero-ammonium fluoride at 25°C and −195°C are shown in Figs. 2 and 3. An extra-thick film of ammonium fluoride is shown at −195°C to give the maximum amount of detail. The film of intermediate thickness in Fig. 2 at −195°C was estimated to be 0.8 micron thick by its interference colors.

The most striking features of the NH_4F spectrum are the sharp lines and the large number of bands, shoulders, and general spectral detail in the low-temperature spectrum. The high-frequency stretching region from 2500 to 3300 cm^{-1} is extremely complicated, with eleven distinct peaks at −195°C. The low-frequency bending region from 1400 to 1600 cm^{-1} shows sharp lines and the strong line at 1494 cm^{-1} has a half-width of only seven cm^{-1}. The region from 1600 to 2500 cm^{-1} would usually be thought to contain an infrared inactive (under T_d) bending mode and lattice frequencies in combination with bending vibrations. The relative intensities of the observed bands are surprising since combination bands are usually less intense than fundamentals.

Bovey observed distinct peaks at 1503 cm^{-1} and 1484 cm^{-1} whereas only one peak of comparable inten-

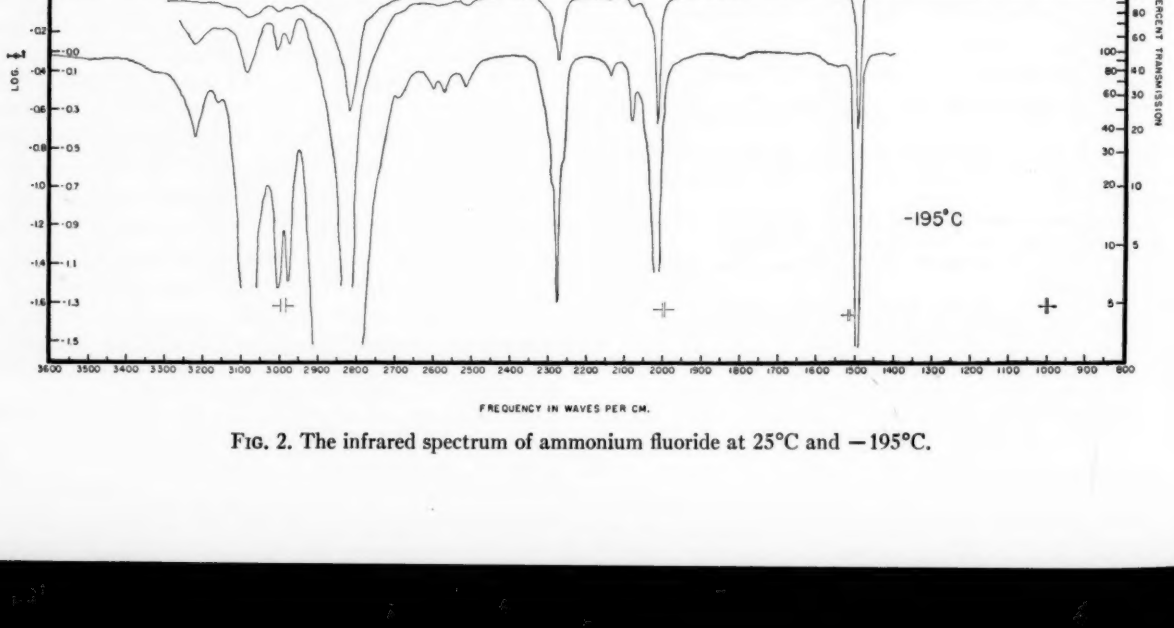

FIG. 2. The infrared spectrum of ammonium fluoride at 25°C and −195°C.

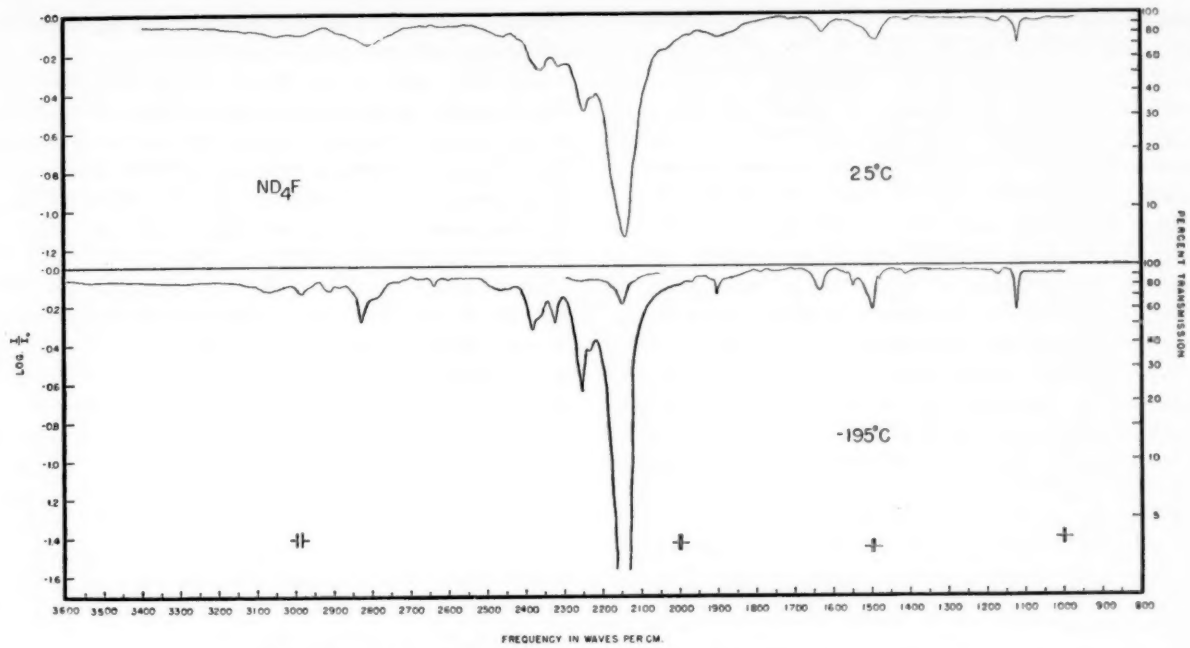

FIG. 3. The infrared spectrum of deutero-ammonium fluoride at 25°C and −195°C.

sity was found in this work. Bovey also found that the 2800 cm^{-1} region was very broad and diffuse. No comparable characteristics were observed in this work.

Most of the detail is lost in the room-temperature spectrum, and all of the line widths increase considerably. The spectrum is therefore consistent with a phase change and may indicate a certain amount of disordering in the room-temperature phase.

IV. STRUCTURE OF AMMONIUM FLUORIDE

The unit cell of ammonium fluoride as commonly represented is shown in Fig. 4. The highest symmetry which an ammonium ion may have in this unit cell is C_{3V}. The nearest-neighbor fluoride ions are arranged about the ammonium ion approximately tetrahedrally. In the event that the axial ratio were 1.63 (hexagonal closest packing), the nearest-neighbor fluoride ions would be arranged exactly tetrahedrally, but the site symmetry would remain C_{3V}. If the axial ratio is 1.60, the nearest-neighbor fluoride ions are not arranged tetrahedrally, and a considerable distortion of the vibrations of a tetrahedral ammonium ion would be expected. Under C_{3V} symmetry, both of the inactive vibrations of a tetrahedral molecule,[9] the symmetric stretching vibration $\nu_1(A_1)$ and the doubly degenerate bending vibration $\nu_2(E)$, may become active while the two triply degenerate vibrations, $\nu_3(T_2)$ and $\nu_4(T_2)$, are split into components of species A_1 and E (under C_{3V}), both of which may be active. A confirmation of C_{3V} symmetry, therefore, would take the form of the observation of ν_1 or ν_2, or of the splitting of ν_3 or ν_4.

[9] G. Herzberg, *Infrared and Raman Spectra of Polyatomic Molecules* (D. Van Nostrand Company, Inc., New York, 1947), p. 100.

By comparison with the other ammonium salts, the most sensitive band should be ν_4, to which the peak at 1494 cm^{-1} must be assigned. This band has a half-width of only 7 cm^{-1}, and if it contains two components, they must be separated by less than 7 cm^{-1}, or it is split by at least 523 cm^{-1}, which would place the second component at 2017 cm^{-1}. Similarly, ν_3 may be assigned as being the most intense band in the spectrum at 2815 cm^{-1}. The only other peak with sufficient intensity to be a second component is that at 3082 cm^{-1}. Since ν_1 probably occurs at 2870 cm^{-1}, the frequency of the intense Raman line, there is no evidence of its having become infrared active. The same holds for ν_2, unless the perturbation is great enough so that its frequency is 2277 cm^{-1} rather than the anticipated value of about 1800 cm^{-1}.

On the other hand, the general pattern of the spectrum is very similar to that of other ammonium salts. If it is assumed that the fluoride ions are arranged tetra-

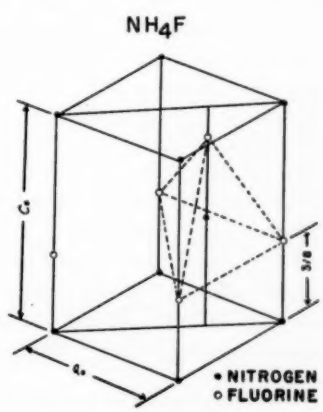

FIG. 4. The unit cell of ammonium fluoride.

hedrally about the ammonium ion the true site symmetry will remain C_{3V}, but as far as the ammonium ion and its nearest neighbors are concerned, T_d symmetry would be a correct description. In the crystal this symmetry is only lowered by longer-range forces and by the coupling between the motions of the various ammonium ions. Since all of the internal vibrations of the ion are hydrogen motions and the ions are separated by the relatively massive fluorine ions, the coupling of the motions can probably be neglected. If the crystalline field is dominated by the nearest-neighbor fluoride ions, the symmetry of the ammonium ion may be described as "essentially" tetrahedral, i.e., described by the group T_d. In that case only ν_3 and ν_4 may be active so that the wealth of detail in the spectrum must originate in combination bands. An assignment of frequencies on this basis is given in Tables I and II.

All of the main aspects of the spectrum are satisfactorily taken into account by this assignment which parallels the other ammonium salts closely. The frequency-product ratios which result are:

Species T_2

$$\frac{\nu_3^{\mathrm{H}}\nu_4^{\mathrm{H}}}{\nu_3^{\mathrm{D}}\nu_4^{\mathrm{D}}}=\frac{2815.1494}{2148.1120}=1.748 \text{ (harmonic value, 1.781).}$$

Species T_1

$$\frac{\nu_6^{\mathrm{H}}}{\nu_6^{\mathrm{D}}}=\frac{523}{376}=1.391 \text{ (harmonic value, 1.414).}$$

Species E

$$\frac{\nu_2^{\mathrm{H}}}{\nu_2^{\mathrm{D}}}=\frac{1754}{1257}=1.394 \text{ (harmonic value, 1.414).}$$

The agreement is satisfactory, and the deviations are in the direction expected from anharmonicity. If the anharmonicity for ν_1 is of the same order of magnitude as in the other vibrations, it may be predicted that ν_1 occurs at about 2050 cm^{-1} in ND_4F.

The detailed assignment of the numerous peaks ascribed to combinations is open to question, however. Corresponding to each active fundamental frequency there is an entire band of inactive frequencies in the crystal. Whereas only one frequency in the band may appear in the spectrum as a fundamental, all of the frequencies in both bands may enter into combinations which appear in the spectrum.[10] Hence a combination which is designated by a single symbol (e.g. $\nu_4+\nu_6$) may appear as a band with any number of maxima, diffuse or sharp as the case may be. It is on this basis that we have assigned both of the peaks at 2974 and 3010 cm^{-1} to $2\nu_4$; in NH_4Cl and NH_4Br, $2\nu_4$ also appears as a band running to high frequencies from the calculated values, although in those cases the bands show only diffuse maxima and not sharp peaks.

Similarly, some of the fine structure near 2000 cm^{-1} may actually be part of the $\nu_4+\nu_6$ band. The problem in that region is further complicated by the probability that Fermi resonance may contribute intensity to minor peaks of $4\nu_6$, $\nu_2+\nu_5$, and $\nu_4+2\nu_6$, all of which are superimposed. There is no simple way to gauge the probable width of these bands, but it may be noted that the band, $3\nu_5$, which lies at the base of ν_4, has a width of roughly 50 cm^{-1}. Finally, although the fundamentals are apparently those of an "essentially tetrahedral" ion, the combination tones may be split by the crystal symmetry.

The biggest problem which arises is the strong band at 3082 cm^{-1} in NH_4F and 2251 cm^{-1} in ND_4F. It has been assigned to $\nu_4+3\nu_6$, but it is startling that such a high combination should appear with such intensity. Furthermore, the observed frequency is some 40 cm^{-1} higher than predicted, and this can only be correct if the frequency is raised by Fermi resonance with some of the slightly lower frequencies. At present, the situation on this peak cannot be considered satisfactory. The only other peak for which no assignment is available is the weak peak at 2688 cm^{-1}.

The ND_4F spectrum fits the same general scheme as NH_4F. Even after the ND_3H^+ lines are eliminated, the peaks do not show a one-to-one correspondence with those of NH_4F, but this is probably because of the numerous overlapping bands mentioned before. There

TABLE I. Observed frequencies, relative intensities, and assignments to the infrared spectrum of NH_4F at −195°C and 25°C.

Infrared			Raman[a]		
−195°C ν (cm^{-1})	Half widths (cm^{-1})	25°C ν (cm^{-1})	25°C ν (cm^{-1})	Inferred[b] frequencies (−195°C)	Assignment "essentially" T_d symmetry
3320 vw[c]		3310		3338	$\nu_3+\nu_6$
3222 m[c]		3218		3248	$\nu_2+\nu_4$
3161 vw		...		3130, 3185	$\nu_3+\nu_5$, $\nu_1+\nu_5$
3082 s[c]		3065		3063	$\nu_4+3\nu_6$
			3088		
3010 m-w		2999		2988	$2\nu_4$
2974 m-w		2969			
2815 vs	53	2820	2870		ν_1
			2820		ν_3
2688 vw		...		2699	$\nu_2+3\nu_5$
2600 vw		2590		2559	$3082-\nu_6$?
2571 vw				2592	$\nu_2+\nu_5+\nu_6$
				2555	$\nu_1-\nu_5$
2516 vw		2485		2540, 2500	$\nu_4+2\nu_6$, $\nu_3-\nu_5$
2277 m		2261	2262	...	$\nu_2+\nu_6$
2159 vw		...		2124	$\nu_4+2\nu_5$
2084 vw		...		2069	$\nu_2+\nu_5$
2017 m	15	2007		...	$\nu_4+\nu_6$
1809 vw		...		...	$\nu_4+\nu_5$
...		...		1754	ν_2
1545 vw		...		1569	$3\nu_6$
1494 m	7	1489			ν_4
...		...		523	ν_6
...		...		315	ν_5

[a] Reference 5.
[b] Sum of fundamental frequencies or values derived from differences of combination and fundamental frequencies.
[c] s=strong, m=medium, w=weak, v=very.

[10] H. Winston and R. S. Halford, J. Chem. Phys. **17**, 607 (1949).

remains, nevertheless, no satisfactory assignment for the weak bands near 1900 cm^{-1} and in the 2600–3100-cm^{-1} region.

It might be argued that since Bovey observed two components of ν_4 and was able to assign separate components of ν_3 the films studied in the present investigation were oriented with the hexagonal axis parallel to the infrared beam, whereas his were unoriented. In that case only the E components of the spectrum would have been observed in the present work. If that were the case, and $\nu_2(E)$ is assigned to either 2017 or 2277 cm^{-1} (1496 or 1633 in ND$_4$F), the frequency-product ratio for the type E vibrations would be either 2.43 or 2.35. The harmonic value of this product is 2.56 and the check is poor.

TABLE II. Observed frequencies, relative intensities, and assignments to the infrared spectrum of ND$_4$F at −195°C and 25°C.

ν (cm^{-1}) −195°C	25°C	Inferred[a] frequencies (−195°C)	Assignment "essentially" T_d symmetry
3070 w[b]	3049	3041	$\nu_2+\nu_4+\nu_5+\nu_6$?
2983 vw[b]	···	2992, 3012	$2(\nu_4+\nu_6)$, $\nu_3+3\nu_5$?
2911 vw	···	2900, 2899	$\nu_3+2\nu_6$?, $\nu_1+3\nu_5$?
2828 m[b]	2810		ND$_3$H[a]
2790 m	···	2812	$\nu_3+\nu_5+\nu_6$
2639 vw	···	2699	$\nu_1+\nu_5+\nu_6$?
2471 w	2469	2514	$2\nu_2$?
2360 m	2363	2377	$\nu_2+\nu_4$
2323 m	2313	···	$\nu_1+\nu_5$
2251 s[b]	2247	2248	$\nu_4+3\nu_6$
2233 m	···	2240	$2\nu_4$
2148 vs	2140		ν_3
···	2042	2089	$\nu_2+\nu_4-\nu_5$
···	···	2035	ν_1
1970 vw	···	1872, 2121	$\nu_4+2\nu_6$, $\nu_2+3\nu_5$
1899 m	1900	1921	$\nu_2+\nu_5+\nu_6$?
1633 m	1627	···	$\nu_2+\nu_6$
1549 vw	···	1545	$\nu_2+\nu_5$
1496 m	1490	···	$\nu_4+\nu_6$
1479 vw	···		ND$_3$H[a]
1412 vw	1407	···	$\nu_4+\nu_5$
···	···	1257	ν_2
1170 vw	1173		ND$_3$H[a]
1120 m	1119		ν_4
···	···	376	ν_6
···	···	288	ν_5

[a] Sum of fundamental frequencies on values derived from differences of combination and fundamental frequencies.
[b] s = strong, m = medium, w = weak, v = very.

We therefore conclude that the symmetry of the NH_4^+ ion site is "essentially" tetrahedral. This cannot be exactly true in a hexagonal crystal but a necessary consequence is that the arrangement of nearest neighbors must be quite precisely tetrahedral.

V. X-RAY CRYSTAL STRUCTURE OF AMMONIUM FLUORIDE

The previous conclusion conflicts with the x-ray structure found by Zachariasen[1] so that it was considered important to carry out a more precise determination of the lattice parameters. This was done by a careful study of the diffraction pattern from the powder.

The ammonium fluoride was purified as described previously. The sublimed salt was in a finely divided state, and no further grinding was necessary to reduce the particle size. The samples were mounted in sealed Pyrex capillary tubes (i.d. = 0.5 mm).

TABLE III. Observed and calculated line spacings in the diffraction pattern from powdered ammonium fluoride.

h	k	l	Weight in least-squares fit	$4\theta_B$ (observed)	$4\theta_B$ (calculated)	error
1	$\bar{1}$	0	1	46.3	46.28	0
0	$\bar{0}$	2	2	49.6	49.68	+0.1
1	$\bar{1}$	1	3	52.7	52.60	−0.1
1	$\bar{1}$	2	4	68.3	68.36	+0.1
1	$\bar{2}$	0	5	81.3	81.28	0
1	$\bar{1}$	3	6	89.2	89.28	+0.1
2	$\bar{2}$	0	7	94.5	94.56	+0.1
1	$\bar{2}$	2	8	96.4	96.40	0
2	$\bar{2}$	1	9	98.2	98.08	−0.1
2	$\bar{2}$	2	10	108.3	108.26	0
2	$\bar{2}$	3	11	123.9	123.88	0
2	$\bar{3}$	2	12	140.0	139.64	−0.4
3	$\bar{3}$	0	13	148.0	147.88	−0.1
2	$\bar{3}$	3	14	153.6	153.52	−0.1

A copper target source was used with a nickel filter and a powder camera which gave 0.5 Bragg degree per mm. For purposes of calibration, the diffraction pattern of sodium chloride was recorded on the same film as that of ammonium fluoride in two separate exposures with half of the film masked with a thin lead strip during the sodium chloride exposure.

The ammonium fluoride showed a tendency to form aggregates giving spotty lines on the film. The effect was noted only on samples allowed to stand at room temperature for more than twelve hours.

The indexing of lines and the observed and calculated positions of lines is given in Table III. The final adjustment of parameters was made by a least-squares fit where the 14 observed angles were weighted by integers from 1–14 with increasing angle in order to minimize the effects of errors from absorption and eccentricity in the movement of the capillary tube.

The resulting parameters were $a = 4.44 \pm 0.005$ A, $c = 7.17 \pm 0.02$ A, and $c/a = 1.62 \pm 0.01$. The axial ratio is within experimental error of 1.63, the value predicted from the infrared spectrum. The N−F distance corresponding to these new parameters is 2.69 A.

VI. HYDROGEN BONDING IN NH$_4$F

The frequencies of the N−H stretching vibrations in a number of ammonium salts are listed in Table IV. It is evident that in structures in which N−H—X hydrogen bonds are weak, if they exist at all, the N−H frequency is in the vicinity of 3300 cm^{-1}. In NH$_4$F, then, the N−H frequency is displaced downwards by about 450 cm^{-1}. Similarly, the two bending frequencies, which lie at 1650 cm^{-1} (ν_2) and 1400 cm^{-1} (ν_4) in the other ammonium salts, are displaced upwards by about 100

TABLE IV. Frequency of N−H stretching lines in ammonium salts.

	ν_1	ν_3
NH_4F	2870	2810
NH_4Cl	3048	3086
NH_4Br	3038	3124
NH_4I	3021	3070
NH_4BF_4[a]	···	3332
NH_4NO_3[b]	···	3200

[a] G. L. Cote and H. W. Thompson, Proc. Roy. Soc. (London) **A210**, 217 (1951).
[b] W. E. Keller and R. S. Halford, J. Chem. Phys. (London) **17**, 26–30 (1949).

cm^{-1}. These shifts are a clear indication of moderately strong hydrogen bonds.

The shift in the stretching frequency is very nearly equal to that observed in passing from water vapor to ice, but whereas the O−H stretching bands in ice are several hundred wave numbers wide at all temperatures, the N−H stretching peak in NH_4F is only 50 cm^{-1} wide at −195°C. It follows, therefore, that broad bands are not necessarily associated with strong hydrogen bonds although this is usually the case.[11,12]

The half-widths of ν_3 in a number of ammonium halides are shown in Table V. It is seen here too that although the hydrogen bonds are much stronger in NH_4F than in the other ammonium halides the line widths are very nearly the same in the ordered low-temperature phase.

On the other hand, a considerable increase in the line width in NH_4Cl, Br, and I is associated with the disordering which takes place in the λ transition. It is not unreasonable to suspect, therefore, that at room temperature NH_4F is also disordered. If so, the mechanism of the disordering is obscure, and it should be noted that our x-ray studies showed a structure at room temperature which is similar to that deduced from the spectrum at −195°C.

One further consequence of the hydrogen bonding is worth noting. In the other ammonium halides, as in methane, the symmetric stretching vibration has a lower frequency than the antisymmetric; in NH_4F this situation is reversed. This difference can be ascribed formally to a large negative stretch-stretch interaction term in the ammonium ion potential function, but this leaves unanswered the question of why the energy required to distort the ion in the antisymmetric motion is less than in the symmetric motion. A possible line of argument runs as follows: during the symmetric stretching motion all of the protons move away from (or toward) the nitrogen atom simultaneously. If carried to an extreme, it would lead to the formation of N^{-3} and FH_4^{+3} ions, an energetically unfavorable configuration. On the other hand, the antisymmetric motion brings three protons toward the nitrogen while one is removed. This motion, when carried far enough, leads to the formation of NH_3 and HF, a relatively more favorable situation. It does not seem unreasonable, therefore, for this motion to require less energy, and it might be suspected that for *this motion* the potential-energy curve possesses two minima, that associated with NH_4^+ and F^- ions and another higher energy minimum corresponding to NH_3+HF.

[11] R. E. Rundle and M. Parasol, J. Chem. Phys. **20**, 1487 (1952).
[12] R. C. Lord and R. E. Merrifield, J. Chem. Phys. **21**, 166 (1953).

VII. *A PRIORI* CALCULATION OF THE TORSIONAL FORCE CONSTANTS IN AMMONIUM HALIDES

Wagner and Hornig[2] calculated the torsional frequency of the ammonium ion in the cubic crystal NH_4Cl by using a simplified point charge model of the ion. They placed point charges at the positions of the nitrogen atom and the protons in the ion under consideration, and at the center of all other ions. A calculation of the purely electrostatic energy of interaction of this ion with the rest of the lattice showed that the experimentally determined value of this frequency could be obtained when a not unreasonable fraction of an electronic charge was placed on the protons.

These results were subsequently extended to the tetragonal crystals, NH_4Br and NH_4I, and to the low-temperature cubic phase of ND_4Br by Millman and Hornig.[13] Their results are summarized in Table VI. The quantity f is the fraction of an electronic charge on the proton. Although the value of f is somewhat higher than might have been anticipated, its constancy is quite reassuring for although the structure of these compounds does not vary greatly, the N−X distance changes from 3.34 A in NH_4Cl to 3.78 A in NH_4I.

It was of some interest, therefore, to test the same model on NH_4F whose structure differs drastically. In the other salts each ammonium ion is surrounded by eight halogen ions; in NH_4F by contrast, there are only four. The expression derived for the force constant was:

$$K_\phi = -3fe^2a^2\alpha \sum_j \frac{Y_j}{[a^2B+c^2D]^{3/2}} - \frac{3a^2\alpha X_j^2}{[a^2B+c^2D]^{5/2}}$$

$$B = X_j^2 + (Y_j - \alpha)^2$$

$$D = (Z_j - \gamma)^2$$

TABLE V. Width of N−H stretching lines (ν_3) in ammonium halides.

	25°C	−195°C
NH_4F	110	53
ND_4F	88	45
NH_4Cl	110	35
ND_4Cl	80	33
NH_4Br	120	52
ND_4Br	78	45
NH_4I	113 (Phase II, −15°C)	42

[13] S. Millman and D. F. Hornig (unpublished).

where a and c are the lattice parameters; ϕ is the angle of rotation about a threefold axis; X_j and Y_j are Cartesian coordinates of the jth ion in units of the lattice parameter a, and Z_j the remaining coordinate in units of c; $\alpha = r_{NH} \cos 19°28'/a$; and $\gamma = -r_{NH} \sin 19°28'/c$. This quantity was summed over 44 neighbors, using $r_{NH} = 1.02$ A, $a = 4.44$ A, and $c = 7.17$ A.

To obtain the experimental frequency of ν_6, 523 cm^{-1}, a value of $f = 0.164$ was necessary. This is drastically different from the previous result and indicates a basic defect in the simple model.

Some insight into the nature of the difficulty came when it was noted that in the cubic or tetragonal structures the four nearest-neighbor halide ions toward which N—H bonds were *not* directed made a very substantial contribution to the force constant, and that their effect was of opposite sign to that of the other four nearest neighbors. Since this set is absent in NH_4F, one might guess that its role had been overemphasized. This would be the case if there are substantial short-range forces between the protons and the nearest four halide ions. To test this a computation was made in which the contribution of only the four nearest neighbors was included, the rest of the lattice being neglected arbitrarily. The contribution of these four ions to the force constant is given by the expression

$$K_\phi = \frac{3fe^2 r_{NH} r_{NX} \cos^2 19°28'}{(r_{NX} - r_{NH})^3}$$

TABLE VI. Charge distribution on ammonium ions necessary to account for torsional lattice vibration frequency.

Compound	Phase	$\nu_{Torsional}$	f
NH_4Cl	III (cubic)	390 cm^{-1}	0.45
NH_4Br	III (tetragonal)	319 cm^{-1}	0.43
ND_4Br	IV (cubic)	248 cm^{-1}	0.42
NH_4I	III (tetragonal)	285 cm^{-1}	0.42

TABLE VII. Effective point charge necessary to give correct torsional frequency for NH_4^+ ion in the field of its four nearest neighbors.

Salt	k_ϕ	ν	f
NH_4F	$36.4\times10^{-12}f$	523	0.123
NH_4Cl (III)	$16.7\times10^{-12}f$	390	0.149
NH_4Br (III)	$14.2\times10^{-12}f$	319	0.118
NH_4I (III)	$11.2\times10^{-12}f$	279	0.114

where f and e have the same meaning as before. The distances used were $r_{NH} = 1.02$ A, $r_{NF} = 2.69$ A, $r_{NCl} = 3.34$ A, $r_{NBr} = 3.50$ A, and $r_{NI} = 3.78$ A. The results are listed in Table VII. The discrepancy between NH_4F and the other salts no longer appears. Of course, this calculation should not be taken too seriously, but it does suggest that the torsional force constants arise primarily from the attraction of the nearest-neighbor ions toward which the N—H bonds are directed and that the effect of the remainder of the lattice is less important than appeared in the simple point-charge electrostatic model. Further refinements of the model must include an allowance for such effects as the nonspherical charge distribution of the nearest-neighbor halide ions.

CONCLUSIONS

The infrared spectrum of NH_4F is remarkable for a compound with moderately strong hydrogen bonds because of the sharpness of the lines. At −195°C it is consistent only with an accurately tetrahedral arrangement of nearest-neighbor fluoride ions about each ammonium ion. At room temperature the x-ray pattern also shows a tetrahedral arrangement, but the spectrum may indicate disorder. If that is the case, the nature of disordering is not clear.

The authors wish to acknowledge the aid of Dr. G. B. Carpenter in obtaining the x-ray diffraction pattern of NH_4F, and one of them (R.C.P.) wishes to thank the E. I. du Pont de Nemours and Company, Inc. for its aid while this work was being carried out.

Electronic Structure of Metal bis-cyclopentadienyls*

J. D. DUNITZ† AND L. E. ORGEL‡§
Gates and Crellin Laboratories of Chemistry, California Institute of Technology, Pasadena, California
(Received September 24, 1954)

Molecular orbital theory has been used to describe the electronic structure of ferrocene and related compounds. It is shown that, provided the valence-state promotion energies are considered, the thermochemistry and magnetic properties may be understood.

SINCE the first proposal of the "sandwich" structure for bis-cyclopentadienyl iron (II)[1] (ferrocene), a number of different explanations of the stability and magnetic behavior of the metal bis-cyclopentadienyls have been advanced. The original tentative suggestion that the stability arises as a result of the central atom achieving a krypton shell[1] was clearly untenable after the preparation of stable bis-cyclopentadienyls containing different numbers of electrons, and the various subsequent attempts to explain these properties by assigning some of the electrons to bonds and others to atomic orbitals have been imprecise, or unsatisfactory for one reason or another.

The bis-cyclopentadienyls have also been discussed in terms of molecular orbital theory,[2–4] although up till now only in a more or less qualitative fashion. Here we shall discuss the problem in a semiquantitative manner and show that molecular orbital theory can give a satisfactory account of the thermochemical and magnetic evidence which has been obtained for these compounds.

The basic theory, which is treated in more detail in Moffitt's paper,[3] is summarized below. In the point group $D_{5d}=C_{5v}\times i$, the π orbitals of the pair of cyclopentadienyl radicals transform as a_{1g}, a_{1u}, e_{1g}, e_{1u}, e_{2g}, e_{2u}, with stabilities $a_1>e_1>e_2$ and g's and u's roughly degenerate; the d orbitals of the metal transform as a_{1g}, e_{1g}, e_{2g}, degenerate for an isolated atom. The $4s$ metal orbital transforms as a_{1g}. The $4p$ metal orbitals transform as a_{1u}, e_{1u}. The molecular orbitals are formed by linear combinations of metal and cyclopentadienyl orbitals of like transformation properties. The most stable molecular orbitals are, in approximate order of stability: $a_{1g}(\pi,3d,4s)$, $a_{1u}(\pi,4p)$, $e_{1g}(\pi,3d)$. The order of the next three levels, $e_{2g}(\pi,3d)$, $a_{1g}'(\pi,3d,4s)$, $e_{1u}(\pi,4p)$ is less certain and will vary from one metal to the next. These orbitals can accommodate exactly 18 electrons and are therefore fully occupied in the iron compound. The remaining orbitals are of relatively low stability but they must accommodate the extra electrons in the bis-cyclopentadienyls of cobalt (II) and nickel (II).

In order to assess more accurately the relative importance of the different molecular orbitals in providing the binding energy in ferrocene and related compounds, we have tried to obtain semiquantitative evidence by calculating the overlap integrals between the metal atom and the ring orbitals. Since the $3d$ and $4s$ electrons on the metal atom have very similar ionization potentials it seems plausible to take the matrix elements for the interactions as roughly proportional to the overlap integrals.

The actual evaluation of the overlap integrals is complicated by the fact that the direction of quantization for the metal orbitals must be taken as the fivefold axis, which is inclined at an angle of about 36° to the Fe−C bond directions.

The first stage is to resolve these orbitals into new orbitals corresponding to quantization about the metal-carbon bond directions, e.g., a p_z orbital in the first system of coordinates becomes $p_z'\cos w-p_x'\sin w$ in a new coordinate system chosen as in Fig. 1 in which the metal-carbon bond direction is taken as the z' axis. The other orbitals transform as follows:

$$\psi_s=\psi_{s'}$$
$$\psi_{p_z}=\psi_{p_{z'}}\cos w-\psi_{p_{x'}}\sin w$$
$$\psi_{d_{z^2}}=\psi_{d_{z'^2}}(\cos^2 w-\tfrac{1}{2}\sin^2 w)-\tfrac{1}{2}\sqrt{3}\psi_{d_{x'z'}}\sin 2w+\tfrac{1}{2}\sqrt{3}\psi_{d_{x'^2-y'^2}}\sin^2 w$$
$$\psi_{d_{xz}}=\tfrac{1}{2}\sqrt{3}\psi_{d_{z'^2}}\sin 2w+\psi_{d_{x'z'}}\cos 2w-\tfrac{1}{2}\psi_{d_{x'^2-y'^2}}\sin 2w$$
$$\psi_{d_{x^2-y^2}}=\tfrac{1}{2}\sqrt{3}\psi_{d_{z'^2}}\sin^2 w+\tfrac{1}{2}\psi_{d_{x'z'}}\sin 2w+\tfrac{1}{2}\psi_{d_{x'^2-y'^2}}(1+\cos^2 w).$$

This enables us to express the overlap integral Σ_μ, between a metal μ-orbital (quantized with respect to the fivefold axis) and a $p_z\pi$-orbital on a single-carbon atom in the xz plane, in terms of conventional overlap integrals. The overlap integrals between metal orbitals and molecular orbitals of a cyclopentadienyl ring are multiples of $\Sigma\mu$ and may be determined from the known forms of the M.O.'s and the transformation properties of the metal orbitals. Thus, for the e_{2g} orbital the molecular overlap integral is seen from Fig. 2 to be $(c_1+2c_2\cos 36°+2c_3\cos 72°)\ \Sigma_{d_{x^2-y^2}}$. (The angles 36° and 72° appear because of the angular dependence of the $d_{x^2-y^2}$ orbital on $\cos 2\phi$.) The coefficients c_i are given

* Contribution No. 1959 from the Gates and Crellin Laboratories.
† Now at National Institutes of Health, Bethesda, Maryland.
‡ Arthur A. Noyes Fellow, 1954.
§ Present address: The Laboratory of Molecular Structure and Spectra, The University of Chicago, Chicago 37, Illinois.
[1] Wilkinson, Rosenblum, Whiting, and Woodward, J. Am. Chem. Soc. **74**, 2125 (1952); E. O. Fischer and W. Pfab, Z. Naturforsch. **78**, 377 (1952).
[2] H. H. Jaffé, J. Chem. Phys. **21**, 156 (1953).
[3] W. Moffitt, J. Am. Chem. Soc. **76**, 3386 (1954).
[4] J. D. Dunitz and L. E. Orgel, Nature **171**, 121 (1953).

by simple LCAO theory and on substituting for them we obtain a value of $\sqrt{\frac{5}{2}}\,\Sigma d_{x^2-y^2}$, provided that we neglect overlap in the LCAO calculations. The final forms of these overlap integrals, multiplied by $\sqrt{2}$ to give *complete* molecular overlap integrals, are:

$$S(a_{1g},4s)=\sqrt{10}S^{2p_\sigma 4s}\cos w$$

$$S(a_{1g},3d_{z^2})=\sqrt{10}\{S^{2p_\sigma 3d_\sigma}\cos w(\cos^2 w-\tfrac{1}{2}\sin^2 w)-\sqrt{\tfrac{3}{2}}S^{2p_\pi 3d_\pi}\sin 2w\sin w\}$$

$$S(e_{1g},3d_{xz})=\sqrt{5}\{\tfrac{1}{2}\sqrt{3}S^{2p_\sigma 3d_\sigma}\sin 2w\cos w+S^{2p_\pi 3d_\pi}\cos 2w\sin w\}$$

$$S(e_{2g},3d_{x^2-y^2})=\sqrt{5}\{\tfrac{1}{2}\sqrt{3}S^{2p_\sigma 3d_\sigma}\sin^2 w\cos w+\tfrac{1}{2}S^{2p_\pi 3d_\pi}\sin 2w\sin w\}.$$

To obtain numerical values for the overlap integrals, we have assumed that $\alpha=1.6$ for the carbon-atom orbitals, in accord with Slater's rules.[5] Unfortunately, Slater's rules are not applicable to the iron $3d$ and $4s$ orbitals, and we have followed the recommendations of Craig *et al.*[6] and taken $\alpha_{Fe3d}=\alpha_{Fe4s}=\alpha_c$. However,

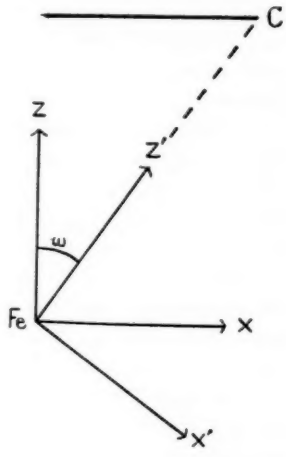

FIG. 1. The relation of the new coordinate system to that based on the five-fold axis.

since the numerical overlap integrals in this range are quite sensitive to the choice of α, we have also made our calculations for a somewhat higher value, $\alpha_{Fe3d}=\alpha_{Fe4s}=2.0$. The changes which occur are significant, but since our interest here is in orders of magnitude rather than in detailed results, we shall confine our future discussion to calculations made with the lower value. We have used the standard tables[7] to obtain values of the overlap integrals. The $4s2p\sigma$ overlaps were obtained by interpolation between $3s2p\sigma$ and $5s2p\sigma$ overlaps.

The final values for the overlap integrals between metal and complete molecular orbitals are given in column I of Table I. These results are valid only if we neglect overlap between π orbitals on the cyclopentadienyl radicals. To include overlap, they must

[5] J. C. Slater, Phys. Rev. **36**, 57 (1930).
[6] Craig, Maccoll, Nyholm, Orgel, and Sutton, J. Chem. Soc. (London) 332 (1954).
[7] Mullikan, Riecke, Orloff, and Orloff, J. Chem. Phys. **17**, 1248 (1949); H. H. Jaffé, *ibid.* **21**, 258 (1953); H. H. Jaffé and G. O. Doak, *ibid.* **21**, 196 (1953).

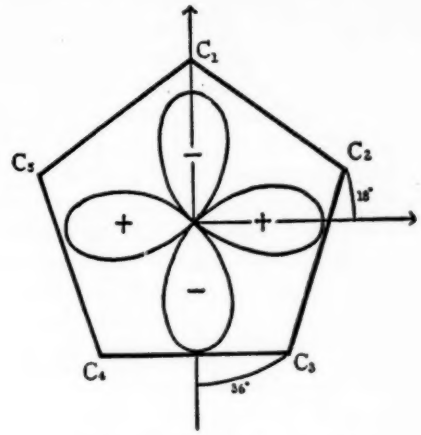

FIG. 2. The orientation of the e_{2g} orbital relative to the molecular framework.

be multiplied by an appropriate normalizing factor $(\sqrt{5}[\sum_{ij}(c_ic_jS_{ij})]^{-\frac{1}{2}})$ for the cyclopentadienyl orbital in question, where $S_{ii}=1$, $S_{ij}=0.25$ if i is adjacent to j, and zero otherwise. The results including overlap are listed in column II.

In order to relate these results to the bonding energies of the molecular orbitals we shall assume (1) that the matrix element for the e_{1g} interaction is 2 ev and (2) that the other matrix elements involving $3d$ or $4s$ electrons may be obtained from our assumption of proportionality of overlaps to matrix elements. Values obtained thus are given in column III. Our choice of 2 ev is empirical and is consistent with values ordinarily adopted for bond energies.

We have omitted any discussion of the $4p$ orbitals. It is difficult to assign α values to them and to make adequate allowance for their low-electron affinity. Although their bonding energies are less than would be suggested by their overlaps, the latter are quite large and so the energy quantities which we are neglecting here may be considerable.

We accept Moffitt's calculations[3] which place the e_{1g} orbital of the cyclopentadienyl pair at about the same level as the e_{1g} orbital of iron. The binding energy provided by the e_{1g} orbitals is therefore 2 ev per electron, or, in all, 8 ev. The binding energies of the other orbitals depend on a choice of a value for β, the conventional parameter of the LCAO theory. The energies of the cyclopentadienyl molecular orbitals, a_{1g}, e_{1g}, and e_{2g} are -2β, -0.62β, and $+1.62\beta$ respectively, and

TABLE I. Column I, values of overlap integrals neglecting overlap between π orbitals on the cyclopentadienyl radicals. Column II, corrected values of overlap integrals. Column III, values of corresponding matrix elements, in ev.

	I	II	III (ev)
$S(a_{1g},4s)$	0.61	0.50	2.7
$S(a_{1g},3d_{z^2})$	0.01	0.01	0.0
$S(e_{1g},3d_{xz})$	0.40	0.37	2.0
$S(e_{2g},3d_{x^2-y^2})$	0.23	0.29	1.6

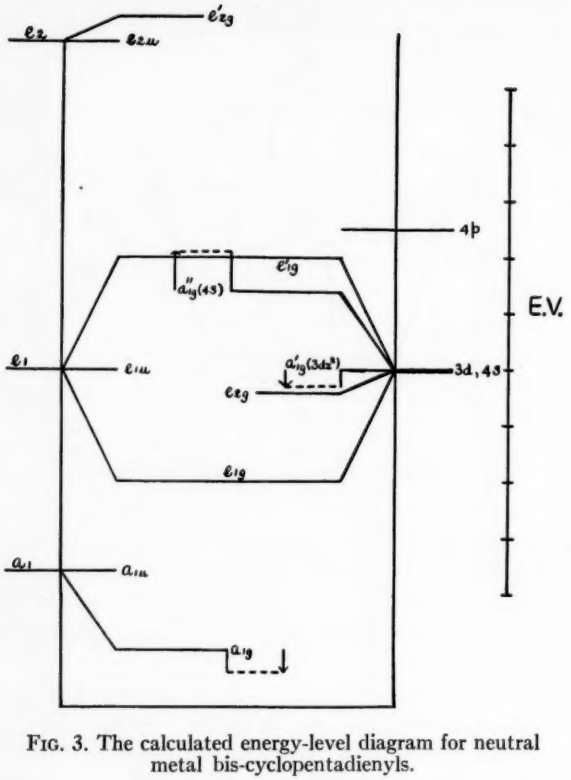

FIG. 3. The calculated energy-level diagram for neutral metal bis-cyclopentadienyls.

taking $\beta=60$ kcal mole^{-1}, the a_{1g} and e_{2g} orbitals lie 3.6 ev below and 5.8 ev above the e_{1g} levels.

The binding energies for the a_{1g} and e_{2g} orbitals are now obtained from the secular equations:[8]

$$\begin{vmatrix} y & 2.7 \\ 2.7 & y-3.6 \end{vmatrix}=0 \qquad \begin{vmatrix} y & 1.6 \\ 1.6 & y+5.8 \end{vmatrix}=0.$$

a_{1g} e_{2g}

We find that for a_{1g} the lower orbital (mostly on the cyclopentadienyl radicals) is stabilized by 1.4 ev per electron (or 2.8 ev for the electron pair), while the upper orbital, largely Fe(4s), is destablized by the same amount. The a_{1g} ($3d_{z^2}$) orbital is hardly affected on this approximation since its matrix element is close to zero. The lower e_{2g} orbital (mostly on the iron atom) is lowered by 0.4 ev per electron (1.6 ev for 4 electrons) while the upper e_{2g} orbital (the antibonding bis-cyclopentadienyl orbital) is raised by a corresponding amount. We find, therefore, that the total bonding energy between the iron atom and the cyclopentadienyl rings is about 12.4 ev or 286 kcal mole^{-1} for ferrocene. It should be clear that bonding in the a_{1g} and e_{2g} orbitals leads to transfer of charge in opposite directions, so that the actual charge separation cannot be very large.

[8] The degeneracy of the 3d and 4s electrons of the metal is implicit in all of these calculations. In the transition-metal series, it is impossible to give an energy-level diagram which correctly predicts the positions of all the different electronic states as these depend strongly on the actual arrangement of electrons within a configuration. On the whole, the evidence suggests that the 4s and 3d orbitals are almost equi-energetic.

Moffitt[3] has postulated a mixing and splitting of the 3d and 4s levels, due to the electrostatic perturbation caused by the cyclopentadienyl electrons. That a splitting must exist is certain, but we feel unable to assess its magnitude. Its effect would be to raise the upper a_{1g} level of the iron atom, and lower the other. The variation of the positions of the three a_{1g} levels with the size of this interaction is obtained from the secular equation

$$\begin{vmatrix} y-3.6 & 0 & 2.7 \\ 0 & y & x \\ 2.7 & x & y \end{vmatrix}=0$$

where x is the matrix element tending to mix the $3d_{z^2}$ and 4s orbitals. In our subsequent discussion, we shall see that there is a further effect tending to mix the $3d_{z^2}$ and 4s orbitals, namely, the lower energy of the d^7s valence state compared with the energies of d^6s^2 and d^8 valence states.

The energy level diagram (Fig. 3) has been drawn in accordance with the arguments and rough calculations presented above. The full lines represent levels calculated neglecting 3d, 4s mixing; the dotted lines represent levels with this interaction taken into account, assuming the matrix element x equal to 1 ev.

In bis-cyclopentadienyl nickel (II) two more electrons must be accommodated in the available orbitals. There are three sets of orbitals which may be used: the e_{1g}' antibonding orbital, the a_{1g}'' orbital, and the metal p-orbitals. We are inclined to think that the e_{1g}' and a_{1g}'' orbitals lie below the 4p-orbitals (which themselves are raised by bonding interactions with the cyclopentadienyl radicals). We cannot calculate whether the e_{1g}' or the a_{1g}'' orbital lies lowest, nor can we be certain that they are indeed below the p-orbitals, but we think that the most probable assignment of these electrons is $(e_{1g}')^1$ $(a_{1g}'')^1$ or $(e_{1g}')^2$.

In any case, since the lowest available orbitals (e_{1g}', a_{1g}'') in bis-cyclopentadienyl nickel (II) lie about 2 ev above the highest occupied orbital in the nickel atom, we expect that the total bonding energy between the metal atom and the cyclopentadienyl rings is about 4 ev less than in ferrocene, or about 8.4 ev (194 kcal mole^{-1}).

The heats of formation of bis-cyclopentadienyl iron (II) and bis-cyclopentadienyl nickel (II) from metal atoms and cyclopentadienyl radicals have been estimated to be 147 and 123 kcal mole^{-1} respectively.[9] These figures cannot be compared directly with the calculated energy of the metal cyclopentadienyl bonds. In order to effect such a comparison, the latter must first be corrected for (1) promotion energy to the valence state of the metal atom, (2) repulsion between nonbonded electrons, and (3) loss of resonance energy in the ring. We cannot calculate (2) and (3), but we guess that, together, they amount to between 2 and 3

[9] Wilkinson, Pauson, and Cotton, J. Am. Chem. Soc. **76**, 1970 (1954).

ev, and are not very different for the iron, cobalt, and nickel compounds. The valence-state promotion energies, on the other hand, vary very much from one metal to another and we have calculated them.

For iron, the lowest configuration able to produce a suitable valence state is $3d^64s^2$ with the particular assignment of electrons $(d_{xy})^2(d_{x^2-y^2})^2[(d_{xz})^1(d_{yz})^1](s)^2$ or $(d_{+2})^2(d_{-2})^2[(d_{+1})^1(d_{-1})^1](s)^2$ where d_{+2} is the $3d$ orbital with 2 units of angular momentum about the five-fold axis, etc. The electrons within the square bracket are valence electrons and have randomly oriented spin. We can now calculate the electrostatic repulsion energy between the $3d$ electrons in such a valence state in terms of Slater-Condon parameters[10] as $15F_0-6F_2-250F_4$. The corresponding energy in the ground state is $15F_0-35F_2-315F_4$ and hence the promotion energy is $29F_2+65F_4$ which we estimate as $48\,000\pm4000$ cm^{-1}, about 140 kcal mole^{-1}, taking $F_2=1430$ cm^{-1} and $F_4=105$ cm^{-1}, values which give a satisfactory interpretation of the iron spectrum.[11] Promotion energies to valence states arising from other configurations will also be required. From the ground state of iron to the valence states of $3d^74s$, $(d_0)^1(d_{+2})^2(d_{-2})^2[(d_{+1})^1(d_{-1})^1](s)^1$ and $3d^8$, $(d_0)^2(d_{+2})^2(d_{-2})^2[(d_{+1})^1(d_{-1})^1]$, the promotion energies are 29 000 cm^{-1} and 53 000 cm^{-1} respectively.

For nickel, we first consider the hypothetical valence state arising from the configuration $3d^84s^2$, $(d_0)^2(d_{+2})^2(d_{-2})^2[(d_{+1})^1(d_{-1})^1](s)^2$. The valence state, ground state, and promotion energies are $28F_0-44F_2-382F_4$, $28F_0-50F_2-387F_4$, and $6F_2+5F_4$ respectively, i.e., the promotion energy is now only about 9500 cm^{-1} or 28 kcal mole^{-1}. The promotion energy to a valence state of nickel arising from $3d^84s4p$ is at least 35 000 cm^{-1} but may be larger.

These values are seen to be reasonable in the following way. The valence state, $3d^64s^2$, of iron in ferrocene is a mixture of singlet and triplet states with weights 1 and 3 respectively. The observed[12] singlet states of the $3d^64s^2$ configuration for iron lie between 29 000 cm^{-1} and 35 000 cm^{-1}, and the triplets between 19 000 cm^{-1} and 29 000 cm^{-1}, above the quintet ground state. A detailed comparison with the spectrum of Fe^{++} and consideration of the calculations of Platt and Laporte[13] show, however, that there must be upper singlets and triplets (not observed in neutral iron itself) which lie as high as 80 000 and 48 000 cm^{-1} respectively. Thus our value of 48 000 cm^{-1} lies near the middle of the possible range. The lower promotion energy in nickel is due to the ground state having the same multiplicity as the greater part of the valence state and contributing heavily to it.

We see that the promotion energy to the valence state of iron in ferrocene depends on the extent to which the $3d_{z^2}$ and $4s$ orbitals are mixed together in the a'_{1g} orbital. It certainly could not be less than 40 000 cm^{-1} (115 kcal mole^{-1}), and a value of about 125 kcal mole^{-1} seems most probable. Adding the heat of formation (147 kcal mole^{-1}) and the correction for (2) and (3) (60 kcal mole^{-1}), we obtain a total bonding energy of about 320 kcal mole^{-1} compared with the calculated 286 kcal mole^{-1}. The agreement is reasonable since we have neglected bonding using $4p$-orbitals and the additional stabilization arising from Moffitt's mixing and splitting. With the matrix element x equal to 1 ev (see Fig. 3) a_{1g} is further stabilized by an extra 0.4 ev per electron and a'_{1g} is stabilized by 0.3 ev per electron, a total additional stabilization of 1.4 ev (32 kcal mole^{-1}). Of course, all this shows only that the various guesses which we have made have been sensible ones. But then our treatment is to be regarded not as an attempt to calculate the bonding energy *a priori* but rather as an indication of how it is made up from the contributions of the different orbitals.

In the same way, for the nickel compound, if we add the valence-state promotion energy (28 kcal mole^{-1}), the observed heat of formation (123 kcal mole^{-1}), and the same correction for (2) and (3) (60 kcal mole^{-1}), we obtain 211 kcal mole^{-1} compared with the calculated 194 kcal mole^{-1} for the total bonding energy. The two values are as close as can be expected, considering the nature of the approximations involved.

Our conclusion that antibonding e_{1g}' and a_{1g}'' orbitals are occupied in bis-cyclopentadienyl nickel (II) is supported by recent structural studies. In ferrocene, the iron-carbon distances are about 2.05 A as found both by x-ray[14] and electron diffraction.[15] In the nickel compound, preliminary electron-diffraction work indicates that the mean nickel-carbon distance is about 0.15 A greater.[15] Comparison of the unit cell dimensions[16] indicates a similar lengthening of about 0.1 A.

Further evidence comes from comparison of the infrared spectra of these compounds.[9,17] The sharp peak at 817 cm^{-1} in the ferrocene spectrum is likely to arise from Fe—C stretching; in the nickel compound, the corresponding peak has moved to 775 cm^{-1}, indicating a weaker and longer metal to ring bond. Furthermore, the peak at 1420 cm^{-1} in ferrocene, attributed to C—C stretching,[18] is moved to slightly higher wave number in bis-cyclopentadienyl nickel (II) (~1440

[10] E. U. Condon and G. H. Shortley, *The Theory of Atomic Spectra* (Cambridge University Press, London, 1935), chapter VI.
[11] L. E. Orgel, J. Chem. Phys. (to be published).
[12] All data on atomic spectra are taken from *Atomic Energy Levels* (Natl. Bur. Standards, Washington, D. C.), Vol. I, 1949, Vol. II, 1952.
[13] O. Laporte and J. Platt, Phys. Rev. **61**, 305 (1942).
[14] Dunitz, Orgel, and Rich (to be published).
[15] Berndt, Hamilton, and Hedberg (to be published).
[16] W. Pfab and E. O. Fischer, Z. anorg. u. allgem. Chem. **274**, 316 (1953).
[17] In the legend to Fig. 1 of the paper by Wilkinson, Pauson, and Cotton, it would appear that a mistake in the labeling of the infrared spectra has occurred; the spectrum ascribed to $(C_5H_5)_2Ni$ coincides with an earlier infrared spectrum of ferrocene [Kaplan, Kester, and Katz, J. Am. Chem. Soc. **75**, 5531 (1952)], and also with the spectrum assigned to ferrocene in Fig. 2 of the paper. Thus, in Fig. 1 of the paper, we believe that we should read $(C_5H_5)_2Fe$ for $(C_5H_5)_2Ni$, and vice versa.
[18] E. Lippincott and R. D. Nelson, J. Chem. Phys. **21**, 1307 (1953).

cm^{-1}), indicating that the carbon-carbon bonds are slightly stronger in the nickel compound than in ferrocene, as would follow from at least partial occupancy of the e_{1g}' orbital. The unit cell lengths[16] and also the electron diffraction evidence[15] likewise suggest a very slight but probably significant shortening of the carbon-carbon bonds.

The energy-level diagram which we have drawn will probably be adequate for the neutral bis-cyclopentadienyls, although even in these there will be slight shifts of the metal orbital energies with respect to the constant energy-level scheme of the bis-cyclopentadienyl radicals. It is clear, however, that for charged compounds the situation is very different. To take an extreme example, the ionization potential of Ti^{++} is 28 ev so that the *d*-orbitals are much more stable than any of the bis-cyclopentadienyl π orbitals. Consequently much of the stability of the bis-cyclopentadienyl titanium (IV) cation[19] must come from the ionic character of the titantium-cyclopentadienyl bonds which will distribute the formal charge of +2 in the titanium atom over the entire molecule. A simple calculation, like those of the previous sections, shows that, electron for electron, the a_{1g} orbital is about as effective as the e_{1g} orbital in bonding. In the bis-cyclopentadienyls of iron (III), cobalt (III) and nickel (III),[1,9] the situation is intermediate, since the metals have ionization potentials of about 16 ev, but the energy-level diagrams are certainly very different from those of the neutral compounds. In all of these, ionic contributions to the bonding must be quite important.

Predictions of the magnetic properties of the bis-cyclopentadienyls follow from the energy-level diagram. It will be seen that in the case of ferrocene all electrons are paired in orbitals up to a_{1g}' and so we get diamagnetism. Addition or removal of one electron, as in bis-cyclopentadienyl cobalt (II)[9,20] and bis-cyclopentadienyl manganese (II),[21] respectively, must give one unpaired spin. Addition of two electrons would give a triplet ground state, as observed for bis-cyclopentadienyl nickel (II),[9,22] provided that they do not both go into the a_{1g}'' orbital. Thus the magnetism does not distinguish between $(e_{1g}')^2$, $(e_{1g}')(a_{1g}'')$, $(4p)(a_{1g}'')$, $(4p)^2$, etc. The a_{1g}' and e_{2g} levels lie very close together. Removal of two electrons from e_{2g} or one each from a_{1g}' and e_{2g} would give a triplet ground state for bis-cyclopentadienyl chromium (II) as is found experimentally.[23] Bis-cyclopentadienyl vanadium (II) has been recently shown to have 3 unpaired spins[24] which must arise from the arrangement $(e_{2g})^2(a_{1g}')^1$. We are unable to find any published results on the magnetic properties of bis-cyclopentadienyl titanium (II). We suspect, however, that it should be paramagnetic, with 2 unpaired spins.

No barrier to rotation of the cyclopentadienyl rings relative to one another is to be expected from the molecular orbital treatment. However, the normal steric repulsion between nonbonded carbon atoms will favor the staggered D_{5d} configuration in ferrocene where the perpendicular distance between the cyclopentadienyl planes is only 3.2 A.[14] The corresponding distance in bis-cyclopentadienyl nickel (II) is about 3.4 A,[15] and hence rotation should occur more readily.

[19] Wilkinson, Pauson, Birmingham, and Cotton, J. Am. Chem. Soc. **75**, 1011 (1953).

[20] E. O. Fischer and R. Jira, Z. Naturforsch. **8B**, 327 (1953).
[21] F. Engelman, Z. Naturforsch. **8B**, 775 (1953); G. Wilkinson and F. A. Cotton, Chemistry and Industry 307 (1954).
[22] E. O. Fischer and R. Jira, Z. Naturforsch. **8B**, 217 (1953).
[23] G. Wilkinson, J. Am. Chem. Soc. **76**, 209 (1954).
[24] E. O. Fischer and W. Hafner, Z. Naturforsch. **9B**, 503 (1954).

Measurement of the Magnetic Susceptibility of Manganese Nitride Mn_5N_2 by a Microvibration Method

Y. L. Yousef, R. K. Girgis, and H. Mikhail
Physics Department, Faculty of Science, University of Cairo, Giza, Egypt

(Received September 10, 1954)

The susceptibility-temperature relationship of carefully prepared manganese nitride Mn_5N_2 was measured over the temperature range -180°C to 530°C. The Curie-Weiss law $\chi=C/(T-\theta)$ was found to hold, with $\theta=-1070$ and $C=0.0316$ emu deg/g. The effective Bohr magneton number is 3.94 per Mn, and is in reasonable agreement with the theoretical value 3.87 for 3 unpaired electrons. This suggests that Mn_5N_2 behaves as a coordination compound with 4 electron-pair bonds.

A new microvibration technique, particularly suitable for susceptibility investigations of materials available in small amounts, has been developed for the present work. The underlying principle is to modulate the magnetic field and to translate the periodic force on the material into a periodic displacement of an elastic strip. The force is measured dynamically in terms of a compensating electrostatic force, an electronic circuit being used as a null detector. Accuracy to 10^{-4} dyne is claimed.

INTRODUCTION

IT has long been known that manganese combines with nitrogen to form compounds with peculiar magnetic properties.[1] In recent times, Guillaud and Wyart[2] prepared nitrided manganese alloys and reported, in conformity with earlier work by Hägg[3] and Schenck and Kortengäber,[4] that for nitrogen content between 8.5 to 28.5 atomic percent, the nitrides are ferromagnetic with maximum saturation at the composition Mn_4N, denoted by the ϵ phase. However, beyond the composition corresponding to the ξ phase Mn_5N_2, the alloys cease to be ferromagnetic.

In the present contribution, it was thought worth while to carry out magnetic investigations on the ξ phase having the composition Mn_5N_2, with a view to elucidating the status in which manganese exists in that structure.

PREPARATION OF Mn_5N_2

The nitride was carefully prepared by Professor Jantsch of the Institut für Anorg. Chem. Technologie und Analytische Chemie, Technische Hochschule, Graz. The method of preparation consisted in the nitriding at 825°C and 10 atmospheres pressure of very pure electrolytic manganese powder (Mn, 99.6 percent, H, 0.4 percent) which was obtained in a finely divided state from the amalgam by distilling off mercury in a stream of pure, dry nitrogen. The formation took place in a bomb calorimeter supplied with a heating coil, and a reaction with 99.9 percent pure compressed nitrogen lasted two minutes. The composition of the nitride was determined by the Kjeldahl micro method. The nitrogen content was 9.47 percent. Homogeneity was stated to have been tested electron optically.

EXPERIMENTAL MEASUREMENTS

In the earlier stages of this work some experiments were perfomed on the temperature dependence of the susceptibility between 20°C and 530°C by the conventional Gouy method. The magnetic pull was measured by a chemical balance. The actual susceptibility at room temperature was determined by comparison with ferrous ammonium sulfate and also with manganese sulfate; the usual correction for ferromagnetic impurity by observations at different fields was applied.[5] When investigating the temperature dependence, the sample was contained in an evacuated and sealed Pyrex-glass vial.

The electromagnet used in the static measurements could supply fields up to 2300 oersteds in a gap of 2.5 cm. The container of the sample was sufficiently loaded by a suspended stretching weight to suppress lateral displacements when the field is established. The temperature was varied by means of a cylindrical furnace and was measured by a platinum-platinum iridium thermocouple.

Obviously, the analytical balance method of determining the magnetic pull does not lend itself readily to measurements at low temperatures (requiring a controlled atmosphere), but it was resorted to here only for the purpose of comparison (in the region of overlap) with our new microvibration method which appears to possess decided flexibility.

Although the Sucksmith ring balance is admirable in its simplicity, and can be adapted for operation under vacuum and over a wide temperature interval,[6] it was felt desirable to develop the dynamic balance which we proposed[7] in 1951, and which was subsequently

[1] E. Wedekind and T. Veit, Ber. deut. chem. Ges. **41**, 3769 (1908); P. Weiss and K. Onnes, Compt. rend. **150**, 686 (1910); and T. Ishiwara, Sci. Repts. Tôhoku Imp. Univ. **5**, 53 (1916).
[2] C. Guillaud and J. Wyart, Compt. rend. **222**, 71 (1946); Rev. Met. **45**, 271 (1948).
[3] G. Hägg, Z. physik. Chem. (B) **4**, 346 (1929).
[4] R. Schenck and A. Kortengräber, Z. anorg. allgem. Chem. **210**, 273 (1933).
[5] K. Honda, Ann. Phys. Lpz. **32**, 1048 (1910); H. Owen, Ann. Phys. Lpz. **37**, 657 (1912); and L. F. Bates and P. F. Illsley, Proc. Phys. Soc. (London) **49**, 511 (1937).
[6] W. P. Van Ort, J. Sci. Instr. **28**, 279 (1951).
[7] Yousef, Mikhail, and Girgis, Rev. Sci. Instr. **22**, 342 (1951).

realized in a practicable form, though of restricted use, by one of us[8] (Y. L. Y.) early in 1953.

Our new microvibration arrangement, which we shall describe in detail in the following section, involves radical modifications in the technique employed in the earlier prototype, particularly as regards the adaptability for temperature dependence investigations. The broad outline of the present method is the use of a small magnetic field with low-frequency modulation to exert on the specimen under test a sinusoidal force which is communicated to a properly damped resonant reed, the resulting mechanical vibrations being detected electronically by the capacity change they produce in a high Q circuit. The alternating magnetic force is counterpoised by a suitably phased esu force measurable on a potentiometer. With this scheme, our preliminary static observations were checked, and the range was conveniently extended down to liquid nitrogen temperature.

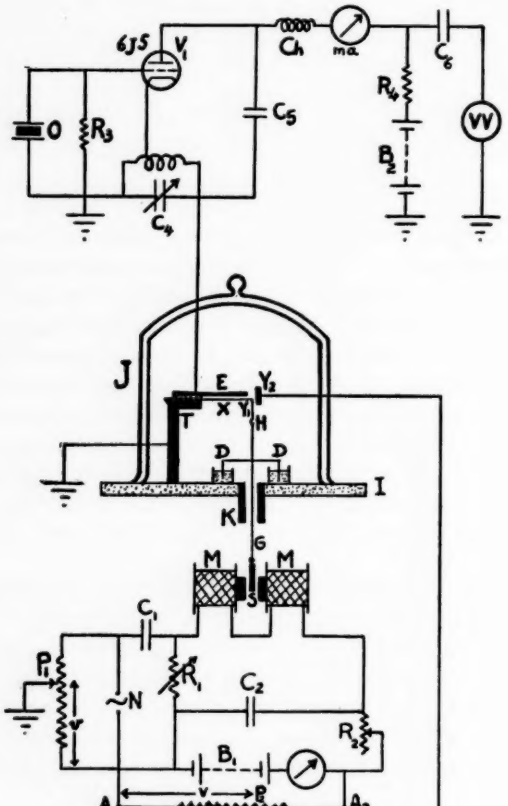

FIG. 1. The reed balance, complete with the power supply for the electromagnet and the electrical detector where X=elastic reed, G=glass suspension rod, S=material under test, Y_1=vibrating end of the reed, Y_2=balancing electrode, D,D=damping vanes, E=capacity electrode, J=gas-tight bell jar, R_1=1000 Ω, 20 watt, adjustable for phase correction, R_2=2000 Ω, 20 watt, regulating rheostat, R_3=50KΩ, R_4=20KΩ, P_1,P_2=100KΩ potential dividers, adjustable at the working middle portions, C_1=25 −100 μf, 250 v, C_2=30 μf, 350 v, C_3=20 μf, 350 v, C_4=300 μμf variable air condenser, C_5=0.0001 μf blocking condenser, C_6=0.1 μf, M,M=two small relay electromagnets, each 200 Ω, the cores being of Permalloy and are included in a magnetic circuit, N=30 V source, 20–60 cps, B_1=250 V ht supply, 200 mA, B_2=100 V ht supply for V_1, V_1=6J5 valve used below normal rating to operate the vibration detector, V,V=ac voltmeter serving as a null detector, O=quartz crystal oscillator, 6–8 Mc/sec, ma=milliammeter, 5 mA range, and Ch=1 mH hf choke.

[8] Y. L. Yousef, Brit. J. Appl. Phys. 4, 46 (1953).

DESCRIPTION OF THE SUSCEPTIBILITY BALANCE

The essential parts of the microbalance and the ancillary equipment are shown in Fig. 1, where X is an elastic reed functioning as a balance and is made of a phosphor bronze strip 2×1×0.005 cm, soldered at one end to an earthed stout brass support T and loaded at the other end Y_1 by the material S under test. The connection between S and Y_1 is effected by means of a thin glass rod G suspended from a hook H and attached to damping aluminum vanes DD dipped in dry oil and serving to reduce, in particular, lateral and rotational motions of S. The total suspended load is about 0.5 g, but may well be as large as few g.

A capacity probe E is situated at about 0.02 cm from X and is connected to the vibration detecting circuit incorporating the valve V_1 and a quartz crystal O. When slightly off-tune, this circuit is extremely sensitive to minute capacity changes, the sensitivity amounting, with reasonable stability, to 0.0005-volt output indication for a capacity change of only 10^{-6} μμf. An adequate description of a similar circuit has been given elsewhere.[8]

The loaded end Y_1 of the reed is bent at right angles to X and is arranged to face a compensating electrode Y_2 which partially overlaps the upper portion of Y_1, with a clearance of about 0.05 cm. The sensitivity and the range of application of the balance may be adjusted by adjusting the distances of E and of Y_2 respectively by means of screws, omitted from the diagram for the sake of simplification.

The balance may be surrounded by an air-tight bell jar J, resting on an ebonite base I, through which all connections can be made. By enclosing the suspension rod G and the specimen S in a test tube communicating to the sleeve K, the balance may be evacuated when necessary—a feature which is particularly important in measurements in a controlled atmosphere and at low temperatures.

The magnetic field may be produced by a small coil or by two relay electromagnets MM. A high-tension source B_1 of 250 volts may be employed to establish a steady (polarizing) field. In a typical case, the electromagnet has a resistance of 400 ohms, and for a current of 0.10 amp it produces a field of 70 oersteds in a gap which is wide enough (1.85 cm) to accomodate a furnace or a cooling bath that may enclose the tube surrounding the container of the material under investigation. Measures have to be taken to prevent serious changes of the temperature of the electromagnet.

A low-frequency mains N of 30 v and 28 cps, resonant

with the loaded reed X and supplying to the electromagnet a modulating current of 15 mA is resistance-capacity coupled to the dc winding of the electromagnet by means of the condenser C_1 and the resistance R_1, the latter being adjustable for phase correction. Mains supply frequency may be employed for modulation if, by appropriate loading for example, the reed is made to resonate with it. By virtue of the damping due partly to the proximity of the electrode E and partly to the action of the vanes DD, the frequency response curve of the reed is substancially flat around the peak, and adjustment to resonance is by no means critical.

Potential dividers P_1 and P_2 are connected respectively across the ac and dc supplies, and are intended to provide voltages to the compensating electrode Y_2. A large by-pass consenser C_2 across B_1 and the current regulating rheostat R_2 will help in minimizing the ac voltage drop due to R_2 and to the internal resistance of B_1.

A capacitance C_3 is joined between Y_2 and the end A_1 of the potentiometer P_2. If the reactance of C_3 is small compared with the resistance of each of the two parts A_1P_2 and P_2A_2 of the dc potentiometer P_2, then any ac component of the voltage V appearing between A_1 and P_2 can be made quite insignificant, provided that the resistance of the source B_1 is sufficiently smaller than the resistance of the part P_2A_2 of the potential divider.

METHOD OF USE AND CALCULATION OF THE SUSCEPTIBILITY

The theoretical performance of the vibrating reed type microbalance has already been briefly discussed by one of the present authors (Y. L. Y.).[8] In the modification here described, the following argument will show how the susceptibility can be deduced.

When the variable contact of the ac potentiometer P_1 is earthed, the resultant potential difference between Y_1 and Y_2 will be $(v+V)$, where v and V are respectively the alternating and the polarizing voltages. This gives rise to an electrostatic force at the reed end with a vertical component whose effective oscillating part is proportional to vV, and would thus induce resonant flexural vibrations in the reed. The modulated magnetic force, too, has a vertical isofrequentic component proportional to hH, where h is the modulating field and H the steady field, also acting at the reed end.

Since the two forces are colinear and act in opposition, then with proper synchronization an adjustment of the product hH or, more simply, vV will suffice to neutralize the vibrations completely. Equilibrium is judged by the null indication of the voltmeter VV (Fig. 1).

In general, the magnetic field in the gap (and accordingly, the magnetic force on the specimen) lags behind the voltage applied to the electromagnet mainly for two reasons, *viz.*, the inductance of the windings and the magnetic viscosity of the core. Appropriate phasing between the magnetic and the opposing electrostatic forces may be brought about by the R_1C_1 coupling between the ac source and the electromagnet. With a core of Permalloy, the magnetic viscosity is small and the phase angle is small and insensitive to changes of temperature, frequency or magnetic history,[9] so that for a given modulating current the alternating field h remains strictly constant—a requirement which is extremely essential.

When required, phase correction without a change of the modulating voltage across the electromagnet may be achieved if the coupling condenser C_1 is joined in series with an inductance shunted by a variable resistance so as to form with C_1 a constant impedance phase shifter.[10]

Since for a fixed circuit resistance the field H, to a first approximation, is proportional to the dc supply voltage, E say, and h is likewise proportional to the ac source voltage, e say, it follows that the effective alternating magnetic force is approximately proportional to eE. As the counter esu force ($\propto vV$) is also proportional to eE, it comes out that slight voltage fluctuations in the power supplies would affect the two opposing forces to the same extent, provided that the material under test does not show pronounced field dependence. The implication of this is that if the forces are balanced, and v and V are expressed in terms of the settings P_1 and P_2 of the potentiometers, the balance point will be almost independent of changes in the power supplies. This becomes strictly true if the magnetic field is produced by an air-cored coil, in which case the compensating voltages may be taken entirely from a part of the drop on R_1.

In investigating the susceptibility χ of a substance under any condition, it is desirable to obtain the product P_1P_2 (which is evidently a measure of χ) from the slope of the straight line giving $1/P_2$ as a function of P_1. The manipulation of the apparatus is so simple and rapid that the data required for the construction of such a curve can be obtained in about one minute.

TABLE I. Typical results for Mn_5N_2. Mass 0.1 g; steady field 70 oersted; modulation frequency 28 cps.

Setting of dc potentiometer P_2 ($K\Omega$)	$1/P_2$	Reading of ac potentiometer P_1 ($K\Omega$)					
		−180°C	−67°C	24°C	130°C	220°C	305°C
21.8	0.0459	39.8	35.5	33.2	31.2	28.7	27.0
25.2	0.0397	34.2	30.3	29.2	26.1	25.0	23.7
29.5	0.0339	29.8	25.9	25.0	22.5	21.0	20.0
33.3	0.0300	25.8	23.2	21.9	20.2	19.1	17.8
37.0	0.0270	23.4	21.0	19.6	17.9	16.6	15.7
40.7	0.0246	21.4	19.0	17.9	16.5	15.4	14.5
43.0	0.0233	20.3	17.9	16.9	15.4	14.5	13.7

[9] R. M. Bozorth, *Ferromagnetism* (D. Van Nostrand Company, Inc., New York, 1951), 796.

[10] G. P. Harnwell, *Principles of Electricity and Electromagnetism* (McGraw-Hill Book Company, Inc., New York, 1949), 477.

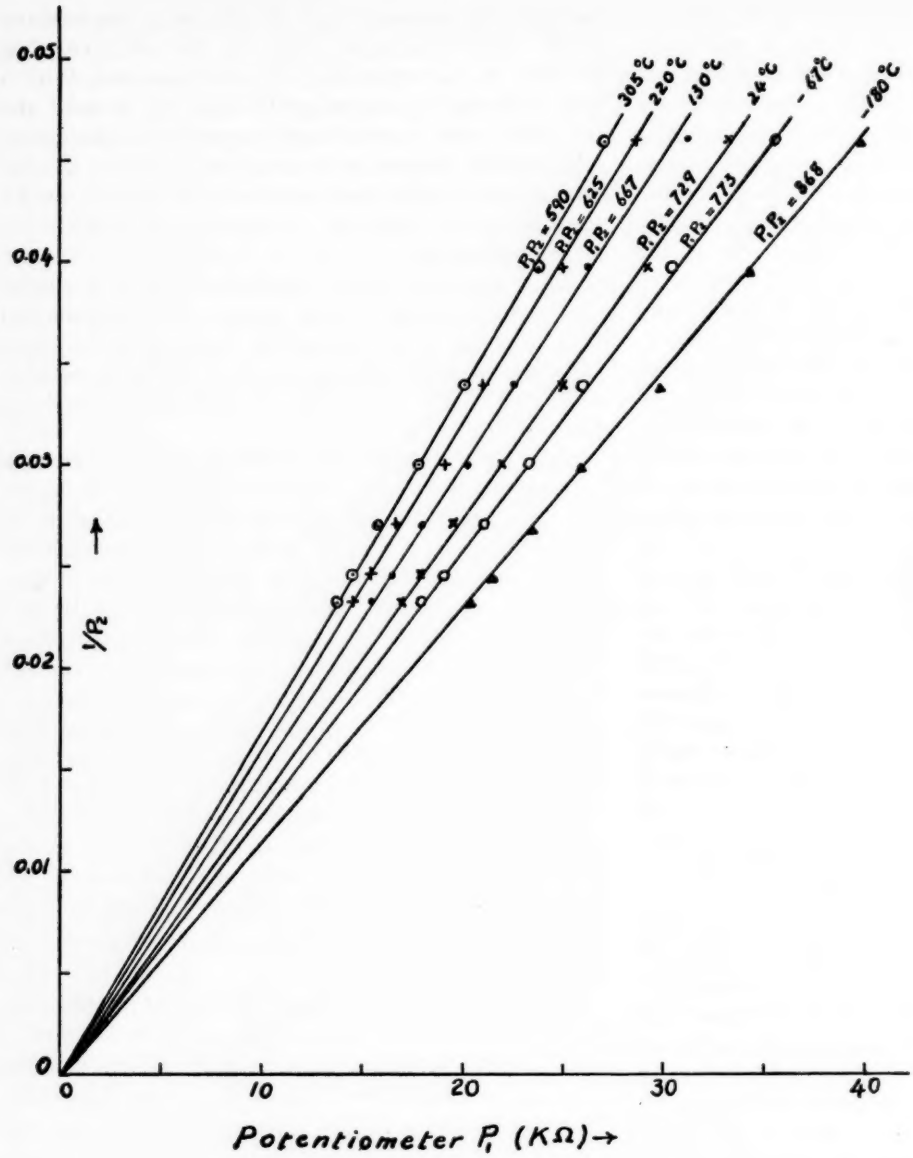

FIG. 2. Inverse proportionality between the direct and the alternating voltages on the compensating electrode. The slope P_1P_2 of each line represents the balancing force at the temperature considered.

One of the outstanding features of the susceptibility measuring equipment we adopted here is that it can be entirely operated from an ac mains with small power consumption (the electromagnet consumes 4 watts). Other features are high sensitivity, flexibility, compactness, accuracy, and rapidity. The indications are nearly independent of voltage supply fluctuations, changes of modulating frequency, of sensitivity of the electronic circuit, of the elastic properties of the reed, or of its distance from the probe electrode. The method offers a delicate test for the presence of ferromagnetic impurities either by observing the lag in magnetization or by comparison of the susceptibility values at a low and at a large field.

RESULTS

With the arrangement described, an oscillating force whose amplitude is only 0.01 dyne would give an output indication of more than one volt. The noise level is normally less than 0.005 volt, and for forces of the order of magnitude mentioned above the potentiometers can be set to give balance accurately to 1 percent.

Table I gives typical results for Mn_5N_2 at various temperatures and Fig. 2 shows a graphical representation of these results.

Figure 3 is derived from the curves of Fig. 2, and it represents the variation of χ with T. Results obtained on the same sample by the conventional Gouy method are inserted for comparison. The same room-temperature value of χ was taken as reference in the two sets of observations.

A very delicate test for the existence of a ferromagnetic impurity in a substance can be performed by the present arrangement. First, the phasing network is adjusted so that a counterbalance of the magnetic force

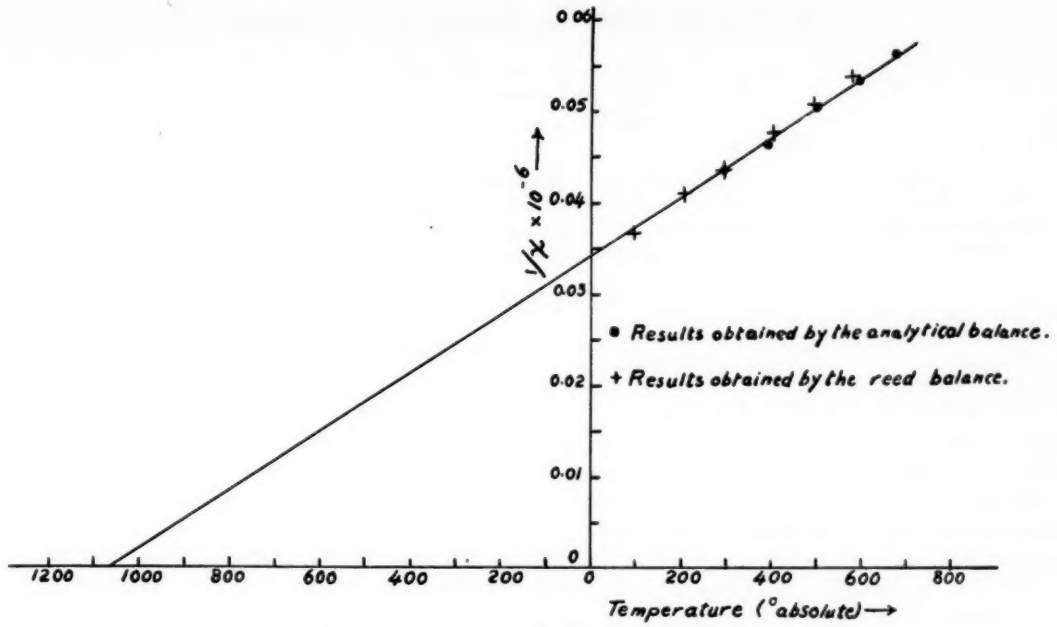

FIG. 3. $1/\chi$ *vs* T relationship for Mn_5N_2.

may be obtained for a material which is known to contain no ferromagnetic impurity. The material under enquiry is then placed in the field. Failure to secure a sharp counterbalance is an indication of the presence of a constituent whose magnetization lags behind the field—a property which is normally ascribed to ferromagnetics due principally to magnetic viscosity.

A test carried in this fashion on fresh Mn_5N_2 gave a distinct sign of ferromagnetism, possibly due to traces of the ϵ phase. However, after heat treatment in vacuum for three hours at 500°C, all evidence of ferromagnetism was found to disappear. The results in Figs. 2 and 3 refer to a heat-treated sample.

CONCLUSION

The data shown in Fig. 3 can be represented by a Curie-Weiss law

$$\chi = C/(T-\theta),$$

where $\theta = -1070$ and $C = 0.0316$ emu deg/g.

The value of the effective Bohr magneton number is 3.94 per Mn, in good agreement with the theoretical value 3.87 for three unpaired electrons. According to Pauling's theory[11] on the nature of the chemical bond, it appears that there is some covalent bonding Mn—Mn or Mn—N in which the Mn nonbonding electrons occupy only 4 of the 5 3*d* orbitals.

[11] L. Pauling, J. Am. Chem. Soc. **53**, 1391 (1931); **54**, 988 (1932).

Linear Association in Nonaqueous Solutions

ROBERT GINELL AND JOEL SHURGAN
Chemistry Department, Brooklyn College, New York
(Received August 24, 1954)

The two-constant theory of linear association has been considered further, and methods have been derived whereby the constants can be evaluated from experimental data. These methods have been applied to data on phenanthrene solutions in ethanol. The agreement of the derived curve with experimental points is excellent. The experimental data go up to ~3 molal solutions (~65 wt percent soln.).

INTRODUCTION

THE basic idea that the deviations from ideality in both gases and solutions is the result of the aggregation of the molecules is a very old one. Many of the pioneers of this branch of science have tried to explain these deviations in these terms.[1,2] Their general approach was to assume the aggregation proceeded to a limited extent and that the equilibrium that existed was one between monomers and dimers or between monomers, dimers, and trimers. Higher species were ignored. These early attempts were not too successful, and with Clausius[3] and Van der Waals[4] the emphasis, especially in gas theory, left aggregation and swung to a consideration of intermolecular forces. Lately the inadequacies of this approach have been recognized and attention has been directed again at aggregation as a cause of the deviations from ideality.[5] An interesting approach of later date applying to gases has been made by Woolley.[6]

In the approach used in this paper, the assumption is made that all types of aggregation are not only possible, but more important, occur to such an extent that they must be considered. The basic theory of linear association has been previously presented,[7–9] as has the n-constant theory.[10] In this paper we shall further develop the theory of linear association, derive methods for applying the theory to experimental data and give some results of the application of this theory to solutions.

THEORETICAL

Modes of Growth and Degradation

In applying the improved two-constant theory to actual data, several points must be elucidated. The first consists of a consideration of the multiplicity of modes of attachment or detachment of a 1-mer particle. The number of ways in which a 1-mer can add to a j-mer will enter into the equation as a coefficient. The question arises as to whether this would affect the form of the final solutions and hence make a comparison of the data with the theory dependent upon choosing the correct mechanism or structure of the j-mer. This is an important consideration since we often know very little about the structure of the higher j-mers, and if our solution depended upon this structure, we would need a great number of sets of equations. It can be shown readily that the final form of the equations is independent of the modes of attachment and detachment.

All the possible reactions under our assumptions are summarized by the following equations (see Table I):

$$n_1+n_1 \underset{l_{11}}{\overset{k_{11}}{\rightleftarrows}} n_2 \tag{1a}$$

$$n_1+n_j \underset{l_{1j}}{\overset{k_{1j}}{\rightleftarrows}} n_{j+1} \quad (j\geqq 2). \tag{1b}$$

The differential equations describing the rates of growth and degradation of the various species are then:

$$\frac{dn_1}{dt}=-Ak_{11}n_1n_1-Gk_{1j}n_1\sum_{x=2}^{M-1}n_x +2Cl_{11}n_2+El_{1j}\sum_{x=3}^{M}n_x \tag{2a}$$

$$\frac{dn_2}{dt}=-Gk_{1j}n_1n_2+\frac{Ak_{11}}{2}n_1n_1+El_{1j}n_3-Cl_{11}n_2 \tag{2b}$$

$$\frac{dn_3}{dt}=-Gk_{1j}n_1n_3+Gk_{1j}n_1n_2+El_{1j}n_4-El_{1j}n_3 \tag{2c}$$

$$\vdots$$

$$\frac{dn_{M-1}}{dt}=-Gk_{1j}n_1n_{M-1}+Gk_{1j}n_1n_{M-2} +El_{1j}n_M-El_{1j}n_{M-1} \qquad [2(m-1)]$$

$$\frac{dn_M}{dt}=+Gk_{1j}n_1n_{M-1}-El_{1j}n_M. \tag{2m}$$

[1] L. Boltzman, Ann. Physik **22**, 39 (1884); L. Natanson, Ann. Physik **38**, 288 (1889); J. J. Thomson, Phil. Mag. **18**, 233 (1884).
[2] This older work is very ably summarized by J. Jeans, *Introduction to the Kinetic Theory of Gases* (The Cambridge University Press, New York, 1940); L. B. Loeb, *Kinetic Theory of Gases* (McGraw Hill Book Company, Inc., New York, 1927).
[3] R. Clausius, For a summary of his work see *Die Kinetische Theorie der Gase* (F. Vierweg und Sohn, Braunschweig, 1889), Chap. II.
[4] Van der Waals, Academisch Proefschrift, Leiden (1873).
[5] For an interesting survey of the many facets of this problem and some of the modes of attack on it see, for instance, the Symposium papers in Chem. Revs. **1**, (February, 1949); especially note the introductory remarks by Otto Redlich.
[6] H. W. Woolley, J. Chem. Phys. **21**, 236 (1953).
[7] P. J. Blatz, and A. V. Tobolsky, J. Phys. Chem. **49**, 77 (1945).
[8] R. Ginell, J. Colloid Sci. **3**, 1 (1948); **5**, 99 (1950).
[9] R. Ginell, J. Polymer Sci. **7**, 413 (1951).
[10] R. Ginell, Ann. N. Y. Acad. Sci. April, 1955.

This set of equations is consistent with the laws of conservation of mass which may be stated as:

$$d\sum_x xn_x/dt=0.$$

An assumption made here is that all j-mers ($j\geqq 2$) have the same number of modes of attachment and detachment which, however, may be different from the modes of attachment of the 1-mer−1-mer combination. This is a plausible assumption and stems directly from the assumption of linear chain formation.

Now, adding Eqs. (2b) through (2m) and setting all the terms dn_x/dt equal to zero since we are considering equilibrium conditions, and solving we get:

$$n_2=\frac{K_{11}'}{2}n_1^2 \qquad (3a)$$

where

$$K_{11}'=\frac{A}{C}K_{11}.$$

Similarly by repeating this process we find that:

$$n_j=\frac{K_{11}'K_{1j}'^{(j-2)}n_1^j}{2}, \qquad j\geqq 2 \quad (3b)$$

where

$$K_{1j}'=\frac{G}{E}K_{1j}.$$

Equations (3a) and (3b) are identical in form to the equations in the paper of Ginell,[9] differing only in a factor of $(\frac{1}{2})^{j-2}$ in the case of Eq. (3b). This difference stems from the fact that the equations in the latter paper assume two modes of degradation, one for each end. The equations in this paper are more general when this is stated in terms of K''s.

Thus we see that while the number of modes of growth and degradation will have a bearing on the true value of the equilibrium constant, the equations can be solved for the over-all equilibrium constants from the generalized equations. Specific mechanisms may then be postulated and inserted to get the value of the true equilibrium constant. This, of course, greatly simplifies the situation since only one general set of equations is needed.

The Largest Particle

In considering the equilibrium state arrived at by the simultaneous growth and degradation, we ask whether there is a maximum size of particle which will not be exceeded no matter how large a system is taken. Upon consideration it will be apparent that there always will be a largest particle if the system is large enough (i.e. contains enough particles). However, practical experiments are often not done with such large samples of matter, and hence the amount of material may have a bearing on the actual size of the largest particle. This

TABLE I. Table of symbols.

A = number of possible modes of combination of a 1-mer.
$B_c=\Sigma xC_x-\Sigma C_x$.
$B_n=\Sigma xn_x-\Sigma n_x$.
C = number of possible modes of degradation of a 2-mer to two 1-mers.
C_1 = concentration (molar or molal) of a 1-mer in solution equals $n_1/N_0\phi$.
C_j = concentration (molar or molal) of a particular j-mer in solution equals $n_j/N_0\phi$.
$D_c=(K_{c11}'-2K_{c1j}')$.
$D_n=(K_{11}'-2K_{1j}')$.
E = number of possible modes of degradation of a j-mer to a 1-mer and a $(j-1)$-mer.
G = number of possible modes of combination of a 1-mer with a j-mer.
$K_{11}=k_{11}/l_{11}$ = true equilibrium constant for the formation of a 2-mer from two 1-mers.
$K_{1j}=k_{1j}/l_{1j}$ = true equilibrium constant for the formation of j-mers ($j\geqq 3$) from a $(j-1)$-mer and a 1-mer.
$K_{11}'=(A/C)K_{11}'$ = generalized equilibrium constant.
$K_{1j}'=(G/E)K_{1j}'$ = generalized equilibrium constant.
$K_{c11}=N_0\phi K_{11}$ = true equilibrium constant in terms of concentration.
$K_{c1j}=N_0\phi K_{1j}$ = true equilibrium constant in terms of concentration.
$K_{c11}'=(A/C)K_{c11}$ = generalized equilibrium constant in terms of concentration.
$K_{c1j}'=(G/E)K_{c1j}$ = generalized equilibrium constant in terms of concentration.
M = the degree of association of the largest particle which will be found in a system of infinite extent.
$M_1^{(0)}$ = molecular weight of 1-mer in grams.
N_0 = Avogadro's number.
N_1 = number of 1-mers in units of Avogadro's number.
N_j = number of j-mers in units of Avogadro's number.
$P_N=\Sigma xn_x/\Sigma n_x=W/M_1^{(0)}\Sigma N_x$ = number average degree of association.
R = universal gas constant.
W = weight of sample in grams.
$Z_n=d\Sigma n_x/dB_n$.
j = degree of association (an integer).
j-mer = a particle of degree of association, j.
k_{11} = second-order specific rate constant for the addition of 1-mer to 1-mer; $n_1+n_1\xrightarrow{k_{11}}n_2$.
k_{1j} = second-order specific rate constant for the addition of 1-mer to j-mer; $n_1+n_j\xrightarrow{k_{1j}}n_{j+1}$.
l_{11} = first-order specific rate constant for the degradation of a 2-mer to two 1-mers; $n_2\xrightarrow{l_{11}}n_1+n_1$.
l_{1j} = first order specific rate constant for the degradation of a $(j+1)$-mer to a j-mer and a 1-mer; $n_{j+1}\xrightarrow{l_{1j}}n_j+n_1$.
m = the degree of association of the largest particle present in a given system.
n_1 = number of 1-mer particles in absolute count.
n_j = number of j-mer particles in absolute count.
t = time.
ϕ = volume of solution or mass of solvent.
ΣC_x = the number of avmoles of particles per liter of solution (avmolarity) or per 1000 g of solvent (avmolality).
ΣxC_x = the stochiometric concentration; formula weights per liter of solution (formolarity) or per 1000 g of solvent (formolality).
$\Sigma N_x=\Sigma n_x/N_0$ = the avmolity = the number of particles measured in multiples of Avogadro's number.
$\Sigma xN_x=\Sigma xn_x/N_0=W/M_1^{(0)}$ = the formolity or the number of 1-mers which would be present if all the associated particles would be completely dissociated, counted in multiples of Avogadro's number. The stochiometric concentration.
Σn_x = the actual number of particles between the limits given.
Σxn_x = the number of 1-mers, which would be found between the given limits if all the associated particles would be completely dissociated.

consideration must be taken into account in the forms of equations and the methods of mathematical solution employed.

For a finite amount of material several cases can be distinguished.

(1) The equilibrium constant of j-mers, K_{1j}, is very large. This means that the rate of growth is very large compared to the rate of degradation. In such a case we may exhaust the concentration of 1-mers before equilibrium is even reached. Then the substance is in a metastable state of pseudo-equilibrium. If this large K_{1j}, implying a large k_{1j}, is accompanied by a small k_{11} then we will produce true high polymers. In this case it is possible to partially neglect the degradation mechanism. Here k_{11} is equivalent to an initiation k (to use the specialized language of high polymer chemistry) and k_{1j} to the rate of growth while l_{1j} functions as a rate of termination.* The mathematics of this case has been extensively investigated[11,12] and will not be considered further here. The state here is that $M>m$.

(2) The equilibrium constant K_{1j} is not so great. Here, while the size of the largest particle present, m, is controlled by the amount of material, nevertheless it is not enough to consider only the growth mechanism since there is always present an appreciable amount of the lower j-mers. The state here is $M>m$.

(3) The equilibrium constant K_{1j} is small. Here, the maximum theoretical size M is attained in normal experimental quantities. Here, $M=m$.

(4) The equilibrium constant K_{1j} is very small. Here, there is little association and the bulk of the molecules are to be found in 1-mers and 2-mers. Here, $M=m$ = small number.

The equations governing these cases can easily be derived from Eq. (3b).

$$\sum_{x=1}^{M} n_x = n_1 + \sum_{x=2}^{M} n_x = n_1 + \sum_{x=2}^{M} \frac{K_{11}' K_{1j}'^{(x-2)} n_1^x}{2}. \tag{4a}$$

This upon expansion gives

$$\sum_{x=1}^{M} n_x = \frac{2n_1 + D_n n_1^2 - K_{11}' n_1^2 (K_{1j}' n_1)^{M-1}}{2(1-K_{1j}' n_1)}. \tag{4b}$$

Similarly from Eq. (3b)

$$\sum_{x=1}^{M} x n_x = n_1 + \sum_{x=2}^{M} x n_x = n_1 + \sum_{x=2}^{M} \frac{x K_{11}' K_{1j}'^{(x-2)} n_1^x}{2}. \tag{4c}$$

This upon expansion gives[12]

$$\sum_{x=1}^{M} x n_x = \frac{2n_1 + 2D_n n_1^2 - K_{1j}' D_n n_1^3 - K_{11}' n_1^2 (K_{1j}' n_1)^{M-1}[M(1-K_{1j}' n_1)+1]}{2(1-K_{1j}' n_1)^2}. \tag{4d}$$

These are the general equations and apply at all times. In the case where $M>m$, this expression can be simplified by taking the upper limit of the sum as infinity rather than M. If, from Eq. (3b), we derive the sums till infinity, we get:

$$\sum_{x=1}^{\infty} n_x = \frac{2n_1 + D_n n_1^2}{2(1-K_{1j}' n_1)} \tag{5a}$$

and

$$\sum_{x=1}^{\infty} x n_x = \frac{2n_1 + 2D_n n_1^2 - K_{1j}' D_n n_1^3}{2(1-K_{1j}' n_1)^2}. \tag{5b}$$

These equations are essentially those given by Ginell.[9] The only way the Eqs. (4) can reduce to Eqs. (5) is if the

$$\lim_{M\to\infty} (K_{1j}' n_1)^M = 0. \tag{6}$$

Since M is always a positive integer, Eq. (6) can be true only if

$$K_{1j}' n_1 < 1.$$

This means that

$$\frac{1}{K_{1j}'} > n_1. \tag{7}$$

Hence, two cases are evident in which it is possible to use the simpler set of equations neglecting M: (1) if the substance is highly associated and M is very large, (2) if the substance is very little associated. Then K_{1j}' is very small, and therefore $K_{1j}' n_1$ may be small. However, there remains a range in which the use of the general equations (4) is imperative.

Conversion of the Equations to the Basis of Concentration

When working with solutions, it is usually more convenient to consider concentrations rather than the absolute numbers of particles as in the previous equations. If we let ϕ equal either the volume of the solution or the mass of the solvent (depending upon whether we choose to express the concentrations in molar or molal

* It is not implied here that this is the sole cause of termination in polymer growth. Other causes, such as interaction with excess free radicals are always present. However in the present treatment of the kinetics of polymerization, the usual procedure is to consider the forward reactions only and totally ignore the backward reactions. In a certain sense this is justified as the forward reaction is far more important than the backward one since the compounds so formed are stable. However, when the reaction approaches completion, the backward reaction may be an important factor in the termination of further growth. The fact that the system can still react with free radicals, impurities, and other extraneous material may have an important bearing on the ageing and consequent modification of the properties of high polymers.

[11] H. Mark and A. V. Tobolsky, *Physical Chemistry of High Polymers* (Interscience Publishers, Inc., New York), second edition.

[12] R. Ginell and R. Simha, J. Am. Chem. Soc. **65**, 706 (1943).

units) then,

$$C_1=\frac{n_1}{N_0\phi}=\frac{N_1}{\phi} \quad (8a)$$

and

$$C_j=\frac{n_j}{N_0\phi}=\frac{N_j}{\phi}. \quad (8b)$$

Substituting Eqs. (8a) and (8b) in Eqs. (3a) and (3b), we get

$$C_2=\frac{N_0\phi K_{11}'C_1^2}{2} \quad (8c)$$

and

$$C_j=\frac{(N_0\phi K_{11}')(N_0\phi K_{1j}')^{j-2}C_1^j}{2}, \quad (j\geqq 2). \quad (8d)$$

Now we can define new constants.

$$K_{c11}'=N_0\phi K_{11}' \quad (8e)$$

and

$$K_{c1j}'=N_0\phi K_{1j}'. \quad (8f)$$

We now have:

$$C_j=\frac{K_{c11}'K_{c1j}'^{(j-2)}C_1^j}{2}, \quad (j\geqq 2) \quad (8g)$$

which is of exactly the same form as Eq. (3b). Hence, we can rewrite all the formulas previously given in terms of the number of particles in terms of concentration:

$$\sum_{x=1}^{M} C_x=\frac{2C_1+D_cC_1^2-K_{c11}'C_1^2(K_{c1j}'C_1)^{M-1}}{2(1-K_{c1j}'C_1)} \quad (9a)$$

$$\sum_{x=1}^{M} xC_x=\frac{2C_1+2D_cC_1^2-K_{c1j}'D_cC_1^3-K_{c11}'C_1^2(K_{c1j}'C_1)^{M-1}[M(1-K_{c1j}'C_1)+1]}{2(1-K_{c1j}'C_1)^2} \quad (9b)$$

and

$$\sum_{x=1}^{\infty} C_x=\frac{2C_1+D_cC_1^2}{2(1-K_{c1j}'C_1)} \quad (10a)$$

$$\sum_{x=1}^{\infty} xC_x=\frac{2C_1+2D_cC_1^2-K_{c1j}'D_cC_1^3}{2(1-K_{c1j}'C_1)^2}. \quad (10b)$$

Application of the Equations to Experimental Data

At the present no exact method is available by means of which an analytic solution of Eqs. (4) or (9) can be obtained. However, in certain cases approximate methods are useful.

M is very large ($M>m$). In this case where the theoretically largest particle, M, is greater than any particle, m, present in the finite amount of solution used, we can use the following analysis. Experimentally, this case is characterized simply by plotting the difference between the formolality and the avmolality, B_e; *versus* the avmolality (i.e., B_e *vs* $\sum C_x$; see Fig. 1). (These quantities are experimentally determined and will be further discussed.) If the value of B_e approaches zero simultaneously with $\sum C_x$, then the system falls into this class. The rationale for this test is clear. Since B_e which is a measure of the concentration of associated particles (actually $B_e=\sum(x-1)C_x$) approaches zero at the same time that the number of particles approaches zero, then the meaning is that this system is highly associated.

In this case, since M is so large we can use Eqs. (5) where the summation is to infinity. Equations (5a) and (5b) are independent equations. Since both quantities $\sum xC_x$ and $\sum C_x$ may be determined experimentally; the first from its definition and an assumption as to what the monomer particle is, and the latter from the experimentally determined molecular degree of association.

Method I

These two equations contain two parameters K_{11}' and K_{1j}', and one variable, n_1, which must be determined. Hence, a third relationship which contains another experimentally measurable quantity must be derived in order to be able to arrive at a solution.

Differentiating Eq. (5a) with respect to n_1 we get:

$$\frac{d\sum_{1}^{\infty} n_x}{dn_1}=\frac{2+2D_nn_1-K_{1j}'D_nn_1^2}{2(1-K_{1j}'n_1)^2}=\frac{\sum_{x=1}^{\infty} xn_x}{n_1}. \quad (11a)$$

Using the definition of B_n and D_n and Eqs. (5a) and (5b) we get:

$$B_n=\sum_{1}^{\infty} xn_x-\sum_{1}^{\infty} n_x=\frac{K_{11}'n_1^2}{2(1-K_{1j}'n_1)^2}. \quad (11b)$$

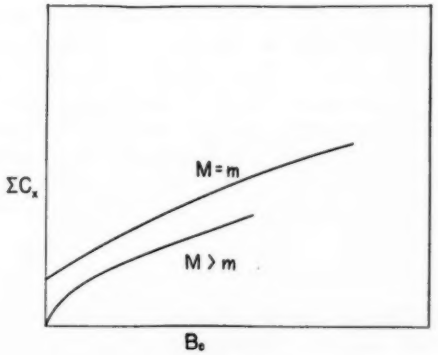

FIG. 1.

Differentiating Eq. (11b) with respect to n_1 we get:

$$\frac{dB_n}{dn_1}=\frac{2K_{11}'n_1}{2(1-K_{1j}'n_1)^3}=\frac{2B_n}{(1-K_{1j}'n_1)n_1}. \tag{11c}$$

We have now from Eqs. (11a) and (11c)

$$Z_n=\frac{d\sum_1^\infty n_x}{dB_n}=\frac{d\sum_1^\infty n_x/dn_1}{dB_n/dn_1}=\frac{(1-K_{1j}'n_1)\sum_1^\infty xn_x}{2B_n}. \tag{11d}$$

From which

$$K_{1j}'=\frac{1}{n_1}-\frac{2B_nZ_n}{n_1\sum_1^\infty xn_x}. \tag{11e}$$

Substituting Eq. (11e) in Eq. (5a) and solving for $D_nn_1^2$ using the definition of P_N we get:

$$D_nn_1^2=\frac{4B_nZ_n-2n_1P_N}{P_N}. \tag{11f}$$

Substituting Eqs. (11e) and (11f) into Eq. (5b) and solving for n_1 we get:

$$n_1=\sum_{x=1}^\infty n_x-\frac{2B_nZ_n(P_N-1)}{P_N}. \tag{11g}$$

Substituting Eq. (11e) into Eq. (11b) and solving for K_{11}' we have:

$$K_{11}'=2B_n\left[\frac{2B_nZ_n}{n_1\sum_1^\infty xn_x}\right]^2. \tag{11h}$$

Equations (11g), (11h), and (11e) are the desired solutions; Eq. (11g) giving n_1 in terms of the experimental quantities; B_n, the difference between the formolity and the avmolity; P_N, the number average degree of association which is the ratio of the formolity to the avmolity; $\sum n_x$, which is the avmolity; and Z_n, the slope of the curve of the avmolity plotted *versus* B_n.

Equations (11h) and (11e) give K_{1j}' and K_{11}' in terms of n_1 and the known experimental quantities. These equations can, of course, be directly rewritten in terms of B_c, Z_c, C_j, K_{c11}' and K_{c1j}' for application to solutions. The modes of growth and degradation do not appear in the equation but are contained in the values of K_{11}' and K_{1j}' and hence the distribution spectra are independent of these modes and may be calculated directly from Eq. (3b).

Method II

This method is usually simpler than Method I since it does not involve obtaining graphical or numerical tangents. Equations (4a) and (4c) can be rewritten in expanded form using the substitution of C's for n's as in Eqs. (9) as

$$\sum_{x=1}^\infty C_x=C_1+C_2+C_3+C_4+\cdots \tag{4a}$$

$$\sum_{x=1}^\infty xC_x=C_1+2C_2+3C_3+4C_4+\cdots \tag{4c}$$

from whence we get

$$\sum_1^\infty xC_x-2\sum_1^\infty C_x=-C_1+C_3+2C_4+\cdots. \tag{12a}$$

From the definition of P_N, we have at $P_N=2$

$$\sum_{x=1}^\infty xC_x=2\sum_{x=1}^\infty C_x. \tag{12b}$$

Hence, substituting Eq. (12b) in Eq. (12a), we have

$$C_1=C_3+2C_4+3C_5+\cdots. \tag{12c}$$

Substituting Eq. (8g) into Eq. (12c) we get

$$1=K_{c1j}'\left(\frac{K_{c11}'}{2}C_1^2+2\frac{K_{c11}'}{2}K_{c1j}'C_1^3+\frac{3K_{c11}'}{2}K_{c1j}'^2C_1^4+\cdots\right). \tag{12d}$$

The term in the parentheses is equal to B_c, hence

$$K_{c1j}'=\frac{1}{B_c}\quad\text{at}\quad P_N=2. \tag{12e}$$

One can now obtain K_{c1j}' graphically from a plot of B_c *versus* P_N, or B_c *versus* $\sum C_x$ (at $P_N=2$, $B_c=\sum C_x$) or any other related pair of variables.

Knowing K_{c1j}' we can now solve for K_{c11}' and C_1. Inserting the definition of D_c into Eqs. (10a) and (10b) and eliminating K_{c11}' between them we get, after rearrangement and utilizing the definitions of P_N and B_c,

$$C_1=\left(\frac{2-P_N}{1-P_N}\right)\left[\frac{1}{K_{c1j}'-\frac{1}{B_c}}\right] \tag{12g}$$

or alternatively

$$C_1=\frac{\sum C_x-B_c}{1-K_{c1j}'B_c}. \tag{12h}$$

Equation (12h) is simpler for computation. Solving Eqs. (10a) and (11b) we get:

$$K_{c11}'=\frac{2}{B_c}\left(\frac{\sum C_x}{C_1}-1\right)^2. \tag{12i}$$

TABLE II. Phenanthrene in ethanol.

Pressure cm Hg	ΔP cm	g solvent	g solute	75°C avmolality ΣC_x	formolality ΣxC_x	B_e	P_N	C_1	K_{c11}'[a]
66.91	1.10	15.78	1.105	0.362811	0.392915	0.03010	1.08298	0.34031	0.29049
	2.15		2.483	0.720632	0.882904	0.16227	1.22518	0.63479	0.22536
	3.00		4.399	1.018906	1.564194	0.54529	1.53517	0.79548	0.28935
	3.92		7.65	1.350817	2.720182	1.36937	2.01372	1.15293	0.46419
66.97	0.90	19.72	1.033	0.295679	0.293925	−0.001753	0.99407[b]	0.29704	−0.02415[c]
	1.19		1.462	0.392676	0.415991	0.02331	1.05937	0.37586	0.17163
	1.87		2.667	0.623509	0.758856	0.13535	1.21707	0.54266	0.32800
	2.75		4.537	0.929489	1.290938	0.36145	1.38887	0.77622	0.21573
	3.28		6.54	1.117852	1.860863	0.74301	1.66468	0.83544	0.30759
	3.59		8.192	1.229487	2.330916	1.10143	1.89584	0.70083	1.03324[c]
	4.03		10.40	1.389825	2.959170	1.56935	2.12917	1.09147	0.95229[c]

[a] Average $K_{c11}' = 0.2865 \pm 0.0617$.
[b] The experimental data scatters and this appears to be a value having a large error. It was disregarded in the computations although shown on the graphs.
[c] These points were disregarded in calculating average.

Equations (12h) and (12i) are indeterminate at $P_N = 2$. However, by utilizing values other than this, K_{c11}' can be evaluated. Having the values of these two constants the whole curve may be computed using Eqs. (10a) and (10b).

Application to a Specific Case

In general it is difficult to find data in the literature to which to apply this theory. Usually, either the data contain too few points, or if enough points are given, the precision of the data is so low that one is at a loss as to how to correlate them since in essence the data must be used to evaluate the constants in the equation. In other cases where both the amount and precision of the data seem satisfactory, the equations seem nevertheless not to hold. We ascribe this departure from this theory to the fact that many substances, while they associate, do not associate in a linear manner. These substances would associate to form three-dimensional aggregates which are the subject of another paper.[10] We have found one case in the literature for which all the requirements have been met. This is solutions of phenanthrene in alcohol.

Phenanthrene in Ethanol

The raw data is that of Innes.[13] These are vapor pressure data obtained at 75°C. Assuming Raoult's law to hold exactly, i.e., that the mole fraction as determined by this law gives us the true avmolality, we have calculated Table II wherein are given also the original data of Innes.

The second method was used and K_{c1j}' was obtained by plotting $\log\sum C_x$ *vs* $\log B_c$. This is a very sensitive curve, the errors being magnified. The points are so scattered that the simplest curve that fits the points is a straight line. The straight line was derived by least squares. It was determined that at $B_c = \sum C_x$ (i.e., $P_N = 2$); $B_c = 1.347683$, and $K_{c1j}' = 0.742014$. Using this value and the experimental points C_1 and K_{c11}' were calculated from Eqs. (12h) and (12i). The values are shown in Table II.

Using these values of K_{c1j}' and K_{c11}' and arbitrary values of C_1, $\sum xC_x$ and $\sum C_x$ were calculated from Eqs. (10a) and (10b). These values are plotted as the theoretical curve on Fig. 2. On Fig. 3 the formolality ($\sum xC_x$) is plotted *versus* P_N. Table III gives the distribution spectrum for various values of the formolality as calculated from Eq. (8g). As can be seen from Figs. 2 and 3, the experimental points agree well with the curve. We also see from Table III that at low concentrations very little of the higher j-mers are present, while at higher concentrations they appear in considerable concentrations.

The calculation of the "true" equilibrium constants from the values of K_{c11}' and K_{c1j}' by means of Eqs. (8e), (8f), (3a), and (3b) presents a definite problem since little is known of the modes of aggregation of phenanthrene in alcohol. From the quality of the agreement of the theoretical curve with the experimental data, we can conclude that in this case the association is linear and hence that two equilibrium constants suffice to represent the aggregation of this substance. However, these equilibrium constants are composite factors which contain such effects as the solute-solvent interactions and the entropy effects in them. The same solute in different solvents will give different equilibrium constants, and these will all differ from the values ob-

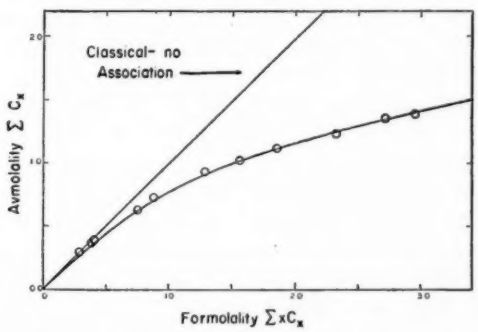

FIG. 2. Phenanthrene in ethanol:—theory; ○ experimental.

[13] W. R. Innes, J. Chem. Soc. **113**, 410 (1918).

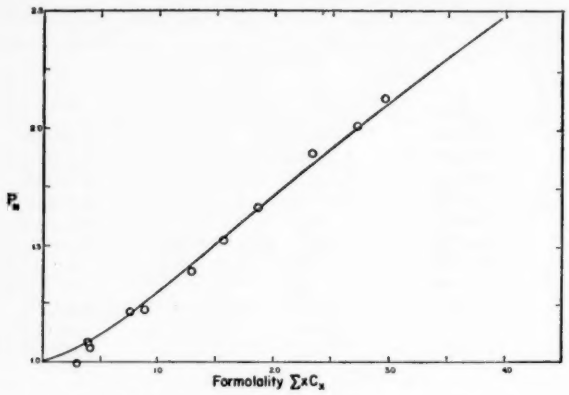

FIG. 3. Phenanthrene in ethanol: $K_{c1j}'=0.742014$, $K_{c11}'=0.28654$; ○ experimental.

TABLE III. Distribution spectrum in weight percent. Phenanthrene in ethanol 75°C.

Formolality	0.103219	0.337922	0.647475	1.150037	2.30100
C_1	96.8813%	88.7778%	77.2230%	60.8676%	39.1135%
C_2	2.7760	7.6315	11.0637	12.2087	10.0868
C_3	0.3090	2.5482	6.1573	9.5120	10.1042
C_4	0.0306	0.7528	3.0458	6.5875	8.9969
C_5	0.0028	0.2105	1.4125	4.2770	7.5103
C_6	0.0003	0.0562	0.6289	2.6658	6.0186
C_7	0.0000	0.0146	0.2722	1.6154	4.6892
C_8	0.0000	0.0037	0.1154	0.9589	3.5788
C_9	0.0000	0.0009	0.0482	0.5603	2.6887
$\sum_{x=10}^{\infty} C_x$	0.0000	0.0038	0.0330	0.7468	7.2130

tainable in the gas phase. Hence getting the "true" equilibrium constants involves first: deriving the modes of aggregation, perhaps from x-ray analyses; and second: dissecting out the effect of the solvent by a simultaneous consideration of the values of the equilibrium constants in different solvents and in the gas phase. Work is proceeding along these lines.

APPENDIX

Reasons for Not Considering Higher Equilibria

In considering these various equilibria, the question arises: is one justified in deriving the differential equations under the implicit assumption that the addition of 1-mers is the only process occurring and totally neglecting the equilibria between higher species? The proof for the case where all the bonds between associated particles are considered to be identical (i.e., linear association), has been given by Blatz,[14] who showed that the treatment of the one-constant theory by Ginell,[8] who neglects all the higher equilibria and that of Blatz and Tobolsky[7] who consider all of them to be present, leads to identical equations at equilibrium.[9] They differ, however, at times before equilibrium. This was formulated by Blatz as a general principle which can be stated thus: the equilibrium equations are unique, if equilibrium between all possible species is allowed, no matter what the formal mechanism by which the equations have been derived.[15]

It is not self-evident from this statement, however, whether this principle also applies to cases where all the equilibrium constants are not identical (e.g. 2-constant theory, n-constant theory). The difference in the constants implies that the bonds between the various species are different. That this principle is applicable can be shown by the following proof. The equilibria involved can be written thus:

$$\begin{array}{llll} n_1+n_1 \rightleftarrows n_2 & & & \\ n_1+n_2 \rightleftarrows n_3 & & & \\ n_1+n_3 \rightleftarrows n_4 & n_2+n_2 \rightleftarrows n_4 & & \\ n_1+n_4 \rightleftarrows n_5 & n_2+n_3 \rightleftarrows n_5 & & \\ n_1+n_5 \rightleftarrows n_6 & n_2+n_4 \rightleftarrows n_6 & n_3+n_3 \rightleftarrows n_6 & \\ n_1+n_6 \rightleftarrows n_7 & n_2+n_5 \rightleftarrows n_7 & n_3+n_4 \rightleftarrows n_7 & \\ n_1+n_7 \rightleftarrows n_8 & n_2+n_6 \rightleftarrows n_8 & n_3+n_5 \rightleftarrows n_8 & n_4+n_4 \rightleftarrows n_8 \text{ etc.} \\ \text{etc.} & \text{etc.} & \text{etc.} & \text{etc.} \end{array} \tag{13a}$$

Writing the equilibrium constants for the individual processes, we have:

$$\begin{array}{llll} K_{11}=\dfrac{n_2}{n_1^2} & & & \\ K_{12}=\dfrac{n_3}{n_1 n_2} & & & \\ K_{13}=\dfrac{n_4}{n_1 n_3}, & K_{22}=\dfrac{n_4}{n_2 n_2} & & \\ K_{14}=\dfrac{n_5}{n_1 n_4}, & K_{23}=\dfrac{n_5}{n_2 n_3} & & \\ K_{15}=\dfrac{n_6}{n_1 n_5}, & K_{24}=\dfrac{n_6}{n_2 n_4}, & K_{33}=\dfrac{n_6}{n_3 n_3} & \\ K_{16}=\dfrac{n_7}{n_1 n_6}, & K_{25}=\dfrac{n_7}{n_2 n_5}, & K_{34}=\dfrac{n_7}{n_3 n_4} & \\ K_{17}=\dfrac{n_8}{n_1 n_7}, & K_{26}=\dfrac{n_8}{n_2 n_6}, & K_{35}=\dfrac{n_8}{n_3 n_5}, & K_{44}=\dfrac{n_8}{n_4 n_4} \end{array} \tag{13b}$$

etc.

From the first column in Eq. (13b), we have

$$n_j=(K_{11}K_{12}K_{13}\cdots K_{1,j-1})n_1^j, \tag{13c}$$

which is the recurrence equation given by Ginell in the n-constant theory.[10] This neglects higher order interactions. Since these are simultaneous equilibria and

[14] P. J. Blatz, private communication.

[15] P. J. Blatz, Ph.D. dissertation, Princeton University (1949).

$n_j \equiv n_j$ hence solving column 1 and 2 of Eq. (13b) simultaneously, we get

$$K_{11}K_{11}K_{22}=K_{11}K_{12}K_{13}$$

$$K_{22}=\frac{K_{12}K_{13}}{K_{11}},$$

$$K_{23}=\frac{K_{13}K_{14}}{K_{11}},$$

$$K_{2j}=\frac{K_{1,j}K_{1,j+1}}{K_{11}}. \tag{13d}$$

Similarly,

$$K_{33}=\frac{K_{13}K_{14}K_{15}}{K_{11}K_{12}},$$

$$K_{34}=\frac{K_{14}K_{15}K_{16}}{K_{11}K_{12}},$$

and

$$K_{44}=\frac{K_{14}K_{15}K_{16}K_{17}}{K_{11}K_{12}K_{13}}.$$

The general expression for any K_{nm} being

$$K_{nm}=\frac{\prod_{x=m}^{m+n-1} K_{1x}}{\prod_{x=1}^{n-1} K_{1x}}. \tag{13e}$$

This shows that all the higher equilibrium constants are functions of the K_{1j}'s and hence need not enter into the equations unless it is convenient that they do so.

The basic equation of the association theory is

$$\sum_{x=1}^{m} n_x=n_1+n_2+n_3+\cdots n_m.$$

In this equation there can be substituted any of the various expressions for the n_x's derived from Eq. (13d) that we wish. The simplest set is the one represented by the recurrence formula

$$n_j=n_1{}^j \prod_{x=1}^{j-1} K_{1x} \tag{13e}$$

which yields

$$n_x=n_1+K_{11}n_1{}^2+K_{11}K_{12}n_1{}^3+\cdots+K_{11}K_{12}\cdots K_{1,m-1}n_1{}^m.$$

This equation is equivalent to that given by Woolley,[6] if one states that

$$K_n{}^{(w)}=\prod_{x=1}^{n-1} K_{1x},$$

where $K_n{}^{(w)}$ is Woolley's constant. The equations given here, give however a deeper insight into the meaning of the constants and show that they are not totally independent of one another. The value of the differential equations in these derivations is mainly in that it clarifies the meaning of the constants and gives the values of the numerical coefficients when various assumptions as to the character of the bonds are made.

Letters to the Editor

THIS section will accept reports of new work, provided these are terse and contain few figures, and especially few half-tone cuts. The Editorial Board will not hold itself responsible for opinions expressed by the correspondents. Contributions to this section should not exceed 600 words in length and must reach the office of the Editor not later than the 15th of the second month preceding that of the issue in which the Letter is to appear. No proof will be sent to the authors. A publication charge of $10.00 per Letter is made which, when honored, will entitle the Institution to 100 free reprints.

New Method for the Kinetic Study of Fast Electrode Reactions

TALIVALDIS BERZINS AND PAUL DELAHAY
Department of Chemistry, Louisiana State University, Baton Rouge, Louisiana
(Received February 1, 1955)

THE kinetics of electrode processes involving a single rate determining step and soluble species can be characterized at the standard potential E^0 by a rate constant k^0 defined by

$$i_c^0 = i_a^0 = nFCk^0, \quad (1)$$

where i_c^0 and i_a^0 are the cathodic and anodic current densities, n is the number of electrons involved in the reaction, F the Faraday, and C the common value of the concentrations of the reactants. The upper limit of k^0 at room temperature is 10^4 to 10^5 cm sec^{-1} (absolute rate theory) or 10^3 to 10^4 cm sec^{-1} (collision theory[1]). Values of k^0 up to approximately 10^{-2} cm sec^{-1} can be determined by conventional polarization experiments, and electrolysis with superimposed sinusoidal voltage[2] can be applied up to $k^0=1$ cm sec^{-1}. *Values of k^0 as large as 1000 cm sec^{-1} can be determined by the method discussed below.*

The potential of the electrode whose kinetics is studied is adjusted at its equilibrium value, and a current impulse represented by a step function is applied to the electrolytic cell. The solution is not stirred and a large excess of supporting electrolyte is present in solution, i.e., diffusion (linear) is virtually the sole mode of mass transfer. The voltage across the cell is recorded during electrolysis, and the rate constant k^0 is determined from voltage-time curves.

The current is

$$i = nFk^0\{C_0 \exp[-\alpha nF(E-E_e)/RT] - C_R \exp[(1-\alpha)nF(E-E_e)/RT]\}, \quad (2)$$

where α is the transfer coefficient for the cathodic process, the C's the concentrations (at the electrode surface) of the species O and R involved in the electrode reaction, E the potential, and E_e the equilibrium potential. By introducing in (2) the values of C_O and C_R obtained by solving the diffusion problem[3] (Sand) one has

$$i_d = nFk^0\left\{\begin{matrix} C_O^0[1-(t/\tau_c)^{\frac{1}{2}}]\exp[-\alpha nF(E-E_e)/RT] \\ -C_R^0[1+(t/\tau_a)^{\frac{1}{2}}]\exp[(1-\alpha)nF(E-E_e)/RT]\end{matrix}\right\}, \quad (3)$$

where the τ's are the transition times, i.e., the times at which C_O and C_R are equal to zero. The times τ_c and τ_a can be measured easily because they correspond to a rapid variation of potential. It follows from (3) that a plot of

$$\ln\frac{C_O^0[1-(E/\tau_c)^{\frac{1}{2}}]-C_R^0[1+(t/\tau_a)^{\frac{1}{2}}]\exp[nF(E-E_e)/RT]}{i_d}$$

against $E-E_e$ should yield a straight line whose slope is $\alpha nF/RT$ and whose intercept at $E=E_e$ is $-\ln nFk^0$; k^0 and α can thus be determined.

The exponentials in (3) can be expanded if $t \leqslant 0.1\tau_c$ (or $0.1\tau_a$). Furthermore, E_e is essentially the standard potential if $C_O^0=C_R^0=C^0$, and

$$E = E^0 - iRT/nF[1/nFC^0k^0 + 2/\pi^{\frac{1}{2}}nFC^0(1/D_O^{\frac{1}{2}}+1/D_R^{\frac{1}{2}})t^{\frac{1}{2}}], \quad (4)$$

where the D's are the diffusion coefficients. A plot of E against $t^{\frac{1}{2}}$ is linear, and k^0 can be determined from the intercept at $t=0$. By introducing numerical data in (4) one concludes that values of k^0 up to 1000 cm sec^{-1} can be determined. The charging of the double layer does not interfere because this process occurs in a time much shorter than that involved in electrolysis. Values of $E-E^0$ in the upper range of k^0 are about 10^{-4} volt, but measurements are still possible ("Tektronix" oscilloscope, model 531 with amplifier 53E, sensitivity 50 microvolts per cm). The ohmic drop in the cell in such measurements is compensated by means of a bridge circuit. Circuits for generation of step function with a very steep front (10^{-6} sec) have been described.[4]

This method should prove valuable in the study of electrolysis in fused salts, the study of so-called reversible electrodes, etc. Applications are now being made.

[1] H. Rubin and F. C. Collins, J. Phys. Chem. **58**, 958 (1954).
[2] For a review see P. Delahay, *New Instrumental Methods in Electrochemistry—Theory, Instrumentation, and Applications to Analytical and Physical Chemistry* (Interscience Publishers, Inc., New York, 1954), pp. 146–178.
[3] Reference 2, p. 180.
[4] W. C. Elmore and M. Sands, *Electronics, Experimental Techniques* (McGraw-Hill Book Company, Inc., New York, 1949), pp. 95–105.

Raman Spectrum of Sulfur Dichloride*

H. STAMMREICH, ROBERTO FORNERIS, AND KÔZÔ SONE†
Department of Physics, Faculty of Philosophy, Science, and Letters, University of São Paulo, São Paulo, Brazil
(Received February 21, 1955)

THE structure of the SCl_2 molecule was investigated by the electron diffraction method by Palmer[1] and by Stevenson and Beach.[2] The internuclear distance S−Cl was found to be 1.99±0.03 A and 2.00±0.02 A, respectively; the same authors obtained for the Cl−S−Cl angle the values of 101±4° and 103 ±2°, respectively. It seems that no spectral data on sulfur dichloride are reported.[3]

We obtained the Raman spectrum of liquid SCl_2 in the red region of the spectrum by excitation with helium radiation.

Sulfur dichloride was prepared by chlorination of sulfur monochloride and purified by fractional distillation, as described in the literature. The processes of chlorination of S_2Cl_2 and of purification of SCl_2 are easily controlled by the Raman spectrum; the shifts corresponding to S_2Cl_2 gradually disappear and the spectrum of the finally used substance showed, at normal exposures, no trace of the strongest Raman line of S_2Cl_2 at 447 cm^{-1}.

Sulfur dichloride is a garnet red liquid with a transmittancy of about 87 percent at 6678.2 A of 1 cm layer; above 7000 A it becomes completely transparent, excitation of the Raman spectrum being therefore possible by the helium radiations 6678.2, 7065.2, and 7281.4 A.

The spectra were taken with a grating spectrograph provided with a Bausch & Lomb C. P. plane transmission grating of 600 grooves mm and a ruled area of 65×76 mm. The first-order blazed region comprised the zone between 6000 and 8000 A that interests us here. The other optical components are the same described briefly in a previous paper[4]; the reciprocal dispersion of the spectrograph was 58 A/mm.

The Raman spectra excited by He 6678.2 A were recorded on Kodak 103 *a* F plates and those excited by He 7065.2 and 7281.4 A on Kodak I N plates. The exposure times in the first case ranged from 5 min to 1 hr and in the second case from 2 to 14 hr. Polari-

TABLE I.

Vibration	Class	Observed value (cm^{-1})
ω_1	A_1	208±1 (5,*p*)
ω_2	A_1	514±1 (10,*p*)
ω_3	B_1	535±2 (1, −)

zation observations were only qualitative in Raman shifts excited by He 6678.2 A and recorded on 103 *a* F plates in a 12-hr exposure.

As is to be expected for a triatonic symmetrical top molecule with symmetry of the C_{2v} point group, we observed three Raman shifts corresponding to the three fundamental modes of vibration. The results are given in Table I.

It was not possible to determine the state of polarization of ω_3 since the intensity of this Raman shift is very weak, but there cannot be any doubt that we have here the antisymmetric mode of vibration and therefore a depolarized line.

By using the known formulas[5] for the simple valence force model we calculate the Cl−S−Cl angle 2θ, the bond stretching force constant K_{S-Cl}, and the bond deformation constant $K_{2\theta}$ without the introduction of interaction constants, and obtained:

$$2\theta = 100°\ 20'$$
$$K_{S-Cl} = 2.58\times10^5 \text{ dyne cm}^{-1}$$
$$K_{2\theta} = 0.294\times10^5 \text{ dyne cm}^{-1}.$$

The calculated value for the Cl−S−Cl angle of 100° 20′ is in good agreement with the results of the aforementioned investigations by electron diffraction method.

Calculating the value of K_{S-Cl} by Siebert's product rule[6] that gives generally good results for interatomic distances corresponding to the sum of the covalent radii, we obtained 2.68×10^5 dyne cm^{-1} which corresponds satisfactorily to our value. Using our value of 2.58×10^5 dyne cm^{-1} in Badger's formula,[7] the S−Cl distance results in 2.02 A which agrees with the observations of Palmer and of Stevenson and Beach.

* This work has been supported partly by the "Conselho Nacional de Pesquisas," Rio de Janeiro; the authors are much indebted for the facilities created with the aid of the C. N. Pq.

† Fellow of the University of São Paulo; permanent address: Aichi College of Liberal Arts, Nagoya, Japan.

[1] K. J. Palmer, J. Am. Chem. Soc. **60**, 2360 (1938).
[2] D. P. Stevenson and J. Y. Beach, J. Am. Chem. Soc. **60**, 2872 (1938).
[3] Observations on the absorption spectrum of SCl_2 in the visible and ultraviolet are reported by T. M. Lowry and G. Jessop, J. Chem. Soc. 1421 (1929) and by H. P. Koch, J. Chem. Soc. 394 (1949).
[4] H. Stammreich and R. Forneris, J. Chem. Phys. **21**, 944 (1953).
[5] v. F. Lechner, Sitzber. Akad. Wiss. Wien, Abt. IIa **141**, 291 (1932).
[6] H. Seibert, Z. anorg. allgem. Chem. **273**, 170 (1953).
[7] R. M. Badger, J. Chem. Phys. **3**, 710 (1935).

Interdiffusion in the Gaseous Systems: BF_3-CCl_4 and BCl_3-CCl_4

C. J. G. Raw
Department of Chemistry and Chemical Technology, University of Natal, Pietermaritzburg, South Africa
(Received February 16, 1955)

THE diffusion coefficients of carbon tetrachloride vapor in gaseous boron trifluoride and boron trichloride have been determined at a temperature of 30°C. It was originally proposed to investigate the interdiffusion of the boron halide vapors themselves, following the recent work[1] in these laboratories on their transport properties. In view of the fact that these gases react[2] to form the mixed halide molecules this proposal was unsatisfactory, and it was decided to investigate the interdiffusion of each of the gaseous boron halides with some convenient vapor with which they did not react. Carbon tetrachloride vapor was chosen for this purpose.

The method used in this investigation was essentially that of Stefan.[3] The diffusion coefficient is determined from the rate of fall of the meniscus of a column of liquid carbon tetrachloride in a small glass tube across the top of which flows a current of the boron halide vapor. The equation used to calculate the diffusion coefficient and references to other experimental determinations (in which essentially the same apparatus was used) are given by Partington.[3]

Commercial boron trifluoride (supplied by the Harshaw Chemical Company) was used. Boron trichloride was prepared by passing boron trifluoride over aluminum chloride at 200°C. The resulting boron trichloride was trapped out with a dry-ice ethanol freezing mixture and purified to a constant vapor pressure of 481 mm of mercury at 0°C by repeated vacuum distillation through a column packed with glass rings (and kept at 0°C), with generous rejection of head and tail fractions. The carbon tetrachloride was prepared for use by distillation of the A. R. Laboratory reagent.

The interdiffusion experiments were all carried out at a temperature of 30±0.05°C and a total pressure of one atmosphere. Each determination was repeated a number of times for different rates of flow of the boron halide vapor.

The following results for the diffusion coefficients (D) were obtained:

$D=0.045$ cm^2 sec^{-1}, for the gas pair BF_3-CCl_4;
$D=0.034$ cm^2 sec^{-1}, for the gas pair BCl_3-CCl_4.

The Lennard-Jones (12,6) intermolecular force constants of boron trifluoride,[4] boron trichloride,[5] and carbon tetrachloride[6] have all been determined from experimental gas viscosity data.

Use is made of the empirical "combining laws,"

$$\epsilon_{ij} = (\epsilon_{ii}\epsilon_{jj})^{\frac{1}{2}},$$
$$\sigma_{ij} = \tfrac{1}{2}(\sigma_{ii}+\sigma_{jj}),$$

to relate the potential parameters between two unlike molecules, i and j, to those between like molecules. (ϵ = the maximum energy of attraction between two gas molecules and σ = the collision diameter for low-energy head-on collisions.) The intermolecular force constants between the pairs of different molecules having been determined, the method of Hirschfelder and his co-workers[6] can be used to calculate theoretical values of the diffusion coefficients.

In Table I, the theoretical and experimental values (D_{theoret} D_{exp}) of the diffusion coefficients are compared.

TABLE I. Theoretical and experimental values of the diffusion coefficients at 30°C.

Gas pair	ϵ_{ij}/k(°K)[a]	σ_{ij}(A)	D_{theoret}(cm^2 sec^{-1})[b]	D_{exp}(cm^2 sec^{-1})[b]
BF_3-CCl_4	235.8	5.07	0.0433	0.045
BCl_3-CCl_4	336.3	5.49	0.0263	0.034

[a] k = Boltzmann's constant.
[b] Total pressure = 1 atmosphere.

The agreement between the experimental and theoretical results can be regarded as satisfactory. It seems that the Lennard-Jones (12,6) model provides a fair approximation to the intermolecular potentials of these molecules in the vapor state, at least as far as the transport properties are concerned.

The author gratefully acknowledges a grant from the South African Council for Scientific and Industrial Research to cover the expenses entailed in this work.

[1] See, for example, Cooke and Mackenzie, J. S. African Chem. Inst. **4**, 12 (1951); Mackenzie and Raw, J. S. African Chem. Inst. **6**, 8 (1953).
[2] R. E. Nightingale and B. Crawford, Jr., J. Chem. Phys. **22**, 1468 (1954).
[3] Partington, *An Advanced Treatise on Physical Chemistry* (Longmans, Green and Company, London, 1949), Vol. I.
[4] C. J. G. Raw, J. S. African Chem. Inst. **7**, 20 (1954).
[5] C. J. G. Raw, J. S. African Chem. Inst. (to be published).
[6] Hirschfelder, Curtiss, and Bird, *Molecular Theory of Gases and Liquids* (John Wiley and Sons, Inc., New York, 1954).

Bond Energies in Organic Fluorine Compounds

Norbert W. Luft
Cheadle Hulme, Cheshire, England
(Received March 4, 1955)

ALTHOUGH the exceptional stability of aliphatic fluorine compounds is a well-established experimental fact,[1,2] the available quantitative information on their bond energies is very scant. It is possible, however, with the aid of recently published data, especially enthalpies of formation, ΔHf, to estimate CF

dissociation energies in a number of important organic fluorine compounds. Hereby $\Delta Hf(F)=19$ kcal/mole is used in agreement with the recently proposed dissociation energy, $D(F_2)=37\pm2$,[3] and 39 ± 1 kcal/mole.[4,5]

The bond dissociation energy $D(F_3C-F)\sim150-195$ kcal/mole, from Hg photosensitation experiments,[6] which corresponds to $-\Delta Hf(CF_3)\equiv A\sim87-42$ kcal/mole, can only be regarded as an upper limit. The failure[6] to observe the reaction $CF_4+H\rightarrow CF_3+HF$ entails that $A>88$ kcal/mole. On the other hand, activation energies determined[7] from Na diffusion flames, for the reactions $CF_3X+Na\rightarrow CF_3+NaX$, with X= (I), Br, Cl, F, and the occurrence of $H_2+CF_3\rightarrow CF_3H+H$, together with presently known or estimated ΔHf values, result in A=94 to 112 kcal/mole i.e., $D(F_3C-F)=125-143$ kcal/mole. Whence

$$D(F_3C-Cl)=D(F_3C-F)-38, \qquad (1)$$

=87–105 kcal/mole from thermochemical data. Moreover, available enthalpies of formation[8,9] (see Table I) furnish the relation

$$D(F_3C-F)=237-A=85+\tfrac{1}{2}D(F_3C-CF_3), \qquad (2)$$

≤147 kcal/mole from the electron impact result $D(F_3C-CF_3)\leq124$ kcal/mole of Dibeler *et al.*[10]

The preceding remarks as well as interpolation of CC bond energies from force constants (and bond lengths) in the series H_3C-CH_3, H_3C-CN, $NC-CN$, F_3C-CF_3, $H_2C=CH_2$ seem to indicate that $D(F_3C-CF_3)$ is smaller though not much smaller than 124 kcal/mole. By identifying the activation energy, $E=74.1$ kcal/mole of cyclo-C_4F_8 depolymerization,[11] with the CC bond energy and allowing 30 kcal/mole for ring-straining and excess repulsion, one obtains $D_{CC}\sim104$ kcal/mole, for perfluoro alkanes, and $D(F_3C-F)\sim137$ kcal/mole. Furthermore the reaction $F_3C-CF_3\rightarrow F_2C=CF_2+2F$, by which two CF bonds are broken, requires $\Delta H=180$ kcal/mole, the excitation energy E^* or the triplet state of $F_2C=CF_2$ is not known, but probably higher than for $H_2C=CH_2$, so that the average CF bond energy, as from $F_3C-CF_3\rightarrow F_2C=CF_2+2F$, is $(\Delta H+E^*)/2\sim125$ kcal/mole, in agreement with the above lower limit in CF_4.

For the CF bond energy in CH_3F, $D(H_3C\cdot CO-F)\sim93+\Delta Hf(F)\sim112$ and $D(H_3C-X)-(DH_3C\cdot CO-X)\sim4-6$ kcal/mole[12] suggests $D(H_3C-F)\sim115-120$ kcal/mole. This is confirmed, *viz.* $D(H_3C-F)\sim120\pm10$ kcal/mole, by plotting $D(H_3C-X)$ against the ionization energy of X or dissociation energy of HX, methods which provide reasonable correlations for other series of compounds.

Szwarc and Sehon[13] give the dissociation energy of the CBr bond in CF_3Br as ~64 kcal/mole, i.e., only slightly less than in CH_3Br. Since, according to preceding considerations, $D(CF_3-F)>D(CH_3-F)$ one may reasonably conclude that $D(F_3C-Cl)>D(H_3C-Cl)\sim83\pm3$ kcal/mole,[13,14] i.e., $D(F_3C-Cl)\sim95-100$ kcal/mole.

TABLE I.

Molecule	$\Delta Hf_{298.16}$ kcal/mole	Dissociation energy, kcal/mole D_{CF}	D_{CX}	D_{CC}
CCl_3F	$-70(\pm)4$[a]	100 ± 5	70 ± 5	
CCl_2F_2	-112 ± 1[a]	107 ± 5	78 ± 5	
$CClF_3$	-171 ± 1[a]	128 ± 4	100 ± 4	
CF_4	-218.3[a,b]	138 ± 4		
CF_3Br	(-132)	(95)	~64[c]	
CH_3F	(-60)	115 ± 5	(104)	
CH_2F_2	(-110)	(120)	(105)	
CHF_3	(-168)	(130)	(125)	
CH_3COF	-104[d]	112		(84)
COF_2	-149[e]	(115)		
$F_3C\cdot CF_3$	-303 ± 2[a]	(130)		107 ± 8
$ClF_2C\cdot CF_2Cl$	-213 ± 3[a]	(120)	(80)	95 ± 10

[a] Reference 8.
[b] Reference 9.
[c] Reference 13.
[d] Reference 12.
[e] Reference 8, see H. von Wartenberg, Z. anorg. u. allgem. Chem. **258**, 356 (1949).

Thermochemical data yield

$$D(Cl_3C-F)=\Delta Hf(CCl_3)+89\pm4, \qquad (3)$$

$=104\pm6$ kcal/mole, *viz.* by $\Delta Hf(CCl_3)=15\pm2$ from dissociation energies[13,14] of trichloro compounds. Then extrapolation of $D(CH_3-X)-D(CCl_3-X)$ leads to $D(CH_3-F)\sim114$ kcal/mole which is close to the figure derived previously.

After the range of CF and CCl bond energies in chloro-fluoro methanes has been fixed provisionally by the preceding results for CF_4, CF_3Cl and CCl_4, the figures can be improved and values for CF_2Cl_2 may be derived (see Table I) by using Eqs. (1) and (2) and four similar relations for the other species together with the postulate that bond energies, upon substitution, ought to vary in a regular manner. The figures given for the fluoro methanes are supported by estimates of the CC bond strength in H_2FC-CH_2OH and HF_2C-CH_2OH, whose enthalpies of formation are known.[15] Figures in parenthesis are tentatively proposed estimates.

[1] L. White and O. K. Rice, J. Am. Chem. Soc. **69**, 267 (1947).
[2] G. C. Rogers and G. H. Cady, J. Am. Chem. Soc. **73**, 3523 (1951).
[3] E. Wicke and H. Friz, Z. Elektrochem. **57**, 9 (1953).
[4] H. Wise, J. Chem. Phys. **20**, 927 (1952).
[5] P. W. Gilles and J. L. Margrave, J. Chem. Phys. **21**, 381 (1953).
[6] J. R. Dacey and J. W. Hodgins, Can. J. Research **28B**, 173 (1950).
[7] J. W. Hodgins and R. L. Haines, Can. J. Chem. **30**, 473 (1952).
[8] F. W. Kirkbride and F. G. Davidson, Nature **174**, 79 (1954).
[9] Scott, Good, and Waddington, J. Am. Chem. Soc. **77**, 245 (1955).
[10] Dibeler, Reese, and Mohler, J. Chem. Phys. **20**, 761 (1952).
[11] B. Atkinson and A. B. Treuwith, J. Chem. Phys. **20**, 754 (1952).
[12] P. W. Allen and L. E. Sutton, Trans. Faraday Soc. **47**, 236 (1951).
[13] M. Szwarc and A. H. Sehon, J. Chem. Phys. **18**, 1685 (1950).
[14] E. Wicke, in Landolt-Börnstein, *Zahlenwerte und Funktionen, II* (Julius Springer, Berlin, 1951), pt. 3.
[15] *Tables of Selected Values of Chemical Thermodynamic Properties* (National Bureau of Standards, Washington 25, D. C., 1952), Circular No. 500.

Exact Method for the Calculation of Coexistent Densities from Van der Waals' Type Equations

SIDNEY W. BENSON AND CHARLES S. COPELAND
Chemistry Department, University of Southern California, Los Angeles 7, California
(Received March 14, 1955)

VAN der Waals' and Berthellot's equations can be subsumed under a general class which can be written as:

$$P=RT/(V-b)-aT^{-n}V^{-2}$$

or, in reduced form as:

$$\pi=8\theta/(3\phi-1)-3\theta^{-n}\phi^{-2}.$$

These equations, although of limited quantitative use, are very useful qualitatively and semiquantitatively for the description of gases and liquids and condensation phenomenon. Calculations concerning the latter are, however, difficult because of the form of the equations which seem to require rather cumbersome, numerical approximations for their solution. In the course of some investigations of the shape of coexistence curves in the neighborhood of the critical it was discovered that by suitable transformations, exact values of the coexistent densities could be quickly obtained.

The condition of equality of free energies (gas and liquid), leads to the equation (in reduced form):

$$0=\int_{\Delta_1}^{\Delta_2}\frac{d\pi}{\Delta}=\frac{8\theta}{3-\Delta_2}-\frac{8\theta}{3-\Delta_1}+\frac{8\theta}{3}\ln\left[\frac{\Delta_2(3-\Delta_1)}{\Delta_1(3-\Delta_2)}\right]-\frac{6(\Delta_2-\Delta_1)}{\theta^n}$$

where $\Delta=1/\phi=$ the reduced density and subscripts 2 and 1 refer to liquid and gas respectively. The original equation of state can now be used together with the last equation and the variables θ and π eliminated to give an equation in Δ_2 and Δ_1. On making the substitution

$$Z=\Delta_2(3-\Delta_1)/\Delta_1(3-\Delta_2);\quad x=(3-\Delta_2)/(3-\Delta_1),$$

this last equation becomes

$$x=(\ln Z-Z+1)/(Z-1-Z\ln Z)$$

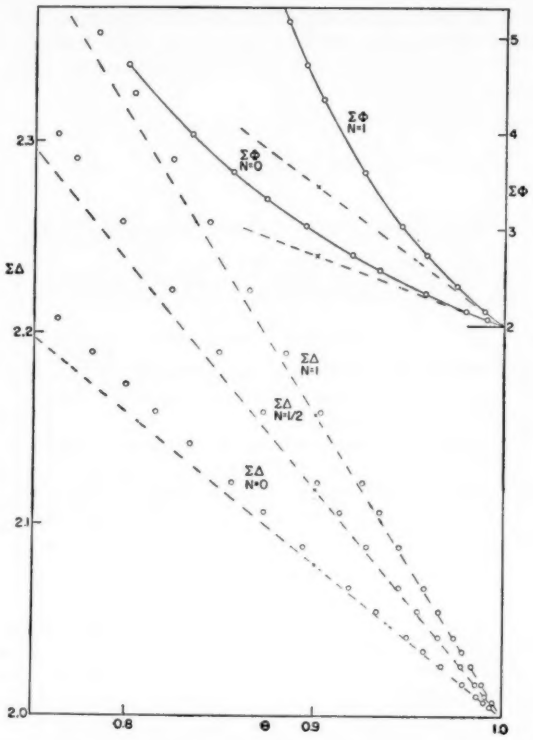

FIG. 1. Plot of the sums of coexistent densities (ordinates on left) and coexistent volumes (upper curves, ordinates on right) against reduced temperature (abscissa) for van der Waal's type equation. The limiting slopes are indicated by dotted lines (Table I). Open circles and full curves represent calculated data. Because of the proximity of the curves and limiting slopes for the densities, the curves have not been drawn in.

so that it is possible to calculate x for any value of Z and from the inverse transformations, the corresponding values of Δ_1 and Δ_2. It is interesting to note that the form of the equations is such that the sets of coexistent densities are simply related to temperature by a scale factor θ^{n+1}.

The behavior of the coexistent densities and volumes is shown in Fig. 1 for different values of the exponent $n=0$, $\frac{1}{2}$, and 1. All three equations indicate reasonably good agreement with the law of rectilinear densities, $\Delta_1+\Delta_2-2=k(1-\theta)$, the best fit over the widest range being given by the Berthellot equation ($n=1$). None of them, however, shows good agreement with the law of rectilinear volumes, $\phi_1+\phi_2-2=k'(1-\theta)$. However, in the immediate vicinity of the critical, (i.e., in the range $\theta=0.998$ to 1) both laws are obeyed to within ± 0.01 percent by all three values of n. Table I gives the limiting slopes (k_0 and k_0') for this region. Guggenheim[1] has proposed an empirical formula for the difference of the coexistent densities, $(\Delta_2-\Delta_1)=7/2(1-\theta)^{\frac{1}{2}}$, while both Guggenheim and Fowler[2] and Landau and Lifschitz[3] have predicted on theoretical grounds a parabolic relation, $(\Delta_2-\Delta_1)=a(1-\theta)^{\frac{1}{2}}$. In fact it has been generally supposed that van der Waals' type equations will have a parabolic coexistence plot in the immediate neighborhood of the critical. However, if $\log(\Delta_2-\Delta_1)$ is plotted against $\log(1-\theta)$, then it is found that in the immediate vicinity of the critical the slope of the curve is 1/1.68 for $n=\frac{1}{2}$ or 1 and 1/1.84 for $n=0$. This seems to indicate some serious difficulty with the expansion methods which have been used in the aforementioned derivations.

TABLE I. Values of limiting slopes for rectilinear plots.

	k_0	k_0'
$n=0$	0.80	7.25
$n=\frac{1}{2}$	1.19	10.9
$n=1$	1.58	14.4

In conclusion it should be noted that the equation with $n=\frac{1}{2}$ gives a reasonably good representation of the properties of non-associated liquids. At $\theta=0.625$ which corresponds to the normal boiling point of most liquids, the Trouton constant is 9.4 (observed 10) and the reduced liquid density is 2.47 (observed 2.68). This is a marked improvement over both van der Waals' and Berthellot's equations.

We are pleased to acknowledge our indebtedness to Mr. David Pearson of this department for his assistance with the computations and to the Office of Naval Research for their support (Contract No. N6-onr-23811).

[1] E. A. Guggenheim, J. Chem. Phys. **13**, 253 (1945).
[2] R. Fowler and E. A. Guggenheim, *Statistical Thermodynamics* (Cambridge University Press, Cambridge, England, 1949), Section 729.
[3] L. Landau and E. Lifschitz, *Statistical Physics* (Oxford University Press, Oxford, England, 1938), Section 50.

Effect of Fermi Resonance on the Centrifugal Stretching Constants in CO_2

C. P. COURTOY* AND G. HERZBERG
Division of Physics, National Research Council, Ottawa, Canada
(Received March 2, 1955)

USUALLY it has been assumed that the centrifugal stretching constants D are essentially the same for all vibrational levels of a polyatomic molecule in its electronic ground state. Since D itself is very small and therefore not measurable with high accuracy, any small changes of D with vibration would normally be expected to be beyond the accuracy of most measurements. We were therefore greatly surprised when we found large differences in the D-values of various Fermi polyads of vibrational levels in CO_2.

The CO_2 bands $\nu_1+\nu_3$, $2\nu_2+\nu_3$; $2\nu_1+\nu_3$, $\nu_1+2\nu_2+\nu_3$, $4\nu_2+\nu_3$; $3\nu_1+\nu_3$, $2\nu_1+2\nu_2+\nu_3$, $\nu_1+4\nu_2+\nu_3$, $6\nu_2+\nu_3$; $\nu_2+2\nu_3$; $3\nu_3$ and most of the corresponding "hot" bands were measured with a high-resolution infrared spectrometer with a PbS receiver using up to 68 traversals through a 1-m absorption cell. The D-values in Table I were obtained for the levels indicated. The relative accuracy of these numbers is much better than the absolute accuracy. The D-values for the Π states (upper and lower states of hot bands, $l=1$) are less accurate than those of the Σ states ($l=0$). Within the accuracy of the determination, the average D-values of the polyads are the same as those of the lowest vibrational level and of the single unperturbed states (monads). However, within a polyad the individual D-values differ greatly, in the case of the tetrad by as much as a factor three.

TABLE I.

v_1	v_2^l	v_3		$D(10^{-8}$ cm$^{-1})$	Mean for polyad
0	0^0	0	Σ	13.7	
1	0^0	1	Σ	11.6	13.8
0	2^0	1	Σ	16.1	
2	0^0	1	Σ	9.8	
1	2^0	1	Σ	13.7	13.8
0	4^0	1	Σ	18.0	
3	0^0	1	Σ	7.6	
2	2^0	1	Σ	10.4	14.0
1	4^0	1	Σ	16.8	
0	6^0	1	Σ	21.4	
0	0^0	3	Σ	13.8	
0	1^1	0	Π	14.2	
0	1^1	2	Π	12	
0	1^1	3	Π	12	
1	1^1	1	Π	12.9	
0	3^1	1	Π	...	
2	1^1	1	Π	11.5	
1	3^1	1	Π	14.6	14.0
0	5^1	1	Π	16	
2	3^1	1	Π	13.8	
1	5^1	1	Π	16.8	

The D-values have been determined by means of the combination sums $R(J)+P(J)$ which, when plotted against $J(J+1)$, would give straight lines if $D'-D''$ were zero. To illustrate the effect of the variation of D within a polyad, Fig. 1 shows $R(J)+P(J)+2(B''-B')J(J+1)$ for the four bands of the tetrad $3\nu_1+\nu_3$. If the D'-values were all the same as in the ground state, four horizontal straight lines should be obtained. The strong

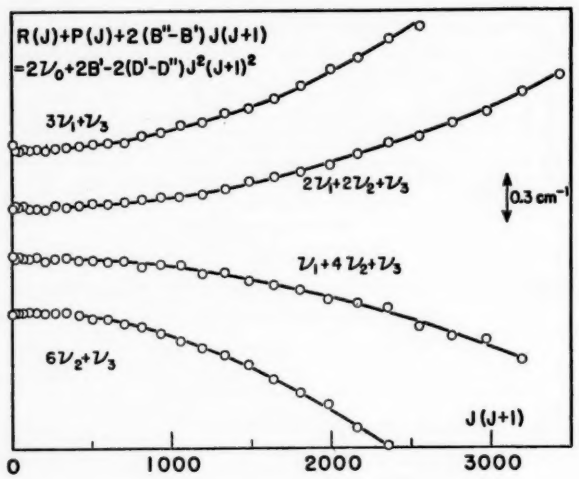

FIG. 1. Combination sums for the Fermi tetrad $3\nu_1+\nu_3$ of CO_2.

deviation from linearity actually found is a measure of the deviation of D' from D_{000}. The symmetrical way in which D' varies for the four components of the tetrad is striking.

If the D-values of the Σ states are plotted against the order of the polyad, the diagram Fig. 2 is obtained. The variation for the Π states is similar but less completely observed. The D-values of the Π states given in Table I are averages of the D-values of the two l-doubling components. Actually there is a systematic difference in the D-values of the two l-doubling components which increases rather rapidly with v_2. However, this difference may equally well be considered as due to a quartic term in the formula for the l-type doubling.

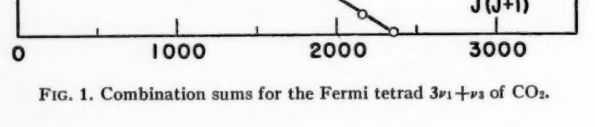

FIG. 2. The D-values of CO_2 in Fermi polyads (Σ states).

It is remarkable that while the B-values in a Fermi polyad approach one another more closely than they would without Fermi resonance, the D-values are pushed apart from one another quite strongly. Following the preliminary report of this work at the Columbus meeting last June, Amat, Goldsmith, and Nielsen have discussed the theory of this effect. We understand that they will report about it shortly.

The detailed analyses of the bands on which the above discussion is based will be submitted for publication shortly. A similar study for $C^{13}O_2$ is in progress and has already yielded similar differences in the D-values.

* National Research Laboratories Postdoctorate Fellow.

Ionization Potential of Benzyl Radical

IKUZO TANAKA* AND CHIMAO KOMATSU
Division of Pure Chemistry, National Research Council, Ottawa, Canada, and Laboratory of Physical Chemistry, Tokyo Institute of Technology, Tokyo, Japan

(Received March 8, 1955)

BENZYL radical has C_{2v} symmetry (see Fig. 1). The electronic structure has already been investigated by Tanaka[1] using simple LCAO approximation.

The authors calculated the energy levels and wave functions by the SCF method. The SCF determinant was constructed for benzyl cation, a six π-electron system, using $2p\pi$ Slater functions for neutral carbon atoms ($Z=3.18$). According to Parr and Mulliken,[2] a solution of SCF determinant is given to be

$$\epsilon_i=I_i+\sum_j(2J_{ij}-K_{ij}). \tag{1}$$

It was assumed here that the lowest three MO's of the benzyl cation obtained can be applied to benzyl radical, a seven π-electron system as approximation. Then, using (1) the energy ϵ_4 was represented as

$$\epsilon_4=I_4+2(J_{14}+J_{24}+J_{34})-(K_{14}+K_{24}+K_{34}) \tag{2}$$

and it can be used for benzyl radical as approximation. Also ϕ_4 can be used for it. Moreover, as the radical is a neutral molecule, use of $Z=3.18$ gives a better approximation to ϵ_4 and ϕ_4 than lower levels and MO's. The energy ϵ_4 and the corresponding ϕ_4 obtained from SCF calculation are

$$\epsilon_4=E_{2p}+3.30 \text{ ev}, \tag{3}$$

$$\phi_4=0.040\chi_1-0.506\chi_4-0.679\chi_7+0.414(\chi_2+\chi_6)+0.002(\chi_3+\chi_5). \tag{4}$$

The ionization potential of benzyl radical becomes immediately from (3),

$$I_p\left(\text{C}_6\text{H}_5\text{—CH}_2\cdot\right)=7.98 \text{ ev}.$$

Recently Lossing and his co-workers[3] obtained by electron impact,

$$I_p\left(\text{C}_6\text{H}_5\text{—CH}_2\cdot\right)=7.73 \text{ ev}.$$

These two values are in good agreement.

Lossing[4] also obtained 7.61 ± 0.05, 7.65 ± 0.05, and 7.46 ± 0.05 ev for the ionization potentials of *ortho-*, *meta-*, and *para*-methyl radicals respectively.

Using the aforementioned orbital, and making simple perturbation calculations, the authors reached the following results. According to second-order perturbation theory,

$$W_k''=\frac{|H_{k1}'|^2}{W_k^0-W_1^0} \tag{5}$$

where W_k'' is second-order perturbation energy, W_k^0 is above ϵ_4, the energy of ϕ_4 orbital, and W_1^0 is the energy of the methyl radical in its ground state. Now

$$K_{k1}'=\int\chi_8H'\phi_4d\tau \tag{6}$$

where χ_8 is $2p\pi$ Slater function of the new-coming eighth carbon atom. Neglecting all $\beta=\int\chi_8H'\chi_jd\tau$ but for the nearest neighbors, it becomes

$$W_k''=\frac{C_j^2\beta^2}{W_k^0-W_1^0}. \tag{7}$$

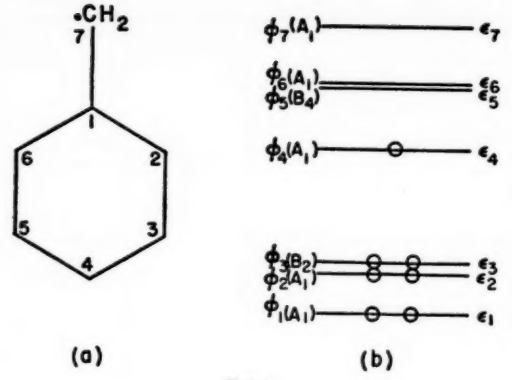

FIG. 1.

In (7) C_j represents the coefficient of χ_j in ϕ_4. So the ionization potentials of *ortho*-, *meta*-, and *para*-methyl benzyl radicals should be lower by $|W_k''|$ than benzyl radical, and their sequence is determined approximately by the squares of C_2, C_3, and C_4 in the ϕ_4 orbital. As

$$C_2^2=0.17(ortho),$$
$$C_3^2=0.00(meta),$$
$$C_4^2=0.26(para),$$

which gives the following results:

$$I_p(\mathrm{CH_3}\text{—}\bigcirc\text{—}\mathrm{CH_2}\cdot) < I_p(\bigcirc\text{—}\mathrm{CH_2}\cdot) \quad (\mathrm{CH_3}) < I_p(\quad\bigcirc\text{—}\mathrm{CH_2}\cdot). \quad (\mathrm{CH_3})$$

This sequence of I_p also agrees with Lossing's experimental results, although very qualitatively.

The authors wish to thank Dr. E. W. R. Steacie, for his interest and support in this work, Dr. F. P. Lossing, for his kindness in making available to them the results of recent investigations in his laboratory, and Dr. J. B. Farmer. They would also like to thank Y. Mori for his hearty discussions during the course of this research.

* Japanese Government Fellow at The National Research Council, Ottawa, Canada.

[1] I. Tanaka, Bull. Tokyo Inst. Tech. A, No. 1, 44 (1954).
[2] R. G. Parr and R. S. Mulliken, J. Chem. Phys. **18**, 1338 (1950).
[3] Lossing, Ingold, and Henderson, J. Chem. Phys. **22**, 621 (1954)
[4] Farmer, Lossing, Marsden, and McDowell (to be published).

Note on the Dodecahedral σ Hybrids*

GIOVANNI GIACOMETTI
Institute of Physical Chemistry, University of Padua, Padua, Italy
(Received October 27, 1954)

IN a communication to the Editor, appearing in this Journal,[1] Higman stated the necessity of using one f orbital to make dodecahedral σ hybrids. This statement is in error and Kimball's Table XXII in the cited paper[2] is correct.

The character table for the group D_{2d} is[3]

	E	C_2	$2S_4$	$2C_2'$	$2\sigma_d$
A_1	1	1	1	1	1
A_2	1	1	1	−1	−1
B_1	1	1	−1	1	−1
B_2	1	1	−1	−1	1
E	2	−2	0	0	0

Higman's error arises from the belief that the p set of orbitals of the central atom transforms, in the D_{2d} group, as A_2+E. In fact this set transforms as $E+B_2$.

The transformation table reads

	E	C_2	S_4	C_2'	σ_d
	x	$-x$	y	x	$-y$
	y	$-y$	$-x$	$-y$	$-x$
	z	z	$-z$	$-z$	z
Char.:	3	−1	−1	−1	1

The C_2 axis has been chosen along the z axis. Only one operation for each class has been listed.

From the character of the reducible representation, x, y, z, we see that it transforms as the two irreducible representations E and B_2.

To support even more this fact one might recall that the dodecahedral hybrids have been actually set up by Duffey[4] by making us only of s, p, and d functions. The directed valency treatment by Linnett and Mellish[5] is also in agreement with our present point of view.

* This work was done while staying at the California Institute of Technology, where the A. was supported by an American Government Grant.

[1] B. Higman, J. Chem. Phys. **21**, 2224 (1953).
[2] G. E. Kimball, J. Chem. Phys. **8**, 188 (1940).
[3] Eyring, Walter, and Kimball, *Quantum Chemistry* (John Wiley and Sons, Inc., New York).
[4] Duffey, J. Chem. Phys. **18**, 1444 (1950).
[5] J. W. Linnett and C. E. Mellish, Trans. Faraday Soc. **50**, 665 (1954).

Note on the Dodecahedral σ Hybrids

BRYAN HIGMAN
43 St. John's Road, Watford, Herts, England
(Received February 24, 1955)

DR. Giocometti is correct in his criticism of the first half of my letter; the group in question is almost unique (there is one other) in that axes equivalent under the corresponding real group are no longer equivalent, and I fell into a trap of my own devising. Kimball's tables are therefore correct apart from the obvious misprints.

The point made in the second half of my letter remains valid, though it seems to have more theoretical than practical importance. The fuller discussion promised will be found in my forthcoming *Applied Group-Theoretic and Matrix Methods in Physics and Chemistry* to be published by Oxford University Press.

Effect of Oxygen on Luminescence of Cadmium Sulfide

S. H. LIEBSON AND E. J. WEST
United States Naval Research Laboratory, Washington, D. C.
(Received February 21, 1955)

BUBE[1] has reported water vapor to be responsible for a decrease in photoconductivity of wurtzite cadmium sulfide. Electronegative gases have been reported[2] to cause a decrease in photoconductivity as well as a decrease in the luminescence of cadmium sulfide excited by ultraviolet light of wavelengths about 3650 A, within the fundamental absorption band of these crystals. The absorption coefficient for ultraviolet at this wavelength is of the order of 2×10^4 cm^{-1} according to Fassbender,[3] limiting the photoelectric production of carriers and excitation of luminescent centers to the surface region. We have examined the red luminescence and photoconductivity of cadmium sulfide single crystals grown by a modified Frerichs method[4] as a function of oxygen pressure at room temperature. An increase or decrease in luminescence is accompanied by an increase or decrease respectively in the photocurrent. Since the earlier measurements[1,2] indicate changes in the rate of recombination of carriers to be responsible for the decrease in photoconductivity, it appears likely that the changes in luminescence intensity are also caused by increased radiationless recombination. To minimize experimental difficulties, we have chosen to measure the luminescence intensity. Of measurements

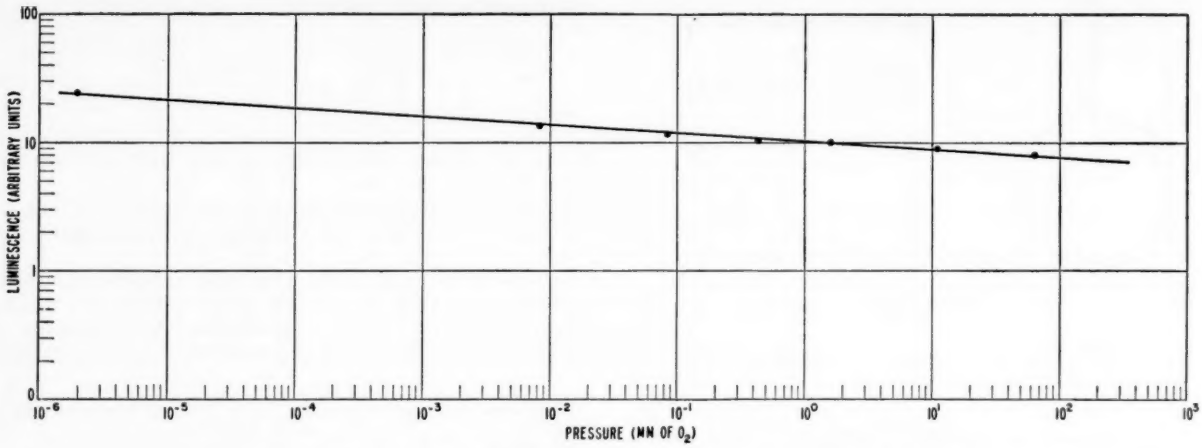

FIG. 1. Variation of luminescence intensity with pressure of oxygen in millimeters of mercury.

made on four groups of crystals, three showed evidence of a dependence of the form

$$\text{luminescence} = p^{-1/k}, \tag{1}$$

where k is a constant for a given phosphor sample and p is the ambient pressure. High impedance, photoconductive crystals, as well as crystals exhibiting appreciable conductivity at room temperature, showed similar behavior. Figure 1 shows the variation of luminescence intensity as a function of ambient pressure after equilibrium has been obtained. The data represent the results after the sample had been cycled through the pressure range four times. The pressure reading at 2×10^{-6} mm Hg was obtained from an ionization gauge and was the lowest obtainable pressure in the system.

The decrease in luminescence has been related to the formation of a surface barrier due to chemisorbed gas,[2] and an increase of recombination processes in the surface region. Figure 2 illustrates the type of barrier to be expected on n-type cadmium sulfide due to chemisorption or oxygen atoms or molecules. For an isomorphic chemically related compound, zinc oxide, the oxygen pressure dependence of the conductivity has been shown[5] to be due to oxygen atom chemisorption, producing a surface barrier of the type shown. In cadmium sulfide the surface barrier may aid recombination by several means. The field is such as to promote the migration of holes to the surface to recombine with electrons in surface traps due to chemisorption, in a manner similar to that proposed for infrared quenching of photoconductivity of cadmium sulfide.[6] The lowering of the Fermi level at the surface will also cause a redistribution of occupied levels within the forbidden band which may affect directly both radiationless and luminescent recombination.

These results also suggest that at least a partial cause for the relative inefficiency of some cathode-ray phosphors at low bombarding voltages[7] may be the formation of a surface barrier region with consequent increased radiationless transitions.

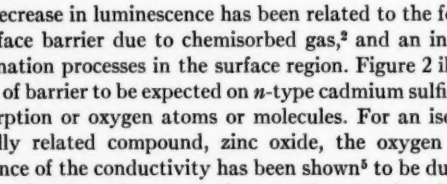

FIG. 2. Surface barrier.

[1] R. H. Bube, J. Chem. Phys. **21**, 1409 (1953).
[2] S. H. Liebson, J. Electrochem. Soc. **101**, 359 (1954).
[3] J. Fassbender, Ann. Physik (6), **5**, 33 (1949).
[4] M. E. Bishop and S. H. Liebson, J. Appl. Phys. **24**, 660, 963 (1953).
[5] K. Hauffe and H. J. Engell, Z. Electrochem. **56**, 366 (1952).
[6] S. H. Liebson, J. Electrochem. Soc. (to be published).
[7] H. W. Leverenz, *An Introduction to Luminescence of Solids* (John Wiley and Sons, Inc., New York, 1950).

Paramagnetic Resonance of X-Rayed Teflon*

E. E. SCHNEIDER†
Department of Physics, Duke University, Durham, North Carolina
(Received March 4, 1955)

PARAMAGNETIC resonance absorption at 23 700 Mc has been observed in specimens of commercial Teflon (polytetrafluorethylene) irradiated with x-rays from a beryllium window 50-kv Machlett tube (AEG 50). Both the irradiation and the resonance observations were carried out at room temperature. A sensitive bridge type K-band resonance spectrometer similar to the X-band spectrometer described by Schneider and England,[1] was used to detect the weak resonances. From the magnitude of the integrated magnetic absorption it was estimated that after irradiation for 3 hours at 40 mA corresponding to a dose of the order of 5.10^5 r the concentration of spins was of the order of 10^{17} cm^{-3}. A typical spectrum is shown in Fig. 1. The position of the resonance corresponds to a g-factor $g=2.021$, i.e., a positive g-shift as compared with the free electron value ($g=2.0023$). Of greatest interest is the structure of the resonances, a triplet with a separation of 19 gauss between peaks. Although this structure is only barely resolved, the existence and magnitude of the splitting has been definitely established by direct observations of the central section of the spectrum on a CRO and by recording the derivative with a phase-sensitive detector. It is suggested that it is a hyperfine structure due to interaction of the resonating electrons with fluorine nuclei and thus similar to the well-resolved structure of the resonance in x-rayed Lucite (polymethylmethacrylate)[2] which has been ascribed by the author to hyperfine interaction with protons in CH_2 groups.[3] It is likely that the resonance is due to unpaired electrons which result from a breaking of C—C bonds in the polymer chain and are localized on the C-atoms at the break. Thus, the observed triplet structure would have to be ascribed to the interaction of the electron with the nuclei of $I=\frac{1}{2}$ of the two F-atoms directly bonded to the C-atom. If the electron were localized in a p-orbital on the C-atom the resonance should have $g=g_{el}$ and, with a C—F distance of 1.33 A, the magnetic moment

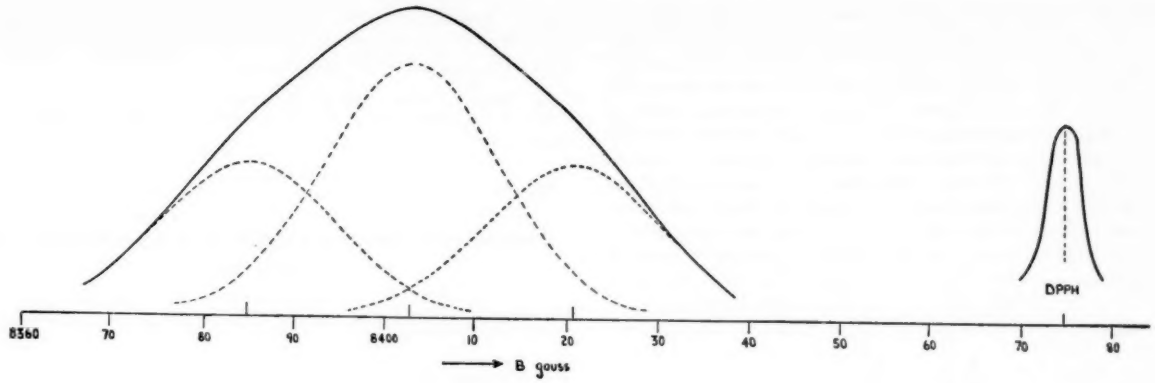

FIG. 1.

of the F-nucleus of 2.6 mm would lead to a triplet splitting of 5.6 gauss. The existence of a g-shift of positive sign characteristic of halogen orbitals and the larger value of the triplet splitting would indicate that the extra electron participates to a certain extent in the CF bonding. Hyperfine interaction of the electron with more distant surrounding the F-nuclei would account for the large width (23 gauss) of the resonance lines.

* Work supported by the U. S. Air Force through the Office of Scientific Research of the Air Research and Development Command.

† Now returned to King's College, Newcastle/Tyne, in the University of Durham, England.

[1] E. E. Schneider and T. S. England, Physica **17**, 221 (1951).
[2] Schneider, Day, and Stein, Nature **168**, 645 (1951).
[3] E. E. Schneider, Trans. Faraday Soc. (to be published); see also Gordy, Smith, and Trambarulo, *Microwave Spectroscopy* (John Wiley and Sons, Inc., New York, 1953), p. 239.

Some Remarks on the Spectra of Nitrites and Nitrosamines

P. TARTE
University of Liège, Liège, Belgium
(Received October 26, 1954)

IN a recent paper,[1] Haszeldine and Jander have reported and briefly discussed the ir and uv spectra of a series of nitroso-compounds. As we have worked for many years in this field, we should like to add some comments to their data and interpretations.

A. Alkyl nitrites.—(1) Haszeldine and Jander have compared the uv spectra of alkyl nitrites in light petroleum and ethanol. This method is not reliable since the mixing of a nitrite, R^1ONO, with an alcohol, R^2OH, is followed by a rather rapid reaction (which is limited to a chemical equilibrium): $R^1ONO+R^2OH \rightleftharpoons R^1OH+R^2ONO$. In the peculiar case studied here (butyl and amyl nitrites in ethanol), the error is not very serious because the uv spectra of ethyl, butyl, and amyl nitrites are very similar. But anyway, the observed spectrum is not the spectrum of a pure compound, and it is evident that another polar solvent should have been chosen.

(2) Rotational isomerism was first proposed by us in 1951[2] and fully confirmed as a general property of alkyl nitrites.[3] We should like to point out that our hypothesis of rotational isomerism is based, not merely upon a study of the doubling and temperature dependence of bands of methyl nitrite in the 6μ region (as it seems to appear from reference 1), but upon (a) a study of the doubling and temperature dependence of *all* the bands (between 3 and 15 μ) of methyl nitrite[3] and monodeuterated methyl nitrite,[4] (b) a systematic study of the uv and ir spectra of 15 alkyl nitrites[5] (rotational isomerism was deduced here from the doubling of the bands of the functional group O—N=O), and (c) a study of the nitrous acid (light and heavy) itself.[5]

B. Dialkylnitrosamines.—We agree with the statement that "The ir spectrum of dimethylnitrosamine dissolved in chloroform . . . is substantially identical with that of the liquid nitrosamine"; but the conclusion "Dimerisation . . . (analogous to *C*-nitrosodimers) . . . is thus improbable" may be considered as premature. We have studied the ir spectra of a series of dialkylnitrosamines in the liquid, dissolved (nonpolar solvent: CCl_4), and gaseous states[6] and, in the case of dimethylnitrosamine, our results are as follows: the band observed at 1317 cm^{-1} in the liquid is significantly weakened in solution and completely disappears in the gas; on the other hand, the band at 1448 cm^{-1} in the liquid is shifted to 1490 cm^{-1}, with a strong increase in intensity in the gas. Such spectral changes are characteristic of strong associations, and our interpretation is the following:

Liquid 1317 cm^{-1} ν_{N-O} frequency of associated molecules
1448 cm^{-1} ν_{N-O} frequency of nonassociated molecules
Gas 1490 cm^{-1} ν_{N-O} frequency of free molecules

(For the discussion of these assignments, see Tarte.[6])

[1] Haszeldine and Jander, J. Chem. Soc. 691 (1954).
[2] D'Or and Tarte, J. Chem. Phys. **19**, 1064 (1951).
[3] P. Tarte, J. Chem. Phys. **20**, 1570 (1952).
[4] P. Tarte, Bull. Soc. Chim. Belges **62**, 401 (1953).
[5] P. Tarte, Bull. Soc. Chim. Belges **59**, 365 (1950). D'Or and Tarte, Bull. Soc. Roy. Sci. e. Liège, **685**, 478 (1951).
[6] P. Tarte, Bull. Soc. Chim. Belges (to be published).

Further Remarks on the Spectra of Nitrites and Nitrosamines

R. N. HASZELDINE AND J. JANDER
University Chemical Laboratory, Pembroke Street, Cambridge, England, and Chemische Laboratorium der Universitat, Freiburg, Germany
(Received November 29, 1954)

(a) The well-known preparative method for methyl nitrite depends on the ready removal of methyl nitrite (b.p. −14°) from the equilibrium:

$$C_5H_{11}ONO+CH_3OH \rightleftharpoons C_5H_{11}OH+CH_3ONO.$$

Escape of any ethyl nitrite (b.p. 17°) produced by a similar equilibrium involving amyl nitrite and ethanol was prevented by deliberate choice of conditions (temperature 10–12°; sealed silica cells) for our measurements. Furthermore, since an independent method (to be published) shows that the amount of ethyl nitrite present at equilibrium is <10–20 percent, the spectrum recorded is in fact predominantly that of amyl nitrite in ethanol. Amyl and butyl nitrites in other solvents (e.g., dimethylformamide; acetonitrile), where equilibria of the above type cannot exist, have spectra identical with those in ethanol and light petroleum.

(b) Dr. Tarte's paper[1] on alkyl nitrites was acknowledged in our publication, but lest this was inadequate it should be made clear that the interpretation given of the infrared spectra of alkyl nitrites is based upon Tarte's original and prior postulate of rotational isomerism in these and similar compounds.

(c) Liquid dimethylnitrosamine shows four strong bands at 6.92, 7.10, 7.60, and 7.76 μ of approximately equal intensity [Fig. 1(a)]. The spectrum of a solution in chloroform [Fig. 1(b)] shows scarcely any change in the position and relative intensities of these bands, or in the band at 9.53 μ, and it was this which led to the conclusion that dimerisation to give $R_2N\cdot N(O^-)\cdot N^+(:O)NR_2$ (analogous to *C*-nitroso-dimers), although it would explain the shift of the N:O vibration, was improbable, since partial dissociation with subsequent change in spectrum was to have been expected. The spectrum of a carbon tetrachloride solution was subsequently found to show appreciable change in several bands; however [Fig. 1(c)], the 6.92 μ band moves to

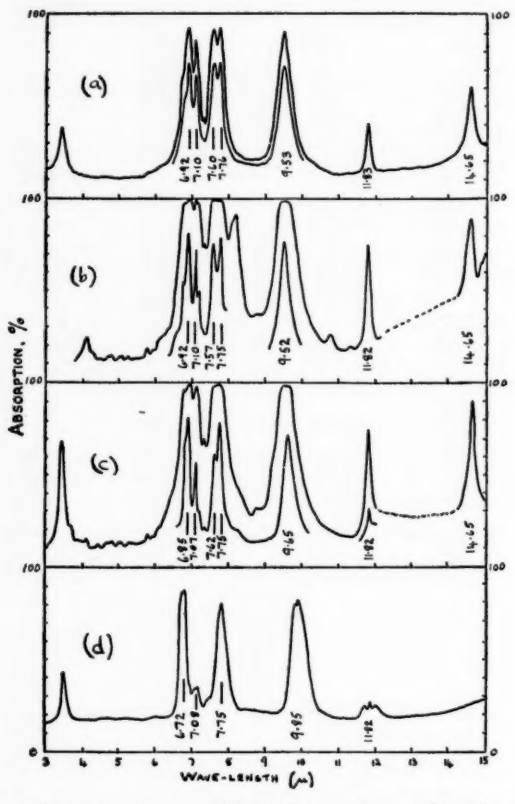

FIG. 1. Absorption spectra of dimethylnitrosamine. (a) Liquid capillary films. (b) Approximately 50 percent and 5 percent solutions in chloroform 0.025 mm cell. (c) Approximately 50 percent and 5 percent solutions in carbon tetrachloride 0.025 mm cell. (d) Vapor in 10 cm gas cell heated at 120°.

6.85 μ, but relative to the 7.76 μ band scarcely changes in intensity and the 7.10 and 7.60 μ bands move to 7.07 and 7.62 μ and are appreciably weakened relative to the 7.76 μ band. The 9.53 μ band shifts to 9.65 μ, but the 11.83 and 14.65 μ bands which appear in the pure liquid remain unchanged in both solutions. Finally the spectrum of dimethylnitrosamine vapor at 120° [Fig. 1(d)] shows the 7.60 μ band as only a weak shoulder, and the 7.1 μ band as a weak peak. The strong bands in the spectrum are now at 6.72, 7.75, and 9.85 μ. We assign the 6.72 μ band to the N:O bond in monomeric dimethylnitrosamine, and agree with the conclusion independently reached by Tarte, namely that in liquid dimethylnitrosamine hydrogen-bonding or association, as suggested earlier but rejected on the basis of the chloroform solution spectrum, must in fact be involved. A detailed discussion of the assignment of the 7.75, 7.07, and 7.62 μ bands, and of the solution and vapor spectra of other nitrosamines, is deferred to a paper to be submitted shortly to the *Journal of the Chemical Society*.

(d) We would take this opportunity of correcting a typographical error in our paper, which was carried through to other papers,[2] namely that the nitrogen-nitrogen vibration, assigned to the strong band in the 9.15–9.55 μ region for liquid nitrosamines, appeared in print as N−O instead of N−N.

[1] P. Tarte, J. Chem. Phys. **20**, 1570 (1952).
[2] R. N. Haszeldine and J. Jander, J. Chem. Soc. 697, 919 (1954).

Pure Rotational Spectrum of H_2Se between 50 and 250 cm^{-1}

E. D. PALIK*
Department of Physics, The Ohio State University, Columbus, Ohio
(Received February 21, 1955)

SEVERAL vibration-rotation bands of H_2Se have been measured by Cameron, Sears, and Nielsen.[1] The fairly simple structure of the observed bands suggests that the molecule is an almost accidently symmetric rotator with the apex angle $2\alpha\approx 90°$ and $a\approx b\approx 2c$ where a, b, and c are the reciprocals of inertia.

The pure rotational spectrum of H_2Se has been observed in the spectral region between 50 and 250 cm^{-1} using the far infrared spectrograph in this laboratory.[2] The gas was prepared by a method involving the chemical reaction

$$Al_2Se_3+6H_2O\rightarrow 2Al(OH)_3+3H_2Se.$$

The gas, dried with P_2O_5, was introduced into a cell 7.5 in. long having polyethylene windows 0.01 in. thick. Several spectrograms were obtained using gas pressures between 3 and 12 cm Hg.

A portion of the observed spectrum is shown in Fig. 1. It consists of a series of strong lines with approximately constant spacing $2c$, with some weaker lines between these main lines. These strong lines are indicated by arrows. Taking into consideration the selection rules $J=0,\pm 1$ and $++\leftrightarrow--$ and $+-\leftrightarrow-+$ for dipole moment along the axis of intermediate moment of inertia,[3] the strong series can be identified with transitions between low τ levels, for example $7_{-6}-6_{-6}$, $8_{-7}-7_{-7}$, $9_{-8}-8_{-8}$. Some of these transitions are indicated in Fig. 1. A weaker series of lines, marked by crosses in Fig. 1, is found to have approximately constant spacing $2a$. These are assigned to high τ transitions, for example 7_6-6_6, 8_7-7_7, 9_8-8_8. The spacing of the lines in these two series give approximate values for a and c, and b was obtained using the fact that $I_c=I_a+I_b$ for a planar figure. Making use of the approximate expression for the energy levels of a slightly asymmetric rotator

$$F(J,K)_{\text{oblate}}=\tfrac{1}{2}(a+b)J(J+1)+[c-\tfrac{1}{2}(a+b)]K^2$$

given by Herzberg,[4] it was possible to calculate the pure rotational spectrum. This approach leads to a tentative assignment of several of the other lines which also form series which are less evident than the two main series.

The analysis was refined by using the Cross, Hainer, King tables[5,6] to calculate energy levels and intensities. It was possible to assign most of the lines between 50 and 150 cm^{-1}. Many of the lines of higher frequency were assigned tentatively, but a quantitative centrifugal stretching correction has not been too successful

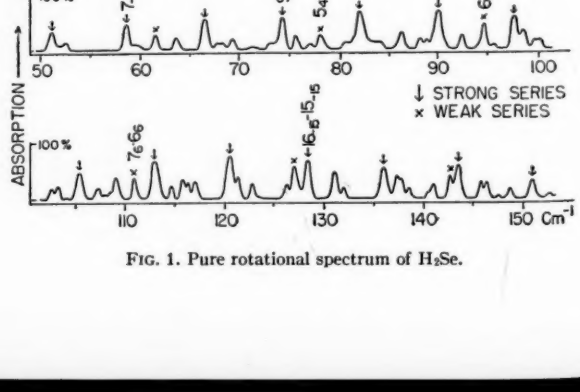

FIG. 1. Pure rotational spectrum of H_2Se.

TABLE I. Molecular constants of H_2Se.

$a=8.16\ cm^{-1}$	$I_a=3.42\times10^{-40}\ g\ cm^2$
$b=7.69$	$I_b=3.64$
$c=3.91$	$I_c=7.16$
$r(H-Se)=1.47\ A$	$2\alpha=91°$

except for the two main series. For these two series, it is found that because of the effect of centrifugal stretching on the energy levels, the observed lines are shifted from the positions of the corresponding rigid rotor lines by an amount proportional to J'.[3] Here J' is the rotational quantum number for the final state involved in the transition.

On the basis of the analysis carried out so far, tentative values for the reciprocals of inertia a, b, c, the moments of inertia I_a, I_b, I_c, the H—Se distance r, and the apex angle 2α can be given. These results are listed in Table I. Since there are several isotopes of selenium, H_2Se^{78}, H_2Se^{80}, etc., there is a slightly different pure rotational spectrum due to each of the molecules because the rotational constants are different, but these spectra essentially coincide for the resolution available in this investigation.

* DuPont Fellow.

[1] Cameron, Sears, and Nielsen, J. Chem. Phys. **7**, 994 (1939).

[2] The spectrograph was available for this investigation through the courtesy of Wright Air Development Center, who, through a contract with The Ohio State University Research Foundation, has provided partial support for its construction and maintenance. This has gratings ruled at the University of Michigan and a Golay detector with a diamond window, the latter being made available through the courtesy of Elias Burstein of the Naval Research Laboratory.

[3] G. Herzberg, *Infrared and Raman Spectra* (D. Van Nostrand Company, Inc., New York, 1945), p. 55.

[4] Reference 3, page 48.

[5] King, Hainer, and Cross, J. Chem. Phys. **11**, 27 (1943).

[6] Cross, Hainer, and King, J. Chem. Phys. **12**, 210 (1944).

Separation of Nitrogen Isotopes by Chemical Exchange between NO and HNO_3*

W. SPINDEL† AND T. I. TAYLOR
Chemistry Department, Columbia University, New York, New York
(Received February 28, 1955)

THE isotopic exchange reaction

$$N^{15}O+N^{14}O_2\rightleftharpoons N^{14}O+N^{15}O_2,$$

first suggested by Urey and Greiff[1] as a possible method of separating nitrogen isotopes, was shown by Leifer[2] to be very rapid even at low temperatures. Using this chemical exchange in a thermal diffusion column, Spindel and Taylor[3,4] obtained an over-all separation of 3.0 in a 2.0 meter column. These results suggested that exchange reactions between gas and liquid phases containing the oxides of nitrogen might also be useful. Calculations from spectroscopic data[2,3,5] indicated favorable equilibrium constants for a number of exchange reactions involving oxy-compounds of nitrogen. Those reactions for which exchange is rapid should yield useful separations if suitable reflux systems are available.

In some preliminary experiments with the exchange reaction[6]

$$N^{15}O(g)+N_2{}^{14}O_3(l)\rightleftharpoons N^{14}O(g)+N_2{}^{15}O_3(l)$$

at 3–5°C in a 2.0 meter column, 1.0 cm i.d., we obtained an over-all separation of 2.1. We have found that the reaction

$$N^{15}O(g)+HNO_3{}^{14}(aq)\rightleftharpoons N^{14}O(g)+HN^{15}O_3(aq)$$

is also rather favorable for the separation of N^{15}. The partial pressures of NO and NO_2 in the gas phase as well as the composition of the liquid phase depends upon the concentration of the nitric acid.[7] The presence of NO_2, N_2O_3, and HNO_2 in the liquid phase apparently speeds up the exchange between NO and HNO_3. When the concentration of NO_2 in the gas phase is too high the over-all separation for the system is lowered. Thus, there appears to be an optimum range of concentration of nitric acid as shown by the following experiments.

The exchange column used for the experiments is shown diagrammatically in Fig. 1. Nitric acid entering the product refluxer is converted to NO and NO_2 by reaction with SO_2; H_2SO_4 being formed in the process. The reaction zone, about 10 cm long, is easily detected by the color of the NO_2 or by the rather marked rise in temperature. A photometer cell is used to automatically control the position of the reaction zone by opening a by-pass solenoid valve in the SO_2 line whenever the color of NO_2 in the cell becomes too intense. A small amount of water (0.05 to 0.1 of the HNO_3 flow) is added at the top of the refluxer to maintain the partial pressure of NO_2 at about that in equilibrium with the nitric acid in the column. The NO from the top of the column is passed into a waste refluxer where it is converted to nitric acid.

The over-all separations obtained in the 1.5 meter column for several concentrations of nitric acid are summarized in Table I. In a similar column 1.2 meters long, Thode and Urey[8] obtained an over-all separation of 1.42 using the $NH_3-NH_4NO_3$ system for which the enrichment factor α is 1.023. For the NO—10M HNO_3 system several preliminary single stage experiments gave an α of 1.045 ± 0.01. Using this value for α, the H.E.T.P. for 10M

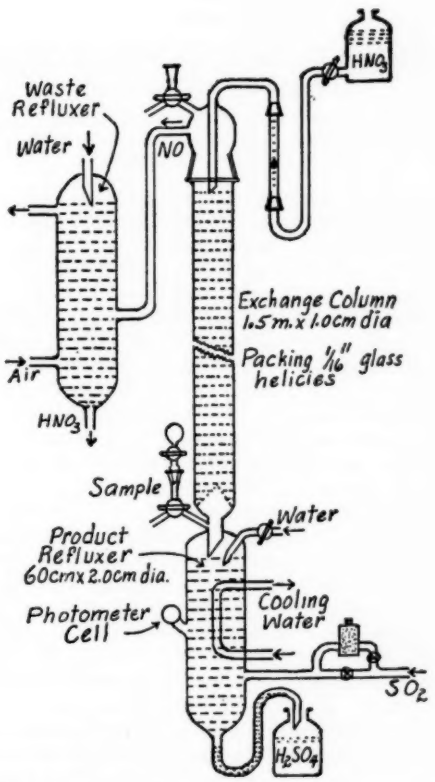

FIG. 1. Exchange column and reflux systems for separation of nitrogen isotopes by exchange of nitric oxide with nitric acid.

TABLE I. Effect of HNO_3 concentration on over-all separation.

Conc. of HNO_3	Flow rate cc/cm²/min	Approx. time for equilibrium, hr	Over-all separation
12 M	1.3	11	1.7–2.0[a]
10 M	1.5	12	2.5
8 M	1.5	10	2.3
6 M	1.3	11	2.0
2 M	0.8	3	1.15

[a] The separations were sensitive to the concentration of NO_2 in the NO from the refluxer.

HNO_3 is 7.2 cm compared to 7.0–7.8 for the $NH_3-NH_4NO_3$ system.[8]

The favorable value of α for the $NO-HNO_3$ exchange considerably reduces the plant size required to produce large quantities of $HN^{15}O_3$. Also the production of a useful chemical, H_2SO_4 in the product refluxer and the low cost of chemicals needed to reflux the waste end of the system, along with the recovery of HNO_3, all serve to reduce the operating cost.

Further experiments are in progress to determine the optimum operating conditions with respect to concentration, temperature, pressure, and flow rates.

* This work was supported by a grant from the U. S. Atomic Energy Commission, AT(30-1) 755.
† On leave from New York State College for Teachers, Albany, New York.
[1] H. C. Urey and L. J. Greiff, J. Am. Chem. Soc. **57**, 321 (1935).
[2] E. Leifer, J. Chem. Phys. **8**, 301 (1940).
[3] W. Spindel, thesis, Columbia University (1950). Paper to be published.
[4] T. I. Taylor and W. Spindel, J. Chem. Phys. **16**, 635 (1948).
[5] W. Spindel, J. Chem. Phys. **22**, 1271 (1954).
[6] A study of this system was started at New York State College for Teachers, Albany, New York by W. Spindel in collaboration with O. E. Lanford. A study of the kinetics of this and similar reactions is being continued there but the isotope separations are being done in this laboratory.
[7] Abel, Schmid, and Stein-Wien, Z. Electrochem. **36**, 692 (1930).
[8] H. G. Thode and H. C. Urey, J. Chem. Phys. **7**, 34 (1939).

Electron Exchange Coupling of Nuclei in Aromatic Systems*

H. S. Gutowsky, L. H. Meyer,† and D. W. McCall‡
Noyes Chemical Laboratory, University of Illinois, Urbana, Illinois
(Received March 2, 1955)

THE high-resolution nuclear magnetic resonance spectra of liquids often exhibit a multiplet structure which arises from an exchange coupling of nonequivalent magnetic nuclei by the bonding electrons.[1] This coupling is greatest for nuclei in atoms bound directly to one another, but it can extend over several bonds. For single bonds, the magnitude of the coupling falls off rapidly with the number of bonds. As an example, we have measured[2] the proton-fluorine coupling in ethyl fluoride and found it to be about 60 and 20 cycles respectively for the CH_2 and CH_3 groups. So the attenuation factor for the additional C–C single bond between the interacting nuclei is the order of $\frac{1}{3}$.

The proton and fluorine spectra observed in several fluorobenzenes are distinctively different from those in aliphatic compounds. Typical results are summarized in Table I, and the proton resonance in fluorobenzene itself is shown in Fig. 1. The latter at first glance is a doublet as would be the case if the fluorine were coupled equally to the *ortho-*, *meta-*, and *para-*protons. The fluorine resonance has apparently six main components with an intensity distribution about as predicted[1] for five protons coupled equally to the fluorine. But the individual components appear broader than in the proton resonance suggesting slightly different coupling with different protons.

Also, the spectra of the di- and tetra-fluorobenzenes require the proton-fluorine coupling to be independent of the proton and fluorine locations in the molecule, but in these compounds no proton-fluorine pair is in the *para-*orientation. The broadened proton and fluorine triplets in 1,3,5-trifluorobenzene show that each proton and fluorine couples mainly with only two nuclei of the opposite species and to a much lesser extent with the third.[3] So the coupling with the *para-*position must be small compared to that with the *ortho-*position.

A small coupling with the *para-*position is compatible with the results for fluorobenzene. In Fig. 1 the left component is definitely broader than the right indicating further, unresolved structure displaced from the center of the resonance by a chemical shift. Moreover, in *para-*substituted monofluorobenzenes (*p*-fluorophenol, -anisole, and -phenetole) the doublet proton resonances are more clearly resolved, even though the splittings are the same as in fluorobenzene.

These results do not appear to have a simple explanation. Coupling via the σ bonds should attenuate rapidly in the *ortho-*, *meta-*, and *para-*sequence, by analogy with aliphatic compounds and as theoretically expected.[1] And if the π electrons predominate in the coupling, the interactions should be comparable at the *ortho-* and *para-*positions, as found for substituent effects.[4] Additional experiments, with higher resolution, are under way to characterize more accurately the exchange coupling in aromatic systems. If the results are amenable to a theoretical analysis, the method should contribute to our understanding of the electronic nature of such systems. In this connection, it is of interest to note the dependence of the coupling constants in Table I on the extent of fluorine substitution. Also, these coupling constants are smaller than that between the CH_3 protons and the fluorine in ethyl fluoride, which are separated by the same number of bonds as a pair of nuclei *ortho* to one another.

TABLE I. Splitting of the nuclear magnetic resonances by the electron coupling of the protons and fluorine nuclei in several fluorobenzenes.

Compound	Proton resonance Line shape[a]	Proton resonance Splitting[b]	Fluorine resonance Line shape[a]	Fluorine resonance Splitting[b]
fluorobenzene[c]	(1-1)	6.8 cycles	6 lines (?)	~6.5 cycles
p-difluorobenzene	(1-2-1)	6.1 cycles	(1-4-6-4-1)	6.5 cycles
1,3,5-trifluorobenzene[c]	(1-2-1)	7.6 cycles	(1-2-1)	7.9 cycles
1,2,4,5-tetrafluorobenzene	(1-4-6-4-1)	9.1 cycles	(1-2-1)	9.3 cycles

[a] The numbers give the relative intensities of the resonance components.
[b] This is the separation between adjacent components; the observed splittings are the same within experimental error for protons and fluorine.
[c] The resonance components for these compounds appear broader than for the others.

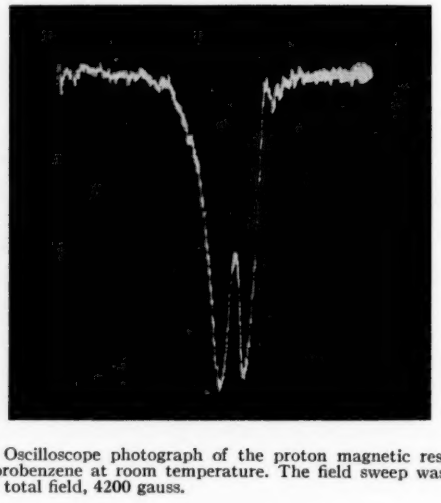

FIG. 1. Oscilloscope photograph of the proton magnetic resonance in liquid fluorobenzene at room temperature. The field sweep was 15 milligauss, the total field, 4200 gauss.

* Supported by the Office of Naval Research and by a grant-in-aid from E. I. du Pont de Nemours and Company.
† U. S. Atomic Energy Commission Predoctoral Fellow. Present address: U. S. Atomic Energy Division, E. I. du Pont de Nemours and Company, Augusta, Georgia.
‡ National Science Foundation Predoctoral Fellow. Present address: Bell Telephone Laboratories, Murray Hill, New Jersey.
[1] Gutowsky, McCall, and Slichter, J. Chem. Phys. **21**, 279 (1953).
[2] Gutowsky, Meyer, and McClure, Rev. Sci. Instr. **24**, 644 (1953).
[3] The three protons are equivalent, group A, and so are the three fluorines, group B, but the fluorobenzenes differ in general from the case described in reference 1, p. 286. The molecular symmetry of the latter case was such that coupling of a (the single) nucleus in group A was the same with all nuclei in group B. However, here the *ortho-*, *meta-*, and *para-*positions are distinguishable from one another when referred to a particular nucleus, so the internuclear coupling can differ at these different sites, even though some of the sites may be identical when considered from the over-all molecular symmetry.
[4] See, for example, C. A. Coulson, *Valence* (Oxford University Press, London, 1952), pp. 247–9.

Free Energy Functions for Gaseous Atoms from Hydrogen ($Z=1$) to Niobium ($Z=41$)

THOMAS J. KATZ AND JOHN L. MARGRAVE
Department of Chemistry, University of Wisconsin, Madison, Wisconsin
(Received March 8, 1955)

ACCURATE thermodynamic functions, especially free energy functions, are needed for all gaseous atoms, but reliable data for their calculation are not always available. The recent critical compilations of Moore[1] include atomic energy levels for neutral and ionized atoms from hydrogen ($Z=1$) to niobium ($Z=41$). With these atomic energy level tables, the chemical atomic weights,[2] and the values of the fundamental constants,[3] one may calculate the free energy function, $(F^0-H_0^0/T)$, for gaseous atoms as described by Giauque.[4] The superscripts indicate that an ideal gas has been assumed. Nuclear spin contributions have not been considered in this work. The free energy function is exceedingly useful for many thermodynamic calculations.[5]

The results of the calculations, which were carried out with an International Business Machines Card-Programmed Electronic Calculator, Model II, in the Numerical Analysis Laboratory of the University of Wisconsin, Madison, Wisconsin, are given in Table I. These values include both translational and electronic contributions to the free energy function. The wiring of the calculator was such that only electronic energy level contributions ≥ 0.0005 were considered. The results agree well with those of Brewer[6] and with the data from the NBS Series III Tables[7] where comparisons are possible. Our results show differences caused by revision of values of the fundamental constants, of chemical atomic weights, and in positions of atomic energy levels. In particular, new or different values are presented for Sc, V, Co, Ga, Zr, and Nb, and should be used for calculations involving these gaseous atoms.

TABLE I. Free energy functions for gaseous atoms.

Element	$-(F^0-H_0^0/T)$ in cal deg^{-1} mole^{-1} 298°K	500°K	1000°K	2000°K
H	22.422	24.993	28.437	31.880
He	25.155	27.726	31.170	34.613
Li	28.173	30.744	34.188	37.631
Be	27.577	30.148	33.592	37.035
B	31.579	34.190	37.664	41.123
C	32.519	35.200	38.727	42.213
N	31.644	34.215	37.658	41.102
O	33.074	35.840	39.459	43.002
F	32.689	35.413	39.057	42.642
Ne	29.978	32.549	35.992	39.436
Na	31.744	34.315	37.759	41.202
Mg	30.534	33.104	36.548	39.992
Al	33.754	36.570	40.209	43.755
Si	34.064	37.102	40.928	44.587
P	34.010	36.581	40.024	43.469
S	34.746	37.538	41.276	44.928
Cl	34.426	37.060	40.688	44.338
A	32.012	34.583	38.027	41.471
K	33.326	35.897	39.340	42.785
Ca	32.023	34.594	38.037	41.481
Sc	35.120	37.691	41.134	46.260
Ti	37.021	40.103	44.033	47.793
V	37.205	40.448	44.663	48.840
Cr	36.666	39.237	42.681	46.151
Mn	36.523	39.094	42.538	45.981
Fe	37.618	40.532	44.504	48.368
Co	37.780	40.489	44.381	48.513
Ni	38.045	40.897	44.822	48.823
Cu	34.775	37.346	40.790	44.235
Zn	33.481	36.052	39.496	42.939
Ga	35.122	37.960	42.011	45.986
Ge	34.171	37.406	41.994	46.390
As	36.642	39.213	42.656	46.102
Se	37.242	39.817	43.334	47.024
Br	36.834	39.406	42.854	46.362
Kr	34.218	36.789	40.232	43.676
Rb	35.658	38.229	41.672	45.116
Sr	34.354	36.925	40.369	43.813
Y	37.371	40.284	44.221	48.015
Zr	37.850	40.798	44.989	49.264
Nb	37.792	41.308	46.015	50.512

The authors wish to acknowledge the aid of the Wisconsin Alumni Research Foundation for funds supporting the use of het computing machines, and the cooperation of the staff of the Numerical Analysis Laboratory of the University of Wisconsin.

[1] C. E. Moore, *Atomic Energy Levels* (National Bureau of Standards, Washington 25, D. C.), Circular 467, Vol. I (1949) and Vol. II (1952).
[2] E. Wichers, J. Am. Chem. Soc. **76**, 2033 (1954).
[3] Rossini, Gucker, Johnston, Pauling, and Vinal, J. Am. Chem. Soc. **74**, 2699 (1952).
[4] W. F. Giauque, J. Am. Chem. Soc. **52**, 4808 (1930).
[5] J. L. Margrave, J. Chem. Educ. (to be published).
[6] L. Brewer, *National Nuclear Energy Series*, edited by L. L. Quill (McGraw-Hill Book Company, Inc., New York, 1950), Paper 3, Vol. 19B.
[7] *Selected Values of Chemical Thermodynamic Properties, Series III* (National Bureau of Standards, Washington, D. C.).

On the Molar Sound Velocity in Liquids and the Liquid State

HERMAN I. LEON
Department of Engineering, University of California, Los Angeles, California
(Received February 21, 1955)

THERE are several proposed theories[1,2] that provide a somewhat simplified mechanical model of liquid structure, but prediction of ultrasonic velocities from these models is not completely satisfactory. There is another technique, completely empirical, for predicting ultrasonic velocities that makes use of the additive property of the molar sound velocity in organic liquids.

Rao[3] observed that the thermal coefficient of sound velocity in organic liquids is about three times the thermal coefficient of density:

$$\frac{1}{v}\left(\frac{\partial v}{\partial T}\right)_P=3\frac{1}{\rho}\left(\frac{\partial \rho}{\partial T}\right)_P \tag{1}$$

where v is the ultrasonic velocity, ρ the density, P the pressure, and T the absolute temperature. The molar sound velocity R follows by integration:

$$R=Vv^{\frac{1}{3}} \tag{2}$$

where V is the molar volume. No theoretical justification for the form of Eqs. (1) and (2) has yet been found.

Theoretical and numerical analysis.—It is known from the derivation of the one-dimensional wave equation in a lossless fluid that the velocity of sound is[4]

$$v^2=\left(\frac{\partial P}{\partial \rho}\right)_S=\gamma\left(\frac{\partial P}{\partial \rho}\right)_T \tag{3}$$

for small amplitude sound waves, in which P is pressure, S is entropy, and γ is the ratio of specific heats. Differentiating with respect to temperature and substituting from (3), we finally derive (for constant γ)

$$\frac{1}{v}\left(\frac{\partial v}{\partial T}\right)_P=\left\{\frac{\rho}{2}\left(\frac{\partial T}{\partial \rho}\right)_P\left(\frac{\partial \rho}{\partial P}\right)_T\left[\frac{\partial}{\partial T}\left(\frac{\partial P}{\partial \rho}\right)_T\right]_P\right\}\frac{1}{\rho}\left(\frac{\partial \rho}{\partial T}\right)_P. \tag{4}$$

In order to give theoretical support to the experimental relation of Eq. (1), we wish to show that the term in brackets in Eq. (4) is numerically equal to three.

A numerical method of calculating the factors in Eq. (4) has been proposed by Watson,[5] who presents a table of values for T_r, P_r, and f, where T_r and P_r are dimensionless ratios to critical values, and f is directly proportional to ρ. This table is claimed to be applicable to calculations for all liquids with good accuracy.

Figure 1 shows the results of graphical and numerical evaluation of Eq. (5).[6] For room temperature and atmospheric pressure, the range of T_r is from 0.50 to 0.65 and of P_r from 0.02 to 0.03 for hydrocarbons. It is seen that for these values the ratio of thermal coefficients of sound velocity to density runs close to 3. For higher temperatures and pressures, the ratio is substantially greater. From these results a ratio of 3 for the temperature coefficients appears to be nothing more than an accident of environmental conditions.

Analytical equations of state.—Of the several equations of state for the liquid phase, one has been used with moderate success by Kittel[1] to predict temperature and pressure coefficients of density,

FIG. 1. Ratio of thermal coefficient of sound velocity to thermal coefficient of density where T_r = temp. (°R)/critical temp., P_r = psia/(psia)$_{crit.}$ For hydrocarbons: room temp.: T_r = 0.5 to 0.65 atmos pressure: P_r = 0.02 to 0.03.

sound velocity, and sound absorption:

$$PV_a = 3RT \tag{5}$$

where R is the perfect gas constant and V_a is the available volume. Furthermore, V_a is the difference between the actual volume and the volume of closest packing. From this expression, Kittel derives expressions for the temperature coefficients of sound velocity and density. The ratio of these coefficients becomes

$$\frac{V}{2V_a}\left[1-\frac{T}{\gamma}\left(\frac{\partial\gamma}{\partial T}\right)_P\right]-1. \tag{6}$$

If we arbitrarily set this ratio of coefficients equal to 3, we merely derive a relationship, $V=8V_a$ (neglecting a term involving γ), that is consistent with Eqs. (1) and (5). It is apparent that theoretical footing for Eq. (1) cannot be found through this approach.

[1] C. Kittel, J. Chem. Phys. **14**, 614 (1946).
[2] W. Schaaffs, Z. physik. Chem. **196**, 397 (1941).
[3] M. R. Rao, Indian J. Phys. **14**, 109 (1940) and J. Chem. Phys. **9**, 682 (1941).
[4] See, for instance, P. Vigoureux, *Ultrasonics* (John Wiley and Sons, Inc., New York, 1951).
[5] K. M. Watson, Ind. Eng. Chem. **35**, 398 (1943).
[6] The variation in γ can be calculated from Watson's tables, and terms involving derivatives of γ are to be negligibly small.

Nuclear Spin-Spin Coupling in Substituted Benzenes

EDWARD B. BAKER
Dow Chemical Company, Midland, Michigan
(Received March 15, 1955)

HIGH resolution nuclear magnetic resonance spectroscopy is capable of contributing greatly to knowledge of the structures of substituted benzenes. Studies based on gross position of the ring hydrogens and of attached fluorines were reported by Gutowsky[1] *et al.* The fine structure of the ring hydrogens caused by chemical differences and by mutal spin-spin splitting[2] studied in the proton spectra, or in spectra of magnetic substituents, can also contribute valuable quantitative information.

A great variety of situations can arise, some too complicated for present resolving power. We present several simple cases to illustrate the method.

The fluorine spectra of *p*-fluoro ethyl benzene (Fig. 1) and fluorobenzene (Fig. 2), show by the multiplicities and intensity distributions that the ring protons all couple equally to the fluorine. Equality of coupling strikingly demonstrates the effect of π-bond resonance, since the coupling is passed undiminished around the ring. In the corresponding proton spectra (not shown) spin-spin doublets are observed, with coupling constant 6.6 cps in both proton and both fluorine spectra. Since no internal chemical shifts are evident in the proton spectra the ring hydrogens are chemically equivalent, and resonating structures bearing formal charges must be proportioned to fulfill this condition or be negligible. The absolute shifts of proton and fluorine spectra are in

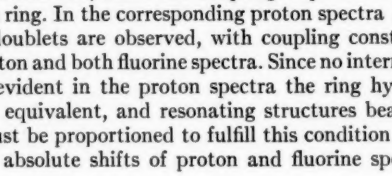

FIG. 1. F^{19} spectrum of *p*-fluoro ethyl benzene at 30 Mc (reference C_4F_8O).

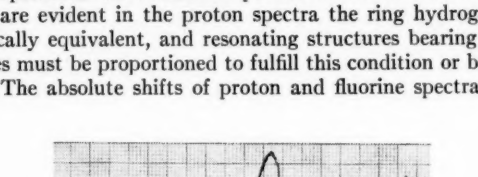

FIG. 2. F^{19} spectrum of fluorobenzene at 30 Mc (reference (C_4F_8O).

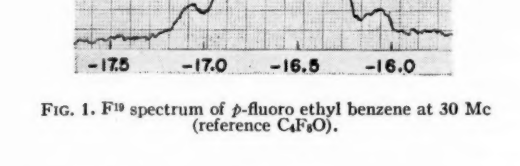

FIG. 3. Ring H′ spectrum of *p*-nitrocumene at 40 Mc (reference H_2O).

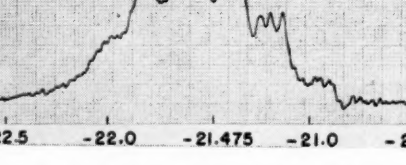

FIG. 4. H′ spectrum of nitrobenzene at 40 Mc (reference H_2O).

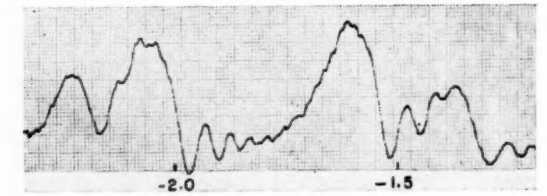

FIG. 5. Ring H′ spectrum of *o*-dibromo benzene at 40 Mc (reference H_2O).

accord with each other and indicate a donation of electrons to the ring by fluorine in the case of fluorobenzene, and a withdrawal in the case of *p*-fluoro ethyl benzene (by comparison with benzene).

Relative chemical shifts of ring hydrogens and destruction of around-the-ring coupling are illustrated by *p*-nitro cumene (Fig. 3). In this case no external magnetic nuclei are needed to demonstrate the inequality of coupling. This pattern is interpreted as a mutual splitting ($J=7.5$ cps) by two nonequivalent protons ($\delta=0.70$ ppm) with duplication on the opposite side of the ring by an independent pair of protons. The nitro group is electron withdrawing, and if one assumes less electron density on *ortho*- than *meta*-hydrogens the *ortho*-hydrogens lie on the low field side.

Nitrobenzene (Fig. 4) appears qualitatively similar except for the superposition of the *para* line between *ortho* and *meta*; it is closer to *meta* according to the assumption made above. The $o-m$ chemical difference is now only $\delta=0.62$ ppm and coupling $J=6.6$ cps. Since the *para* is unsplit, it is not coupled to *ortho*. Since *para* and *meta* are nearly the same chemically, the *para-meta* splitting would be nearly forbidden.

Finally, *o*-dibromo benzene (Fig. 5) is an example of an intermediate case in which around-the-ring coupling is still present but internal chemical shifts are apparent. The spectrum shows two spin-spin multiplets ($J=3.5$ cps) of three components separated by a chemical shift of $\delta=0.47$ ppm. Thus both J and δ are intermediate between the fluoro and nitro compounds discussed above. The absolute position indicates a withdrawal of electrons from the ring close to that for nitrobenzene although the manner of withdrawal is quite different. The two spin groups of two protons apiece are evidently the pair adjacent to the bromines and the pair opposite, from symmetry. Since the absolute position of the line center ($\delta=-2.0$) indicates the bromines are electron withdrawing, the pair of protons adjacent to the bromines should have lessened electron density and thus are assigned to the low field triplet.

[1] Gutowsky, McCall, McGarvey, and Meyer, J. Am. Chem. Soc. **74**, 4809 (1952).
[2] N. F. Ramsey and E. M. Purcell, Phys. Rev. **85**, 143 (1952); E. L. Hahn and D. E. Maxwell, Phys. Rev. **88**, 1070 (1952); Gutowsky, McCall, and Slichter, J. Chem. Phys. **21**, 279 (1953).

Note on the Branching Condition in the One-Dimensional Free Electron Gas Model

ARTHUR A. FROST
Department of Chemistry, Northwestern University, Evanston, Illinois
(Received February 8, 1955)

KUHN,[1] in a letter to this Journal with the above title as well as elsewhere[2,3] has discussed a modified relation between first derivatives of the wave function along the one-dimensional branches in a free-electron system at the branching point. He proves that the necessary and sufficient condition for conservation of probability current[1] and that there be a system of orthogonal functions[3] is

$$\Sigma_i(d\psi s_i/ds_i)_P=\mathrm{K}\psi_P, \qquad (1)$$

where the s_i are coordinates along the several branches meeting at the point P; these coordinates are defined as all increasing in a direction away from this point. The ψs_i are the wave functions along these branches with ψ_P their common value at the point of intersection. K is a constant which must be the same for all acceptable wave functions at the point P but can be different for other branching points.

The previously used branching condition of Kuhn[4] and of Griffith[5] and Ruedenberg and Scherr[6] is Eq. (1) but with $K=0$.

It is to be noted that Kuhn has not used in his proofs any specific assumption about the potential energy of the electron as a function of position. Equation (1) is therefore more general than required for the free electron method and applies regardless of whether or not the potential energy is constant. It will now be argued that K differs from zero only if there is a delta function discontinuity in the potential energy and that therefore for the free electron method K must be zero as in the original calculations.

First consider a branching point with only two branches. This, of course, is a case of really no branching at all. Nevertheless, the proofs apply equally well. Equation (1) then states that in the neighborhood of any point there may be a discontinuity in the derivative. Now it would ordinarily be concluded that such a discontinuity would not be permitted in any acceptable wave function and therefore K must be zero. Nevertheless, a finite value of K can have significance even in this nonbranching case, as discussed recently by this author[7] in connection with a delta potential function model where $K=-2\ mg/\hbar^2$, m being the mass of the electron and g the strength of the delta potential function.

Now consider a branching point with three or more branches. The simplest example is a hydrogen-like atom in its 1_s state. Replace the usual three-dimensional problem by one involving a wave function along n one-dimensional straight line branches radiating out from the nucleus. With $n=2$ as pointed out in reference 7 the correct energy and wave function along the line are obtained if $g=Ze^2$, the magnitude of the charge product of nucleus and electron. In order for the same correct solution for energy and wave function to be obtained for n branches, Eq. (1) must be satisfied with $K=-nmg/\hbar^2$.

The conclusion is that the new Kuhn condition (1) with K not zero applies only if the potential energy involves delta functions. If the electrons are free or have only continuous changes in potential then $K=0$, in which case the old condition is applicable.

This research was supported by the National Science Foundation.

[1] H. Kuhn, J. Chem. Phys. **22**, 2098 (1954).
[2] H. Kuhn, Z. Elektrochem. **58**, 219 (1954).
[3] H. Kuhn, Z. Naturforsch. **9a**, 989 (1954).
[4] H. Kuhn, Helv. Chim. Acta **32**, 2247 (1949).
[5] J. S. Griffith, Trans. Faraday Soc. **49**, 345 (1953).
[6] K. Ruedenberg and C. W. Scherr, J. Chem. Phys. **21**, 1565 (1953).
[7] A. A. Frost, J. Chem. Phys. **22**, 1613 (1954).

Infrared Spectrum of Iridium Hexafluoride

H. C. MATTRAW, N. J. HAWKINS, D. R. CARPENTER, AND W. W. SABOL
Knolls Atomic Power Laboratory, Schenectady, New York*
(Received March 10, 1955)

ALL of the Group VI hexafluorides have been shown to have the symmetrical structures of regular octahedra. Since rhenium hexafluoride in Group VII has been shown to be octahedral it is interesting to see if this symmetry is retained by IrF_6 a Group VIII hexafluoride.

Iridium hexafluoride was prepared at KAPL by direct combination of the elements. Purification of the golden yellow gas was accomplished by vacuum distillation in a copper and nickel vacuum system.

The infrared spectrum of iridium hexafluoride was recorded over the range of 2 to 40 μ. Nickel cells with silver chloride windows were used in the range from 2 to 23 μ. The cells were heated externally and spectra recorded at temperatures from 25°C to 100°C. The instrument used for this part of the investigation was a standard Baird Spectrophotometer with sodium chloride and potassium bromide prisms. In the range from 23 to 40μ a Perkin-Elmer single-beam instrument utilizing a KRS-5 prism was used.†

The spectrum of iridium hexafluoride is typical of the other heavy metal hexafluorides of O_h symmetry.[1] That is, there are a total of six fundamental vibrations, two of which (ν_3 and ν_4) are infrared active. Both of these fundamental vibrations were ob-

served directly; the other four fundamental vibrations were derived from the binary combination bands.

In the sodium chloride region the two highest frequency combinations are $\nu_1+\nu_3$ and $\nu_2+\nu_3$; ν_4 has less intense bands in combination with ν_1 and ν_2. Although the $\nu_3+\nu_5$ is always observed in molecules of this type, its frequency is practically identical with $\nu_1+\nu_4$. The value for ν_6, the inactive vibration, was determined from the combination band $\nu_2+\nu_6$.

Iridium hexafluoride is apparently more reactive than the Group VI hexafluorides, for the gas attacks both silver chloride and KRS-5. The attack was apparently a tightly bonded surface "corrosion," for soon after the initial attack the band produced at 16.1 μ with silver chloride and the band at 18.4 μ with KRS-5 neither increased nor decreased with changes in pressure within the cells. It was noted also, in preliminary experiments, that the gas dissolved slowly in Teflon and reacted to give some CF_4. This necessitated the removal of inner Teflon gaskets from the cells.

The observed frequencies and their assignments are presented in Table I.

TABLE I. Infrared spectrum of IrF_6.

Observed band, cm^{-1}	Intensity[a]	Assignment
1414	M	$\nu_1+\nu_3$
1361	M	$\nu_2+\nu_3$
972	W	$\nu_1+\nu_4$
		$\nu_3+\nu_5$
918	W	$\nu_2+\nu_4$
850	MW	$\nu_2+\nu_6$
785	VW	$3\nu_4$
718	VS	ν_3
465	VW	$\nu_5+\nu_6$
450	VW	$\nu_3-\nu_5$
440	VW	$\nu_2-\nu_6$
324	W	$2\nu_5-\nu_6$
276	VS	ν_4

[a] Symbols: M = medium, W = weak, MW = medium weak, VW = very weak, VS = very strong.

The P-, Q-, R-branches of ν_4 were observed at 272, 276, and 281 cm^{-1}, respectively.

The fundamentals for the fluorides of tungsten, rhenium, and iridium are listed in Table II.

An unsuccessful attempt was made to determine the Raman spectrum. Because of the yellow color and reactivity of IrF_6 it will require more than normal effort. However, ν_5 is still open to question since $\nu_3+\nu_5$ apparently coincides with $\nu_1+\nu_4$.

TABLE II. Fundamental vibrations.

	Species	WF_6[a]	ReF_6[b]	IrF_6
ν_1	A_{1g}	769	753	696
ν_2	E_g	670	600	643
ν_3	F_{1u}	712	716	718
ν_4	F_{1u}	256	393	276
ν_5	F_{2g}	322	246	260
ν_6	F_{2u}	216	170	205

[a] Burke, Smith, and Nielsen, J. Chem. Phys. **20**, 447 (1952).
[b] J. Gaunt, Trans. Faraday Soc. **50**, 209 (1954).

The data presented in Table II indicate that Gaunt's value of ν_4 in ReF_6 may be too high.

Because of the lack of knowledge of the electronic ground state and the internuclear distances in IrF_6, it was thought unwise to compute thermodynamic properties.

* Operated by the General Electric Company for the U. S. Atomic Energy Commission.
† This instrument is owned by the General Electric Research Laboratory and is operated by Dr. R. S. McDonald who had borrowed the prism through the generosity of M. I. T.
[1] G. Herzberg, *Molecular Spectra and Molecular Structure. II. Infrared and Raman Spectra of Polyatomic Molecules* (D. Van Nostrand Company, Inc., New York, 1945), p. 122.

Use of Partially Oriented Solid Samples and Unpolarized Radiant Energy in the Analysis of Infrared Absorption Spectra

JAMES E. STEWART
National Bureau of Standards, Washington 25, D. C.
(Received February 10, 1955)

THE infrared spectrum of an unoriented solid sample, e.g., alkali halide pellet, is frequently different from a spectrum of an oriented sample, e.g., film deposited on a window.

The absorption coefficient (for a particular vibration with its transition dipole moment, p, making an angle, θ, with the plane of the incident energy wave front and with the projection of p on the wave front plane, making an angle, ϕ, with a particular electric field vector) can be written:

$$a=K\int_{-\pi/2}^{\pi/2}\int_{0}^{2\pi}(p\cos\theta\cos\phi)^2 n_i(\theta)\,d\phi\,d\theta,$$

where $n_i(\theta)$ is the distribution function expressing the density of transition moments in direction θ, and the incident electric field vectors are assumed randomly distributed over all angles ϕ. For perfect orientation relative to the plane of the wave front $n_i(\theta)=N_i$, $a_0{}^i=K'N_ip^2\cos^2\theta$. For completely random orientation $a_r{}^i=K'N_ip^2/2$. Molecular vibrations of a given symmetry species have their transition moments in the same direction in the molecule, provided the species is such that the representation of the motions is $+1$ under C_n for $n>1$, -1 under σ, or -1 under S_n, and in general the direction varies from one species to another. But the direction of transition moments for the same vibration may vary from molecule to molecule in the lattice, and it is the lattice which is oriented. Hence, a_0 is determined from a sum of $a_0{}^i$ with a term for each set of equivalent molecules in the lattice, i.e., sets which can be generated by translation of a single molecule. N_i is then interpreted as the number of equivalent molecules in the ith set per lattice unit and $N=\Sigma N_i$. The ratio a_0/a_r should be the same for absorption bands belonging to the same vibration symmetry species.

In practice a_r is influenced by scatter, the effect of particle size on absorption even in the absence of scatter,[1] and the formation of different isomeric, polymorphic, or chemical species.[2] However, a qualitative inspection of spectra is often informative.

An example of the application of the proposed technique occurs in the vibrational assignment for p-dichlorobenzene. Free molecules are in point group V_h, and the infrared active fundamentals are distributed in species: $5b_{1u}+3b_{2u}+5b_{3u}$. Two b_{2u} vibrations and one b_{3u} vibration lie outside the rocksalt region. The rest are easily assigned by analogy with benzene, p-difluorobenzene, etc. (see Table I), except for two close bands at about 820 K. One of these is $\sigma_{20}(b_{2u})$, an out-of-plane hydrogen bending mode, and the other is $\sigma_{14}(b_{1u})$, the carbon-chlorine antisymmetric stretching mode. In the monoclinic crystal lattice[3] of space group $C_{2h}{}^5$ (factor group C_{2h}), the site group is C_i with two molecules per unit cell oriented in slightly different directions. Consequently the b_{1u}, b_{2u}, b_{3u}, and also the two infrared inactive a_u modes of point

TABLE I. Infrared spectrum of para-dichlorobenzene.

Frequency (K or cm^{-1})	Species, assignment, description	a_0/a_r
3021	b_{1u}: σ_{10} CH stretch	—
1475	σ_{11} CC stretch	0.28
1085	σ_{12} CH in-plane bend	0.29
1014	σ_{13} ring deform.	0.34
818	σ_{14} CCl stretch	0.33
821	b_{2u}: σ_{20} CH out-of-plane bend	1.2
<400 not observed	σ_{21} ring bend	—
406 ?	σ_{22} CCl out-of-plane bend	>1
3096	b_{3u}: σ_{26} CH stretch	—
1393	σ_{27} CC stretch	1.1
1221	σ_{28} ring deform.	2.3
1124	σ_{29} CH in-plane bend	1.5
<400 not observed	σ_{30} CCl in-plane bend	—

group V_h are converted to infrared active species a_u of point group C_i. One of the additional vibrations lies beyond the rocksalt region and the other, a CH out-of-plane bending mode, is probably weak because it is rendered active only by crystal forces.

Comparison of the spectrum of a partially oriented film of *p*-dichlorobenzene prepared by crystallization from the liquid phase on a rocksalt window with a spectrum of an equivalent amount of the same sample crushed, finely ground with potassium iodide, and pressed into a clear disk shows that the shoulder at 821 K increases in intensity ($a_0/a_r=1.2$), whereas the band at 818 K decreases ($a_0/a_r=0.33$) in the oriented form. Furthermore, intensities of all of the bands assigned to b_{1u} vibrations are seen to decrease in the oriented form. Therefore 818 K is assigned to $\sigma_{14}(b_{1u})$.

[1] J. E. Stewart, J. Research Natl. Bur. Standards **54**, 41 (1955).
[2] J. E. Tyler and S. A. Ehrhardt, Anal. Chem. **25**, 390 (1953).
[3] S. B. Hendricks, Z. Krist. **84**, 85 (1932).

Relative Intensities of Anthracene and Naphthacene Emissions under Cathode-Ray, Ultraviolet, and X-Ray Excitations

B. D. SAKSENA, *National Physical Laboratory of India, New Delhi, India*
AND
L. M. PANT, *Department of Physics, University of Allahabad, Allahabad, India*

(Received October 25, 1954)

IT is well known that ultraviolet light[1,2] (of wavelength <3900 A), γ radiation or α particles[3] excite a very strong fluorescence of naphthacene dissolved at very low concentrations (10^{-4} percent) in anthracene crystals. The phenomenon is due to an excitation migration (Förster[4]) in which the energy is first absorbed by anthracene molecules, and a certain proportion is then transferred to naphthacene molecules depending on their concentration. Since, according to Pringsheim,[5] the intensity of fluorescence and also the energy distribution of the fluorescent spectrum are both independent of the type of excitation, it may be expected that the relative intensities of anthracene and naphthacene emission for a given contaminated specimen would not depend upon the type of excitation but, experimentally, such is not the case.

We have studied the luminescence of the same specimen of anthracene (a Merck chemical) under ultraviolet, cathode-ray, and x-ray excitations. Six bands are obtained. Their peak-wavelengths and band widths are the same in all the cases but the relative intensities differ. (See Fig. 1 and Table I.)

Since the fluorescent bands of naphthacene in solution occur between 4600–5800 A (4680, 4980, 5330, 5740), we may attribute the bands at 4976, 5342, and 5735 A observed by us to naphthacene and call them naphthacene bands. The main result from Table I is that naphthacene bands are much stronger than anthracene bands with x-ray and cathode-ray excitation than with ultraviolet.

We have also investigated the fluorescence of a different sample of anthracene with 3650, 3131, and 2536 radiations from a Hanovia mercury arc using a quartz spectrograph as monochromator. The

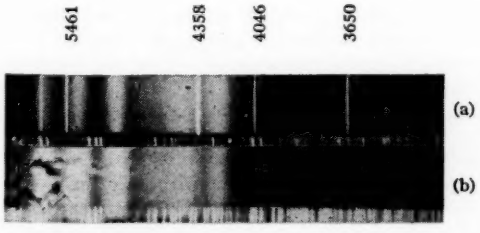

FIG. 1. Luminescence of anthracene. (a) Ultraviolet excitation. (b) Cathodo excitation.

TABLE I.[a]

Peak-wavelength (A)	5735	5342	4976	4645	4471	4236
Band width (A)	5859–5611	5466–5220	5085–4866	4705–4587	4574–4371	4303–4170
Intensity under cathode rays	10	10	10	1	3	4
X-rays	5	5	5	1	2	1
Ultraviolet (3650 A)	1	3	4	1	3	4

[a] (Intensity estimates are only visual and relative to the strongest band.)

fluorescence was photographed by another quartz spectrograph. The microphotometer curves are shown in Fig. 2. It may be seen that anthracene band at 4236 A is slightly stronger than naphthacene band at 4976 A for 3650 and 3131 A excitations, but the reverse happens with 2536 A excitation. (See Table II.)

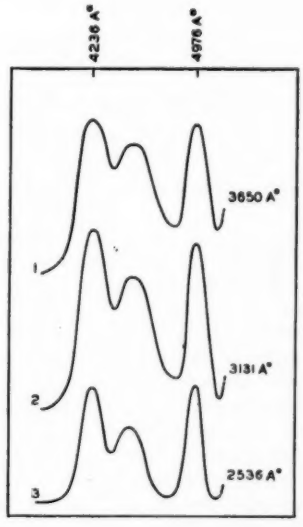

FIG. 2. Microphotometer curves for ultraviolet luminescence of anthracene with 3650, 3131, 2536.

The results stated in the above paragraph may be explained as follows. The different exciting radiations have different penetrating powers depending on their wavelength and, therefore, the fluorescence produced has to traverse different thicknesses of the crystal before it is emitted. Due to the overlap of fluorescence and absorption bands in solid anthracene,[6] the fluorescent radiation would be partly absorbed by its passage through the crystal especially at its short wavelength end. Therefore, relative to the band at 4976 A the band at 4236 A would suffer greater diminution of intensity on irradiation with 2536 A than with 3650 A because the former radiation penetrates deeper into the crystal.

The results of x-ray and cathode-ray excitation are, however, not explained by this reasoning. Firstly, in these cases, the long wavelength region does not possess the same distribution of intensity as in the ultraviolet excitation, which it should if the short wavelength end alone is absorbed by overlap reabsorption effects. Secondly in cathode-ray excitation, the penetration of the electrons in the crystal[7] is extremely small and, therefore, relative to the long wavelength end the 4236 A band should have a larger intensity in this case than in ultraviolet excitation.

There may be other factors that affect the migration of excitation energy. It has been reported[3,8] that on irradiation with x-rays, the system containing terphenyl and diphenyl-hexatriene in

TABLE II. Ratio of the density of the 4236 band and 4976 band in various excitations.

Excitation wavelength	3650	3131	2536 A
Density ratio	1.21	1.14	0.96

xylene solutions at 293°K shows only fluorescence characteristic of diphenyl-hexatriene which is of greater intensity than that from a system containing only hexatriene, but on irradiation with 2537 or 3131 radiations no such result is obtained—the spectrum being that to be expected if the two substances are absorbed or emitted independently of each other.

Thanks are due to C.S.I.R. for a scholarship to one of us (L.M.P.).

[1] P. Pringsheim, *Fluorescence and Phosphorescence* (Interscience Publishers, Inc., New York, 1949), pp. 365, 407–8.
[2] G. F. J. Garlick, *Luminescent Materials* (Oxford University Press, New York, 1949), pp. 234.
[3] H. Kallmann and M. Furst, Phys. Rev. **79**, 857 (1950) and Phys. Rev. **81**, 853 (1951).
[4] Th. Forster, Ann. physik. **2**, 55 (1948); Z. Naturforsch. **4a**, 321 (1949).
[5] P. Pringsheim, see reference 1, pp. 307 and 310.
[6] E. J. Bowen and F. Wokes, *Fluorescence of Solutions* (Longmans Green and Company, New York, 1953), pp. 21.
[7] H. W. Leverenz, *Introduction to Luminescence of Solids* (John Wiley and Sons, Inc., New York, 1950), pp. 157–59.
[8] C. Reid and M. M. Moodie, J. Chem. Phys. **22**, 1126 (1954).

Tritium Isotope Effect in the Isomerization of Cyclopropane*

RALPH E. WESTON, JR.
Chemistry Department, Brookhaven National Laboratory, Upton, Long Island, New York
(Received March 10, 1955)

THE generally accepted mechanism for homogeneous unimolecular gaseous reactions is some form of that originally proposed by Lindemann.[1] According to this, a reactant molecule obtains the necessary activation energy by collision with a second molecule (reactant or added inert gas). At sufficiently high pressure, the activated molecules have a Maxwell-Boltzmann energy distribution and the rate-determining step is the decomposition of an activated molecule. At very low pressure this energy distribution is not maintained, and the slow step becomes the transfer of energy by collision. While many of the reactions once used as experimental support for this mechanism have since fallen into disrepute, recent work[2,3] has given new proof of its validity.

We have sought for a new type of evidence concerning this mechanism: the variation in the kinetic isotope effect as a function of pressure.[4] At high pressure the isotope effect will be that for the decomposition of an activated molecule. If this involves breaking a bond to an isotopically labeled atom, the effect for this step can be predicted by the usual methods.[5] For the activation and deactivation steps involving only collisional transfer of energy, the rates may be considered classical, to a first approximation, and hence without isotope effect. Therefore, the effect is expected to decrease from the value for bond-breaking to zero as the pressure decreases.

The reaction studied was the isomerization of tritium-labeled cyclopropane to propylene. All evidence points to this as a clean, unimolecular isomerization.[3,6] Cyclopropane-t was allowed to react in a 2-l flask at ~500°C, and samples of the reaction mixture were removed at different times. For analysis of the mixture, propylene was absorbed in a solution of mercuric sulfate. The remaining cyclopropane was placed in a counting tube, and the specific activity (SA) was measured using standard techniques. The original cyclopropane-t has a SA of ~0.5 mc/mole. The isotope effect is defined as $\epsilon=1-(k'/k)=-\log S/\log(1-f)$, where $S\equiv(SA)_f/(SA)_o$ and f is the fractional completion of the reaction.[4] The results are summarized in Table I. In addition, some preliminary experiments with a 100-ml reaction vessel and a slightly different analytical procedure gave $\epsilon=0.125$ at ~1 atmosphere.

The complete disappearance of the isotope effect in the low pressure region indicates the validity of the Lindemann mechanism, and of the assumption about the rates of collisional energy transfer. The high pressure effect is interesting because of theoretical calculations by Slater,[7] in which the "critical coordinate" for this reaction is found to be a C—H rather than a C—C distance.

TABLE I. Tritium isotope effect in the isomerization of cyclopropane.

P, mm	T, °C	No. of samples	$1-f$	S	100ϵ
0.40–0.43	493	7	0.439–0.515	1.004±0.010	0.4±1.0
45	470	1	0.502	1.063	8.9
77	493	4	0.438±0.011	1.067±0.009	7.9±1.1
80	493	3	0.725±0.006	1.031±0.006	8.8±1.7
700	470	1	0.797	1.039	17.0
		2	0.620	1.056±0.014	11.3±3.0
		4	0.481±0.009	1.097±0.017	12.7±2.3
		Weighted mean at 700 mm			12.9±2.7

Our results confirm this since the other choice of critical coordinate would not give a hydrogen isotope effect. If a correction is made for the five paths by which a labeled molecule can react by breaking a C—H rather than a C—T bond, $k_T/k_H=0.28$. While it is impossible to make an accurate *a priori* calculation of this ratio, a reasonable model of the transition state will fit the experimental value.

Details of the cyclopropane-t synthesis, the experimental procedure, and the results will be published later. Similar experiments using cyclopropane-d_6 are contemplated; the larger isotope effect for the completely labeled molecule would be subject to less experimental error, and would provide a more rigorous test of Slater's calculations.

I am indebted to Dr. Jacob Bigeleisen for many helpful discussions during the course of this work.

* Research performed under the auspices of the U. S. Atomic Energy Commission.
[1] For discussion, see L. S. Kassel, *The Kinetics of Homogeneous Gas Reactions* (The Chemical Catalog Company, Inc., New York, 1932), Chap. V.
[2] R. L. Mills and H. S. Johnston, J. Am. Chem. Soc. **73**, 938 (1951); H. S. Johnston and R. L. Perrine, 4782.
[3] Pritchard, Sowden, and Trotman-Dickenson, Proc. Roy. Soc. (London) **A217**, 563 (1953).
[4] R. B. Bernstein [J. Phys. Chem. **56**, 893 (1952)] mentions this possibility.
[5] J. Bigeleisen, J. Chem. Phys. **17**, 675 (1949).
[6] T. S. Chambers and G. B. Kistiakowsky, J. Am. Chem. Soc. **56**, 399 (1934); E. S. Corner and R. N. Pease, *ibid.* **67**, 2067 (1945).
[7] N. B. Slater, Proc. Roy. Soc. (London) **A218**, 224 (1953).

Diffusion of Radioactive Calcium in $Ca_3Si_2O_7$

R. LINDNER AND ARTHUR S. OBERMAYER*
Chalmers University of Technology, Gothenburg, Sweden, and Massachusetts Institute of Technology, Cambridge 39, Massachusetts
(Received February 28, 1955)

IN connection with a program of investigations on the mechanism of solid-state reactions[1] the formation of silicates has been studied. During the reaction between lime and silica, several silicates are found in the reaction layer,[2] and the mobility of calcium ions in one of them, namely $Ca_3Si_2O_7$, has been measured in the following way.

The silicate was produced by the powder reaction between very pure calcium carbonate and pulverized quartz crystals. After reaction at 1000°C the mixture was compressed to pellets, which were heated for several days at about 1350°C. After repeated pulverizations, compressions, and heat treatments the initial instability of the pellets (produced by traces of *ortho*-silicate which undergo a transformation followed by an increase in volume) disappeared and from the x-ray powder pattern no evidence of the *ortho*-silicate could be found.

The diffusion of Ca^{45} was measured by three different methods. At higher temperatures a single pellet with a thin radioactive layer was used. This layer had been produced by transfer of Ca^{45} from a radioactive pellet in contact with an inactive one under influence of an electric field. During the experiment the activity measured at the surface decreased as a consequence of diffusion of the active material to the interior and self-absorption of the soft β radiation within the silicate. At lower temperatures the

diffusion coefficients were evaluated according to the amount of radioactivity exchanged between a homogeneous radioactive sintered pellet and an inactive one kept in firm contact with it at diffusion temperatures.[3] The values obtained are shown in Fig. 1

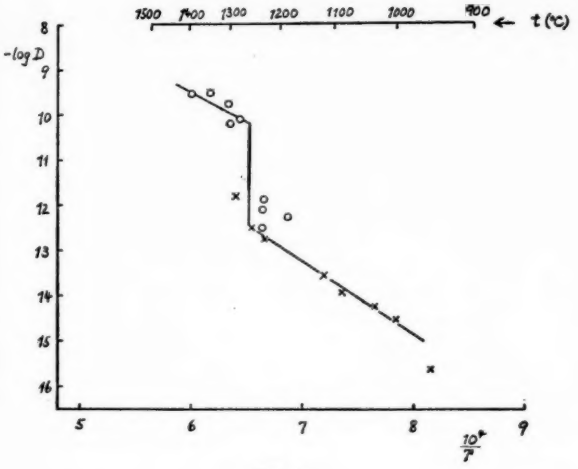

FIG. 1.

where the logarithm of the diffusion coefficient is plotted against the inverse absolute temperature. At lower temperatures that function can be approximately described by the expression: $D=10^{-2}\exp(-73\,000/RT)$. At about 1260°C the diffusion coefficient increases with about 2 orders of magnitude. (A considerable scattering of the values is observed, and they must be considered as preliminary.) No information is available about a possible transformation at that temperature.

The ionic conductivity was determined by application of a dc field of about 1000 volts to a system of radioactive and inactive pellets. The transfer number was found to be a logarithmic function of temperature and varies between 10^{-3} at 830°C and 10^{-1} at 1205°C. The specific electric conductivity changed by about one order of magnitude abruptly near 1280°C.

The self-diffusion coefficients calculated from the data for ionic conductivity do not agree with the coefficients measured with radioactive tracers. The assumption that the Einstein relation is not valid can, however, not be made before the details of the assumed transformation process have been investigated, as e.g. a freezing-in of high-temperature modifications could be possible.

* Massachusetts Institute of Technology Overseas Summer Fellow, 1953.
[1] R. Lindner, J. Chem. Phys. **23**, 410 (1955).
[2] W. Jander, and E. Hoffmann, Z. anorg. u. allgem. Chem. **128**, 211 (1934).
[3] R. Lindner, J. Chem. Soc. 395 (1949).

Cathodo-Luminescence Spectrum and Energy Levels in MgO

B. D. SAKSENA AND L. M. PANT
National Physical Laboratory of India, New Delhi, India
(Received February 22, 1955)

RECENTLY we reported[1] that the cathodo-luminescence spectrum, at room temperature, of a fresh specimen of MgO cleaved from a natural crystal shows a strong and broad band having peak at 2.75 ev and a weaker one having peak at 2.16 ev. As exposure continues, the former band gets weaker and the latter stronger and there is also an extension of the former towards the ultraviolet. These results may be explained qualitatively on the basis of an energy scheme for Mg-colored crystals.

We assume that oxygen is liberated from oxides under cathode-ray bombardment[2,3] producing an oxygen deficit or a stoichiometric excess of metal. This assumption is also supported by the fact that the absorption bands produced by electron[4,5] and neutron[6] bombardment and ultraviolet irradiation[6] are the same as those observed for Mg-colored crystals.[7]

There is reason to believe that the gap between the top of the uppermost filled band of the crystal and the bottom of the conduction band may be 5.9 ev.[8–10] Although Johnson[11] thinks that this width is greater than 7.3 ev, his conclusions need reconsideration because MgO is found to be transparent from 9μ to 0.22μ.[7,12,13] Other absorption bands beyond 0.22μ may be the fundamental band[8] (peak at 1850 A) and a band due to the first

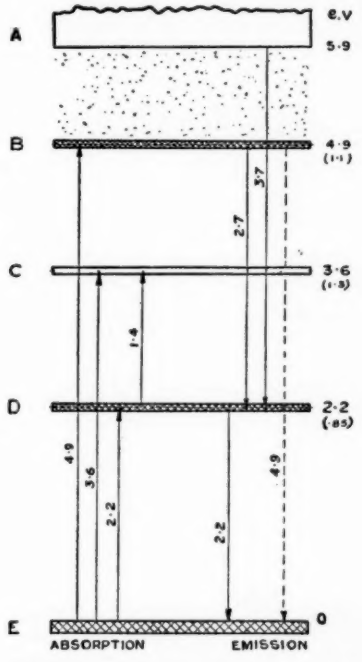

FIG. 1. Schematic representation of energy levels in Mg-colored MgO. *A* is the conduction band, and *E* the filled band while *B*, *C*, *D* are bands due to excess Mg impurity centers. The widths of these bands are indicated in small brackets. The dotted region between *A* and *B* indicates that the *B* levels when fully developed will overlap the conduction band *A*.

excited state of the crystal (tail at 7 ev and peak at 12 ev from the valence band[8,14]).

Following the work of Day[6] and Weber[7] we postulate, with reference to the valence band, three energy levels at 4.9, 3.6, and 2.2 ev in the forbidden zone (Fig. 1) and consider that the 2.2- and 4.9-ev levels are occupied and the 3.6-ev levels empty and that there is a large preponderance of the latter over the former.

In cathode-ray excitation the electrons are raised to the conduction band creating holes in the valence band and luminescence occurs when an electron combines with a hole. Since even a pure specimen has a small concentration of 2.2-ev levels (Day[6]), we expect two bands close to 2.2 and 3.7 ev in the emission spectrum of a pure specimen. If the 4.9-ev occupied level is also present, as may happen at small concentration of excess Mg, we will have an additional band close to 2.7 ev. The 3.7-ev band appears very weakly in our spectrograms but it appears strongly in the emission spectra of pure normal crystals obtained by Eisenstein.[15]

The relative intensities of these bands will depend greatly on the concentration of excess Mg for the following reasons: (1) The 4.9-ev levels screen the conduction band from the 2.2-ev levels

and therefore produce a diminution in the intensity of the 3.7-ev band relative to the 2.7-ev band. When fully developed, this (4.9-ev) band (semi-width 1.1 ev[7]) would merge into the conduction band and electronic transitions between the two bands would be possible even thermally producing a considerable weakening of the 3.7-ev band and an extension of the 2.7-ev band into the ultraviolet. This may account for the very small intensity of the 3.7-ev band in our spectrograms. (2) The numerous unoccupied 3.6-ev levels in Mg-colored specimens capture electrons from the occupied 4.9-ev levels which are therefore unable to produce luminescence by combining with holes in the 2.2-ev levels. This greatly reduces the intensity of the 2.7-ev band while the 2.2-ev band increases in intensity due to an increase in the concentration of excess Mg. The intensity variations observed in these bands with continued cathode-ray excitation are possibly due to this cause.

[1] B. D. Saksena and L. M. Pant, Proc. Phys. Soc. (London) **67**, 811 (1954)
[2] Headrick and Lederer, Phys. Rev. **50**, 1094 (1936).
[3] Jacobs, J. Appl. Phys. **17**, 596 (1946).
[4] Boyd, Rich, and Avery, Atomic Energy Commission Report No. MDMC-1508, 1947 (unpublished).
[5] Pringsheim and Nelson, Arr. Natl. Lab. Report 4232, 1948 (unpublished).
[6] H. R. Day, Phys. Rev. **91**, 822 (1953).
[7] R. Weber, Z. Physik **130**, 392 (1951).
[8] D. A. Wright, Proc. Phys. Soc. (London) **60**, 13 (1948).
[9] J. B. Johnson and K. G. Mckay, Phys. Rev. **91**, 582 (1953).
[10] Lempicki, Proc. Phys. Soc. (London) **66**, 278 (1953).
[11] P. D. Johnson, Phys. Rev. **94**, 845 (1954).
[12] J. Strong and R. T. Brice, J. Opt. Soc. Am. **25**, 207 (1935).
[13] Barnes, Brattain, and Seitz, Phys. Rev. **48**, 582 (1935).
[14] N. F. Mott and R. W. Gurney, *Electronic Processes in Ionic Crystals*, (Clarendon Press, Oxford, England, 1950), pp. 76–78.
[15] A. Eisenstein, Phys. Rev. **93**, 1017 (1953).